GHENT UNIVERSITY

FACULTY OF SCIENCES

The role of Nanos3 in tumor progression

Evi De Keuckelaere

Thesis submitted in partial fulfillment of the requirements for the degree of

Doctor of Science: Biochemistry and Biotechnology

2017-2018

Promoters: Prof. Dr. em. Frans Van Roy and Prof. Dr. Geert Berx

dbmb department of biomedical molecular biology

CRIG

VIB

The research described in this doctoral thesis was performed at the Department of Biomedical Molecular Biology, Faculty of Sciences, Ghent University, and at the Inflammation Research Center (IRC), Flanders Institute for Biotechnology (VIB).

Evi De Keuckelaere was supported by a personal fellowship of the Research Foundation Flanders (FWO-Vlaanderen).

The role of Nanos3 in tumor progression

By Evi De Keuckelaere

Molecular and Cellular Oncology Lab

Department of Biomedical Molecular Biology, Ghent University

Cancer Research Institute Ghent (CRIG)

Inflammation Research Center, Flanders Institute for Biotechnology (VIB)

Technologiepark 927

B-9052 Gent-Zwijnaarde, Belgium

Academic year: 2017-2018

Promoters:	Prof. Dr. em. Frans Van Roy[1, 2]
	Prof. Dr. Geert Berx[1, 3]
Examination committee:	
Chair:	Prof. Dr. Peter Brouckaert[1]
Secretary:	Prof. Dr. Wim Declercq[1, 2]
Examination board	Prof. Dr. Kris Vleminckx[1, 3, 4]
	Prof. Dr. Philippe Birembaut[5, 6]
	Prof. Dr. Pieter Mestdagh[7]
	Prof. Dr. Nadine Van Roy[7]

[1] Department of Biomedical Molecular Biology, Ghent University, Ghent, Belgium

[2] VIB Inflammation Research Center, Ghent University, Ghent, Belgium

[3] Cancer Research Institute Ghent, Ghent University, Belgium

[4] Center for Medical Genetics, Ghent University, Ghent, Belgium

[5] INSERM UMR-S 903, SFR CAP-Santé, University of Reims Champagne-Ardenne, France

[6] Laboratory of Histology, CHU Reims, France

[7] Department of Pediatrics and Medical Genetics, Ghent University, Ghent, Belgium

SUMMARY

Nanos genes encode RNA-binding proteins (RBPs) that form a post-transcriptional repressor complex together with a Pumilio protein. This complex regulates transcript stability and translation upon binding Nanos regulatory/response elements (NREs), Pumilio-binding elements (PBEs), or both in the 3'UTR of mRNA targets.

Nanos proteins belong to a highly conserved protein family found in both vertebrates and invertebrates. Since a general overview of the extent of this conservation was missing, we created a phylogenetic tree based on the C-terminal zinc finger domain, which is the only conserved domain among all nanos proteins.

The normal physiologic expression of nanos proteins is mainly restricted to the gonads and the brain. As such, they have generally been studied with regard to their role in germ cell development. However, in humans, Nanos1 and Nanos3 are both upregulated in non-small cell lung cancers (NSCLCs). In NSCLC cell lines, overexpression and silencing of Nanos3 are linked to epithelial-mesenchymal transition (EMT) and mesenchymal-epithelial transition (MET), respectively. This occurs partly by negatively influencing E-cadherin transcription and stimulating vimentin expression.

In this project, we investigated the expression of Nanos3 in several human cancer cell lines and we made use of NSCLC cell lines with and without Nanos3 overexpression to identify new mRNA targets. To examine the contribution of Nanos3 to tumor progression *in vivo* we generated a conditional Nanos3-expressing mouse, which was crossed with mice from established lung cancer mouse models and a prostate cancer mouse model. Prostate cancer was chosen since preliminary data in our group demonstrated a correlation between Nanos3 expression levels and tumor aggressiveness in human prostate cancer tissues.

Both lung cancer and prostate cancer are frequently diagnosed cancers that are responsible for around 23% of the cancer deaths worldwide. Any research that focuses on better understanding the tumorigenesis of these cancers can be relevant in the search for better treatments for these cancers.

In both LSL-KRas^{G12D};p53$^{fl/fl}$;CCSP-rtTA$^{+/-}$;TetO-Cre$^{+/-}$ and LSL-KRas^{G12D};CCSP-rtTA$^{+/-}$;TetO-Cre$^{+/-}$ NSCLC models, after doxycycline induction, mice with ectopic Nanos3 expression (Nanos3$^{LSL/-}$

;LSL-KRas^{G12D};p53$^{fl/fl}$;CCSP-rtTA$^{+/-}$;TetO-Cre$^{+/-}$ and Nanos3$^{LSL/-}$;LSL-KRas^{G12D};CCSP-rtTA$^{+/-}$;TetO-Cre$^{+/-}$) died earlier than the control mice (LSL-KRas^{G12D};p53$^{fl/fl}$;CCSP-rtTA$^{+/-}$;TetO-Cre$^{+/-}$ and LSL-KRas^{G12D};CCSP-rtTA$^{+/-}$;TetO-Cre$^{+/-}$). Mice from the LSL-KRas^{G12D};p53$^{fl/fl}$;CCSP-rtTA$^{+/-}$;TetO-Cre$^{+/-}$ NSCLC mouse model were used to further investigate this.

The only notable difference between the lungs of both genotypes seemed to be the enhanced bronchiolar dysplasia observed in the Nanos3-expressing mice compared to the control mice. Several primary cell lines were established from the lung of a control and a Nanos3 NSCLC mouse. These were used in an allograft experiment and showed that Nanos3 expression did not seem to influence the ectopic tumor growth. Both mice, injected with either control or Nanos3-expressing lung tumor-derived (LuTD) cell lines, demonstrated lung metastases. Although lymph node metastases were observed in both mice injected with control or Nanos3-expressing LuTD cell lines, these metastases were bigger and differentiated in mice injected with the latter.

Prostate-specific ectopic Nanos3 expression did not appear to effect the survival of Hi-Myc transgenic mice, as comparable prostate cancer progression was observed in Hi-Myc control mice and Nanos3-expressing mice.

To further look into the mechanisms and possible pathways involved in the function of Nanos3 we used several approaches in search of interaction partners of Nanos3, including MAPPIT, co-immunoprecipitation and proximity-dependent biotin identification (BioID). This revealed DDX1 and several Argonaute proteins as new interaction partners of Nanos3. DDX1 seems to be involved in Nanos3-mediated post-transcriptional regulation. The interaction of Nanos3 with members of the Argonaute family further establishes the link between Nanos proteins and the miRNA regulatory network. Additionally, other interesting complexes, involved in mRNA regulation, were identified in the Nanos3 proxeome.

In summary, the *Nanos* genes constitute a highly conserved gene family with a role in germ cell development. Recently, evidence for ectopic expression of Nanos proteins in human cancer is growing. We have clearly shown that expression of Nanos3 influences the survival of NSCLC mice and uncovered a link between Nanos3 expression and lymph node metastatic propensity. Further research will be necessary to further elucidate the molecular functions

of Nanos proteins and the involved molecular interaction partners, and to verify whether Nanos proteins are potent promoters of tumor formation and progression.

SAMENVATTING

Nanos genen coderen voor RNA-bindende eiwitten die een posttranscriptioneel repressorcomplex vormen met een Pumilio eiwit. Dit complex reguleert de stabiliteit van de mRNA sequentie en de translatie na het binden van Nanos-regulatorische elementen, Pumilio-bindende elementen, of beide in de 3'UTR van de mRNA doelwitten.

Nanos eiwitten behoren tot een sterk geconserveerde eiwitfamilie die zowel in gewervelde als in ongewervelde dieren voorkomt. Gezien een algemeen overzicht van de omvang van deze conservatie nog niet gerapporteerd was, hebben we een fylogenetische boom gemaakt op basis van het C-terminale zinkvinger domein, wat tevens het enige geconserveerde domein is van alle nanos eiwitten.

De normale fysiologische synthese van nanos eiwitten is voornamelijk beperkt tot de geslachtsklieren en de hersenen. Zodoende worden ze voornamelijk bestudeerd met betrekking tot hun rol in de ontwikkeling van kiemcellen. In mensen worden Nanos1 en Nanos3 echter beide opgereguleerd in niet-kleincellige longcarcinomen (NSCLCs). In cellijnen van dit soort kanker zijn overexpressie en neerregulatie van Nanos3 respectievelijk gelinkt aan epitheliale-mesenchymale transitie (EMT) en mesenchymale-epitheliale transitie (MET). Dit gebeurt gedeeltelijk door de negatieve regulatie van E-cadherine transcriptie en het stimuleren van vimentine expressie.

In dit project gingen we de expressie van Nanos3 na in verschillende humane kankercellijnen en maakten we gebruik van NSCLC cellijnen met en zonder overexpressie van Nanos3 met als doel nieuwe mRNA doelwitten te identificeren. Om de bijdrage van Nanos3 na te gaan in "*in vivo* tumorprogressie" hebben we een conditionele Nanos3-expresserende muis gecreëerd. Deze muis werd vervolgens gekruist met muizen van gevestigde muismodellen voor longkanker en een muismodel voor prostaatkanker. Dit laatste werd gekozen aangezien voorafgaande data in onze groep een correlatie aantoonde tussen Nanos3 expressie en de kwaadaardigheid van de tumor in humane prostaatkankerweefsels.

Longkanker en prostaatkanker zijn vaak gediagnosticeerde kankers en zijn wereldwijd verantwoordelijk voor ongeveer 23% van alle sterfgevallen die te wijten zijn aan kanker. Elk onderzoek dat zich richt op een beter begrip van het ontstaan en de progressie van tumoren

van deze kankers kan relevant zijn bij het zoeken naar betere behandelingen voor deze kankers.

In beide onderzochte NSCLC modellen stierven muizen met ectopische expressie van Nanos3 (Nanos3$^{LSL/-}$;LSL-KRas^{G12D};p53$^{fl/fl}$;CCSP-rtTA$^{+/-}$;TetO-Cre$^{+/-}$ en Nanos3$^{LSL/-}$;LSL-KRas^{G12D};CCSP-rtTA$^{+/-}$;TetO-Cre$^{+/-}$), na doxycycline inductie, eerder dan de controle muizen (LSL-KRas^{G12D};p53$^{fl/fl}$;CCSP-rtTA$^{+/-}$;TetO-Cre$^{+/-}$ en LSL-KRas^{G12D};CCSP-rtTA$^{+/-}$;TetO-Cre$^{+/-}$). Muizen van het LSL-KRas^{G12D};p53$^{fl/fl}$;CCSP-rtTA$^{+/-}$;TetO-Cre$^{+/-}$ NSCLC muismodel werden gebruikt om dit verder te onderzoeken.

Nanos3 muizen vertonen een sterkere bronchiolaire dysplasie dan de controle muizen en dit is schijnbaar het enige opvallende verschil tussen de longen van beide genotypen. Er werden verschillende primaire cellijnen gemaakt van de long van een controle en een Nanos3 NSCLC muis. Deze cellijnen werden subcutaan geïnjecteerd in naakte muizen en demonstreerden dat Nanos3 expressie schijnbaar geen invloed heeft op de ectopische tumorgroei. Zowel muizen geïnjecteerd met controle of Nanos3-expresserende cellen, afgeleid van primaire tumoren van onze NSCLC muizen, vertonen uitzaaiingen naar de long (longmetastasen). Lymfekliermetastasen werden gedetecteerd in zowel muizen die geïnjecteerd waren met controle tumor-afgeleide cellijnen als muizen die geïnjecteerd waren met Nanos3-expresserende tumor-afgeleide cellijnen. De metastasen waren echter groter en gedifferentieerd in muizen geïnjecteerd met deze laatste cellijnen.

Wanneer Nanos3 specifiek tot expressie werd gebracht in de prostaat, observeerden we geen effect van Nanos3 op de overleving van Hi-Myc transgene muizen. Zowel in de Hi-Myc controle muizen als in de Nanos3-expresserende muizen verliep de tumorprogressie gelijkaardig.

In een zoektocht naar de door Nanos3 gebruikte mechanismes en pathways hebben we verschillende technieken gebruikt met als doel het ontdekken van interactiepartners van Nanos3, zoals MAPPIT, co-immunoprecipitatie en proximiteit-afhankelijke biotine-identificatie (BioID). DDX1 en verschillende Argonaute eiwitten kwamen naar boven als nieuwe interactiepartners van Nanos3. DDX1 is betrokken in de posttranscripitonele regulatie van Nanos3. De aangetoonde interactie tussen Nanos3 en leden van de Argonaute familie onderbouwen de link tussen Nanos eiwitten en het miRNA netwerk. Verder werden

er ook andere interessante complexen teruggevonden in het Nanos3-proxeoom. Deze waren voornamelijk betrokken in mRNA regulatie.

Kort samengevat vormen *Nanos* genen een sterk geconserveerde genfamilie met een rol in kiemcelontwikkeling. Ectopische expressie van Nanos eiwitten werd ook reeds gedetecteerd in humane tumorweefsels. We hebben duidelijk aangetoond dat expressie van Nanos3 de overleving van NSCLC muizen beïnvloedt en hebben een verband ontdekt tussen Nanos3 expressie en de geneigdheid voor lymfekliermetastasen. Verder onderzoek is nodig om de moleculaire functies van Nanos eiwitten en de betrokken interactiepartners verder op te helderen. Verder moet er ook nog worden nagegaan of Nanos eiwitten wel degelijk het ontstaan van tumoren en tumorprogressie kunnen bevorderen.

Table of contents

List of abbreviations

A

AA	amino acid
ACC	adrenocortical carcinoma
ACK	Ammonium-Chloride-Potassium
AcyC	adenoid cystic *c*arcinoma
Adeno	adenovirus
Ago	argonaute
AML	acute myeloid leukemia
AR	androgen receptor
ArgoL1	argonaute linker 1 domain
ArgoN	N-terminal domain of argonaute
AT1/2	alveolar type 1/2 cell

B

BAC	bronchioloalveolar carcinoma
BADJ	bronchoalveolar duct junction
BASC	bronchioalveolar stem cell
BBB	blood-brain barrier
BCCM	Belgian coordinated collections of microorganisms
BiFc	bimolecular fluorescence complementation
BioID	proximity-dependent biotin identification
BLOC-1	biogenesis of the lysosome-related organelle complex 1
BORC	BLOC-1-related complex

BPB	bromophenol blue
BPDE	benzo(a)pyrene diol epoxide
BPE	bovine pituitary extract
BPH	benign prostatic hyperplasia
Brat	brain tumor
BRET	bioluminescence resonance energy transfer
Bron	bronchioles
BS3	bis(sulfosuccinimidyl)suberate
BTB	blood-testis barrier

C

CC10	Club cell 10 kDa protein
CCDS	consensus coding sequence
CCLE	cancer cell line encyclopedia
CCSP	Club cell secretory protein
CCT	chaperonin-containing TCP-1
CCT5	T-complex protein subunit epsilon
CD44v6	CD44 variant 6
CNA	copy number alteration
CNRQ	calibrated normalized relative quantity
Co-IP	co-immunoprecipitation
CPEB	cytoplasmic polyadenylation element binding protein
CTA	cancer testis antigen
CTNNBL1	β-catenin-like protein 1

D

Dimer	dimerization
DLBC	diffuse large B-cell lymphoma
DNA-PKcs	DNA-dependent protein kinase catalytic subunit
Dox	doxycycline
dREAM	*Drosophila* Rb, E2F and Myb-associated protein
DREAM	dimerization partner (DP), Rb-like, E2F and MuvB
dsRNA	double-stranded RNA
DTA	Diphtheria toxin A
DTT	Dithiothreitol

E

ECL	enhanced chemiluminescence
ECM	extracellular matrix
EGF	epidermal growth factor
eGFP	enhanced green fluorescent protein
ELISA	enzyme-linked immunosorbent assay
EMT	epithelial-mesenchymal transition
ER	estrogen receptor
ERT	tamoxifen-dependent estrogen receptor
ES cell	embryonic stem cell

F

FBF	fem-3 binding factor
FCS	fetal calf serum
FDA	food and drug administration

Fl	floxed, flanked with loxP sites
Flp	flippase
FRET	fluorescence resonance energy transfer
FRT	Flp Recombinase/Recognition Target site

G

GBM	glioblastoma
GEMMS	genetically engineered mouse models
GO	Gene Ontology

H

HAT-medium	hypoxanthine-aminopterin-thymidine medium
HBE	human bronchial epithelium
HDAC1	histone deacetylase 1
Hid	head involution defective
HIFU	high intensity focused ultrasounds
HOS	human osteosarcoma
HPV-16	human papilloma virus 16

I

IF	immunofluorescence
IHC	immunohistochemistry
IP	immunoprecipitation
IRES	internal ribosomal entry site

K

KLH	keyhole limpet hemocyanin

L

l(3)mbt	lethal (3) malignant brain tumor
LFQ	label-free quantification
LGG	low-grade glioma
L-Gln	L-Glutamine
LHRH	luteinizing hormone-releasing hormone
Lkb1	liver kinase B1
LPb	large probasin promotor
LSL	floxed stop cassette
Lung squ	lung squamous cell carcinoma

M

M domain	middle domain
MBL	medulloblastoma
MBP	maltose binding protein
MET	mesenchymal-epithelial transition
mLIF	mouse leukemia inhibitory factor
MMP-14	matrix metalloproteinase-14
MNNG	N-methyl-N’-nitro-N-nitrosoguanidine
mRNP	messenger RNP

N

N.A.	not available
NBR	NOT module binding region
NCBI	National Center for Biotechnology
ncRNAs	non-coding RNAs

Nd	not determined
NEAA	non-essential AA
NED	nanos effector domain
Neo	neomycine
NEPC	neuroendocrine prostate cancer
NIM	NOT1 interacting motif
NRE	Nanos regulatory/response element
Ns	not significant
NSCLC	non-small cell lung cancer
NuRD	nucleosome remodeling and histone deacetylation

O

ON	overnight
Osr-1	odd skipped related 1

P

PABP	poly(A) binding protein
Para	paralytic
PARP-1	poly [ADP-ribose] polymerase 1
PAZ	PIWI/Argonaute/Zwille
Pb	probasin
PBE	Pumilio-binding element
P-bodies	processing bodies
PBST	PBS with 0.1% Tween 20
PCM	Pumilio conserved motif
PCPG	pheochromocytoma and paraganglioma

PD-1	programmed cell death 1
PD-L1	PD-1 ligand
PFA	paraformaldehyde
PGK	phosphoglycerine kinase
PIN	prostatic intraepithelial neoplasia
piRNAs	PIWI-interacting RNAs
PIWI	P-element-induced whimpy testes
PKP4	plakophilin-4
PLAK	plakoglobin
PMSF	phenylmethylsulfonyl fluoride
PSA	prostate-specific antigen
PSF	Protein Service Facility
PVDF	polyvinylidene fluoride

R

RBP	RNA-binding protein
RCC2	regulator of chromosome condensation 2
RIBOc	ribonuclease III
RIP	RNA immunoprecipitation
RISC	RNA-induced silencing complex
RLU	relative light units
Rnc	ribonuclease
RNP	ribonucleoprotein
RRM	RNA recognition motif
rRNAs	ribosomal RNAs

RT	room temperature
RTK	receptor tyrosine kinase
rtTA	reverse tetracycline transactivator

S

s.c.	subcutaneous(ly)
SA	splice acceptor site
Sca1	stem cell antigen-1
SCC	squamous cell carcinomas
SCLC	small cell lung cancer
SDS	sodium dodecyl sulfate
SFM	serum-free medium
Sftpc	surfactant protein C
siRNAs	short-interfering RNAs
SMN	survival motor neuron
snRNA	small nuclear RNA
snRNP	small nuclear ribonucleoprotein
SOD	sodium deoxycholate
SPC	surfactant protein C
SPRY	Spla and Ryanodine receptor
SRB	sulforhodamine B
SrmB	Superfamily II DNA and RNA helicases
SSC	saline-sodium citrate
STK11	serine-threonine kinase 11
SV40 Tag and tag	Simian Virus 40 large/small T antigen

T

TAP	tandem affinity purification
TCA	trichloroacetic acid
TCGA	The Cancer Genome Atlas
tetO	tetracycline operator
TGCT	testicular germ cell tumors
TGFβ	transforming growth factor β
TNM	tumor, node and metastasis
TRAMP	transgenic adenocarcinoma mouse prostate
Trim-NHL	tripartite motif and Ncl-1, HT2A and Lin-41
tRNAs	transfer RNAs
TSA	tyramide signal amplification
TβRII	TGFβ type II receptor

U

3'UTR	3'untranslated region
uPA	urokinase-type plasminogen activator
USPSTF	U.S. Preventive Services Task Force

V

VEGFR2	vascular endothelial growth factor receptor 2

W

WB	western blotting

Z

Zf-nanos	zinc finger motif of Nanos proteins

INTRODUCTION

Chapter 1.1

Nanos genes and their role in cancer

Evi De Keuckelaere[1,2,3,4], Paco Hulpiau[1,2], Yvan Saeys[1,5], Geert Berx[3,4] and Frans van Roy[1,2*]

1. VIB-UGent Center for Inflammation Research, Technologiepark 927, 9052 Ghent, Belgium
2. Molecular Cell Biology Unit, Department of Biomedical Molecular Biology, Ghent University, Technologiepark 927, 9052 Ghent, Belgium
3. Molecular and Cellular Oncology laboratory, Department of Biomedical Molecular Biology, Ghent University, Technologiepark 927, 9052 Ghent, Belgium
4. Cancer Research Institute Ghent (CRIG), Ghent, Belgium
5. Department of Applied Mathematics, Computer Science and Statistics, Ghent University, Krijgslaan 281, S9, 9000 Ghent, Belgium

This Chapter is adapted from De Keuckelaere E., Hulpiau P., Saeys Y., Berx G. and van Roy F. (2018) *Nanos* genes and their role in cancer. Cell Mol Life Sci. 2018 Feb 3. doi: 10.1007/s00018-018-2766-3 [Epub ahead of print].

Contributions

This review was written by Evi De Keuckelaere and corrected by Prof. Dr. em. Frans Van Roy and Prof. Dr. Geert Berx. The phylogenetic analysis of Nanos zinc finger domains (Figure 1.2) was done by Paco Hulpiau.

The hallmark of Nanos proteins is their typical $(CCHC)_2$ zinc finger motif (Zf-nanos). Animals have one to four *nanos* genes. For example, the fruit fly and demosponge have only one *nanos* gene, zebrafish and humans have three, and *Fugu rubripes* has four. *Nanos* genes are mainly known for their evolutionarily preserved role in germ cell survival and pluripotency. Nanos proteins have been reported to bind the C-terminal RNA-binding domain of Pumilio to form a post-transcriptional repressor complex. Several observations point to a link between the miRNA-mediated repression complex and the Nanos/Pumilio complex. Repression of the E2F3 oncogene product is indeed mediated by cooperation between the Nanos/Pumilio complex and miRNAs. Another important interaction partner of Nanos is the CCR4-NOT deadenylase complex. Besides the tissue-specific contribution of Nanos proteins to normal development, their ectopic expression has been observed in several cancer cell lines and various human cancers. An inverse correlation between the expression levels of human Nanos1, Nanos3 and E-cadherin was observed in several cancer cell lines. Loss of E-cadherin, an important cell–cell adhesion protein, contributes to tumor invasion and metastasis. Overexpression of Nanos3 induces epithelial-mesenchymal transition (EMT) in lung cancer cell lines partly by repressing E-cadherin. Other than some most interesting data from *Nanos* knockout mice, little is known about mammalian Nanos proteins, and further research is needed. In this review, we summarize the main roles of Nanos proteins and discuss the emerging concept of Nanos proteins as oncofetal antigens.

1.1.1 Introduction

Nanos was originally discovered and studied in *Drosophila melanogaster* (fruit fly) [1]. Nanos proteins belong to a highly conserved protein family found in both vertebrates and invertebrates. In *D. melanogaster*, the *nanos* gene was primarily found to be essential for anterior-posterior axis polarity, abdomen formation and germ cell development [1-3]. The Nanos protein establishes a multisubunit translation-inhibitory complex with Pumilio, its RNA-binding partner. The genomes of mouse and other mammals contain three Nanos-encoding genes, *Nanos1*, *Nanos2* and *Nanos3*. Nanos homologs exist in several other species, such as *Caenorhabditis elegans*, *Xenopus laevis* and *Danio rerio* (summarized in Table 1.1).

Table 1.1. Overview of reported nanos homologs in vertebrates and invertebrates.

Scientific name	Common name	Name of nanos homolog	Reference
Vertebrates			
Homo sapiens	Human	Nanos1, Nanos2 and Nanos3	[4]
Mus musculus	Mouse	Nanos1, Nanos2 and Nanos3	[5,6]
Rattus norvegicus	Rat	Nanos1, Nanos2 and Nanos3	[7]
Xenopus laevis	Frog	Xcat-2 and nanos3	[8] GenBank accession number XM_018251758.1
Xenopus tropicalis	Frog	Xtcat-2 and nanos3	[9] GenBank accession numbers XM_004919168.3, XM_004919167.3
Danio rerio	Zebrafish	nos1, nos2 and nos3	[10] GenBank accession number NM_131878.1
Invertebrates			
Helobdella robusta	Leech	Hro-nos	[11]
Drosophila melanogaster	Fruit fly	nanos (nos)	[1]
Caenorhabditis elegans	Roundworm	nos1, nos2 and nos3	[12]
Apis mellifera	Honeybee	nanos	[13]
Bombyx mori	Silkmoth	nanosM, nanosN, nanosO and nanosP	[14]
Schistocerca americana	Grasshopper	nanos	[15]
Gryllus domesticus	Cricket	nanos	[15]
Anopheles gambia, Anopheles stephensi and Aedes aegypti	Mosquito	Anga nos, Anst nos and Aeae nos	[16]
Hydra magnipapillata	Fresh-water polyp	Cnnos1 and Cnnos2	[17]
Podocoryne	Jellyfish	nanos	[18]
Nematostella vectensis	Sea anemone	NvNanos1 and NvNanos2	[19]
Sycon ciliatum	Sponge	SciNanos	[20]

The germ stem cell function of Nanos orthologs is conserved from invertebrates to mammals such as *Mus musculus* (Nanos2 and Nanos3) [6] and *Homo sapiens* (Nanos3) [21]. Two essential characteristics of germline cells is that they are pluripotent and immortal, passing

on their genetic information to an endless series of generations. Nanos protein expression has also been linked to increased cell migration and invasion [7,22]. Ectopic expression of *Nanos1* mRNA and Nanos3 protein have been observed in human lung carcinomas [23,22], suggesting a functional link between Nanos proteins and lung cancer.

We present a general overview of the Nanos proteins in different organisms, their structures, and their roles in development and cancer in *Drosophila* and mammals. Since Nanos proteins are linked to essential molecular processes and characteristics such as the cell cycle, pluripotency, epithelial-mesenchymal transition, and cell survival *versus* apoptosis, further research on *Nanos* genes and proteins could shed more light on various biological phenomena, especially cancer.

1.1.2 Structures of *Nanos* genes and proteins

Nanos genes encode proteins with a typical carboxy-terminal zinc finger motif $(CCHC)_2$ (Figure 1.1A), which is the only domain that is evolutionarily conserved between mammalian Nanos family members and those in lower organisms such as the fruit fly and the roundworm [24]. Likewise, it is the most conserved sequence among the three mammalian Nanos paralogs (Nanos family members of the same species). This domain is crucial for Nanos function because it mediates binding with RNA as well as with interaction partners such as Pumilio [25,4]. Nanos proteins from vertebrates and some invertebrates (such as sponge, fresh-water polyp and jellyfish) share an additional N-terminal region of 17 amino acids (AA) called NIM (NOT1 interacting motif) [24,26] (Figure 1.1B). In contrast to the C-terminal domain (Zf-nanos), the sequences of the N-terminal domains of the various Nanos proteins are not conserved.

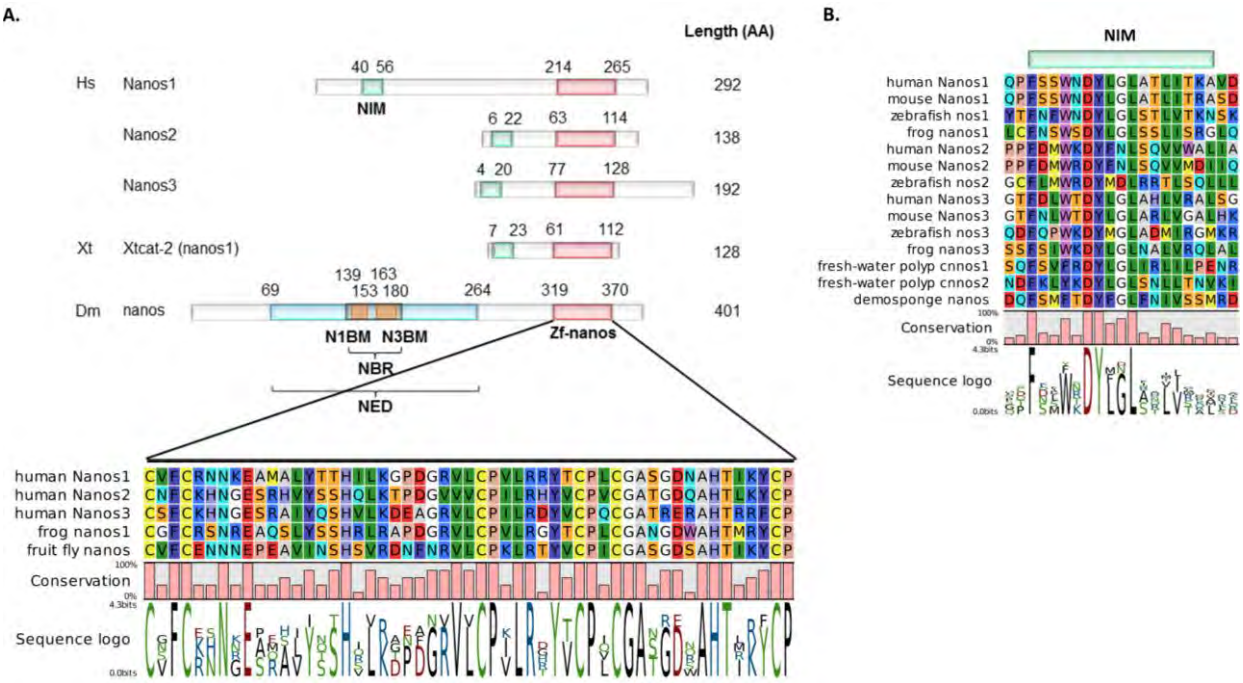

Figure 1.1. Nanos protein domains. A. All Nanos proteins contain a C-terminal $(CCHC)_2$ zinc finger domain (Zf-nanos). Nanos proteins of all vertebrates and a few invertebrates have an additional N-terminal NOT1-interacting motif (NIM). *Drosophila melanogaster* (Dm) has a nanos effector domain (NED) with a central region (NOT module binding region, NBR) that can bind NOT1 and NOT3, components of the CCR4-NOT complex. N1BM, NOT1 binding motif; N3BM, NOT3 binding motif; Hs, *Homo sapiens*, Xt, *Xenopus tropicalis*. Amino acid (AA) positions of the domains are given on top of the sequences. The figure was adapted from [27] **B.** Alignment of the NIM domain in several vertebrate and invertebrate organisms.

Zf-nanos is the only conserved domain that can be used to create a reliable phylogenetic tree. By browsing the gene and genome databases of UCSC, Ensembl and NCBI, we observed that there is at least one *nanos* gene in all animals, even in the comb jellies, which are among the most ancestral animals (Table 1.2). Depending on the species, the genome encodes one (*D. melanogaster*), two (*Hydra vulgaris*), three (*C. elegans*, *M. musculus*, *H. sapiens*) or four (*Fugu rubripes*) *nanos* genes (Tables 1.1 and 1.2). Most vertebrates have three *nanos* genes whereas some reptiles have lost a *nanos* gene and birds seem to have lost two. *Xenopus tropicalis* has only two annotated *nanos* genes, although a third gene has been reported [24]. Similarly, a *nanos2* gene that has not been annotated is found in stickleback.

Tabel 1.2. Overview of Nanos protein sequences, predicted from genomic and transcriptomic databases.

Taxonomy		Species (common name)	*Nanos* gene(s)
Deuterostomes	Primates	*Homo sapiens* (human)	Nanos1 (NP_955631) Nanos2 (NP_001025032) Nanos3 (NP_001092092)
	Rodentia	*Mus musculus* (mouse)	Nanos1 (NP_848508) Nanos2 (NP_918953) Nanos3 (NP_918948)
	Carnivora	*Canis lupus familiaris* (dog)	Nanos1 (XP_005637940) Nanos2 (XP_541547) Nanos3 (ENSCAFT00000026271.3)
	Metatheria	*Monodelphis domestica* (opossum)	Nanos1 (XP_001376960) Nanos2 (XP_007492184) Nanos3 (XP_007489148)
	Aves	*Gallus gallus* (chicken)	Nanos1 (XP_015144398)
	Reptilia	*Chrysemys picta* (turtle)	Nanos1 (XP_005284212) Nanos2 (XP_005283826) Nanos3 (XP_005310751)
	Reptilia	*Alligator sinensis* (alligator)	Nanos1 (XP_014373968) Nanos3 (XP_006023461)
	Amphibia	*Xenopus tropicalis* (frog)	Nanos1 (NP_988857) Nanos3 (XP_004919224)
	Fish	*Danio rerio* (zebrafish)	Nos1 (NP_001292590) Nos2 (XP_009300191) Nos3 (NP_571953)
	Fish	*Gasterosteus aculeatus* (stickleback)	Nanos1a (ENSGACT00000022078) Nanos1b (ENSGACT00000006526) Nanos3 (ENSGACT00000025168)
	Fish	*Fugu rubripes* (fugu)	Nanos1a (XP_011609291) Nanos1b (XP_011618819) Nanos2 (XP_011606249) Nanos3 (XP_011610763)
	Urochordata	*Ciona intestinalis* (sea squirt)	Nanos (XP_002130327)
	Cephalochordata	*Branchiostoma floridae* (amphioxus)	Nanos (XP_002608940)
	Hemichordata	*Saccoglossus kowalevskii* (acorn worm)	Nanos (NP_001161595)
	Echinodermata	*Strongylocentrotus purpuratus* (sea urchin)	Nanos1a (XP_001177221) Nanos1b (NP_001073023)

Tabel 1.2. Overview of Nanos protein sequences, predicted from genomic and transcriptomic databases. (Continued)

Protostomes	Lophotrochozoa	*Aplysia californica* (sea hare)	Nanos1 (XP_005096656) Nanos2 (XP_012937610)
	Lophotrochozoa	*Helobdella robusta* (leech)	Nanos1a (XP_009018920) Nanos1b (XP_009013101)
	Ecdysozoa	*Drosophila melanogaster* (fruit fly)	Nanos (Nos) (NP_476658)
	Ecdysozoa	*Caenorhabditis elegans* (roundworm)	Nos1 (NP_496358) Nos2 (NP_495452) Nos3 (NP_496101)
	Ecdysozoa	*Solenopsis invicta* (red fire ant)	Nanos1a (XP_011159578) Nanos1b (XP_011159747) Nanos1c (LOC105205302)
	Ecdysozoa	*Bombyx mori* (silkmoth)	NanosM (NP_001098700) NanosN (NP_001098702) NanosO (NP_001093314) NanosP (NP_001093313)
Non-bilaterian animals	Cnidaria	*Nematostella vectensis* (sea anemone)	Cnnos1 (XP_001637175) Cnnos2 (XP_001641215)
	Cnidaria	*Hydra vulgaris* (fresh-water polyp)	Cnnos1 (XP_002161850) Cnnos2 (XP_002159764)
	Cnidaria	*Acropora digitifera* (acroporid coral)	Cnnos1 (XP_015755666) Cnnos2 (XP_015758550)
	Placozoa	*Trichoplax adhaerens* (placozoan)	Nanos (XP_002114667)
	Porifera	*Amphimedon queenslandica* (demosponge)	Nanos (XP_003384296)
	Ctenophora	*Mnemiopsis leidyi* (comb jelly)	Nanos1a (ML130210a) Nanos1b (ML22086a)

Based on the phylogenetic analysis of Zf-nanos, vertebrate nanos1, -2 and -3 proteins mainly cluster together with nanos1, -2 and -3 proteins from other species (orthologs), respectively, rather than with their paralogs (Figure 1.2). This indicates that the *nanos* gene had undergone duplications and that the resulting paralogs probably evolved new functions. Some *nanos* genes, such as those of *H. vulgaris* and other cnidarians, cannot be classified within the branches of vertebrate *nanos1*, *-2* or *-3* genes. Their *nanos* genes were probably duplicated independently during evolution. The *nanos* genes in red fire ant, fugu and silkmoth had also undergone lineage specific duplications and this resulted in four *nanos* genes in the latter two animals (Table 1.2). The fourth *nanos* gene of fugu is probably a duplicated *nanos1* homolog (Figure 1.2).

The large sequence differences between the non-Zf part of Nanos orthologs and paralogs are manifested in a major difference in protein length between Nanos sequences (Figure 1.1A).

The *nanos* gene of *Drosophila* encodes the largest protein sequence (401 AA), which is considerably larger than Nanos proteins from mouse and human (Nanos1: 267 and 292 AA; Nanos2: 136 and 138 AA; and Nanos3 178 and 192 AA, respectively). In *Xenopus*, nanos1 (Xtcat-2) comprises only 128 AA, including the 16-AA NIM region and the 52-AA zinc finger domain (Figure 1.1A). These differences might be linked with different molecular interaction partners and functions.

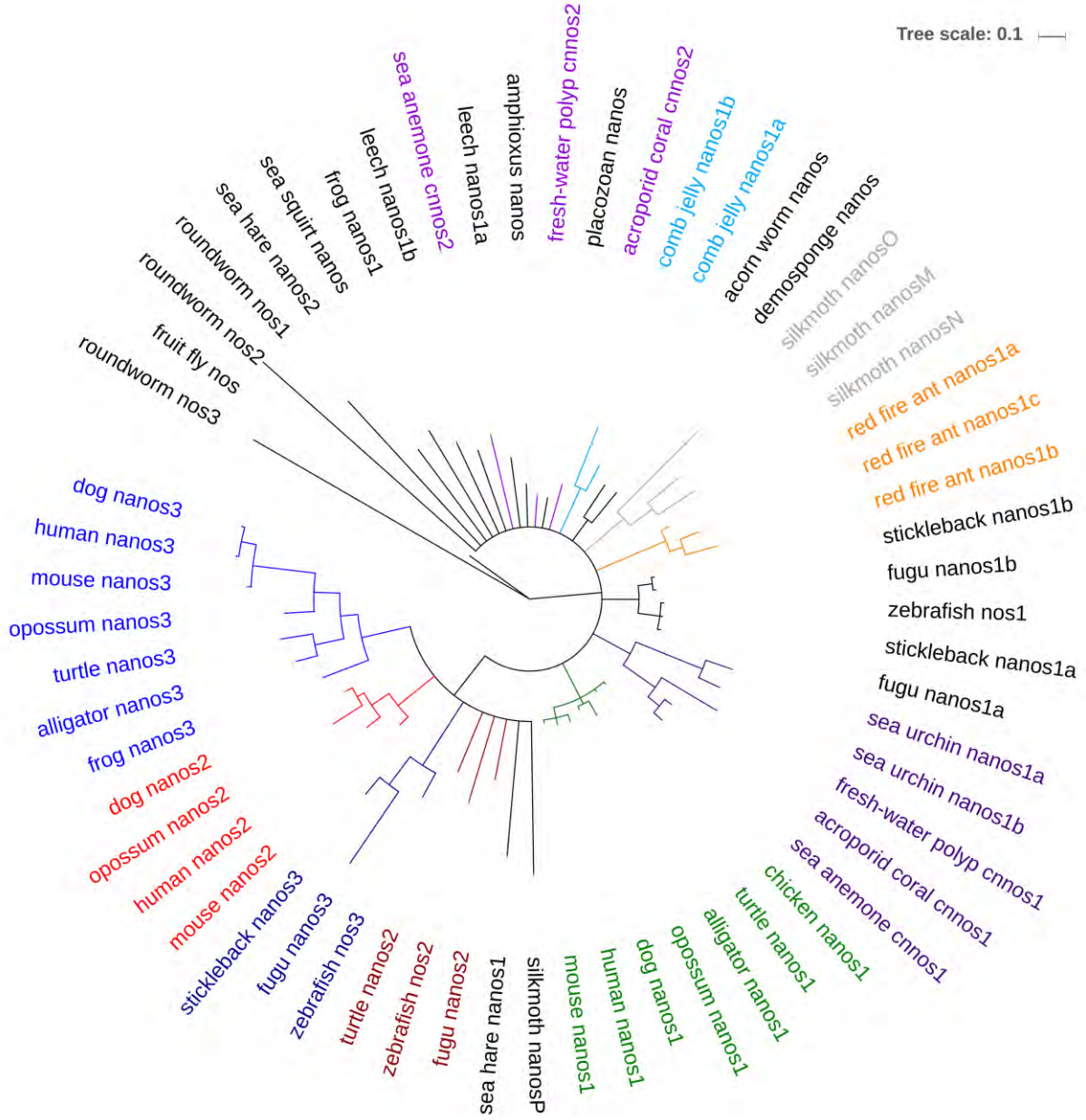

Figure 1.2. Phylogenetic tree based on the zinc finger domain of Nanos proteins. The Zf-nanos domains of metazoan nanos homologs were aligned with MUSCLE [28]. With this alignment as input a Bayesian inference (BI) consensus tree was built using MrBayes 3 [29]. Convergence (<0.01) was reached after 5,000,000 generations. The circular BI tree shown here was visualized with iTOL [30].

1.1.3 Nanos interaction partners

Few nanos interaction partners have been identified. See Table 1.3 for the known interaction partners of human Nanos proteins.

Table 1.3. Known interaction partners of human Nanos proteins.

Nanos protein	Interaction partner	Interaction domains[a]	Reference
Nanos1	Pumilio2	Zf-nanos	[4]
	p120-catenin	N-terminal domain (including NIM)	[7]
	β-catenin	nd	[7]
	SNAPIN	N-terminal domain & Zf-nanos are needed	[31]
	GEMIN3	N-terminal domain (without NIM)	[32]
	CNOT1	NIM domain	[24]
Nanos2	CNOT1	NIM domain	[24]
Nanos3	CNOT1	NIM domain	[24]

[a] Interaction domains: Zf-nanos, zinc finger domain of nanos proteins; NIM, NOT1 interacting motif; nd: not determined.

Pumilio proteins

Pumilio is at the origin of the PUF family, which is named after its founders Pumilio (*Pum*) of *D. melanogaster* and *FBF* of *C. elegans*. PUF proteins are RNA-binding proteins (RBPs) found in eukaryotes ranging from plants to yeasts, invertebrates and humans [33]. The number of PUF family members varies from multiple in *C. elegans*, *Saccharomyces cerevisiae* and *Arabidopsis thaliana* to only one member in insects, such as *D. melanogaster*. Humans and mice have two Pumilio-encoding genes. They all share a highly conserved C-terminal RNA-binding domain comprising eight tandem repeats, collectively called the PUM homology domain (PUM-HD) (Figure 1.3) [34]. Each repeat binds to one RNA base in the mRNA target [35].

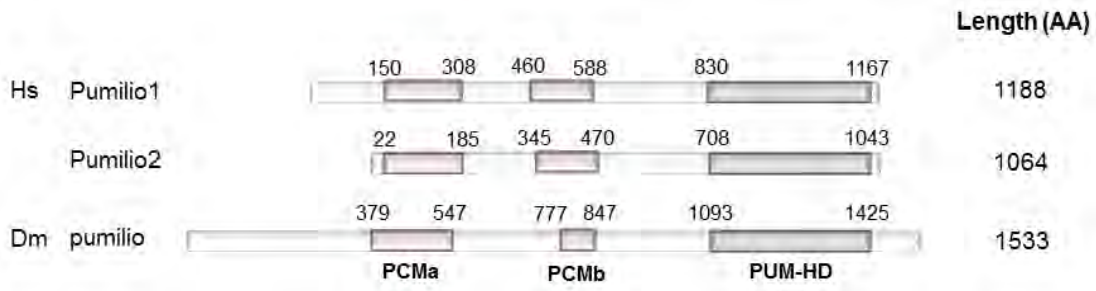

Figure 1.3. Pumilio protein structure. All pumilio proteins contain a pumilio homology domain (PUM-HD) and some family members contain two additional N-terminal pumilio conserved motifs (PCMs). Both human (Hs, *Homo sapiens*) Pumilio proteins and the *Drosophila melanogaster* (Dm) pumilio protein are shown.

Pumilio has been reported to bind both Pumilio-binding elements (PBEs, 5'-UGUANAUA-3') and Nanos regulatory/response elements (NREs) in the 3' untranslated region (UTR) of their target mRNAs and recruits, among other proteins, deadenylation and decapping proteins. The NREs are composed of two sequences, called box A (5'-GUUGU-3') and box B (5'-AUUGUA-3'). Nanos binds to the first part of the box B sequence [36]; the last part of this NRE box B sequence shares identity with the first part of the PBE.

Tandem affinity purification (TAP) and a DNA microarray were used to identify mRNAs associated with the pumilio protein in adult ovaries and embryos of *Drosophila* [37]. For this analysis, a TAP-tagged C-terminal fragment of pumilio was expressed under the control of an ovary-specific promoter. A PBE was present in 54% of the adult and 22% of the embryonic pumilio targets identified. Unlike for the human Pumilio proteins, *Drosophila* pumilio binds *nanos* mRNA in the embryo. Nonetheless, *nanos* mRNA lacks the UGUA(A/U/C)AUA motif [37], and another non-canonical motif in *nanos* mRNA was found to mediate pumilio binding [38].

Besides binding RNA, the PUM-HD domain can bind various proteins, such as nanos [25], CNOT8 [39] and DAZ [40]. Nanos binding is mediated through the loop region between the last two pumilio repeats [41]. Nanos determines the location in the embryo or the postnatal cell type where the specific translation inhibition of the nanos/pumilio complex occurs [42-44].

In *Drosophila*, the interaction between nanos and pumilio is stabilized by a NRE-containing RNA fragment and is therefore RNA-dependent [25]. However, human Nanos1 was found to interact with Pumilio2 in the absence of RNA [4]. Likewise, mouse Nanos3 was shown to

interact with Pumilio in an RNA-independent manner [45]. The interaction between Xcat-2/nanos and pumilio was also confirmed in *Xenopus*, but RNA dependence was not investigated here [46].

Although the N-terminal sequence of PUF proteins is very variable, in some family members it contains two conserved pumilio motifs (PCMs) that can be traced back from humans to *Drosophila* (Figure 1.3) [47]. Multiple domains in the N-terminus confer repressive activity [47]. The N-terminus is also important for dimerization of Pumilio2 [4] and for specific protein interactions, such as the interaction between Pumilio2 and SNAPIN [31]. SNAPIN is a widely expressed protein that is part of BLOC-1 (biogenesis of the lysosome-related organelle complex 1) and BORC (BLOC-1-related complex) and associates with the SNARE complex [48-50]. It is involved in several functions involving intracellular vesicles, such as endosomes and lysosomes [51-53]. The relevance of the interaction between Pumilio2 and SNAPIN is unknown.

PUF proteins have the conserved role of maintaining stem cells [54-56], but other roles, such as in sperm/oocyte switch [57], long-term memory [58] and anterior-posterior patterning [42], have been acquired during evolution. PUF proteins perform these functions by post-transcriptional regulation of their targets, as reviewed in [59]. This occurs in cooperation with interaction partners such as nanos [25], CPEB [46,60] and the CCR4-NOT complex [61]. Although PUF proteins are generally believed to repress mRNA translation by deadenylation [39] or interference with translation initiation [62], PUF proteins can also stimulate mRNA translation [63,64]. Further research is needed to understand how these repressive and activating functions are integrated, which could vary with the target or the interaction partner, or depend on extracellular or intracellular signals.

The identification of mRNA targets of the human Pumilio proteins in HeLaS3 cancer cells led to the discovery of extensive interactions with the miRNA regulatory system [65]. Pumilio-associated mRNAs were identified using RNA immunoprecipitation (RIP) followed by a microarray-based analysis. RNA sequences that specifically bind Pumilio (PBE, Pumilio-binding elements) are more likely to be located near miRNA-binding sites; similarly mRNA targets of Pumilio are enriched in miRNA binding sites. Links between Pumilio-mediated and miRNA-mediated repression have indeed been discovered [66,67,43]. It would be interesting to

further investigate the link between the miRNA regulatory complex and the Nanos/Pumilio complex. This might reveal new interaction partners of the Nanos proteins.

Additionally, many Pumilio targets are associated with pathways involved in cancer, such as angiogenesis, cell proliferation and cell survival [65]; Pumilio-mediated regulation is indeed disturbed in several cancers [68-70].

Other proteins with PUM repeats, i.e. non-canonical PUF proteins, have been reported, such as the human Puf-A (Pum3) with orthologs such as pum3 (in mice), pufa (in zebrafish) and Puf6 (in yeast) [71,72]. Unlike the classical PUF proteins, they have 11 PUM repeats and bind double-stranded RNA or DNA in a sequence-independent manner [71]. Nanos binding to these non-canonical PUF proteins has not been reported.

The CCR4-NOT complex

The N-terminals of all human Nanos proteins interact with the C-terminal domain of CNOT1 (Figure 1.4) [24]. CNOT1 is part of the CCR4-NOT deadenylase complex, which is a common partner of Nanos proteins in some species [73,24,74]. The CCR4-NOT complex is a highly conserved, multisubunit complex that facilitates gene regulation in diverse ways. This complex was first studied in yeast, in which it consists of nine core proteins. Except for Caf130, homologs of these proteins exist, for instance in *D. melanogaster* and *H. sapiens* (Table 1.4). The CNOT1 subunit is the scaffold that keeps the complex together (Figure 1.4). The smaller complex, consisting of CNOT1 to -3 in humans and of Not1, Not2 and Not5 in yeast, is referred to as the NOT module [75,76]. Proteins CCR4 and Caf1 contribute to the deadenylation activities of the CCR4-NOT protein complex (Figure 1.4B). The complex can also interact with diverse proteins, such as the poly(A) binding protein (PABP) through binding of BTG/TOB proteins [77-79], eIF4A2 [80], and proteins of the decapping complex through binding of DDX6 [81], which leads to inhibition of transcription or translation of their target genes/mRNAs, or to both. The CCR4-NOT complex is also involved in miRNA-mediated repression through binding with the GW182 protein [82,83]. More information about the CCR4-NOT complex can be found in the following reviews [84,85].

In mice, Nanos2 also binds the CCR4-NOT complex through CNOT1, but Nanos3 does this mainly by interacting with POP2 [86]. The different ways in which Nanos2 and Nanos3 interact with components of the mouse CCR4-NOT complex could be responsible for the weaker

deadenylase activity of Nanos3 compared to Nanos2, and might explain why Nanos3 cannot fully compensate for loss of Nanos2, as described below. The Nanos NIM region and its interaction with the CCR4-NOT complex proved to be essential for Nanos-mediated translational repression and mRNA degradation [24]. Binding of the CCR4-NOT complex is functionally conserved: also *Drosophila* nanos has been shown to bind to this complex though it has no NIM region [27]. *Drosophila* nanos interacts with NOT1 and NOT3 of the CCR4-NOT complex *via* a central region (called NBR, for NOT module binding region) situated in the nanos effector domain (NED) [27] (Figure 1.1).

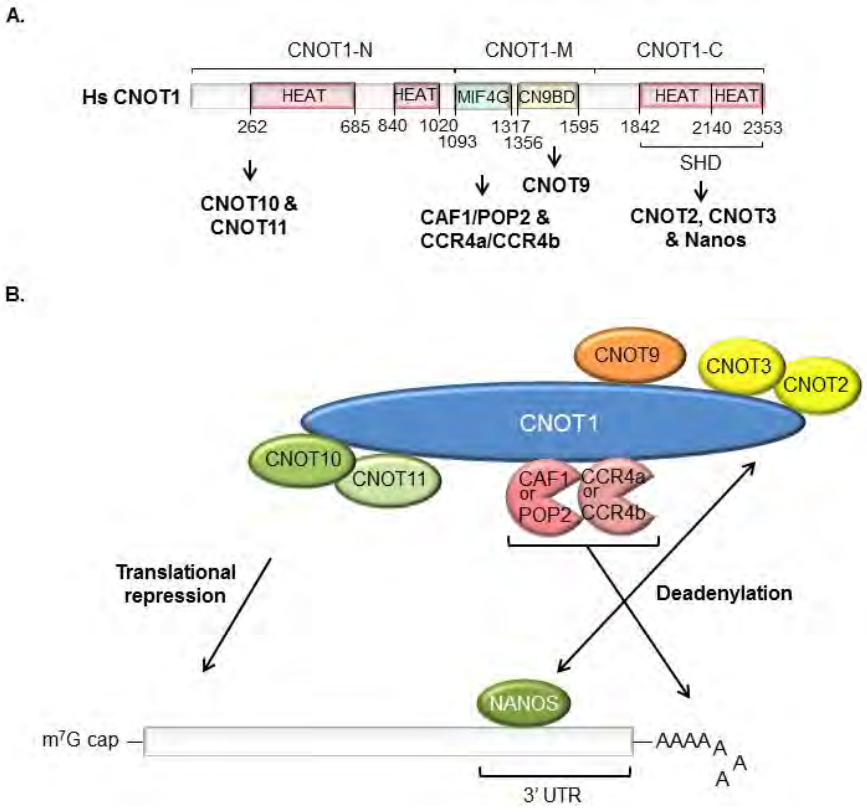

Figure 1.4. CNOT1 is the scaffold protein of the CCR4-NOT deadenylase complex. A. Schematic representation of human CNOT1. The N-terminal region (CNOT1-N) consists of two HEAT repeats and provides binding sites for CNOT10 and CNOT11 [87]. The middle region (CNOT-M) contains the MIF4G domain, structurally related to the middle domain of eIF4G, and the CNOT9 binding domain [81], also called DUF3819 domain. The MIF4G domain binds the catalytic subunits, CAF1 or POP2 along with CCR4a or CCR4b deadenylases [88]. The C-terminal region (CNOT1-C) contains the superfamily homology domain (SHD) required for binding to CNOT2, CNOT3 [75] and Nanos proteins [24]. AA positions of the domains are given below the sequences. Hs, *Homo sapiens.* **B.** Translation regulators such as Nanos bind the 3'UTR of their mRNA targets and recruit the CCR4-NOT complex. This complex stimulates deadenylation and translational repression by recruiting additional proteins.

Table 1.4. Subunits of the CCR4-NOT deadenylation complex in yeast and their orthologs in *Drosophila* and humans.

Saccharomyces cerevisiae	*Drosophila melanogaster*	*Homo sapiens*
Not1	NOT1	CNOT1
Not2	NOT2	CNOT2
Not3	NOT3	CNOT3
Not5[a]		
Ccr4	CCR4	CCR4a = CNOT6C
		CCR4b = CNOT6L
Pop2/Caf1	POP2	Caf1a = CNOT7 = CAF1
		Caf1b = CNOT8 = CALIF = POP2
Caf40	CAF40	CAF40 = CNOT9 = Rcd1 = RQCD1
Caf130	-	-
-	NOT10	CNOT10
-	NOT11	CNOT11
Not4	NOT4[b]	CNOT4[b]

[a] There is no clear homolog to Not5 in *D. melanogaster* or *H. sapiens.* However, there is an extensive amount of sequence homology between NOT3 and CNOT3 and yeast Not5.

[b] NOT4 and CNOT4 are not a standard component of the CCR4-NOT complex in *Drosophila* and humans.

Other interaction partners

Unlike the CCR4-NOT complex, other Nanos partners often differ depending on the paralog, the organism or the mRNA target. For example, the nos-3 protein in *C. elegans* was found to bind the fem-3 binding factor (FBF), but neither nos-1 nor nos-2 bound FBF [57]. Another example is the Nanos1-p120-catenin interaction mediated through the NIM region, which is present in humans but not in lower organisms such as *Drosophila* [7]. Further, human Nanos1 has been reported to interact with SNAPIN [31] and GEMIN3, an RNA DEAD box

helicase [32]. GEMIN3 is a component of the SMN (Survival Motor Neuron) complex, which is essential for formation of small nuclear ribonucleoproteins (snRNPs), which are essential for correct splicing [89]. GEMIN3 was also detected in miRNP particles, and its involvement in miRNA-mediated repression has been suggested [90,91]. The interaction between Nanos1 and GEMIN3 seems to take place in the chromatoid body of germ cells, which also contains several miRNAs and components involved in miRNA regulation, such as Dicer and Argonaute proteins [32].

1.1.4 Nanos functions

Nanos genes are especially known for their roles in germ cell development, which are conserved between basic model organisms and mammals. Reproductive pathways usually evolve faster than somatic pathways, which emphasizes the importance of the role of *nanos* genes in germ cell development. Current models for discovering the target mRNAs of Nanos-containing translation-inhibitory complexes are based on identifying both NREs and PBEs in the 3'UTR of candidate transcripts.

mRNA targets of the Nanos/Pumilio complex in *D. melanogaster* and humans

An overview of targets of the nanos/pumilio complex in the germline of model organisms has been published by Lai and King [92]. The nanos/pumilio complex was found to repress somatic gene expression, the cell cycle and apoptosis; this repression correlates perfectly with its function in germ cell development and survival. A short overview of the mRNA targets of *Drosophila* nanos and human Nanos proteins discussed below and involving a PBE or NRE sequence, or both, is given in Table 1.5 and Table 1.6, respectively.

Hunchback. In *D. melanogaster*, nanos-encoding mRNA was first discovered as a maternal factor localized to the posterior pole of the unfertilized egg [1] (Figure 1.5). Whereas nanos represents the abdominal determinant, the bicoid protein is the anterior determinant. Posterior localization of nanos mRNA is dependent on signals present in its 3’UTR [93,94]. Both bicoid and nanos mRNAs are translated after fertilization. During oogenesis, several genes, such as *oskar*, *vasa* and *aub*, contribute to the posterior localization of *nanos* RNA [95-97]. This ensures a nanos protein gradient decreasing from the posterior pole to the anterior pole. The bicoid protein activates hunchback protein expression, while nanos in association with pumilio and brain tumor (brat) represses hunchback translation (Figure 1.5).

This generates an anterior-posterior gradient of the hunchback protein, which blocks abdomen formation at the anterior pole, thus allowing development of the head and thorax [98]. Likewise, bicoid inhibits *caudal* mRNA translation, causing a posterior-anterior gradient of the caudal protein. Together, these gradients ensure correct anterior-posterior patterning of the embryo. Nanos can also repress translation of *bicoid* mRNA if the latter is not correctly restricted to the anterior pole [99].

Table 1.5. Overview of mRNA targets of *Drosophila* nanos.

mRNA target	Complex	Determining factor	Effect	Reference
hunchback	nanos/pumilio/brat	nanos	Abdomen formation	[100,62]
cyclin B	nanos/pumilio	nanos	Blocking mitosis in the pole cells	[101,102]
hid	nanos/pumilio	nanos	Blocking apoptosis of the pole cells	[103]
para	nanos/pumilio	pumilio	Regulates neuronal membrane excitability	[104,105]
mei-P26	nanos/pumilio	nanos	Regulates self-renewal of ovarian stem cells	[74]
dE2F1	nanos/pumilio/brat	nanos	Ensuring correct E2F regulation	[43,68]

Table 1.6. Overview of mRNA targets of human Nanos.

mRNA target	Complex	Effect	Reference
E2F3	Nanos/Pumilio	Ensuring correct E2F regulation	[43]
MAP3K1 and MAP2K3	Nanos/Pumilio	Influencing p53 expression (and thereby suppressing apoptosis)	[68]

Repression of hunchback mRNA translation by nanos depends on two NREs in the 3'UTR of hunchback mRNA [99]. Pumilio, as well as nanos and brat, were found to bind these NRE sequences [42,41,36]. Brat was convincingly shown to bind box A of the NRE sequence [36,106-108]. Prior RNA binding of brat or pumilio facilitates the binding of the other protein [106]. Nanos is recruited only when pumilio is bound to the NRE sequence (Figure 1.5) [25].

This nanos-brat-pumilio complex blocks hunchback translation by promoting the deadenylation of hunchback mRNA [100] and inhibiting its translation [62]. Translation inhibition is mediated by brat-dependent recruitment of d4EHP, which binds the 5' cap structure of hunchback mRNA and thereby inhibits the binding of the homologous eIF4E protein (Figure 1.5).

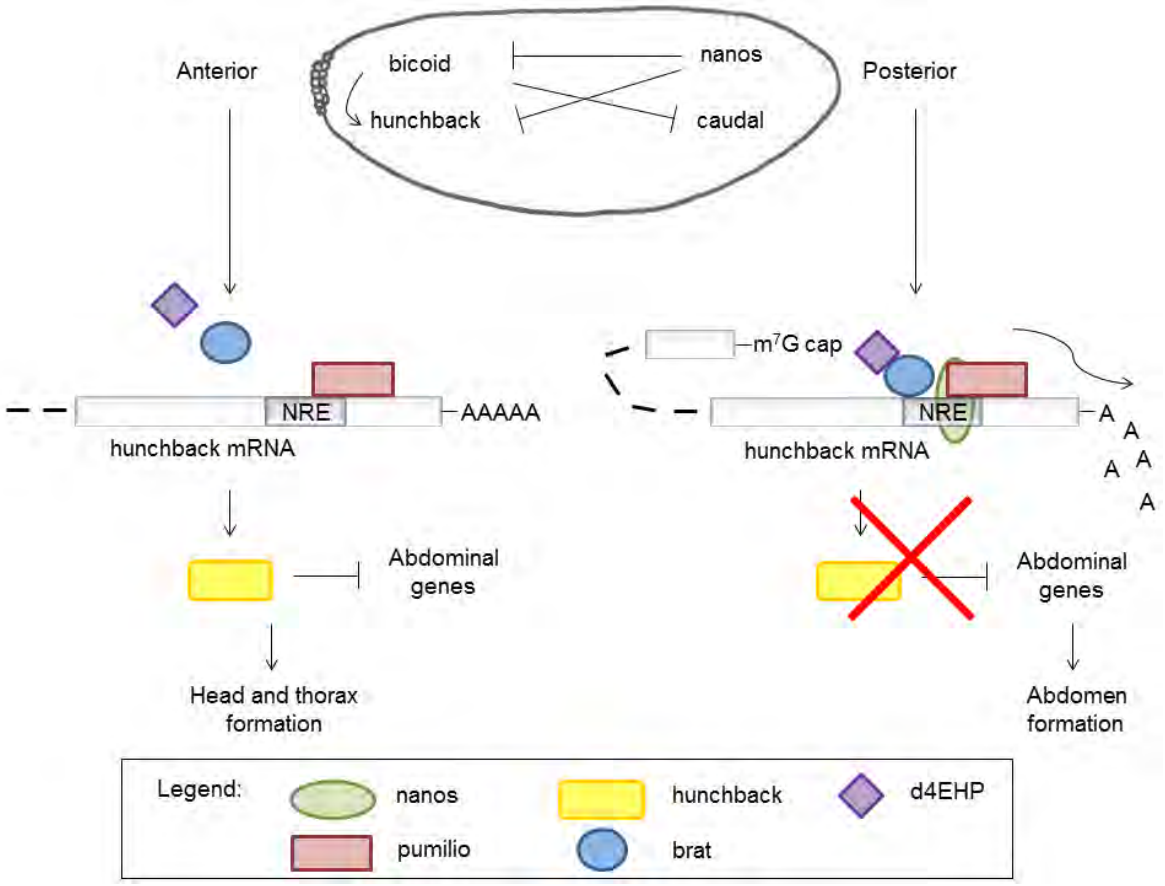

Figure 1.5. Anterior-posterior patterning of the *Drosophila* embryo. Nanos is an important posterior determinant in *Drosophila* development. Nanos expression induces abdomen formation by inhibiting, in cooperation with pumilio and brat, translation of hunchback mRNA. Hunchback has two nanos response elements (NREs) in its 3' untranslated region, but for simplicity only one is drawn. See text for further explanation.

Cyclin B. In addition to the above-mentioned role of the posterior pole plasm of the *Drosophila* embryo in abdomen formation, this pole is also responsible for germline formation [109]. Nanos expression is seen in the pole cells, also called primordial germ cells (PGCs), and a functional maternal nanos protein is indeed important for correct migration of these pole cells into the gonads and thus for germ cell formation [3,56]. During this migration, pole cell mitosis is blocked by nanos- and pumilio-dependent translational

repression of cyclin B RNA [101,102]. In this case, unlike for hunchback regulation, pumilio apparently functions merely by recruiting nanos. Nanos then represses cyclin B RNA by interacting with its conserved interaction partner, the CCR4-NOT complex [110]. Though pumilio mediates nanos recruitment *in vivo*, the experimentally linking of nanos to the cyclin B mRNA sequence efficiently downregulates cyclin B in the absence of pumilio. Association of Nanos with cyclin B1 mRNA was found to be conserved in *Xenopus* [46,26].

Hid. Nanos suppresses somatic gene expression and apoptosis in the pole cells [111], the latter by repressing translation of the pro-apoptotic head involution defective (*hid*) gene [103].

Para. The nanos/pumilio complex in *D. melanogaste*r also seems to play a role in neurogenesis. Nanos and pumilio mutants and double mutants have similar effects on dendrite morphogenesis of class-III and class-IV dendritic arborization neurons [112]. Nanos was found to colocalize with RNA granules in these dendrites, which might be where the nanos/pumilio complex is located. This complex also regulates neuronal membrane excitability by repressing transcription of paralytic (*para*) mRNA [104,105,113]. Intriguingly, the PBE sequence, which is both essential and sufficient for pumilio binding, was found in the open reading frame (ORF) instead of the 3'UTR [104]. *Para* encodes a voltage-gated Na^+ channel. Increased pumilio expression or reduced *para* mRNA consequently reduces voltage-gated Na^+ current and membrane excitability [105,104]. Pumilio seems to be the determining factor of the *para* mRNA repression by the nanos/pumilio complex [104]. Overexpression of pumilio negatively influences *nanos* mRNA expression, what might serve as a negative feedback mechanism, preventing excessive repression of *para* mRNA [37,104,38].

Mei-P26. Mei-P26 is a Trim-NHL (Tripartite motif and Ncl-1, HT2A and Lin-41) protein, restricting cell growth and self-renewal of ovarian stem cells [114]. The nanos/pumilio complex targets *mei-P26* mRNA in the ovarian stem cells, thereby allowing self-renewal of these stem cells. This is mediated by recruitment of the CCR4-NOT deadenylase complex [74].

E2F3. The Nanos/Pumilio complex has been shown to repress E2F3 translation in primary human fibroblasts (IMR90) [43]. *E2F3* is an oncogene found to be overexpressed or

dysregulated in several cancers, such as bladder [115], prostate [116] and lung cancer [117]. The E2F family includes both transcriptional activators (dE2F1 in *Drosophila* and E2F1 to -3 in humans) and transcriptional repressors (dE2F2 in *Drosophila* and E2F4 to -8 in humans).

E2F transcription factors play an important role in progression of the cell cycle and induction of apoptosis (reviewed in [118] and [119]). *E2F3* mRNA contains two functional PBE sequences, and ectopic expression in IMR90 cells of any combination of a Nanos protein (Nanos1 or Nanos3) and a Pumilio protein (Pumilio1 or Pumilio2) decreased E2F3 expression levels [43]. Nanos/Pumilio-mediated regulation of E2F is conserved from *Drosophila* (where it regulates dE2F1 expression) to humans (where it controls the expression levels of the orthologous E2F3) [43]. Proximal to the PBEs, several miRNA seed sequences were found, and their corresponding miRNAs were shown to repress E2F3. Interestingly, this miRNA-mediated repression of E2F3 has been found to depend on the presence of these PBEs in the 3'UTR, and thus on Nanos/Pumilio-mediated regulation.

MAP3K1 and **MAP2K3.** *MAP3K1* and *MAP2K3* mRNAs are repressed by Nanos1 in combination with Pumilio1 or Pumilio2, as detailed below [68].

Functions of the nanos and pumilio proteins in *Drosophila*

The above-mentioned targets of the nanos/pumilio complex point out most of the known functions of the nanos protein in *D. melanogaster*. Furthermore, *nanos* RNA and protein are expressed during several stages of *Drosophila* oogenesis [120]. In adult ovaries, nanos is important for proliferation and survival of germline stem cells, and for cyst development [56]. Accordingly, female nanos mutants with severely reduced or no protein expression produce very few eggs [121]. Ovaries and testes from nanos-deficient embryos are devoid of germ cells. This function of nanos in germ cell development and survival is conserved in *C. elegans* [12] and zebrafish [10].

Also loss of pumilio causes loss of germ cells in the ovaries, and this occurs even earlier than in the ovaries of nanos mutants [56]. Other phenotypic changes caused by loss of either pumilio or nanos suggest that other nanos partners may be involved in the germline. Although, as mentioned above, the nanos/pumilio complex has been shown to regulate mei-P26, nanos and pumilio might have other partners to regulate specific mRNA targets. For

instance, interaction between cup and nanos seems to be important in the female germline [122]. Cup has been shown to be important for several functions during oogenesis [123-125].

Also at the pre- and postsynaptic sites of the larval neuromuscular junction, pumilio and nanos seem to have divergent functions [38]. Pumilio was found to repress *GluRIIA* mRNA translation and thereby stimulate the switch from GluRIIA to GluRIIB receptors, which influences the amount of current through the synapses. This regulation is even more tightly controlled because pumilio also reduces nanos protein levels, while nanos downregulates GluRIIB.

Functions of mammalian Nanos proteins

Mouse. Unlike germ cell-specific expression of mouse Nanos2 and Nanos3 [6], mouse Nanos1 is predominantly expressed in the central nervous system [5]. *Nanos1* knockout mice seem to develop normally without any obvious differences from wild type mice [5]. Mouse Nanos3 clearly plays a role in maintaining PGCs from the migration phase onwards [6]. Nanos3-deficient mice initially have a normal number of PGCs, but these cells are gradually lost and are absent in ovaries and testes at E12.5 [6]. Ectopic expression of Nanos2 from E8.0 onwards partially counteracted the loss of both male and female germ cells in Nanos3 knockout mice, and thus partially compensated for the loss of Nanos3 [126]. Nanos2 is normally detectable only at E13.5.

On the other hand, although Nanos3 is upregulated in Nanos2-null mice, male PGCs in these mice undergo apoptosis from E15.5 onwards, resulting in deficiency in male germ cells. *Nanos3* transgene expression under control of the Nanos2 enhancer could not prevent this loss of spermatogonia. Nevertheless, *Nanos3* transgene expression or upregulation might at least partly rescue Nanos2 deficiency. For instance, mutation of the zinc fingers in Nanos2 results in loss of Nanos3 expression and is associated with an even more severe phenotypic abnormality than complete Nanos2 deficiency [86]. Nonetheless, the inability of Nanos3 to fully compensate for Nanos2 loss indicates that these two related proteins have different functions.

Nanos3 is also expressed in undifferentiated spermatogonia in the prepubertal testis [45]. By regulating the cell cycle of these spermatogonial cells, their differentiation is blocked until

puberty. Given that Nanos3 interacts with Pumilio2 in spermatogonia, it is likely that also Pumilio2 is involved in this regulation [45].

Both Nanos2 and Nanos3 mouse proteins were found to be associated with ribonucleoproteins (RNPs), suggesting translational regulation. Nanos2 is also present in RNPs, where it recruits and represses mRNAs important for germ cell differentiation [127]. More precisely, in mouse, Nanos2 and Nanos3 are expressed in processing bodies (P-bodies) [73,86], which are cytoplasmic mRNPs (messenger RNPs) linked with miRNA-mediated repression and contain many proteins involved in mRNA deadenylation, decapping and decay [128,129]. Nanos3 seems to be important for the assembly of these P-bodies in male germ cells [86], whereas Nanos2 is involved in their maintenance [73]. It would be interesting to investigate the functional association between Nanos proteins and regulatory proteins, which are generally found in the P-bodies.

Human. The first human *NANOS* gene was discovered in 2003 [4]. In contrast to murine nanos1 [5], human Nanos1 is not expressed in the adult brain. RT-qPCR analysis revealed *NANOS1* mRNA expression in embryonic stem cells, fetal testis and ovary, and adult testis [4]. Later, others showed that *NANOS1* mRNA was expressed more ubiquitously but also confirmed protein expression in fetal testis and ovary, and in adult testis [21]. However, in contrast to the original report, the latter authors also showed Nanos1 protein expression in the adult ovary. Nanos2 expression in adults was found to be restricted to the testis, in line with the findings for the mouse homologue [130]. Therefore, a possible link between *NANOS2* mutations and male infertility was investigated, but the detected mutations did not seem to have a causative role in male infertility [130].

More recently, human Nanos2 was found to be expressed in the adult ovary as well [21]. Nanos3 was not only found in the fetal and adult testis and ovary, like human Nanos1 and Nanos2, but also in the adult brain. Reducing Nanos3 expression levels in human embryonic stem cells significantly decreased germ cell numbers and the expression levels of genes important for germ cell development [21]. *NANOS3* mutations were also studied in a cohort of sterile men, again revealing no causative role in sterility [131]. On the other hand, a plausible, pathological link has been found for *NANOS3* mutations in patients with premature ovarian insufficiency [132,133]. Unlike what has been reported for *NANOS2* and *NANOS3* mutations, *NANOS1* mutations were convincingly linked to male infertility [134].

1.1.5 *Nanos* genes, tumor invasion and cancer

Germ cells and cancer cells share several characteristics, such as self-renewal and rapid proliferation. *Nanos* genes are responsible for germline traits such as pluripotency and survival, which are also important for tumor cells. Hence, Nanos overexpression might be a logical asset for cancer tissues.

In ***D. melanogaster***, nanos overexpression was only reported in the lethal (3) malignant brain tumor model (*l(3)mbt*) [135]. *Nanos* was only one of many genes essential in the germline that were upregulated in this model. These results point out that nanos expression is advantageous for brain tumor growth, at least in this invertebrate model.

In the **mouse**, an interaction between the *Dmrt1* and *Nanos3* genes was discovered [136]. In mice that are heterozygous for both genes, incidence of teratoma formation was significantly more elevated than in singly heterozygous mice. Like Nanos3, Dmrt1 controls male germ cell proliferation [137]. Dmrt1 additionally regulates male germ cell pluripotency by repressing *Sox2*.

In **humans**, Nanos1 is a potential effector in E-cadherin-negative cancer cells, contributing to tumor migration and invasion [7]. The mRNA expression levels of *NANOS1* and *CDH1* are inversely correlated in several cancer cell lines, which led to the discovery that E-cadherin represses *NANOS1* [7].

Nanos3 has been found to be ectopically expressed in a variety of human cancers [138]. So far, this was further investigated only in NSCLCs, in which Nanos3 expression levels correlated with patient outcome [22]. Immunostaining of lung tumors revealed Nanos3 overexpression, particularly at the invasion front and especially in squamous cell carcinomas (SCCs). When comparing primary tumors with their metastases, Nanos3 expression levels were found to be higher in the latter. Furthermore, ectopic expression of Nanos3 has been observed in several invasive NSCLC cell lines, in which it was associated with higher invasiveness. Moreover, Nanos3 overexpression causes clear-cut EMT in human lung cancer cells, thereby reinforcing the hypothesis that ectopic Nanos expression is involved in cancer progression [22].

A likely mechanism for malignancy caused by ectopic Nanos expression involves Nanos3-mediated repression of E-cadherin, occludin and β-catenin, combined with Nanos3-induced

stimulation of expression of vimentin, slug, urokinase-type *plasminogen* activator (uPA) and matrix metalloproteinase-14 (MMP-14) [22]. Both transcriptional regulation (uPA, slug and E-cadherin) and post-transcriptional regulation (MMP-14, occludin and vimentin) have been found to be involved in these Nanos3 effects. Nanos3 does not bind *CDH1* mRNA, suggesting that repression is at the transcriptional level. This has not yet been reported for the Nanos/Pumilio complex and should be investigated further. Nanos3 transcriptionally regulates the E-cadherin encoding *CHD1* gene independently of the E-boxes in its promoter region [138]. Other transcriptional repressors, such as Slug, Snail and ZEB proteins, depend on these E-boxes to repress E-cadherin expression.

Remarkably, Nanos3 stabilizes vimentin mRNA by increasing its poly(A)-tail length. Furthermore, Nanos3 protects vimentin mRNA from being bound by miR-30a, which would otherwise repress translation of vimentin. This mechanism of *VIM* mRNA regulation is the first demonstration that binding of a Nanos protein to an mRNA sequence leads to its upregulation. Further investigation of a possible activating role for Nanos proteins is needed. Such activating role might be a specific function executed by mammalian Nanos proteins only. We must note that it has not been investigated whether Pumilio proteins are needed for the Nanos-mediated regulation of E-cadherin and vimentin. In complex organisms the proposed Nanos role as transcriptional regulator and activator might depend as well on other interaction partners besides Pumilio. As Pumilio can act also independently of Nanos, it is conceivable that interaction of Nanos with other regulating proteins can expand its repertoire of specific mRNA targets.

The mechanism underlying increased uPA and MMP-14 levels upon Nanos3 expression has not been elucidated. The role of the malignancy-promoting matrix metalloproteinase MMP-14 (an ECM degrading enzyme) in EMT is unmistakable. Nanos1 expression has been linked to MMP-14 induction [23]. Nanos1 is similarly overexpressed in lung carcinomas [23], where its expression is higher at the invasion front of SCCs and is linked to increased invasiveness. In addition, the expression levels of Nanos1 correlated with tumor aggressiveness (TNM stage). Evidently, identifying target mRNAs of the human Nanos1 and Nanos3 proteins could reveal more about its molecular role and how its overexpression can contribute to tumorigenesis.

The Nanos/Pumilio complex has an interesting role in Rb1-deficient and p53 wild type cancer cells. Functional *RB1*/pRb inactivation is often seen in cancers, and it can be achieved in several ways, such as *E2F* or *CDK4/6* amplification, and inactivating mutations of *p16INK4A* or *RB1* [139] (Figure 1.6A). However, *RB1*/pRb inactivation can be associated with cellular stress and apoptosis, which are deleterious for cancer cell growth. Nonetheless, pRb-deficient cells often seem to evade these stress responses. pRb deletion is associated with upregulation of *nanos* in flies, and of *NANOS1* and *NANOS3* in humans [68]. Rb1 expression is needed for regulation of Nanos expression by the DREAM complex [68]. This complex, consisting of dimerization partner (DP), Rb-like, E2F and MuvB, is evolutionarily conserved with minor variations in its components [140]. The DREAM complex contributes to a balanced gene expression during the different stages of the cell cycle, thereby influencing proliferation [140]. As in humans, the *nanos* gene is strongly bound by components of the *Drosophila* dREAM complex, consisting of Rb, E2F and Myb-associated protein [68].

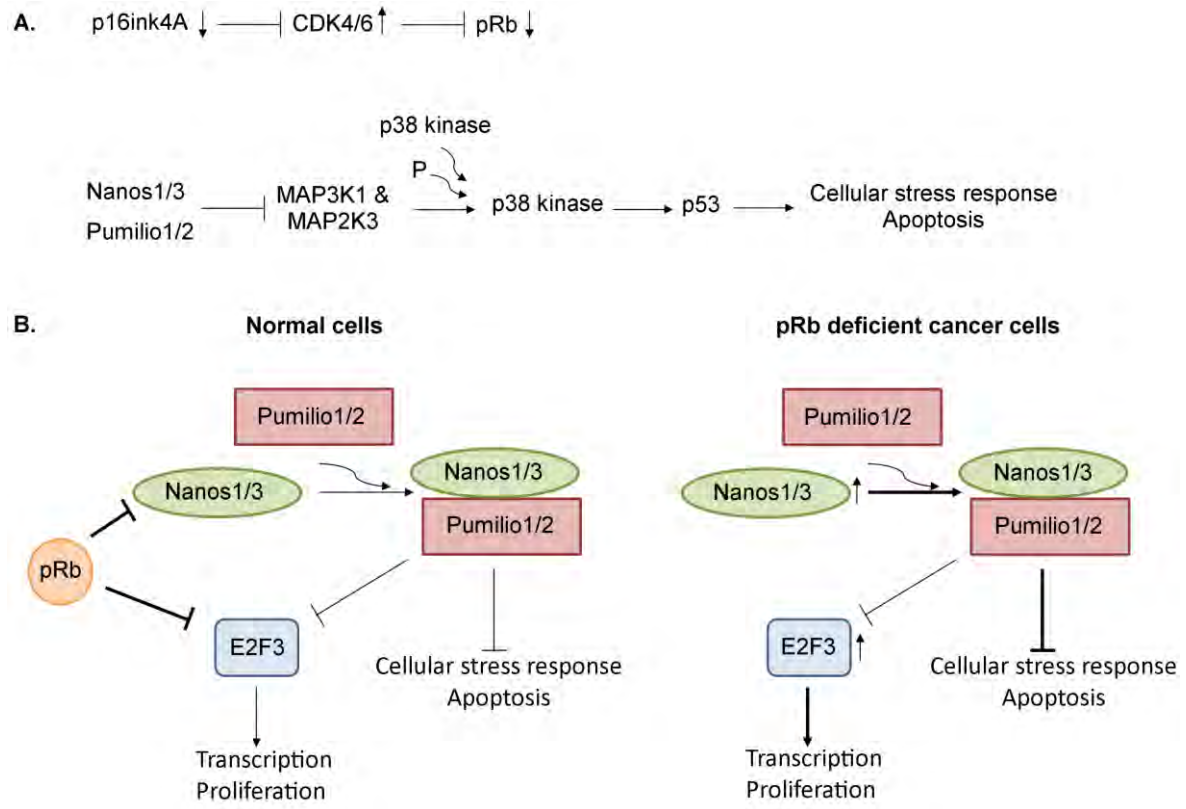

Figure 1.6. pRb deregulation in cancer cells. A. pRb inactivation can be obtained in several ways, for example by down- or upregulation of upstream regulators. Upon loss of Rb1 the Nanos/Pumilio complex is important in cancer cells to repress p53-mediated cellular stress and apoptosis. **B.** Schematic representation of the role of Nanos proteins in pRb-deficient cells retaining a functional p53 protein. See text for further explanation.

This inverse correlation between pRb and Nanos1 or Nanos3 expression is seen in diverse human tumor cell lines. When depleting Nanos1 in pRb-deficient cells, such as the NSCLC cell line NCI-H1666, the cell number is reduced gradually [68]. However, this was only observed in pRb-deficient cells harboring a wild-type p53 gene, suggesting that Nanos1 can repress p53-mediated inhibition of cell growth (Figure 1.6B). Nanos1 was indeed found to downregulate *MAP3K1* and *MAP2K3* genes, which encode kinases upstream of p53 (Figure 1.6A) [68]. Additionally, Nanos1 leads to suppression of apoptosis and thus allows oncogenic growth of pRb-deficient cells. Nanos1 expression can therefore enable pRb-deficient cells lacking p53 mutations to evade stress responses. Though p53 is the most frequently mutated gene in human cancers, p53 mutations are rare in some cancers, such as retinoblastoma and cervical cancer. Many genes that are downregulated in retinoblastoma tumors compared to normal retinal tissue indeed contain PBE motifs. These genes encode proteins such as MAP3K1 and MAP2K3, which are involved in signaling and apoptotic pathways.

1.1.6 Conclusions and perspectives

Nanos proteins originated a long time ago and are represented in all animals. Their primary function in germ cell maintenance is generally conserved, but several other functions have been added during evolution. It would be interesting to gain a deeper understanding of these functions acquired during evolution and in which species. Nanos members form protein complexes with interaction partners such as Pumilio and the CCR4-NOT complex in order to mediate transcriptional and translational regulation of their target mRNAs [25,24,27]. Several studies reported a link between the Nanos/Pumilio complex and miRNA-mediated regulation [43,65,32]. The CCR4-NOT complex is also recruited by GW182 proteins and contributes to miRNA-mediated repression [82,83]. A functional interaction between the Nanos/Pumilio complex and the miRNA regulatory complex has been reported to mediate E2F3 repression [43]. In view of the close interaction between miRNAs and the Nanos/Pumilio complex in regulating specific targets, miRNA silencing might also affect the efficiency with which the Nanos/Pumilio complex regulates these targets [43]. Further correlations between these complexes should be investigated.

Research on Nanos protein expression in cancer is limited. Given that expression of Nanos proteins is mainly restricted to the testis or to the testis and brain, and that they are overexpressed in human cancer, they are potential candidates as cancer testis antigens (CTA). In malignant tumors of epithelial origin, a key event of high diagnostic and prognostic value is inactivation or complete loss of the cell-adhesion protein E-cadherin, generally during EMT. Expression levels of Nanos1 or Nanos3 proteins are inversely correlated to E-cadherin expression levels in several cancer cell lines [7], and Nanos3 was even reported to repress E-cadherin expression [22]. Additionally, as the physical and functional interaction between the DREAM complex and the Nanos/Pumilio complex is conserved, this complex might play an important role in Rb-deficient cancer cells retaining a wild-type p53 (Figure 1.6) [68]. In general, the Nanos/Pumilio complex modulates the expression levels of genes important in both development and disease, and most likely their influence depends on the "cellular context," such as protein complex composition and miRNA levels.

Clearly, Nanos protein members can act as oncofetal agents in the progression of human cancers, although this should be elucidated further. Novel *in vivo* mouse models would be valuable for elucidating the effects of Nanos overexpression and the mechanistic pathways used by Nanos proteins to stimulate tumor progression. Identification and characterization of mRNA targets and interaction partners of mammalian Nanos proteins could also identify pathways that might be triggered in cancer cells. Furthermore, as both Nanos1 and Nanos3 play roles in lung carcinoma, the interplay between Nanos paralogs might be relevant. On the other hand, no cancer-specific expression of Nanos2 has been reported to date. *In vitro* and *in vivo* experiments could show whether Nanos2 overexpression also increases the tumorigenic potential of cancer cells.

Besides investigating the roles of Nanos proteins in cancer, the normal functions of mammalian Nanos proteins need further research. For instance, Nanos1 knockout mice seem perfectly normal. Given the function of *Drosophila* nanos in dendrite morphogenesis [112] and neuronal excitability [104], it could be interesting to study this in more detail in the mouse. Besides its expression in the testis, Nanos3 is also expressed in the brain, although also here no specific function has been identified. Additionally, the implications of the interactions between Nanos1 and GEMIN3 and SNAPIN should be elucidated, and it would be interesting to check whether these interactions are conserved in other species.

Chapter 1.2

Lung cancer

1.2.1 Introduction

Cancer is a worldwide phenomenon caused by environmental and genetic factors. The number of reported cancer patients is increasing, partially because of the population growth and the increased life expectancy. Increasing trends in incidence of obesity and in air pollution are also contributing. Lung cancer is the leading cause of cancer death in men worldwide [141]. This is also the case for women in developed countries, while breast cancer is still the leading cause of cancer death in women in developing countries. Lung cancer is also one of the most aggressive human cancers and is mostly diagnosed in an advanced disease stage. On the other hand, it is one of the most preventable cancers by avoiding exposure to risk factors such as tobacco smoke, asbestos and air pollution [142].

1.2.2 The physiological function of the lung

The lungs are respiratory organs present in vertebrates with the exception of most fish and some amphibians, which take up oxygen through their gills or skin. Humans have two lungs of which the right one consists of three lobes and is bigger than the left one, which only has two lobes, due to the inclination of the heart to the left (Figure 1.7A). In mice the left lung consists of only one lobe and the right lung counts four lobes (Figure 1.7B). The key function of lungs is gas exchange between the air and the blood, which is essential for the metabolism. Oxygen diffuses into the blood stream whereas carbon dioxide is released from the venous blood to the outside. This process is called external respiration. Transport of oxygen from the arterial blood to the cell and the release of carbon dioxide from the cell to the blood occurs throughout the body and is called the internal respiration.

The air enters the lungs through the trachea that ends in the left and the right bronchi, which further branch into secondary and tertiary bronchi, which then branch into bronchioles (Figure 1.7A). The bronchioles end in the alveoli where the gas exchange takes place. Alveolar type-1 cells are responsible for the gas exchange, while alveolar type-2 cells secrete surfactant proteins and other ECM components to maintain the alveolar space and to regulate the surface tension, enabling gas exchange. Mucus produced by goblet cells in the nose, trachea, bronchi and larger bronchioles captures airborne particles such as dust and allergens as well as bacteria. The mucus layer continuously moves towards the oropharynx due to the action of ciliated cells, and thus prevents these particles from

entering the lungs. Non-ciliated club cells, which are mainly found in the bronchioles, protect the lungs by metabolizing inhaled toxic chemicals. Pulmonary neuroendocrine cells have a sensory role, controlling the immune response in the lung [143].

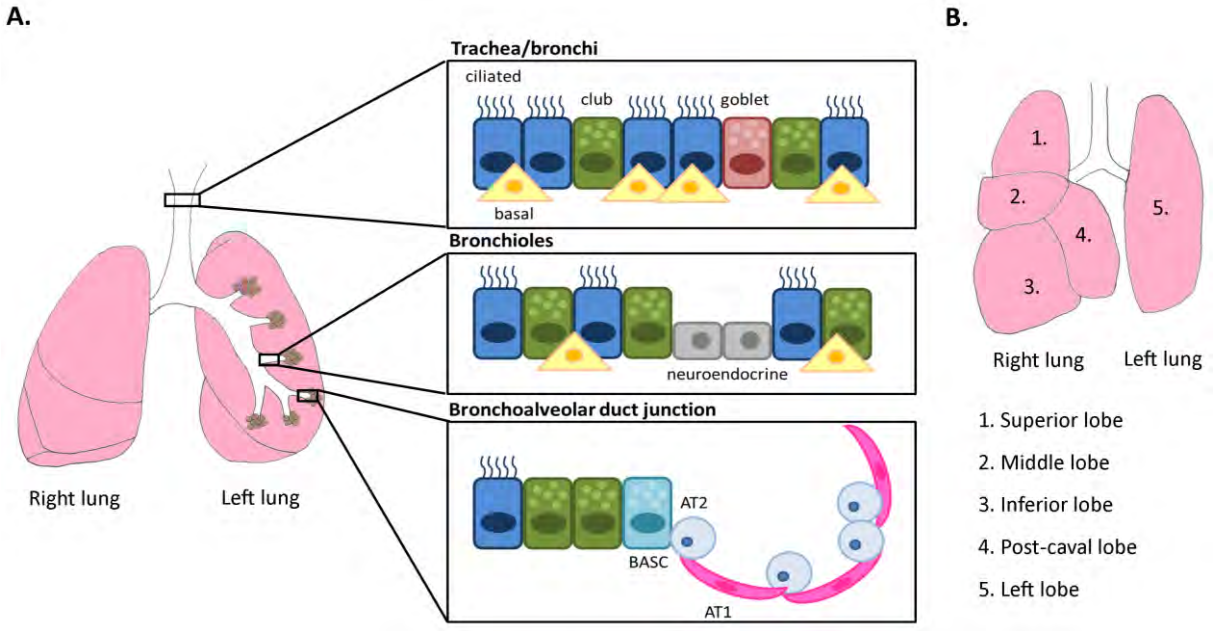

Figure 1.7. Anatomy of the lung in man and mouse. A. A representation of the human lungs and the distribution of lung cells. **B.** In mice the right lung counts four lobes and the left lung counts only one lobe unlike three and two lobes in humans, respectively. Contrasting to the human situation, basal cells are not found in the bronchioles of mice. BASC, bronchioalveolar stem cell; AT1, alveolar type 1 cell; AT2, alveolar type 2 cell.

1.2.3 Classification of lung cancers

Lung cancers are classified in two major groups: small cell lung cancer (SCLC) and NSCLC. The former cancer type is highly metastatic and covers approximately 15% of all lung cancers [142]. NSCLC accounts for the other 85% and was, until recently, divided in three main subgroups: adenocarcinoma, squamous cell carcinoma and large cell carcinoma. The latter subgroup became disputable on the basis of genomic analyses [144,145]. Adenocarcinoma is the most common subgroup of NSCLC. Recently, a new adenocarcinoma classification was suggested eliminating the terms bronchioloalveolar carcinoma (BAC) and mixed subtype adenocarcinoma [146]. A new class, lepidic predominant adenocarcinoma, was introduced, referring to a non-mucinous tumor with minimal invasion. This new adenocarcinoma classification was implemented in the 2015 WHO Classification of Lung Tumors [147]. The new classification depends for a greater extent on immunohistochemical characterization,

including adenocarcinoma markers (e.g. TTF-1 or Napsin A), squamous markers (e.g. p40, p65 or cytokeratin 5/6) and mucin stains, and on genetic studies. This should help in optimizing tailored cancer treatment.

Another classification, the TNM (tumor, node and metastasis) classification, depends on the stage of the tumor with respect to tumor growth and metastasis formation. In 2017 an updated version of the TNM classification was implemented (Tables 1.7 and 1.8). The effectiveness of this updated staging system was already confirmed on a cohort of NSCLC patients [148]. The correlated prognostic value of the updated classification proved to be better than this of the previous edition. Similarly to the abovementioned immunohistochemical and genetic classification, the updated TNM should help in choosing the correct treatment strategy for each lung cancer patient.

Table 1.7. TNM classification for lung cancer. This table is adapted from [149].

T: Primary tumor	
Tx	Primary tumor cannot be assessed
T0	No evidence of primary tumor
Tis	Carcinoma *in situ*
T1	Tumor ≤ 3 cm, surrounded by lung or visceral pleura without bronchoscopic evidence of invasion more proximal than the lobar bronchus (i.e. not in the main bronchus)
T1a(mi)	Minimally invasive adenocarcinoma
T1a	Tumor ≤ 1 cm
T1b	Tumor > 1-2 cm
T1c	Tumor > 2-3 cm
T2	Tumor > 3-5 cm or if the tumor - involves the main bronchus, without involvement of the carina - invades the visceral pleura - is associated with atelectasis or obstructive pneumonitis that extends to the hilar region, involving part or all of the lung
T2a	Tumor > 3-4 cm
T2b	Tumor > 4-5 cm
T3	Tumor > 5-7 cm or associated with separate tumor nodule(s) in the same lobe as the primary tumor or directly invades any of the following structures: chest wall, phrenic nerve or parietal pericardium
T4	Tumor > 7 cm or associated with separate tumor nodule(s) in a different ipsilateral lobe than that of the primary tumor or invades any of the following structures: diaphragm, mediastinum, heart, great vessels, trachea, recurrent laryngeal nerve, esophagus, vertebral body and carina
N: Regional lymph node involvement	
Nx	Regional lymph nodes cannot be assessed
N0	No regional lymph node metastasis
N1	Metastasis in ipsilateral peribronchial and/or ipsilateral hilar lymph nodes and intrapulmonary nodes, including involvement by direct extension
N2	Metastasis in ipsilateral mediastinal and/or subcarinal lymph nodes(s)
N3	Metastasis in contralateral mediastinal, contralateral hilar, ipsilateral or contralateral scalene, or supraclavicular lymph node(s)
M: Distant metastasis	
M0	No distant metastasis
M1	Distant metastasis
M1a	Separate tumor nodule(s) in contralateral lobe; tumor with pleural or pericardial nodule(s) or malignant pleural or pericardial effusion
M1b	Single metastasis in a single organ
M1c	Multiple metastases in one or more organs

Table 1.8. Staging according to the 8th edition of the TNM classification [149].

		N0	N1	N2	N3	M1a	M1b	M1c
T1	**T1a**	IA1	IIB	IIIA	IIIB	IVA	IVA	IVB
	T1b	IA2	IIB	IIIA	IIIB	IVA	IVA	IVB
	T1c	IA3	IIB	IIIA	IIIB	IVA	IVA	IVB
T2	**T2a**	IB	IIB	IIIA	IIIB	IVA	IVA	IVB
	T2b	IIA	IIB	IIIA	IIIB	IVA	IVA	IVB
T3	**T3**	IIB	IIIA	IIIB	IIIC	IVA	IVA	IVB
T4	**T4**	IIIA	IIIA	IIIB	IIIC	IVA	IVA	IVB

The colors mark the four different stage groups.

1.2.4 Genetic landscape of NSCLC

Several major somatic mutations are linked to lung cancer. Part of these are elicited by exposure to tobacco smoke. Mutations in the tumor suppressor gene *TP53* are the most widespread mutations in lung cancer. Besides *TP53* other genes such as *EGFR*, *NF1* and *CDKN2A* are also often mutated in adenocarcinoma [150]. Another set of affected genes in adenocarcinoma, such as *KRAS*, *BRAF* and *PI3KC,* show 'gain-of-function' mutations while the *MYC* gene is often amplified. Unlike other mutated genes such as *EGFR* and *EML4-ALK* translocation, *KRAS* mutations are more frequent in smokers versus non-smokers [150]. Benzo(a)pyrene diol epoxide (BPDE), a mutagen found in cigarette smoke, causes G to T conversion in *TP53* [151]. The occurrence of these mutagenic conversions for *TP53* in lung cancer was higher in smokers than in non-smokers. Similarly, these G to T conversions were also found in *KRAS* [152].

1.2.5 Mouse models for NSCLC

The generation of mouse models aids in finding better ways to treat cancer. Mouse models contribute to identifying the driver mutations for a specific cancer, to analyze synergistic or antagonistic interactions between cancer-associated genes, by making it possible to study the influence of certain genes on tumor progression and metastasis, and to test drugs on these models.

Several types of models exist such as xenograft and syngeneic models where cancer cells are injected orthotopically, subcutaneously, intraperitoneally or intravenously. Xenograft models in which human tumors and tumor-derived cell lines are implanted or injected in mice are most frequently used to evaluate treatment methods before starting clinical trials. Mouse models for spontaneous or carcinogen-induced lung cancer involve susceptible mouse strains such as A/J and SWR [153]. Intraperitoneal injection of carcinogens such as urethane, benzo(a)pyrene and dimethylhydrazine induces adenoma formation [154].

Transgenic mouse models are widely used in cancer research. The first transgenic mice described for lung cancer include mice overexpressing a certain oncogene such as cMyc, H-Ras and Simian Virus 40 large-T antigen (SV40 Tag) [155]. SV40 Tag inactivates p53 of which the corresponding gene is often mutated in lung cancer. Oncogene expression can also be conditional, regulated by using the Cre/lox system or a tetracycline-controlled system or a combination of both. Using the Cre/lox system, oncogene expression can be induced by removing a 5' positioned floxed stop cassette (LSL). Gene knockout of a tumor suppressor gene can also be induced by Cre-expression if (part of) the gene is flanked by loxP sites (floxed). For instance, Cre-dependent deletion of *TP53* gives rise to lung adenocarcinomas [156]. Cre can be administered in lungs by using Cre-encoding viruses, often adenoviruses, or its expression can be made lung-specific by using gene promoters such as those of surfactant protein C (SPC) and club cell specific protein (CCSP, also known as CC10). Two tetracycline-dependent systems exist. These are based on the resistance mechanism in *Escherichia coli* bacteria against the tetracycline antibiotic. In the Tet-Off system the transcription of a gene under control of a tetracycline response element (TRE) is activated in the absence of tetracycline or its derivative, doxycycline. The tetracycline transactivator (tTA) binds to tetracycline operator (tetO) sequences in the TRE. In the Tet-On system transcription depends on the reverse tTA (rtTA) and is activated in the presence of doxycycline. These techniques have the advantage that gene activation or silencing is reversible while this is not the case for the Cre/lox system. A combination of these systems involves tetracycline-inducible Cre expression where the Cre gene is under control of the TRE, and where the rtTA required for Cre activation is expressed from a tissue-specific promoter (Tet-On system). This will be explained in more detail in Chapter 3. The Cre-recombinase can also be fused to an estrogen receptor (ER) or a modified ER, tamoxifen-dependent ER (ERT), while expression of

the fusion protein can be made tissue-specific. Cre recombinase activity is hence regulated by estrogen or tamoxifen, respectively. Examples of mouse models using the (modified) ER are given below in Table 1.9. Besides overexpression of oncogenes such as *MYC*, mutated *PIK3CA, HRAS* or *KRAS* mutants and the EML4-ALK fusion protein, also overexpression of frequently mutated growth factor receptors such as EGFR is used to model lung cancer [157,158]. Overexpression of the receptor tyrosine kinase RON under control of the SPC promotor has also been linked to lung tumor formation, with an interesting progression from adenomas to adenocarcinomas [159]. Besides overexpressing RON, Ras expression was significantly increased in these tumors. Overexpression of RON can indeed lead to activation of the Ras-MAPK and PI3K-AKT pathway [160]. Also, overexpression of mutant KRas in combination with deletion of a tumor suppressor gene such as *TP53* and *PTEN* is often used to model human lung cancer. Overexpression of mutated KRas in combination with knockout of tumor suppressor liver kinase B1 (lkb1), also known as serine-threonine kinase 11 (STK11), gives rise to both adenocarcinomas and squamous cell carcinomas [161]. Rarely also large cell carcinoma was observed in these mice.

1.2.6 Cells at the origin of adenocarcinoma

Human tissue samples from adenocarcinomas often stain positive for alveolar type-II markers such as SPC and for club cell markers such as CC10. Both alveolar type-II cells and club cells were consequently considered as candidate cells of origin for adenocarcinoma formation. A series of elegant studies in genetically engineered mice has investigated this by cell-specific overexpression of the *LSL-KRas*^{G12D} or *LSL-KRas*^{G12V} oncogenes [162-164] (summarized in Table 1.9). Tumor initiation was seen in both alveolar type-II and club cell types upon overexpression of oncogenic KRas. However, mainly engineered alveolar type-II cells seem to show a sustained proliferative response, eventually giving rise to KRas-driven adenocarcinoma (Figure 1.8).

The promotor sequence of Stem cell antigen-1, *Sca-1*, encoding a marker for BASCs and lung epithelial precursor cells [165], was similarly used to express the Cre recombinase. The Cre recombinase will remove the floxed stop cassette in front of the oncogenic *KRas* transgene and thus initiate oncogene expression. LSL-KRas^{G12V};Sca-1-Cre mice gave rise to hyperplasia and adenoma formation at the bronchioles, which mainly stained CC10-positive [162]. The

mice died too early to observe any progression to adenocarcinoma. When *KRas* oncogene expression is induced at weaning, under control of the same promotor (LSL-KRas^{G12V};Sca-1-CreERT2$^{+/-}$), SPC-positive alveolar adenomas were seen. The cells able to initiate cancer can consequently differ depending on the timing of oncogenic induction.

Table 1.9. Experiments concerning the cells of origin in lung cancer.

Oncogenic driver(s)[1]	Initiation method[a]	Major phenotype[b]	Cell markers[c]	(Proposed) cell(s) of origin	Reference
LSL-KRas^{G12V}	Adeno-Cre (intratracheal infection)	Alveoli: adenoma, adenocarcinoma; Bronchioles, BADJ: hyperplasia, adenoma	Alveoli: SPC Bron/BADJ: SPC, CC10, CC10/SPC	Alveoli: AT2 cell Bron/BADJ: club cell/BASC	[162]
LSL-KRas^{G12V}	Sca1-Cre	Bronchioles: hyperplasia, adenoma	CC10, CC10/SPC	Club cell precursor	[162]
LSL-KRas^{G12V}	Sca1-CreERT2 + tamoxifen	Alveoli: adenoma	SPC	AT2 cell	[162]
LSL-KRas^{G12D}	Adeno SPC-Cre	Alveolar hyperplasia	SPC	AT2 cell	[163]
LSL-KRas^{G12D}	Adeno CC10-Cre	BADJ papilloma	CC10, SPC, CC10/SPC	Club cell/BASC	[163]
LSL-KRas^{G12D};p53$^{fl/fl}$	Adeno SPC-Cre	Alveoli adenoma, adenocarcinoma	N.A.	AT2 cell	[163]
LSL-KRas^{G12D};p53$^{fl/fl}$	Adeno CC10-Cre	BADJ papillary carcinoma	N.A.	Club cell/BASC	[163]
LSL-KRas^{G12D};p53$^{fl/+}$	CC10-CreER + tamoxifen	BADJ: hyperplasia; Alveoli: adenoma/adenocarcinoma	BADJ: CC10, CC10/Foxj1, CC10/SPC; alveoli: SPC	BADJ: club cell/BASC; Alveoli: AT2/BASC	[164]
LSL-KRas^{G12D};p53$^{fl/+}$	Sftpc-CreER + tamoxifen	BADJ: only very rarely, small hyperplasia at late stage; Alveoli: adenoma/adenocarcinoma	alveoli: SPC	AT2	[164]

[a] Adeno, adenovirus; Sca1, Stem cell antigen-1; ERT2, tamoxifen-dependent estrogen receptor 2; SPC, surfactant protein C; CC10, club cell 10 kDa protein; Sftpc, surfactant protein C; ER, estrogen receptor

[b] BADJ, bronchoalveolar duct junction

[c] Bron, bronchioles; AT2, alveolar type 2 cell; N.A., not available

[d] BASC, bronchioalveolar stem cell

[1] The floxed stop cassette (LSL) in front of the oncogenic *KRas* transgenes is removed by the Cre-recombinase. Similary, the Cre-recombinase removes the floxed (fl, flanked with loxP sites) *p53* gene.

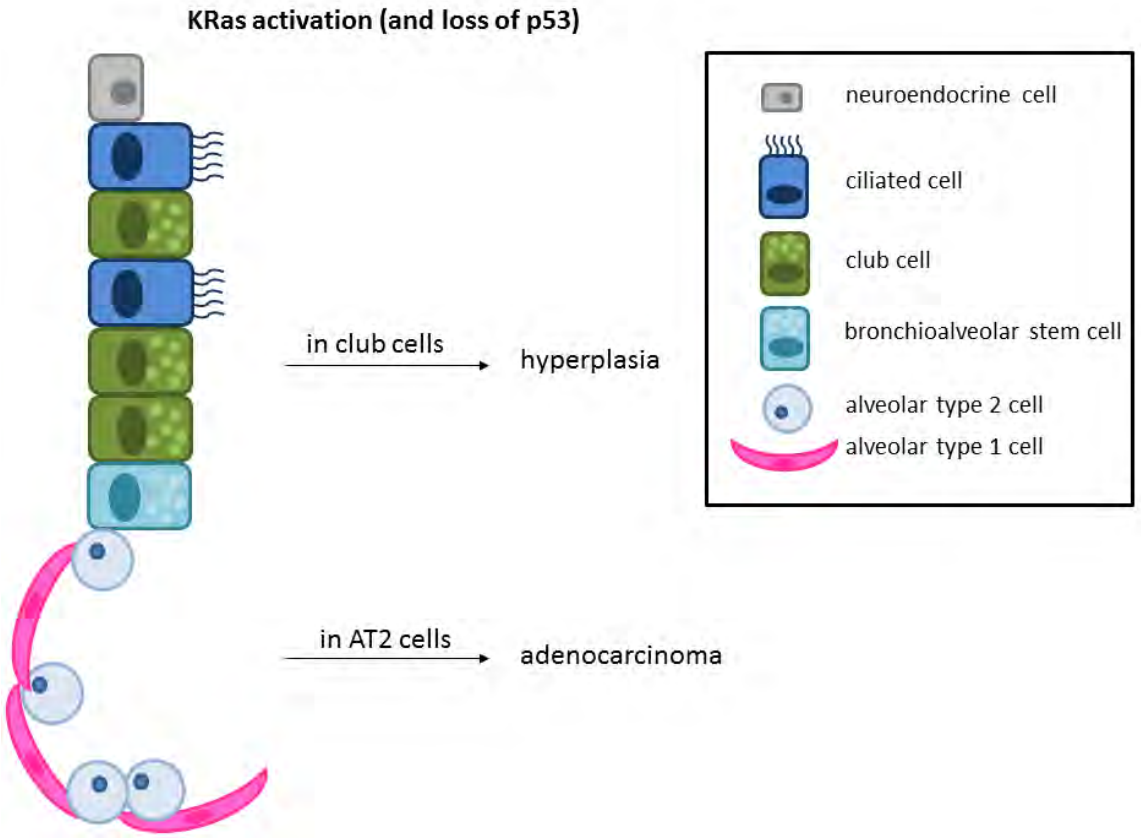

Figure 1.8. Cell-specific effects of KRas activation, with or without loss of p53, on lung epithelial cells. AT2 cells, alveolar type 2 cells.

1.2.7 NSCLC treatments

The treatment modalities for NSCLC patients are mainly based on the stage and the genetic background of the cancer. Surgery, radiotherapy, chemotherapy and combinations of these, are the primary treatment methods. Stage 0 NSCLC, i.e. carcinoma in situ, is easy to cure and is mostly treated by surgery alone. The other stages often require additional radio- or chemotherapy or both. These can be applied as a neoadjuvant to shrink the tumor before surgery, or as adjuvant therapy after surgery to kill the remainder of cancer cells. In some advanced tumors or if surgery is not an option, radio- and chemotherapy will be applied as main treatment.

When the cancer has metastasized, the tumor will be checked for common gene mutations. For instance, several genes involved in the receptor tyrosine kinase (RTK) pathways, such as *EGFR* and *ALK*, are often dysregulated in NSCLC and therefore will be checked. Drugs targeting *EGFR*, such as erlotinib, gefitinib and afatinib, and drugs targeting *ALK*, such as crizotinib and ceritinib, have already been approved as NSCLC treatments by the Food and

Drug Administration (FDA) [150]. However, resistance to for instance *EGFR*-inhibitors is common (reviewed in [166]). Chemotherapy is often combined with other drugs such as antibodies against VEGF (bevacizumab) or EGFR (nicitumumab). Although *TP53* and *KRAS* mutations are the most frequent genomic alterations in NSCLC, these are hard to target.

If the primary treatment did not inhibit tumor progression or if the tumor has recurred, second line treatments will be started. For instance, ramucirumab, directed against vascular endothelial growth factor receptor 2 (VEGFR2), has been approved as a second-line treatment of NSCLC in combination with the cytotoxic chemotherapy drug docetaxel [167].

NSCLC is one of the most responsive cancers to immunotherapy. The immunogenic tumor microenvironment and the high mutagenic burden of these tumors contribute to this (Figure 1.9). The prevalence of somatic mutations likely correlates with neoantigen formation in the tumor [168].

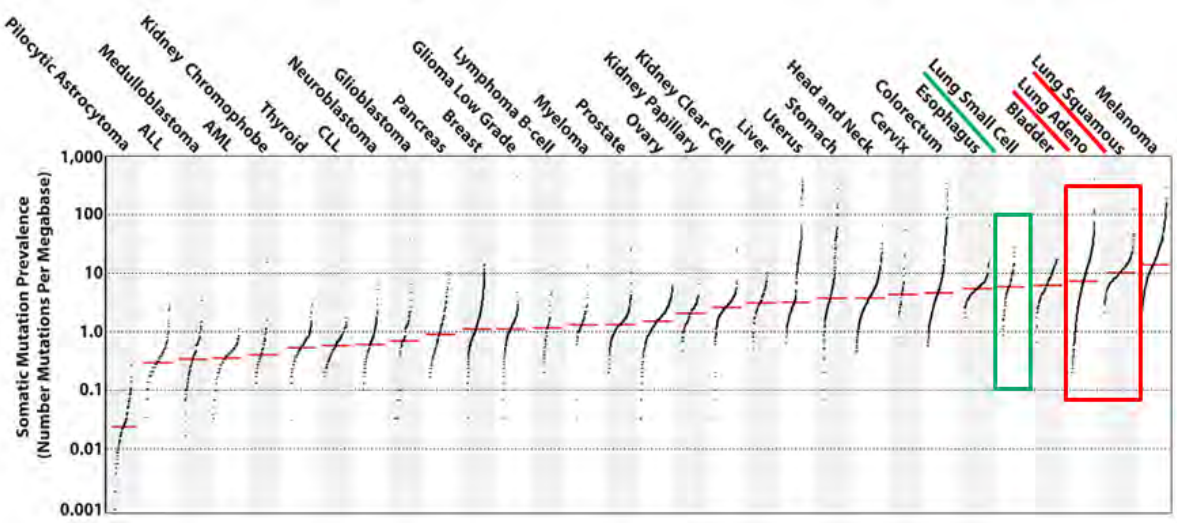

Figure 1.9. The occurrence of somatic mutations in various human cancer types. Small cell lung cancer and non-small cell lung cancer are depicted in green and red, respectively, and show high somatic mutation prevalence. Figure adapted from [169].

Immunotherapy is often used when driver mutations or rearrangements are apparently absent, and as a second-line treatment. Patients with driver mutations such as *EGFR* and *ALK* mutations generally respond less to immunotherapy compared to those exposed to tobacco smoke. Immunotherapeutical drugs such as nivolumab have been approved as a second-line treatment for NSCLC. Pembrolizumab can only be used for non-squamous cell type NSCLC.

Both nivolumab and pembrolizumab block the immune checkpoint protein programmed cell death 1 (PD-1).

PD-1 is a receptor expressed on the surface of activated T cells. If this receptor binds PD ligand 1 (PD-L1), the T cells become inactive. The PD-1/PD-L1 pathway regulates the immune response, preventing chronic activation and thus the possibility of autoimmune inflammation. Tumor cells commonly overexpress PD-L1 in order to evade immune detection and the following immune response. PD-1 inhibitors block binding of PD-L1, preventing T cell inhibition and hence stimulating the T-cell mediated immune response. The effectivity of PD-1 blocking immunotherapy in NSCLC was shown to depend on the acquired mutations [170]. Since the mutational burden is also determined by the smoking behavior, smokers respond better to PD-1 blocking drugs *versus* non-smokers [171].

Despite the positive evolution in NSCLC treatment, most patients with advanced NSCLC are not completely cured after treatment.

Chapter 1.3

Prostate cancer

1.3.1 Introduction

In developed countries prostate cancer is the most frequently diagnosed cancer in men, with almost 3/5 more new cases in 2012 than for lung cancer which ranks second [141]. At the worldwide level prostate cancer follows lung cancer as the second most diagnosed cancer in men. When considering cancer deaths, prostate cancer ends up at the third and fifth place in developed countries and worldwide, respectively. There is a lot of variation in prostate cancer incidence rates of different countries, and countries with the highest incidence rates do not correlate with those with the highest mortality rates (Figure 1.10). The difference in incidence rates can partially be explained by the use of prostate-specific antigen (PSA) testing or not. PSA detection allows a better diagnosis of prostate cancer patients and consequently increases incidence rates in the countries that use it [172]. Different treatment methods, life styles and genetic factors are likely to contribute to the difference in mortality rates. Nonetheless, the PSA test has been seriously criticized given the high percentage of false diagnoses [173]. Discontinuing PSA screening for men that reached the age of 70 was estimated to eliminate around 65% of overdiagnosis [174]. In April 2017 the U.S. Preventive Services Task Force (USPSTF) has set new guidelines for prostate cancer screening; men between 55 and 69 should discuss the matter with their doctor and decide individually whether to do a PSA screening or not. Previously USPSTF discouraged the screening test for all men.

The current clinical testing enables early detection of prostate cancer; with most tumors exhibiting a relatively slow degree of proliferation that contributes to the very high survival rates. However, aggressive forms of prostate cancer, which spread to surrounding tissues (e.g. seminal vesicle and lymph nodes) and to other organs, exist. The bone is the most common site of metastasis but other organs such as the liver, lung and brain should also be checked.

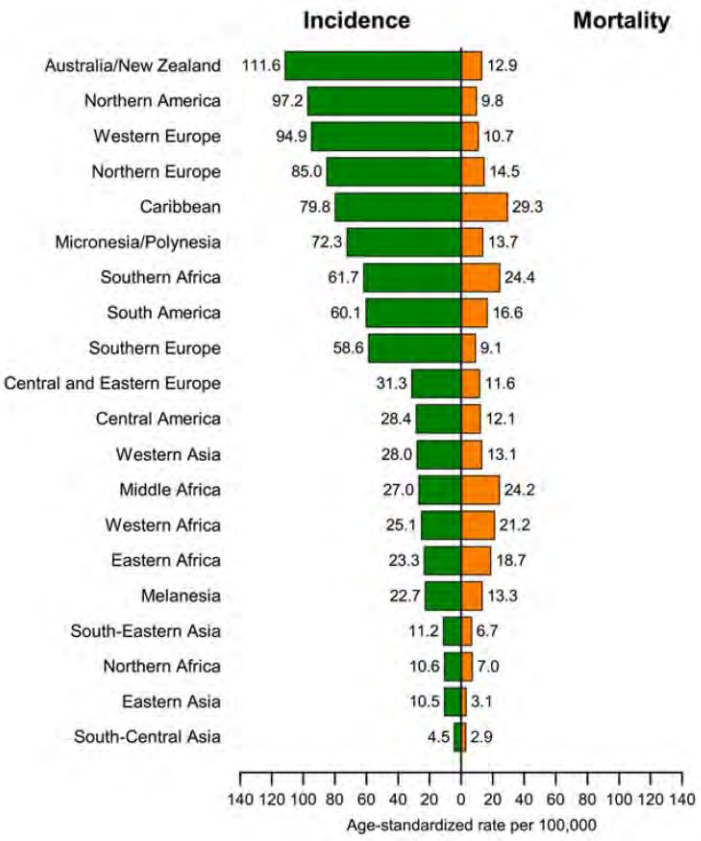

Figure 1.10. Estimated incidence and mortality rates for prostate cancer in 2012. Figure reproduced from [141].

1.3.2 The physiology and anatomy of the prostate

The prostate is a fairly small gland located underneath the bladder. It is part of the urogenital system, which combines the reproductive organs and the urinary system. The primary function of the prostate is fluid production, which is subsequently mixed with the sperm cells from the testicles and with other secretions; together they form the semen. Prostate fluid is a mixture of sugars, enzymes and alkaline chemicals. It serves as nutrition for the sperm while the enzymes allow the sperm cells to leave the semen after ejaculation. Prostate cells express PSA, also known as the enzyme kallikrein-3, which liquefies the semen after ejaculation, enabling the sperm to swim freely. The PSA level is increased in prostate cancer and can be measured through a simple blood test. However, other causes and in particular benign prostatic hyperplasia (BPH; see below) can increase the PSA levels; therefore, a PSA increase should be seen as a warning rather than a firm indication of prostate cancer. Finally, the alkaline chemicals in the prostate secretion contribute to the survival of the sperm cells after ejaculation by neutralizing acidic vaginal secretions.

In humans the prostate is an unilobular organ subdivided into three zones - the transition zone, the central zone and the peripheral zone (Figure 1.11A). The transition zone encircles the urethra. The prostate grows gradually during a man's life which can cause problematic urinating at an older age (BPH). If the urethra becomes completely blocked the prostate will be removed, while medications might help in less severe cases. The central zone surrounds the ejaculatory ducts and the peripheral zone comprises the largest part of the prostate. Most prostate cancers arise in this peripheral zone [175]. In mice the prostate comprises four pairs of lobes, the anterior, dorsal, ventral and lateral prostate (Figure 1.11B), which cannot be linked to the zones in the human prostate.

The epithelial cell layers of the prostate mainly comprise basal and secretory luminal cells with few intermediate and neuroendocrine cells (Figure 1.12). This is the case in both the human and mouse prostate, although fewer basal cells are present in the prostate epithelium of mice.

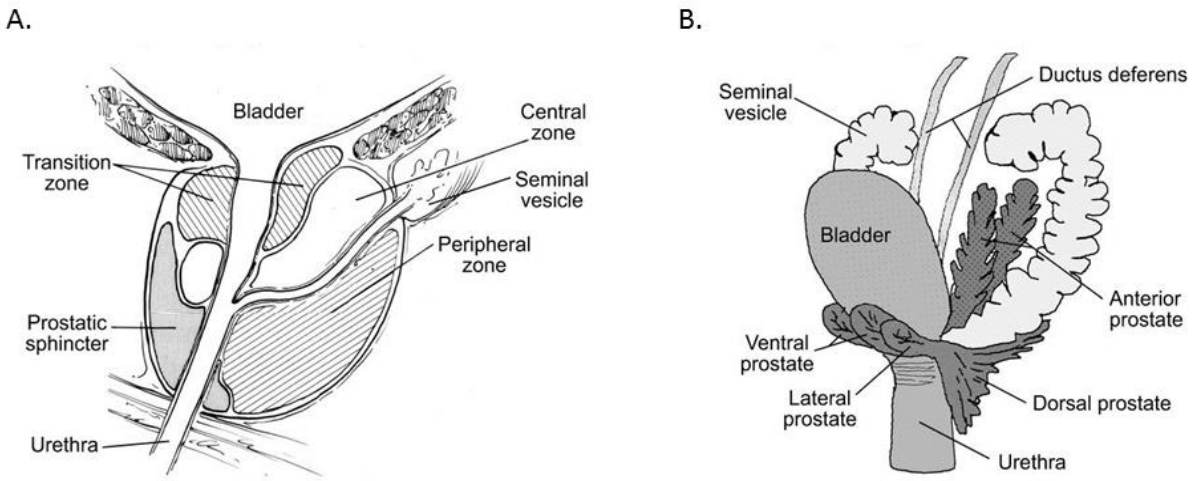

Figure 1.11. Anatomy of the prostate. Schematic representation of the adult human prostate (sagittal section) **(A)** and the mouse prostate (lateral view) **(B).** Picture adapted from [176].

Figure 1.12. Schematic representation of the human prostate epithelium.

1.3.3 Classification and genetic landscape of prostate cancers

As for lung cancer the TNM classification for prostate cancer has recently been updated [177] (Table 1.10). Staging is a way of classifying a cancer, and is generally based on the size of the tumor (T) and whether the cancer has spread (N and M). Prostate cancer staging now also takes the Gleason grade groups into account (Table 1.11 and Table 1.12). Grading is a way to classify cancer cells, depending on their degree of differentiation and their growth rate. Prostate biopsies can be used to give a Gleason score and to determine the grade group (Table 1.11). Assigning a prostate cancer stage further depends on the PSA levels in the blood and other methods to analyze the growth and metastasis of the tumor (Table 1.12). The Gleason score is based on the observed histological grades in the tumor, ranging from grade 1 for a well differentiated tumor to grade 5 for a very poorly differentiated tumor. The two most prevalent grades are added, yielding a score ranging from two to ten. Combining abovementioned parameters leads to an optimal staging of prostate cancer, helps to select the best treatment for the patient and can be used to estimate a patient's prognosis.

Table 1.10. TNM classification for prostate cancer. This table is adapted from [177].

Category	Criteria
Clinical (cT)	
T (Primary tumor)	
TX	Primary tumor cannot be assessed
T0	No evidence of primary tumor
T1	Clinically inapparent tumor that is not palpable or visible by imaging
T1a	Tumor incidental histologic finding in ≤ 5% of tissue resected
T1b	Tumor incidental histologic finding in > 5% of tissue resected
T1c	Tumor identified by needle biopsy found in one or both sides, but not palpable
T2	Tumor is palpable and confined within prostate
T2a	Tumor involves one-half of one side or less
T2b	Tumor involves more than one-half of one side but not both lobes
T2c	Tumor involves both sides
T3	Extraprostatic tumor that is not fixed or does not invade adjacent structures
T3a	Extracapsular extension (unilateral or bilateral)
T3b	Tumor invades seminal vesicle(s)
T4	Tumor is fixed or invades adjacent structures other than seminal vesicles such as bladder, rectum, external sphincter, levator muscles and/or pelvic wall
Pathologic (pT)	
T (Primary tumor)	
pT2	Organ confined
pT3	Extraprostatic extension
pT3a	Extraprostatic extension (unilateral or bilateral) or microscopic invasion of the bladder neck
pT3b	Tumor invades seminal vesicle(s)
pT4	Tumor is fixed or invades adjacent structures other than seminal vesicles such as bladder, rectum, external sphincter, levator muscles and/or pelvic wall
N (Regional lymph nodes)	
NX	Regional lymph nodes were not assessed
N0	No regional lymph node metastasis
N1	Metastasis in regional lymph node(s)
M (Distant metastasis)	
M0	No distant metastasis
M1	Distant metastasis
M1a	Nonregional lymph nodes(s)
M1b	Bone(s)
M1c	Other site(s) with or without bone disease

Table 1.11. Criteria to determine the correct grade group. This table is adapted from [178].

Grade group 1: Gleason score ≤ 6
Only individual discrete well-formed glands
Grade group 2: Gleason score 3+4=7
Predominantly well-formed glands with lesser component of poorly formed/fused/cribriform glands
Grade group 3: Gleason score 4+3=7
Predominantly poorly formed/fused/cribriform glands with lesser component of well-formed glands
Grade group 4: Gleason score 4+4=8; 3+5=8, 5+3=8
Only poorly formed/fused/cribriform glands Predominantly well-formed glands and lesser component lacking glands Predominantly lacking glands and lesser component of well-formed glands
Grade group 5: Gleason scores 9-10
Lack gland formation (or with necrosis) with or without poorly formed/fused/cribriform glands

Table 1.12. The stage group according to the TNM categories, the PSA level and the grade group. This table is adapted from [177].

Prognostic stage group	T	N	M	PSA (in ng/ml)	Grade group
I	cT1a-c, cT2a	N0	M0	< 10	1
	pT2	N0	M0	< 10	1
IIA	cT1a-c, cT2a	N0	M0	≥ 10 < 20	1
	pT2	N0	M0	≥ 10 < 20	1
	cT2b-c	N0	M0	< 20	1
IIB	T1-2	N0	M0	< 20	2
IIC	T1-2	N0	M0	< 20	3
	T1-2	N0	M0	< 20	4
IIIA	T1-2	N0	M0	≥ 20	1-4
IIIB	T3-4	N0	M0	Any	1-4
IIIC	Any T	N0	M0	Any	5
IVA	Any T	N1	M0	Any	Any
IVB	Any T	Any	M1	Any	Any

Although environmental and dietary factors play a role in prostate cancer initiation, genetic factors are also important. The risk for prostate cancer is higher when a man has multiple first-degree relatives with either prostate cancer or a combination of prostate cancer with other related cancers such as breast and ovarian cancer. Early-onset prostate cancer (diagnosed at or before the age of 55) also suggests a genetic contribution. Somatic genetic

and epigenetic changes in tumor suppressor genes (such as *NKX3.1*, *PTEN* and *TP53*), oncogenes (such as *MYC*, *ERG* and *AR*) and caretaker genes (such as *GSTP1*) are commonly found in prostate cancer [175]. Overexpression of ERG is almost always paired with chromosomal rearrangements involving the fusion of the 5'-UTR of *TMPRSS2* to *ERG* [179,180]. Germline mutations in *HOXB13* and the mismatch repair genes *BRCA1* and *BRCA2* are also associated with a high risk of prostate cancer [181-183]. Furthermore, amplification of *MYC*, *EZH2* and *BRAF* and loss of *RB1* is often seen in prostate cancer [184].

Prostate cancers are primarily adenocarcinomas (95%) with few other tumor types such as small cell tumors and mucinous carcinomas. Adenocarcinoma formation is preceded by prostatic intraepithelial neoplasia (PIN) (Figure 1.13).

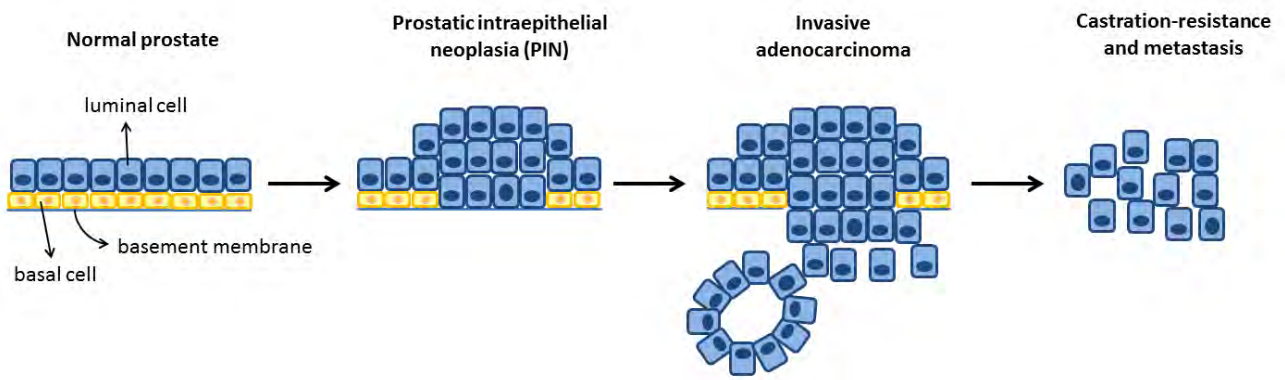

Figure 1.13. Schematic illustration of prostate tumor progression to adenocarcinoma and metastasis formation.

1.3.4 Mouse models for prostate cancer

Unlike rats and dogs, which develop spontaneous prostate cancer similarly to the situation in humans, this is rarely the case in mice. Mice and humans also have a completely different anatomy concerning the prostate (see above). However, mice remain the preferred animals for modeling prostate cancer. This is because of several general advantages such as the small size of the mouse, the relatively short gestation period, a fully sequenced genome, which is 99% similar to the human genome, and several available techniques for genetic engineering. Mouse xenograft and allograft models also exist for prostate cancer using, respectively, either human prostate tissues and cancer cell lines such as LNCaP and PC3, or cell lines derived from transgenic mouse models such as TRAMP-C1 and PNEC30 [185].

Several genetically engineered mouse models (GEMMs) exist for prostate cancer in which oncogenes, growth factors, growth factor receptors, hormone receptor genes and genes involved in the cell cycle, apoptosis or Wnt signaling are overexpressed or deleted (reviewed in [186]).

Several models are based on the SV40 tumor antigens. Prostate-specific expression of the SV40 large and small tumor antigens (Tag/tag) resulted in the transgenic adenocarcinoma mouse prostate (TRAMP) model [187,188]. Prostate-specific expression was mediated here by the rat probasin (Pb) promoter. Lymph node metastases were detected in all mice and pulmonary metastases were detected in most mice, while bone metastasis, albeit commonly observed in humans, were rare. TRAMP is a good model for castration resistant prostate cancer but has a neuroendocrine origin [189], while in humans most cells in prostate adenocarcinoma are of epithelial origin. Another SV40-based model only involves the expression of Tag from the large Pb promoter (LPb), hence called LPb-Tag (LADY) [190]. In this model, the rat Pb promoter has been modified to give higher transgene expression. Tumorigenesis in this model is similar to that observed in the human prostate, although metastasis cannot be reproduced.

The ARR_2/Pb promoter is another variant of the rat Pb promoter, and results in the highest transgene expression in comparison to the Pb and LPb promoters. The ARR_2/Pb promoter is for instance used to overexpress the *Myc* oncogene in the luminal epithelial cells of the prostate, resulting in prostatic adenocarcinoma [191]. This model is explained in more detail in Chapter 4. Other proto-oncogenes such as *Ras*, *Neu* and *ERG* have also been overexpressed in epithelial cells of the mouse prostate, regulated by the Pb promoter [192-194]. Overexpression of the androgen receptor (AR) has been achieved by using Osr(odd skipped related)1-Cre mice with induced expression in the urogenital sinus epithelium [195]. This caused PIN development in 50% of the analyzed mice and adenocarcinoma formation in 10% of the analyzed mice.

The Cre/lox system is also used in combination with a prostate-specific promoter of which the Pb promoter is mainly used. Besides the traditional knockout models, this system permits conditional knockout of tumor suppressor genes such as *APC*, *PTEN*, *NKX3.1* and *TP53*. PTEN is an important tumor suppressor in many human cancers including prostate cancer. PTEN negatively regulates the PI3K/AKT pathway and heterozygous knockout of

PTEN went along with PIN formation in the prostate [196]. Prostate-specific homozygous *PTEN* knockout mice showed PIN, invasive adenocarcinoma and metastasis [197]. Several heterozygous and homozygous *PTEN* knockout models exist in combination with other genes such as *TP53*, *p27* and *NKX3.1*, as reviewed in [198] and [199]. These models are suitable for identifying metastasis promoting pathways and the influence of specific genes on tumor progression. *PTEN* knockout mice have also been combined with *TP53* knockout and Myc-overexpressing mice [200]. Instead of using the ARR_2/Pb promoter mentioned above, an androgen-independent strategy was used to overexpress the *Myc* gene in the Z-Myc mouse [201]. This mouse continuously expresses the *LacZ* gene. The silent *Myc* gene is expressed after Cre-mediated recombination, removing the *LacZ* gene. Pb-Cre4;Z-Myc;$Pten^{fl/+}$;$p53^{fl/fl}$ mice turned out to show a more aggressive prostate cancer than the Pb-Cre4;Z-Myc;$Pten^{fl/fl}$;$p53^{fl/+}$ mice, while in Pb-Cre4;Z-Myc;$Pten^{fl/+}$;$p53^{fl/+}$ mice the WT *PTEN* allele is more often lost than the WT *TP53* allele [200]. Furthermore, prostate-specific loss of both p53 and Rb1 resulted in metastatic adenocarcinoma while only PIN lesions were observed upon deletion of either *TP53* or *RB1* [202].

While both basal and luminal cells can give rise to prostate cancer, the latter seem to be the preferred cells of origin [203]. The important role of the tumor stroma has also been shown by generally deleting the transforming growth factor β (TGFβ) type II receptor (TβRII) in fibroblast cells [204,205]. This resulted in PIN development with progression to adenocarcinoma within seven months.

The ideal prostate cancer model shows a transition from the normal prostate to PIN lesions, followed by localized and invasive adenocarcinoma, progressing to a final castration-resistant, androgen-independent tumor with metastases to the lymph nodes, bones and other organs such as the lungs. Even though such a mouse model would be the ideal representation of human prostate cancer development, the mouse model used in practice strongly depends on the specific research question that needs to be solved. For instance, will tumor initiation or rather metastasis be investigated.

1.3.5 Prostate cancer therapy

Surgical removal of the prostate, prostatectomy, is frequently used to treat prostate cancer. The type of surgery used depends on several factors such as the age and health of the

patient. Besides classical surgery, laparoscopic surgery, also called minimally invasive or keyhole surgery, is an option. This surgery goes hand in hand with some advantages such as a shorter recovery time and a faster recovery of urinary incontinence. Besides incontinence, surgery is often associated with a risk for impotence and narrowing of the urinary tract. Surgery can be followed by radiotherapy to target the remaining cancer cells. In some cases radiotherapy can be applied as the standard treatment. Hormone therapy can also be used in combination with the previously mentioned treatments but is mainly used as palliative treatment. The male hormones, also called androgens, are important for the function and growth of the prostate and are also necessary for the growth of hormone-dependent prostate cancers [206]. Hormone therapy or androgen deprivation therapy arrests the testosterone production, leading to shrinkage of the tumor as far as the tumor has not become hormone-independent or androgen-resistant. Androgen deprivation can be achieved by injection of or by placing implants with luteinizing hormone-releasing hormone (LHRH)-antagonists or -analogs or by intake of anti-androgens. LHRH stimulates LH production, which in turn stimulates testosterone production. Weight gain, dizziness, mood swings and higher blood pressure are a few side effects of hormone therapy. If androgen resistant tumors arise, chemotherapy can be used to slow down tumor growth. Other less used techniques are cryotherapy and HIFU (High Intensity Focused Ultrasounds) treatment. To this end, probes are inserted into the prostate and will kill the tumor cells by freezing or thermal shock, respectively.

Follow-up treatment includes measuring the patient's PSA levels. These can be used to test the effectiveness of the treatment, which should cause a drop in the patient's PSA level.

1.4 References

1. Irish V, Lehmann R, Akam M (1989) The *Drosophila* posterior-group gene nanos functions by repressing hunchback activity. Nature 338 (6217):646-648. doi:10.1038/338646a0
2. Wang C, Lehmann R (1991) Nanos is the localized posterior determinant in *Drosophila*. Cell 66 (4):637-647
3. Kobayashi S, Yamada M, Asaoka M, Kitamura T (1996) Essential role of the posterior morphogen nanos for germline development in *Drosophila*. Nature 380 (6576):708-711. doi:10.1038/380708a0
4. Jaruzelska J, Kotecki M, Kusz K, Spik A, Firpo M, Reijo Pera RA (2003) Conservation of a Pumilio-Nanos complex from *Drosophila* germ plasm to human germ cells. Dev Genes Evol 213 (3):120-126. doi:10.1007/s00427-003-0303-2
5. Haraguchi S, Tsuda M, Kitajima S, Sasaoka Y, Nomura-Kitabayashid A, Kurokawa K, Saga Y (2003) nanos1: a mouse nanos gene expressed in the central nervous system is dispensable for normal development. Mech Dev 120 (6):721-731
6. Tsuda M, Sasaoka Y, Kiso M, Abe K, Haraguchi S, Kobayashi S, Saga Y (2003) Conserved role of nanos proteins in germ cell development. Science 301 (5637):1239-1241. doi:10.1126/science.1085222
7. Strumane K, Bonnomet A, Stove C, Vandenbroucke R, Nawrocki-Raby B, Bruyneel E, Mareel M, Birembaut P, Berx G, van Roy F (2006) E-cadherin regulates human Nanos1, which interacts with p120ctn and induces tumor cell migration and invasion. Cancer Res 66 (20):10007-10015. doi:10.1158/0008-5472.CAN-05-3096
8. Mosquera L, Forristall C, Zhou Y, King ML (1993) A mRNA localized to the vegetal cortex of *Xenopus* oocytes encodes a protein with a nanos-like zinc finger domain. Development 117 (1):377-386
9. Sekizaki H, Takahashi S, Tanegashima K, Onuma Y, Haramoto Y, Asashima M (2004) Tracing of *Xenopus tropicalis* germ plasm and presumptive primordial germ cells with the Xenopus tropicalis DAZ-like gene. Dev Dyn 229 (2):367-372. doi:10.1002/dvdy.10448
10. Koprunner M, Thisse C, Thisse B, Raz E (2001) A zebrafish nanos-related gene is essential for the development of primordial germ cells. Genes Dev 15 (21):2877-2885. doi:10.1101/gad.212401
11. Pilon M, Weisblat DA (1997) A nanos homolog in leech. Development 124 (9):1771-1780
12. Subramaniam K, Seydoux G (1999) nos-1 and nos-2, two genes related to *Drosophila* nanos, regulate primordial germ cell development and survival in *Caenorhabditis elegans*. Development 126 (21):4861-4871

13. Dearden PK (2006) Germ cell development in the Honeybee (*Apis mellifera*); vasa and nanos expression. BMC Dev Biol 6:6. doi:10.1186/1471-213X-6-6

14. Nakao H, Matsumoto T, Oba Y, Niimi T, Yaginuma T (2008) Germ cell specification and early embryonic patterning in *Bombyx mori* as revealed by nanos orthologues. Evol Dev 10 (5):546-554. doi:10.1111/j.1525-142X.2008.00270.x

15. Lall S, Ludwig MZ, Patel NH (2003) Nanos plays a conserved role in axial patterning outside of the Diptera. Curr Biol 13 (3):224-229

16. Calvo E, Walter M, Adelman ZN, Jimenez A, Onal S, Marinotti O, James AA (2005) Nanos (nos) genes of the vector mosquitoes, *Anopheles gambiae*, *Anopheles stephensi* and *Aedes aegypti*. Insect Biochem Mol Biol 35 (7):789-798. doi:10.1016/j.ibmb.2005.02.007

17. Mochizuki K, Sano H, Kobayashi S, Nishimiya-Fujisawa C, Fujisawa T (2000) Expression and evolutionary conservation of nanos-related genes in *Hydra*. Dev Genes Evol 210 (12):591-602

18. Torras R, Yanze N, Schmid V, Gonzalez-Crespo S (2004) nanos expression at the embryonic posterior pole and the medusa phase in the hydrozoan *Podocoryne carnea*. Evol Dev 6 (5):362-371. doi:10.1111/j.1525-142X.2004.04044.x

19. Torras R, Gonzalez-Crespo S (2005) Posterior expression of nanos orthologs during embryonic and larval development of the anthozoan *Nematostella vectensis*. Int J Dev Biol 49 (7):895-899. doi:10.1387/ijdb.051980rt

20. Leininger S, Adamski M, Bergum B, Guder C, Liu J, Laplante M, Brate J, Hoffmann F, Fortunato S, Jordal S, Rapp HT, Adamska M (2014) Developmental gene expression provides clues to relationships between sponge and eumetazoan body plans. Nat Commun 5:3905. doi:10.1038/ncomms4905

21. Julaton VT, Reijo Pera RA (2011) NANOS3 function in human germ cell development. Hum Mol Genet 20 (11):2238-2250. doi:10.1093/hmg/ddr114

22. Grelet S, Andries V, Polette M, Gilles C, Staes K, Martin AP, Kileztky C, Terryn C, Dalstein V, Cheng CW, Shen CY, Birembaut P, Van Roy F, Nawrocki-Raby B (2015) The human NANOS3 gene contributes to lung tumour invasion by inducing epithelial-mesenchymal transition. J Pathol 237 (1):25-37. doi:10.1002/path.4549

23. Bonnomet A, Polette M, Strumane K, Gilles C, Dalstein V, Kileztky C, Berx G, van Roy F, Birembaut P, Nawrocki-Raby B (2008) The E-cadherin-repressed hNanos1 gene induces tumor cell invasion by upregulating MT1-MMP expression. Oncogene 27 (26):3692-3699. doi:10.1038/sj.onc.1211035

24. Bhandari D, Raisch T, Weichenrieder O, Jonas S, Izaurralde E (2014) Structural basis for the Nanos-mediated recruitment of the CCR4-NOT complex and translational repression. Genes Dev 28 (8):888-901. doi:10.1101/gad.237289.113

25. Sonoda J, Wharton RP (1999) Recruitment of Nanos to hunchback mRNA by Pumilio. Genes Dev 13 (20):2704-2712

26. Lai F, Zhou Y, Luo X, Fox J, King ML (2011) Nanos1 functions as a translational repressor in the *Xenopus* germline. Mech Dev 128 (1-2):153-163. doi:10.1016/j.mod.2010.12.001

27. Raisch T, Bhandari D, Sabath K, Helms S, Valkov E, Weichenrieder O, Izaurralde E (2016) Distinct modes of recruitment of the CCR4-NOT complex by *Drosophila* and vertebrate Nanos. EMBO J 35 (9):974-990. doi:10.15252/embj.201593634

28. Edgar RC (2004) MUSCLE: multiple sequence alignment with high accuracy and high throughput. Nucleic Acids Res 32 (5):1792-1797. doi:10.1093/nar/gkh34032/5/1792 [pii]

29. Huelsenbeck JP, Ronquist F (2001) MRBAYES: Bayesian inference of phylogenetic trees. Bioinformatics 17 (8):754-755

30. Letunic I, Bork P (2007) Interactive Tree Of Life (iTOL): an online tool for phylogenetic tree display and annotation. Bioinformatics 23 (1):127-128. doi:btl529 [pii]; 10.1093/bioinformatics/btl529

31. Ginter-Matuszewska B, Spik A, Rembiszewska A, Koyias C, Kupryjanczyk J, Jaruzelska J (2009) The SNARE-associated component SNAPIN binds PUMILIO2 and NANOS1 proteins in human male germ cells. Mol Hum Reprod 15 (3):173-179. doi:10.1093/molehr/gap004

32. Ginter-Matuszewska B, Kusz K, Spik A, Grzeszkowiak D, Rembiszewska A, Kupryjanczyk J, Jaruzelska J (2011) NANOS1 and PUMILIO2 bind microRNA biogenesis factor GEMIN3, within chromatoid body in human germ cells. Histochem Cell Biol 136 (3):279-287. doi:10.1007/s00418-011-0842-y

33. Wickens M, Bernstein D, Crittenden S, Luitjens C, Kimble J (2001) PUF proteins and 3'UTR regulation in the *Caenorhabditis elegans* germ line. Cold Spring Harb Symp Quant Biol 66:337-343

34. Zamore PD, Williamson JR, Lehmann R (1997) The Pumilio protein binds RNA through a conserved domain that defines a new class of RNA-binding proteins. RNA 3 (12):1421-1433

35. Wang X, McLachlan J, Zamore PD, Hall TM (2002) Modular recognition of RNA by a human pumilio-homology domain. Cell 110 (4):501-512

36. Arvola RM, Weidmann CA, Tanaka Hall TM, Goldstrohm AC (2017) Combinatorial control of messenger RNAs by Pumilio, Nanos and brain tumor proteins. RNA Biol:1-12. doi:10.1080/15476286.2017.1306168

37. Gerber AP, Luschnig S, Krasnow MA, Brown PO, Herschlag D (2006) Genome-wide identification of mRNAs associated with the translational regulator PUMILIO in *Drosophila melanogaster*. Proc Natl Acad Sci U S A 103 (12):4487-4492. doi:10.1073/pnas.0509260103

38. Menon KP, Andrews S, Murthy M, Gavis ER, Zinn K (2009) The translational repressors Nanos and Pumilio have divergent effects on presynaptic terminal growth and postsynaptic glutamate receptor subunit composition. J Neurosci 29 (17):5558-5572. doi:10.1523/JNEUROSCI.0520-09.2009

39. Goldstrohm AC, Hook BA, Seay DJ, Wickens M (2006) PUF proteins bind Pop2p to regulate messenger RNAs. Nat Struct Mol Biol 13 (6):533-539. doi:10.1038/nsmb1100

40. Moore FL, Jaruzelska J, Fox MS, Urano J, Firpo MT, Turek PJ, Dorfman DM, Pera RA (2003) Human Pumilio-2 is expressed in embryonic stem cells and germ cells and interacts with DAZ (Deleted in AZoospermia) and DAZ-like proteins. Proc Natl Acad Sci U S A 100 (2):538-543. doi:10.1073/pnas.0234478100

41. Weidmann CA, Qiu C, Arvola RM, Lou TF, Killingsworth J, Campbell ZT, Tanaka Hall TM, Goldstrohm AC (2016) *Drosophila* Nanos acts as a molecular clamp that modulates the RNA-binding and repression activities of Pumilio. Elife 5. doi:10.7554/eLife.17096

42. Murata Y, Wharton RP (1995) Binding of pumilio to maternal hunchback mRNA is required for posterior patterning in *Drosophila* embryos. Cell 80 (5):747-756

43. Miles WO, Tschop K, Herr A, Ji JY, Dyson NJ (2012) Pumilio facilitates miRNA regulation of the E2F3 oncogene. Genes Dev 26 (4):356-368. doi:10.1101/gad.182568.111

44. Weidmann CA, Raynard NA, Blewett NH, Van Etten J, Goldstrohm AC (2014) The RNA binding domain of Pumilio antagonizes poly-adenosine binding protein and accelerates deadenylation. RNA 20 (8):1298-1319. doi:10.1261/rna.046029.114

45. Lolicato F, Marino R, Paronetto MP, Pellegrini M, Dolci S, Geremia R, Grimaldi P (2008) Potential role of Nanos3 in maintaining the undifferentiated spermatogonia population. Dev Biol 313 (2):725-738. doi:10.1016/j.ydbio.2007.11.011

46. Nakahata S, Katsu Y, Mita K, Inoue K, Nagahama Y, Yamashita M (2001) Biochemical identification of *Xenopus* Pumilio as a sequence-specific cyclin B1 mRNA-binding protein that physically interacts with a Nanos homolog, Xcat-2, and a cytoplasmic polyadenylation element-binding protein. J Biol Chem 276 (24):20945-20953. doi:10.1074/jbc.M010528200

47. Weidmann CA, Goldstrohm AC (2012) *Drosophila* Pumilio protein contains multiple autonomous repression domains that regulate mRNAs independently of Nanos and brain tumor. Mol Cell Biol 32 (2):527-540. doi:10.1128/MCB.06052-11

48. Ilardi JM, Mochida S, Sheng ZH (1999) Snapin: a SNARE-associated protein implicated in synaptic transmission. Nat Neurosci 2 (2):119-124. doi:10.1038/5673

49. Falcon-Perez JM, Starcevic M, Gautam R, Dell'Angelica EC (2002) BLOC-1, a novel complex containing the pallidin and muted proteins involved in the biogenesis of melanosomes and platelet-dense granules. J Biol Chem 277 (31):28191-28199. doi:10.1074/jbc.M204011200

50. Pu J, Schindler C, Jia R, Jarnik M, Backlund P, Bonifacino JS (2015) BORC, a multisubunit complex that regulates lysosome positioning. Dev Cell 33 (2):176-188. doi:10.1016/j.devcel.2015.02.011

51. Pan PY, Tian JH, Sheng ZH (2009) Snapin facilitates the synchronization of synaptic vesicle fusion. Neuron 61 (3):412-424. doi:10.1016/j.neuron.2008.12.029

52. Somanath S, Partridge CJ, Marshall C, Rowe T, Turner MD (2016) Snapin mediates insulin secretory granule docking, but not trans-SNARE complex formation. Biochem Biophys Res Commun 473 (2):403-407. doi:10.1016/j.bbrc.2016.02.123

53. Khatamzas E, Hipp MM, Gaughan D, Pichulik T, Leslie A, Fernandes RA, Muraro D, Booth S, Zausmer K, Sun MY, Kessler B, Rowland-Jones S, Cerundolo V, Simmons A (2017) Snapin promotes HIV-1 transmission from dendritic cells by dampening TLR8 signaling. EMBO J 36 (20):2998-3011. doi:10.15252/embj.201695364

54. Zhang B, Gallegos M, Puoti A, Durkin E, Fields S, Kimble J, Wickens MP (1997) A conserved RNA-binding protein that regulates sexual fates in the *C. elegans* hermaphrodite germ line. Nature 390 (6659):477-484. doi:10.1038/37297

55. Lin H, Spradling AC (1997) A novel group of pumilio mutations affects the asymmetric division of germline stem cells in the *Drosophila* ovary. Development 124 (12):2463-2476

56. Forbes A, Lehmann R (1998) Nanos and Pumilio have critical roles in the development and function of *Drosophila* germline stem cells. Development 125 (4):679-690

57. Kraemer B, Crittenden S, Gallegos M, Moulder G, Barstead R, Kimble J, Wickens M (1999) NANOS-3 and FBF proteins physically interact to control the sperm-oocyte switch in *Caenorhabditis elegans*. Curr Biol 9 (18):1009-1018

58. Dubnau J, Chiang AS, Grady L, Barditch J, Gossweiler S, McNeil J, Smith P, Buldoc F, Scott R, Certa U, Broger C, Tully T (2003) The staufen/pumilio pathway is involved in *Drosophila* long-term memory. Curr Biol 13 (4):286-296

59. Quenault T, Lithgow T, Traven A (2011) PUF proteins: repression, activation and mRNA localization. Trends Cell Biol 21 (2):104-112. doi:10.1016/j.tcb.2010.09.013

60. Nakahata S, Kotani T, Mita K, Kawasaki T, Katsu Y, Nagahama Y, Yamashita M (2003) Involvement of *Xenopus* Pumilio in the translational regulation that is specific to cyclin B1 mRNA during oocyte maturation. Mech Dev 120 (8):865-880

61. Van Etten J, Schagat TL, Hrit J, Weidmann CA, Brumbaugh J, Coon JJ, Goldstrohm AC (2012) Human Pumilio proteins recruit multiple deadenylases to efficiently repress messenger RNAs. J Biol Chem 287 (43):36370-36383. doi:10.1074/jbc.M112.373522

62. Cho PF, Gamberi C, Cho-Park YA, Cho-Park IB, Lasko P, Sonenberg N (2006) Cap-dependent translational inhibition establishes two opposing morphogen gradients in *Drosophila* embryos. Curr Biol 16 (20):2035-2041. doi:10.1016/j.cub.2006.08.093

63. Pique M, Lopez JM, Foissac S, Guigo R, Mendez R (2008) A combinatorial code for CPE-mediated translational control. Cell 132 (3):434-448. doi:10.1016/j.cell.2007.12.038

64. Kaye JA, Rose NC, Goldsworthy B, Goga A, L'Etoile ND (2009) A 3'UTR pumilio-binding element directs translational activation in olfactory sensory neurons. Neuron 61 (1):57-70. doi:10.1016/j.neuron.2008.11.012

65. Galgano A, Forrer M, Jaskiewicz L, Kanitz A, Zavolan M, Gerber AP (2008) Comparative analysis of mRNA targets for human PUF-family proteins suggests extensive interaction with the miRNA regulatory system. PLoS One 3 (9):e3164. doi:10.1371/journal.pone.0003164

66. Nolde MJ, Saka N, Reinert KL, Slack FJ (2007) The *Caenorhabditis elegans* pumilio homolog, puf-9, is required for the 3'UTR-mediated repression of the let-7 microRNA target gene, hbl-1. Dev Biol 305 (2):551-563. doi:10.1016/j.ydbio.2007.02.040

67. Kedde M, van Kouwenhove M, Zwart W, Oude Vrielink JA, Elkon R, Agami R (2010) A Pumilio-induced RNA structure switch in p27-3' UTR controls miR-221 and miR-222 accessibility. Nat Cell Biol 12 (10):1014-1020. doi:10.1038/ncb2105

68. Miles WO, Korenjak M, Griffiths LM, Dyer MA, Provero P, Dyson NJ (2014) Post-transcriptional gene expression control by NANOS is up-regulated and functionally important in pRb-deficient cells. EMBO J 33 (19):2201-2215. doi:10.15252/embj.201488057

69. Miles WO, Lembo A, Volorio A, Brachtel E, Tian B, Sgroi D, Provero P, Dyson N (2016) Alternative polyadenylation in triple-negative breast tumors allows NRAS and c-JUN to bypass PUMILIO posttranscriptional regulation. Cancer Res 76 (24):7231-7241. doi:10.1158/0008-5472.CAN-16-0844

70. Fernandez S, Risolino M, Mandia N, Talotta F, Soini Y, Incoronato M, Condorelli G, Banfi S, Verde P (2015) miR-340 inhibits tumor cell proliferation and induces apoptosis by targeting multiple negative regulators of p27 in non-small cell lung cancer. Oncogene 34 (25):3240-3250. doi:10.1038/onc.2014.267

71. Qiu C, McCann KL, Wine RN, Baserga SJ, Hall TM (2014) A divergent Pumilio repeat protein family for pre-rRNA processing and mRNA localization. Proc Natl Acad Sci U S A 111 (52):18554-18559. doi:10.1073/pnas.1407634112

72. Kuo MW, Wang SH, Chang JC, Chang CH, Huang LJ, Lin HH, Yu AL, Li WH, Yu J (2009) A novel puf-A gene predicted from evolutionary analysis is involved in the development of eyes and primordial germ-cells. PLoS One 4 (3):e4980. doi:10.1371/journal.pone.0004980

73. Suzuki A, Igarashi K, Aisaki K, Kanno J, Saga Y (2010) NANOS2 interacts with the CCR4-NOT deadenylation complex and leads to suppression of specific RNAs. Proc Natl Acad Sci U S A 107 (8):3594-3599. doi:10.1073/pnas.0908664107

74. Joly W, Chartier A, Rojas-Rios P, Busseau I, Simonelig M (2013) The CCR4 deadenylase acts with Nanos and Pumilio in the fine-tuning of Mei-P26 expression to promote germline stem cell self-renewal. Stem Cell Reports 1 (5):411-424. doi:10.1016/j.stemcr.2013.09.007

75. Boland A, Chen Y, Raisch T, Jonas S, Kuzuoglu-Ozturk D, Wohlbold L, Weichenrieder O, Izaurralde E (2013) Structure and assembly of the NOT module of the human CCR4-NOT complex. Nat Struct Mol Biol 20 (11):1289-1297. doi:10.1038/nsmb.2681

76. Bhaskar V, Roudko V, Basquin J, Sharma K, Urlaub H, Seraphin B, Conti E (2013) Structure and RNA-binding properties of the Not1-Not2-Not5 module of the yeast Ccr4-Not complex. Nat Struct Mol Biol 20 (11):1281-1288. doi:10.1038/nsmb.2686

77. Bogdan JA, Adams-Burton C, Pedicord DL, Sukovich DA, Benfield PA, Corjay MH, Stoltenborg JK, Dicker IB (1998) Human carbon catabolite repressor protein (CCR4)-associative factor 1: cloning, expression and characterization of its interaction with the B-cell translocation protein BTG1. Biochem J 336 (Pt 2):471-481

78. Morel AP, Sentis S, Bianchin C, Le Romancer M, Jonard L, Rostan MC, Rimokh R, Corbo L (2003) BTG2 antiproliferative protein interacts with the human CCR4 complex existing in vivo in three cell-cycle-regulated forms. J Cell Sci 116 (Pt 14):2929-2936. doi:10.1242/jcs.00480

79. Ezzeddine N, Chang TC, Zhu W, Yamashita A, Chen CY, Zhong Z, Yamashita Y, Zheng D, Shyu AB (2007) Human TOB, an antiproliferative transcription factor, is a poly(A)-binding protein-dependent positive regulator of cytoplasmic mRNA deadenylation. Mol Cell Biol 27 (22):7791-7801. doi:10.1128/MCB.01254-07

80. Meijer HA, Kong YW, Lu WT, Wilczynska A, Spriggs RV, Robinson SW, Godfrey JD, Willis AE, Bushell M (2013) Translational repression and eIF4A2 activity are critical for microRNA-mediated gene regulation. Science 340 (6128):82-85. doi:10.1126/science.1231197

81. Chen Y, Boland A, Kuzuoglu-Ozturk D, Bawankar P, Loh B, Chang CT, Weichenrieder O, Izaurralde E (2014) A DDX6-CNOT1 complex and W-binding pockets in CNOT9 reveal direct links between miRNA target recognition and silencing. Mol Cell 54 (5):737-750. doi:10.1016/j.molcel.2014.03.034

82. Braun JE, Huntzinger E, Fauser M, Izaurralde E (2011) GW182 proteins directly recruit cytoplasmic deadenylase complexes to miRNA targets. Mol Cell 44 (1):120-133. doi:10.1016/j.molcel.2011.09.007

83. Chekulaeva M, Mathys H, Zipprich JT, Attig J, Colic M, Parker R, Filipowicz W (2011) miRNA repression involves GW182-mediated recruitment of CCR4-NOT through conserved W-containing motifs. Nat Struct Mol Biol 18 (11):1218-1226. doi:10.1038/nsmb.2166

84. Collart MA, Panasenko OO (2012) The Ccr4-not complex. Gene 492 (1):42-53. doi:10.1016/j.gene.2011.09.033

85. Shirai YT, Suzuki T, Morita M, Takahashi A, Yamamoto T (2014) Multifunctional roles of the mammalian CCR4-NOT complex in physiological phenomena. Front Genet 5:286. doi:10.3389/fgene.2014.00286

86. Suzuki A, Niimi Y, Saga Y (2014) Interaction of NANOS2 and NANOS3 with different components of the CNOT complex may contribute to the functional differences in mouse male germ cells. Biol Open 3 (12):1207-1216. doi:10.1242/bio.20149308

87. Bawankar P, Loh B, Wohlbold L, Schmidt S, Izaurralde E (2013) NOT10 and C2orf29/NOT11 form a conserved module of the CCR4-NOT complex that docks onto the NOT1 N-terminal domain. RNA Biol 10 (2):228-244. doi:10.4161/rna.23018

88. Petit AP, Wohlbold L, Bawankar P, Huntzinger E, Schmidt S, Izaurralde E, Weichenrieder O (2012) The structural basis for the interaction between the CAF1 nuclease and the NOT1 scaffold of the human CCR4-NOT deadenylase complex. Nucleic Acids Res 40 (21):11058-11072. doi:10.1093/nar/gks883

89. Meister G, Buhler D, Laggerbauer B, Zobawa M, Lottspeich F, Fischer U (2000) Characterization of a nuclear 20S complex containing the survival of motor neurons (SMN) protein and a specific subset of spliceosomal Sm proteins. Hum Mol Genet 9 (13):1977-1986

90. Mourelatos Z, Dostie J, Paushkin S, Sharma A, Charroux B, Abel L, Rappsilber J, Mann M, Dreyfuss G (2002) miRNPs: a novel class of ribonucleoproteins containing numerous microRNAs. Genes Dev 16 (6):720-728. doi:10.1101/gad.974702

91. Nelson PT, Hatzigeorgiou AG, Mourelatos Z (2004) miRNP:mRNA association in polyribosomes in a human neuronal cell line. RNA 10 (3):387-394

92. Lai F, King ML (2013) Repressive translational control in germ cells. Mol Reprod Dev 80 (8):665-676. doi:10.1002/mrd.22161

93. Gavis ER, Lehmann R (1994) Translational regulation of nanos by RNA localization. Nature 369 (6478):315-318. doi:10.1038/369315a0

94. Bergsten SE, Gavis ER (1999) Role for mRNA localization in translational activation but not spatial restriction of nanos RNA. Development 126 (4):659-669

95. Gavis ER, Curtis D, Lehmann R (1996) Identification of cis-acting sequences that control nanos RNA localization. Dev Biol 176 (1):36-50. doi:10.1006/dbio.1996.9996

96. Ephrussi A, Lehmann R (1992) Induction of germ cell formation by oskar. Nature 358 (6385):387-392. doi:10.1038/358387a0

97. Becalska AN, Kim YR, Belletier NG, Lerit DA, Sinsimer KS, Gavis ER (2011) Aubergine is a component of a nanos mRNA localization complex. Dev Biol 349 (1):46-52. doi:10.1016/j.ydbio.2010.10.002

98. Hulskamp M, Schroder C, Pfeifle C, Jackle H, Tautz D (1989) Posterior segmentation of the *Drosophila* embryo in the absence of a maternal posterior organizer gene. Nature 338 (6217):629-632. doi:10.1038/338629a0

99. Wharton RP, Struhl G (1991) RNA regulatory elements mediate control of *Drosophila* body pattern by the posterior morphogen nanos. Cell 67 (5):955-967

100. Wreden C, Verrotti AC, Schisa JA, Lieberfarb ME, Strickland S (1997) Nanos and pumilio establish embryonic polarity in *Drosophila* by promoting posterior deadenylation of hunchback mRNA. Development 124 (15):3015-3023

101. Dalby B, Glover DM (1993) Discrete sequence elements control posterior pole accumulation and translational repression of maternal cyclin B RNA in *Drosophila*. EMBO J 12 (3):1219-1227

102. Asaoka-Taguchi M, Yamada M, Nakamura A, Hanyu K, Kobayashi S (1999) Maternal pumilio acts together with nanos in germline development in *Drosophila* embryos. Nat Cell Biol 1 (7):431-437. doi:10.1038/15666

103. Sato K, Hayashi Y, Ninomiya Y, Shigenobu S, Arita K, Mukai M, Kobayashi S (2007) Maternal Nanos represses hid/skl-dependent apoptosis to maintain the germ line in *Drosophila* embryos. Proc Natl Acad Sci U S A 104 (18):7455-7460. doi:10.1073/pnas.0610052104

104. Muraro NI, Weston AJ, Gerber AP, Luschnig S, Moffat KG, Baines RA (2008) Pumilio binds para mRNA and requires Nanos and Brat to regulate sodium current in *Drosophila* motoneurons. J Neurosci 28 (9):2099-2109. doi:10.1523/JNEUROSCI.5092-07.2008

105. Mee CJ, Pym EC, Moffat KG, Baines RA (2004) Regulation of neuronal excitability through pumilio-dependent control of a sodium channel gene. J Neurosci 24 (40):8695-8703. doi:10.1523/JNEUROSCI.2282-04.2004

106. Loedige I, Stotz M, Qamar S, Kramer K, Hennig J, Schubert T, Loffler P, Langst G, Merkl R, Urlaub H, Meister G (2014) The NHL domain of BRAT is an RNA-binding domain that directly contacts the *hunchback* mRNA for regulation. Genes Dev 28 (7):749-764. doi:10.1101/gad.236513.113

107. Loedige I, Jakob L, Treiber T, Ray D, Stotz M, Treiber N, Hennig J, Cook KB, Morris Q, Hughes TR, Engelmann JC, Krahn MP, Meister G (2015) The Crystal Structure of the NHL Domain in Complex with RNA Reveals the Molecular Basis of *Drosophila* Brain-Tumor-Mediated Gene Regulation. Cell Rep 13 (6):1206-1220. doi:10.1016/j.celrep.2015.09.068

108. Laver JD, Li X, Ray D, Cook KB, Hahn NA, Nabeel-Shah S, Kekis M, Luo H, Marsolais AJ, Fung KYY, Hughes TR, Westwood JT, Sidhu SS, Morris Q, Lipshitz HD, Smibert CA (2015) Brain tumor is a sequence-specific RNA-binding protein that directs maternal mRNA clearance during the *Drosophila* maternal-to-zygotic transition. Genome Biol 16. doi:10.1186/s13059-015-0659-4

109. Illmensee K, Mahowald AP (1974) Transplantation of posterior polar plasm in *Drosophila*. Induction of germ cells at the anterior pole of the egg. Proc Natl Acad Sci U S A 71 (4):1016-1020

110. Kadyrova LY, Habara Y, Lee TH, Wharton RP (2007) Translational control of maternal Cyclin B mRNA by Nanos in the *Drosophila* germline. Development 134 (8):1519-1527. doi:10.1242/dev.002212

111. Hayashi Y, Hayashi M, Kobayashi S (2004) Nanos suppresses somatic cell fate in *Drosophila* germ line. Proc Natl Acad Sci U S A 101 (28):10338-10342. doi:10.1073/pnas.0401647101

112. Ye B, Petritsch C, Clark IE, Gavis ER, Jan LY, Jan YN (2004) Nanos and Pumilio are essential for dendrite morphogenesis in *Drosophila* peripheral neurons. Curr Biol 14 (4):314-321. doi:10.1016/j.cub.2004.01.052

113. Schweers BA, Walters KJ, Stern M (2002) The *Drosophila melanogaster* translational repressor pumilio regulates neuronal excitability. Genetics 161 (3):1177-1185

114. Neumuller RA, Betschinger J, Fischer A, Bushati N, Poernbacher I, Mechtler K, Cohen SM, Knoblich JA (2008) Mei-P26 regulates microRNAs and cell growth in the *Drosophila* ovarian stem cell lineage. Nature 454 (7201):241-245. doi:10.1038/nature07014

115. Feber A, Clark J, Goodwin G, Dodson AR, Smith PH, Fletcher A, Edwards S, Flohr P, Falconer A, Roe T, Kovacs G, Dennis N, Fisher C, Wooster R, Huddart R, Foster CS, Cooper CS (2004) Amplification and overexpression of E2F3 in human bladder cancer. Oncogene 23 (8):1627-1630. doi:10.1038/sj.onc.1207274

116. Foster CS, Falconer A, Dodson AR, Norman AR, Dennis N, Fletcher A, Southgate C, Dowe A, Dearnaley D, Jhavar S, Eeles R, Feber A, Cooper CS (2004) Transcription factor E2F3 overexpressed in prostate cancer independently predicts clinical outcome. Oncogene 23 (35):5871-5879. doi:10.1038/sj.onc.1207800

117. Cooper CS, Nicholson AG, Foster C, Dodson A, Edwards S, Fletcher A, Roe T, Clark J, Joshi A, Norman A, Feber A, Lin D, Gao Y, Shipley J, Cheng SJ (2006) Nuclear overexpression of the E2F3

transcription factor in human lung cancer. Lung Cancer 54 (2):155-162. doi:10.1016/j.lungcan.2006.07.005

118. Bracken AP, Ciro M, Cocito A, Helin K (2004) E2F target genes: unraveling the biology. Trends Biochem Sci 29 (8):409-417. doi:10.1016/j.tibs.2004.06.006
119. Iaquinta PJ, Lees JA (2007) Life and death decisions by the E2F transcription factors. Curr Opin Cell Biol 19 (6):649-657. doi:10.1016/j.ceb.2007.10.006
120. Wang C, Dickinson LK, Lehmann R (1994) Genetics of nanos localization in *Drosophila*. Dev Dyn 199 (2):103-115. doi:10.1002/aja.1001990204
121. Lehmann R, Nusslein-Volhard C (1991) The maternal gene nanos has a central role in posterior pattern formation of the *Drosophila* embryo. Development 112 (3):679-691
122. Verrotti AC, Wharton RP (2000) Nanos interacts with cup in the female germline of *Drosophila*. Development 127 (23):5225-5232
123. Keyes LN, Spradling AC (1997) The *Drosophila* gene fs(2)cup interacts with otu to define a cytoplasmic pathway required for the structure and function of germ-line chromosomes. Development 124 (7):1419-1431
124. Wilhelm JE, Hilton M, Amos Q, Henzel WJ (2003) Cup is an eIF4E binding protein required for both the translational repression of oskar and the recruitment of Barentsz. J Cell Biol 163 (6):1197-1204. doi:10.1083/jcb.200309088
125. Nakamura A, Sato K, Hanyu-Nakamura K (2004) *Drosophila* cup is an eIF4E binding protein that associates with Bruno and regulates oskar mRNA translation in oogenesis. Dev Cell 6 (1):69-78
126. Suzuki A, Tsuda M, Saga Y (2007) Functional redundancy among Nanos proteins and a distinct role of Nanos2 during male germ cell development. Development 134 (1):77-83. doi:10.1242/dev.02697
127. Zhou Z, Shirakawa T, Ohbo K, Sada A, Wu Q, Hasegawa K, Saba R, Saga Y (2015) RNA Binding Protein Nanos2 Organizes Post-transcriptional Buffering System to Retain Primitive State of Mouse Spermatogonial Stem Cells. Dev Cell 34 (1):96-107. doi:10.1016/j.devcel.2015.05.014
128. Liu J, Rivas FV, Wohlschlegel J, Yates JR, 3rd, Parker R, Hannon GJ (2005) A role for the P-body component GW182 in microRNA function. Nat Cell Biol 7 (12):1261-1266. doi:10.1038/ncb1333
129. Macfarlane LA, Murphy PR (2010) MicroRNA: biogenesis, function and role in cancer. Curr Genomics 11 (7):537-561. doi:10.2174/138920210793175895
130. Kusz KM, Tomczyk L, Sajek M, Spik A, Latos-Bielenska A, Jedrzejczak P, Pawelczyk L, Jaruzelska J (2009) The highly conserved NANOS2 protein: testis-specific expression and significance for the human male reproduction. Mol Hum Reprod 15 (3):165-171. doi:10.1093/molehr/gap003

131. Kusz K, Tomczyk L, Spik A, Latos-Bielenska A, Jedrzejczak P, Pawelczyk L, Jaruzelska J (2009) NANOS3 gene mutations in men with isolated sterility phenotype. Mol Reprod Dev 76 (9):804. doi:10.1002/mrd.21070

132. Wu X, Wang B, Dong Z, Zhou S, Liu Z, Shi G, Cao Y, Xu Y (2013) A NANOS3 mutation linked to protein degradation causes premature ovarian insufficiency. Cell Death Dis 4:e825. doi:10.1038/cddis.2013.368

133. Santos MG, Machado AZ, Martins CN, Domenice S, Costa EM, Nishi MY, Ferraz-de-Souza B, Jorge SA, Pereira CA, Soardi FC, de Mello MP, Maciel-Guerra AT, Guerra-Junior G, Mendonca BB (2014) Homozygous inactivating mutation in NANOS3 in two sisters with primary ovarian insufficiency. Biomed Res Int 2014:787465. doi:10.1155/2014/787465

134. Kusz-Zamelczyk K, Sajek M, Spik A, Glazar R, Jedrzejczak P, Latos-Bielenska A, Kotecki M, Pawelczyk L, Jaruzelska J (2013) Mutations of NANOS1, a human homologue of the *Drosophila* morphogen, are associated with a lack of germ cells in testes or severe oligo-astheno-teratozoospermia. J Med Genet 50 (3):187-193. doi:10.1136/jmedgenet-2012-101230

135. Janic A, Mendizabal L, Llamazares S, Rossell D, Gonzalez C (2010) Ectopic expression of germline genes drives malignant brain tumor growth in *Drosophila*. Science 330 (6012):1824-1827. doi:10.1126/science.1195481

136. Krentz AD, Murphy MW, Zhang T, Sarver AL, Jain S, Griswold MD, Bardwell VJ, Zarkower D (2013) Interaction between DMRT1 function and genetic background modulates signaling and pluripotency to control tumor susceptibility in the fetal germ line. Dev Biol 377 (1):67-78. doi:10.1016/j.ydbio.2013.02.014

137. Krentz AD, Murphy MW, Kim S, Cook MS, Capel B, Zhu R, Matin A, Sarver AL, Parker KL, Griswold MD, Looijenga LH, Bardwell VJ, Zarkower D (2009) The DM domain protein DMRT1 is a dose-sensitive regulator of fetal germ cell proliferation and pluripotency. Proc Natl Acad Sci U S A 106 (52):22323-22328. doi:10.1073/pnas.0905431106

138. Grelet S (2014) Implication de Nanos-3 dans l'invasion tumorale broncho-pulmonaire. Dissertation, University of Reims Champagne-Ardenne

139. Di Fiore R, D'Anneo A, Tesoriere G, Vento R (2013) RB1 in cancer: different mechanisms of RB1 inactivation and alterations of pRb pathway in tumorigenesis. J Cell Physiol 228 (8):1676-1687. doi:10.1002/jcp.24329

140. Sadasivam S, DeCaprio JA (2013) The DREAM complex: master coordinator of cell cycle-dependent gene expression. Nat Rev Cancer 13 (8):585-595. doi:10.1038/nrc3556

141. Torre LA, Bray F, Siegel RL, Ferlay J, Lortet-Tieulent J, Jemal A (2015) Global cancer statistics, 2012. CA Cancer J Clin 65 (2):87-108. doi:10.3322/caac.21262

142. Molina JR, Yang P, Cassivi SD, Schild SE, Adjei AA (2008) Non-small cell lung cancer: epidemiology, risk factors, treatment, and survivorship. Mayo Clin Proc 83 (5):584-594. doi:10.4065/83.5.584

143. Branchfield K, Nantie L, Verheyden JM, Sui P, Wienhold MD, Sun X (2016) Pulmonary neuroendocrine cells function as airway sensors to control lung immune response. Science 351 (6274):707-710. doi:10.1126/science.aad7969

144. Clinical Lung Cancer Genome P, Network Genomic M (2013) A genomics-based classification of human lung tumors. Sci Transl Med 5 (209):209ra153. doi:10.1126/scitranslmed.3006802

145. Johnson L, Mercer K, Greenbaum D, Bronson RT, Crowley D, Tuveson DA, Jacks T (2001) Somatic activation of the K-ras oncogene causes early onset lung cancer in mice. Nature 410 (6832):1111-1116. doi:10.1038/35074129

146. Travis WD, Brambilla E, Noguchi M, Nicholson AG, Geisinger K, Yatabe Y, Powell CA, Beer D, Riely G, Garg K, Austin JH, Rusch VW, Hirsch FR, Jett J, Yang PC, Gould M, American Thoracic S (2011) International Association for the Study of Lung Cancer/American Thoracic Society/European Respiratory Society: international multidisciplinary classification of lung adenocarcinoma: executive summary. Proc Am Thorac Soc 8 (5):381-385. doi:10.1513/pats.201107-042ST

147. Travis WD, Brambilla E, Nicholson AG, Yatabe Y, Austin JHM, Beasley MB, Chirieac LR, Dacic S, Duhig E, Flieder DB, Geisinger K, Hirsch FR, Ishikawa Y, Kerr KM, Noguchi M, Pelosi G, Powell CA, Tsao MS, Wistuba I, Panel WHO (2015) The 2015 World Health Organization Classification of Lung Tumors: Impact of Genetic, Clinical and Radiologic Advances Since the 2004 Classification. J Thorac Oncol 10 (9):1243-1260. doi:10.1097/JTO.0000000000000630

148. Chen K, Chen H, Yang F, Sui X, Li X, Wang J (2017) Validation of the eighth edition of the TNM staging system for lung cancer in 2043 surgically treated patients with non-small-cell lung cancer. Clin Lung Cancer. doi:10.1016/j.cllc.2017.04.001

149. Goldstraw P, Chansky K, Crowley J, Rami-Porta R, Asamura H, Eberhardt WE, Nicholson AG, Groome P, Mitchell A, Bolejack V, International Association for the Study of Lung Cancer S, Prognostic Factors Committee AB, Participating I, International Association for the Study of Lung Cancer S, Prognostic Factors Committee Advisory B, Participating I (2016) The IASLC Lung Cancer Staging Project: Proposals for Revision of the TNM Stage Groupings in the Forthcoming (Eighth) Edition of the TNM Classification for Lung Cancer. J Thorac Oncol 11 (1):39-51. doi:10.1016/j.jtho.2015.09.009

150. Shtivelman E, Hensing T, Simon GR, Dennis PA, Otterson GA, Bueno R, Salgia R (2014) Molecular pathways and therapeutic targets in lung cancer. Oncotarget 5 (6):1392-1433. doi:10.18632/oncotarget.1891

151. Lewis PD, Parry JM (2004) In silico p53 mutation hotspots in lung cancer. Carcinogenesis 25 (7):1099-1107. doi:10.1093/carcin/bgh068

152. Slebos RJ, Kibbelaar RE, Dalesio O, Kooistra A, Stam J, Meijer CJ, Wagenaar SS, Vanderschueren RG, van Zandwijk N, Mooi WJ, et al. (1990) K-ras oncogene activation as a prognostic marker in adenocarcinoma of the lung. N Engl J Med 323 (9):561-565. doi:10.1056/NEJM199008303230902

153. de Seranno S, Meuwissen R (2010) Progress and applications of mouse models for human lung cancer. Eur Respir J 35 (2):426-443. doi:10.1183/09031936.00124709

154. Kellar A, Egan C, Morris D (2015) Preclinical Murine Models for Lung Cancer: Clinical Trial Applications. Biomed Res Int 2015:621324. doi:10.1155/2015/621324

155. Meuwissen R, Berns A (2005) Mouse models for human lung cancer. Genes Dev 19 (6):643-664. doi:10.1101/gad.1284505

156. Meuwissen R, Linn SC, Linnoila RI, Zevenhoven J, Mooi WJ, Berns A (2003) Induction of small cell lung cancer by somatic inactivation of both Trp53 and Rb1 in a conditional mouse model. Cancer Cell 4 (3):181-189

157. Politi K, Zakowski MF, Fan PD, Schonfeld EA, Pao W, Varmus HE (2006) Lung adenocarcinomas induced in mice by mutant EGF receptors found in human lung cancers respond to a tyrosine kinase inhibitor or to down-regulation of the receptors. Genes Dev 20 (11):1496-1510. doi:10.1101/gad.1417406

158. Regales L, Balak MN, Gong Y, Politi K, Sawai A, Le C, Koutcher JA, Solit DB, Rosen N, Zakowski MF, Pao W (2007) Development of new mouse lung tumor models expressing EGFR T790M mutants associated with clinical resistance to kinase inhibitors. PLoS One 2 (8):e810. doi:10.1371/journal.pone.0000810

159. Chen YQ, Zhou YQ, Fu LH, Wang D, Wang MH (2002) Multiple pulmonary adenomas in the lung of transgenic mice overexpressing the RON receptor tyrosine kinase. Recepteur d'origine nantais. Carcinogenesis 23 (11):1811-1819

160. Wang MH, Zhang R, Zhou YQ, Yao HP (2013) Pathogenesis of RON receptor tyrosine kinase in cancer cells: activation mechanism, functional crosstalk, and signaling addiction. J Biomed Res 27 (5):345-356. doi:10.7555/JBR.27.20130038

161. Ji H, Ramsey MR, Hayes DN, Fan C, McNamara K, Kozlowski P, Torrice C, Wu MC, Shimamura T, Perera SA, Liang MC, Cai D, Naumov GN, Bao L, Contreras CM, Li D, Chen L, Krishnamurthy J, Koivunen J, Chirieac LR, Padera RF, Bronson RT, Lindeman NI, Christiani DC, Lin X, Shapiro GI, Janne PA, Johnson BE, Meyerson M, Kwiatkowski DJ, Castrillon DH, Bardeesy N, Sharpless NE,

Wong KK (2007) LKB1 modulates lung cancer differentiation and metastasis. Nature 448 (7155):807-810. doi:10.1038/nature06030

162. Mainardi S, Mijimolle N, Francoz S, Vicente-Duenas C, Sanchez-Garcia I, Barbacid M (2014) Identification of cancer initiating cells in K-Ras driven lung adenocarcinoma. Proc Natl Acad Sci U S A 111 (1):255-260. doi:10.1073/pnas.1320383110
163. Sutherland KD, Song JY, Kwon MC, Proost N, Zevenhoven J, Berns A (2014) Multiple cells-of-origin of mutant K-Ras-induced mouse lung adenocarcinoma. Proc Natl Acad Sci U S A 111 (13):4952-4957. doi:10.1073/pnas.1319963111
164. Xu X, Rock JR, Lu Y, Futtner C, Schwab B, Guinney J, Hogan BL, Onaitis MW (2012) Evidence for type II cells as cells of origin of K-Ras-induced distal lung adenocarcinoma. Proc Natl Acad Sci U S A 109 (13):4910-4915. doi:10.1073/pnas.1112499109
165. Kim CF, Jackson EL, Woolfenden AE, Lawrence S, Babar I, Vogel S, Crowley D, Bronson RT, Jacks T (2005) Identification of bronchioalveolar stem cells in normal lung and lung cancer. Cell 121 (6):823-835. doi:10.1016/j.cell.2005.03.032
166. Morgillo F, Della Corte CM, Fasano M, Ciardiello F (2016) Mechanisms of resistance to EGFR-targeted drugs: lung cancer. ESMO Open 1 (3):e000060. doi:10.1136/esmoopen-2016-000060
167. Thomas A, Liu SV, Subramaniam DS, Giaccone G (2015) Refining the treatment of NSCLC according to histological and molecular subtypes. Nat Rev Clin Oncol 12 (9):511-526. doi:10.1038/nrclinonc.2015.90
168. Schumacher TN, Schreiber RD (2015) Neoantigens in cancer immunotherapy. Science 348 (6230):69-74. doi:10.1126/science.aaa4971
169. Alexandrov LB, Nik-Zainal S, Wedge DC, Aparicio SA, Behjati S, Biankin AV, Bignell GR, Bolli N, Borg A, Borresen-Dale AL, Boyault S, Burkhardt B, Butler AP, Caldas C, Davies HR, Desmedt C, Eils R, Eyfjord JE, Foekens JA, Greaves M, Hosoda F, Hutter B, Ilicic T, Imbeaud S, Imielinski M, Jager N, Jones DT, Jones D, Knappskog S, Kool M, Lakhani SR, Lopez-Otin C, Martin S, Munshi NC, Nakamura H, Northcott PA, Pajic M, Papaemmanuil E, Paradiso A, Pearson JV, Puente XS, Raine K, Ramakrishna M, Richardson AL, Richter J, Rosenstiel P, Schlesner M, Schumacher TN, Span PN, Teague JW, Totoki Y, Tutt AN, Valdes-Mas R, van Buuren MM, van 't Veer L, Vincent-Salomon A, Waddell N, Yates LR, Australian Pancreatic Cancer Genome I, Consortium IBC, Consortium IM-S, PedBrain I, Zucman-Rossi J, Futreal PA, McDermott U, Lichter P, Meyerson M, Grimmond SM, Siebert R, Campo E, Shibata T, Pfister SM, Campbell PJ, Stratton MR (2013) Signatures of mutational processes in human cancer. Nature 500 (7463):415-421. doi:10.1038/nature12477

170. Rizvi NA, Hellmann MD, Snyder A, Kvistborg P, Makarov V, Havel JJ, Lee W, Yuan J, Wong P, Ho TS, Miller ML, Rekhtman N, Moreira AL, Ibrahim F, Bruggeman C, Gasmi B, Zappasodi R, Maeda Y, Sander C, Garon EB, Merghoub T, Wolchok JD, Schumacher TN, Chan TA (2015) Cancer immunology. Mutational landscape determines sensitivity to PD-1 blockade in non-small cell lung cancer. Science 348 (6230):124-128. doi:10.1126/science.aaa1348

171. Hellmann M, Rizvi N, Wolchok JD, Chan TA (2016) Genomic profile, smoking, and response to anti-PD-1 therapy in non-small cell lung carcinoma. Mol Cell Oncol 3 (1):e1048929. doi:10.1080/23723556.2015.1048929

172. Center MM, Jemal A, Lortet-Tieulent J, Ward E, Ferlay J, Brawley O, Bray F (2012) International variation in prostate cancer incidence and mortality rates. Eur Urol 61 (6):1079-1092. doi:10.1016/j.eururo.2012.02.054

173. Draisma G, Etzioni R, Tsodikov A, Mariotto A, Wever E, Gulati R, Feuer E, de Koning H (2009) Lead time and overdiagnosis in prostate-specific antigen screening: importance of methods and context. J Natl Cancer Inst 101 (6):374-383. doi:10.1093/jnci/djp001

174. Gulati R, Tsodikov A, Etzioni R, Hunter-Merrill RA, Gore JL, Mariotto AB, Cooperberg MR (2014) Expected population impacts of discontinued prostate-specific antigen screening. Cancer 120 (22):3519-3526. doi:10.1002/cncr.28932

175. De Marzo AM, Platz EA, Sutcliffe S, Xu J, Gronberg H, Drake CG, Nakai Y, Isaacs WB, Nelson WG (2007) Inflammation in prostate carcinogenesis. Nat Rev Cancer 7 (4):256-269. doi:10.1038/nrc2090

176. Toivanen R, Shen MM (2017) Prostate organogenesis: tissue induction, hormonal regulation and cell type specification. Development 144 (8):1382-1398. doi:10.1242/dev.148270

177. Buyyounouski MK, Choyke PL, McKenney JK, Sartor O, Sandler HM, Amin MB, Kattan MW, Lin DW (2017) Prostate cancer - major changes in the American Joint Committee on Cancer eighth edition cancer staging manual. CA Cancer J Clin 67 (3):245-253. doi:10.3322/caac.21391

178. Moch H, Humphrey PA, Ulbright TM, Reuter VE (2016) WHO Classification of Tumours of the Urinary System and Male Genital Organs. Fourth edition. International Agency for Research on Cancer, Lyon. ISBN 928322437X, 9789283224372.400

179. Tomlins SA, Rhodes DR, Perner S, Dhanasekaran SM, Mehra R, Sun XW, Varambally S, Cao X, Tchinda J, Kuefer R, Lee C, Montie JE, Shah RB, Pienta KJ, Rubin MA, Chinnaiyan AM (2005) Recurrent fusion of TMPRSS2 and ETS transcription factor genes in prostate cancer. Science 310 (5748):644-648. doi:10.1126/science.1117679

180. Perner S, Mosquera JM, Demichelis F, Hofer MD, Paris PL, Simko J, Collins C, Bismar TA, Chinnaiyan AM, De Marzo AM, Rubin MA (2007) TMPRSS2-ERG fusion prostate cancer: an early

molecular event associated with invasion. Am J Surg Pathol 31 (6):882-888. doi:10.1097/01.pas.0000213424.38503.aa

181. Ewing CM, Ray AM, Lange EM, Zuhlke KA, Robbins CM, Tembe WD, Wiley KE, Isaacs SD, Johng D, Wang Y, Bizon C, Yan G, Gielzak M, Partin AW, Shanmugam V, Izatt T, Sinari S, Craig DW, Zheng SL, Walsh PC, Montie JE, Xu J, Carpten JD, Isaacs WB, Cooney KA (2012) Germline mutations in HOXB13 and prostate-cancer risk. N Engl J Med 366 (2):141-149. doi:10.1056/NEJMoa1110000
182. Mersch J, Jackson MA, Park M, Nebgen D, Peterson SK, Singletary C, Arun BK, Litton JK (2015) Cancers associated with BRCA1 and BRCA2 mutations other than breast and ovarian. Cancer 121 (2):269-275. doi:10.1002/cncr.29041
183. Castro E, Goh C, Olmos D, Saunders E, Leongamornlert D, Tymrakiewicz M, Mahmud N, Dadaev T, Govindasami K, Guy M, Sawyer E, Wilkinson R, Ardern-Jones A, Ellis S, Frost D, Peock S, Evans DG, Tischkowitz M, Cole T, Davidson R, Eccles D, Brewer C, Douglas F, Porteous ME, Donaldson A, Dorkins H, Izatt L, Cook J, Hodgson S, Kennedy MJ, Side LE, Eason J, Murray A, Antoniou AC, Easton DF, Kote-Jarai Z, Eeles R (2013) Germline BRCA mutations are associated with higher risk of nodal involvement, distant metastasis, and poor survival outcomes in prostate cancer. J Clin Oncol 31 (14):1748-1757. doi:10.1200/JCO.2012.43.1882
184. Taylor BS, Schultz N, Hieronymus H, Gopalan A, Xiao Y, Carver BS, Arora VK, Kaushik P, Cerami E, Reva B, Antipin Y, Mitsiades N, Landers T, Dolgalev I, Major JE, Wilson M, Socci ND, Lash AE, Heguy A, Eastham JA, Scher HI, Reuter VE, Scardino PT, Sander C, Sawyers CL, Gerald WL (2010) Integrative genomic profiling of human prostate cancer. Cancer Cell 18 (1):11-22. doi:10.1016/j.ccr.2010.05.026
185. Rea D, Del Vecchio V, Palma G, Barbieri A, Falco M, Luciano A, De Biase D, Perdona S, Facchini G, Arra C (2016) Mouse Models in Prostate Cancer Translational Research: From Xenograft to PDX. Biomed Res Int 2016:9750795. doi:10.1155/2016/9750795
186. Wu X, Gong S, Roy-Burman P, Lee P, Culig Z (2013) Current mouse and cell models in prostate cancer research. Endocr Relat Cancer 20 (4):R155-170. doi:10.1530/ERC-12-0285
187. Gingrich JR, Barrios RJ, Morton RA, Boyce BF, DeMayo FJ, Finegold MJ, Angelopoulou R, Rosen JM, Greenberg NM (1996) Metastatic prostate cancer in a transgenic mouse. Cancer Res 56 (18):4096-4102
188. Greenberg NM, DeMayo F, Finegold MJ, Medina D, Tilley WD, Aspinall JO, Cunha GR, Donjacour AA, Matusik RJ, Rosen JM (1995) Prostate cancer in a transgenic mouse. Proc Natl Acad Sci U S A 92 (8):3439-3443
189. Chiaverotti T, Couto SS, Donjacour A, Mao JH, Nagase H, Cardiff RD, Cunha GR, Balmain A (2008) Dissociation of epithelial and neuroendocrine carcinoma lineages in the transgenic

adenocarcinoma of mouse prostate model of prostate cancer. Am J Pathol 172 (1):236-246. doi:10.2353/ajpath.2008.070602

190. Kasper S, Sheppard PC, Yan Y, Pettigrew N, Borowsky AD, Prins GS, Dodd JG, Duckworth ML, Matusik RJ (1998) Development, progression, and androgen-dependence of prostate tumors in probasin-large T antigen transgenic mice: a model for prostate cancer. Lab Invest 78 (6):i-xv
191. Ellwood-Yen K, Graeber TG, Wongvipat J, Iruela-Arispe ML, Zhang J, Matusik R, Thomas GV, Sawyers CL (2003) Myc-driven murine prostate cancer shares molecular features with human prostate tumors. Cancer Cell 4 (3):223-238
192. Scherl A, Li JF, Cardiff RD, Schreiber-Agus N (2004) Prostatic intraepithelial neoplasia and intestinal metaplasia in prostates of probasin-RAS transgenic mice. Prostate 59 (4):448-459. doi:10.1002/pros.20020
193. Li Z, Szabolcs M, Terwilliger JD, Efstratiadis A (2006) Prostatic intraepithelial neoplasia and adenocarcinoma in mice expressing a probasin-Neu oncogenic transgene. Carcinogenesis 27 (5):1054-1067. doi:10.1093/carcin/bgi324
194. Tomlins SA, Laxman B, Varambally S, Cao X, Yu J, Helgeson BE, Cao Q, Prensner JR, Rubin MA, Shah RB, Mehra R, Chinnaiyan AM (2008) Role of the TMPRSS2-ERG gene fusion in prostate cancer. Neoplasia 10 (2):177-188
195. Zhu C, Luong R, Zhuo M, Johnson DT, McKenney JK, Cunha GR, Sun Z (2011) Conditional expression of the androgen receptor induces oncogenic transformation of the mouse prostate. J Biol Chem 286 (38):33478-33488. doi:10.1074/jbc.M111.269894
196. Di Cristofano A, Pesce B, Cordon-Cardo C, Pandolfi PP (1998) Pten is essential for embryonic development and tumour suppression. Nat Genet 19 (4):348-355. doi:10.1038/1235
197. Wang S, Gao J, Lei Q, Rozengurt N, Pritchard C, Jiao J, Thomas GV, Li G, Roy-Burman P, Nelson PS, Liu X, Wu H (2003) Prostate-specific deletion of the murine Pten tumor suppressor gene leads to metastatic prostate cancer. Cancer Cell 4 (3):209-221
198. Grabowska MM, DeGraff DJ, Yu X, Jin RJ, Chen Z, Borowsky AD, Matusik RJ (2014) Mouse models of prostate cancer: picking the best model for the question. Cancer Metastasis Rev 33 (2-3):377-397. doi:10.1007/s10555-013-9487-8
199. Ittmann M, Huang J, Radaelli E, Martin P, Signoretti S, Sullivan R, Simons BW, Ward JM, Robinson BD, Chu GC, Loda M, Thomas G, Borowsky A, Cardiff RD (2013) Animal models of human prostate cancer: the consensus report of the New York meeting of the Mouse Models of Human Cancers Consortium Prostate Pathology Committee. Cancer Res 73 (9):2718-2736. doi:10.1158/0008-5472.CAN-12-4213

200. Kim J, Roh M, Doubinskaia I, Algarroba GN, Eltoum IE, Abdulkadir SA (2012) A mouse model of heterogeneous, c-MYC-initiated prostate cancer with loss of Pten and p53. Oncogene 31 (3):322-332. doi:10.1038/onc.2011.236

201. Roh M, Kim J, Song C, Wills M, Abdulkadir SA (2006) Transgenic mice for Cre-inducible overexpression of the oncogenes c-MYC and Pim-1 in multiple tissues. Genesis 44 (10):447-453. doi:10.1002/dvg.20235

202. Zhou Z, Flesken-Nikitin A, Corney DC, Wang W, Goodrich DW, Roy-Burman P, Nikitin AY (2006) Synergy of p53 and Rb deficiency in a conditional mouse model for metastatic prostate cancer. Cancer Res 66 (16):7889-7898. doi:10.1158/0008-5472.CAN-06-0486

203. Wang ZA, Toivanen R, Bergren SK, Chambon P, Shen MM (2014) Luminal cells are favored as the cell of origin for prostate cancer. Cell Rep 8 (5):1339-1346. doi:10.1016/j.celrep.2014.08.002

204. Bhowmick NA, Chytil A, Plieth D, Gorska AE, Dumont N, Shappell S, Washington MK, Neilson EG, Moses HL (2004) TGF-beta signaling in fibroblasts modulates the oncogenic potential of adjacent epithelia. Science 303 (5659):848-851. doi:10.1126/science.1090922

205. Li X, Placencio V, Iturregui JM, Uwamariya C, Sharif-Afshar AR, Koyama T, Hayward SW, Bhowmick NA (2008) Prostate tumor progression is mediated by a paracrine TGF-beta/Wnt3a signaling axis. Oncogene 27 (56):7118-7130. doi:10.1038/onc.2008.293

206. Massie CE, Lynch A, Ramos-Montoya A, Boren J, Stark R, Fazli L, Warren A, Scott H, Madhu B, Sharma N, Bon H, Zecchini V, Smith DM, Denicola GM, Mathews N, Osborne M, Hadfield J, Macarthur S, Adryan B, Lyons SK, Brindle KM, Griffiths J, Gleave ME, Rennie PS, Neal DE, Mills IG (2011) The androgen receptor fuels prostate cancer by regulating central metabolism and biosynthesis. EMBO J 30 (13):2719-2733. doi:10.1038/emboj.2011.158

AIMS AND OBJECTIVES

Lung cancer and prostate cancer are the most diagnosed cancers worldwide and in developed countries, respectively [1]. They also contribute extensively to the amount of cancer deaths worldwide. For lung cancer, this is the case in both men and women. My research laboratory found evidence that Nanos3 might play an important role in the tumor progression of these major human cancers, indicating its relevance for cancer research. Nanos3 is encoded by one of the three mammalian *NANOS* genes, so far mainly investigated in the germ line. Nanos3 expression is mainly brain- and testis-restricted. However, sections of several human cancer tissues including prostate and non-small cell lung cancer (NSCLC) stained positive for Nanos3, suggesting *NANOS3* as a possible, ectopically expressed oncogene [2]. Furthermore, in lung cancer cell lines Nanos3 appears to be involved in epithelial-mesenchymal transition (EMT) [3], an important step during metastasis formation, which is the major cause of cancer deaths.

It is the ultimate goal of this project to verify conclusively whether human Nanos3 is a novel potent promoter of tumor formation or tumor progression *in vivo*, and whether Nanos3 can be considered a novel cancer therapeutic target. My Ph.D. project more specifically aimed at further elucidating the putative oncogenic role of Nanos3 in epithelial cancers, in particular lung and prostate cancers.

First, the expression of Nanos3 was measured in several mouse organs to corroborate the restricted expression pattern observed in humans [4,3]. Additionally, Nanos3 expression was investigated in several human cancer cell lines. Lung cancer cell lines with and without Nanos3 overexpression were further used to gain more insight in the Nanos3-induced changes in protein expression and to identify target mRNAs of Nanos3.

To address the tumorigenic potential of Nanos3, *in vivo* studies were initiated. For this the human *NANOS3* open reading frame was targeted to the Rosa26 locus preceded by a floxed (loxP) transcriptional stop (PGK-neo-3xpA) cassette and followed by an IRES-EGFP reporter sequence as described previously [5]. The human cDNA was chosen because of the reported relevance of ectopic Nanos3 expression in human cancers [3,6]. Furthermore the longest, second transcript of *NANOS3* was chosen as this is the only transcript that has been annotated in the curated human consensus coding sequence set (CCDS) [7]. These mice were

bred to mice from established mouse models for lung and prostate cancer in order to analyze the effects of ectopic Nanos3 expression on tumor progression.

Finally, several experiments were performed in order to identify novel interaction partners of Nanos3 as a way to further elucidate its roles in cancer and normal cells, respectively. Functional characterization of these interactions might reveal new molecular mechanisms in which Nanos3 is involved.

References

1. Torre LA, Bray F, Siegel RL, Ferlay J, Lortet-Tieulent J, Jemal A (2015) Global cancer statistics, 2012. CA Cancer J Clin 65 (2):87-108. doi:10.3322/caac.21262
2. Grelet S (2014) Implication de Nanos-3 dans l'invasion tumorale broncho-pulmonaire. Dissertation, University of Reims Champagne-Ardenne
3. Grelet S, Andries V, Polette M, Gilles C, Staes K, Martin AP, Kileztky C, Terryn C, Dalstein V, Cheng CW, Shen CY, Birembaut P, Van Roy F, Nawrocki-Raby B (2015) The human NANOS3 gene contributes to lung tumour invasion by inducing epithelial-mesenchymal transition. J Pathol 237 (1):25-37. doi:10.1002/path.4549
4. Julaton VT, Reijo Pera RA (2011) NANOS3 function in human germ cell development. Hum Mol Genet 20 (11):2238-2250. doi:10.1093/hmg/ddr114
5. Nyabi O, Naessens M, Haigh K, Gembarska A, Goossens S, Maetens M, De Clercq S, Drogat B, Haenebalcke L, Bartunkova S, De Vos I, De Craene B, Karimi M, Berx G, Nagy A, Hilson P, Marine JC, Haigh JJ (2009) Efficient mouse transgenesis using Gateway-compatible ROSA26 locus targeting vectors and F1 hybrid ES cells. Nucleic Acids Res 37 (7):e55. doi:10.1093/nar/gkp112
6. De Keuckelaere E, Hulpiau P, Saeys Y, Berx G, van Roy F (2018) Nanos genes and their role in development and beyond. Cell Mol Life Sci:e-pub ahead of print 3 February 2018; doi:2010.1007/s00018-00018-02766-00013. doi:10.1007/s00018-018-2766-3
7. Pruitt KD, Harrow J, Harte RA, Wallin C, Diekhans M, Maglott DR, Searle S, Farrell CM, Loveland JE, Ruef BJ, Hart E, Suner MM, Landrum MJ, Aken B, Ayling S, Baertsch R, Fernandez-Banet J, Cherry JL, Curwen V, Dicuccio M, Kellis M, Lee J, Lin MF, Schuster M, Shkeda A, Amid C, Brown G, Dukhanina O, Frankish A, Hart J, Maidak BL, Mudge J, Murphy MR, Murphy T, Rajan J, Rajput B, Riddick LD, Snow C, Steward C, Webb D, Weber JA, Wilming L, Wu W, Birney E, Haussler D, Hubbard T, Ostell J, Durbin R, Lipman D (2009) The consensus coding sequence (CCDS) project:

Identifying a common protein-coding gene set for the human and mouse genomes. Genome Res 19 (7):1316-1323. doi:10.1101/gr.080531.108

RESULTS

Chapter 2

Nanos3 (over)expression

Contributions

Evi De Keuckelaere designed, performed and analyzed experiments (Figure 2.1-2.16). Dr. Vanessa Andries provided overall support in the design of the study, performed experiments (Figure 2.5 and 2.9) and was involved in the analysis of the Nanos3-expressing mice (section 2.2.3). Katrien Staes provided technical assistance concerning Figure 2.2 and 2.4 and for the experiments performed in section 2.2.3. ES cell work and the generation of transgenic mice was performed by the Transgenic Core Facility of the IRC under Dr. Tino Hochepied. Dr. Simon Grelet and Dr. Béatrice Nawrocki-Raby (Reims) provided the HBE4-E6/7, SK-LU-1-GFP and Calu-1-GFP cell lines with and without stable Nanos3 overexpression. Prof. Dr. Marnik Vuylsteke provided statistical support.

2.1 Nanos3 expression

2.1.1 Introduction

Numerous aspects are important in the study of a protein. Where is the protein expressed, in which tissues or cell types, and more specifically in which subcellular location? What is the function of the protein and which molecular partners does it need to fulfill this function? Is this protein conserved in other species and do homologous proteins have a similar function? With respect to Nanos proteins, several of these questions were already addressed in the Introduction section , including a phylogenetic study. Concerning the subcellular localization, this was shown for mammalian Nanos3 to be both nuclear and cytoplasmic [1-3]. More specifically an association with RNP particles such as P-bodies and stress granules has been reported for mouse Nanos2 and Nanos3 proteins [4-6,2]. In the nucleus, human Nanos3 was mainly expressed in the nucleoli [3].

I will study Nanos3 making use of human cancer cell lines and specific mouse models. I have investigated the expression of Nanos3 in several human cancer cell lines and mouse tissues as summarized in this Chapter. Such analysis is important for choosing a strategy to study the function or influence of the protein of interest. Additionally, our exclusive Nanos3-expressing mouse is introduced in this Chapter. This mouse will be further used in combination with murine cancer models.

2.1.2 Mouse Nanos3 expression is mainly testis- and brain-specific

Human *NANOS3* mRNA expression is mainly observed in the brain and the testis of adults [1,3]. To assess the mRNA expression of mouse *Nanos3*, diverse tissues from 12-week old FVB/N mice were analyzed by RT-qPCR. As in humans, *Nanos3* mRNA was found to be mainly expressed in the brain and testis (Figure 2.1). In addition, *Nanos3* mRNA expression was seen in the uterus. The latter is not yet investigated/reported in humans. Protein expression was also tested by immunohistochemistry (IHC), but the Proteintech Nanos3-specific antibody gave a lot of background and specific protein detection could not be detected in the brain, testis or uterus (data not shown). We also tried to make our own Nanos3-specific polyclonal and monoclonal antibodies, however, these antibodies did not outperform the commercial antibody from Proteintech (see addendum 1).

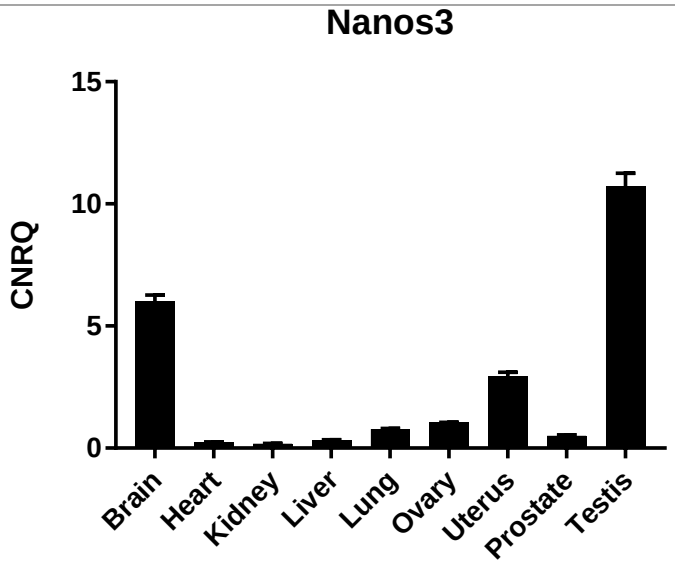

Figure 2.1. *Nanos3* mRNA expression is restricted to the brain, testis and uterus in adult mouse tissues. RT-qPCR analysis of *Nanos3* mRNA levels in mouse (FVB/N) tissue samples. CNRQ**,** calibrated normalized relative quantity; error bars, SEM; n=3.

Similarly, western blot detection of Nanos3, using the Proteintech Nanos3-specific antibody, gave a lot of background when using tissue lysates (data not shown).

Human Nanos1 was found to be expressed in several E-cadherin-negative cancer cell lines [7]. To check whether *NANOS3* is similarly ectopically activated in human cancer, cancer cell lines from the liver, skin, prostate and the ovary were investigated (Table 2.1 and Figure 2.2A). HEK cells transfected with a *NANOS3* cDNA construct were used as a positive control. Since the *NANOS3* mRNA levels of this positive control were very high compared to those in the cell lines, they were omitted from the figures. Then, another cell line with high endogenous *NANOS3* mRNA expression, the neuroblastoma cell line SMS-KAN, was used as a positive control and showed more comparable expression levels. The Hela cell line, which is frequently used in research, was also taken along. Additional investigation of *NANOS1* and *NANOS2* mRNA expression levels in skin and liver cancer cell lines indicated that both Nanos1 and Nanos3 are expressed in several cancer cell lines while Nanos2 expression is observed to a smaller extent (Figure 2.2B). In addition, *CDH1* (E-cadherin) and *VIM* (vimentin) mRNA expression levels were checked in these cancer cell lines. No clear correlation could be found between *CDH1* or *VIM* and *NANOS* mRNA expression levels, whereas E-cadherin and vimentin levels were inversely related in almost all cancer cell lines tested (Figure 2.2C).

Table 2.1. Human cancer cell lines checked for *NANOS* mRNA expression levels.

Tissue	Cell line	Cancer/cell type	Metastatic site
Liver	**HepG2**	hepatocellular carcinoma	
	PLC/PRF/5	hepatoma	
Skin	**Colo16**	skin squamous cell carcinoma	
	HaCat	immortalized keratinocytes	
	A431	epidermoid carcinoma	
	SEB1	sebaceous gland cells*	
	NHEK	normal human epidermal keratinocytes (neonatal)	
Ovary	**AZ224**	ovarian serous adenocarcinoma	
	AZ364	ovarian serous adenocarcinoma	
	OVCAR-3	ovarian adenocarcinoma	
	SK-OV-3	ovarian adenocarcinoma	ascites
Prostate	**PC3**	grade IV, adenocarcinoma	bone
	PNT1A	prostate cells*	
	LNCaP	prostate carcinoma	left supraclavicular lymph node
	BPH1	benign prostate hyperplasia*	
	DU145	prostate carcinoma	brain
	Vcap	prostate carcinoma	vertebra
Nerve	**SMS-KAN**	neuroblastoma	
Cervix	**Hela**	adenocarcinoma	

* Immortalized with SV40.

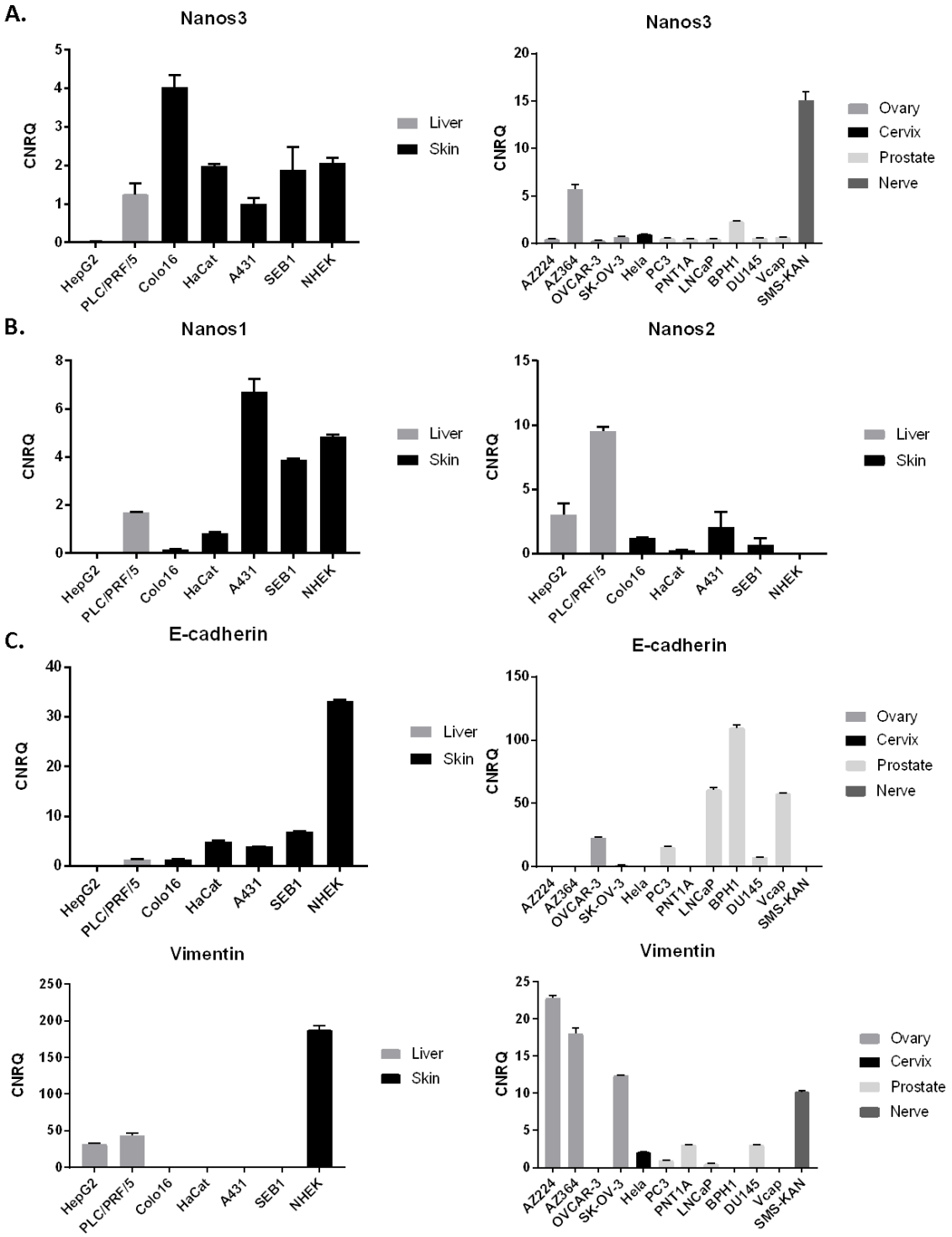

Figure 2.2. *NANOS*, *CDH1* and *VIM* mRNA expression levels in several human cancer cell lines. A. RT-qPCR was used to look at the *NANOS3* mRNA levels in cancer cell lines originating from the liver (HepG2 and PLC/PRF/5), skin (Colo16, HaCat, A432 and SEB1), ovary (AZ224, AZ364, OVCAR-3 and SK-OV-3), cervix (Hela), prostate (PC3, PNT1A, LNCaP, DU145 and Vcap) and nerve (SMS-KAN). **B.** *NANOS1* and *NANOS2* mRNA expression levels in various skin and liver cancer cell lines. **C.** *CDH1* (E-cadherin) and *VIM* (vimentin) mRNA expression levels in several cancer cell lines. CNRQ, calibrated normalized relative quantity; error bars, SEM; n=3.

2.2 Nanos3 overexpression

2.2.1 Introduction

The Cancer Genomics database, cBioPortal (*http://cbioportal.org*), provides a list of cancer-associated gene alterations of human genes [8,9]. This database contains data from both published and unpublished (TCGA, The Cancer Genome Atlas), large-scale cancer genomics studies. A query considering all studies reveals gene amplification as the most common gene alteration for *NANOS3* in diverse cancer types (Figure 2.3). Neuroendocrine prostate cancer (NEPC) has the highest frequency of *NANOS3* gene alterations. This cancer type comes second when considering *NANOS1* and *NANOS2* alterations. NEPC progresses from castration-resistant metastatic prostate adenocarcinoma and is possibly triggered by hormone treatment [10,11]. In general, carcinomas, cancer types with an epithelial origin, seem to be more susceptible to gene alterations for *NANOS3* than non-epithelial cancer types.

Since Nanos3 overexpression or overabundance is observed in several human cancer types we wanted to investigate the influence of ectopic Nanos3 expression. This was done more specifically for lung cancer by comparing lung cancer cell lines with and without ectopic Nanos3 expression. Furthermore, a Nanos3-expressing mouse was generated to analyze *NANOS3* activation *in vivo*, using mouse models for epithelial cancer such as lung cancer and prostate cancer.

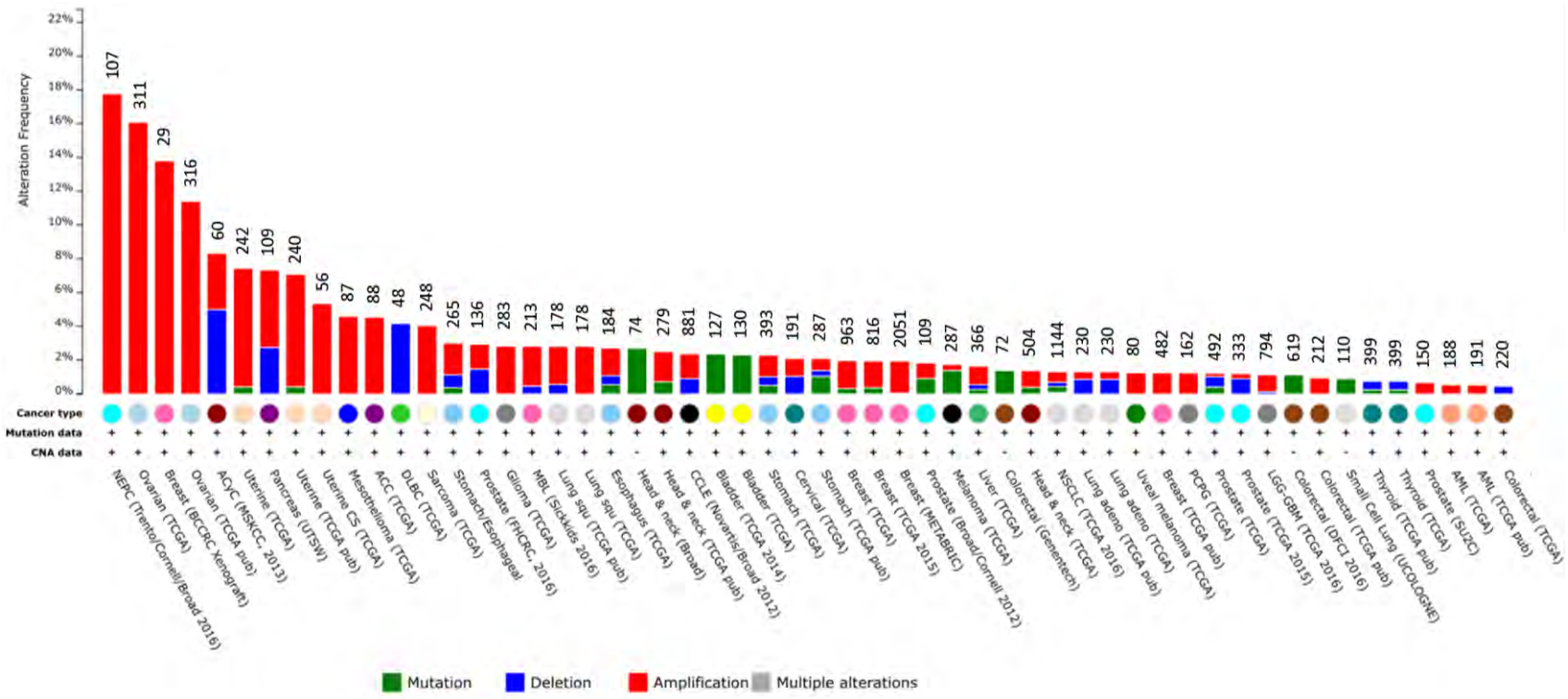

Figure 2.3. *NANOS3* gene alterations across human cancer studies. This graph displays the frequency of observed alternations in the *NANOS3* gene in various human cancer types. The study associated with each bar is mentioned between brackets at the bottom. Each cancer type was given a color code (circles). The color code associated with the bars depicts the type of gene alternation. The number of patients included in each dataset is indicated above the columns. Underneath the graph, it is indicated whether mutation data and/or copy number alteration (CNA) data is available in the dataset summarized by the bars. NEPC: neuroendocrine prostate cancer; AcyC: adenoid cystic *c*arcinoma; ACC: adrenocortical carcinoma; DLBC: diffuse large B-cell lymphoma; MBL: medulloblastoma; Lung squ: lung squamous cell carcinoma; CCLE: cancer cell line encyclopedia; NSCLC: non-small cell lung cancer; PCPG: pheochromocytoma and paraganglioma; LGG-GBM: merged cohort of low-grade glioma and glioblastoma; AML: acute myeloid leukemia. Obtained from cBioPortal, *http://cbioportal.org*, on 10/2017.

2.2.2 mRNA targets of Nanos3 and Nanos3-induced changes in protein expression in human lung cell lines

Although every somatic cell in the human body has generally the same DNA content, not every gene is expressed in all cells. Gene expression is not only cell type-specific but will also depend on the cell state. Gene expression is regulated at multiple levels to ensure coordinated synthesis of the cells' macromolecular components. Besides transcriptional regulation also post-transcriptional control has a substantial impact on gene expression, with widespread physiological implications. This regulation is mediated by hundreds of RBPs, which can bind certain sequences in mRNAs, thereby regulating the localization, translation or stability of mRNAs [12,13]. Finding the specific mRNA targets of an RBP is important to attribute a role or function to this protein. Many RBPs bind specific sequences in their mRNA targets. However, the secondary structure of the RNA sequence is also of importance since it determines the accessibility for the RBP [14]. To identify possible mRNA targets of Nanos3, a proteome analysis of different lung cell lines, HBE4-E6/7, Calu-1-GFP and SK-LU-1-GFP, with or without the expression of a Nanos3 construct (pdest 12.2 Nanos3cl1), was done (Table 2.2). The control cell lines were transfected with a backbone vector (pdest 12.2). These lung cell lines were chosen since overexpression of Nanos3 was associated with a clear-cut EMT in these cells [3]. This occurred at least partly by downregulating E-cadherin and by stimulating vimentin expression. The current analysis might identify other proteins involved in the migratory and invasive features of these lung cell lines upon Nanos3 expression.

Table 2.2. Lung cell lines used in the proteome analysis. The cell lines were kindly provided by the lab of Dr. Nawrocki-Raby (INSERM, UMR-S 903, University of Reims Champagne-Ardenne).

Cell line	Cancer/cell type	Comment
SK-LU-1-GFP-pdest 12.2 SK-LU-1-GFP-pdest 12.2 Nanos3	adenocarcinoma	
Calu-1-GFP-pdest 12.2 Calu-1-GFP-pdest 12.2 Nanos3	squamous cell carcinoma	derived from metastatic site: pleura
HBE4-E6/E7-pdest 12.2 HBE4-E6/E7-pdest 12.2 Nanos3	bronchial cells	HPV-16 E6/E7 transformed

HBE: Human bronchial epithelium; HPV-16: Human papilloma virus 16

Our compositional proteomic analysis was performed in collaboration with Prof. Dr. Kris Gevaert of the VIB Department of Medical Protein Research, Proteome Analysis and Bioinformatics Unit (see Materials and methods section 2.4). Our proteomic analysis

identified 26 proteins being significantly downregulated and 25 being significantly upregulated, in at least two lung cancer cell lines, upon stable Nanos3 overexpression (Supplementary data; Figure S2.1 and Table S2.1-2.2). When only considering proteins represented by more than one unique peptide, 14 and 2 proteins were significantly downregulated and upregulated, respectively (Figure 2.4). This is in accordance with the primary role of Nanos3 in translation inhibition. mRNAs corresponding to proteins downregulated upon Nanos3 overexpression are likely to be direct targets for Nanos3 repression. The presence of the binding sites of the Nanos/Pumilio complex, NREs and PBEs, in the 3'UTR of candidate mRNA targets can be used to identify such new mRNA targets. The mRNA transcripts of 8/14 downregulated and 2/2 upregulated proteins showed a NRE (5'-GUUGU-3') and/or PBE (5'-UGUANRUA-3', with 'N' standing for any nucleotide and 'R' standing for an A or G) in their 3'UTR. Six mRNAs encoding proteins significantly downregulated upon Nanos3 overexpression had both binding sites. In three of these transcripts the last part of the NRE and the first part of the PBE overlapped. Nanos proteins are able to regulate translation by stimulating deadenylation of the poly(A) tail [15,16], or by protecting this tail [3], thus promoting translation in the latter case. Nanos3 expression was previously reported to have a positive influence on vimentin expression in the same three lung cell lines [3]. The latter could not be confirmed in our proteome analysis, as increased expression of vimentin after Nanos3 overexpression could only be validated in the Calu-1 lung cancer cell line (Table 2.3). However, given the fact that vimentin was only represented by one unique peptide in this analysis, this finding is not reliable. In the other two cell lines, only a marginal and therefore insignificant downregulation was observed (Table 2.3). A protein is found to be significantly up/down-regulated if the absolute z-score (see Table 2.3) is higher than 1.96 and is thus outside the 95% confidence interval.

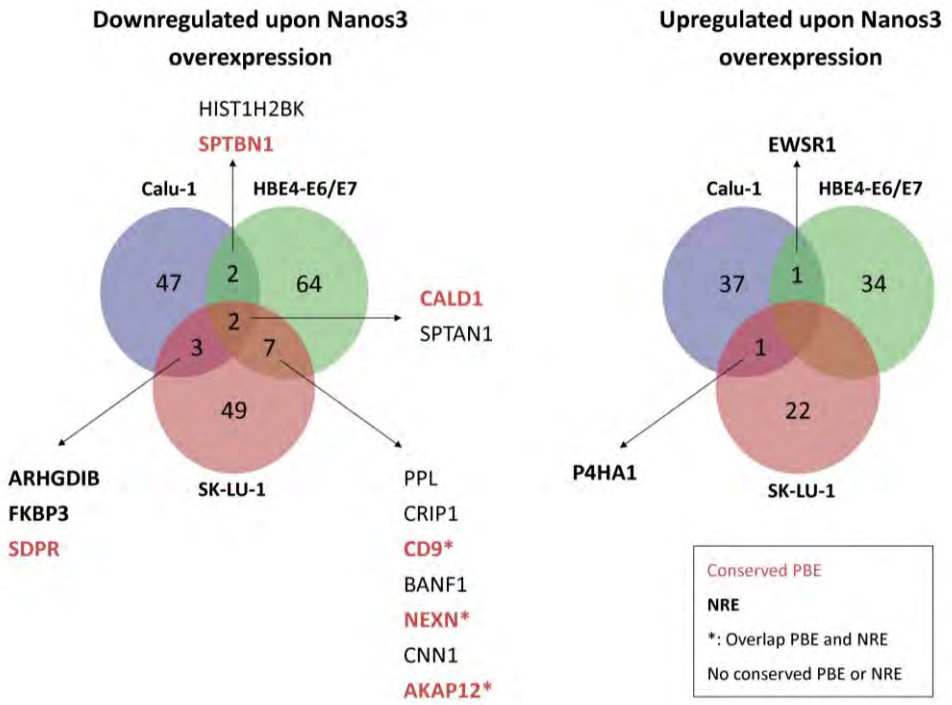

Figure 2.4. Proteins significantly down- or upregulated upon Nanos3 overexpression in lung cell lines. The gene names of the proteins that were significantly down- or upregulated in at least two lung cell lines are given. The proteins that were only represented by one unique peptide were excluded from the figure. The 3'UTR of the corresponding mRNAs was checked for the presence of a Pumilio-binding element (PBE, 5'-UGUANRUA-3') and a Nanos responsive element (NRE, 5'-GUUGU-3'). N can be any nucleotide (A, U, G, C) while R can be A or G. The mRNA transcripts corresponding to the gene names written in bold have an NRE sequence in their 3'UTR.

Table 2.3. Regulation of vimentin protein levels upon Nanos3 overexpression.

Cell line	Protein median (log_2 L/H)	Standard deviation	z-score	up/down with Nanos3	significant up/down	sequence count
HBE4-E6/E7	0,28	0,19	0,33	down	no	9
CALU-1-GFP	-3,17	0,00	-13,50	up	significant	1
SK-LU-1-GFP	-1,73	0,31	0,24	down	no	10

The z-score is calculated as follows: z-score = ((log_2 L/H) - median)/ standard deviation, where log_2 L/H is the median ratio of the peptide log_2 L/H ratios with L and H standing for the protein levels of the protein labeled with the light and heavy isotope, respectively. The median and standard deviation used to calculate the z-score are those of the protein ratio levels for each cell line.

Then the corresponding mRNA expression levels for the proteins found to be significantly regulated upon Nanos3 overexpression (from Figure 2.4 and few from Figure S2.1), were

analyzed in the same cell lines. This was done to check if the regulation of these potential Nanos3 targets is likely to be at the transcriptional or post-transcriptional level, while serving as a confirmation in case of transcriptional regulation. To this end, RNA from three biological replicates from the lung cell lines with and without Nanos3 overexpression were subjected to RT-qPCR analysis (Figures 2.5 and 2.6). Besides the RNA expression levels of the proteins detected in the proteome analysis, those of a few EMT-related genes and *NANOS* and *PUM* genes were additionally checked. In general, the RNA levels corresponding to proteins up- or downregulated upon ectopic Nanos3 expression were similarly up- or downregulated (Figure 2.6). However, the observed changes were rarely significant and differed from cell line to cell line. Whenever significant differences were seen, these were in line with the expectations on the basis of the proteome analysis. So, mRNA levels were up- or downregulated when the encoded protein was found to be, respectively, up- or downregulated (Figure 2.5A-B). E-cadherin, Slug, uPA, vimentin, occludin and MMP-14 were previously shown to be regulated by Nanos3 in these lung cancer cell lines [3]. For vimentin, occludin and MMP-14, Nanos3 regulation was post-transcriptional while transcriptional regulation was reported for uPA, slug and E-cadherin. Hence, we expected an increase in *PLAU* and *SLUG* RNA levels and a decrease in *CDH1* RNA levels and no changes in the *MMP-14*, *OCLN* and *VIM* RNA levels. This is, however, not exactly what we observed in our RT-qPCR experiment (Figure 2.5C). E-cadherin expression seemed to be significantly downregulated only in the Calu-1 cell line upon ectopic Nanos3 expression. E-cadherin levels were, however, very low in both the Calu-1 and the SK-LU-1 cell line with and without Nanos3 overexpression (Figure 2.7). No difference was seen in *SLUG* mRNA expression but overexpression of Nanos3 significantly increased *PLAU* mRNA expression levels in the lung cancer cell lines, Calu-1 and SK-LU-1 (Figure 2.5C). As expected, almost no differences were observed in the *VIM*, *OCLN* and *MMP-14* mRNA levels. Vimentin seems to be significantly upregulated in HBE4-E6/E7-Nanos3, but unlike for the Calu-1 and SK-LU-1 cell lines, the protein levels of vimentin were very low in HBE4-E6/E7 (Figure 2.7). *OCLN* mRNA was only significantly upregulated in the SK-LU-1-Nanos3 cell line. Finally the expression levels of the *PUM* genes and *NANOS1* and *NANOS3* genes were analyzed (Figure 2.5D). *NANOS1* RNA expression levels were not correlated with Nanos3 expression. Upon Nanos3 overexpression, *NANOS1* mRNA levels were found to be down- or upregulated in, respectively, Calu-1 cells and SK-LU-1 cells (Figure

2.5D). Nanos1 was not expressed in the HBE4-E6/E7 cell line. *NANOS3* mRNA levels were significantly upregulated in all the Nanos3 transfected cell lines confirming the correct set-up of the experiment. Nanos3 overexpression was also confirmed via western blot (Figure 2.7). In general, these results suggest that Nanos3 does not directly regulate transcription of the mRNAs that encode the proteins identified in the proteome analysis.

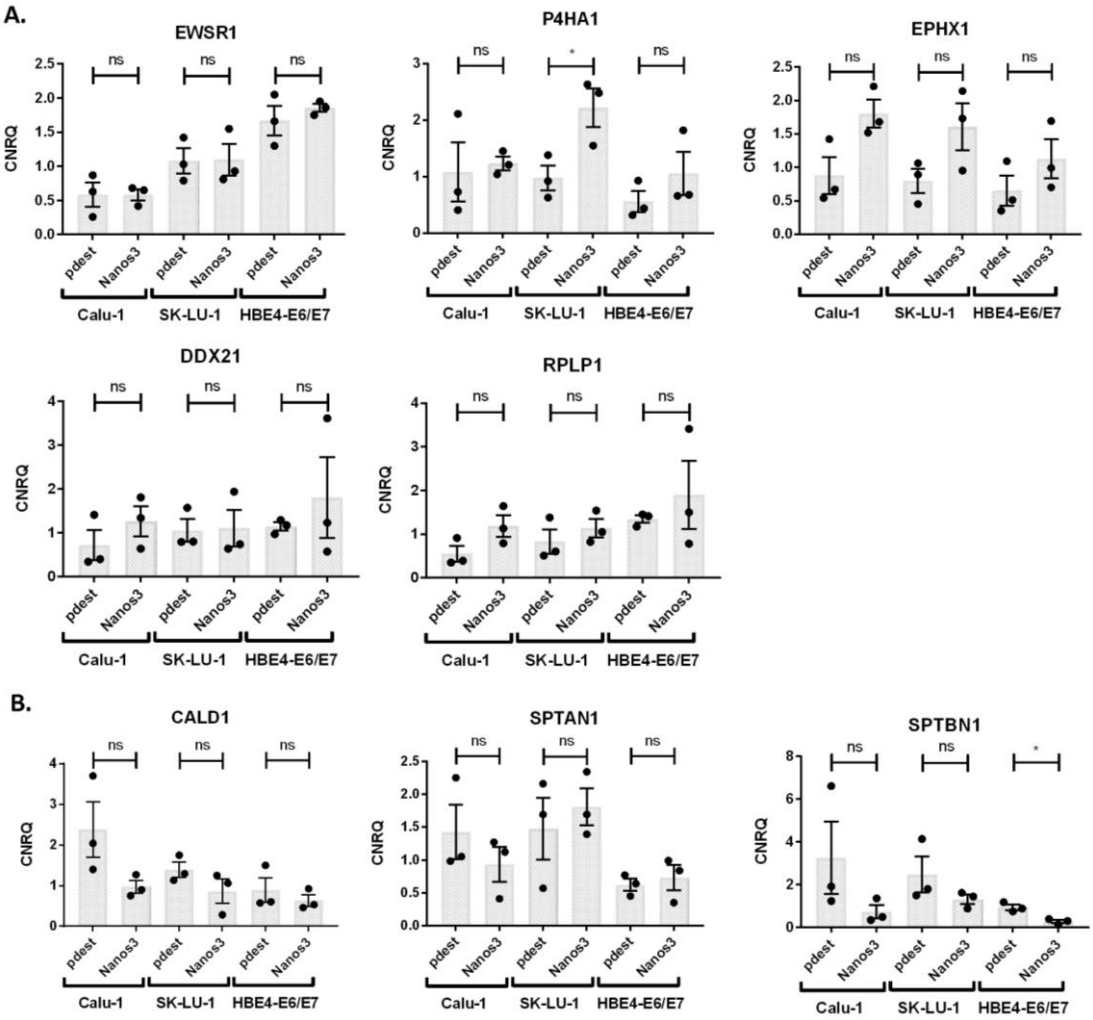

Figure 2.5. The influence of Nanos3 overexpression on expression levels of several mRNAs. mRNA expression levels corresponding to proteins found to be upregulated **(A)** or downregulated **(B)** in our proteome analysis (Figure 2.4) were analyzed with RT-qPCR. For each cell line, with and without Nanos3 overexpression, biological triplicates were made. For each of these, additional technical triplicates were made. CNRQ**,** calibrated normalized relative quantity; error bars, SEM; n=3.

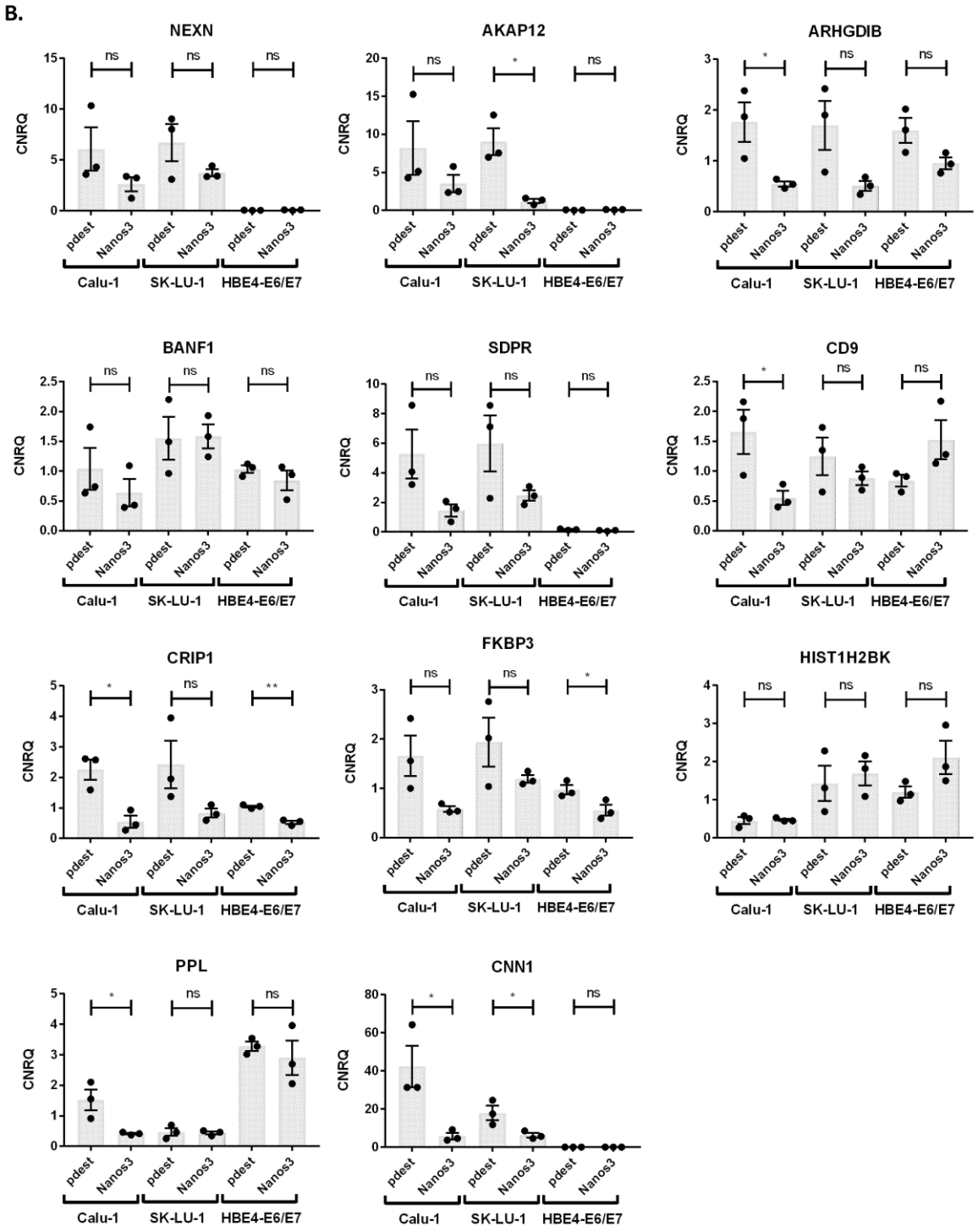

Figure 2.5. The influence of Nanos3 overexpression on expression levels of several mRNAs. (Continued)

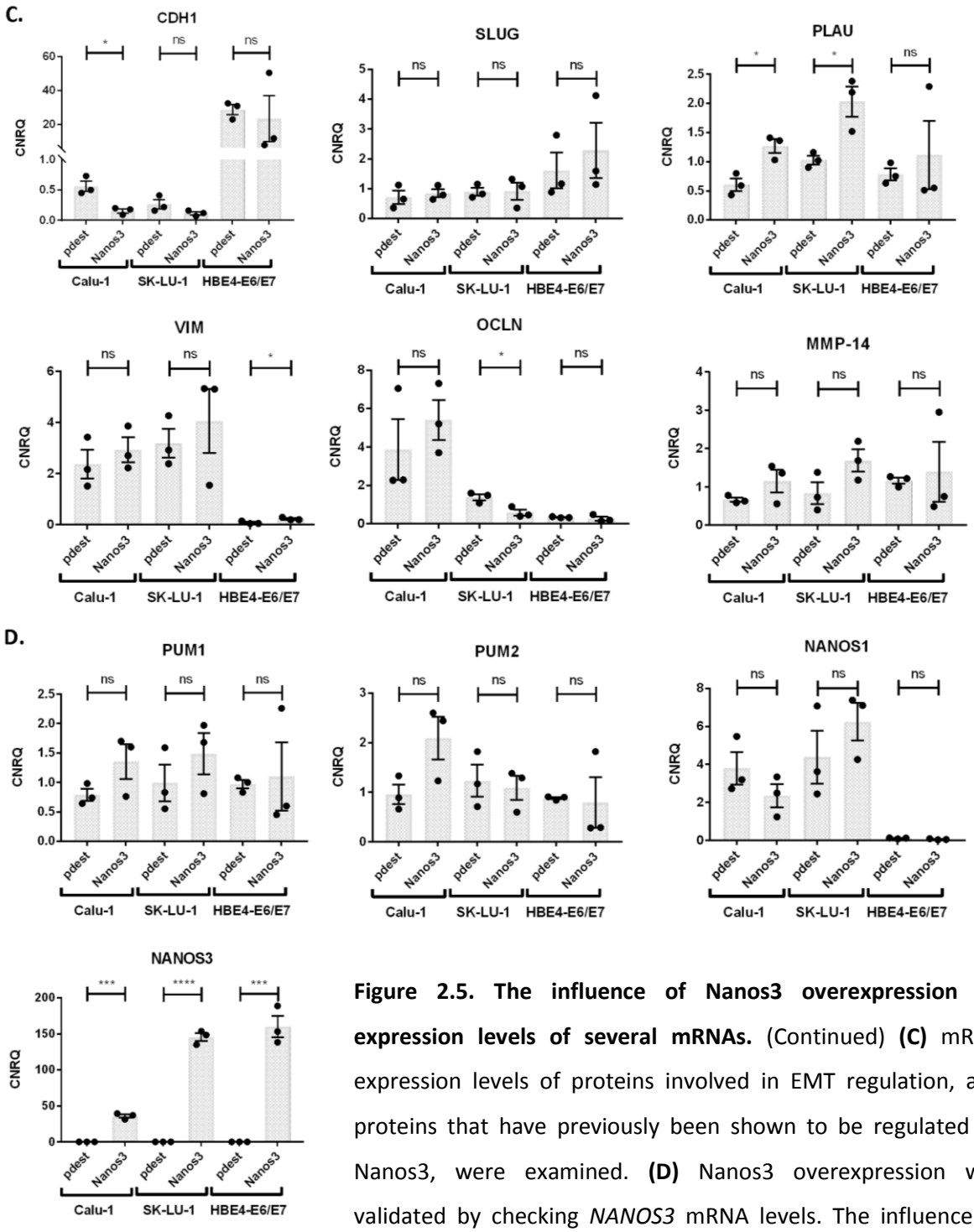

Figure 2.5. The influence of Nanos3 overexpression on expression levels of several mRNAs. (Continued) **(C)** mRNA expression levels of proteins involved in EMT regulation, and proteins that have previously been shown to be regulated by Nanos3, were examined. **(D)** Nanos3 overexpression was validated by checking *NANOS3* mRNA levels. The influence of Nanos3 on the expression of the human *PUM* genes and *NANOS1* was also investigated. Ns: not significant, *: P≤0.05, **: P≤0.01, ***: P≤0.001 and ****: P≤0.0001.

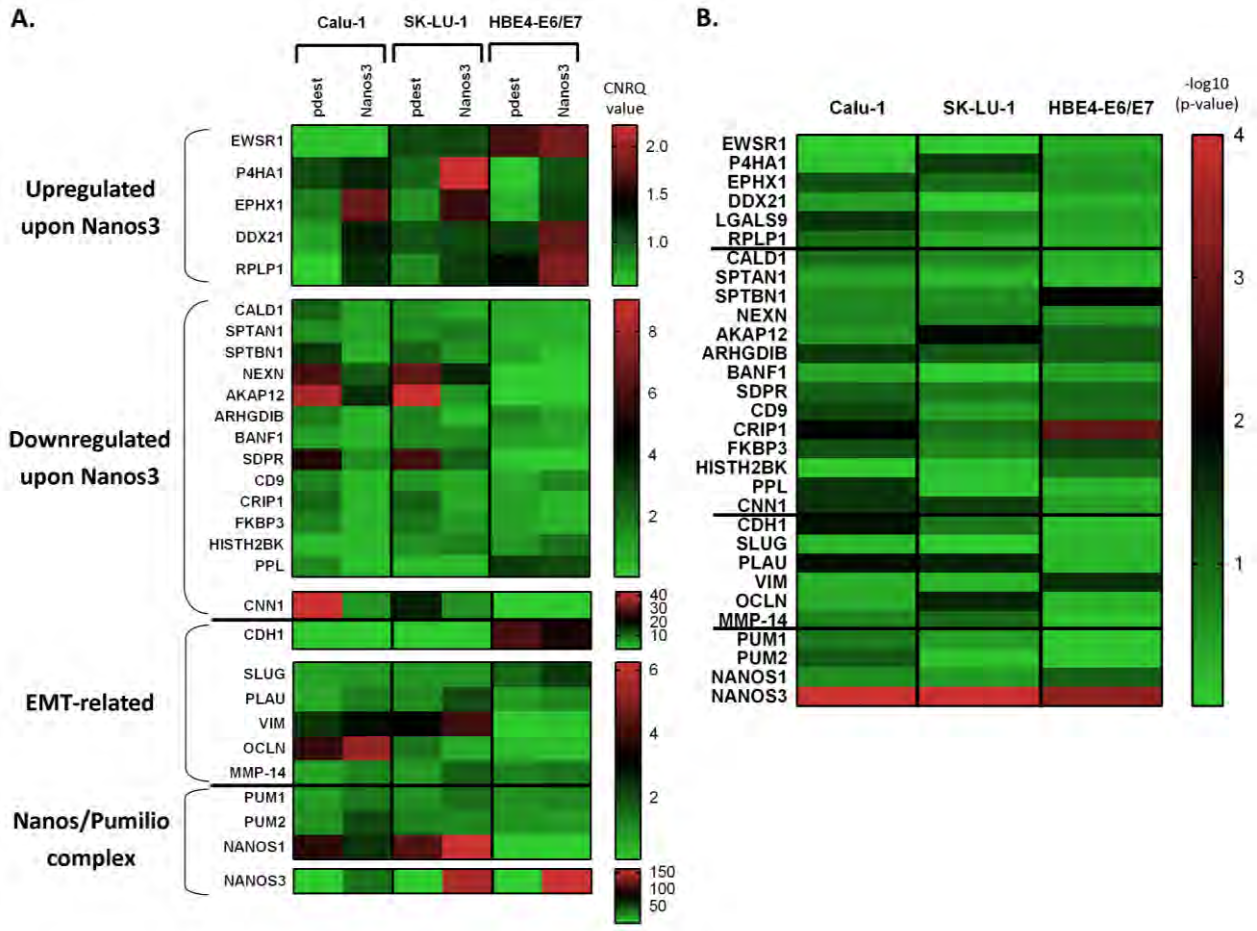

Figure 2.6. Gene expression profiles of lung cells stably transfected with either pdest 12.2 backbone plasmids or pdest 12.2 Nanos3cl1 plasmids. Transcription of genes of which the corresponding proteins were found to be down- or upregulated upon Nanos3 overexpression, EMT-related genes and Nanos/Pumilio genes were analyzed with RT-qPCR. **A.** The CNRQ values are displayed, ranging from light green to red, corresponding to low and high CNRQ values, respectively. **B.** The -log10(p-values) are visualized in a second heat map.

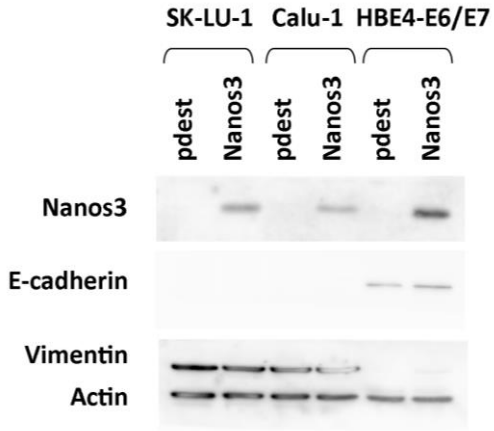

Figure 2.7. Nanos3 overexpression in three lung cell lines. Western blot was used to confirm Nanos3 overexpression and to check for E-cadherin and vimentin expression in both control and Nanos3-expressing cell lines. Actin was used as a loading control.

RNA immunoprecipitations (RIPs) were executed to discover which of the proteins in the proteome analysis are post-transcriptionally regulated by Nanos3 (Figure 2.8). For these experiments only the lung cancer cell lines SK-LU-1-Nanos3 and Calu-1-Nanos3 were analyzed. Vimentin was taken along as a positive control. RIP with a control rabbit IgG or with a Nanos3-specific antibody was followed by an RT-qPCR analysis for the genes corresponding to candidate Nanos3 targets as suggested by the proteome analysis (Figure 2.9). Besides our positive control vimentin, *PPL* mRNA, encoding periplakin, and especially *SPTAN1* mRNA, encoding spectrin alpha, non-erythrocytic 1, also called alpha-fodrin, arose as possible Nanos3 targets. Western blot was done on part of the bead suspension after RIP to test the efficiency of immunoprecipitation. Nanos3 was indeed found in the samples immunoprecipitated with the Nanos3-specific antibody and was missing in those immunoprecipitated with the control rabbit IgG antibody (Figure 2.10).

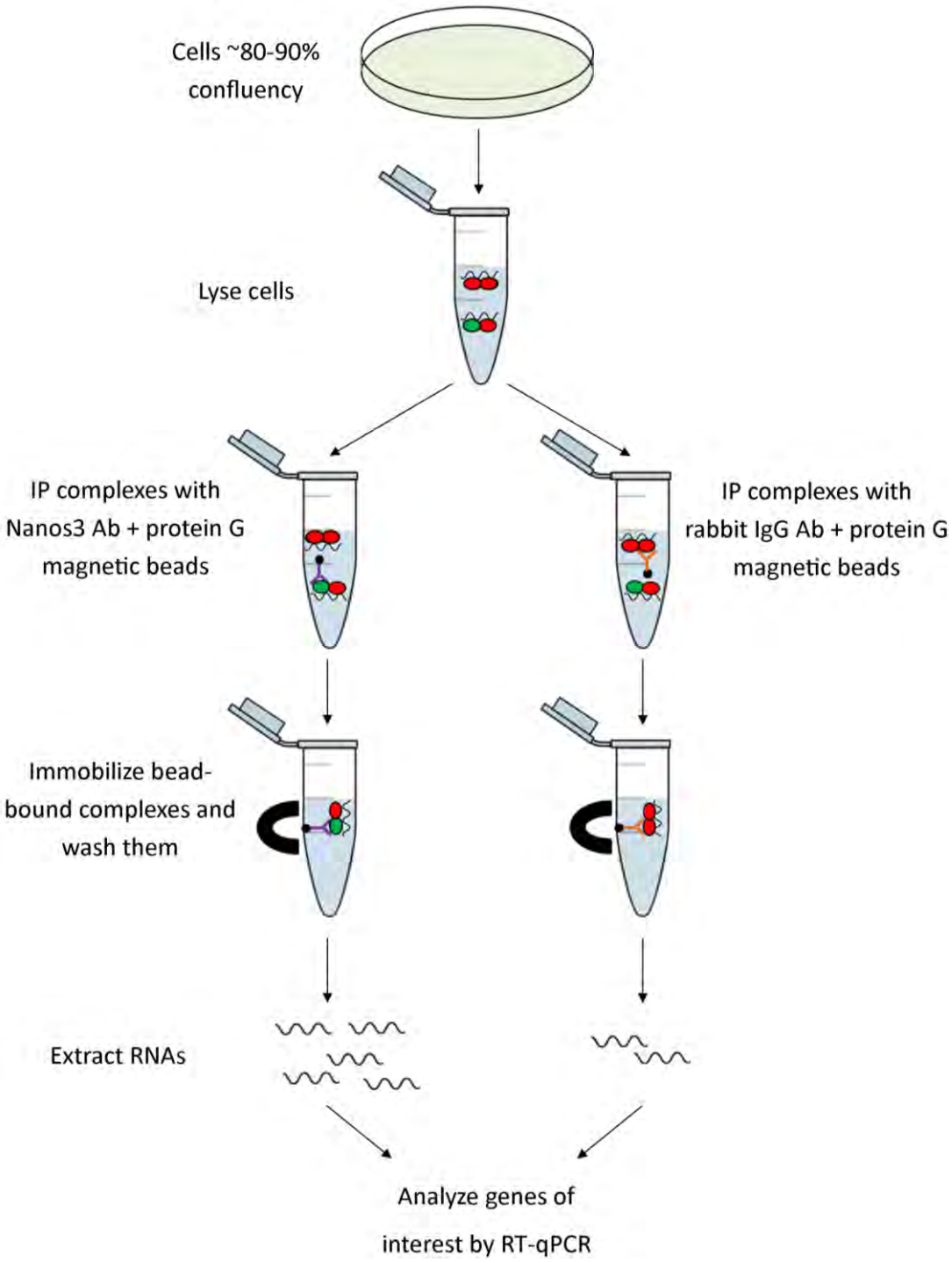

Figure 2.8. Schematic representation of the RNA immunoprecipitation (RIP) protocol. RNase inhibitors were added to the RIP lysis and immunoprecipitation (IP) buffers. Ab, antibody.

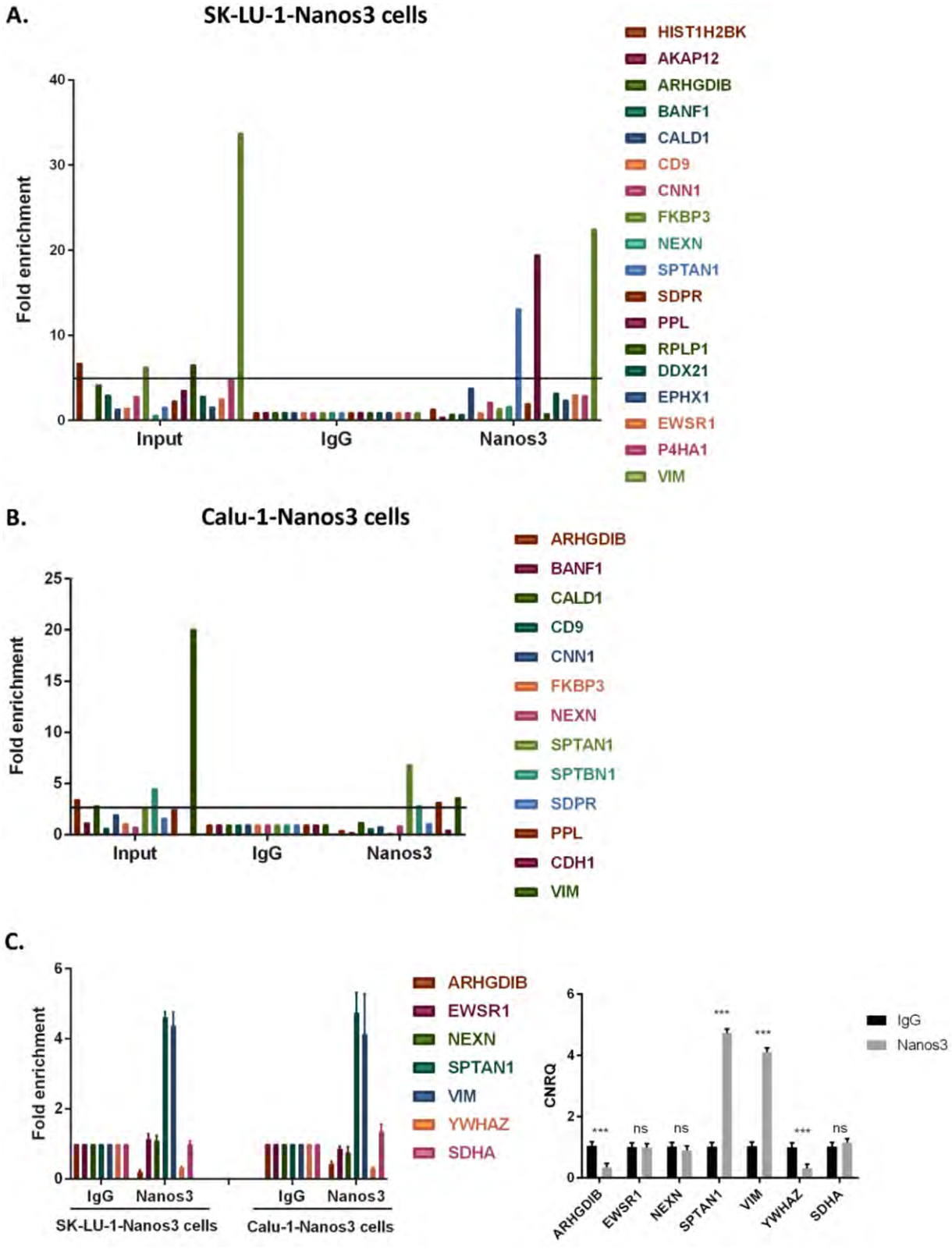

Figure 2.9. *SPTAN1* and *PPL* mRNAs are promising new Nanos3 targets. Figure legend on the next page.

Figure 2.9. *SPTAN1* and *PPL* mRNAs are promising new Nanos3 targets. RNA immunoprecipitation (RIP) of SK-LU-1-GFP-Nanos3 cells **(A)** and Calu-1-GFP-Nanos3 cells **(B)** with a control IgG or Nanos3-specific antibody. RNA expression levels of selected genes were checked with RT-qPCR and normalization was done with qbase+ (Biogazelle) using the global mean. **C.** RIP analysis of lung cancer cells with Nanos3 overexpression to confirm binding of Nanos3 to *SPTAN1* mRNA. RT-qPCR values were normalized with qbase+ using the global mean. YWHAZ and SDHA are irrelevant reference targets. The right graph represents the outcome of the two-way ANOVA assessing the Nanos3 effect on all the target genes at once across both cell lines. Error bars represent the SEM (n=3); ns: not significant; ***: P≤0.001.

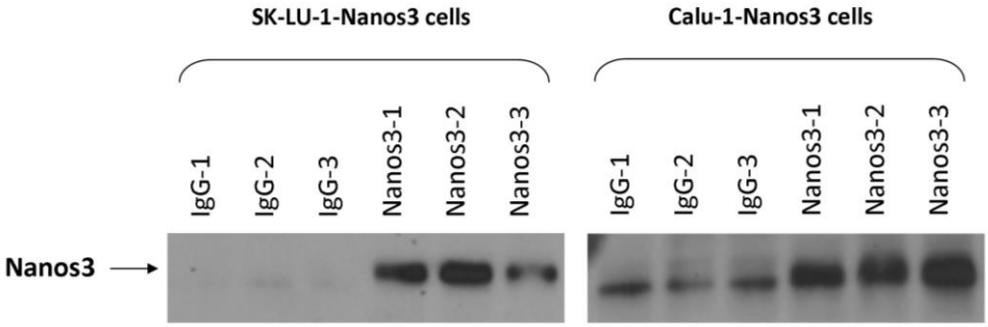

Figure 2.10. Western blotting to test the efficiency of Nanos3 immunoprecipitation in the RIP experiment. Biological triplicates of the SK-LU-1-Nanos3 and the Calu-1-Nanos3 cells were analyzed by RIP with the control rabbit IgG and the Nanos3-specific antibody. Nanos3 expression was checked in the RIP lysates after immunoprecipitation.

To check if Nanos3 overexpression downregulates *SPTAN1* mRNA, a reporter plasmid was made with the 3'UTR of *SPTAN1* recombined with the 3'UTR of the firefly luciferase gene (pGL3-SPTAN1). This reporter construct was transfected into HEK293T cells along with an increasing concentration of the pdest 12.2 Nanos3 plasmid. Untransfected HEK293T cells and cells transfected with a pdest 12.2 backbone vector were used as negative controls. Increasing luciferase activity could be seen upon overexpression of Nanos3, rather indicating upregulation of spectrin alpha-1 by Nanos3 instead of downregulation (Figure 2.11A). To test the influence of the pdest 12.2 and pGL3 plasmid transfection on this assay, HEK293T cells were transfected with an equal amount of either the pdest 12.2 or the pdest 12.2 Nanos3 plasmid along with two different concentrations of pGL3-control or pGL3-SPTAN1 (Figure 2.11B). These results suggest that the upregulation is specific for the pGL3-SPTAN1 plasmid.

The concentration used for the pGL3-SPTAN1 plasmid strongly influenced the observed luciferase signal.

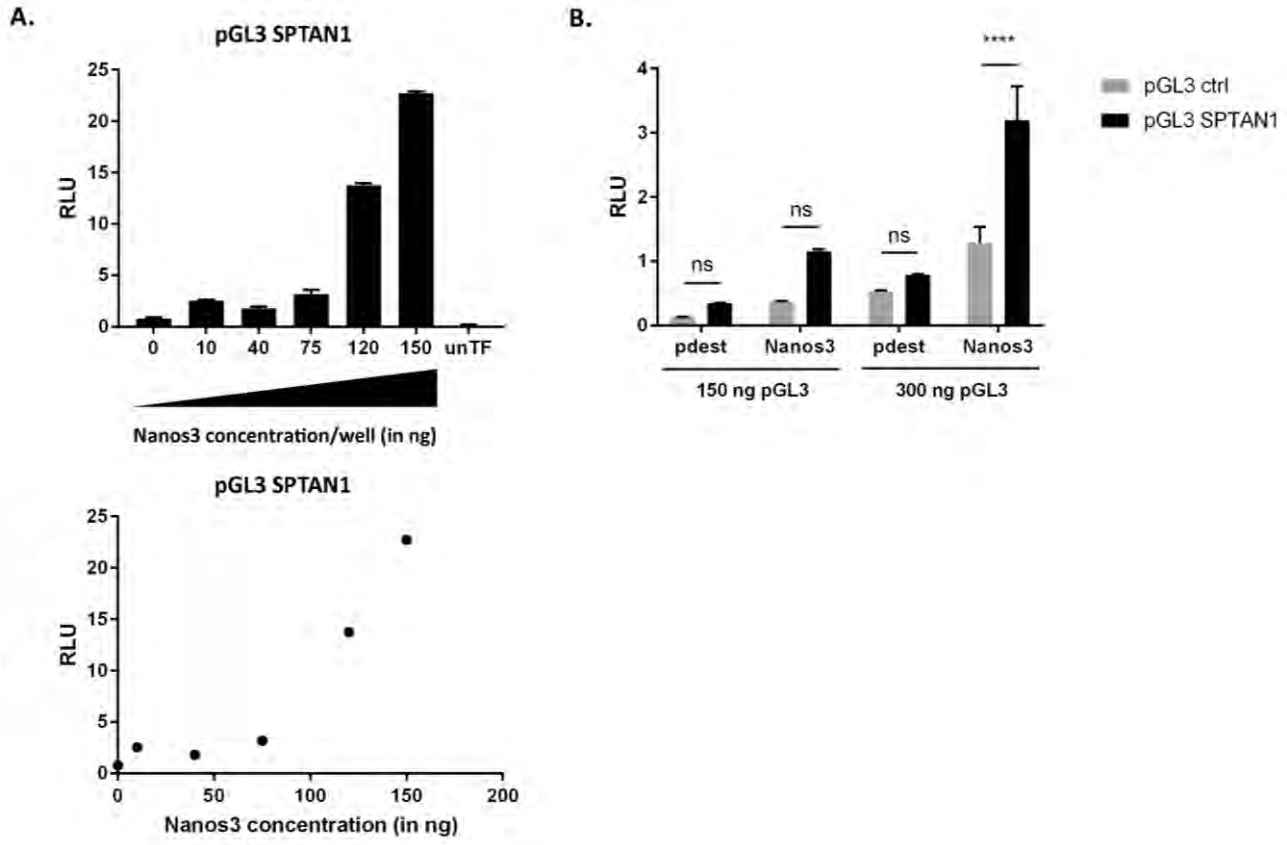

Figure 2.11. The *SPTAN1* 3'UTR increases luciferase expression upon Nanos3 expression. A. HEK293T cells were grown in a 96-well plate and cotransfected with pGL3-SPTAN1 (300 ng) and either pdest 12.2 or different concentrations of pdest 12.2-Nanos3. A luciferase assay was done to detect the effect of Nanos3 on translation of the luciferase gene extended with the 3'UTR of *SPTAN1*. The graph at the bottom offers a different representation of the same results. **B.** HEK293T cells (96-well plate) were cotransfected with two different concentrations of either pGL3-control or pGL3-SPTAN1, together with either pdest 12.2 or pdest 12.2 Nanos3 (each at 75 ng). RLU, relative light units. Error bars, SEM; n=6; ns, not significant; ****: P≤0.0001.

Unfortunately, upon repetition of the RIP analysis including the Calu-1-pdest cells, *SPTAN1* seemed to be a false positive that was also found to interact with the Nanos3-specific antibody in Calu-1-pdest cells (Figure 2.12). Endogenous Nanos3 levels in Calu-1 cells are very low and are unlikely to give these results.

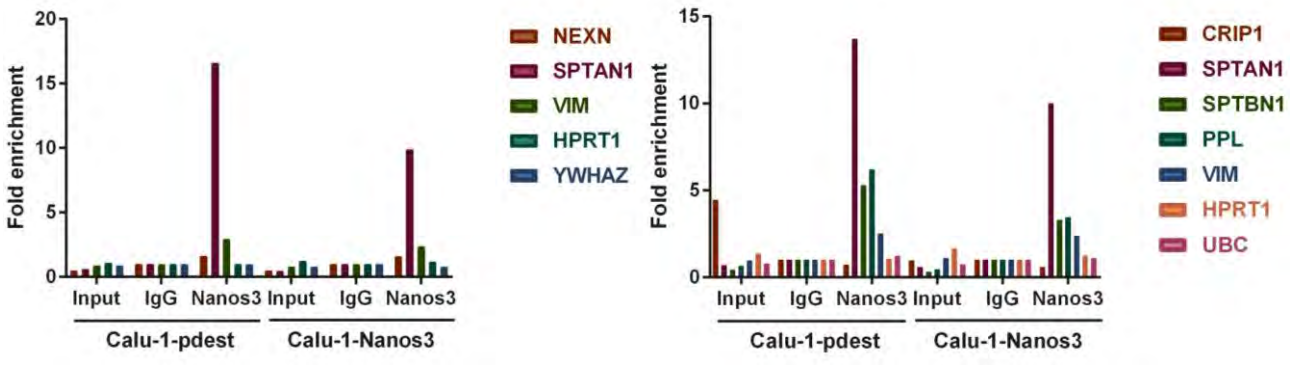

Figure 2.12. *SPTAN1* as a false mRNA target for Nanos3. RNA immunoprecipitation of Calu-1-GFP-pdest 12.2 cells and Calu-1-GFP-Nanos3 cells with a control IgG or Nanos3-specific antibody. RNA expression levels were checked with RT-qPCR and normalization was done with qbase+ using HPRT1 and YWHAZ or HPRT1 and UBC as reference targets.

2.2.3 Conditional Nanos3-expressing mouse

Introduction

NANOS3 is one of the three members of the mammalian *Nanos* gene family. Nanos proteins share a C-terminal zinc finger domain (Zf-nanos; $(CCHC)_2$), which is moreover the only evolutionary conserved domain between Nanos proteins from lower organisms to mammals [17]. Also between paralogs, this Zf-nanos domain is the region with the highest conservation. Vertebrate and some invertebrate Nanos proteins share an additional short N-terminal motif called NOT1 interacting motif or NIM [17]. NOT1 in *Drosophila* or its paralog CNOT1 in humans is part of the CCR4-NOT deadenylase complex, a highly conserved protein complex facilitating gene regulation. Human Nanos3 counts 192 amino acids (AA) including the N-terminal 17-AA long NIM region and the Zf-nanos motif, in case of Nanos3 localized internally from AA 77-128 (Figure 2.13A). Another shorter isoform of human Nanos3 exists. In this shorter isoform, AAs 43-61 (NH_2-VSALEPMPAPESVPVPGPK-COOH) are spliced out. Only the transcript resulting in the 192 AA-long protein is part of the human consensus coding sequence set (CCDS; *https://www.ncbi.nlm.nih.gov/CCDS/*) and was used to generate our conditional Nanos3-expressing mouse.

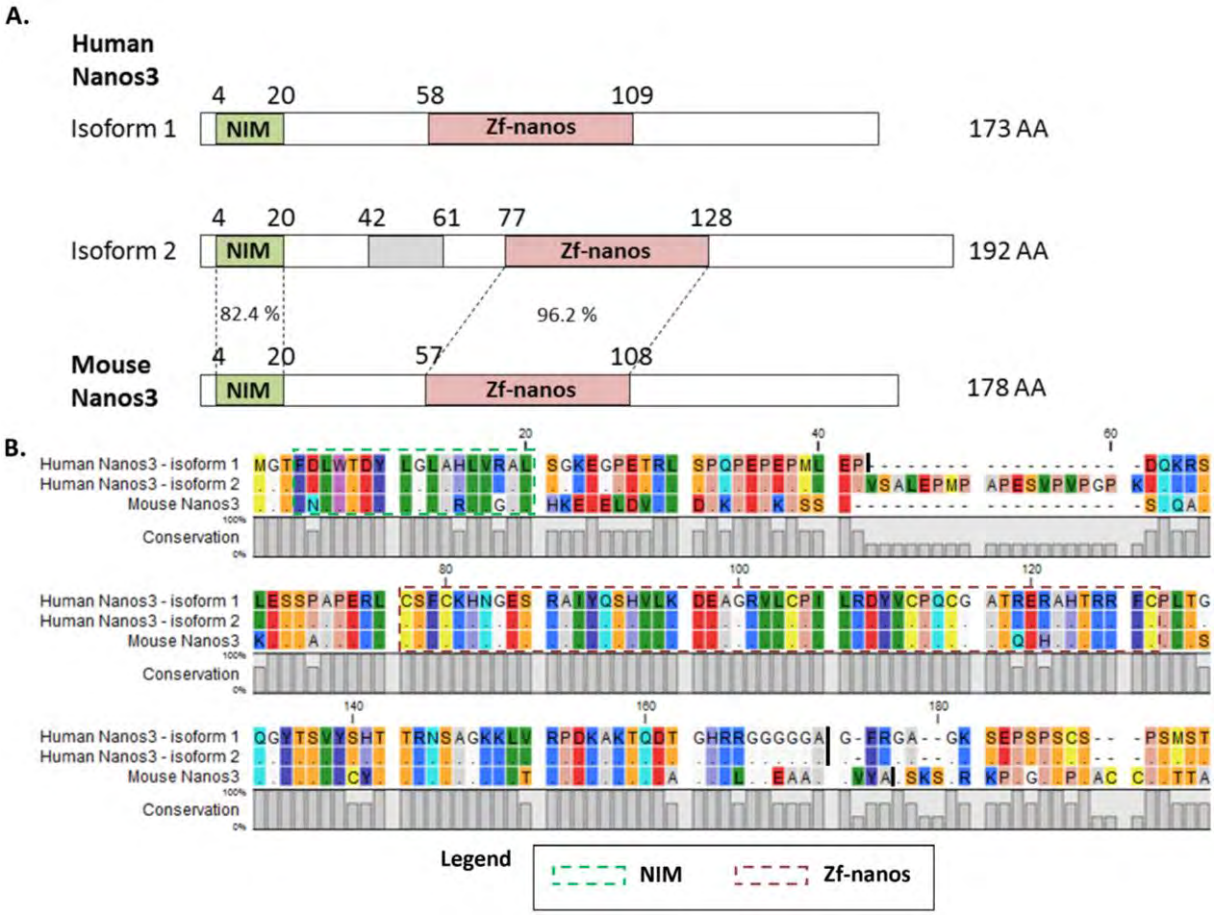

Figure 2.13. Nanos3 protein domains and sequences. A. Human *NANOS3* is transcribed in two protein encoding mRNAs. Both translated protein isoforms include the conserved $(CCHC)_2$ zinc finger domain (Zf-nanos) present in all *Nanos* genes. In common with all vertebrate and a few invertebrate nanos proteins, these isoforms have an additional N-terminal NOT1 interacting motif (NIM). The only difference between these two proteins is an insertion of 19 amino acids (AA) (grey rectangle), which corresponds to a retained intron by alternative splicing. This intron is absent in mouse *Nanos3*. The vertical black lines indicate the exon boundaries. The percentages represent the sequence identity between either the NIM or the ZnF motifs of human and mouse Nanos3 proteins. **B.** Alignment of the Nanos3 protein sequences in human and mouse. The Rasmol color code for AA is used. Identical residues in human and mouse Nanos3 are marked with a dot.

Nanos3, and Nanos proteins in general, are principally identified as post-transcriptional repressors. Nanos proteins exert this function mainly in concert with their conserved interaction partner, Pumilio. Regarding the human Nanos paralogs an interaction between Nanos2 and Pumilio2 has been demonstrated [18]. The highly conserved Zf domain of Nanos2 was by itself sufficient to interact with Pumilio2, indicating the high probability that also Nanos3 interacts with Pumilio2. For the mouse ortholog, Nanos3, interaction with Pumilio2

has already been confirmed [4]. Mouse and human Nanos3 (isoform 2) proteins are 66.2% (131/198) identical and show 70.7% (140/198) similarity (Figure 2.13B). These percentages even increase to 73.2% (131/179) and 78.2% (140/179), respectively, when omitting the 19-AA insertion in human Nanos3 (isoform 1). The NIM motifs of both proteins show 82.4% identity and 88.2% similarity and the zinc finger domain even demonstrates 96.2% (50/52) identity and 98.1% (51/52) similarity (Figure 2.13). The strong conservation between human and mouse Nanos3 suggest common interaction partners and functions in both species. In spermatogonia mouse Nanos3 and Pumilio2 have been mainly localized in ribonucleoprotein (RNP) particles [4]. Since mouse Nanos3 can bind to an mRNA fraction of the testis it is thought to act as a translational repressor in germ cells similar to the *Drosophila* nanos protein. The key role of nanos proteins is germ cell development [19-21]. On the other hand, a growing number of articles provide a link between Nanos proteins and tumor progression and cancer [22,7,23-25,3]. Some of these studies specifically observe ectopic expression of Nanos in tumors [22,3,23]. Considering the putatively important roles of Nanos proteins in malignant cancers, the mechanisms and pathways involved in ectopic Nanos expression remain essentially elusive. We present here a conditional mouse model which allows to ectopically activate *NANOS3* in a tissue- and time-specific manner. In this way ectopic Nanos3 expression can be investigated *in vivo*, ideally opening interesting avenues to a new possible cancer target.

Results and discussion

We used an improved transgenesis system, based on cointegration of the transgene of interest with a floxed STOP (LSL) cassette in the *ROSA26* locus, to efficiently create our transgenic mouse line [26]. Our gateway compatible entry clone containing the human *NANOS3* cDNA (lacking the 3'UTR sequence) was inserted into the previously described pROSA26 destination vector [26] (Figure 2.14A). As such our gene of interest is located in between a PGK-neo-3xpA (STOP) cassette, in which the neomycine (neo) gene is driven by the phosphoglycerine kinase (PGK) promoter, and an internal ribosomal entry site (IRES) placed ahead of an enhanced green fluorescence (eGFP) sequence. This bicistronic vector allows simultaneous expression of our gene of interest and the eGFP reporter protein, this only in Cre recombinase-expressing cells. The obtained targeting vector was introduced into F1 hybrid derived (G4) embryonic stem (ES) cells. Primary ES cell screening was done by positive (neomycin resistance) and negative (diphtheria toxin A [DTA]) selection. Genomic DNA

extracted from the surviving clones was used for PCR screening to check for correct insertion of the 5’ part of the targeting vector (G1 and G2 primers in Figure 2.14A). The genomic DNA of validated clones was subsequently subjected to Southern blot analysis (Figure 2.14B). Two probes designed to detect correct 5’ integration (5’ probe) and single-copy insertion (neo probe) into the *ROSA26* locus, were used.

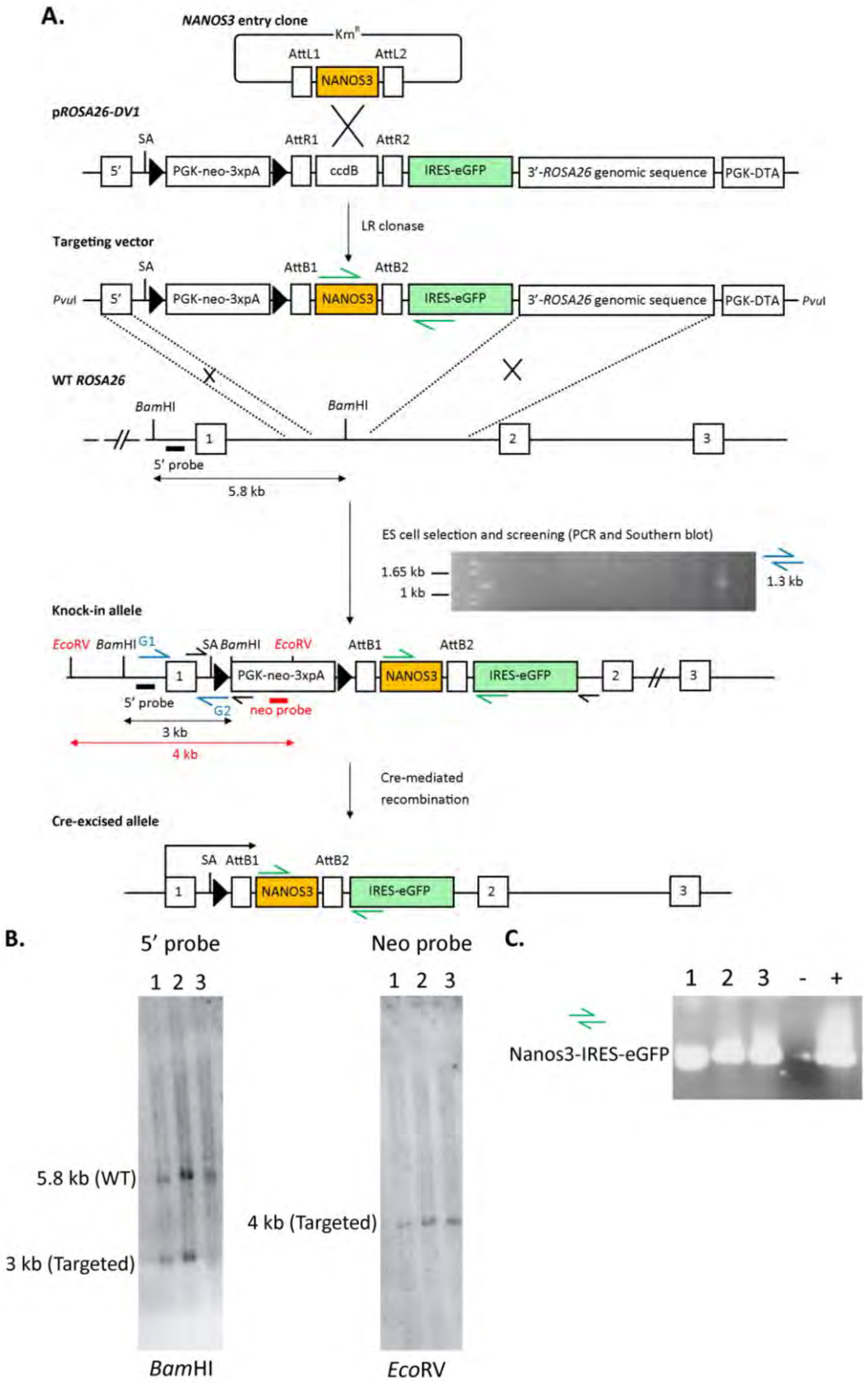

Figure 2.14. Generation by homologous recombination into the *ROSA26* locus and analysis of a human *NANOS3* allele with conditional ectopic expression. Figure legend on the next page.

Figure 2.14. Generation by homologous recombination into the *ROSA26* locus and analysis of a human *NANOS3* allele with conditional ectopic expression. **A.** The Nanos3 entry clone is recombined with the *ROSA26* destination vector (p*ROSA26-DV1*, [26]) using LR clonase. The targeting vector was replicated in bacteria. The targeting vector was subsequently linearized (*Pvu*I) and electroporated in ES cells, where homologous recombination with the wild type (WT) *ROSA26* locus took place. Correctly targeted ES cells were selected (resistance to geneticin [neomycin-resistant cells] and diphtheria toxin A [DTA]) and screened with PCR and Southern blot analyses. The blue and green arrows represent the sequencing primers used. The black and red rectangles represent the 5' and neo probe, respectively, used for Southern blot analysis. The expected band sizes after genomic DNA digestion of the WT or knock-in allele, with the corresponding restriction enzymes, are displayed by the double-headed arrows. Cre-mediated loxP recombination allows expression of Nanos3 and the IRES-eGFP reporter under control of the *ROSA26* promoter. The resulting mice were genotyped using the primers represented as black and green arrows. LoxP sites are represented by triangles. SA, splice acceptor site. **B.** Southern blot analysis of PCR confirmed targeted ES cells. **C.** PCR analysis to confirm the presence of the *NANOS3* gene.

PCR detection of *NANOS3* and the IRES-eGFP cassette sequences was done as a final confirmation (Figure 2.14C). Correctly targeted ES cells were used to make conditional transgenic Nanos3 mice. In such a transgenic line, expression of *NANOS3* is driven by the *ROSA26* promoter providing a moderate level of expression. We further refer to these new transgenic mice as Nanos3$^{LSL/LSL}$ and Nanos3$^{LSL/-}$ lines, with homozygous and heterozygous expression of the transgene, respectively. Depending on the Cre line used to breed with a transgenic line, transgene expression can be ubiquitous or tissue-specific. First, Nanos3 transgenic mice were crossed with the Sox2-Cre transgenic mouse line [27] to activate Nanos3 expression in all tissues and to test the functionality of the system. Interestingly, this experiment showed that transgenic expression of Nanos3 in all tissues was embryonically lethal. Second, these Nanos3 transgenic mice were crossed with an albumin-Cre (Alb-Cre) transgenic line [28], inducing hepatocyte-specific Cre expression. Cre-dependent expression of Nanos3 and GFP specifically in the liver was confirmed by genotyping, western blotting, RT-qPCR and confocal imaging, which proved the reliability of the induction system (Figure 2.15).

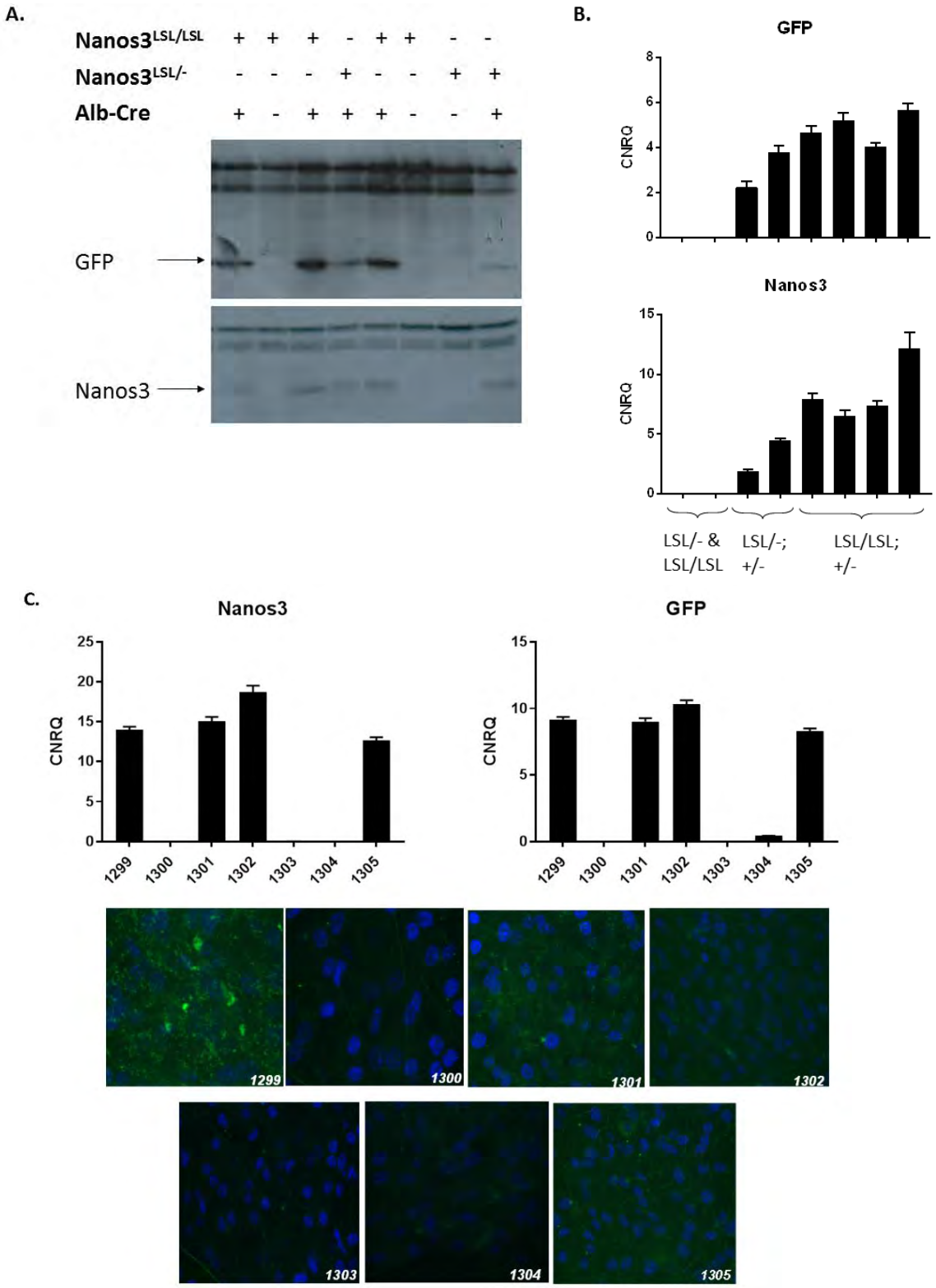

Figure 2.15. Analysis of the livers of Alb-Cre mice with heterozygous or homozygous human Nanos3 expression. Figure legend on the next page.

Figure 2.15. Analysis of the livers of Alb-Cre mice with heterozygous or homozygous human Nanos3 expression. Western blot **(A)** and RT-qPCR analysis **(B)** of liver lysates from control mice and mice with liver-specific heterozygous or homozygous ectopic Nanos3 expression. **C.** RT-qPCR analysis for Nanos3 and GFP expression (top) and confocal pictures showing GFP expression (bottom) in livers from Nanos3$^{LSL/-}$;Alb-Cre$^{+/-}$ (1299, 1301, 1302 and 1305) or Nanos3$^{LSL/-}$;Alb-Cre$^{-/-}$ mice (1300, 1303 and 1304). CNRQ, calibrated normalized relative quantity; error bars, SEM; n=3.

Third, we made use of a K5-Cre line [29], to obtain epidermis-specific Cre and consequently Nanos3 and GFP expression. Similarly as in the previous mouse model, Nanos3 and GFP expression were checked, confirming epidermis-specific expression depending on the presence of the Cre recombinase (Figure 2.16).

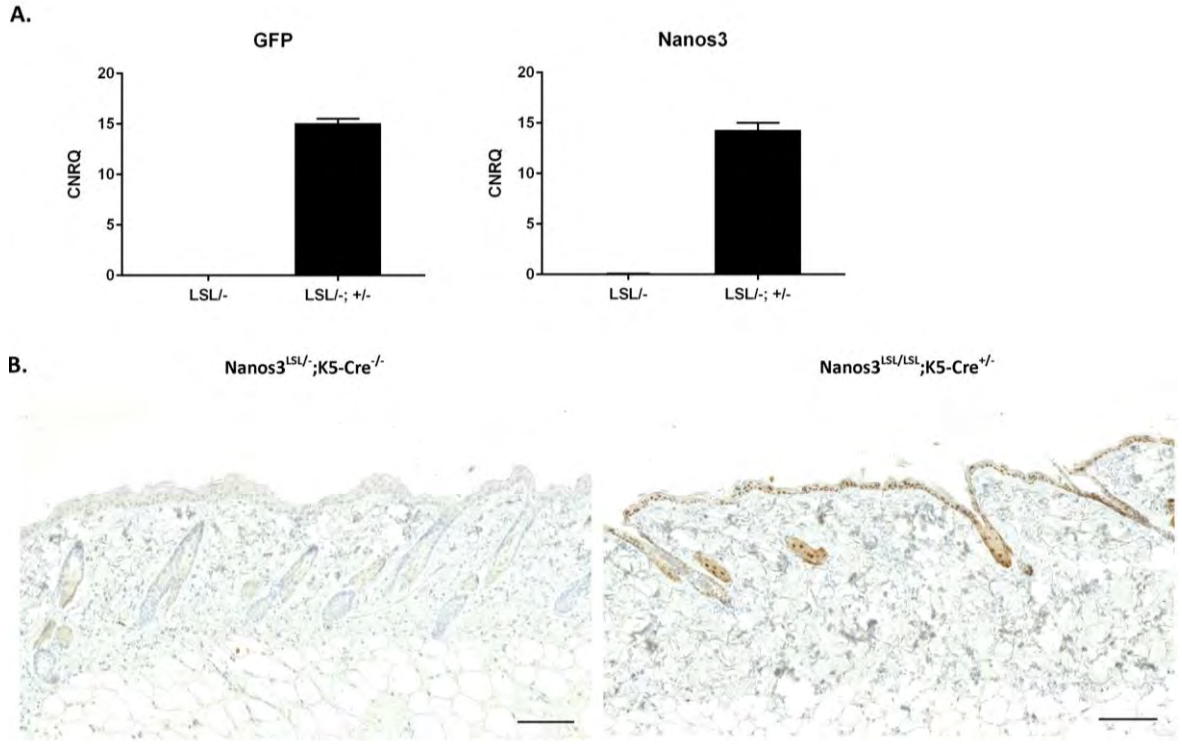

Figure 2.16. Analysis of skin from K5-Cre mice with heterozygous or homozygous human Nanos3 expression. A. RT-qPCR analysis was done to check for *GFP* and *NANOS3* RNA expression in RNA lysates of skin from a Nanos3$^{LSL/-}$;K5-Cre$^{+/-}$ or Nanos3$^{LSL/-}$;K5-Cre$^{-/-}$ mouse. CNRQ, calibrated normalized relative quantity; error bars, SEM; n=3. **B.** GFP expression in skin sections of a Nanos3$^{LSL/-}$;K5-Cre$^{-/-}$ or Nanos3$^{LSL/LSL}$;K5-Cre$^{+/-}$ mouse were analyzed by immunohistochemical staining. Bars; 100 µm.

Finally, it is also possible to activate Nanos3 expression at a specific time point using the Tet-on system [30]. In this case expression of the Cre recombinase would be controlled by the

reverse tetracycline transactivator (rtTA). In the presence of doxycycline, rtTA will bind the tetracycline operator (tetO) preceding the Cre recombinase gene allowing transcription of the latter. Expression of the transactivator can be driven by a tissue-specific promoter, as such permitting spatio-temporally controlled Cre expression. This would be necessary if ectopic expression of Nanos3 leads to embryonic lethality in a specific tissue/cell type. The latter system is also ideal to combine inducible Nanos3 expression with inducible loss of a tumor suppressor gene or activation of an oncogene or both. This makes it possible to analyze the influence of ectopic Nanos3 expression in various cancer models.

We made these Nanos3^{LSL} mice in both a C57BL/6 background and an FVB/N background, by crossing for at least ten generations to the appropriate breeding partners. FVB/N mice are generally more susceptible to carcinogenesis than other strains [31-33].

In summary this mouse model allows spatio-temporally controlled ectopic human Nanos3 expression. The natural testis- and brain-specific expression of this interesting protein and the fact that ectopic expression has been reported in various human cancers makes Nanos3 a potential CTA candidate. Our mouse model allows further analysis of the influence of ectopic Nanos3 expression in cancer and in normal tissues. This system can also contribute much to discovering Nanos3 molecular interaction partners and mRNA targets with physiological relevance. In addition, it allows to further investigate the effect of Nanos3 on germ cell development in mammals and the pathways involved. Since ubiquitous expression of Nanos3 turns out to be embryonically lethal, the correct localization of Nanos3 protein expression seems to be of importance in the mammalian embryo, as is seen in *Drosophila.* It would be interesting to reveal how ubiquitous Nanos3 expression affects embryonic development.

2.3 Discussion

Several databases have been made on which general information about genes and gene products is listed. The cBioportal website (*http://cbioportal.org*), NCBI (*https://www.ncbi.nlm.nih.gov*), Ensembl (*https://ensembl.org*), the human protein atlas (*http://proteinatlas.org*) and UniProt (*http://www.uniprot.org*) are only a few examples of this. They include information based on published articles and on large-scale datasets and form a good starting point when investigating a protein. The Nanos3 protein is mainly expressed in the brain and testis, both in human and in mouse. Nanos3 plays an important role in the germ cells, which is widely conserved as discussed in Chapter 1. The importance of Nanos3 expression in the brain remains elusive. Both brain and testis are hidden from the immune system by the blood-brain barrier (BBB) and the blood-testis barrier (BTB), respectively. The BTB consists of Sertoli cells linked by basally located tight junctions, ectoplasmic specializations, desmosomes and gap junctions, and divides the seminiferous epithelium in a basal and apical or adluminal part [34]. The basal compartment comprises the spermatogonia-containing space while the apical compartment comprises the seminiferous tubule lumen and the adluminal compartment, where the spermatocytes, spermatids and spermatozoa reside and mature (Figure 2.17). Indeed, the post-meiotic spermatogenesis and spermiogenesis take place in the latter compartment, isolated from blood and lymph (Figures 2.17 and 2.18). The BTB, or better the Sertoli cell barrier, protects the sperm cells from toxic substances and allows a specific composition of the fluid in the lumen that is different from that of blood plasma. Nanos3 is expressed in both spermatogonia and spermatocytes and is thus expressed on both sides of the BTB (Figure 2.19). The immune-privileged state is, however, extended to the complete testis. The production of anti-inflammatory cytokines by for instance Sertoli and Leydig cells plays an important role in this [35,36]. The testis also has a high concentration of androgens which have an immunosuppressive role [37].

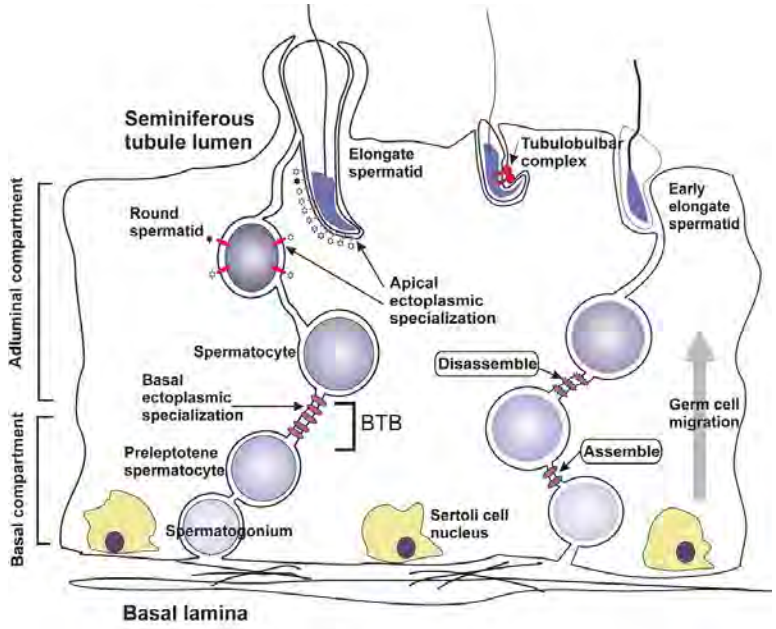

Figure 2.17. A schematic representation of the movement of germ cells across the blood-testis barrier (BTB) along the Sertoli cells. Germ cells move from the basal to the adluminal compartment of the testis for maturation. The BTB and other junctional complexes are continuously disassembled and assembled. Figure modified from [38].

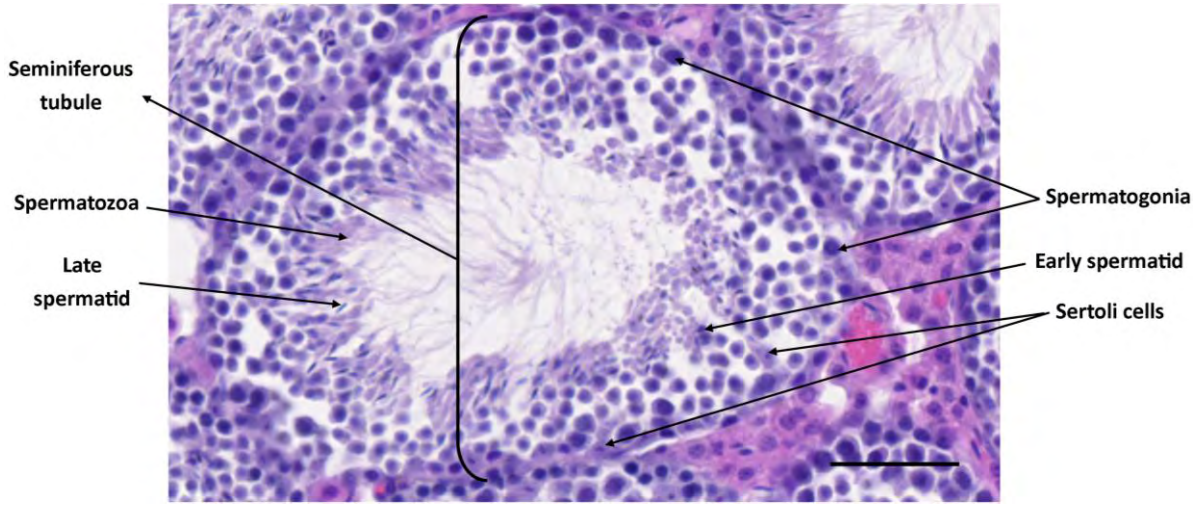

Figure 2.18. The structure of a seminiferous tubule in the mouse testis. H&E staining of the testis. Bar: 50 µm.

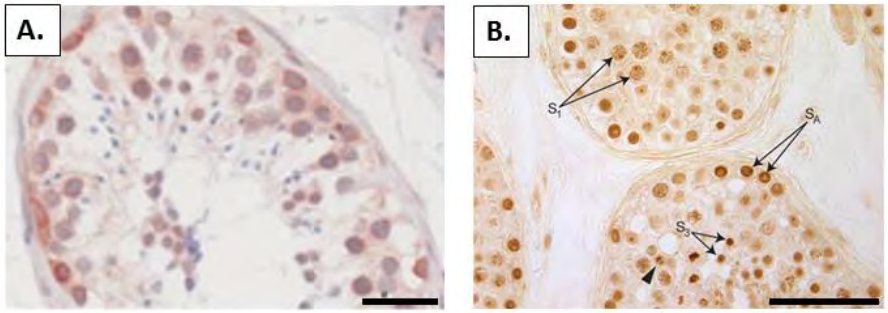

Figure 2.19. Nanos3 expression in the human adult testis. Perinuclear **(A)** and nuclear **(B)** expression of Nanos3 in the human testis. Nanos3 expression is expressed during diverse stages of spermatogenesis. Nanos3 can be detected in type-A spermatogonia (S_A), primary spermatocytes (S_1) and round spermatids (S_3) **(B)**. Figure modified from [39] and [1]. Bars: 50 µm.

The BBB is located at the endothelial tight junctions, which are apically positioned. Gases and lipid-soluble substances such as steroids and fatty acids can freely pass the BBB. Other molecules such as glucose, amino acids, thyroid hormones and several organic acids are transported through carriers in the brain endothelium [40]. Besides nutrient transporters, efflux transporters are also expressed by this endothelium, providing an extra barrier to a wide range of substrates such as small lipophilic molecules. Transcytosis is rare in endothelial cells of the brain. Cationization of plasma proteins such as albumin stimulates their uptake by adsorptive transcytosis. These mechanisms are exploited to deliver drugs inside the brain [41,42].

Nanos3 staining in the human brain is mainly nuclear. Our immunohistochemical staining of FVB/N mouse tissues showed a lot of background and could not confirm specific testis- or brain-specific staining. The staining protocol should therefore be further optimized, and other Nanos3 antibodies should be tested to examine this. Nevertheless, RT-qPCR analysis confirmed *NANOS3* mRNA expression in both organs. The brain- and testis-specific expression of Nanos3 in normal tissues and the observed ectopic expression in several human cancers [3] suggest that Nanos3 is a potential CTA candidate. Nanos1 was already found to be expressed in E-cadherin-deficient breast cancer, colon cancer and neuroblastoma cell lines [7]. Checking Nanos3 expression in several cancer cell lines showed Nanos3 expression in various skin cancer cell lines and in the SMS-KAN neuroblastoma cell line. Unlike previously shown, expression of Nanos1 or Nanos3 could not be linked to E-cadherin expression in the cell lines analyzed [7,3]. Prostate cancer cell lines and ovarian cancer cell lines generally had

low expression levels of Nanos3. The influence of Nanos3 overexpression can consequently be investigated in these cell lines by transfection with an (inducible) Nanos3 expression plasmid.

NANOS3 amplification in cancer has been mainly reported for epithelial cancers. In squamous cell carcinomas Nanos3 is expressed at a higher level at the invasion front and correlates with increased invasiveness and poor prognosis in NSCLC patients [3]. Nanos3 is expressed at different levels in several lung cancer cell lines and is associated with increased invasion and proliferation. Mass spectrometry was used to identify the protein content of samples of three lung cell lines, Calu-1, SK-LU-1 and HBE4-E6/E7, transfected with either a control or a Nanos3 expression plasmid. These cell lines have low to undetectable endogenous Nanos3 expression levels. This analysis was done to give an idea about the possible mRNA targets of Nanos3 and the proteins that could possibly be associated with the observed change in invasive and proliferative behavior. Proteins found to be downregulated upon Nanos3 expression might possibly be encoded by mRNA targets of Nanos3-mediated repression. In accordance with the described role of Nanos proteins as transcriptional repressors together with their interaction partner Pumilio, more proteins were found to be downregulated than upregulated upon Nanos3 expression (Figure 2.4). Results obtained after RT-qPCR analysis were in line with those from the proteome analysis. Significant changes in mRNA expression were however rarely observed and varied from cell line to cell line for the different mRNA sequences (Figure 2.5A-B). Therefore it seems that transcription of most of the mRNAs, encoding the proteins identified by the proteome analysis, is not directly regulated by Nanos3. However, this does not exclude a direct effect by Nanos3 as post-transcriptional regulation is plausible. The latter was investigated using RIP. Unfortunately, our RIP protocol needs further optimization (see below). This optimization could for instance involve the use of a shorter incubation step, more washing steps, the use of another antibody concentration or another Nanos3-specific antibody.

There was also a clear difference visible between the lung cancer cell lines SK-LU-1 and Calu-1 on the one hand and the transformed HBE4-E6/E7 cell line on the other hand. *CNN1* and *PLAU* transcription was for instance significantly regulated in the two cancer cell lines only, suggesting that the influence of Nanos3 depends largely on the “cellular context”. It would be interesting to compare the proteomes of several normal cell populations from the lung

with lung cancer cells with and without ectopic Nanos3 expression to further investigate this.

Nanos3 overexpression in these lung cancer cell lines has previously been linked to EMT and this was associated with an increase in uPA, slug, vimentin and MMP-14 protein levels and a decrease in E-cadherin and occludin protein levels [3,43]. Additionally Nanos3 overexpression was reported to result in an increased *PLAU*, *SLUG* and *CDH1* expression at the mRNA level. In the Calu-1 and SK-LU-1 lung cancer cell lines Nanos3 overexpression is indeed linked to an increased *PLAU* mRNA expression (Figure 2.5C). This was not the case for *SLUG* and *CDH1* mRNAs. When analyzing the expression levels of genes of the Nanos/Pumilio complex no specific correlations could be discovered (Figure 2.5D). RNA expression analysis of the lung cell lines revealed that the lung cancer cell lines Calu-1 and SK-LU-1 are more comparable to each other than the HPV-16 E6/E7 transformed HBE4-E6/E7 lung cell line (Figure 2.6). *NANOS1*, *NEXN*, *AKAP12*, *SDPR*, *CNN1* and *VIM* are for instance not expressed in the last cell line (Figure 2.5B-D). Western blot analysis confirmed vimentin expression in the Calu-1 and SK-LU-1 cell line and its absence in the HBE4-E6/E7 cell line. The opposite was observed for E-cadherin (Figure 2.7).

RIP was used to check the binding of Nanos3 to selected transcripts. Repeated RIP analysis on the Calu-1 and SK-LU-1 lung cancer cell lines with Nanos3 overexpression suggested *SPTAN1* as a possible mRNA target of Nanos3. Both *SPTAN1* mRNA and *VIM* mRNA were immunoprecipitated with the Nanos3-specific antibody in lung cancer cells and absent in the immunoprecipitates using the rabbit IgG control antibody. *VIM* mRNA was used as a positive control as binding of Nanos3 to this transcript has been reported [3].

There is, however, no conserved PRE or NRE sequence present in the *SPTAN1* 3'UTR. In follow-up experiments including the lung cancer cell line Calu-1 without Nanos3 overexpression, the interaction between *SPTAN1* mRNA and Nanos3 seemed to be a false positive one. Experiments involving the use of the *SPTAN1* 3'UTR in a luciferase reporter construct (pGL3-SPTAN1) rather implied upregulation instead of downregulation under influence of Nanos3. However, further experiments are needed to confirm this.

To study the ectopic activation of *NANOS3 in vivo*, a Nanos3 overexpressing mouse model was made. This mouse can be used in combination with cancer models to analyze the effect

of ectopic Nanos3 expression on the tumor progression of different cancer types. The resulting tumors of these *in vivo* mouse models can be used to check for the expression of candidate mRNA targets of Nanos3 and to investigate interaction partners involved in its function.

In conclusion, in a normal situation Nanos3 expression is mostly restricted to the brain and the testis. In human tumors and derived cancer cells, it can be ectopically expressed. It might be interesting to study the effect of Nanos3 overexpression on tumor progression in view of discovering a new therapeutic target and revealing novel mechanisms and pathways involved in tumor progression. Furthermore, we found that Nanos3 overexpression has mainly a negative influence on expression levels of specific protein.

2.4 Materials and methods

Cell culture

HEK293T cells were cultured in DMEM containing 10% FCS, supplemented with L-Gln and Na-pyruvate. PC3, PNT1A, LNCaP, BPH1, DU145 and SMS-KAN cells were cultured in RPMI medium supplemented with 10% FCS and L-Gln. For SMS-KAN cells, Na-pyruvate was added, while for BPH1 cells 70 nM testosterone and 1% insulin-transferrin-selenium mix was added. OVCAR-3 cells were also cultured in RPMI medium but this was supplemented with 20% FCS, L-Gln and Na-pyruvate. HaCat, A431, A224, A364, HepG2, SK-OV-3 and Hela cells were cultured in DMEM medium supplemented with 10% FCS and L-Gln. For HepG2 cells Na-pyruvate was added and for Hela cells both Na-pyruvate and NEAA were added. Vcap cells were cultured in DMEM/F12 medium supplemented with 10% FCS. PLC/PRF/5 cells were cultured in MEM Alpha medium supplemented with 10% FCS. SK-LU-1-GFP, Calu-1-GFP and HBE-E6/7 cells with and without Nanos3 overexpression were generated and provided by the lab of Dr. Nawrocki-Raby (INSERM, UMR-S 903, University of Reims Champagne-Ardenne). SK-LU-1-GFP-pdest 12.2, SK-LU-1-GFP-pdest 12.2 Nanos3, Calu-1-GFP-pdest 12.2 and Calu-1-GFP-pdest 12.2 Nanos3 cells were cultured in EMEM medium supplemented with 10% FCS, L-Gln, Na-pyruvate, NEAA and geneticin (G418; 500 µg/ml, Gibco). HBE4-E6/E7-pdest 12.2 and HBE4-E6/E7-pdest 12.2 Nanos3 cells were cultured in Keratinocyte Serum-Free medium (SFM) supplemented with 0.2 ng/ml human recombinant epidermal growth factor (EGF), 30 µg/ml bovine pituitary extract (BPE) and geneticin (100 µg/ml). Cells were kept at 37°C in a CO_2 incubator (5%) or CO_2 was manually added to 5% in closed recipients, after which cells were grown in a hot room (37°C).

Transient transfection of HEK293T cells

Calcium phosphate ($Ca_3(PO_4)_2$) transfection was done to overexpress Nanos3 (expression construct pdest 12.2 Nanos3cl1) in HEK293T cells. Briefly, 2.5 million cells were seeded in a 75-cm^2 cell culture flask in 15 ml medium. The following day the cells were transfected with the Nanos3 construct and refreshed six hours later. 48 hours after transfection, cells were harvested for western blotting and RT-qPCR analyses. For the luciferase assay, cells were seeded in a 96-well plate and cotransfected with luciferase reporter vectors (pGL3-control or

pGL3-SPTAN1) and pdest 12.2 Nanos3cl1 or pdest 12.2. The model plasmid UT651, containing the *Escherichia coli LacZ* gene, was cotransfected for transfection normalization.

Western blotting

Tissues and cells were washed with PBS and lysed in Laemmli buffer (50 mM Tris-HCl pH 6.8, 10% glycerol and 2% SDS) supplemented with protease inhibitors (Complete Mini, Roche) for half an hour on ice. Tissue lysates were homogenized with the Polytron PT 1600E (Kinematica AG). Lysates were sonicated (Sonics vibra cell^{TM}) for one minute with one-second intervals after which cell debris was removed by centrifugation. Protein concentration of the supernatants was measured using the DC protein assay kit (Bio-Rad) and total protein (40 µg for the samples used in section 2.2.2 and 120 µg for the samples used in section 2.2.3) was separated by SDS-PAGE on a 12-15% polyacrylamide gel. Wet blotting was used to transfer proteins to polyvinylidene fluoride (PVDF) membranes (Millipore). After blocking of the blots in 5% non-fat milk/PBS solution (one hour, RT), blots were incubated in primary antibody (addendum 2) in blocking solution for ON at 4°C. After three washing steps blots were incubated in an HRP-coupled secondary antibody solution (1:3000 anti-mouse/rabbit Ig antibody; GE Healthcare). Following three washes in PBST, detection was performed using the ECL detection system (enhanced chemiluminescence, Thermo scientific or Millipore).

Immunohistochemistry

Tissue sections (5 µm) were deparaffinized by two xylene washes of 3 min followed by two isopropanol washes of 3 min. Rehydration was done in washes with different concentrations of ethanol (2x 100%, 1x 70%; 3 min each) after which the slides were rinsed with tap water and PBS. A citrate buffer was used for antigen retrieval in a 2100 Retriever pressure cooker (PickCell Laboratories), followed by three washes of 5 min in PBS. Endogenous peroxidase activity was blocked by incubating the slides for ten minutes in hydrogen peroxidase (3% in methanol), followed by another three washes in PBS. Tissues were blocked in 5% goat serum in PBS with 1% BSA (bovine serum albumin) for 30 min at RT after which they were incubated with primary antibodies (addendum 2) (in 5% goat serum in PBS with 1% BSA), ON at 4°C in a humid chamber. Slides were then washed three times in PBS and incubated with biotin-conjugated secondary antibodies to rabbit immunoglobulins (Dako, E0432, 1:500) for

30-45 min at RT. The signal was enhanced by use of the ABC-kit (Vector) according to the manufacturer's protocols. Protein localization was imaged using DAB substrate (Dako). The reaction was stopped by incubating the slides with water. Slides were dehydrated by sequential washes with 70% ethanol, 100% ethanol, isopropanol and xylene. Entellan® (Merck Millipore) was used to mount the slides.

Immunofluorescence

For section 2.2.3 liver sections were deparaffinized and rehydrated as mentioned above (see immunohistochemistry). After three washes of 5 min in PBS the slides were stained with Hoechst 33342 for half an hour at RT. After several washes the tissue sections were mounted and images were taken with a Leica SP5 confocal microscope.

RNA isolation and RT-qPCR

Tissues were homogenized in TRIZOL (Invitrogen) with the Polytron PT 1600E (Kinematica AG) and by passing the sample ten times through a 20-gauge needle. For cell lysates only the latter was done. The RNeasy Plus Mini kit (Qiagen) was used to collect total RNA from these tissue and cell lysates. cDNA was prepared using a SuperScript^{TM} III First-strand Synthesis system (Thermo Fisher) according to the manufacturer's protocol. Expression levels of the genes of interest and reference genes were analyzed by real-time quantitative PCR using the SensiFast SYBR No-ROX kit (GC Biotech). Gene expression was normalized to reference genes using qbase+ (Biogazelle) [44]. The primer sequences used are listed in addendum 3.

Proteome analysis

The proteome analysis was outsourced to Prof. Dr. Kris Gevaert and Mrs. Evy Timmerman of the VIB Department of Medical Protein Research, Proteome Analysis and Bioinformatics Unit. First, cell lysates were prepared and this protein extract was denatured and S-alkylated. Then, endo-LysC digestion was performed. After digestion, the control samples (pdest 12.2) were labelled with a light label (sulfo-N-hydroxysuccinimide propionate ($3x^{12}C$)) and the Nanos3 expressing samples with a heavy label (sulfo-N-hydroxysuccinimide propionate ($3x^{13}C$)). In the following step equal amounts of the samples were mixed. Finally, a RP-HPLC run was performed and 60 1-minute fractions were collected for further LC-MS/MS analysis. Mass spectrometry was done on all peptide fractions, which were pooled to

obtain a total of 20 fractions per experiment as to reduce LC-MS/MS time. Mass spectrometry was performed on the LTQ-Orbitrap XL mass spectrometer operating in LC-MS/MS mode. The MS/MS data, obtained by the Orbitrap XL, were presented against the *Homo sapiens* subsection from Swiss-Prot. To identify the proteins, each MS/MS-spectrum was challenged to get linked to a peptide sequence by the Mascot algorithm. Each reported MS/MS spectrum was identified with 99% confidence settings. All the identifications were validated by Peptizer [45] operating in automatic mode. The quantitation was done automatically with Mascot Distiller 2.4. This software tries to fit an ideal isotopic distribution on the experimental data based on the peptide average amino acid composition. This was followed by extraction of the XIC signal (extracted ion current) of both peptide components (light and heavy) from the raw data. Ratios were calculated from the area below the light and heavy isotopic envelope of the corresponding peptide. To calculate this ratio value, a least squares fit to the component intensities from the different scans in the XIC peak was created. MS scans used for this ratio calculation are situated in the elution peak of the precursor determined by the Distiller software (XIC threshold 0.3, XIC smooth 1, Max XIC width250). To validate the calculated ratio, the standard error on the least square fit has to be below 0.16 and the correlation coefficient of the isotopic envelope should be above 0.97. More detailed information can be provided upon request.

RNA immunoprecipitation

RNA immunoprecipitations (RIPs) were done with the Magna RIP^{TM} RNA-binding protein immunoprecipitation kit (Millipore) according to the manufacturer's protocol. Briefly, cells were grown in 14-cm-diameter culture dishes (Thermo scientific) until ~80-90% confluency, then washed in PBS and collected by centrifugation at 1500 rpm for 5 min at 4°C. Cells were resuspended in an equal pellet volume of complete RIP lysis buffer, homogenized and incubated on ice for 5 min. After a freezing step at -80°C, 100 µl of this lysate was used per RIP. The beads were equilibrated in RIP wash buffer and incubated with the Nanos3-specific antibody (Proteintech) or the negative control normal rabbit IgG for 30 min at RT. The anti-SNRNP70 and negative control antibody, included in the kit, were tested on HEK293T cells to evaluate the efficiency of the RIP. After a few washes, 100 µl of the supernatant of the RIP lysate was added in a total of 1 ml RIP immunoprecipitation buffer. 10 µl of the supernatant of the RIP lysate was kept for RNA purification as "input" fraction. The samples were

incubated ON at 4°C. After a few washes part of the bead suspensions was removed to test the efficiency of immunoprecipitation by western blotting. The rest was incubated with a proteinase K buffer to digest the proteins. RNA purification was done with phenol:chloroform:isoamyl alcohol (25:24:1). Finally, RNA was dissolved in 20 µl of RNase-free water and further used for RT-qPCR analysis.

Cloning

The pGL3-control vector (U47296) was purchased from Promega. The *SPTAN1* 3'UTR sequence (5'-GCCACTCCCTGGGTCACCCACCCCTCGCTGCTTGCCCTGCGTCGCCTTGCTGCATGTCCGCTCCTCTG TGTGCTCTCACTTTCCACTGTAACCTTAAGCCTGCTTAGCTTGGAATAAGACTTAGGAGAAAATGGTG CTTCACTAACCCGCTTCCGGTCCAGTCACAATCATCATGTCACTGTGGGGACCCAGATCTGTGTCTTG AAGCAGCTGCCCTCATTCCGACTTCAGAAAATCGAAGCAGCTGGCTCCTCCCCTTGTTCTCTCTCCCAC CCTCCCCCAAATCTGTTTTCATGTAAAAGACAAATAAATGATGACTTCCCCCAAAGCT-3') was cloned from the SK-LU-1 cell line and inserted 3' of the luciferase reporter. This was done by RT-qPCR using primers with terminal *Xba*I restriction sites for cloning of the 3'UTR sequence (forward primer: 5'-TATTCTAGAGCCACTCCCTGGGTCACCCA-3', reverse primer: 5'-ATATCTAGAAGCTTTGGGGGAAGTCATCATT-3'), followed by ligation of the product with the *Xba*I linearized pGL3-control vector. Restriction digests and sequencing confirmed correct integration of the *SPTAN1* 3'UTR sequence. Both in the pGL3-SPTAN1 and pGL3-control vector used, the SV40 late poly(A) signal and the SV40 enhancer sequence were removed since these were first thought to influence the results. Similar results were, however, obtained both with and without these sequences.

Luciferase assay

48 hours after transfection, HEK293T cells were used for a luciferase assay using the Galacto-star kit (Applied biosystems). Cells were washed with 1x PBS and lysed with 50 µl Tropix® lysis solution and put at -70°C for 30 min. After thawing, the lysate was divided over two black 96-well plates (Nunc). Galacto-star™ reaction buffer was added to one plate and left for 40 min at RT after which β-gal activity was measured with a luminometer (Glomax 96 microplate, Promega) using an exposure time of 5 seconds. Luciferase buffer was added to

the other plate and immediately measured with the luminometer, also with an exposure time of 5 seconds. The luciferase buffer was made as follow:

	Concentration	**For 500 ml**
Tricine	40 mM	3.58 g
$(MgCO_3)4Mg(OH)_2{\cdot}5H_2O$	2.14 mM	0.52 g
$MgSO_4{\cdot}7H_2O$	5.34 mM	0.655 g
Dithiothreitol (DTT)	66.6 mM	5.15 g
EDTA	0.2 mM	200 µl 0.5 M stock
Filter sterilize this solution and add the following to 100 ml of this solution		
Coenzym A (MW= 767.2)	521.2 µM	40 mg
ATP (MW= 551.1)	734 µM	697.3 µl 100 mM ATP
Luciferin (MW = 280)	940 µM	26.32 mg

Southern blot analysis

The gDNA obtained from the ES cell clones (section 2.2.3) was cut with *Bam*HI, *Kpn*I or *Eco*RV restriction enzymes, at 37°C ON. The next day the digest was precipitated with 1M NH_4AC and 100% ethanol at -20°C for a minimum of two hours. The supernatant was removed after centrifugation and the pellet was washed with 70% ethanol after which it was dissolved in distilled water with the addition of loading buffer (0.25% bromophenol blue (BPB) and 30% glycerol) to become analyzed on a 0.8% agarose gel. The gel was run ON at +/- 38V. A preliminary check was done by staining the gel with ethidium bromide. Then the gel was depurinated (0.25 M HCl) for 10-15 min. This was followed by denaturation (1.5 M NaCl and 0.5 M NaOH) and neutralization (1.5 M NaCl, 0.5 M Tris, pH 7.2 and 0.001 M EDTA, pH 8.0), 30 min each. The gel was put on a shaker during these steps. The blotting construction was made as explained in [46]. The Whatman papers used were first moistened with 10x SSC (saline-sodium citrate, Lonza). Plastic foil was put on the edges of the gel, before placing the nylon membrane (Amersham Hybond-XL, GE Healthcare), to create a barrier between the Whatman paper and paper towels that come on top. In this way capillary flow is maintained through the gel instead of around it. The next day the membrane was dipped in 2x SSC and dried on Whatman paper followed by crosslinking of the DNA to the membrane by UV irradiation to 150 mJ (GS Gene linker™ UV Chamber, Bio-Rad). The membrane was pre-hybridized in a tube with preheated hybridization buffer (GE Healthcare) for 1-2 hours at 65°C. 25 ng of the corresponding probe (see Figure 2.14) was diluted in 45 µl TE buffer and

denatured for 5 min at 95-99°C. After a snap cool it was centrifuged and added to an Amersham Rediprime reaction tube. 5 µl ^{32}P dCTP was added to the tube and incubation was then for 30-60 min incubation at 37°C. The labeled probe was added to a Microspin™ S-300 HR column (GE Healthcare) according to the manufacturer's instructions. The probe was finally denatured (5 min at 95°C) and added to the blot in fresh hybridization buffer, ON at 65°C.

Finally, the membrane was washed with 0.4x SSC; 0.1% SDS and 0.2x SSC; 0.1% SDS at 65°C and sealed in plastic. The packed membrane was put into a cassette with a cleared phosphor imaging screen (Bio-Rad) on top of it and left to develop for 3-4 days. The Molecular Imager® FX (Bio-Rad) and the Quantify One software version 4.3.1 were used to quantify the signal.

Mice and genotyping

Mice expressing Cre recombinase under control of the rat albumin promoter (Alb-Cre) [28] or the keratin-5 promoter (K5-Cre) [29] were used. All mice were bred and housed at the Vlaams Instituut voor Biotechnologie (VIB, Ghent University) in a specific pathogen-free facility. Mice experiments were performed in accordance with the ethical committee of the Faculty of Science of Ghent University. For genotyping, gDNA was obtained from mice at around 2-3 weeks of age by cutting a piece of the tail or ear. These tissues were lysed ON at 55°C (see below for buffer composition) followed by a 10-min incubation at 95°C. 1 µl of this mixture was used for the PCR reaction. In section 2.2.3 a small part of the liver was also used for genotyping to check liver-specific transgenesis. See addendum 4 and 5 for the used genotyping primers and the associated PCR programs, respectively. Tissues were dissected and fixed in 4% Paraformaldehyde (PFA) ON. Paraffin embedding was done with the *Citadel* 2000 Tissue Processor (Thermo Scientific) and 5 µm sections were made with a Microm H360 microtome (Prosan).

Lysis buffer was made as follow (240 ml):

- 24 ml Buffer A 10x
    - For 200 ml 10x Buffer A:
        - 134 ml 2 M Tris, pH 8.8

- 33.2 ml 1 M $(NH_4)_2SO_4$
- 21.4 ml 0.5 M $MgCl_2$
- 11.4 ml bidi

- 12 ml 10% Triton x-100
- 204 ml bidi

Statistical analysis

The data was analyzed with GraphPad Prism 7. An unpaired student's t-test or two-way ANOVA (luciferase assay) was performed.

Statistics was performed on all the quantification data from the proteomics data. To do robust statistics, the log_2 ratio was used which makes it possible to come close to a normal distribution. Median and Huber scales were calculated. Following this, outliers outside a 95% confidence interval could be identified.

For analyzing the RIP data the two-way ANOVA was performed as implemented in Genstat v18 [47].

2.5 Supplementary data

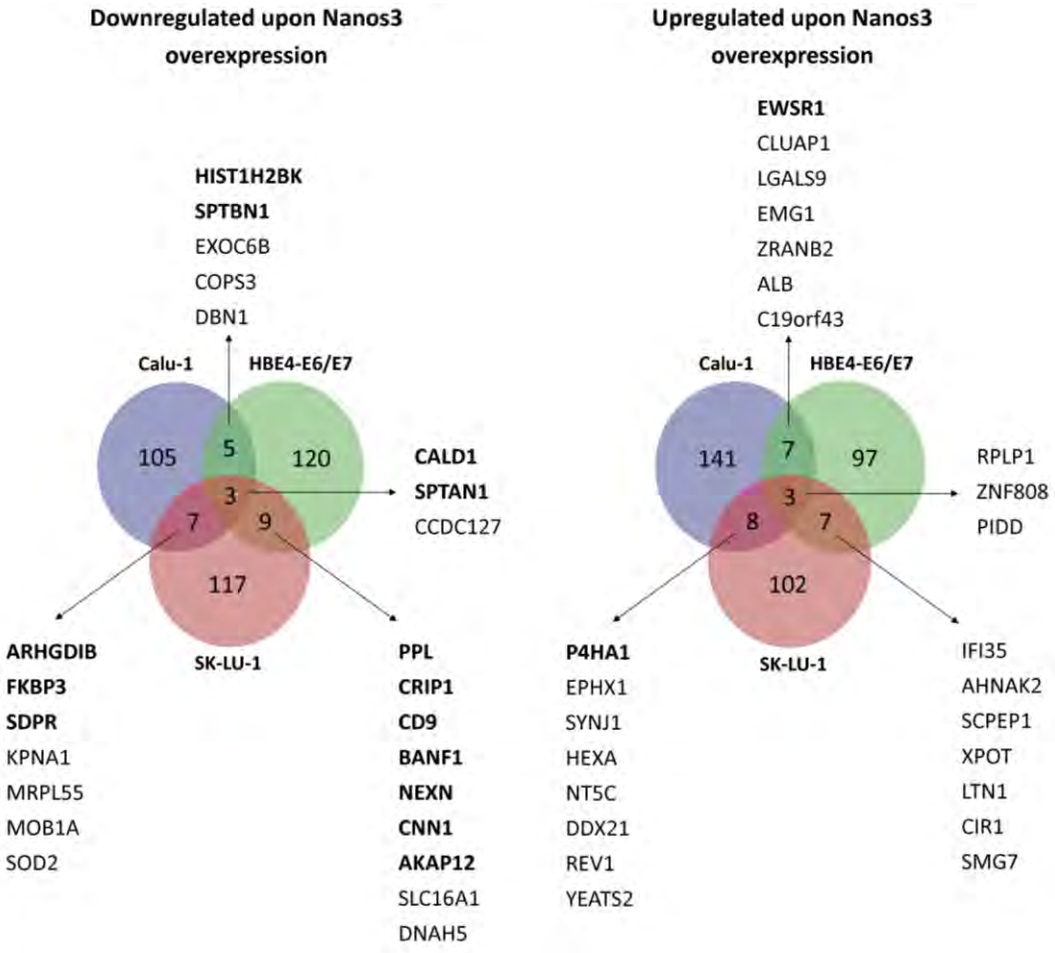

Figure S2.1. Proteome analysis of lung cell lines with and without Nanos3 overexpression. The gene names of the proteins that were significantly down- or upregulated in at least two lung cell lines are given. The names in bold represent those that are identified by more than one peptide.

Table S2.1. A list of the proteins found to be significantly downregulated in at least two lung cell lines with Nanos3 overexpression compared to the control cell lines.

Accession	Description	HBE4-E6/E7 *versus* HBE4-E6/E7-Nanos3					Calu-1-GFP *versus* Calu-1-GFP-Nanos3					SK-LU-1-GFP *versus* SK-LU-1-GFP-Nanos3				
		Protein median (log2 L/H)	SD[a].Median(log 2 L/H)	z-score	up/down with Nanos3	sequence count	Protein median (log2 L/H)	SD.Median(log2 L/H)	z-score	up/down with Nanos3	sequence count	Protein median (log2 L/H)	SD.Median(log2 L/H)	z-score	up/down with Nanos3	sequence count
Significantly downregulated in Calu-1-GFP-Nanos3 and SK-LU-1-GFP-Nanos3																
O95810	**SDPR_HUMAN Serum deprivation-response protein GN[b]=SDPR**	0.32	0.26	0.49	D	10	0.58	0.11	5.15	D	2	-0.42	0.36	2.49	D	12
Q00688	**FKBP3_HUMAN Peptidyl-prolyl cis-trans isomerase FKBP3 GN=FKBP3**	0.48	0.07	1.08	D	4	0.55	0.01	5.00	D	2	-0.64	0.12	2.11	D	5
P04179	**SODM_HUMAN Superoxide dismutase [Mn], mitochondrial GN=SOD2**	-0.11	0.00	-1.15	U	1	0.34	0.00	3.96	D	1	-0.23	0.39	2.83	D	4
P17096	**HMGA1_HUMAN High mobility group protein HMG-I/HMG-Y GN=HMGA1**	0.50	3.69	1.18	D	4	-0.05	0.00	2.02	D	1	-0.02	0.70	3.17	D	3
P52566	**GDIR2_HUMAN Rho GDP-dissociation inhibitor 2 GN=ARHGDIB**	0.02	0.11	-0.66	U	5	0.25	0.00	3.47	D	2	-0.15	0.10	2.95	D	2
Q9H8S9	**MOB1A_HUMAN MOB kinase activator 1A GN=MOB1A**	-0.17	0.00	-1.37	U	1	0.04	0.00	2.44	D	1	1.86	0.00	6.42	D	1
P52294	**IMA1_HUMAN Importin subunit alpha-1 GN=KPNA1**						-0.01	0.00	2.19	D	1	1.32	5.84	5.49	D	2

Q7Z7F7	**RM55_HUMAN 39S ribosomal protein L55, mitochondrial GN=MRPL55**						0.85	0.00	6.48	D	1	-0.46	0.00	2.43	D	1
Q8TC92	**ENOX1_HUMAN Ecto-NOX disulfide-thiol exchanger 1 GN=ENOX1**						0.69	0.00	5.69	D	1	-0.49	0.00	2.37	D	1
Significantly downregulated in HBE4-E6/E7-Nanos3 and Calu-1-GFP-Nanos3																
Q01082	**SPTB2_HUMAN Spectrin beta chain, brain 1 GN=SPTBN1**	1.07	0.94	3.34	D	21	0.05	0.19	2.51	D	13	-1.39	0.20	0.82	D	32
Q16643	**DREB_HUMAN Drebrin GN=DBN1**	1.80	0.11	6.09	D	3	0.55	0.00	4.98	D	1	-0.93	0.27	1.61	D	5
Q9UNS2	**CSN3_HUMAN COP9 signalosome complex subunit 3 GN=COPS3**	6.82	0.00	25.19	D	1	4.63	0.00	25.30	D	1	-1.55	4.98	0.54	D	3
O60814	**H2B1K_HUMAN Histone H2B type 1-K GN=HIST1H2BK**	0.88	0.30	2.60	D	2	0.19	0.21	3.21	D	2	-1.96	0.00	-0.15	U	1
Q9Y2D4	**EXC6B_HUMAN Exocyst complex component 6B GN=EXOC6B**	0.74	0.16	2.06	D	2	-0.04	0.00	2.07	D	1	-1.97	0.00	-0.17	U	1
Significantly downregulated in HBE4-E6/E7-Nanos3 and SK-LU-1-GFP-Nanos3																
P53985	**MOT1_HUMAN Monocarboxylate transporter 1 GN=SLC16A1**	11.63	0.00	43.48	D	1	-0.44	0.00	0.06	D	1	5.37	0.00	12.45	D	1
O60437	**PEPL_HUMAN Periplakin GN=PPL**	2.08	0.20	7.18	D	5	-0.46	0.16	-0.04	U	29	-0.26	0.56	2.77	D	3
O75531	**BAF_HUMAN Barrier-to-autointegration factor GN=BANF1**	0.76	0.00	2.15	D	2	-0.58	0.19	-0.64	U	3	-0.69	0.15	2.03	D	5
P21926	**CD9_HUMAN CD9 antigen GN=CD9**	1.14	0.18	3.59	D	4	-0.50	0.40	-0.26	U	4	-0.38	0.40	2.56	D	3
P50238	**CRIP1_HUMAN Cysteine-rich protein 1 GN=CRIP1**	1.66	0.06	5.58	D	2						0.21	0.26	3.58	D	2

P51911	**CNN1_HUMAN Calponin-1 GN=CNN1**	2.89	1.48	10.27	D	3						-0.59	1.02	2.20	D	2
Q02952	**AKA12_HUMAN A-kinase anchor protein 12 GN=AKAP12**	0.90	0.20	2.68	D	10						0.16	6.65	3.50	D	6
Q0ZGT2	**NEXN_HUMAN Nexilin GN=NEXN**	1.97	0.10	6.75	D	7						-0.26	0.63	2.77	D	6
Q8TE73	**DYH5_HUMAN Dynein heavy chain 5, axonemal GN=DNAH5**	6.36	0.00	23.46	D	1						5.97	0.00	13.49	D	1
Significantly downregulated in HBE4-E6/E7-Nanos3, Calu-1-GFP-Nanos3 and SK-LU-1-GFP-Nanos3																
Q05682	**CALD1_HUMAN Caldesmon GN=CALD1**	0.74	0.11	2.08	D	16	-0.02	0.15	2.14	D	10	-0.57	0.14	2.23	D	15
Q13813	**SPTA2_HUMAN Spectrin alpha chain, brain GN=SPTAN1**	0.87	0.15	2.55	D	37	0.12	0.30	2.84	D	19	-0.57	1.18	2.24	D	47
Q96BQ5	**CC127_HUMAN Coiled-coil domain-containing protein 127**	5.26	0.00	19.25	D	1	5.40	0.00	29.14	D	1	6.31	0.00	14.08	D	1

[a] Standard deviation

[b] Gene name

Table S2.2. A list of the proteins found to be significantly upregulated in at least two lung cell lines with Nanos3 overexpression compared to the control cell lines.

Accession	Description	HBE4-E6/E7 *versus* HBE4-E6/E7-Nanos3					Calu-1-GFP *versus* Calu-1-GFP-Nanos3					SK-LU-1-GFP *versus* SK-LU-1-GFP-Nanos3				
		Protein median (log2 L/H)	SD[a].Median(log 2 L/H)	z-score	up/down with Nanos3	sequence count	Protein median (log2 L/H)	SD.Median(log2 L/H)	z-score	up/down with Nanos3	sequence count	Protein median (log2 L/H)	SD.Median(log2 L/H)	z-score	up/down with Nanos3	sequence count
Significantly upregulated in Calu-1-GFP-Nanos3 and SK-LU-1-GFP-Nanos3																
P07099	**HYEP_HUMAN Epoxide hydrolase 1 GN[b]=EPHX1**	-0.08	0.00	-1.05	U	1	-0.93	0.00	-2.40	U	1	-3.07	0.65	-2.07	U	2
P13674	**P4HA1_HUMAN Prolyl 4-hydroxylase subunit alpha-1 GN=P4HA1**	0.27	0.10	0.28	D	4	-1.06	0.49	-3.01	U	2	-3.02	0.65	-1.98	U	9
O43426	**SYNJ1_HUMAN Synaptojanin-1 GN=SYNJ1**						-5.55	0.00	-25.34	U	1	-7.14	0.00	-9.07	U	1
P06865	**HEXA_HUMAN Beta-hexosaminidase subunit alpha GN=HEXA**						-0.90	0.00	-2.22	U	1	-3.33	0.00	-2.52	U	1
Q8TCD5	**NT5C_HUMAN 5'(3')-deoxyribonucleotidase, cytosolic type GN=NT5C**						-16.61	0.00	-80.39	U	1	-3.28	0.41	-2.43	U	2
Q9NR30	**DDX21_HUMAN Nucleolar RNA helicase 2 GN=DDX21**						-0.91	0.00	-2.29	U	1	-3.09	1.20	-2.11	U	6
Q9UBZ9	**REV1_HUMAN DNA repair protein REV1 GN=REV1**						-15.61	0.00	-75.41	U	1	-15.02	0.00	-22.64	U	1
Q9ULM3	**YETS2_HUMAN YEATS domain-containing protein 2 GN=YEATS2**						-6.74	0.00	-31.28	U	1	-7.12	0.00	-9.04	U	1

Significantly upregulated in HBE4-E6/E7-Nanos3 and Calu-1-GFP-Nanos3																
O95218	**ZRAB2_HUMAN Zinc finger Ran-binding domain-containing protein 2 GN=ZRANB2**	-0.84	0.14	-3.95	U	2	-0.91	0.00	-2.29	U	1	-1.17	0.19	1.20	D	4
Q01844	**EWS_HUMAN RNA-binding protein EWS GN=EWSR1**	-0.59	0.56	-2.97	U	2	-0.88	0.55	-2.12	U	2	-1.76	0.00	0.19	D	1
Q92979	**NEP1_HUMAN Ribosomal RNA small subunit methyltransferase NEP1 GN=EMG1**	-0.32	0.00	-1.97	U	1	-1.28	0.00	-4.13	U	1	-1.57	0.00	0.52	D	1
Q9BQ61	**CS043_HUMAN Uncharacterized protein**	-0.38	0.00	-2.19	U	1	-0.90	0.00	-2.25	U	1	-0.99	0.06	1.52	D	3
P02768	**ALBU_HUMAN Serum albumin GN=ALB**	-0.42	0.06	-2.34	U	2	-0.93	0.00	-2.37	U	1	-2.00	0.17	-0.23	U	2
O00182	**LEG9_HUMAN Galectin-9 GN=LGALS9**	-5.01	0.00	-19.78	U	1	-6.45	0.00	-29.84	U	1					
Q96AJ1	**CLUA1_HUMAN Clusterin-associated protein 1**	-8.55	0.00	-33.24	U	1	-6.11	0.00	-28.15	U	1					
Significantly upregulated in HBE4-E6/E7-Nanos3 and SK-LU-1-GFP-Nanos3																
P80217	**IN35_HUMAN Interferon-induced 35 kDa protein**	-0.64	0.00	-3.17	U	1	-0.33	1.82	0.60	D	4	-8.70	9.78	-11.75	U	2
Q8IVF2	**AHNK2_HUMAN Protein AHNAK2 GN=AHNAK2**	-0.41	0.00	-2.29	U	1	-0.26	0.18	0.95	D	21	-4.67	3.98	-4.82	U	2
Q9HB40	**RISC_HUMAN Retinoid-inducible serine carboxypeptidase GN=SCPEP1**	-0.64	0.00	-3.18	U	1	-0.70	0.12	-1.22	U	2	-3.04	0.00	-2.02	U	1
O43592	**XPOT_HUMAN Exportin-T GN=XPOT**	-0.40	0.00	-2.25	U	1						-5.64	0.00	-6.48	U	1
O94822	**LTN1_HUMAN E3 ubiquitin-protein ligase listerin GN=LTN1**	-7.10	0.00	-27.72	U	1						-7.62	0.00	-9.90	U	1

Q86X95	**CIR1_HUMAN Corepressor interacting with RBPJ 1 GN=CIR1**	-3.94	0.00	-15.73	U	1						-7.32	0.00	-9.38	U	1
Q92540	**SMG7_HUMAN Protein SMG7 GN=SMG7**	-5.12	0.00	-20.20	U	1						-4.58	2.91	-4.66	U	2
Significantly upregulated in HBE4-E6/E7-Nanos3, Calu-1-GFP-Nanos3 and SK-LU-1-GFP-Nanos3																
P05386	**RLA1_HUMAN 60S acidic ribosomal protein P1 GN=RPLP1**	-3.08	0.00	-12.46	U	1	-0.91	0.00	-2.30	U	1	-3.06	0.00	-2.05	U	1
Q8N4W9	**ZN808_HUMAN Zinc finger protein 808 GN=ZNF808**	-5.93	0.00	-23.27	U	1	-6.35	0.00	-29.32	U	1	-7.03	0.00	-8.89	U	1
Q9HB75	**PIDD_HUMAN p53-induced protein with a death domain GN=PIDD**	-3.64	0.00	-14.59	U	1	-4.31	0.00	-19.19	U	1	-5.49	0.00	-6.24	U	1

[a] Standard deviation

[b] Gene name

2.6 References

1. Julaton VT, Reijo Pera RA (2011) NANOS3 function in human germ cell development. Hum Mol Genet 20 (11):2238-2250. doi:10.1093/hmg/ddr114

2. Yamaji M, Tanaka T, Shigeta M, Chuma S, Saga Y, Saitou M (2010) Functional reconstruction of NANOS3 expression in the germ cell lineage by a novel transgenic reporter reveals distinct subcellular localizations of NANOS3. Reproduction 139 (2):381-393. doi:10.1530/REP-09-0373

3. Grelet S, Andries V, Polette M, Gilles C, Staes K, Martin AP, Kileztky C, Terryn C, Dalstein V, Cheng CW, Shen CY, Birembaut P, Van Roy F, Nawrocki-Raby B (2015) The human NANOS3 gene contributes to lung tumour invasion by inducing epithelial-mesenchymal transition. J Pathol 237 (1):25-37. doi:10.1002/path.4549

4. Lolicato F, Marino R, Paronetto MP, Pellegrini M, Dolci S, Geremia R, Grimaldi P (2008) Potential role of Nanos3 in maintaining the undifferentiated spermatogonia population. Dev Biol 313 (2):725-738. doi:10.1016/j.ydbio.2007.11.011

5. Suzuki A, Igarashi K, Aisaki K, Kanno J, Saga Y (2010) NANOS2 interacts with the CCR4-NOT deadenylation complex and leads to suppression of specific RNAs. Proc Natl Acad Sci U S A 107 (8):3594-3599. doi:10.1073/pnas.0908664107

6. Suzuki A, Niimi Y, Saga Y (2014) Interaction of NANOS2 and NANOS3 with different components of the CNOT complex may contribute to the functional differences in mouse male germ cells. Biol Open 3 (12):1207-1216. doi:10.1242/bio.20149308

7. Strumane K, Bonnomet A, Stove C, Vandenbroucke R, Nawrocki-Raby B, Bruyneel E, Mareel M, Birembaut P, Berx G, van Roy F (2006) E-cadherin regulates human Nanos1, which interacts with p120ctn and induces tumor cell migration and invasion. Cancer Res 66 (20):10007-10015. doi:10.1158/0008-5472.CAN-05-3096

8. Cerami E, Gao J, Dogrusoz U, Gross BE, Sumer SO, Aksoy BA, Jacobsen A, Byrne CJ, Heuer ML, Larsson E, Antipin Y, Reva B, Goldberg AP, Sander C, Schultz N (2012) The cBio cancer genomics portal: an open platform for exploring multidimensional cancer genomics data. Cancer Discov 2 (5):401-404. doi:10.1158/2159-8290.CD-12-0095

9. Gao J, Aksoy BA, Dogrusoz U, Dresdner G, Gross B, Sumer SO, Sun Y, Jacobsen A, Sinha R, Larsson E, Cerami E, Sander C, Schultz N (2013) Integrative analysis of complex cancer genomics and clinical profiles using the cBioPortal. Sci Signal 6 (269):pl1. doi:10.1126/scisignal.2004088

10. Ismail AH, Landry F, Aprikian AG, Chevalier S (2002) Androgen ablation promotes neuroendocrine cell differentiation in dog and human prostate. Prostate 51 (2):117-125. doi:10.1002/pros.10066

11. Ito T, Yamamoto S, Ohno Y, Namiki K, Aizawa T, Akiyama A, Tachibana M (2001) Up-regulation of neuroendocrine differentiation in prostate cancer after androgen deprivation therapy, degree and androgen independence. Oncol Rep 8 (6):1221-1224

12. Gebauer F, Hentze MW (2004) Molecular mechanisms of translational control. Nat Rev Mol Cell Biol 5 (10):827-835. doi:10.1038/nrm1488

13. Dreyfuss G, Kim VN, Kataoka N (2002) Messenger-RNA-binding proteins and the messages they carry. Nat Rev Mol Cell Biol 3 (3):195-205. doi:10.1038/nrm760

14. Li X, Quon G, Lipshitz HD, Morris Q (2010) Predicting in vivo binding sites of RNA-binding proteins using mRNA secondary structure. RNA 16 (6):1096-1107. doi:10.1261/rna.2017210

15. Wreden C, Verrotti AC, Schisa JA, Lieberfarb ME, Strickland S (1997) Nanos and pumilio establish embryonic polarity in *Drosophila* by promoting posterior deadenylation of hunchback mRNA. Development 124 (15):3015-3023

16. Joly W, Chartier A, Rojas-Rios P, Busseau I, Simonelig M (2013) The CCR4 deadenylase acts with Nanos and Pumilio in the fine-tuning of Mei-P26 expression to promote germline stem cell self-renewal. Stem Cell Reports 1 (5):411-424. doi:10.1016/j.stemcr.2013.09.007

17. Bhandari D, Raisch T, Weichenrieder O, Jonas S, Izaurralde E (2014) Structural basis for the Nanos-mediated recruitment of the CCR4-NOT complex and translational repression. Genes Dev 28 (8):888-901. doi:10.1101/gad.237289.113

18. Jaruzelska J, Kotecki M, Kusz K, Spik A, Firpo M, Reijo Pera RA (2003) Conservation of a Pumilio-Nanos complex from *Drosophila* germ plasm to human germ cells. Dev Genes Evol 213 (3):120-126. doi:10.1007/s00427-003-0303-2

19. Tsuda M, Sasaoka Y, Kiso M, Abe K, Haraguchi S, Kobayashi S, Saga Y (2003) Conserved role of nanos proteins in germ cell development. Science 301 (5637):1239-1241. doi:10.1126/science.1085222

20. Suzuki A, Tsuda M, Saga Y (2007) Functional redundancy among Nanos proteins and a distinct role of Nanos2 during male germ cell development. Development 134 (1):77-83. doi:10.1242/dev.02697

21. Kusz-Zamelczyk K, Sajek M, Spik A, Glazar R, Jedrzejczak P, Latos-Bielenska A, Kotecki M, Pawelczyk L, Jaruzelska J (2013) Mutations of NANOS1, a human homologue of the *Drosophila* morphogen, are associated with a lack of germ cells in testes or severe oligo-astheno-teratozoospermia. J Med Genet 50 (3):187-193. doi:10.1136/jmedgenet-2012-101230

22. Janic A, Mendizabal L, Llamazares S, Rossell D, Gonzalez C (2010) Ectopic expression of germline genes drives malignant brain tumor growth in *Drosophila*. Science 330 (6012):1824-1827. doi:10.1126/science.1195481

23. Bonnomet A, Polette M, Strumane K, Gilles C, Dalstein V, Kileztky C, Berx G, van Roy F, Birembaut P, Nawrocki-Raby B (2008) The E-cadherin-repressed hNanos1 gene induces tumor cell invasion by upregulating MT1-MMP expression. Oncogene 27 (26):3692-3699. doi:10.1038/sj.onc.1211035

24. Krentz AD, Murphy MW, Zhang T, Sarver AL, Jain S, Griswold MD, Bardwell VJ, Zarkower D (2013) Interaction between DMRT1 function and genetic background modulates signaling and pluripotency to control tumor susceptibility in the fetal germ line. Dev Biol 377 (1):67-78. doi:10.1016/j.ydbio.2013.02.014

25. Jorgensen A, Nielsen JE, Almstrup K, Toft BG, Petersen BL, Rajpert-De Meyts E (2013) Dysregulation of the mitosis-meiosis switch in testicular carcinoma in situ. J Pathol 229 (4):588-598. doi:10.1002/path.4154

26. Nyabi O, Naessens M, Haigh K, Gembarska A, Goossens S, Maetens M, De Clercq S, Drogat B, Haenebalcke L, Bartunkova S, De Vos I, De Craene B, Karimi M, Berx G, Nagy A, Hilson P, Marine JC, Haigh JJ (2009) Efficient mouse transgenesis using Gateway-compatible ROSA26 locus targeting vectors and F1 hybrid ES cells. Nucleic Acids Res 37 (7):e55. doi:10.1093/nar/gkp112

27. Hayashi S, Lewis P, Pevny L, McMahon AP (2002) Efficient gene modulation in mouse epiblast using a Sox2Cre transgenic mouse strain. Mech Dev 119 Suppl 1:S97-S101

28. Postic C, Shiota M, Niswender KD, Jetton TL, Chen Y, Moates JM, Shelton KD, Lindner J, Cherrington AD, Magnuson MA (1999) Dual roles for glucokinase in glucose homeostasis as determined by liver and pancreatic beta cell-specific gene knock-outs using Cre recombinase. J Biol Chem 274 (1):305-315

29. Ramirez A, Page A, Gandarillas A, Zanet J, Pibre S, Vidal M, Tusell L, Genesca A, Whitaker DA, Melton DW, Jorcano JL (2004) A keratin K5Cre transgenic line appropriate for tissue-specific or generalized Cre-mediated recombination. Genesis 39 (1):52-57. doi:10.1002/gene.20025

30. Gossen M, Freundlieb S, Bender G, Muller G, Hillen W, Bujard H (1995) Transcriptional activation by tetracyclines in mammalian cells. Science 268 (5218):1766-1769

31. Hennings H, Glick AB, Lowry DT, Krsmanovic LS, Sly LM, Yuspa SH (1993) FVB/N mice: an inbred strain sensitive to the chemical induction of squamous cell carcinomas in the skin. Carcinogenesis 14 (11):2353-2358

32. Coussens LM, Hanahan D, Arbeit JM (1996) Genetic predisposition and parameters of malignant progression in K14-HPV16 transgenic mice. Am J Pathol 149 (6):1899-1917

33. Rose-Hellekant TA, Gilchrist K, Sandgren EP (2002) Strain background alters mammary gland lesion phenotype in transforming growth factor-alpha transgenic mice. Am J Pathol 161 (4):1439-1447

34. Mruk DD, Cheng CY (2015) The Mammalian Blood-Testis Barrier: Its Biology and Regulation. Endocr Rev 36 (5):564-591. doi:10.1210/er.2014-1101

35. Meinhardt A, Hedger MP (2011) Immunological, paracrine and endocrine aspects of testicular immune privilege. Mol Cell Endocrinol 335 (1):60-68. doi:10.1016/j.mce.2010.03.022

36. Mital P, Kaur G, Dufour JM (2010) Immunoprotective sertoli cells: making allogeneic and xenogeneic transplantation feasible. Reproduction 139 (3):495-504. doi:10.1530/REP-09-0384

37. Trigunaite A, Dimo J, Jorgensen TN (2015) Suppressive effects of androgens on the immune system. Cell Immunol 294 (2):87-94. doi:10.1016/j.cellimm.2015.02.004

38. Wang CQ, Cheng CY (2007) A seamless trespass: germ cell migration across the seminiferous epithelium during spermatogenesis. J Cell Biol 178 (4):549-556. doi:10.1083/jcb.200704061

39. Jorgensen A, Nielsen JE, Blomberg Jensen M, Graem N, Rajpert-De Meyts E (2012) Analysis of meiosis regulators in human gonads: a sexually dimorphic spatio-temporal expression pattern suggests involvement of DMRT1 in meiotic entry. Mol Hum Reprod 18 (11):523-534. doi:10.1093/molehr/gas030

40. Daneman R, Prat A (2015) The blood-brain barrier. Cold Spring Harb Perspect Biol 7 (1):a020412. doi:10.1101/cshperspect.a020412

41. Upadhyay RK (2014) Drug delivery systems, CNS protection, and the blood brain barrier. Biomed Res Int 2014:869269. doi:10.1155/2014/869269

42. Pardridge WM (2017) Delivery of Biologics Across the Blood-Brain Barrier with Molecular Trojan Horse Technology. BioDrugs. doi:10.1007/s40259-017-0248-z

43. Grelet S (2014) Implication de Nanos-3 dans l'invasion tumorale broncho-pulmonaire. Dissertation, University of Reims Champagne-Ardenne

44. Vandesompele J, De Preter K, Pattyn F, Poppe B, Van Roy N, De Paepe A, Speleman F (2002) Accurate normalization of real-time quantitative RT-PCR data by geometric averaging of multiple internal control genes. Genome Biol 3 (7):RESEARCH0034

45. Helsens K, Timmerman E, Vandekerckhove J, Gevaert K, Martens L (2008) Peptizer, a tool for assessing false positive peptide identifications and manually validating selected results. Mol Cell Proteomics 7 (12):2364-2372. doi:10.1074/mcp.M800082-MCP200

46. Sambrook J, Russell DW (2001) Southern blotting: Capillary transfer of DNA to membranes. In: Sambrook J, Russell DW (eds) Molecular Cloning: A Laboratory Manual. Cold Spring Harbor Laboratory Press, New York, USA,

47. Payne RW, Murray DA, Harding SA, Baird DB, Soutar DM (2009) GenStat for Windows (12th Edition) Introduction. VSN International, Hemel Hempstead

Chapter 3

Nanos3 in lung cancer

Contributions

Evi De Keuckelaere designed, performed and analyzed experiments (Figure 3.1-3.51). Dr. Vanessa Andries provided overall support concerning the design, performance and analysis of the experiments. Katrien Staes provided overall technical assistance. Gillian Blancke supported the Indian ink experiment. Kelly Lemeire and Amanda Gonçalves provided technical assistance with histology and microscopy, respectively. Benjamin Pavie provided a script to determine the tumor mass of the lungs from H&E slides. Prof. Dr. Marnik Vuylsteke provided statistical support.

3.1 Introduction

Lung carcinoma is the most frequent cause of cancer-related death, see Chapter 1 [1]. The Van Roy research group has previously reported that Nanos1 is implicated in the acquisition of invasive properties by lung cancer cells [2,3]. Recently, Nanos3 was similarly identified as a prognostic marker for NSCLCs, which contributes to lung cancer invasion by inducing EMT [4]. Several somatic mutations are known to contribute to lung cancer. Mouse models with floxed *TP53* and *RB1* alleles display SCLC tumors after Cre-mediated recombination by intratracheal injection or intubation of adeno-Cre [5]. If only *TP53* was lost in this way, lung adenocarcinomas developed in these mice, but with a long latency of 350-530 days. *KRAS* mutations give rise to lung adenocarcinomas [6], which occur earlier in case of additional loss of *TP53* [7-9].

3.2 Lung cancer mouse models

Mice carrying conditional alleles for LSL-KRas^{G12D} [10] or p53$^{fl/fl}$ (floxed exons 2-10) [11] or for both were chosen to study the role of Nanos3 in tumor progression of NSCLC. The mutated *KRAS* allele, KRas^{G12D}, is only expressed in the presence of a Cre recombinase that removes the LSL stop cassette that lies in front of the gene. A region consisting of exon 2 to -10 of the *TP53* gene is likewise only deleted upon Cre recombinase expression, which is not only tissue- but also time-dependent in this model (see further). The Nanos3-expressing mouse, described in Chapter 2 section 2.2.3, was used to conditionally express human Nanos3. An IRES-eGFP sequence is localized C-terminal of the *NANOS3* gene enabling to use GFP as a reporter.

In order to activate Nanos3 expression specifically in the lung, Nanos3 transgenic mice were crossed with the CCSP-rtTA/TetO-Cre transgenic line [12]. In these mice, the expression of Cre recombinase is controlled by the tetO, which is activated by rtTA and this only in the presence of dox (Figure 3.1). In this setup, the rtTA transgene is driven by the rat CCSP promoter, which is active in club cells, in the bronchioles and in type-II cells in the alveoli [12]. To focus on the role of Nanos3 in tumor invasion during bronchopulmonary carcinoma progression, these mice were crossed to the conditional LSL-KRas^{G12D};p53$^{fl/fl}$ mouse model

[9] and to the LSL-KRas^{G12D} mouse and the p53$^{fl/fl}$ mouse separately. These crossings gave us the following three lung cancer models:

1) Nanos3$^{LSL/LSL}$//p53$^{fl/fl}$//CCSP-rtTA$^{+/-}$//TetO-Cre$^{+/-}$
2) Nanos3$^{LSL/-}$//LSL-KRas^{G12D}//CCSP-rtTA$^{+/-}$//TetO-Cre$^{+/-}$
3) Nanos3$^{LSL/-}$//LSL-KRas^{G12D}//p53$^{fl/fl}$//CCSP-rtTA$^{+/-}$//TetO-Cre$^{+/-}$

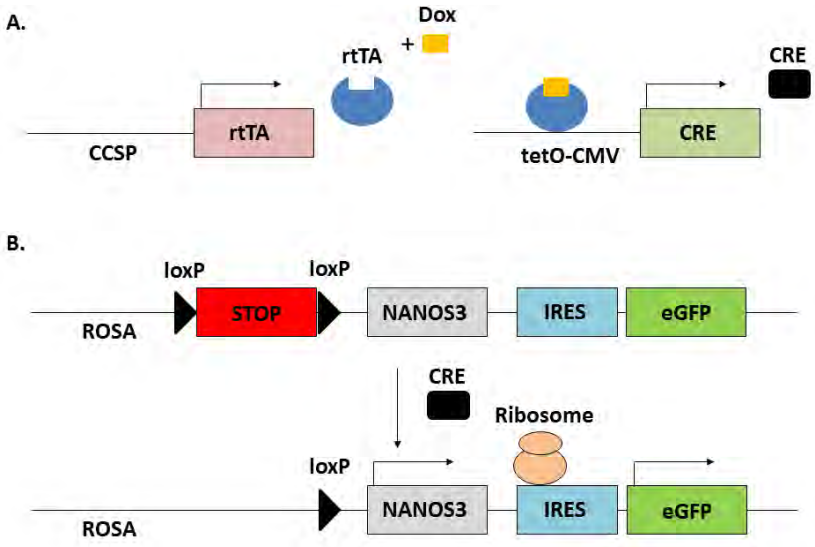

Figure 3.1. Tet-on system. A. The club cell secretory protein (CCSP) promoter is active in club cells and type-II alveolar cells leading to the transcription of the reverse tetracycline transactivator (rtTA) gene. In the presence of doxycycline (dox), rtTA will bind the tetracycline operator (tetO) in the tetO-CMV promoter leading to Cre recombinase expression. **B.** Cre recombinase mediates recombination between loxP sites thereby deleting the floxed STOP cassette (LSL) and allowing transcription of *NANOS3* and enhanced green fluorescent protein (eGFP). IRES: internal ribosomal entry site.

For all models, the various control mice (p53$^{fl/fl}$;CCSP-rtTA$^{+/-}$;TetO-Cre$^{+/-}$, LSL-KRas^{G12D};CCSP-rtTA$^{+/-}$;TetO-Cre$^{+/-}$ and LSL-KRas^{G12D};p53$^{fl/fl}$;CCSP-rtTA$^{+/-}$;TetO-Cre$^{+/-}$), as well as the Nanos3-expressing mice (Nanos3$^{LSL/LSL}$;p53$^{fl/fl}$;CCSP-rtTA$^{+/-}$;TetO-Cre$^{+/-}$, Nanos3$^{LSL/-}$;LSL-K Ras^{G12D};CCSP-rtTA$^{+/-}$;TetO-Cre$^{+/-}$ and Nanos3$^{LSL/-}$;LSL-KRas^{G12D};p53$^{fl/fl}$;CCSP-rtTA$^{+/-}$;TetO-Cre$^{+/-}$) were fed normal food supplemented with doxycycline (625 mg/kg) for two weeks starting after weaning (around the age of two weeks). These mice are further referred to as control and Nanos3 NSCLC mice.

Lung lysates of transgene mice from the first model were checked for Nanos3 and GFP expression in order to validate the functionality of the system. As expected, RT-qPCR

confirmed Nanos3 and GFP expression in the lungs of the Nanos3 transgenic mice that were fed with food containing doxycycline (Figure 3.2). However, transgenic mice that were not placed on a dox food diet showed some leaky expression.

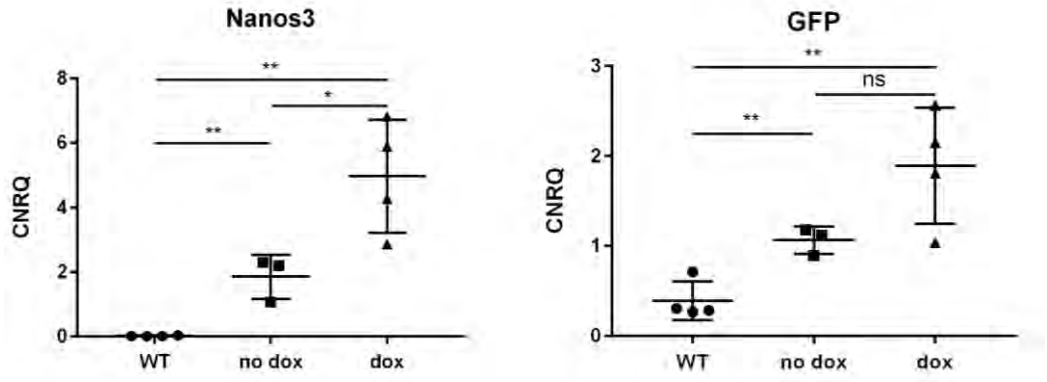

Figure 3.2. Nanos3 transgenic mice showed transgene expression upon doxycycline induction with some leaky expression in the lungs of transgenic mice that were given normal food. RNA lysates were prepared from lungs of Nanos3 transgenic mice (Nanos3$^{LSL/LSL}$;p53$^{fl/fl}$;CCSP-rtTA$^{+/-}$;TetO-Cre$^{+/-}$) and control (WT) mice without TetO-Cre expression. Four Nanos3 transgenic mice were fed doxycycline (dox) food for a period of two weeks. RT-qPCR analysis was used to analyze *NANOS3* and *GFP* mRNA expression**.** CNRQ, calibrated normalized relative quantity; ns, not significant, *: P≤0.05 and **: P≤0.01.

Histological sections from the lungs were submitted to H&E staining, demonstrating that mice from the first model mainly developed lymphomas instead of the anticipated adenocarcinomas (Table 3.1 and Figure 3.3) [5]. Adenocarcinoma formation was though seen in two control mice (Table 3.1 and Figure 3.3). As it was unlikely that this model would have helped us solve our question whether Nanos3 could act as an oncogene in NSCLC, it was abandoned.

Table 3.1. Evaluation of tumor formation in 16-month old mice from the p53$^{fl/fl}$ lung tumor model, with and without Nanos3 induction.

	Gender[a]	CCSP-rtTA	TetO-Cre	p53	Nanos3	Tumor
Control	F	+/-	+/-	fl/fl	-/-	Lymphoma
	F	+/-	+/-	fl/fl	-/-	Lymphoma and adenocarcinoma
	M	+/-	+/-	fl/fl	-/-	Lymphoma
	M	+/-	+/-	fl/fl	-/-	Lymphoma and adenocarcinoma
Nanos3	F	+/-	+/-	fl/fl	LSL/LSL	Lymphoma
	F	+/-	+/-	fl/fl	LSL/LSL	Lymphoma
	M	+/-	+/-	fl/fl	LSL/LSL	Lymphoma
	M	+/-	+/-	fl/fl	LSL/LSL	Lymphoma

[a] F, female; M, male

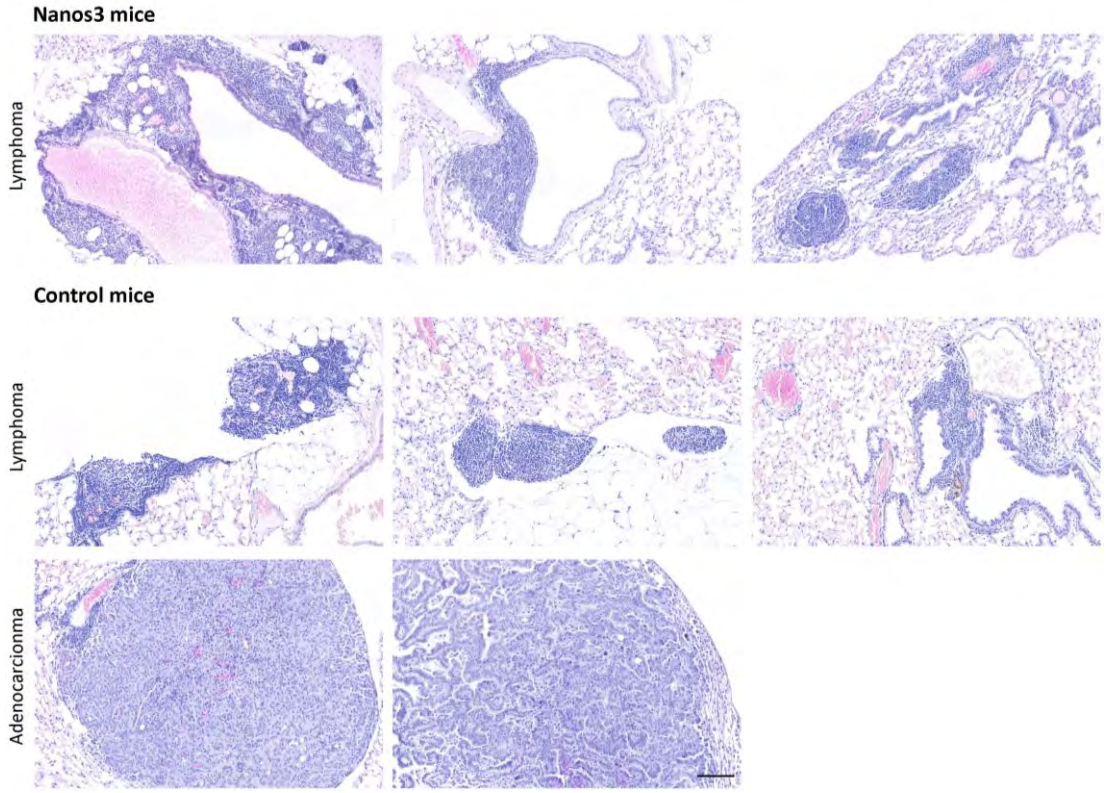

Figure 3.3. Lung-specific loss of *TP53* (model #1) results mainly in lymphoma formation and this does not seem to be influenced by Nanos3 induction. H&E staining of lung sections from control (p53$^{fl/fl}$;CCSP-rtTA$^{+/-}$;TetO-Cre$^{+/-}$) and Nanos3 mice (Nanos3$^{LSL/LSL}$;p53$^{fl/fl}$;CCSP-rtTA$^{+/-}$;TetO-Cre$^{+/-}$) sacrificed 68 weeks after dox induction. Lymphomas are observed in both genotypes while two of the four analyzed control mice showed an additional adenocarcinoma. Bar: 100 µm.

In contrast, mice from tumor models #2 and #3 did give the expected adenocarcinomas (Figure 3.4). The lungs of mice with the induced Nanos3 transgene (Nanos3$^{LSL/-}$;LSL-

KRas^{G12D};CCSP-rtTA$^{+/-}$;TetO-Cre$^{+/-}$ and Nanos3$^{LSL/-}$;LSL-KRas^{G12D};p53$^{fl/fl}$;CCSP-rtTA$^{+/-}$;TetO-Cre$^{+/-}$) were compared to those without (LSL-KRas^{G12D};CCSP-rtTA$^{+/-}$;TetO-Cre$^{+/-}$ and LSL-KRas^{G12D};p53$^{fl/fl}$;CCSP-rtTA$^{+/-}$;TetO-Cre$^{+/-}$). A difference in tumor progression might be expected. In these models, Nanos3-expressing mice express only one exogenous human *NANOS3* allele. Homozygous expression of this transgene was not possible in a straightforward way since the mutant *KRAS* allele was located on chromosome 6 as is the *ROSA* locus from which the *NANOS3* gene is expressed. Heterozygous expression, however, proved to be sufficient to obtain high Nanos3 and GFP expression levels in the lung (Figure 3.5 and 3.6).

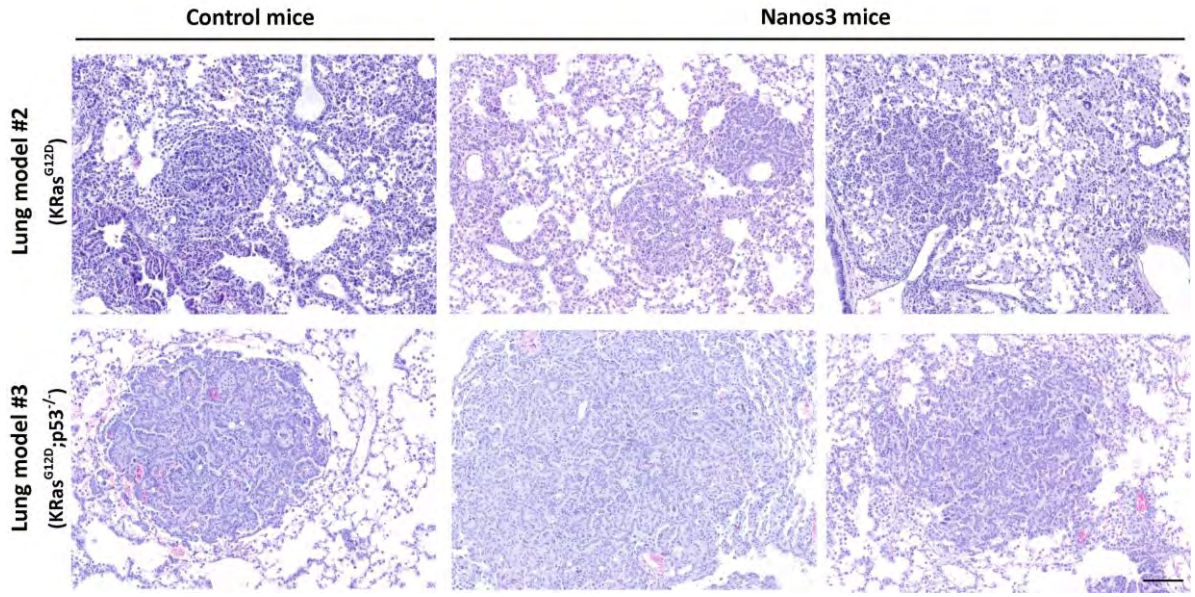

Figure 3.4. Adenocarcinoma formation in control mice and Nanos3-expressing mice with mutant KRas expression and with or without additional loss of *TP53* (models #2 and #3). H&E staining was done on lung sections from dox-induced LSL-KRas^{G12D};CCSP-rtTA$^{+/-}$;TetO-Cre$^{+/-}$ and LSL-KRas^{G12D};p53$^{fl/fl}$;CCSP-rtTA$^{+/-}$;TetO-Cre$^{+/-}$ mice with and without the Nanos3 transgene (Nanos3$^{LSL/-}$). Bar: 100 µm.

Immunohistochemistry, western blot, and RT-qPCR confirmed Nanos3 and GFP expression in the lungs of the Nanos3 transgenic mice from model #3 (Figures 3.5, 3.6, 3.7 and 3.8). The lungs of Nanos3 transgenic mice stained positive for Nanos3 and GFP, although a minority of the tumors lack Nanos3 expression (Figure 3.5). Both alveolar and bronchiolar cells were stained. Lungs from control mice, including the tumors, were negative for Nanos3 and GFP staining. Further on in this chapter, mainly GFP stainings are shown since these give less

background, although both stainings gave the same results. Western blot was done on total lung lysates of wild type, control and Nanos3-expressing mice with actin as loading control (Figure 3.7). When detecting Nanos3 protein levels in the lung lysates from Nanos3 transgenic mice, a background band is seen just above the Nanos3 protein (Figure 3.7). It is therefore important to achieve a good separation on the SDS-PAGE gel. This background band has nothing to do with the Nanos3 construct since it is also seen in the lung lysates from Nanos3$^{LSL/-}$;LSL-KRas^{G12D};p53$^{fl/fl}$;CCSP-rtTA$^{+/-}$;TetO-Cre$^{-/-}$ mice, that lack Cre expression.

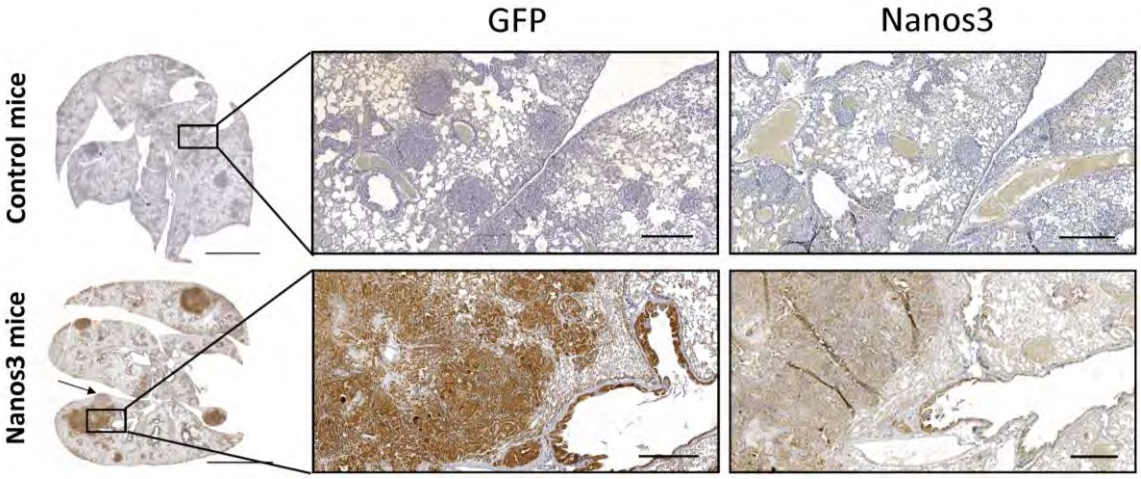

Figure 3.5. Nanos3 and GFP stainings in the lung. Tumors in Nanos3-expressing mice (Nanos3$^{LSL/-}$;LSL-KRas^{G12D};p53$^{fl/fl}$;CCSP-rtTA$^{+/-}$;TetO-Cre$^{+/-}$) are mostly positive for Nanos3 and also for GFP expressed from the IRES-eGFP reporter. Both control and Nanos3 mice were fed doxycycline food to induce transgene expression and were killed 38 days after dox induction. Arrow: A rare Nanos3 and GFP negative tumor in the Nanos3-expressing mice. Bars: 5 mm for the total lungs and 500 µm for the magnifications.

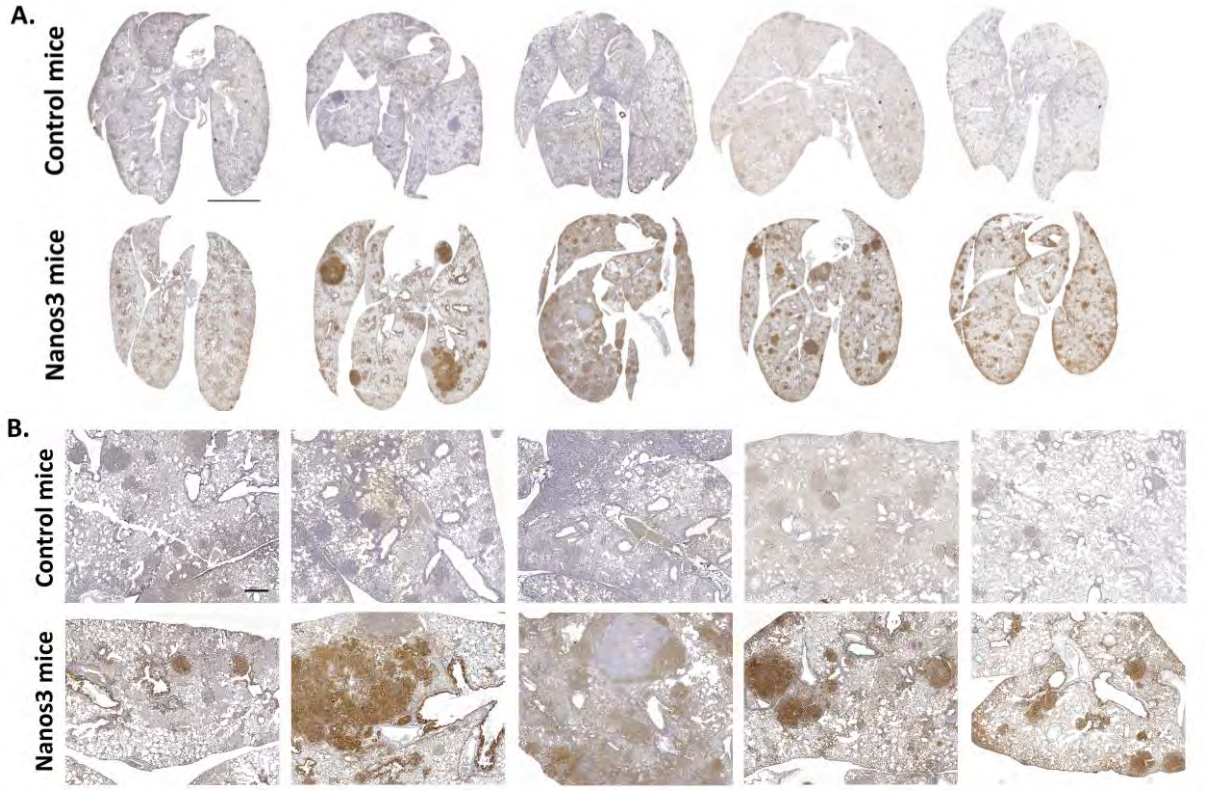

Figure 3.6. GFP expression in the lungs of control and Nanos3 transgenic mice. Immunohistochemical staining for GFP was done on lung sections of dox-induced control (LSL-KRas^{G12D};p53$^{fl/fl}$;CCSP-rtTA$^{+/-}$;TetO-Cre$^{+/-}$) and Nanos3 (Nanos3$^{LSL/-}$;LSL-KRas^{G12D};p53$^{fl/fl}$;CCSP-rtTA$^{+/-}$;TetO-Cre$^{+/-}$) transgenic mice sacrificed around 40 days after dox induction. Bars: 5 mm in **A** and 500 µm in **B**.

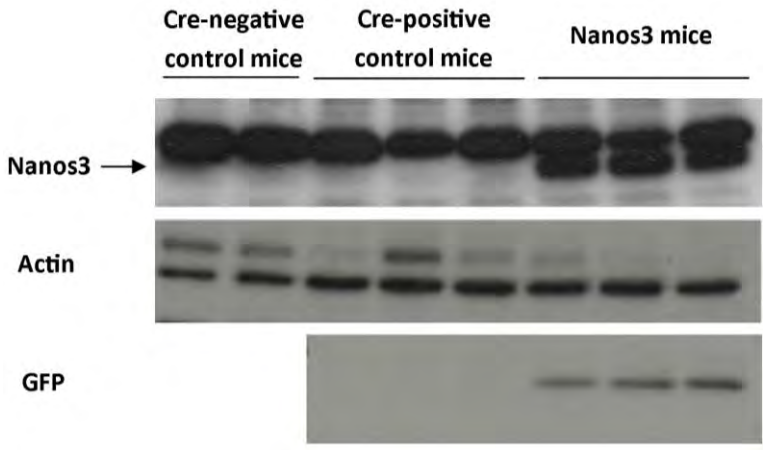

Figure 3.7. Nanos3 and GFP expression in the total lungs. Total lung lysates of two Cre-negative control, three Cre-positive control (LSL-KRas^{G12D};p53$^{fl/fl}$;CCSP-rtTA$^{+/-}$;TetO-Cre$^{+/-}$) and three Nanos3-expressing mice (Nanos3$^{LSL/-}$;LSL-KRas^{G12D};p53$^{fl/fl}$;CCSP-rtTA$^{+/-}$;TetO-Cre$^{+/-}$) were tested for Nanos3 and the correlated GFP expression by means of western blot. Both control and Nanos3 mice were fed doxycycline food to induce transgene expression. Actin was used as a loading control.

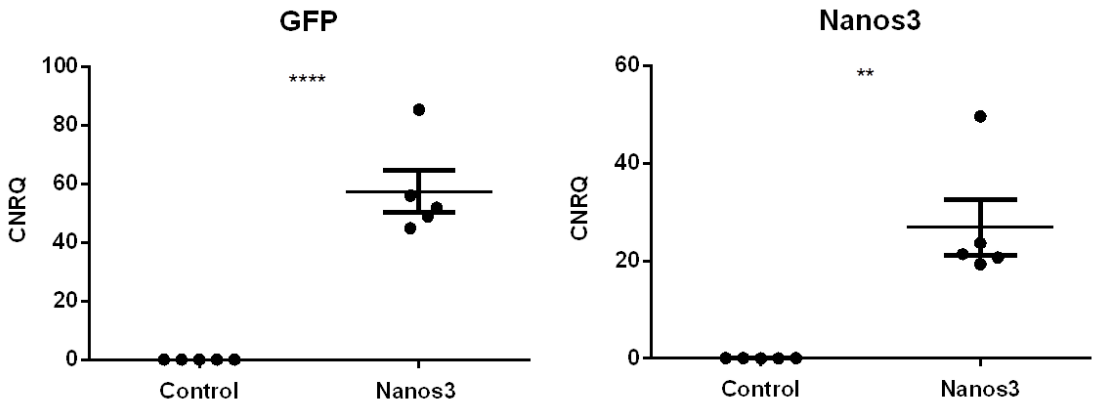

Figure 3.8. Confirmation of transgenic expression. RNA prepared from total lung lysates of control and Nanos3-expressing mice was used to detect GFP and Nanos3 through RT-qPCR. Both control and Nanos3 mice were fed doxycycline food to induce transgene expression. CNRQ, calibrated normalized relative quantity, error bars, SEM; n=3, **: P≤0.01 and ****: P≤0.0001.

3.3 Nanos3 accelerates death in mice with NSCLC

LSL-KRas^{G12D};CCSP-rtTA$^{+/-}$;TetO-Cre$^{+/-}$ and LSL-KRas^{G12D};p53$^{fl/fl}$;CCSP-rtTA$^{+/-}$;TetO-Cre$^{+/-}$ transgenic mice develop lung tumors, which are similar to those seen in BAC, recently called lepidic carcinoma, in humans. These tumors remain noninvasive without any stromal reaction. Grelet et al. [4] demonstrated the positive effect of Nanos3 on the invasion rate of NSCLC cell lines and its involvement in EMT regulation. In line with this, we were curious whether ectopic Nanos3 expression has an effect on tumor development and progression. In our mouse models, both with and without Nanos3 expression, no metastasis was observed. Nevertheless, mice with ectopic Nanos3 expression died significantly earlier (Figures 3.9 and 3.10). When comparing male and female control mice with male and female Nanos3-expressing mice, respectively, a significant difference can only be seen between the female mouse populations. While female control mice have a median survival of 85 days after dox (n=17) that of female Nanos3-expressing mice is only 66 days after dox (n=12) for model #2. For the female mice of model #3 this is 61 days after dox (n=13) and only 37 days after dox (n=13) for the control and Nanos3-expressing mice, respectively. Transgene expression is however clearly visible in the lungs of male transgenic mice (Figure 3.11).

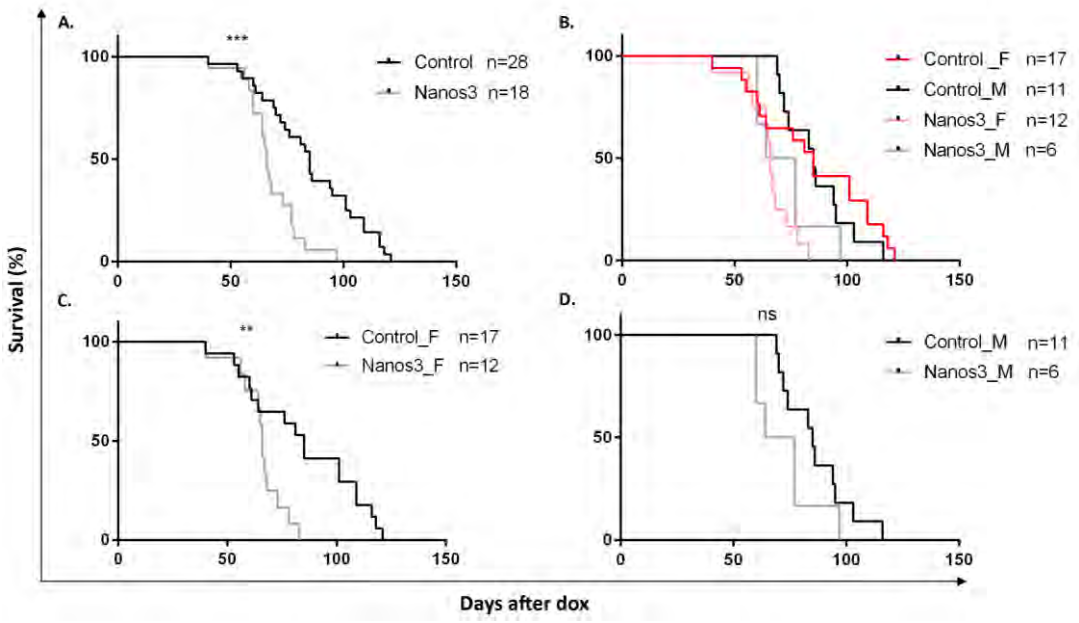

Figure 3.9. Kaplan-Meier curves for the KRas^{G12D} lung cancer model (model #2) with and without ectopic Nanos3 expression. A. The survival curves of control mice compared to Nanos3-expressing mice. **B.** Subdivision of the female (F) and male (M) control and Nanos3-expressing mice. **C-D**. In contrast to the significant difference in survival between female control and Nanos3-expressing mice **(C)**, there is no significant difference in survival between the different male mice **(D)**. All mice were fed doxycycline food to induce transgene expression. Ns: not significant, **: P≤0.01 and ***: P≤0.001.

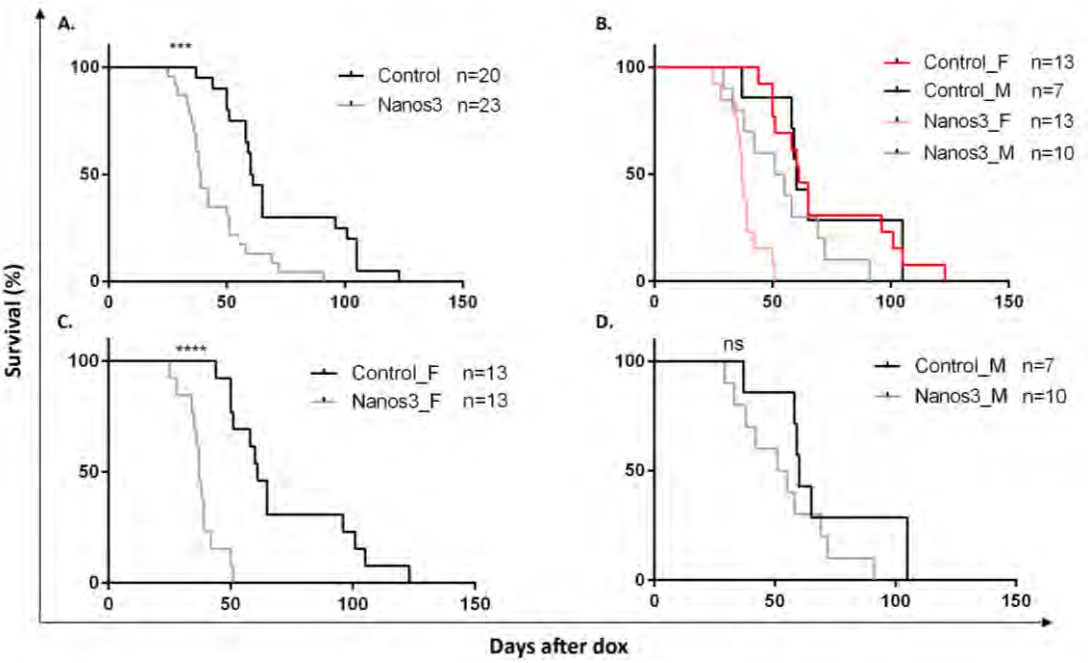

Figure 3.10. Kaplan-Meier curves for the KRas^{G12D};p53$^{-/-}$ lung cancer model (model #3) with and without ectopic Nanos3 expression. Figure legend on the next page.

Figure 3.10. Kaplan-Meier curves for the KRas^{G12D};p53$^{fl/fl}$ lung cancer model (model #3) with and without ectopic Nanos3 expression. A. The survival curves of the control mice compared to the Nanos3-expressing mice. **B.** Subdivision of the female (F) and male (M) control and Nanos3-expressing mice. **C**-**D**. In contrast to the significant difference in survival between female control and Nanos3-expressing mice **(C)**, there is no significant difference in survival between the different male mice **(D)**. All mice were fed doxycycline food to induce transgene expression. Ns: not significant, ***: P≤0.001 and ****: P≤0.0001.

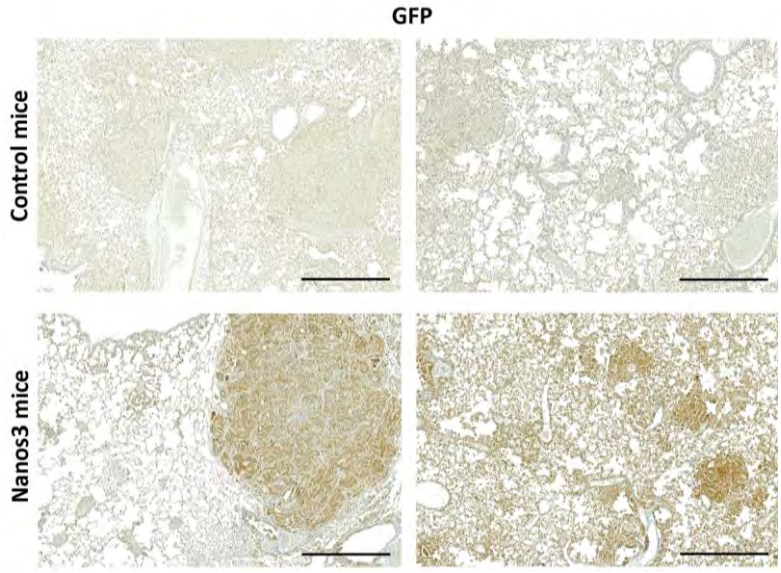

Figure 3.11. GFP expression in the lungs of male transgenic mice. Lung sections from dox-induced control (LSL-KRas^{G12D};p53$^{fl/fl}$;CCSP-rtTA$^{+/-}$;TetO-Cre$^{+/-}$) and Nanos3-expressing mice (Nanos3$^{LSL/-}$;LSL-KRas^{G12D};p53$^{fl/fl}$;CCSP-rtTA$^{+/-}$;TetO-Cre$^{+/-}$) were stained for GFP. Bars: 500 µm.

When comparing both models #2 and #3, Nanos3 mice with expression of the mutant *KRAS* allele died significantly earlier when *TP53* is additionally lost (Figure 3.12). Further experiments were therefore done with female mice from the faster lung model #3.

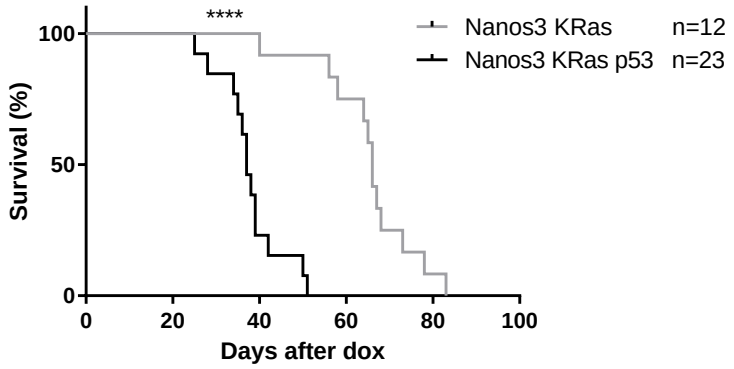

Figure 3.12. Nanos3-expressing mice with lung-specific loss of *TP53* in addition to harboring a *KRAS* mutation died significantly earlier than those that only carry the *KRAS* mutation. Two different mouse models for lung cancer were used, the LSL-KRas^{G12D};CCSP-rtTA$^{+/-}$;TetO-Cre$^{+/-}$ model (model #2), and the LSL-KRas^{G12D};p53$^{fl/fl}$;CCSP-rtTA$^{+/-}$;TetO-Cre$^{+/-}$ model (model #3). The survival curves of dox-induced Nanos3-expressing mice from both models were compared. ****: P≤0.0001.

3.4 Bronchiolar hyperplasia is more pronounced upon ectopic Nanos3 expression

Both control and Nanos3-expressing mice were sacrificed around 40 days after initiation of the dox treatment. Lungs were inflated with 4% PFA resulting in nice sections after paraffin embedding. The lungs were completely sectioned after which H&E staining was done on 5 µm sections throughout the entire lung (Figure 3.13).

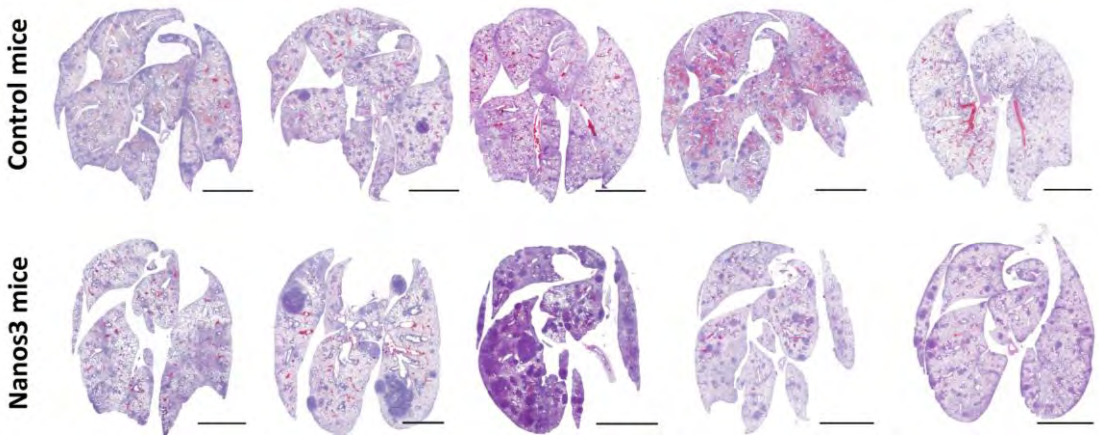

Figure 3.13. H&E staining of the lungs from control and Nanos3 transgenic NSCLC mice, around 40 days after initiation of dox administration. H&E staining was performed on slides of dox-induced control (LSL-KRas^{G12D};p53$^{fl/fl}$;CCSP-rtTA$^{+/-}$;TetO-Cre$^{+/-}$) and Nanos3 (Nanos3$^{LSL/-}$;LSL-KRas^{G12D};p53$^{fl/fl}$;CCSP-rtTA$^{+/-}$;TetO-Cre$^{+/-}$) transgenic mice. Bars: 5 mm.

With the naked eye, we could not distinguish NSCLC mice with or without ectopic Nanos3 expression. Macroscopically, lungs of both mouse genotypes were enlarged compared to those from the corresponding Cre-negative control mice (Nanos3$^{LSL/-}$;LSL-KRas^{G12D};p53$^{fl/fl}$;CCSP-rtTA$^{+/-}$;TetO-Cre$^{-/-}$). Microscopically, different stages of tumor progression were seen (Figure 3.14). Alveolar hyperplasia, premalignant atypical adenomatous hyperplasia (AAH) and adenocarcinoma were observed in the alveolar spaces (Figure 3.14A-C and F-H). Focal and papillary hyperplasia were observed at the bronchioles (Figure 3.14D-E and I-J). While the lungs of both genotypes of NSCLC mice showed bronchiolar hyperplasia compared to the lungs of Cre-negative control mice, Nanos3-expressing mice showed this more frequently (Figure 3.15). This was quantified by measuring the amount of tumor tissue and dividing this by the perimeter of the bronchiole (Figures 3.15B and 3.16). The latter was readily done by measuring the perimeter of the surrounding smooth muscle layer. Representative sections were used for this. The bronchiolar phenotype was also investigated in younger mice (at 21 days after initiating the dox treatment), and already by then a trend was revealed towards a stronger bronchiolar phenotype in Nanos3-expressing mice compared to control mice (Figure 3.17).

With respect to lung tumor model #2, also here bronchiolar hyperplasia was seen (Figure 3.18). However, the effect of Nanos3 on the bronchiolar hyperplasia was not investigated in these mice. Adenocarcinomas were rather rare in this model, but bronchiolar hyperplasia was widespread over the complete lung.

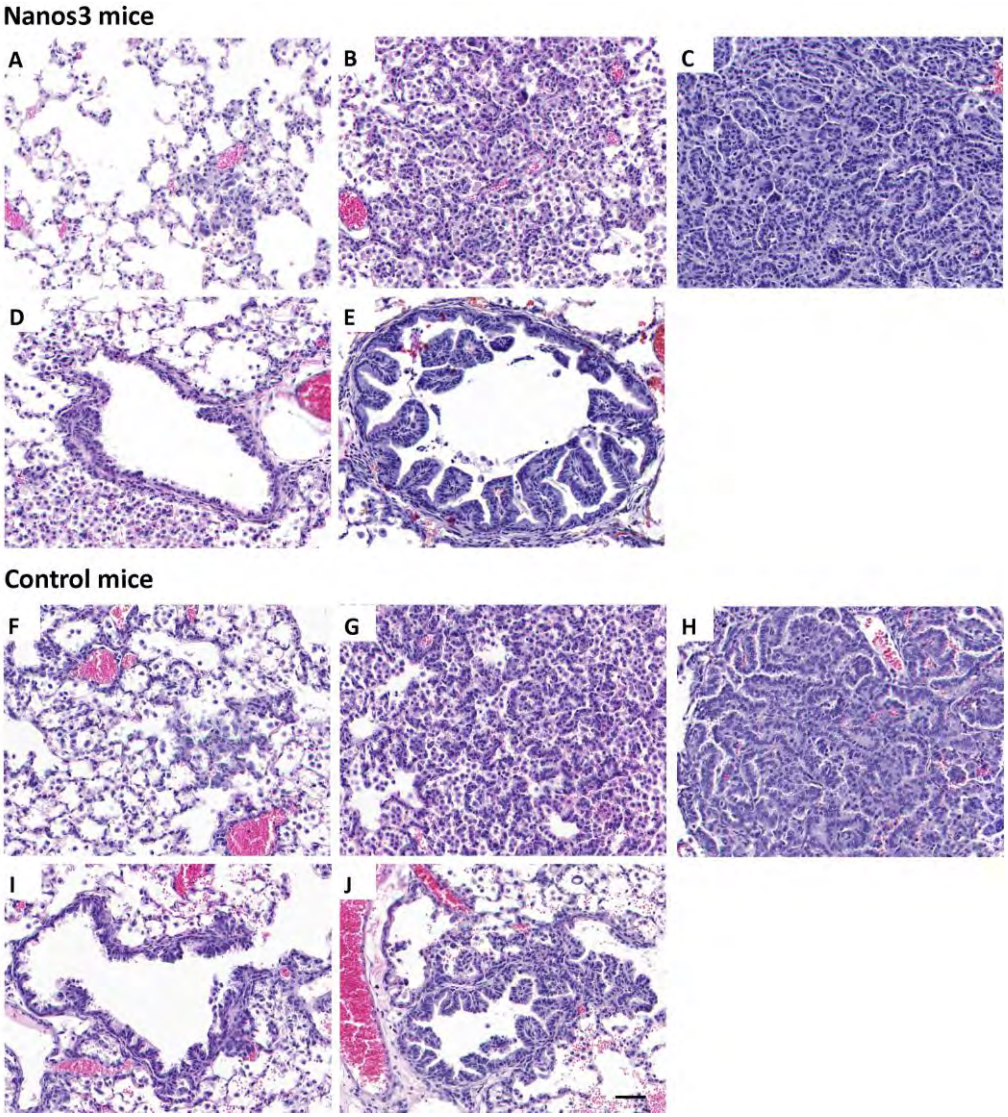

Figure 3.14. Lung tumor initiation and formation in NSCLC mice. Microscopic pictures of H&E stained sections from dox-induced Nanos3-expressing (Nanos3$^{LSL/-}$;LSL-KRas^{G12D};p53$^{fl/fl}$;CCSP-rtTA$^{+/-}$;TetO-Cre$^{+/-}$) **(A-E)** and control (LSL-KRas^{G12D};p53$^{fl/fl}$;CCSP-rtTA$^{+/-}$;TetO-Cre$^{+/-}$) **(F-J)** NSCLC mice. These show alveolar hyperplasia **(A** and **F)**, atypical adenomatous hyperplasia **(B** and **G)** and adenocarcinoma formation **(C** and **H)**. At the bronchioles, focal hyperplasia **(D** and **I)** and papillary hyperplasia **(E** and **J)** of bronchiolar epithelial cells is seen. Bar: 50 µm.

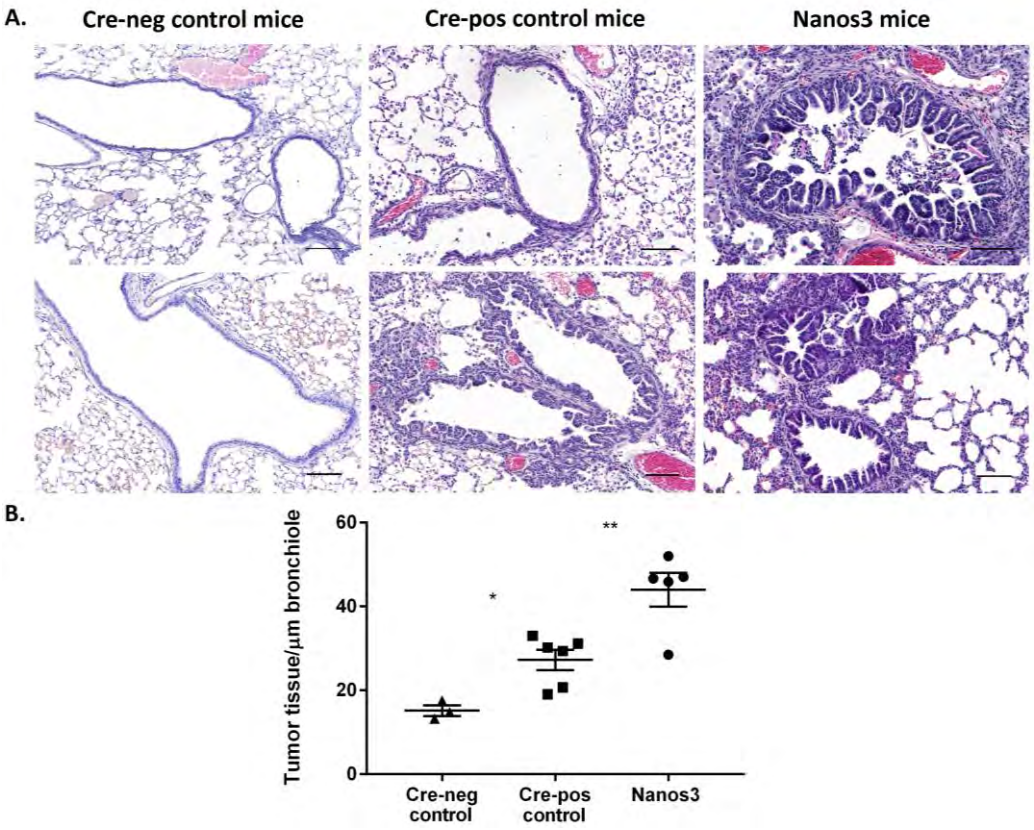

Figure 3.15. Nanos3 expression aggravates bronchiolar hyperplasia seen in NSCLC mice. A. After dox induction, our mouse model for NSCLC shows bronchiolar hyperplasia compared to Cre-negative control mice. Nanos3 overexpression enhances this bronchiolar phenotype. Representative sections are shown. **B.** Three Cre-negative control mice (Nanos3$^{LSL/-}$;LSL-KRas^{G12D};p53$^{fl/fl}$;CCSP-rtTA$^{+/-}$;TetO-Cre$^{-/-}$) and five Cre-positive control (LSL-KRas^{G12D};p53$^{fl/fl}$;CCSP-rtTA$^{+/-}$;TetO-Cre$^{+/-}$) and Nanos3 (Nanos3$^{LSL/-}$;LSL-KRas^{G12D};p53$^{fl/fl}$;CCSP-rtTA$^{+/-}$;TetO-Cre$^{+/-}$) mice were analyzed. The ratio of bronchiolar tumor tissue *versus* the perimeter of the bronchiole was measured for four bronchioles per mouse. The average per mouse is plotted in this figure. Error bars, SEM; *: P≤0.05 and **: P≤0.01. Bars: 100 µm.

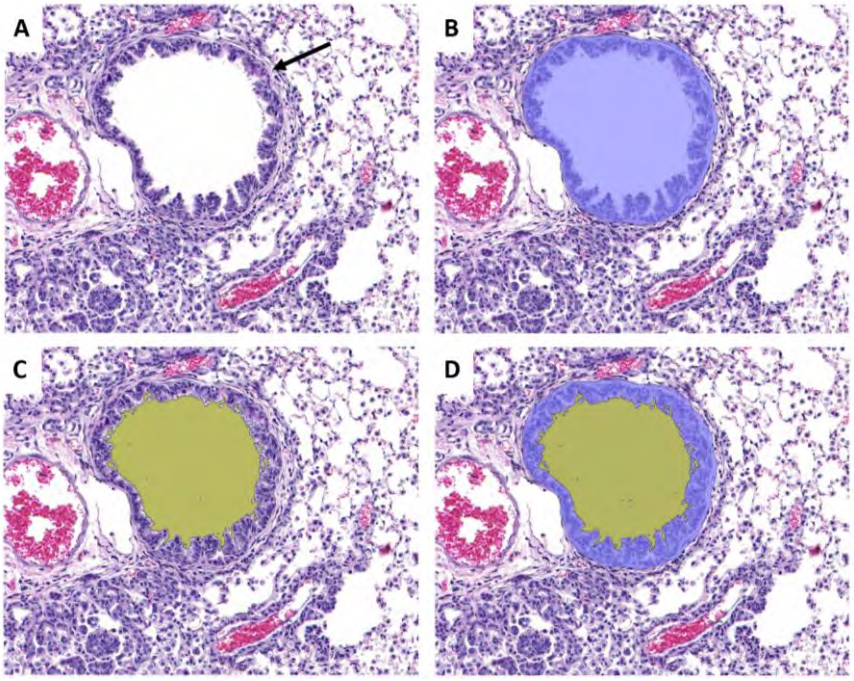

Figure 3.16. Procedure followed to measure the extent of bronchiolar hyperplasia. A. A picture of a bronchiole used for quantification of bronchiolar hyperplasia. The arrow points to the perimeter which was followed to obtain the complete surface area of the bronchiole, depicted in blue in **B**. **C.** The inside of the bronchiole (yellow) was measured using the magic wand ROI tool in Volocity. **D.** Subtracting the area obtained in C from the one obtained in B gives us the area of the bronchiolar hyperplasia (in blue).

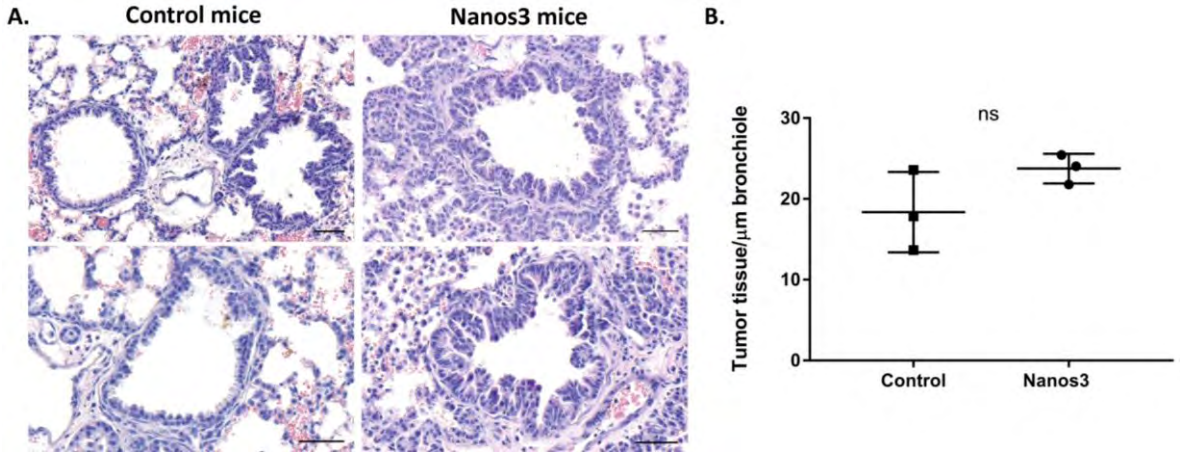

Figure 3.17. At younger age there is already a tendency towards a more advanced bronchiolar phenotype in the Nanos3 mice compared to the control mice. A. Pictures of H&E stained bronchioles from dox-induced control (LSL-KRas^{G12D};p53$^{fl/fl}$;CCSP-rtTA$^{+/-}$;TetO-Cre$^{+/-}$) and Nanos3 (Nanos3$^{LSL/-}$;LSL-KRas^{G12D};p53$^{fl/fl}$;CCSP-rtTA$^{+/-}$;TetO-Cre$^{+/-}$) mice, 21 days after dox treatment**.** Bars: 50 µm. **B.** Quantification of bronchiolar hyperplasia**.** Ns: not significant, P>0.05. Error bars, SEM; n=3.

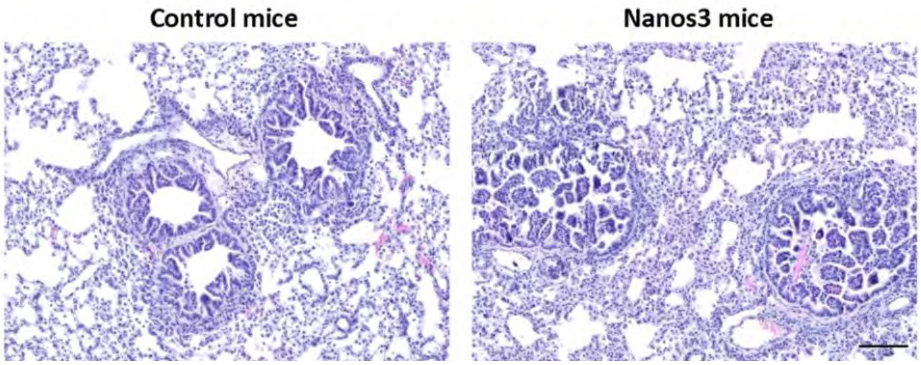

Figure 3.18. Bronchiolar hyperplasia in mice with mutant KRas expression (mouse model #2) with or without ectopic Nanos3 expression. H&E staining of the lungs of a dox-induced control (LSL-KRas^{G12D};CCSP-rtTA$^{+/-}$;TetO-Cre$^{+/-}$) and Nanos3 mouse (Nanos3$^{LSL/-}$;LSL-KRas^{G12D};CCSP-rtTA$^{+/-}$;TetO-Cre$^{+/-}$) of the KRas^{G12D} lung model. Bar: 100 µm.

At first sight it also seemed that the alveolar tumors were more prominent in the Nanos3-expressing mice compared to the control NSCLC mice (Figure 3.13). A preliminary experiment using Indian ink to visualize the lung tumors *ex vivo* showed more white, ink-impenetrable tumor tissue in the Nanos3-expressing lungs compared to control lungs (Figure 3.19). This experiment also suggested a difference between mice carrying one or two *TP53* alleles. However, when using the H&E slides for quantification of the tumor mass (see Materials and methods section 3.9), no significant difference between both genotypes was observed (Figure 3.20).

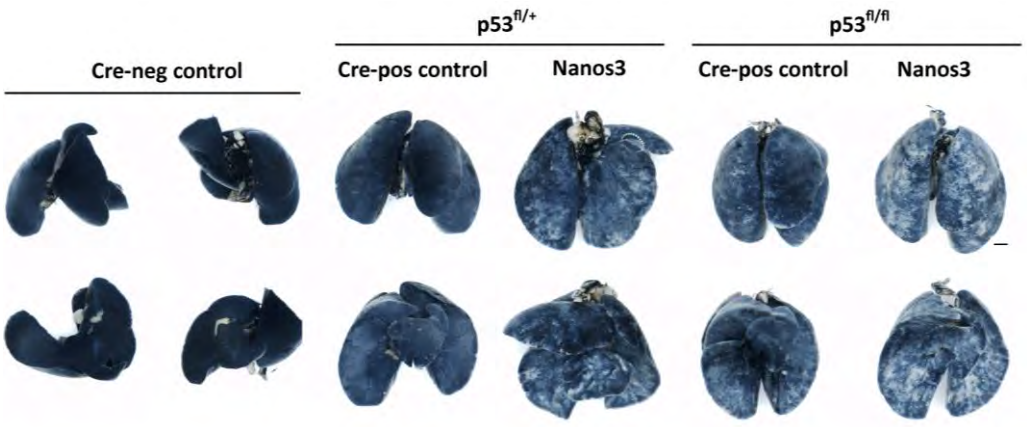

Figure 3.19. Indian ink staining shows more tumor tissue in the Nanos3-expressing lungs. The lungs were perfused with Indian ink and washed in Fekete's solution. The lungs of dox-induced Cre-negative control, Cre-positive control (LSL-KRas^{G12D};p53$^{fl/+}$;CCSP-rtTA$^{+/-}$;TetO-Cre$^{+/-}$ and LSL-KRas^{G12D};p53$^{fl/fl}$;CCSP-rtTA$^{+/-}$;TetO-Cre$^{+/-}$) and Nanos3 mice (Nanos3$^{LSL/-}$;LSL-KRas^{G12D};p53$^{fl/+}$;CCSP-rtTA$^{+/-}$;TetO-Cre$^{+/-}$ and Nanos3$^{LSL/-}$;LSL-KRas^{G12D};p53$^{fl/fl}$;CCSP-rtTA$^{+/-}$;TetO-Cre$^{+/-}$) were analyzed. Bar: 2 mm.

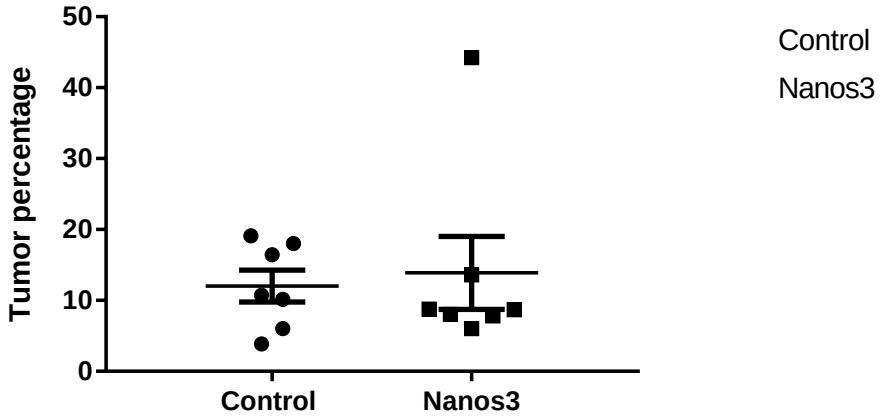

Figure 3.20. The tumor percentage between control and Nanos3 NSCLC mice is comparable. Five H&E sections throughout the complete lungs of dox-induced control (LSL-KRas^{G12D};p53$^{fl/fl}$;CCSP-rtTA$^{+/-}$;TetO-Cre$^{+/-}$) and Nanos3 mice (Nanos3$^{LSL/-}$;LSL-KRas^{G12D};p53$^{fl/fl}$;CCSP-rtTA$^{+/-}$;TetO-Cre$^{+/-}$) were used for quantification of the tumor mass. Quantification was done with ImageJ. Error bars, SEM.

3.5 Mitotic activity in tumors from NSCLC mice with and without Nanos3 expression

Besides the difference in hyperplasia of the bronchioles, our collaborator Prof. Dr. Birembaut (INSERM UMRS 903, Reims), a lung tumor specialist, observed more cellular atypias in tumors from the Nanos3-expressing mice compared to those of the control mice (Figure 3.21). This could be due to more mitotic activity, which was checked by staining for the proliferation markers Ki67 and phospho-histone H3 (pH3) (Figure 3.22). However, quantification of these proliferating cells revealed no significant differences between the lungs of control and Nanos3-expressing NSCLC mice (Figure 3.23). More Ki67-positive than pH3-positive cells were detected. This is in accordance with the fact that Ki67 is expressed in all stages of the cell cycle [13] while pH3 is more specifically expressed in late G2 and mitosis [14].

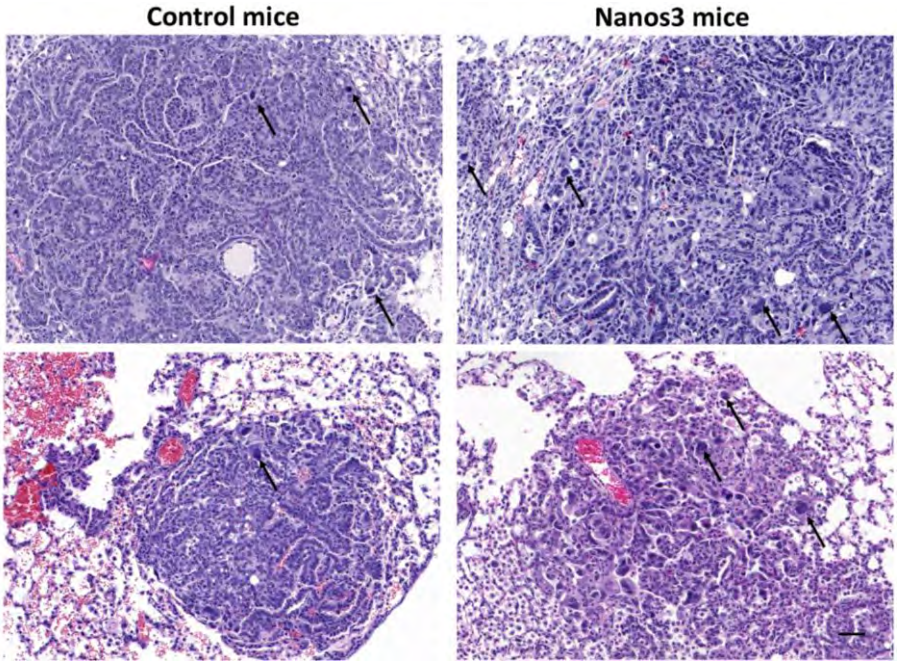

Figure 3.21. Lung tumors from both control and Nanos3-expressing transgenic mice contain tumor cells with irregular nuclei. H&E stainings of lung sections from both dox-induced control (LSL-KRas^{G12D};p53$^{fl/fl}$;CCSP-rtTA$^{+/-}$;TetO-Cre$^{+/-}$) and Nanos3 (Nanos3$^{LSL/-}$;LSL-KRas^{G12D};p53$^{fl/fl}$;CCSP-rtTA$^{+/-}$;TetO-Cre$^{+/-}$) mice. Arrows, atypical cells; bar, 50 µm.

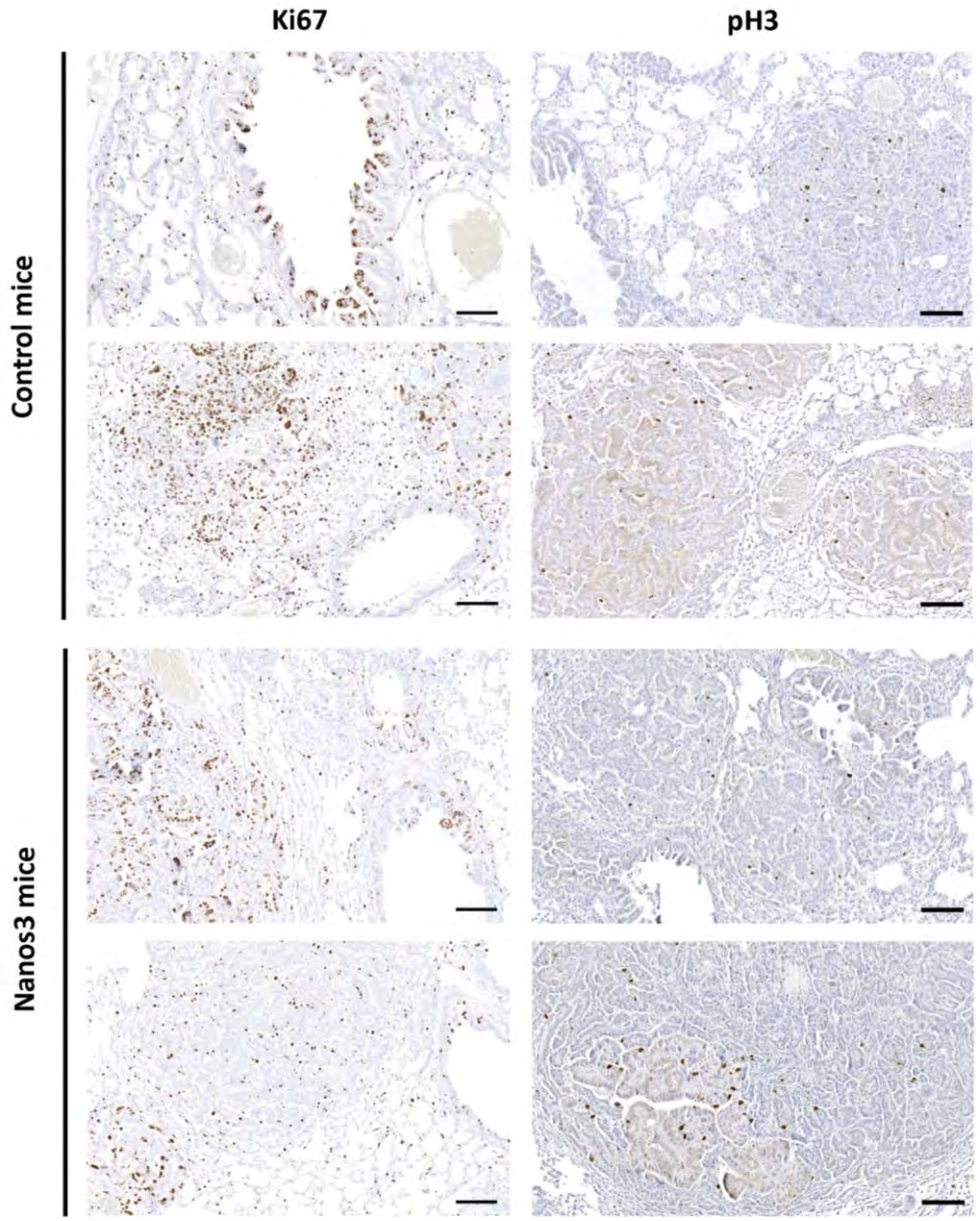

Figure 3.22. Ki67 (A) and pH3 (B) staining of lung sections from control mice and Nanos3 NSCLC mice. Immunohistochemical staining of lung sections from both dox-induced control (LSL-KRas^{G12D};p53$^{fl/fl}$;CCSP-rtTA$^{+/-}$;TetO-Cre$^{+/-}$) and Nanos3 (Nanos3$^{LSL/-}$;LSL-KRas^{G12D};p53$^{fl/fl}$;CCSP-rtTA$^{+/-}$;TetO-Cre$^{+/-}$) mice using a Ki67-specific and phospho-histone H3-specific antibody. Bars: 100 µm.

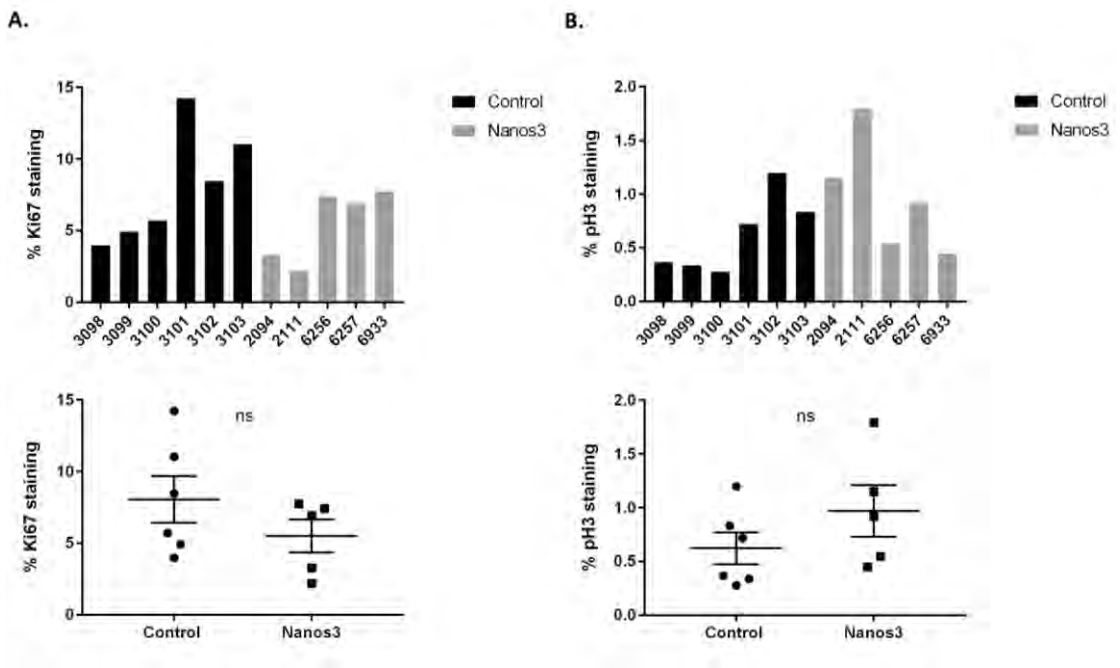

Figure 3.23. The lungs of control and Nanos3-expressing NSCLC mice demonstrate similar levels of proliferation markers. Lung sections from six dox-induced control mice and five dox-induced Nanos3 NSCLC mice were stained for Ki67 (**A**) and pH3 (**B**). Quantification of the stained cells was done with Qupath, see material and methods. Error bars, SEM; ns, not significant.

3.6 Immunohistochemical analysis of the lungs of control and Nanos3-expressing NSCLC mice

Nanos3 was shown to transcriptionally repress E-cadherin expression in lung cancer cell lines [4]. In our model both Nanos3-positive and Nanos3-negative adenocarcinomas showed apparently similar levels of E-cadherin staining (Figure 3.24). E-cadherin expression could therefore not be correlated to Nanos3 expression, contrarily to what was found in the lung cancer cell lines.

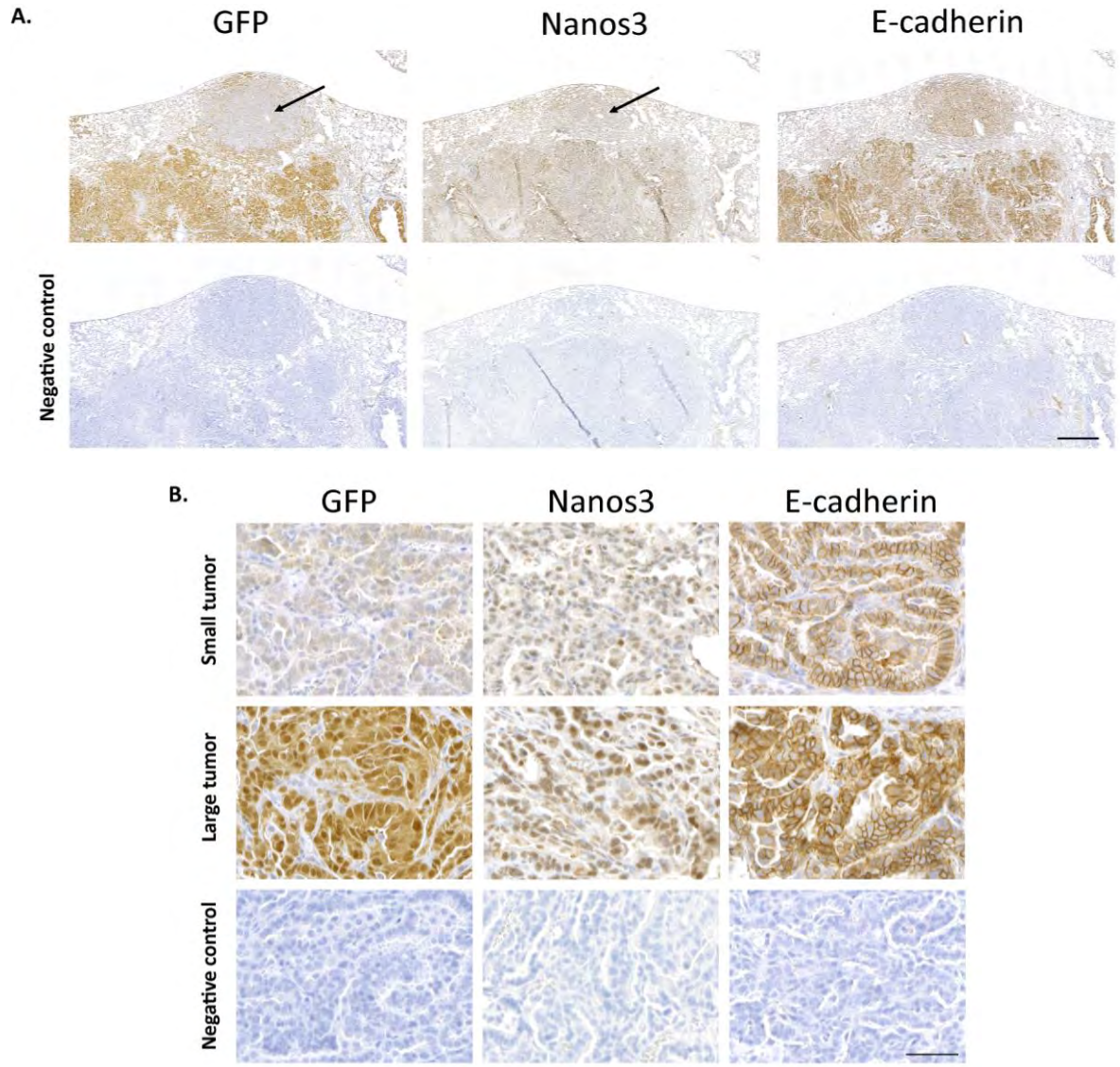

Figure 3.24. E-cadherin expression in Nanos3-positive and Nanos3-negative adenocarcinomas. A. Lung sections of a dox- induced Nanos3$^{LSL/-}$;LSL-KRas^{G12D};p53$^{fl/fl}$;CCSP-rtTA$^{+/-}$;TetO-Cre$^{+/-}$ mouse were stained for GFP, Nanos3 and E-cadherin. Arrow, small tumor lacking GFP and Nanos3 expression; bar, 500 µm. **B.** Magnifications of the small and large tumor shown in A. Bar, 50 µm. The negative controls represent sections only stained with the secondary antibodies.

As can be discerned from Figure 3.24, all alveolar tumors stained positive for E-cadherin at the cell-cell junctions. Also bronchioles, both normal and hyperplastic bronchioles, stained positive for E-cadherin (Figure 3.25). Vimentin expression was mostly absent in these lungs (Figure 3.25).

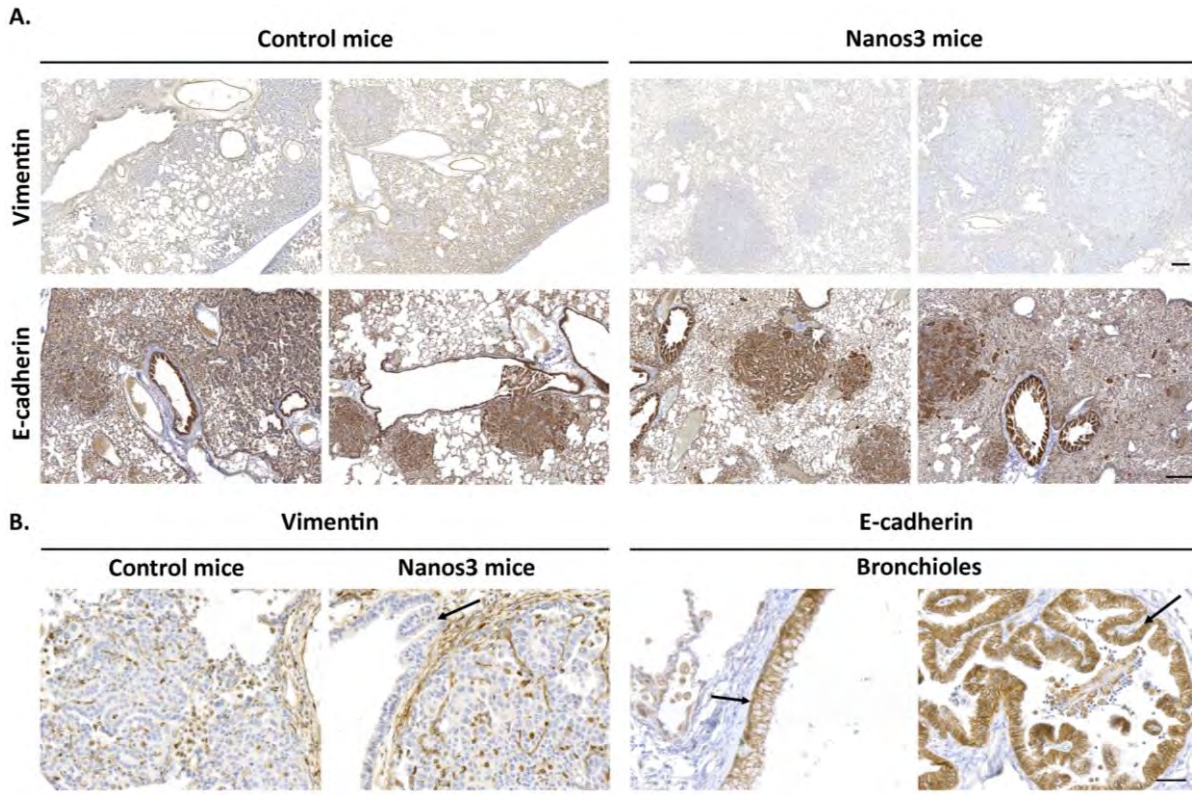

Figure 3.25. Tumor tissue in the lungs of NSCLC mice stains positive for E-cadherin and shows almost no vimentin expression. E-cadherin and vimentin staining of lung sections from dox-induced control (LSL-KRas^{G12D};p53$^{fl/fl}$;CCSP-rtTA$^{+/-}$;TetO-Cre$^{+/-}$) and Nanos3 (Nanos3$^{LSL/-}$;LSL-KRas^{G12D};p53$^{fl/fl}$;CCSP-rtTA$^{+/-}$;TetO-Cre$^{+/-}$) NSCLC mice. **A.** Bars, 200 µm. **B.** Left, magnifications of tumor sections stained with a vimentin-specific antibody showing limited staining of alveolar tumors. Right, magnifications of bronchioles stained with an E-cadherin-specific antibody. Arrows, bronchioles. Bar, 50 µm.

Several immunohistochemical stainings were performed on lung sections of both types of NSCLC mice, with and without Nanos3 expression. Lung sections were for instance stained for Sox2, an epithelial marker of the bronchioles [15], used by us to identify which lesions are derived from transformed CC10-expressing club cells (Figure 3.26). Sox2 is also a cancer stem cell marker [16,17] and is upregulated in carcinomas of different organs [18]. Sox2 expression is associated with a poor prognosis for lung adenocarcinoma patients [19]. As expected the bronchiolar cells were completely stained. In addition, few alveolar tumors showed Sox2-positive cells (Figure 3.26B). When quantifying Sox2-positive cells in alveolar tumors of seven control and seven Nanos3-expressing NSCLC mice (five tumors per mouse) no significant difference was observed between both genotypes (Figure 3.27).

Lung sections were also stained for SPC and CC10, which are markers for AT2 and club cells, respectively. Most bronchiolar cells, from both normal and hyperplastic bronchioles, were CC10-positive and alveolar tumors mostly stained for SPC (Figure 3.28). Immunohistochemical staining for CD44 variant 6 (CD44v6) was also done. High CD44v6 expression is correlated with a poor tumor differentiation, high clinical TNM stage and poor survival of NSCLC patients [20,21]. Both bronchioles and adenocarcinomas in control and Nanos3-expressing NSCLC mice expressed CD44v6, and no significant differences were found between both genotypes (Figure 3.29). In WT mice only the bronchioles showed CD44v6 expression.

Related to the proteome analysis data of several lung cell lines in Chapter 2 (section 2.2.2), expression of spectrin alpha-1 was also analyzed. However no obvious difference between lungs of control and Nanos3 transgenic NSCLC mice were seen (data not shown).

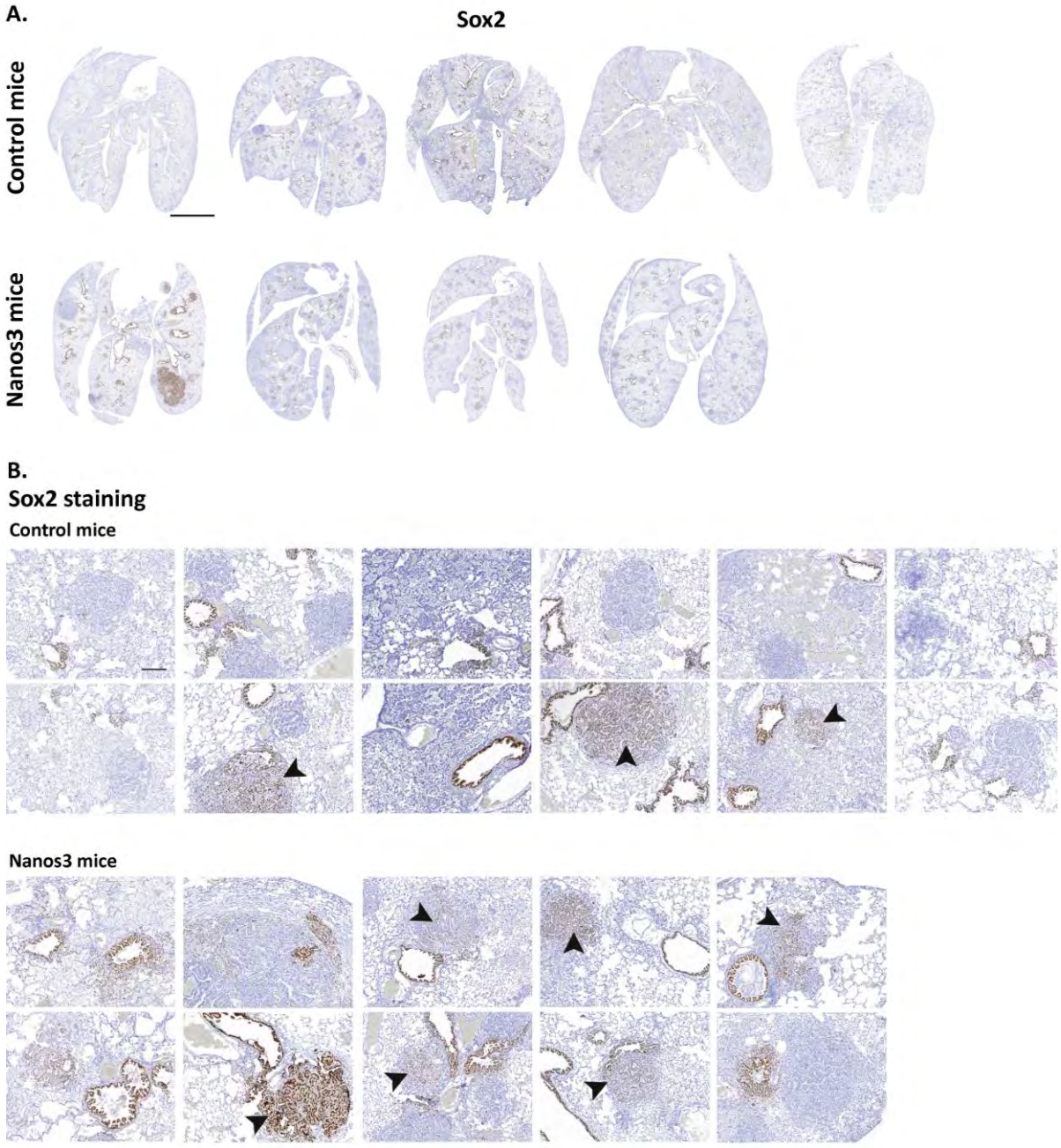

Figure 3.26. Sox2 staining of lungs from NSCLC mice. Lung sections of dox-induced control (LSL-KRas^{G12D};p53$^{fl/fl}$;CCSP-rtTA$^{+/-}$;TetO-Cre$^{+/-}$) and Nanos3 (Nanos3$^{LSL/-}$;LSL-KRas^{G12D};p53$^{fl/fl}$;CCSP-rtTA$^{+/-}$;TetO-Cre$^{+/-}$) mice were stained for Sox2. Arrowhead, Sox2-positive alveolar tumors varying from weak to strong Sox2-staining. **A.** Bar: 5 mm. **B.** Bar: 200 µm

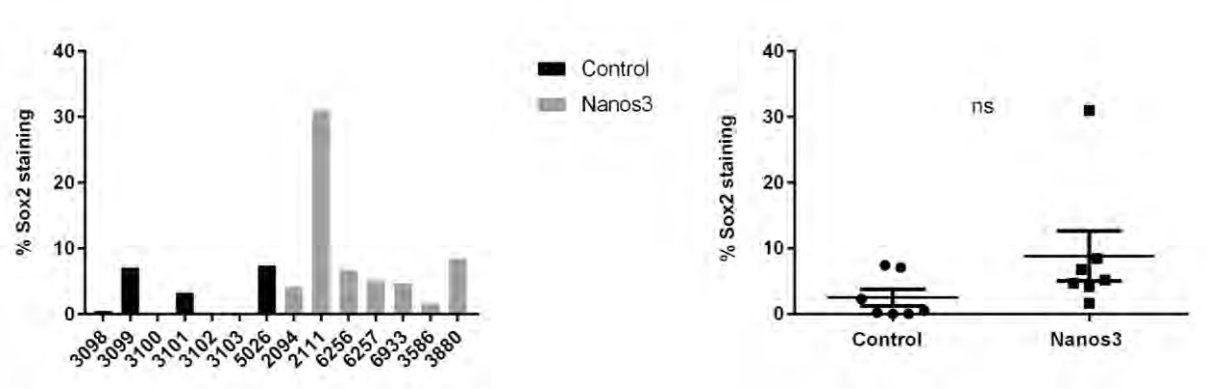

Figure 3.27. Quantification of Sox2 staining in NSCLC mice with and without ectopic Nanos3 expression. Five alveolar tumors per mouse for both dox-induced control (LSL-KRas^{G12D};p53$^{fl/fl}$;CCSP-rtTA$^{+/-}$;TetO-Cre$^{+/-}$) and Nanos3 (Nanos3$^{LSL/-}$;LSL-KRas^{G12D};p53$^{fl/fl}$;CCSP-rtTA$^{+/-}$;TetO-Cre$^{+/-}$) mice were quantified for Sox2-expressing (brown, stained) cells using Qupath. Error bars: SEM; ns, not significant.

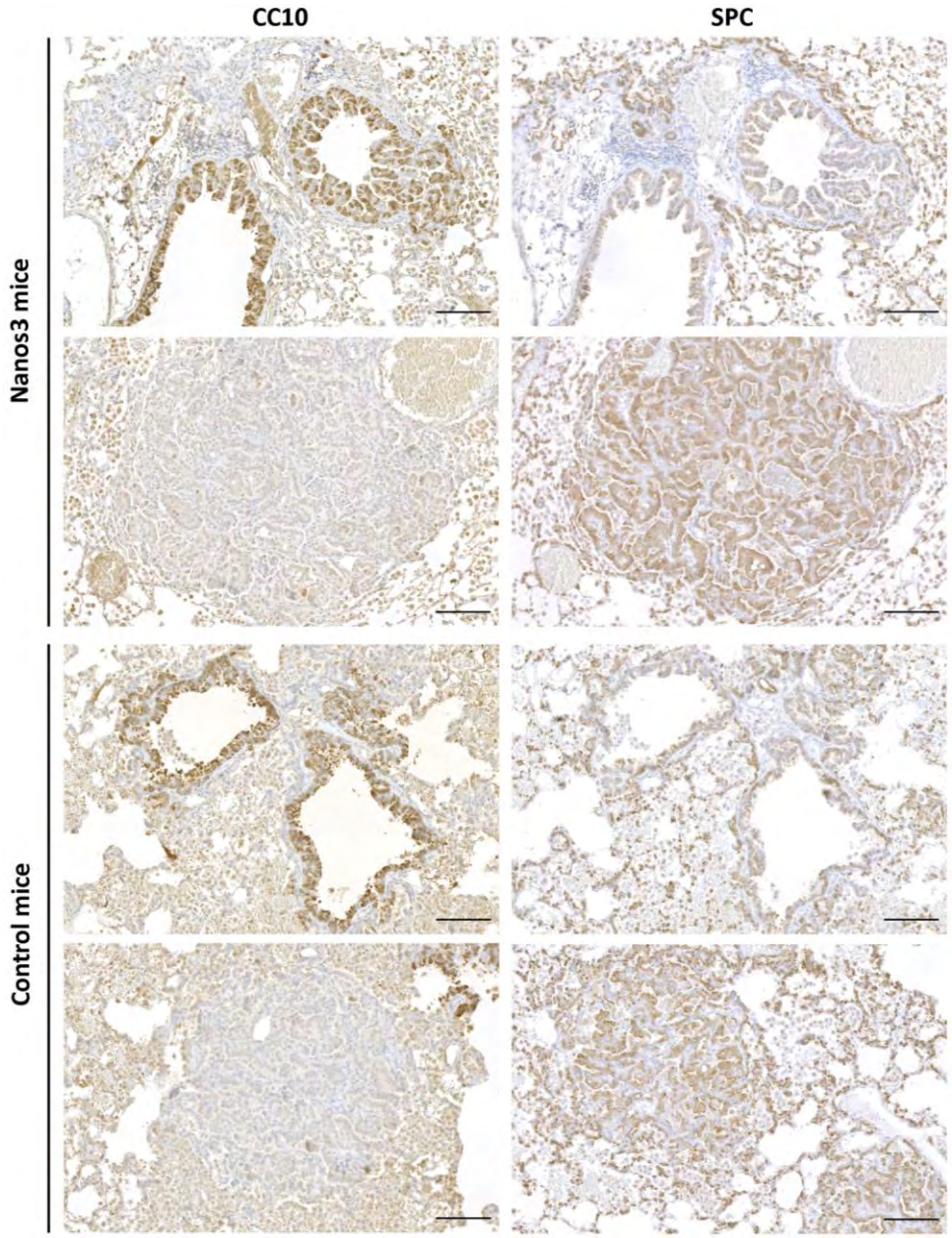

Figure 3.28. Immunohistochemical staining of bronchioles and adenocarcinomas in NSCLC mice. Sections of bronchioles and adenocarcinomas, from dox-induced Nanos3 and control NSCLC mice, were stained for CC10 and SPC. Bars, 100 µm.

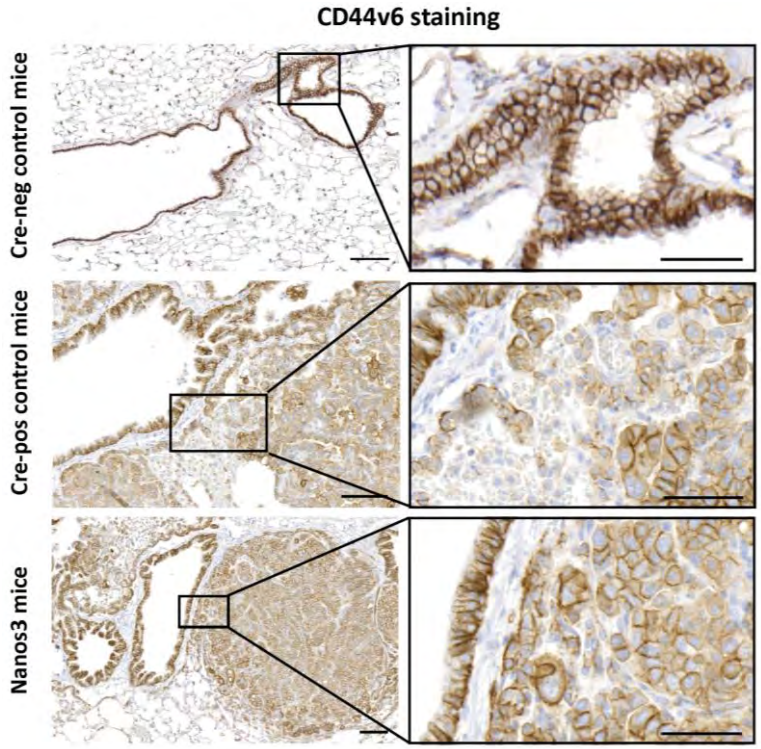

Figure 3.29. Bronchiolar cells and adenocarcinomas from NSCLC mice are CD44v6-positive. Immunohistochemical staining of lung sections of dox-induced Cre-negative control (Nanos3$^{LSL/-}$;LSL-KRas^{G12D};p53$^{fl/fl}$;CCSP-rtTA$^{+/-}$;TetO-Cre$^{-/-}$), Cre-positive control (LSL-KRas^{G12D};p53$^{fl/fl}$;CCSP-rtTA$^{+/-}$;TetO-Cre$^{+/-}$) and Nanos3 (Nanos3$^{LSL/-}$;LSL-KRas^{G12D};p53$^{fl/fl}$;CCSP-rtTA$^{+/-}$;TetO-Cre$^{+/-}$) mice. Bars, 100 µm and 50 µm for the magnifications.

3.7 Primary lung tumor cell lines

Primary cell cultures were established from lung tumors from a control and a Nanos3-expressing mouse (Figure S3.1). From one lung of either genotype, different primary cell lines were obtained, further referred to as LuTDco (lung tumor-derived control) and LuTDNa3 (lung tumor-derived Nanos3), respectively. Nanos3 and GFP protein expression was analyzed in the different primary cell lines (LuTDco: cl3, D5, B3, B5, B6 and B7 and LuTDNa3: E7, D10, G11, F5 and F6) and was indeed only found in those cell lines originating from the Nanos3-expressing lung (Figure 3.30A). RT-qPCR analysis confirmed these results at the mRNA level (Figure 3.30B). Immunofluorescent staining mainly showed cytoplasmic Nanos3 staining (Figure 3.31). β-catenin expression was also investigated since Nanos3 overexpression was previously shown to be paired with β-catenin translocation to the nucleus [22]. This was however not detected in our primary lung tumor cell lines (Figure 3.32). E-cadherin expression was also investigated, however, unlike the expected

downregulation upon Nanos3 overexpression [4], the staining was similar in both LuTDco and LuTDNa3 cell lines (Figure 3.33).

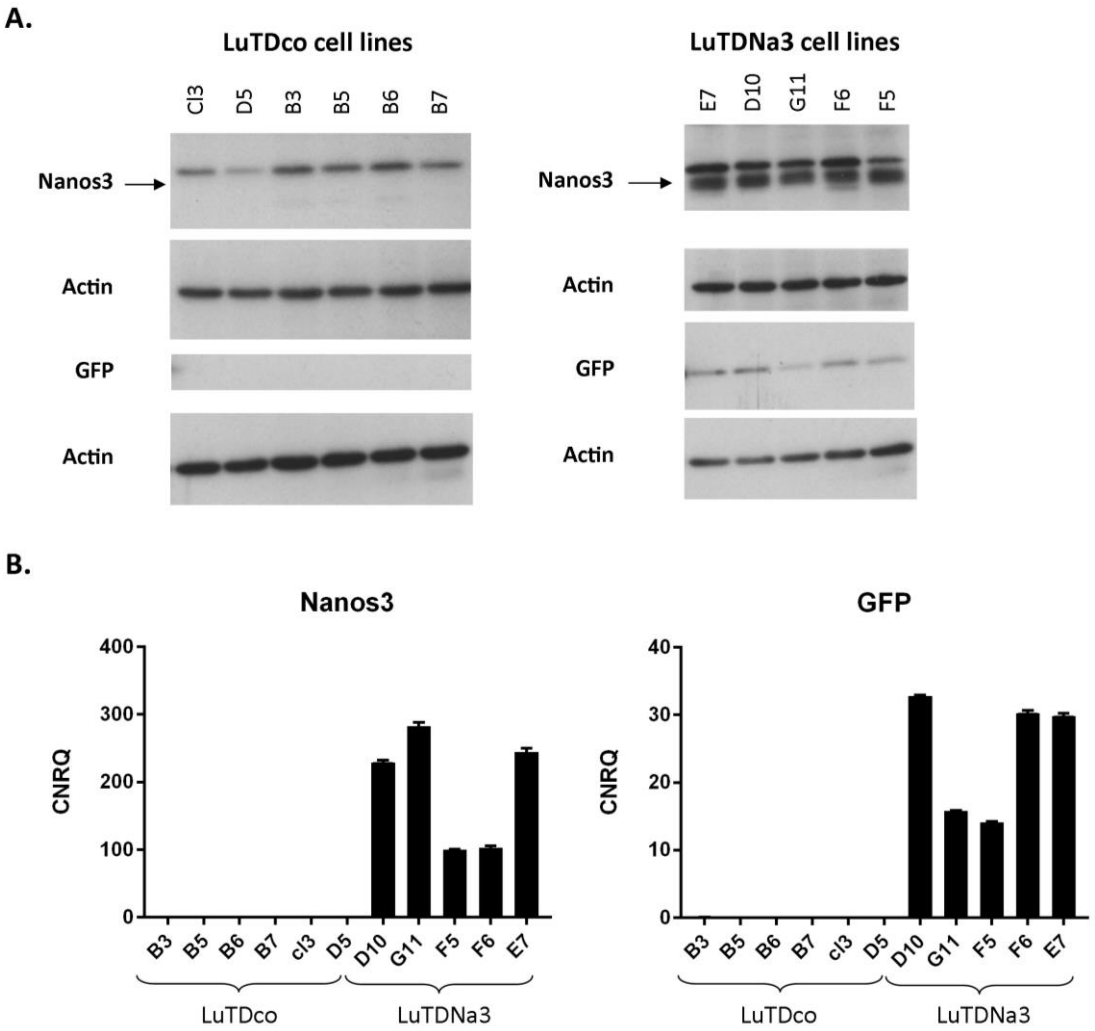

Figure 3.30. Nanos3 and GFP expression of primary lung cancer cell lines. Primary cell lines derived from the lung of either a control (LuTDco) or a Nanos3-expressing mouse (LuTDNa3) were tested for Nanos3 and GFP expression using western blot **(A)** and RT-qPCR **(B)**. Actin was used as a loading control for western blot analysis. CNRQ, calibrated normalized relative quantity, error bars, SEM; n=3.

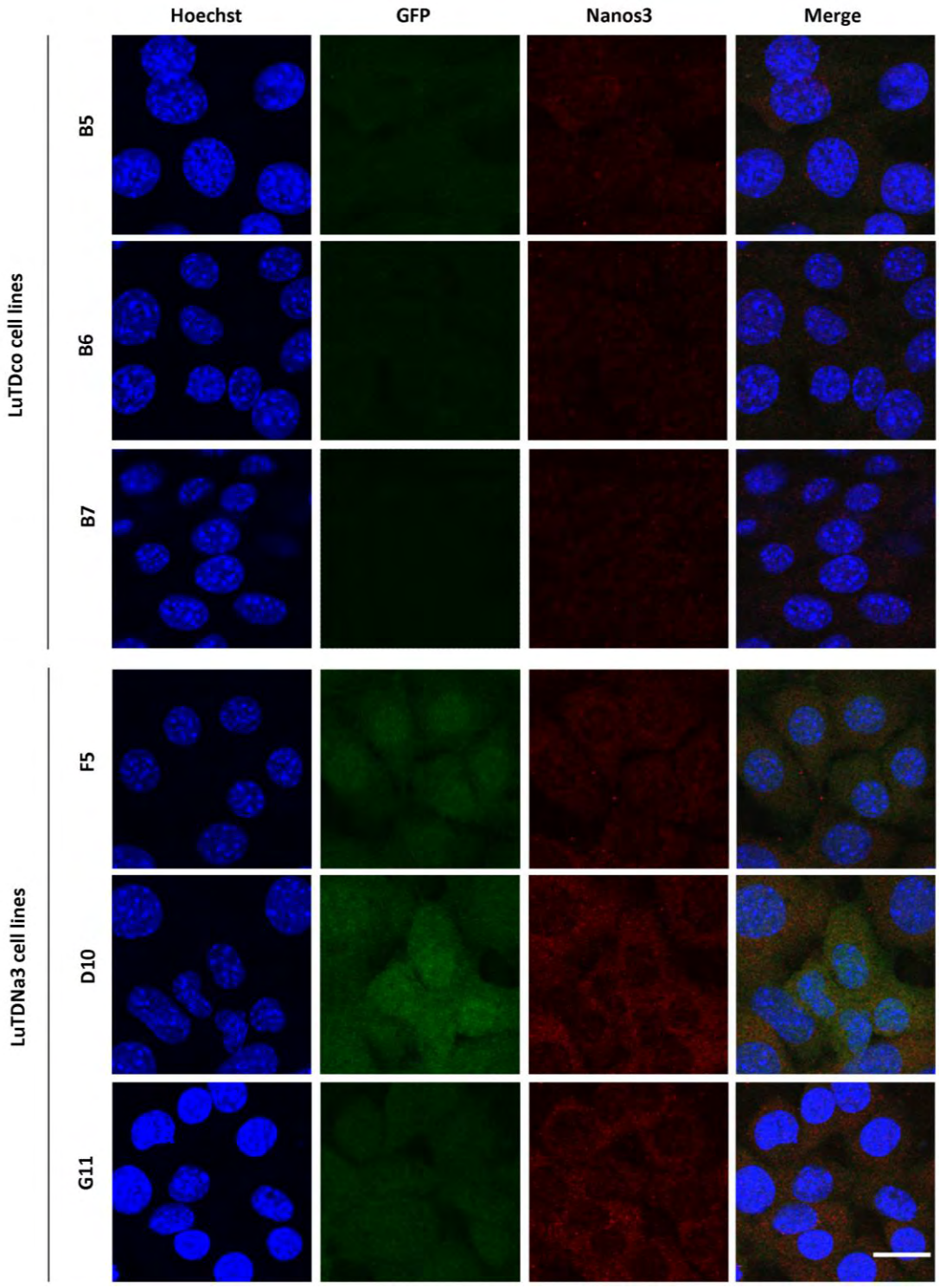

Figure 3.31. Nanos3 and GFP staining in primary lung tumor-derived cells from control and Nanos3 NSCLC mice. Lung tumor-derived cell lines with and without Nanos3 expression, LuTDNa3 and LuTDco cell lines, respectively, were stained with GFP- and Nanos3-specific antibodies. Hoechst 33342 was used as a nuclear stain. Bar, 20 µm.

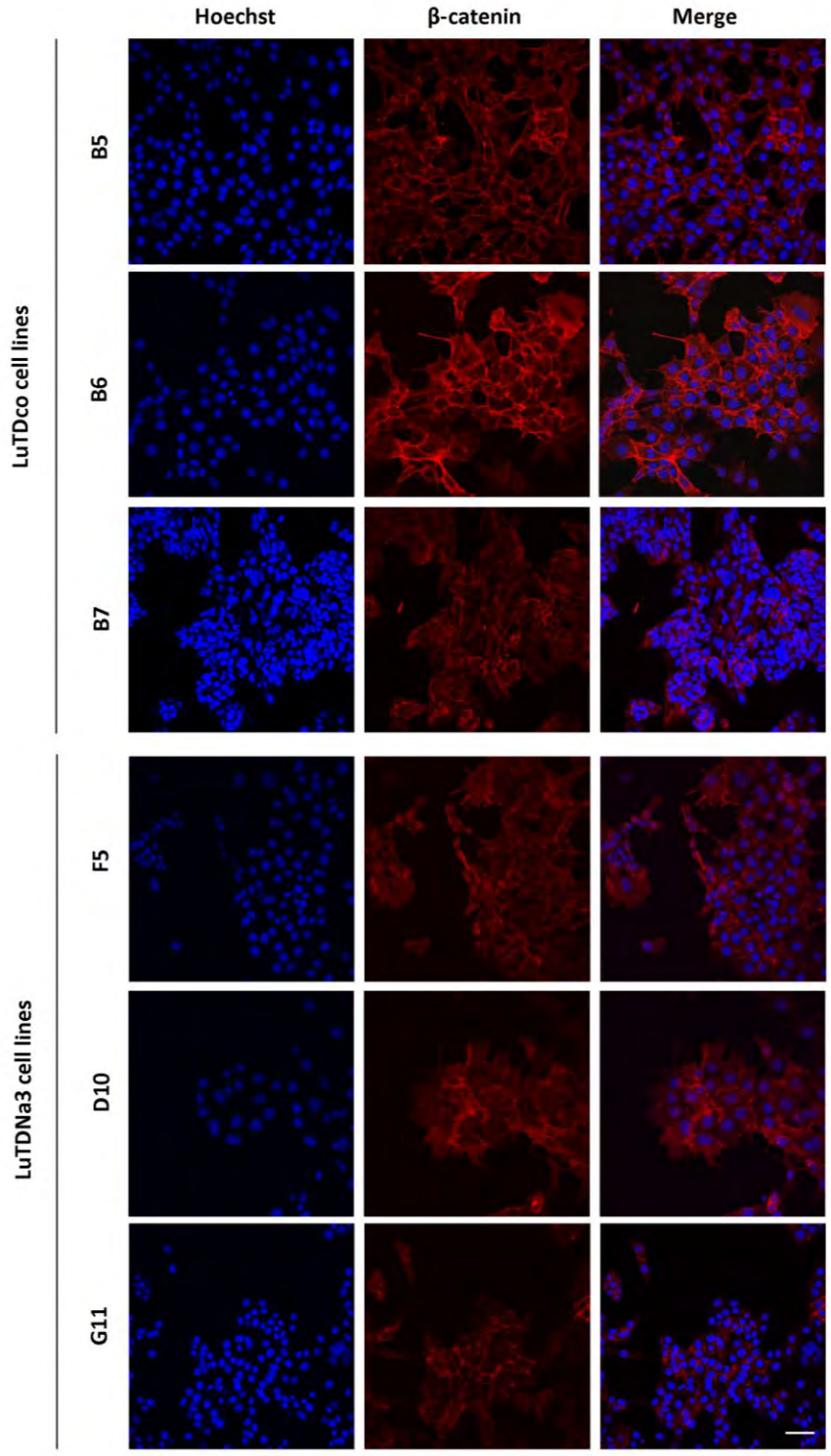

Figure 3.32. β-catenin staining in primary lung tumor-derived cells from control and Nanos3 NSCLC mice. Lung tumor-derived cell lines with and without Nanos3 expression, LuTDNa3 and LuTDco cell lines, respectively, were stained for β-catenin. Hoechst 33342 was used as a nuclear stain. Bar, 50 µm.

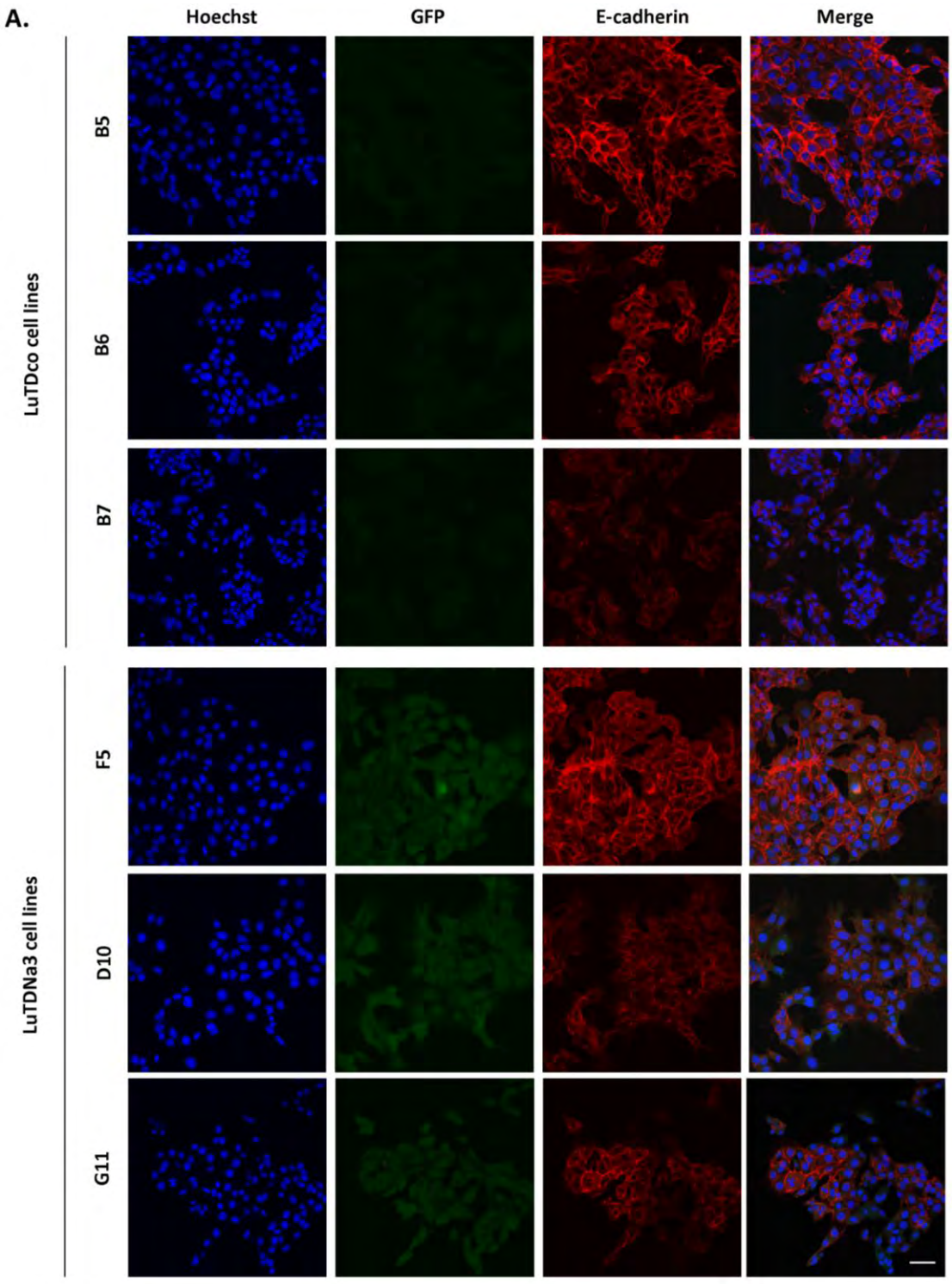

Figure 3.33. Panel A.

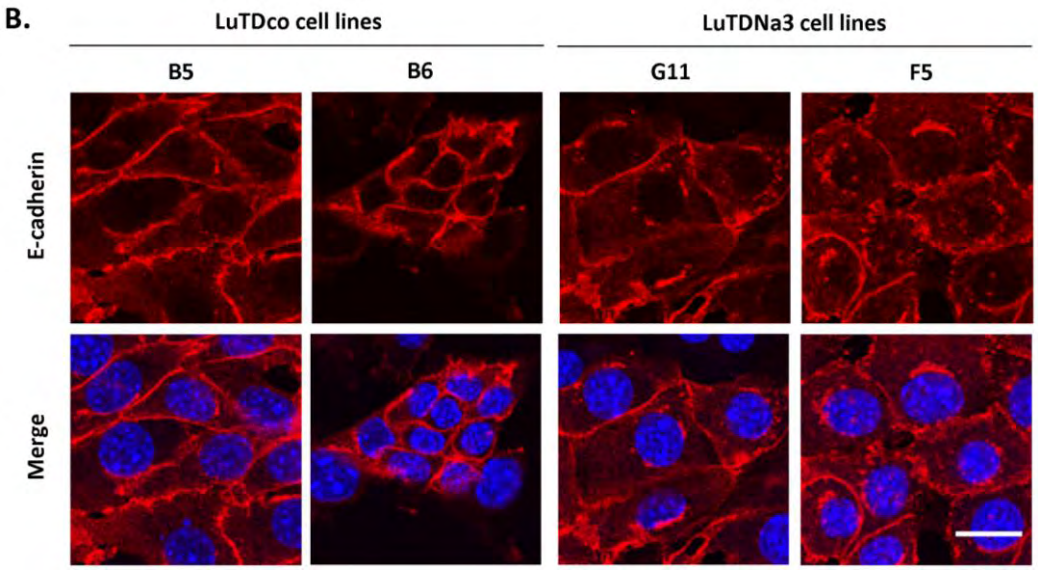

Figure 3.33. E-cadherin expression is expressed in both control and Nanos3-expressing primary lung tumor-derived cell lines. A. Primary lung tumor-derived cell lines with (LuTDNa3: F5, D10 and G11) and without (LuTDco: B5-7) Nanos3 expression were stained by IF using GFP- and E-cadherin-specific antibodies. Hoechst 33342 was used to counterstain nuclei. Bar, 50 µm. **B.** Magnifications of the E-cadherin stainings shown in A. Bar, 20 µm.

3.7.1 Ectopic Nanos3 expression increases anchorage-independent growth of lung tumor cells

A soft agar colony formation assay was used to analyze cellular anchorage-independent growth *in vitro*. Five (E7, D10, G11, F5 and F6) and six (cl3, D5, B3, B5, B6 and B7) primary cell lines from the Nanos3-expressing and the control lung, respectively, were analyzed (Figure 3.34). Compared to the LuTDco cell lines, those from the Nanos3-expressing lung proved to have a higher potential for anchorage-independent growth (Figure 3.35). The parental and N-methyl-N'-nitro-N-nitrosoguanidine (MNNG) transformed HOS (human osteosarcoma) cell lines were taken along as a negative and positive control, respectively. At a dilution of 10^4 cells per ml, the number of colonies and the colony size were significantly higher in those from the Nanos3 mouse. At a lower dilution of 10^5 cells per ml there was merely a trend visible.

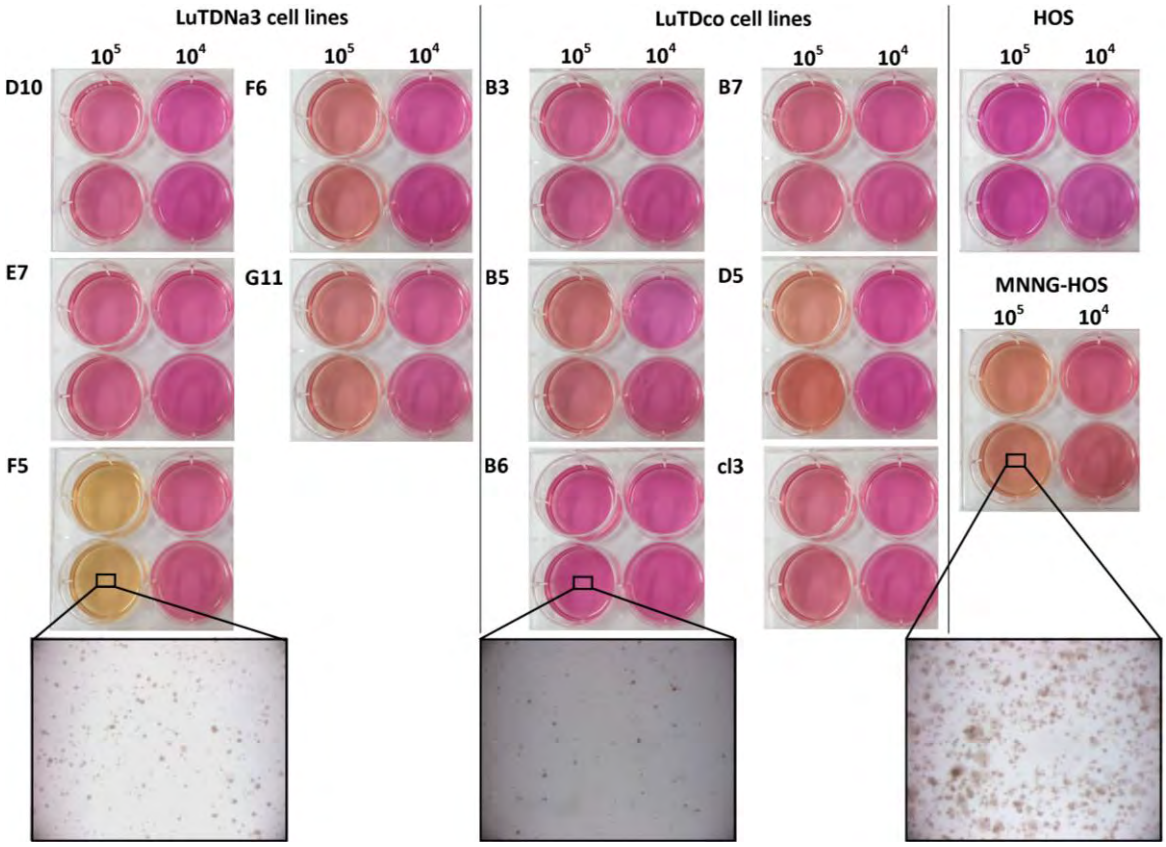

Figure 3.34. Anchorage-independent growth of control and Nanos3-expressing lung tumor-derived cell lines. Primary lung tumor-derived cell lines from mice with (LuTDNa3) or without (LuTDco) transgenic Nanos3 expression were seeded in a soft agar solution in a 6-well plate. This was done in duplicate for two different concentrations (10^4 and 10^5 cells/ml). HOS and MNNG-HOS were used as a negative and positive control, respectively. Pictures were taken after two weeks.

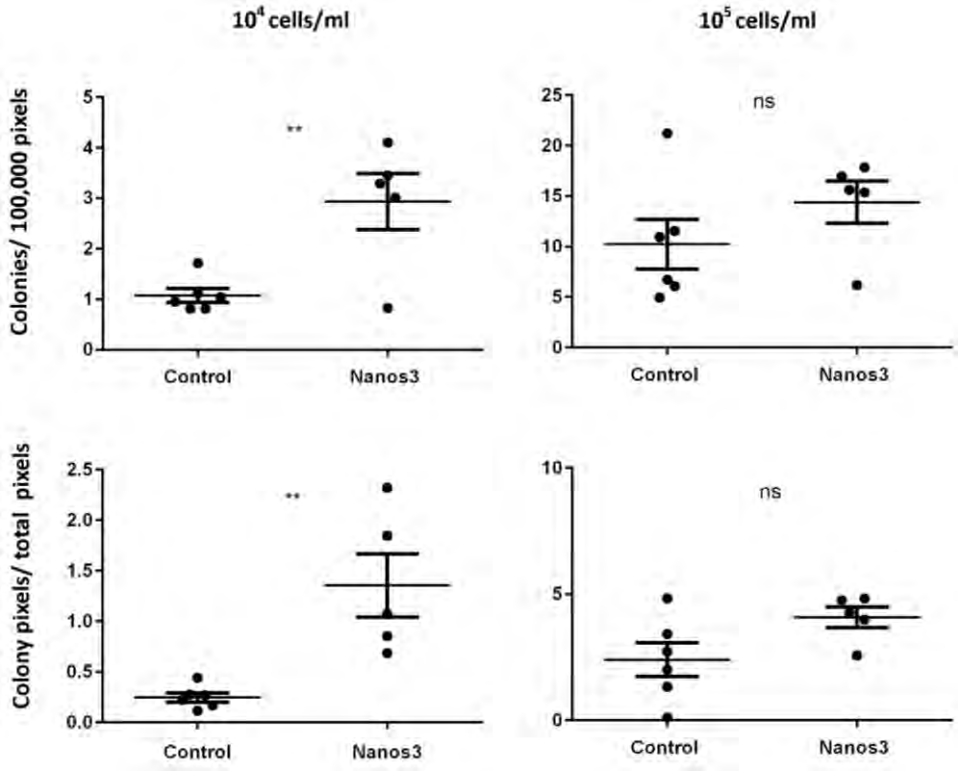

Figure 3.35. Nanos3-expressing lung tumor-derived cells form more and larger colonies in a soft agar assay. Cell lines from a LSL-KRas^{G12D};p53$^{fl/fl}$;CCSP-rtTA$^{+/-}$;TetO-Cre$^{+/-}$ mouse (control) and a Nanos3$^{LSL/-}$;LSL-KRas^{G12D};p53$^{fl/fl}$;CCSP-rtTA$^{+/-}$;TetO-Cre$^{+/-}$ mouse (Nanos3) were grown in a soft agar solution at a dilution of 10^4 or 10^5 cells/ml. Pictures were taken with a Leica microscope and quantified with Volocity. Only colonies bigger than 100 μm^2 were taken into account. Error bars, SEM; ns, not significant and **: P≤0.01.

3.7.2 Ectopic tumor growth analysis of control and Nanos3-expressing lung tumor-derived cell lines

Three primary cell lines originating from either the control or the Nanos3-expressing lung were further used in a mouse allograft experiment. This experiment was performed with the aim of comparing ectopic tumor formation and the potential for accelerated progression to invasive cancer and metastasis between LuTDco and LuTDNa3 cell lines. To this end, the primary lung cell lines were subcutaneously (s.c.) injected into five athymic mice each. Mice injected with one of the three LuTDNa3 cell lines, line G11, showed a clear-cut increase in tumor growth compared to the others (Figure 3.36). In contrast, mice injected with one of the control lung tumor-derived cell lines, line B6, displayed a distinctively slower tumor growth compared to the others. The ectopic tumors (allografts) originating from the other two LuTDNa3 cell lines and two LuTDco cell lines grew at a similar rate.

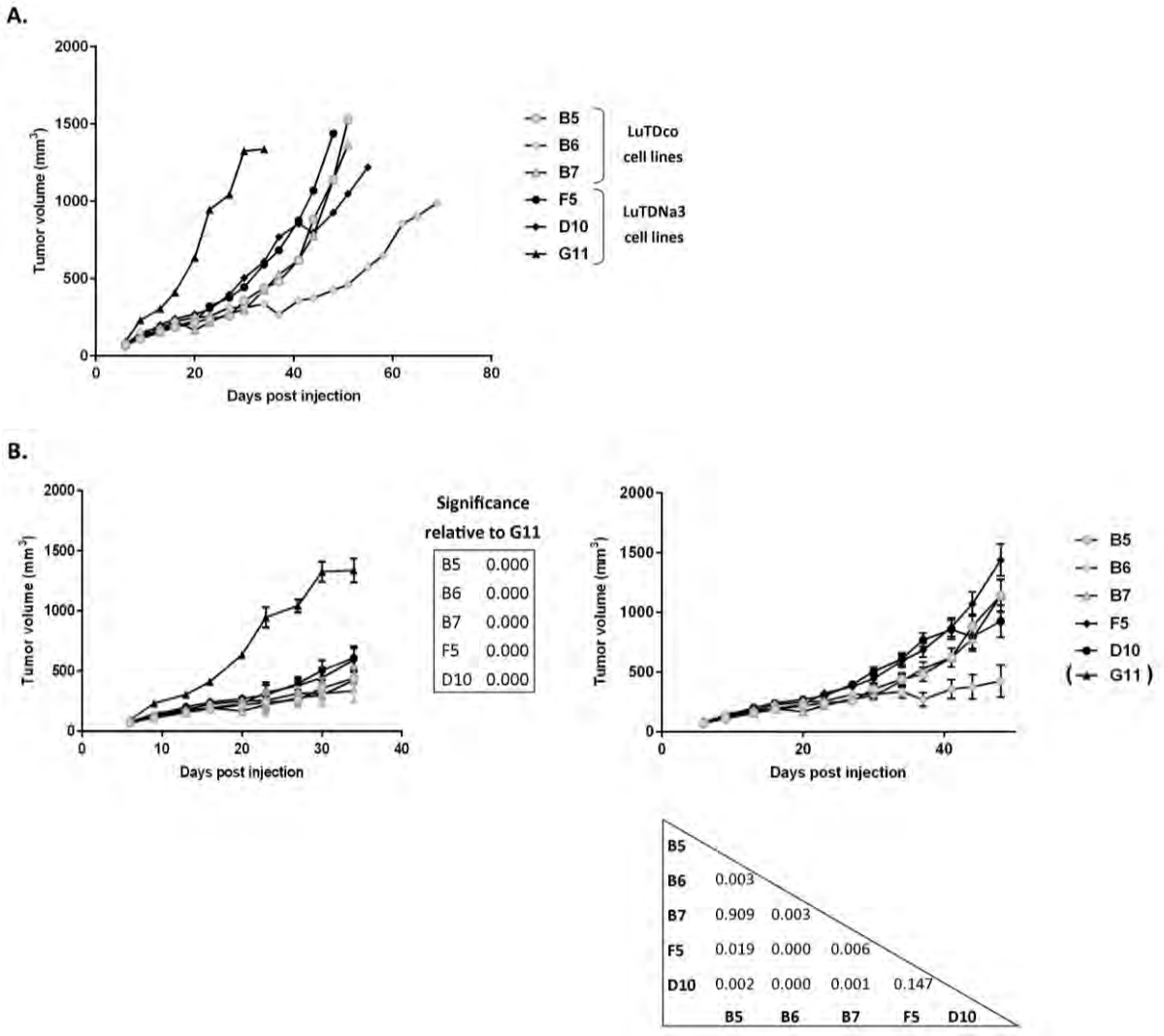

Figure 3.36. Ectopic tumor growth of athymic mice injected with primary lung tumor cell lines. Five athymic mice (M0-4) were subcutaneously injected with 2.5 million cells of a primary cell line from the lung of a control or Nanos3 transgenic mouse (control: LSL-KRas^{G12D};p53$^{fl/fl}$;CCSP-rtTA$^{+/-}$;TetO-Cre$^{+/-}$ and Nanos3: Nanos3$^{LSL/-}$;LSL-KRas^{G12D};p53$^{fl/fl}$;CCSP-rtTA$^{+/-}$;TetO-Cre$^{+/-}$). Tumor volume was measured twice a week. **A.** A graph of all the average tumor growth curves of mice injected with the same cell line. **B.** Mean tumor volume ± SEM (n=5) obtained from repeated measurements analysis of tumor volumes measured in mice in a 34 days period and 48 days period after injection of cell lines. In the latter analysis, the G11 mice were excluded (enclosed in parentheses) since these mice died significantly earlier. P-values refer to the significances of the difference in the change of tumor volume either relative to G11 across the time span of 34 days, or between pairs of cell lines used for injection across the time span of 48 days.

3.7.3 Tumors originating from Nanos3-expressing NSCLC cells show enhanced E-cadherin protein expression levels compared to those from control NSCLC cells

The ectopic tumors were further investigated by western blotting, RT-qPCR and immunohistochemical staining. To minimize variability in results depending on the different parts of the ectopic tumor, the tumor was cut into six fragments with parts from different locations in the tumor to be used for paraffin embedding and protein and RNA experiments (Figure 3.37). H&E staining showed adenocarcinoma tumor formation with some parts of the ectopic tumors from LuTDNa3 cell lines showing tumor differentiation (Figure 3.38). The differentiated tissue observed in tumors from these mice is GFP-positive (Figure 3.39A), CD31-negative (Figure 3.39B), demonstrating that these are neither blood nor lymph vessels, and E-cadherin-positive (Figure 3.39C). Immunohistochemical staining for GFP was only visible in the ectopic tumors from mice injected with LuTDNa3 cell lines (Figure 3.39A).

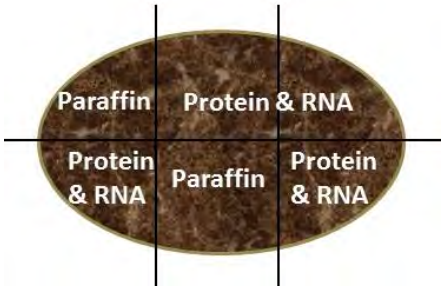

Figure 3.37. Scheme of how the ectopic tumors (allografts) were cut and used in further experiments. The ectopic tumors were cut in six pieces which were used for H&E and immunohistochemical staining and further protein and RNA experiments.

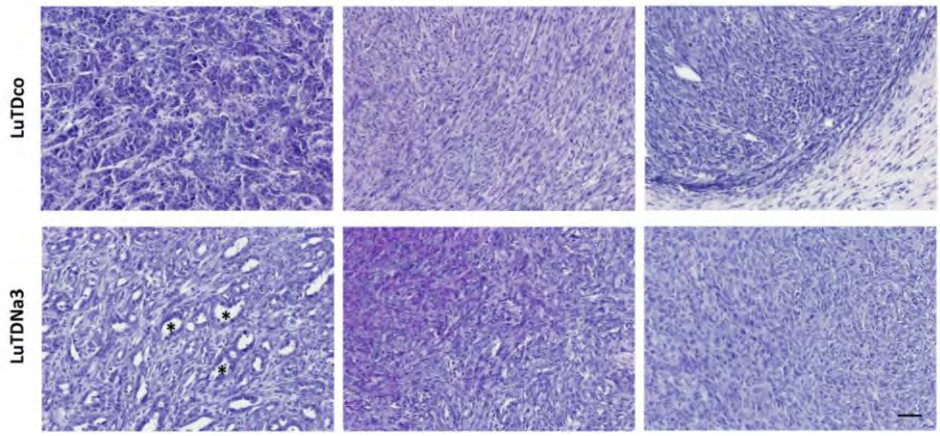

Figure 3.38. H&E pictures of ectopic tumors (allografts) originating from subcutaneous injection of control (LuTDco) and Nanos3 (LuTDNa3) NSCLC cell lines. *, differentiated tissue; bar, 50 µm.

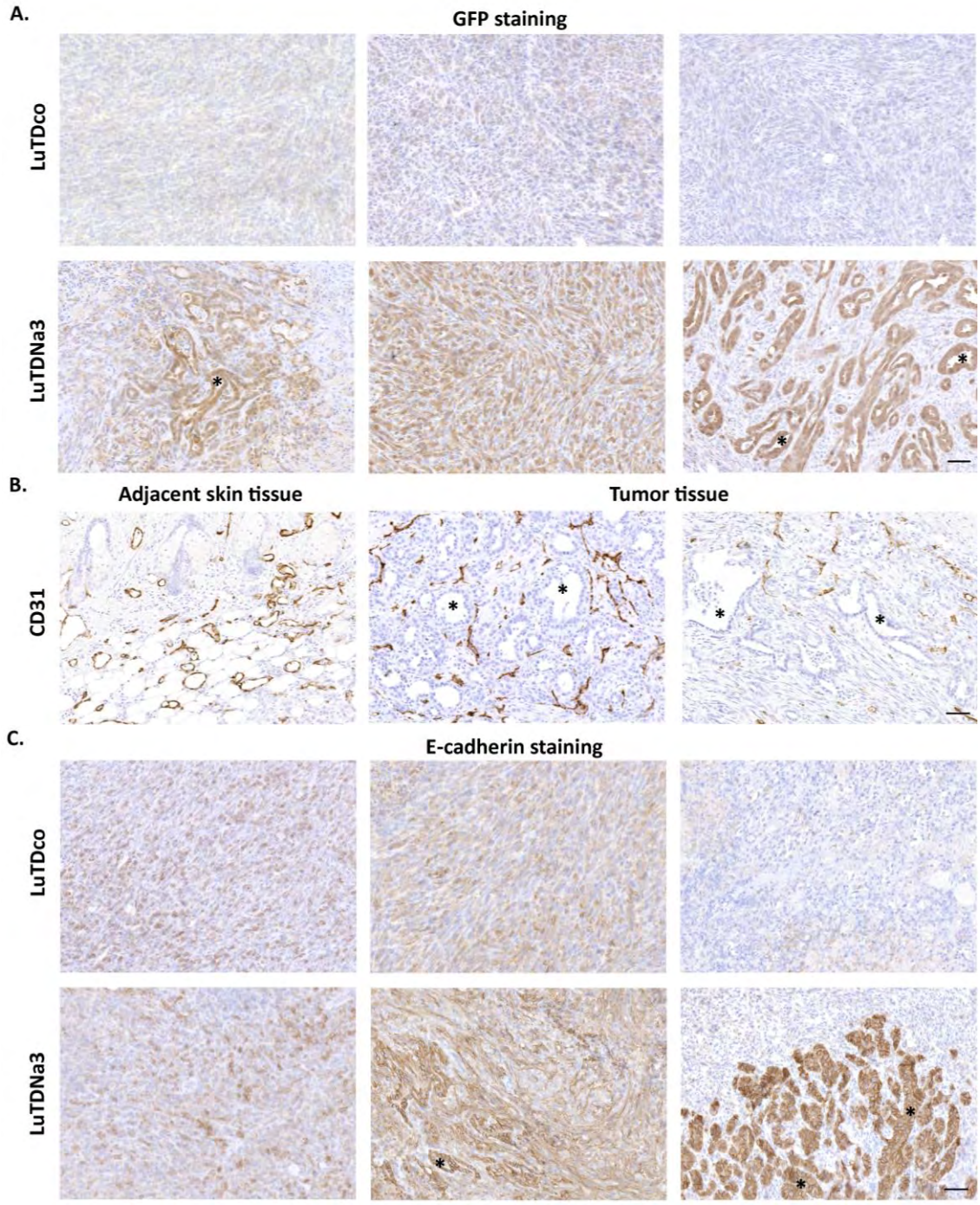

Figure 3.39. The differentiated tissue observed in the tumors from mice injected with LuTDNa3 cell lines was GFP-positive (A), CD31-negative (B) and E-cadherin-positive (C). Tumor sections from ectopic tumors from mice injected with LuTDco and LuTDNa3 cell lines were stained with a GFP-specific **(A)**, CD31-specific **(B)** and E-cadherin-specific **(C)** antibody. In **B** only tumor sections from mice injected with LuTDNa3 cell lines were shown. The differentiated tumor tissue is depicted by the asterisks. Bars, 50 μm.

Similarly, *NANOS3* and *GFP* mRNA expression were clearly detected in the ectopic tumors originating from the LuTDNa3 cell lines and were absent in those from the LuTDco cell lines as expected (Figure 3.40). A difference in Nanos3 protein expression between ectopic tumors from LuTDNa3 line G11 and those from other LuTDNa3s cell lines did not turn out to be the underlying reason for the slower ectopic tumor growth of the latter (Figure 3.41A).

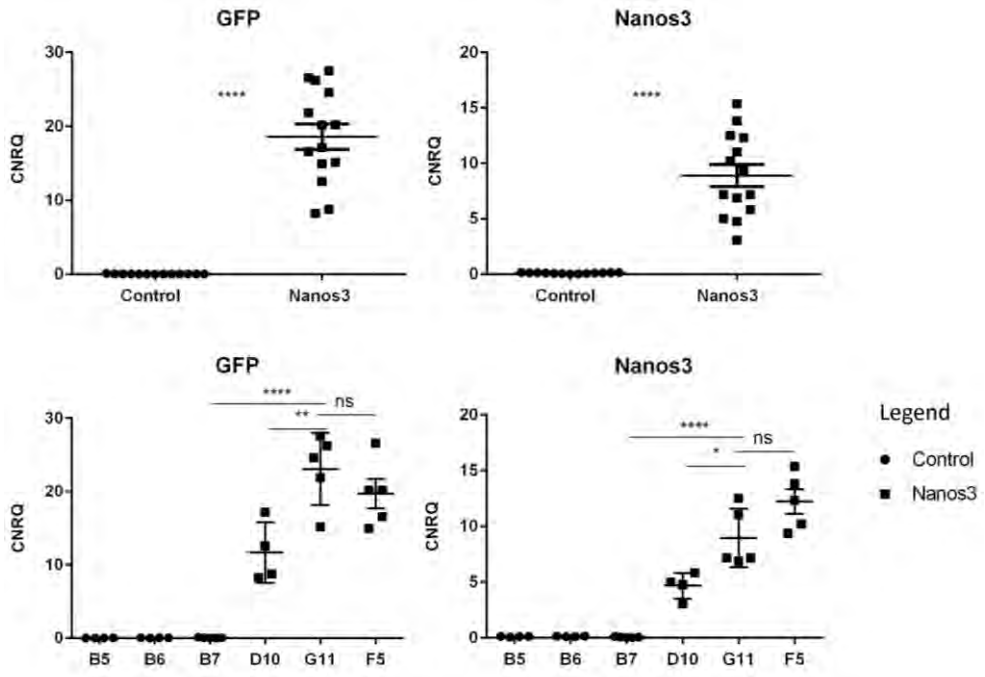

Figure 3.40. Analysis of *GFP* and *NANOS3* mRNA expression in ectopic tumors (allografts) from control and Nanos3-expressing lung tumor-derived cell lines. RNA lysates were made from part of the ectopic tumors originating from Nanos3 and control tumor-derived cell lines. CNRQ, calibrated normalized relative quantity. Error bars, SEM; ns: not significant, *: P≤0.05, **: P≤0.01 and ****: P≤0.0001.

Furthermore, the effect of ectopic Nanos3 expression on E-cadherin expression was examined in these ectopic tumors. Surprisingly, E-cadherin protein expression was found to be significantly higher in those originating from the LuTDNa3 cell lines than those from the LuTDco cell lines (Figure 3.41). This seemed to be regulated at the translational level since E-cadherin mRNA expression was not enriched in all ectopic tumors originating from LuTDNa3 cell lines (Figure 3.42). Ectopic tumors from mice injected with LuTDNa3 cell line F5 were the only ones to show a significantly higher mRNA expression of *CDH1* and *OCLN* (Figure 3.42). This is very surprising given the fact that Nanos3 was previously associated with transcriptional repression of E-cadherin in lung cancer cells [4]. Immunohistochemical

staining of the ectopic tumors with an E-cadherin-specific antibody showed that mainly the differentiated tumor tissue, in the allografts from mice injected with LuTDNa3, stains positive (Figure 3.39C).

Similar differences in E-cadherin expression were not observed in the original LuTD cell lines (Figure 3.33 and Figure 3.43). Fibronectin, a mesenchymal marker, was accordingly decreased in ectopic tumors from LuTDNa3 cell lines compared to those from LuTDco cell lines (Figure 3.44A). Other mesenchymal markers such as vimentin and N-cadherin were also analyzed at the mRNA level (Figure 3.44A). *VIM* mRNA expression was comparable in both groups, N-cadherin was only significantly decreased in the fastest growing ectopic tumor, i.e. LuTDNa3 line G11. Except for this, no clear differences were found between this seemingly more aggressive tumor and the other ectopic tumors originating from Nanos3-expressing lung tumor cell lines. mRNA expression of *PLAU* was equally found to be significantly downregulated in the more aggressive tumor compared to those from the LuTDco cell lines and LuTDNa3 line F5. Even though there was a trend, the difference in *PLAU* mRNA expression was not significant between the ectopic tumor from LuTDNa3 line G11 and that from LuTDNa3 line D10 (P-value: 0.0818) (Figure 3.44A).

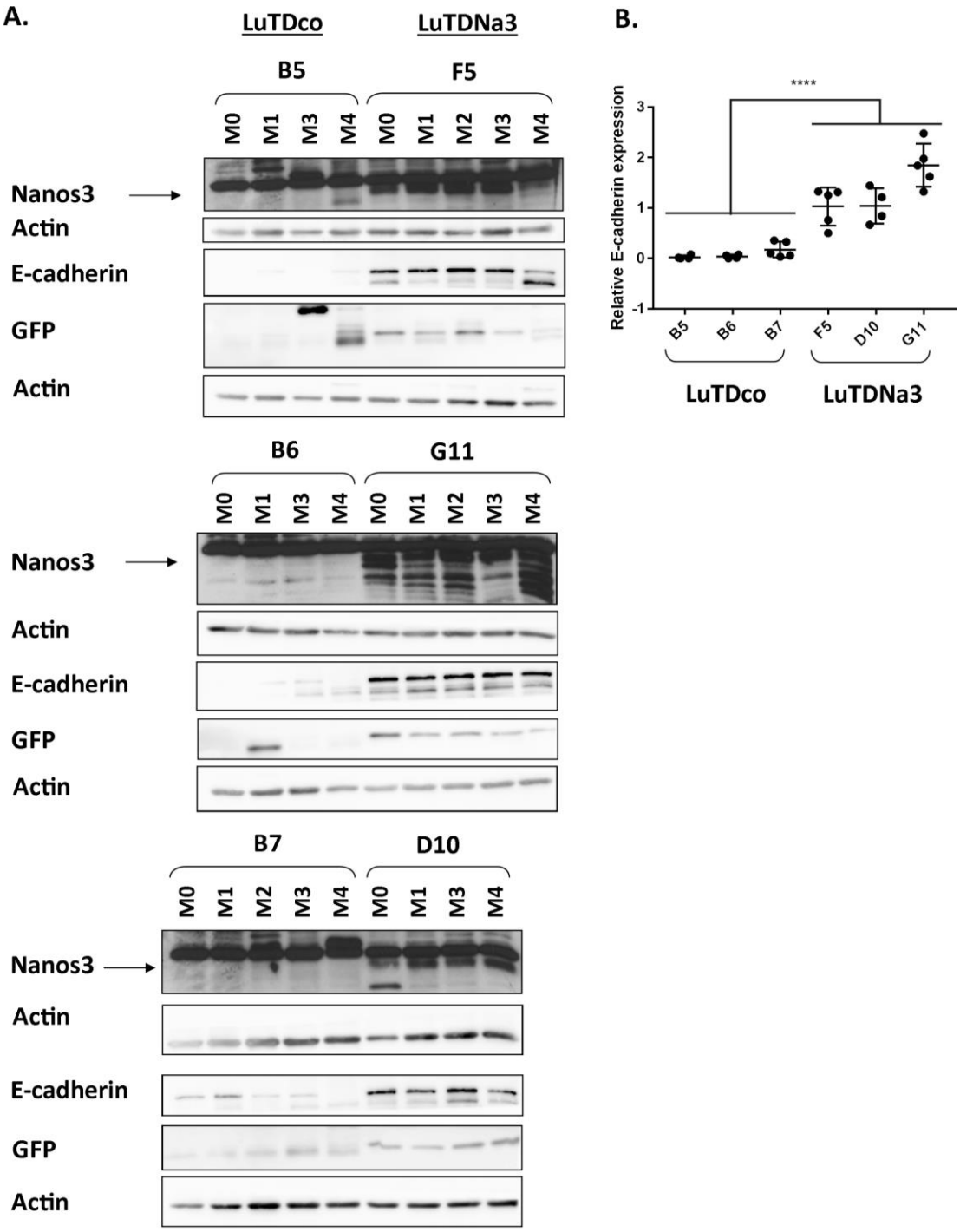

Figure 3.41. E-cadherin expression levels are higher in ectopic tumors from mice injected with Nanos3-expressing primary lung tumor cell lines compared to control cell lines. A. Ectopic tumors were dissected from athymic mice injected s.c. with primary lung cancer cell lines derived from either a LSL-KRas^{G12D};p53$^{fl/fl}$;CCSP-rtTA$^{+/-}$;TetO-Cre$^{+/-}$ mouse (LuTDco) or a Nanos3$^{LSL/-}$;LSL-KRas^{G12D};p53$^{fl/fl}$;CCSP-rtTA$^{+/-}$;TetO-Cre$^{+/-}$ mouse (LuTDNa3). Protein lysates from these tumors were checked for Nanos3, GFP and E-cadherin expression by western blotting. Actin was used as a loading control. **B.** A graph of the relative E-cadherin protein expression levels (E-cadherin/Actin). ImageJ was used for quantification. ****: P≤0.0001.

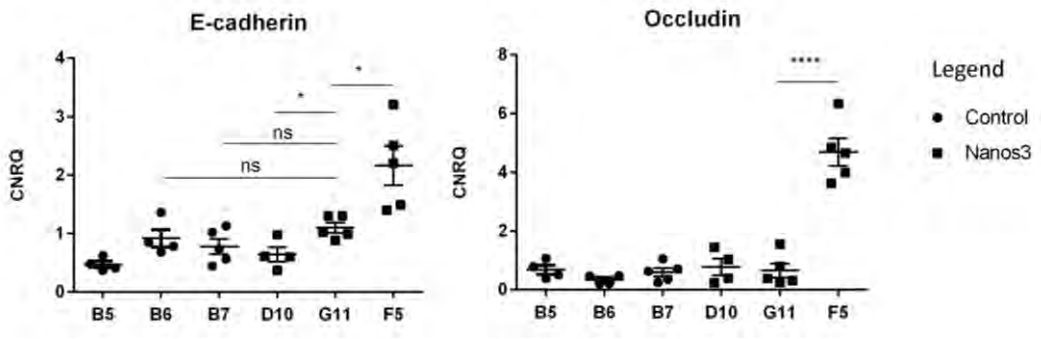

Figure 3.42. Ectopic tumors (allografts) from mice injected with one Nanos3-expressing cell line showed unexpected, higher *CDH1* and *OCLN* mRNA expression levels. Each symbol represents the CNRQ (calibrated normalized relative quantity) value obtained for the RNA lysate of the ectopic tumor from a different mouse. Error bars, SEM; ns, not significant; *: P≤0.05 and ****: P≤0.0001.

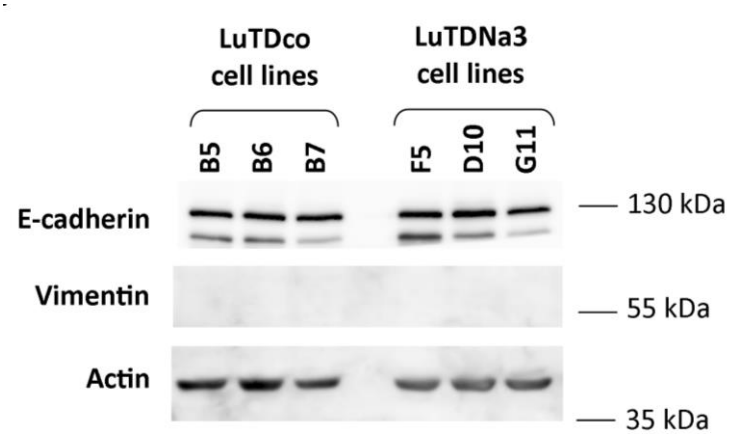

Figure 3.43. E-cadherin expression is expressed in both control and Nanos3-expressing primary lung tumor-derived cell lines. Western blotting was used to detect E-cadherin and vimentin expression in the primary lung tumor-derived cell lines. Calu-1 and HBE4-E6/E7 cells which do not express E-cadherin and vimentin, respectively (see Chapter 2, Figure 2.7), were taken along (not shown). Actin was used as a loading control.

Finally RNA expression of ZEB1 and ZEB2, two transcription factors known to be master regulators of EMT, was analyzed (Figure 3.44B). No difference in RNA expression was found between the two groups though.

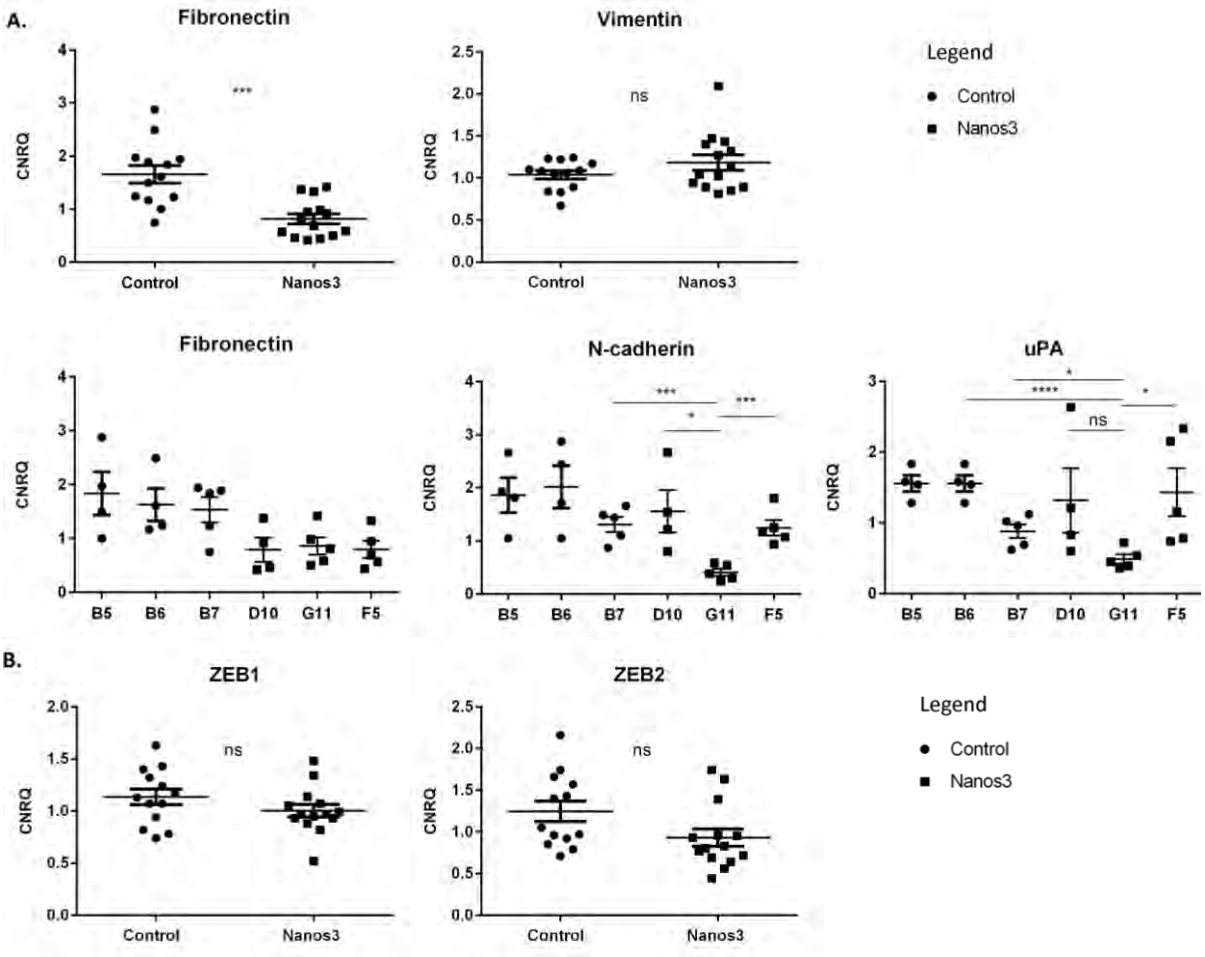

Figure 3.44. Fibronectin mRNA levels are downregulated in ectopic tumors (allografts) originating from Nanos3-expressing lung tumor-derived cells. RNA lysates were made of ectopic tumors induced by control and Nanos3-expressing lung tumor cells. RT-qPCR analysis was done for mesenchymal markers, fibronectin, vimentin and N-cadherin, a serine protease, uPA (**A**) and the ZEB transcription factors (**B**). CNRQ, calibrated normalized relative quantity. Error bars, SEM; ns, not significant; *: P≤0.05; ***: P≤0.001 and ****: P≤0.0001.

3.7.4 Nanos3 expression might positively influence lymph node metastasis formation

Lymph nodes of mice s.c. injected with the Nanos3-expressing primary cell lines F5 and D10 were visibly enlarged compared to those from the other mice. Mice injected with LuTDNa3 line G11 were sacrificed two to three weeks earlier than those injected with the other LuTDNa3 cell lines, which might explain why their lymph nodes were not swollen. Two enlarged lymph nodes from mice injected with LuTDNa3 line F5 were analyzed by western blotting and RT-qPCR. Similarly the lungs of a mouse injected with LuTDNa3 line G11 were subjected to western blotting and RT-qPCR. Both lymph nodes showed high Nanos3 and GFP

expression suggesting lymph node metastasis (Figure 3.45). The other lymph nodes of both control and Nanos3 mice were sectioned after paraffin embedding. Lymph nodes were not available for the mice injected with LuTDNa3 line G11. Clear lymph node metastasis was indeed seen in mice injected with LuTDNa3 line F5 and line D10 (Figure 3.46). In all cases the observed lymph node metastases, originating from LuTDNa3 cell lines, showed clear evidence of cancer tissue differentiation (Figure 3.46C). Lymph node metastases were, however, also visible in mice injected with LuTDco cell lines. Unlike those from the LuTDNa3 cell lines, which mostly covered the complete lymph node, those of LuTDco cell lines were visible as small groups of neoplastic cells in an otherwise, seemingly normal lymph node (Figure 3.46). These neoplastic cells were also rarely seen in lymph nodes from mice injected with LuTDNa3. These cells do not shown any GFP or Nanos3 expression (data not shown).

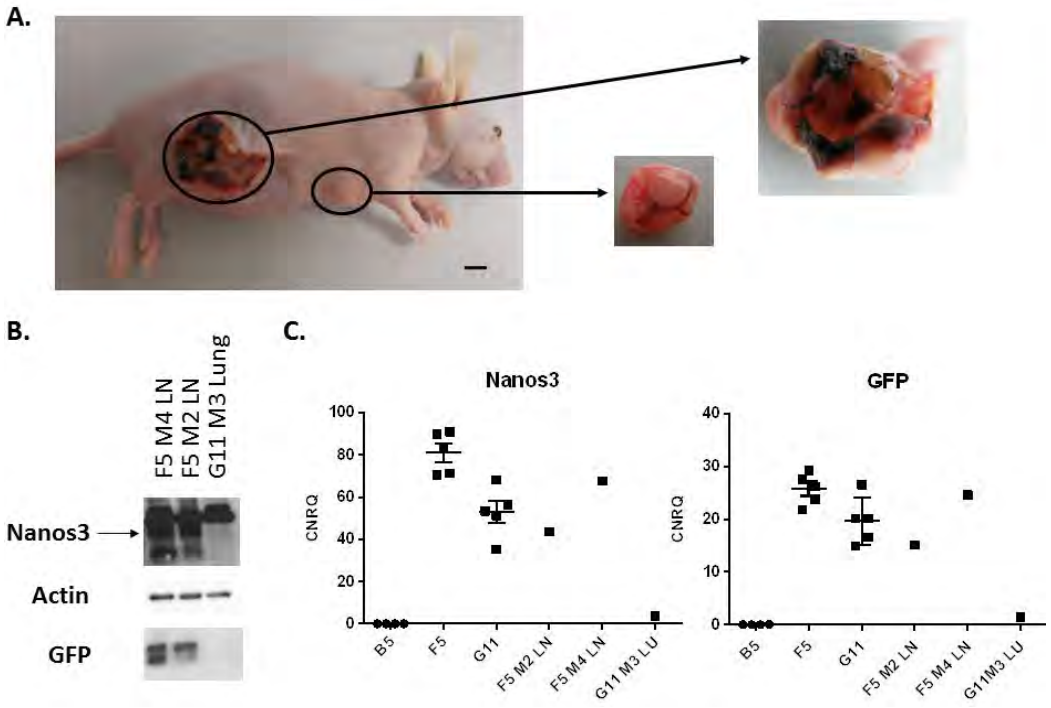

Figure 3.45. Lymph node metastasis upon injection of Nanos3-expressing lung tumor-derived cancer cells. Athymic mice were injected with lung tumor cell lines derived from a NSCLC mouse with ectopic Nanos3 expression (Nanos3$^{LSL/-}$;LSL-KRas^{G12D};p53$^{fl/fl}$;CCSP-rtTA$^{+/-}$;TetO-Cre$^{+/-}$). Axillary Lymph nodes (LN) were dissected **(A)** and subjected to western blotting **(B)** and RT-qPCR analysis **(C)** for *NANOS3* and *GFP* expression. Bar: 5 mm. Actin was used as a loading control. The lungs (LU) of one mouse s.c. injected with a Nanos3-expressing lung tumor-derived cell line (G11) were similarly analyzed. RNA lysates from ectopic tumors dissected from mice injected with a control (B5) or Nanos3-expressing (F5 and G11) lung tumor cell line were used as a negative and positive control(s), respectively. CNRQ**,** calibrated normalized relative quantity; error bars, SEM.

GFP and Nanos3 expression were not visible in the protein lysate from the lungs of the mouse s.c. injected with LuTDNa3 line G11 but very low mRNA levels are detected by RT-qPCR. This could still point to a small metastasis in the lung not detectable when looking at the complete lung lysate. Small lung nodules were detected on the lungs of several other mice (Table 3.2). Metastasis formation is however not consistent for all mice injected with the same cell line. This was observed despite the fact that primary tumor growth was quite similar for all mice injected with the same cell line (Figure S3.2). Although more mice injected with LuTDNa3 cell lines showed exteriorly visible lung metastasis compared to those from LuTDco cell lines, big metastases were found in a few mice injected with LuTDco cell lines (Figure 3.47). Also here the different time points of death could play a role.

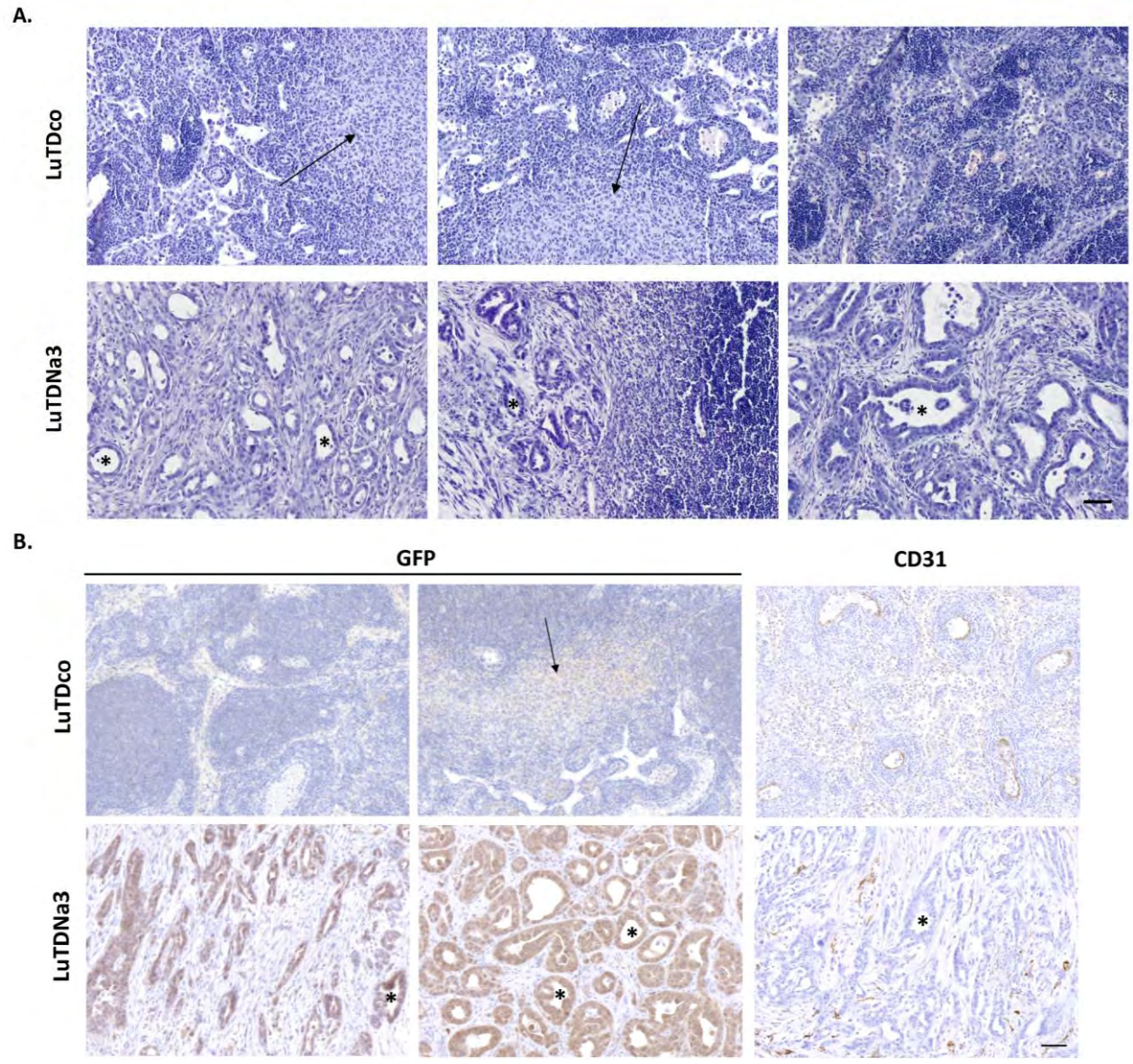

Figure 3.46. Panels A and B.

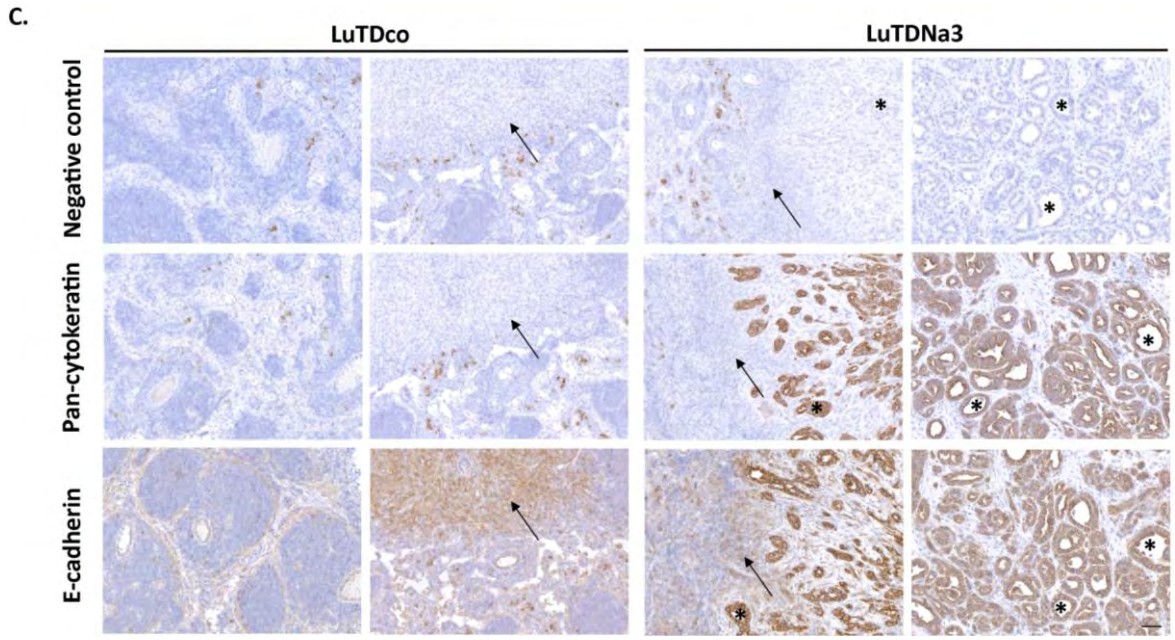

Figure 3.46. Differentiated lymph node metastasis in athymic mice injected with Nanos3-expressing tumor-derived cell lines F5 and D10. A. H&E stained lymph nodes showing metastatic lesions. These are strongly differentiated ones (asterisks) in mice injected with Nanos3-expressing tumor-derived cell lines F5 and D10. **B.** Lymph node sections were stained with a GFP-specific and CD31-specific antibody. **C.** Lymph node sections were stained for E-cadherin and pan-cytokeratin to analyze the differentiation and proof the epithelial origin of the lymph node metastases. Arrows, neoplastic cells. The negative controls represent sections only stained with the secondary antibodies. Bars: 50 µm.

Table 3.2. Metastasis count from the metastases visible at the surface of the lungs of mice injected with control or Nanos3-expressing lung tumor-derived cell lines.

Mice	LuTDco			LuTDNa3		
	B5	B6	B7	F5	D10	G11
Mouse0	/	4[a]	2	3	7[b]	/
Mouse1	/	1	7[a]	/	6[b]	/
Mouse2	/	nd[c]	/	10[b]	nd[c]	2
Mouse3	2	/	/	2	/	/
Mouse4	/	/	/	9[b]	2[b]	2[b]

[a] Big metastases

[b] Several metastases were visible as small white dots

[c] not determined. Mice were found dead in the cage, unable to inspect the lungs.

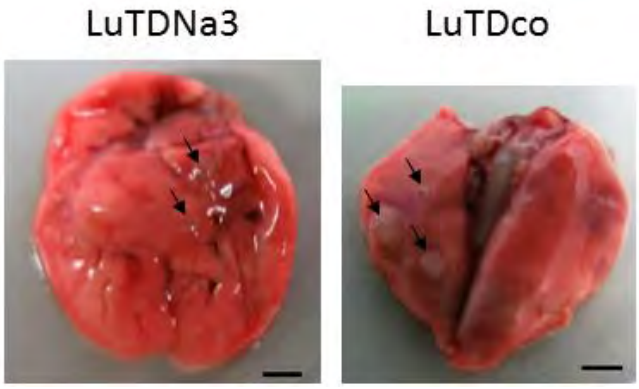

Figure 3.47. Lung metastases after subcutaneous injection of control or Nanos3-expressing lung tumor-derived cell lines in athymic mice. Lungs were dissected from athymic mice s.c. injected with a control (B7, mouse 1) or Nanos3 expressing (D10, mouse 0) tumor-derived cell line. Bar: 2 mm.

Lung metastases (Figure 3.48A) originating from the LuTDNa3 cell lines stained positive for GFP unlike those from the LuTDco cell lines (Figure 3.48B). Both lung metastases from mice injected with LuTDco and LuTDNa3 cell lines stain positive for pan-cytokeratin and E-cadherin (Figure 3.48C).

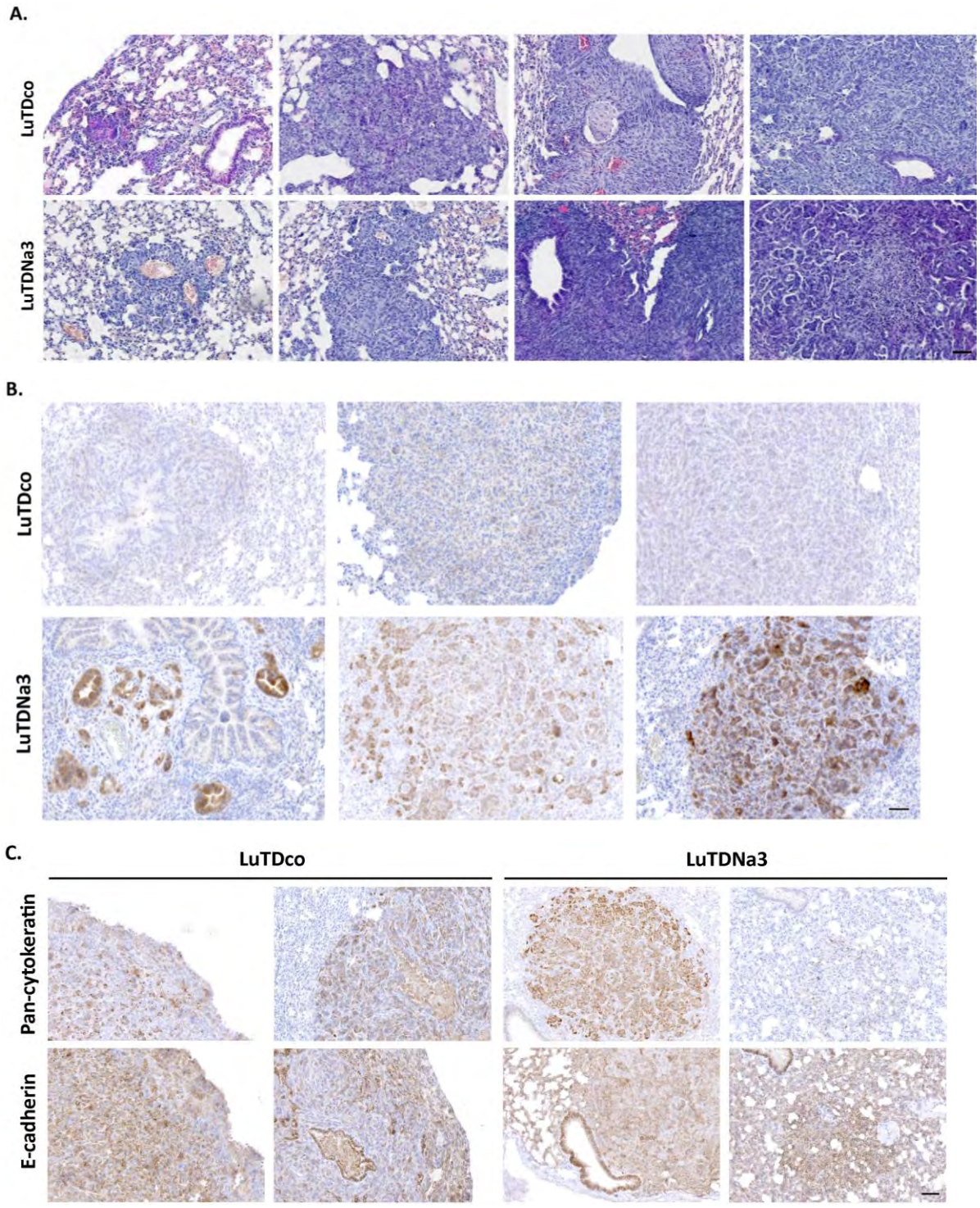

Figure 3.48. Subcutaneous injection of control and Nanos3-expressing lung tumor-derived cell lines results in lung metastasis. A. H&E stained lung sections. **B.** Immunohistochemical staining of GFP was only visible in lung metastases originating from LuTDNa3 cell lines. **C.** Lung metastases from mice injected with LuTDco or LuTDNa3 cell lines stained positive after staining with a pan-cytokeratin- and E-cadherin-specific antibody. Bars: 50 µm

3.7.5 *In vitro* proliferation, migration and invasion assays for the lung tumor-derived cell lines

Besides the soft agar analysis and the allograft experiment analyzing anchorage-dependent growth and the capacity to form tumors, respectively, other cancer-related parameters were investigated for our panel of primary lung tumor-derived cell lines. To assess the proliferative potential upon ectopic Nanos3 expression, primary tumor cell lines with and without Nanos3 expression were seeded in a 96-well plate. Confluency was monitored every two hours over almost three days as displayed in Figure 3.49A. Although differences between the cell lines were minor, these were reproducible, with LuTDNa3 line D10 showing the highest proliferative rate and LuTDco line B7 and LuTDNa3 line G11 showing the lowest proliferative rates (Figure 3.49A-B). The legends next to the graphs in Figure 3.49 were placed in an order corresponding to the displayed curves from left to right.

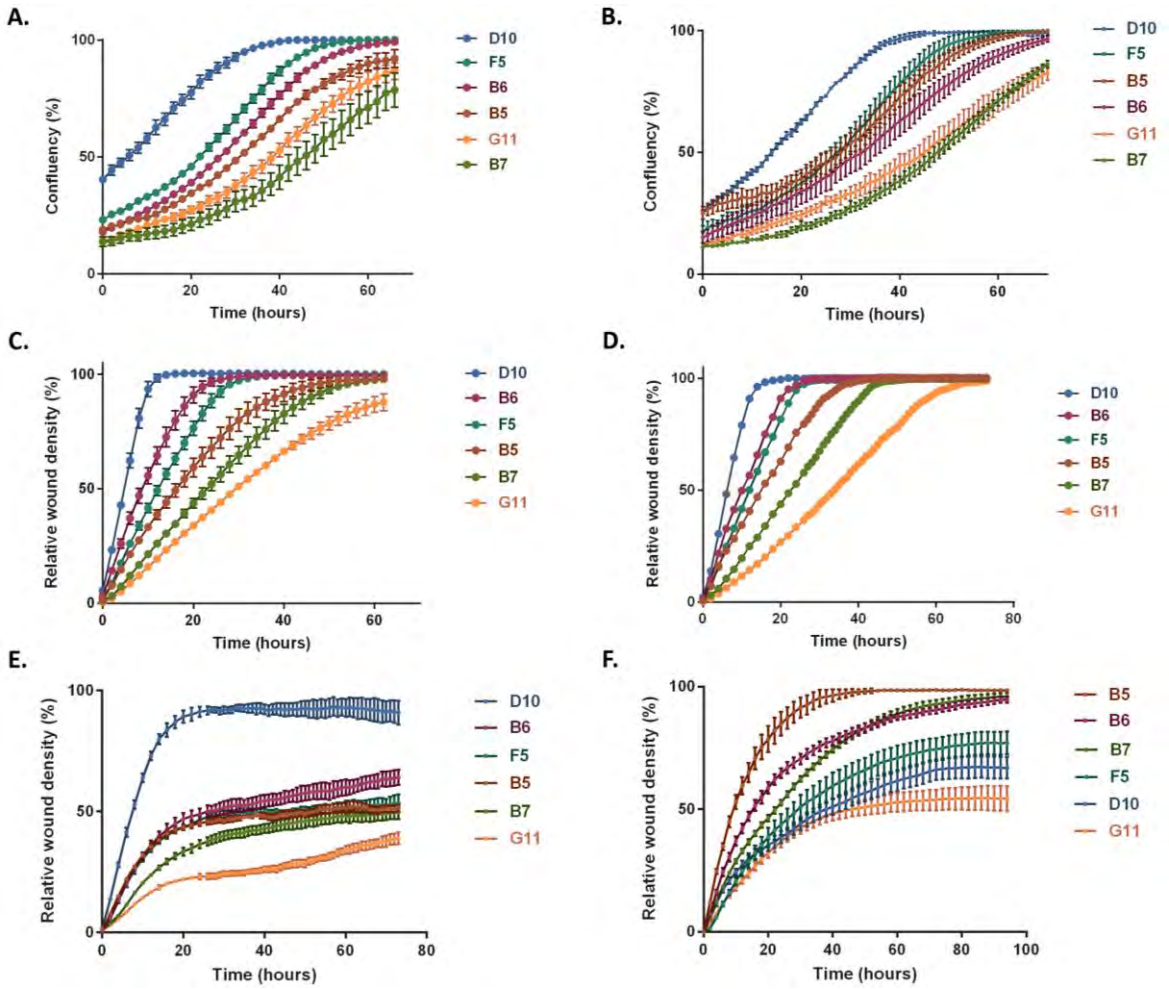

Figure 3.49. Proliferation, migration and invasion assays for control and Nanos3-expressing lung tumor-derived cells. A and **B** represent graphs of two different cell proliferation assays for control (B5, B6 and B7) and Nanos3-expressing (F5, D10 and G11) lung tumor-derived cell lines. **C** and **D** represent graphs showing migration of the indicated cell lines through media after controlled scratching the monolayers. For the migration assay in **D**, cells were treated with DMSO. This was performed simultaneously with and serves as a control for the migration assay in **E** in which the cells were treated with aphidicolin (2 µg/ml), which was dissolved in DMSO. **F** represents a graph showing the invasion of the indicated cell lines through 3D-Matrigel. Error bars, SEM; n=3 for A and B and n=4 for C, E and F.

A scratch assay has been performed to investigate the migratory capacities of these cell lines. The observed results were similar to those obtained from the proliferation experiment (Figure 3.49C). The scratch wound had closed within 10 hours for LuTDNa3 line D10 while within the same time period about 30% to 40% of the scratch wound was closed for LuTDNa3 lines G11 and F5. Since the migration rates are similar to the proliferation rates, we

decided to repeat the experiment using the proliferation blocker aphidicolin to separate the potential proliferation effects from the migratory capacity. The migration rate of cells treated with aphidicolin was significantly reduced, keeping the same order though, with LuTDNa3 line D10 having the highest migratory rate and LuTDNa3 line G11 having the slowest migratory rate (Figures 3.49E and 3.50). After around 24 hours, the aphidicolin-treated cells started to die, as is also evident from the increasing error bars in Figure 3.49E. This is however not caused by the DMSO used to dissolve aphidicolin since this was not observed in our DMSO controls (Figure 3.49D). These controls were comparable with the previously performed migration experiment without aphidicolin (Figure 3.49C).

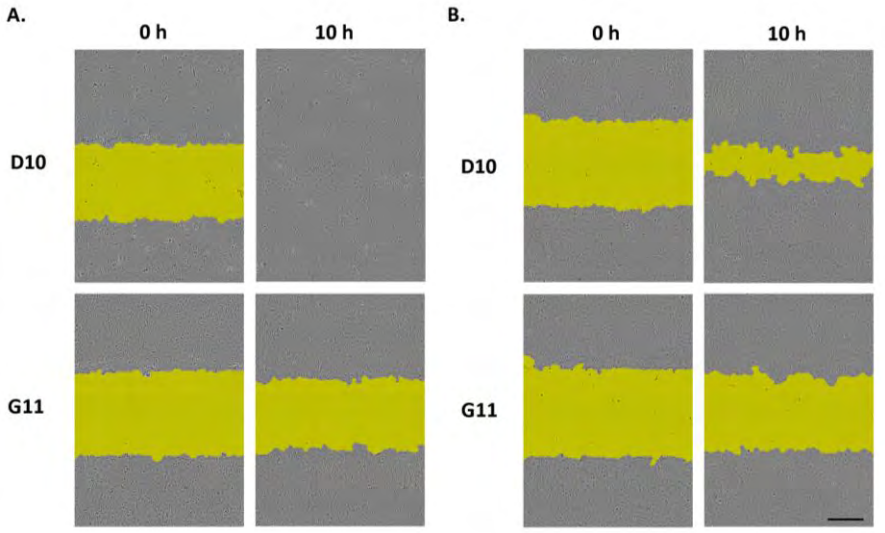

Figure 3.50. Inhibition of proliferation reduces the migration rate. A-B Pictures from the scratch assay of the fastest and slowest migrating cell line, LuTDNa3 line D10 and G11, respectively. In **B** the cells were treated with aphidicolin (2 µg/ml). Bar: 300 µm.

A similar experiment was performed to study invasion. After making the scratch in the monolayers a 1:1 mix of medium and Matrigel was added to the cells allowing to analyze their invasion capacity through Matrigel. Quite surprisingly, this yielded observations suggesting a higher invasive capacity for the three control cell lines compared to the Nanos3 cell lines (Figure 3.49F). GenStat was used to analyze the raw data obtained from the Incucyte, indeed revealing a significant difference between the invasive potential of control and Nanos3-expressing lung tumor-derived cell lines (Figure 3.51).

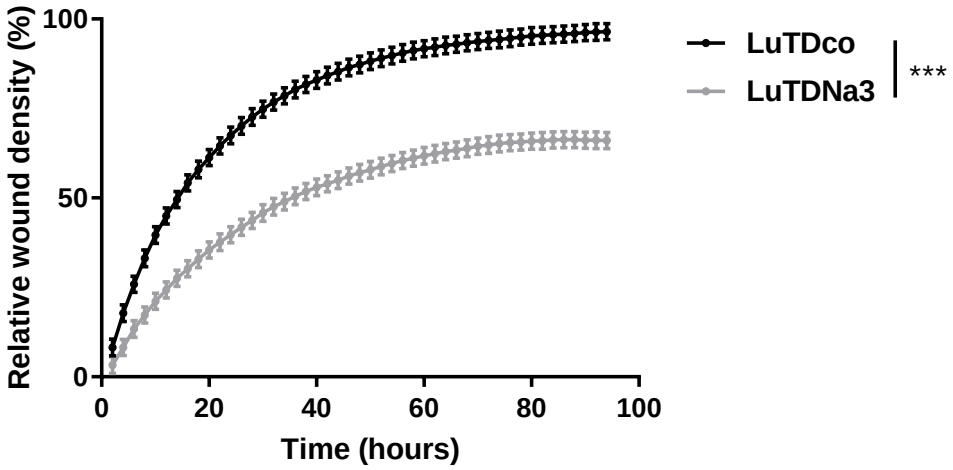

Figure 3.51. The control primary lung tumor cell lines are more invasive than those expressing Nanos3. Mean relative wound density ± SEM (n=12) obtained from repeated measurements analysis of relative wound densities over a time span of 94 hours. ***: P<0.001.

3.8 Discussion

3.8.1 NSCLC mouse model

Ectopic Nanos3 expression has been observed in several human cancers [4,23]. In NSCLC it was recently linked to an increased invasiveness and high Nanos3 expression levels are significantly correlated with a poor prognosis for the patient [4]. In human lung cancer cells, ectopic Nanos3 expression was associated with an increased invasiveness and induction of EMT. In my research described in this chapter, Nanos3 was further investigated using an *in vivo* NSCLC mouse model. For this we made use of a NSCLC mouse model driven by lung-specific mutant *KRAS* expression and loss of *TP53*.

3.8.2 Nanos3-positive NSCLC mice died significantly earlier than control mice but both NSCLC mice were metastasis-free

Unlike another research article reporting a NSCLC model through combined *KRAS* mutation and *TP53* loss [9], in our mouse models, both with and without Nanos3 expression, metastasis was not observed. This could be due to the difference in administration of the Cre recombinase, in time points of sacrifice or the genetic background of the mice. In our case the Cre recombinase is expressed exclusively in cells with an active CCSP promoter while in the article reporting metastasis they used intranasal administration of adenoviruses expressing Cre recombinase, allowing expression in diverse cell types of the pulmonary system [9]. In the published study, mice were sacrificed at 19 weeks after infection, demonstrating that the other model is slower than ours, and consequently there was more time to develop metastases. Another group using CCSP-dependent mutant *KRAS* expression combined with loss of *TP53* did not report any metastasis either [8]. The timing of tumor formation in this last article was similar as observed in our mouse model. Even though *in vivo* Nanos3 overexpression in the lungs did not cause metastasis in our model, it was associated with significantly shorter survival (Figure 3.10). Possibly, the mice with ectopic Nanos3 expression died too soon to develop metastases. Other, more slowly developing cancer models might reveal a metastasis promoting role for Nanos3. Mice only expressing the mutated *KRAS* allele in the lungs also develop NSCLC, but in these mice tumor progression is slower compared to mice with additional loss of *TP53* [8,9,7]. Nanos3-expressing mice from our second NSCLC model, only expressing the mutant *KRAS* allele,

indeed died later compared to those with an additional lung-specific knockout of *TP53* (Figure 3.12). Similarly as was seen in the faster NSCLC model (model #3), in model #2 Nanos3-expressing mice died earlier compared to the control mice without Nanos3 expression (Figure 3.9). Remarkably, in both models, a significant difference between the Nanos3 and control NSCLC mice was only seen in female mice. Our NSCLC models are reminiscent of lepidic carcinoma in humans, which is more common in women [24,25]. However, this does not offer a full explanation for our observed difference since the survival of male and female control mice (tumors without Nanos3 expression) is similar in both models #2 and #3. It rather seems that female mice are more prone to Nanos3-induced changes. Discovering the mechanism behind the Nanos3-induced changes might offer an explanation to this intriguing gender preference. Interestingly, a similar and unexplained shorter survival has been reported for female mice in a model for metastatic lung adenocarcinomas based on the combination of a mutant *KRAS* allele and a mutant *TP53* allele [26]. Hence, other tumor models using the Nanos3^{LSL} alleles may add to our knowledge of the *in vivo* roles of Nanos3 in various cancers.

Also in our slower model #2, metastasis was missing unlike previously reported [6]. Also in this article reporting metastasis, Cre recombinase expressing adenoviruses were used to induce the mutant allele. Lymph node metastasis was seen in half of the mice analyzed at 9-13 weeks after adeno-Cre administration [6]. This was not observed in our mice expressing the mutant *KRAS* allele. The median survival of our mice was 85 and 66 days after dox treatment for control mice and Nanos3-expressing mice, respectively. Since the authors did not mention any mice dying, one can assume that our model is faster than theirs. Therefore the reasoning that our mice die before being able to develop metastasis is still plausible. However, our model using CCSP-dependent Cre-induction is not completely comparable with a model using adenovirus-dependent induction. The former induces Cre expression over the entire lungs while adenoviruses induce Cre expression more focally.

Transgenic mice with a lung-specific *TP53* knockout alone (model #1) were also analyzed. However, against expectation these mice developed lymphomas in both control and Nanos3-expressing mice and an occasional adenocarcinoma only in the control mice. Breedings for this model were therefore discontinued.

3.8.3 Nanos3 expression enhances the hyperplastic bronchiolar phenotype seen in NSCLC mice

Nanos3 overexpression seemed to affect in particular the club cells since our mice with ectopic Nanos3 expression (model #3) showed significantly more hyperplastic bronchioles (Figure 3.15). Besides a clear expression in the club cells, the used CCSP promotor is also active in type-II cells in the alveoli [12]. A more advanced stage, bronchiolar papilloma was not observed in any of the analyzed mice. Alveolar tumor formation of both control and Nanos3 NSCLC mice turned out to be similar (Figure 3.20), despite some promising results from the Indian ink assay for a Nanos3 effect. Indian ink staining is, however, more suitable for *ex vivo* lung metastasis quantification and not for visualizing primary lung tumors.

Somewhat in line with the abovementioned observations, immunohistochemical stainings for proliferation markers showed no difference between the lungs of Nanos3-expressing and control mice (Figure 3.22). Although there seems to be a tendency, no significant difference was observed in Sox2 staining of the alveolar tumors. The reason why female Nanos3-expressing mice die earlier than the control mice can seemingly be narrowed down to more severe bronchiolar hyperplasia. This might have an important impact on the lung function of these mice, hence leading to an early death.

The bronchiolar phenotype was also investigated in younger mice of 21 days after dox treatment, and here already a trend was observed towards a stronger bronchiolar phenotype in Nanos3-expressing mice compared to control mice (Figure 3.17). However, more mice should be investigated to conclude about the significance of the difference in bronchiolar hyperplasia between both genotypes at this age.

Although some carcinomas were observed in control mice from lung model #1, $p53^{-/-}$, bronchiolar hyperplasia was missing in these mice despite their old age at the time of analysis. Since bronchiolar hyperplasia was also clearly visible in lung model #2, $KRas^{G12D}$, and was even more prominent than adenocarcinoma formation, the mutant *KRAS* allele is likely to play a major role in this phenotype. Nanos3 might use similar pathways to enhance development of hyperplasia. *KRAS* activation stimulates several pathways of which the MAP-kinase cascade (RAF-MEK-ERK) leads to cell cycle progression and prominent changes in transcription. Diverse targets are activated through this signaling cascade including c-Myc.

Myc inhibition has been shown to reduce KRas-induced NSCLC tumors [27,28]. The exact relationship between KRas and Myc is, however, rather complicated [29].

3.8.4 Immunohistochemical staining of the lungs of both control and Nanos3 NSCLC mice revealed no major influences of Nanos3 expression

KRas-induced oncogenesis was similarly diminished upon CD44 deletion [30]. The expression of CD44 variants is upregulated in KRas-dependent lung adenocarcinomas [30] and their expression is associated with cancer stem cell-like characteristics [31]. A positive feedback loop has been discovered between CD44v6 splicing and KRas-dependent MAPK signaling [32]. Although CD44 is essentially a transmembrane protein, its intracellular domain can be cleaved, followed by nuclear translocation where it regulates transcription [33,34]. Nuclear expression of the full-length protein is also observed [35]. CD44v expression was also observed in transgenic NSCLC mice, both at the protein level (CD44v6) and at the mRNA level (CD44v5/v6 and vCD44v8/v9; data not shown), but there was no significant difference in CD44v expression between our control and Nanos3 NSCLC mice.

Moreover, staining for CC10, a club cell marker, was clear-cut in the bronchiolar hyperplasias, while staining for SPC, an AT2 cell marker, was nicely positive in the adenocarcinomas. This was the case both in the control and in the Nanos3 genotypes. These hyperplasias and adenocarcinomas also stained positive for E-cadherin, while they showed almost no vimentin expression.

A link between Nanos3 and EMT has been made in lung cancer cells [4], beyond the fact that it is essential for PGC migration in the embryo [36,37], which is an interesting example of non-pathological invasive behavior. Although we have demonstrated by means of our transgenic mouse models that Nanos3 acts as a potential oncogene in NSCLC, our *in vivo* data does not support the role of Nanos3 in EMT induction in lung cancer. Nanos3 and E-cadherin expression were not found by us to be inversely correlated in the tumor tissues, indicating that Nanos3 expression is not linked to EMT induction, at least not directly. The exact mechanism driven by Nanos3 expression in the NSCLC tumors remains elusive.

3.8.5 The influence of Nanos3 expression on the behavior of primary lung tumor-derived cell lines

Primary tumor cell lines derived from the lungs (LuTD) were obtained from control and Nanos3 mice of mouse model #3. Soft agar analysis demonstrated anchorage-independent growth of these tumor-derived cells with LuTDNa3 cell lines displaying more and bigger colonies after two weeks of growth. There was only a significant difference at a dilution of 10^4 cells per ml. Acidification of the medium and shortage of fresh medium supplements needed for growth at higher cell densities can explain this.

An allograft experiment with three control and three Nanos3 LuTD cell lines revealed no reproducible difference in ectopic tumor growth upon ectopic expression of Nanos3. In contrast to those from LuTDco cell lines, all ectopic tumors originating from LuTDNa3 cell lines revealed enhanced E-cadherin expression by western blotting. This was apparently regulated at the post-transcriptional level and was not observed in the original cell lines i*n vitro*. Only ectopic tumors from one LuTDNa3 cell line showed significant *CDH1* and *OCLN* mRNA expression levels, which did not seem to influence the growth of these tumors. Although no difference was seen in *VIM* mRNA expression, all tumors originating from LuTDNa3 showed lower *FN1* mRNA levels compared to those from LuTDco. The ectopic tumor with the fastest growth, originating from LuTDNa3 line G11, did show a significant decrease in *CDH2* mRNA levels and a decreased *UPA* mRNA level compared to the other ectopic tumors. No difference in gene expression has been uncovered yet between the control cell lines even though one of them grew slower *in vivo* than the other two. Subcutaneous injections of these cell lines also led to lung and lymph node metastasis. For the lung metastasis no significant difference was observed between mice injected with LuTDco or LuTDNa3 cell lines. Although lymph node metastases were observed in all mice, these were significantly bigger in mice injected with LuTDNa3 cell lines. This points to a potential role for Nanos3 in promoting lymph node metastasis. The lymph node metastases observed in mice injected with LuTDNa3 cell lines showed tumor differentiation, which was analyzed by performing E-cadherin and pan-cytokeratin stainings. These stainings proofed the epithelial origin of the lymph node metastases and this seems to be in line with the E-cadherin induction in the primary tumors of LuTDNa3 allografts. The lymph node metastases originating from LuTDco cell lines, were represented as small groups of neoplastic cells that

are pan-cytokeratin-negative. As such these neoplastic cells do not have an epithelial origin and it should be further investigated if these originate from wrongly-targeted mesenchymal cells.

The ectopic tumor experiment (s.c. injection) and a lung colonization assay (tail vein injection) with Nanos3-expressing tumor cell lines could be optimized by treatment with a control or Nanos3 shRNA. The comparative analysis of the same tumor cell line treated with different silencing constructs reduces the variability between the analyzed cell lines. Using tumor cell lines from different Nanos3-expressing mice would also give a more general view. For analysis of metastasis, it would be more appropriate to sacrifice all mice at the same time point instead of waiting until the primary tumor reaches a certain size. We should hence be cautious when interpreting our results concerning lymph node and lung metastasis. Nonetheless, the mice injected with LuTDNa3 cell lines were generally sacrificed earlier suggesting that Nanos3 expression stimulates lymph node metastasis formation. Concerning lung metastasis, no difference was seen between both genotypes. We only counted lung metastases visible on the lung surface. A more correct way to analyze metastasis formation is to completely slice the lungs. However, our experimental setup was anyhow not ideal for metastasis analysis and slicing the complete lungs would probably not have influenced the obtained results. Another option is the introduction of luciferase reporter constructs in our cell lines, which would allow us to visualize metastasis formation by performing *in vivo* imaging.

When investigating proliferation and migration of our primary lung tumor-derived cell lines, these gave similar curves for all cell lines analyzed. Moreover, any differences between the cell lines could not be attributed to Nanos3 expression. Although proliferation was shown to have an effect on the migration curves, aphidicolin-treated cells gave analogous results. In the same experiments, cells treated with a DMSO concentration equal to this used to dissolve aphidicolin, were used to check the possible effect of DMSO on the migration rates. This did not seem to have an effect on the migration rates of the cell lines. Against expectation, the invasion experiment suggested a negative influence of Nanos3 on cell invasion. This should however be repeated before drawing definite conclusions, preferably with more comparable Nanos3 knockdown cell lines. The results of our invasion experiment do not correlate with the allograft experiment, in which lymph node metastasis was solely

observed upon s.c. injection of LuTDNa3 cell lines. Clearly, *in vitro* experiments can give deviating results in comparison to what is observed *in vivo*. The surrounding stromal tissue in tumors also plays an important role in the proliferation, migration and invasion potential of the cancer cells. The transwell migration or Boyden chamber assay is an alternative to determine migration. The latter assay involves the vertical migration of cells through a porous membrane [38]. A disadvantage of that assay is the fact that it uses an endpoint analysis, requiring the determination of the optimal time of analysis for each cell type. A modified Boyden chamber assay is widely used and implies ECM components such as Matrigel to be invaded by the cancer cells [39,40]. This technique was shown to correlate nicely with *in vivo* invasive behavior. However, none of these *in vitro* assays recapitulates all the steps involved in metastasis, even though they might give interesting insight into some capacities of the examined cell lines.

Despite cloning, our primary lung tumor-derived cell lines were still quite heterogeneous and were originally made from part of the complete lungs. It would be better to sort the tumor cells for specific markers or features and establish cell lines from the sorted cells only. An antibody recognizing mouse CD44v6 and being suitable for flow cytometry would be ideal to sort the tumor cells of our interest. This together with the use of Nanos3 knockdown would offer a better way to study the Nanos3 controlled differences in protein and RNA expression and cancer-related characteristics. The insertion of (inducible) shRNA plasmids is still preferred to transient siRNA transfection. We obtained shRNAs against human *NANOS3*, but these did not demonstrate a consistent downregulation upon testing of several Nanos3-expressing cell lines (data not shown). We also purchased a Nanos3-specific siRNA (siTOOLs Biotech) which was verified to downregulate Nanos3 expression in several lung cancer cell lines (data not shown).

In conclusion, ectopic expression of Nanos3 by itself does not give rise to tumors, but it contributes to the morbidity in our lung cancer model in cooperation with genuine oncogenes. Furthermore, an allograft experiment, using either Nanos3-expressing or control lung tumor-derived cell cultures, suggested a role for Nanos3 in lymph node metastasis.

3.9 Materials and methods

Mice and genotyping

The mice from our lung tumor models were breedings from the following mice: Nanos3$^{LSL/LSL}$, tetO-Cre$^{+/-}$, CCSP-rtTA$^{+/-}$ [12], p53$^{fl/fl}$/Trp53^{tm1Brn} [11] and LSL-KRas^{G12D} [10]. Mice from lung tumor model #3 were for instance derived from parental strains Nanos3$^{LSL/LSL}$;tetO-Cre$^{+/?}$;CCSP-rtTA$^{+/?}$ and p53$^{fl/fl}$;LSL-KRas^{G12D}. All mice were bred and housed in individually ventilated cages in a specific pathogen-free facility. Genotyping was done as mentioned in Chapter 2 or in the following way. The tissue to be genotyped was placed in a 96-well plate and 100 µl of 50 mM NaOH was added, followed by incubation of the plate at 95°C for 1.5 hours. The plate was then cooled down on ice after which 10 µl 1.5 M Tris (pH 8.8) was added. After a short spin-down the lysates were ready for use in specific PCR reactions. The primers used are listed in addendum 4. The used PCR programs are given in addendum 5. In case of dox induction, mice were fed with normal food supplemented with doxycycline (625 mg/kg, Special Diets Services, Tecnilab-BMI) at the age of 2 weeks, this for a duration of another 2 weeks.

RNA isolation and RT-qPCR

RNA isolation and RT-qPCR were performed as mentioned in Chapter 2. Primer sequences are listed in addendum 3.

Immunohistochemistry

The protocol for IHC stainings is described in detail in Chapter 2. Biotin-conjugated secondary antibodies to rabbit, mouse or rat immunoglobulins (Dako, 1:500) were used. For CD31 detection we used a biotin-conjugated secondary antibody to rat immunoglobulins from BD Pharmingen (1:100). Antibody-specific adaptations to the general protocol can be obtained upon simple request. For the antibodies used and their dilutions, see addendum 2.

Western blotting

Western blotting of primary lung tumor-derived cells and lung tissues was carried out as described in detail in Chapter 2, with one adaptation. The cells and tissues were lysed in a lysis buffer containing 10 mM Tris pH 8.0, 150 mM NaCl and 0.5% NP-40 supplemented with

protease inhibitors (Complete Mini, Roche). Lysis was performed by rotating the tubes for half an hour at 4°C. For the primary antibodies used and their dilutions, see addendum 2. In addition to the anti-mouse and anti-rabbit Ig secondary antibodies mentioned in Chapter 2, also anti-rat Ig HRP-conjugated secondary antibody was used (1:3000, GE Healthcare).

Measurement of bronchiolar hyperplasia and tumor volume

H&E sections of the lungs of both control and Nanos3 transgenic mice of lung tumor model #3 were scanned with the Slide Scanner Axio Scan.Z1. For measurement of the amount of bronchiolar hyperplasia the surrounding perimeter of the bronchioles was manually drawn, the areas were measured using Volocity. The inside of the bronchioles, the inner lining of the bronchiolar hyperplasias, was measured using the magic wand ROI tool of Volocity, again giving a measurement of the area. The bronchiolar hyperplasia area was estimated by subtracting the areas of both surfaces measured. This value was divided by the perimeter. The mean value of four randomly chosen bronchioles for each mouse was plotted in a graph.

The total tumor volume was estimated using ImageJ 1.51j. A program was written to calculate the tumor percentage making use of a classifier model manually trained on H&E sections of both control and Nanos3-expressing mice, using the Trainable Weka Segmentation plugin in ImageJ.

Indian ink staining

Mice were killed by means of CO_2. Around 3 ml of a 15% Indian ink solution (in distilled water) was injected into the lungs via the trachea. The lungs were dissected and transferred to Fekete's solution (63% technical ethanol, 3.33% formaldehyde and 1.5% glacial acetic acid). This was refreshed after around two hours. For taking pictures Fekete's solution was replaced by PBS and afterwards the lungs were also kept in PBS for further storage. Pictures were taken with the Nikon AZ100M Fluorescence macroscope.

Quantification of DAB stainings

Slides stained with antibodies specific for pH3, Ki67 or Sox2 were first scanned with the Slide Scanner Axio Scan.Z1. Quantification of these DAB stainings was done by using the positive

cell detection program from Qupath-0.1.2. The optimal setting was checked for each staining.

Primary cell culture

Primary lung tumor cell lines were derived from the lungs of control (LSL-KRas^{G12D};p53$^{fl/fl}$;CCSP-rtTA$^{+/-}$;TetO-Cre$^{+/-}$) and Nanos3 (Nanos3$^{LSL/-}$;LSL-KRas^{G12D};p53$^{fl/fl}$;CCSP-rtTA$^{+/-}$;TetO-Cre$^{+/-}$) NSCLC mice. After dissection the lungs were incubated in PBS with geneticin (250 µg/ml) for one hour at RT. The lungs were then thoroughly cut into small pieces using sterile scalpel blades. All solutions and recipients in the following steps were sterile. Lung fragments were incubated during 2 to 3 hours in 5 ml dissociation buffer (250 µg/ml gentamycin, 0.5% glucose, 0.125 units/ml dispase II, 0.2% collagenase in DMEM containing 10% FCS) at 37°C while rotating. The almost uniform cell suspension was consecutively run through a 70-µm and 40-µm cell strainer after which the cells are centrifuged at 400 x g for 7 min at 4°C. After addition of 1 ml of ACK (Ammonium-Chloride-Potassium) lysing buffer (Lonza) to the pellet, this was incubated for 5 min followed by a centrifugation. The pellet was washed twice with PBS and seeded in complete medium (see below).

Cell lines

The primary lung tumor-derived cell lines (LuTDs) were cultured in RPMI supplemented with 10% FCS, L-Gln, Na-pyruvate, NEAA, 100 u/ml penicillin and 100 µg/ml streptomycin. MNNG-HOS cells were cultured in DEMEM supplemented with 10% FCS, L-Gln, and NEAA. HOS cells were cultured in MNNG-HOS medium with the addition of Na-pyruvate. Cells were kept at 37°C in a CO_2 incubator (5%) or CO_2 was manually added to 5% in closed recipients, after which cells were grown in a hot room (37°C).

Immunofluorescence

Immunofluorescence was performed as described in Chapter 2 with a few adaptations. Briefly, slides were fixed with 4% PFA for 20 min at RT. After fixation the coverslips were washed with PBS and incubated with primary antibody (addendum 2). After three washes with PBS, coverslips were incubated with fluorescent secondary antibodies (goat anti-rabbit

IgG Dylight® 594 and goat anti-mouse IgG Dylight® 488; 1/1000) and with Hoechst 33342 for nuclear staining. Pictures were taken with a Leica TCS SP5 Confocal microscope.

Soft agar assay

Anchorage-independent growth was determined in 0.35% agarose (Bioline) on top of a 0.76% agarose layer. Single-cell suspensions of the lung tumor-derived cell lines (control and Nanos3-expressing cells) were plated in a semisolid medium (DMEM supplemented with 10% FCS, Penicillin-Streptomycin, Sodium Pyruvate, NEAA and 0.35% agar). Plates were incubated at 37°C in a humidified atmosphere containing 5% CO_2. An additional top-agar layer was added after one week. After 14 days pictures were taken with a Leica microscope (Leica DC300F digital microscope camera) using XnView software and colonies were counted with Volocity. Experiments were performed in duplicate and the mean value was used for further analysis.

Allograft experiment

Athymic mice (*NMRI*-Foxn1$^{nu/nu}$) were subcutaneously injected with primary tumor cell lines derived from a control NSCLC mouse (LSL-KRas^{G12D};p53$^{fl/fl}$;CCSP-rtTA$^{+/-}$;TetO-Cre$^{+/-}$) or from a Nanos3 NSCLC mouse (Nanos3$^{LSL/-}$;LSL-KRas^{G12D};p53$^{fl/fl}$;CCSP-rtTA$^{+/-}$;TetO-Cre$^{+/-}$) with five replicates per cell line. For each mouse 2.5 million tumor cells (in 100 µl PBS) were mixed with an equal volume of Matrigel (Corning® Matrigel® Basement Membrane Matrix, VWR) before injection. The length (L), width (W) and height (H) of the tumor were measured twice a week with a caliper till the tumor reached approximately 1250 mm³, or otherwise for a period of maximum 70 days. Tumor volumes were calculated by using the following equation: (π/6) x L x W x H of the tumor.

Proliferation, migration and invasion assays

To determine cell proliferation, cell lines were seeded at 2,500 cells/well in a 96-well flat bottomed plate (Falcon). Three replicates were used per cell line. Cell proliferation was visualized using a real-time cell imaging system (IncuCyte™ live-cell Essen BioScience Inc, Michigan, USA). Images were taken every (two) hour(s). The percentage of confluency was determined using the IncuCyte imaging system, following the manufacturer's protocol.

A cell scratch assay was performed to analyze cell migration. This was done by use of the IncuCyte system. Cells were seeded in Imagelock plates from Essen Biosciences in order to reach 100% confluency the next morning. Four replicates were used per cell line. Scratches were made with a 96-well WoundMaker™ after which the cells were washed with PBS to remove residual cell debris. Culture medium was added to the wells and images were taken every two hours. The relative wound density was measured using the IncuCyte imaging system according to the manufacturer's protocol. In a second migration experiment, aphidicolin (Sigma-Aldrich, 2 μg/ml) was added to the cells. Since aphidicolin was dissolved in DMSO, an equal amount of DMSO was added to the control cells (0.05% DMSO).

The invasion experiment was performed similarly as the migration experiment. However, after making the scratch, a 1:1 mixture of medium and Matrigel (Corning® Matrigel® basement membrane matrix growth factor reduced, phenol free, Falcon/Corning) was added to the cells. Four replicates were used per cell line.

Statistical analysis

The data was analyzed with GraphPad Prism 7. An unpaired student's t-test was performed for analyzing the RT-qPCR data and the western blot data from Figure 3.41. A log-rank (Mantel-Cox) test was performed to analyze the survival curves.

Allograft and invasion data were analyzed as repeated measurements using the residual maximum likelihood (REML) approach as implemented in Genstat v18 [41]. Briefly, a linear mixed model with cell lines, time and cell lines x time interaction as fixed terms, and subject.time used as residual term, was fitted to data. Times of measurement were set at equal intervals and an autoregressive correlation structure of either order 1 (AR1) or order 2 (AR2) was selected as best model fit, based on the Akaike Information Coefficient. Significances of the fixed terms and changes in differences across time were assessed by an F-test.

3.10 Supplementary data

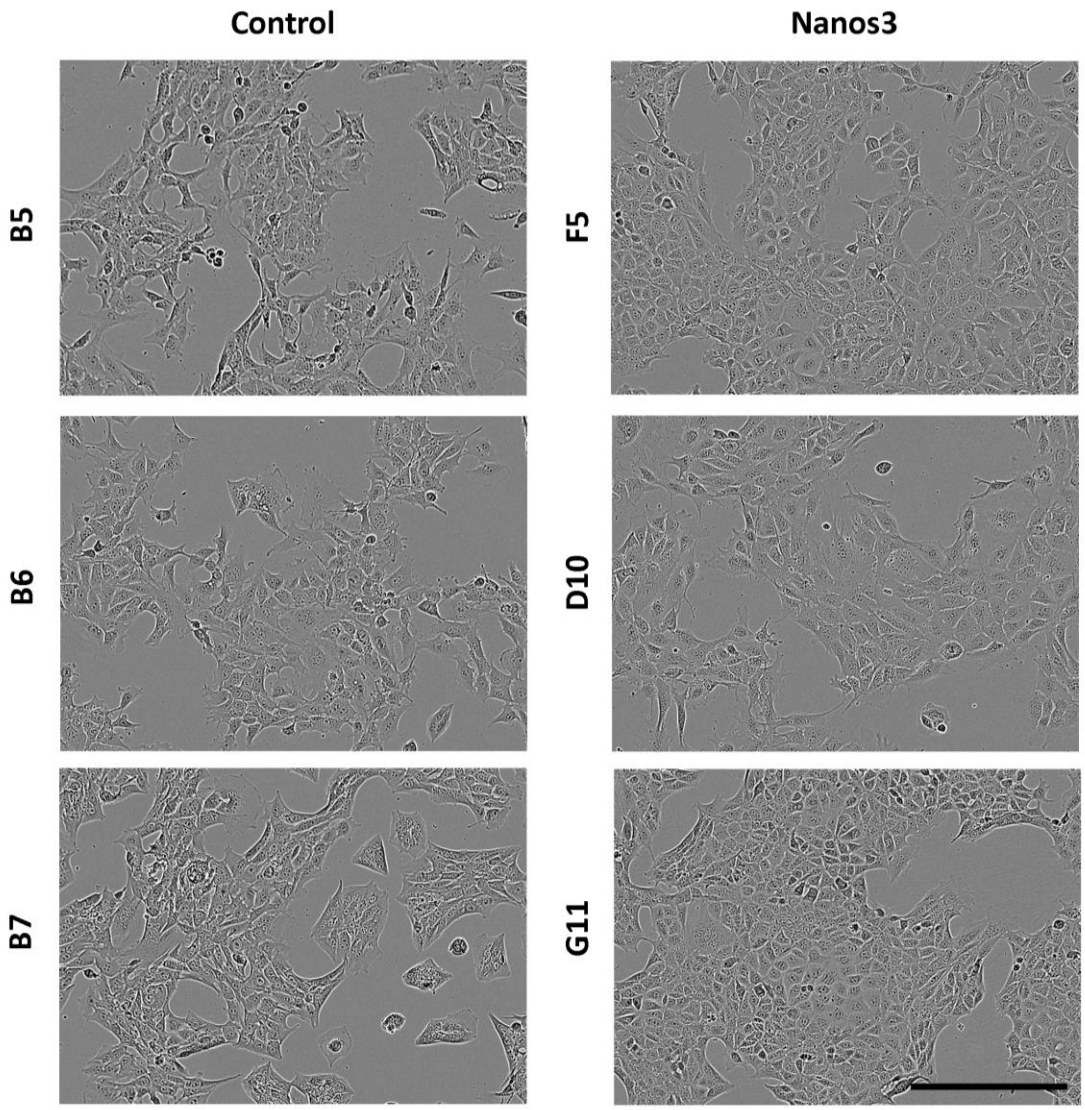

Figure S3.1. Phase contrast pictures of lung tumor-derived cell lines from a control and a Nanos3-expressing NSCLC mouse. Primary cell lines were derived from the lungs of control (LSL-KRas^{G12D};p53$^{fl/fl}$;CCSP-rtTA$^{+/-}$;TetO-Cre$^{+/-}$; B5, B6 and B7) and Nanos3 (Nanos3$^{LSL/-}$;LSL-KRas^{G12D};p53$^{fl/fl}$;CCSP-rtTA$^{+/-}$;TetO-Cre$^{+/-}$; F5, D10 and G11) NSCLC mice. Bar: 300 µm.

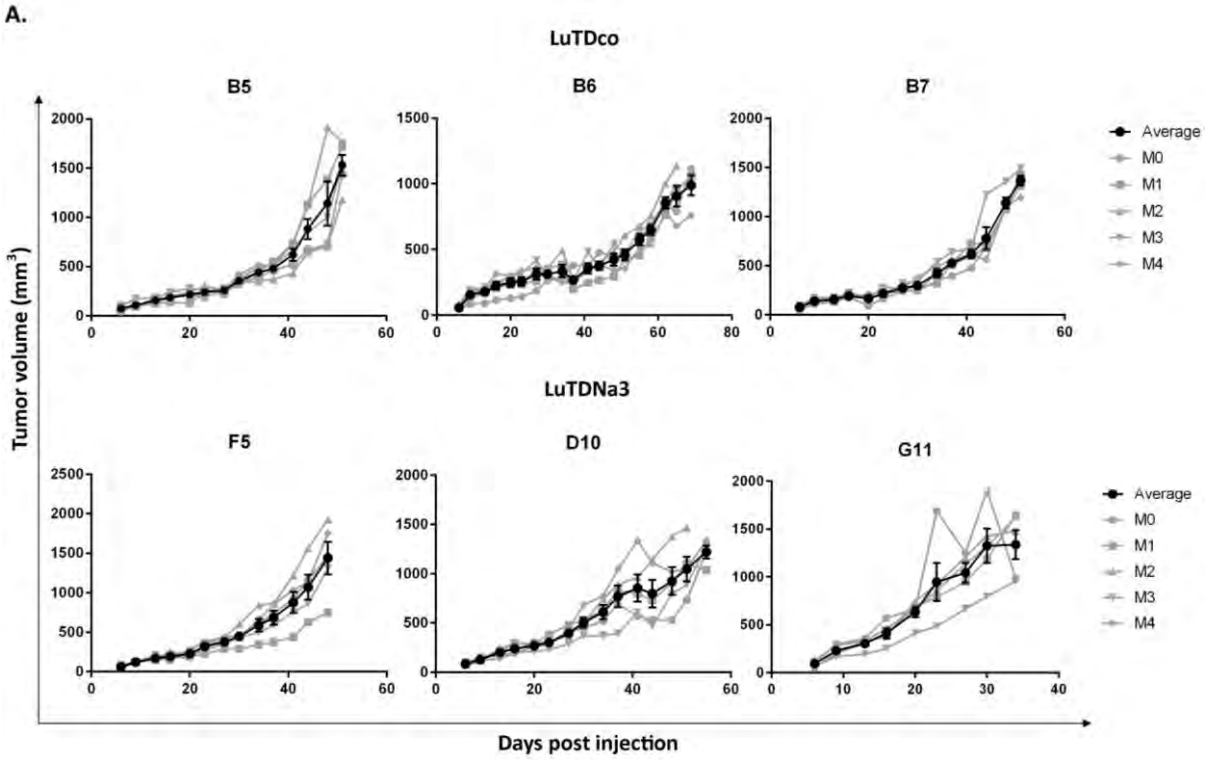

Figure S3.2. Ectopic tumor growth of athymic mice injected with primary lung tumor cell lines. Five athymic mice (M0-4) were subcutaneously injected with 2.5 million cells of a primary cell line from the lung of a control (LuTDco) or Nanos3-expressing mouse (LuTDNa3). Tumor volume was measured twice a week. The average tumor volume and corresponding standard error of the mean for mice injected with the same cell line is represented by the black line and error bar, respectively.

3.11 References

1. Torre LA, Bray F, Siegel RL, Ferlay J, Lortet-Tieulent J, Jemal A (2015) Global cancer statistics, 2012. CA Cancer J Clin 65 (2):87-108. doi:10.3322/caac.21262

2. Strumane K, Bonnomet A, Stove C, Vandenbroucke R, Nawrocki-Raby B, Bruyneel E, Mareel M, Birembaut P, Berx G, van Roy F (2006) E-cadherin regulates human Nanos1, which interacts with p120ctn and induces tumor cell migration and invasion. Cancer Res 66 (20):10007-10015. doi:10.1158/0008-5472.CAN-05-3096

3. Bonnomet A, Polette M, Strumane K, Gilles C, Dalstein V, Kileztky C, Berx G, van Roy F, Birembaut P, Nawrocki-Raby B (2008) The E-cadherin-repressed hNanos1 gene induces tumor cell invasion by upregulating MT1-MMP expression. Oncogene 27 (26):3692-3699. doi:10.1038/sj.onc.1211035

4. Grelet S, Andries V, Polette M, Gilles C, Staes K, Martin AP, Kileztky C, Terryn C, Dalstein V, Cheng CW, Shen CY, Birembaut P, Van Roy F, Nawrocki-Raby B (2015) The human NANOS3 gene contributes to lung tumour invasion by inducing epithelial-mesenchymal transition. J Pathol 237 (1):25-37. doi:10.1002/path.4549

5. Meuwissen R, Linn SC, Linnoila RI, Zevenhoven J, Mooi WJ, Berns A (2003) Induction of small cell lung cancer by somatic inactivation of both Trp53 and Rb1 in a conditional mouse model. Cancer Cell 4 (3):181-189

6. Meuwissen R, Linn SC, van der Valk M, Mooi WJ, Berns A (2001) Mouse model for lung tumorigenesis through Cre/lox controlled sporadic activation of the K-Ras oncogene. Oncogene 20 (45):6551-6558. doi:10.1038/sj.onc.1204837

7. Johnson L, Mercer K, Greenbaum D, Bronson RT, Crowley D, Tuveson DA, Jacks T (2001) Somatic activation of the K-ras oncogene causes early onset lung cancer in mice. Nature 410 (6832):1111-1116. doi:10.1038/35074129

8. Fisher GH, Wellen SL, Klimstra D, Lenczowski JM, Tichelaar JW, Lizak MJ, Whitsett JA, Koretsky A, Varmus HE (2001) Induction and apoptotic regression of lung adenocarcinomas by regulation of a K-Ras transgene in the presence and absence of tumor suppressor genes. Genes Dev 15 (24):3249-3262. doi:10.1101/gad.947701

9. Jackson EL, Olive KP, Tuveson DA, Bronson R, Crowley D, Brown M, Jacks T (2005) The differential effects of mutant p53 alleles on advanced murine lung cancer. Cancer Res 65 (22):10280-10288. doi:10.1158/0008-5472.CAN-05-2193

10. Tuveson DA, Shaw AT, Willis NA, Silver DP, Jackson EL, Chang S, Mercer KL, Grochow R, Hock H, Crowley D, Hingorani SR, Zaks T, King C, Jacobetz MA, Wang L, Bronson RT, Orkin SH, DePinho

RA, Jacks T (2004) Endogenous oncogenic K-ras(G12D) stimulates proliferation and widespread neoplastic and developmental defects. Cancer Cell 5 (4):375-387

11. Marino S, Vooijs M, van Der Gulden H, Jonkers J, Berns A (2000) Induction of medulloblastomas in p53-null mutant mice by somatic inactivation of Rb in the external granular layer cells of the cerebellum. Genes Dev 14 (8):994-1004
12. Perl AK, Wert SE, Loudy DE, Shan Z, Blair PA, Whitsett JA (2005) Conditional recombination reveals distinct subsets of epithelial cells in trachea, bronchi, and alveoli. Am J Respir Cell Mol Biol 33 (5):455-462. doi:10.1165/rcmb.2005-0180OC
13. Verheijen R, Kuijpers HJ, Schlingemann RO, Boehmer AL, van Driel R, Brakenhoff GJ, Ramaekers FC (1989) Ki-67 detects a nuclear matrix-associated proliferation-related antigen. I. Intracellular localization during interphase. J Cell Sci 92 (Pt 1):123-130
14. Prigent C, Dimitrov S (2003) Phosphorylation of serine 10 in histone H3, what for? J Cell Sci 116 (Pt 18):3677-3685. doi:10.1242/jcs.00735
15. Tompkins DH, Besnard V, Lange AW, Wert SE, Keiser AR, Smith AN, Lang R, Whitsett JA (2009) Sox2 is required for maintenance and differentiation of bronchiolar Clara, ciliated, and goblet cells. PLoS One 4 (12):e8248. doi:10.1371/journal.pone.0008248
16. Sarkar A, Hochedlinger K (2013) The sox family of transcription factors: versatile regulators of stem and progenitor cell fate. Cell Stem Cell 12 (1):15-30. doi:10.1016/j.stem.2012.12.007
17. Lundberg IV, Edin S, Eklof V, Oberg A, Palmqvist R, Wikberg ML (2016) SOX2 expression is associated with a cancer stem cell state and down-regulation of CDX2 in colorectal cancer. BMC Cancer 16:471. doi:10.1186/s12885-016-2509-5
18. Maier S, Wilbertz T, Braun M, Scheble V, Reischl M, Mikut R, Menon R, Nikolov P, Petersen K, Beschorner C, Moch H, Kakies C, Protzel C, Bauer J, Soltermann A, Fend F, Staebler A, Lengerke C, Perner S (2011) SOX2 amplification is a common event in squamous cell carcinomas of different organ sites. Hum Pathol 42 (8):1078-1088. doi:10.1016/j.humpath.2010.11.010
19. Karachaliou N, Rosell R, Viteri S (2013) The role of SOX2 in small cell lung cancer, lung adenocarcinoma and squamous cell carcinoma of the lung. Transl Lung Cancer Res 2 (3):172-179. doi:10.3978/j.issn.2218-6751.2013.01.01
20. Jiang H, Zhao W, Shao W (2014) Prognostic value of CD44 and CD44v6 expression in patients with non-small cell lung cancer: meta-analysis. Tumour Biol 35 (8):7383-7389. doi:10.1007/s13277-014-2150-3
21. Luo Z, Wu RR, Lv L, Li P, Zhang LY, Hao QL, Li W (2014) Prognostic value of CD44 expression in non-small cell lung cancer: a systematic review. Int J Clin Exp Pathol 7 (7):3632-3646

22. Grelet S (2014) Implication de Nanos-3 dans l'invasion tumorale broncho-pulmonaire. Dissertation, University of Reims Champagne-Ardenne

23. Cerami E, Gao J, Dogrusoz U, Gross BE, Sumer SO, Aksoy BA, Jacobsen A, Byrne CJ, Heuer ML, Larsson E, Antipin Y, Reva B, Goldberg AP, Sander C, Schultz N (2012) The cBio cancer genomics portal: an open platform for exploring multidimensional cancer genomics data. Cancer Discov 2 (5):401-404. doi:10.1158/2159-8290.CD-12-0095

24. Bracci PM, Sison J, Hansen H, Walsh KM, Quesenberry CP, Raz DJ, Wrensch M, Wiencke JK (2012) Cigarette smoking associated with lung adenocarcinoma in situ in a large case-control study (SFBALCS). J Thorac Oncol 7 (9):1352-1360. doi:10.1097/JTO.0b013e31825aba47

25. Sun S, Schiller JH, Gazdar AF (2007) Lung cancer in never smokers--a different disease. Nat Rev Cancer 7 (10):778-790. doi:10.1038/nrc2190

26. Zheng S, El-Naggar AK, Kim ES, Kurie JM, Lozano G (2007) A genetic mouse model for metastatic lung cancer with gender differences in survival. Oncogene 26 (48):6896-6904. doi:10.1038/sj.onc.1210493

27. Soucek L, Whitfield J, Martins CP, Finch AJ, Murphy DJ, Sodir NM, Karnezis AN, Swigart LB, Nasi S, Evan GI (2008) Modelling Myc inhibition as a cancer therapy. Nature 455 (7213):679-683. doi:10.1038/nature07260

28. Soucek L, Whitfield JR, Sodir NM, Masso-Valles D, Serrano E, Karnezis AN, Swigart LB, Evan GI (2013) Inhibition of Myc family proteins eradicates KRas-driven lung cancer in mice. Genes Dev 27 (5):504-513. doi:10.1101/gad.205542.112

29. Ischenko I, Zhi J, Hayman MJ, Petrenko O (2017) KRAS-dependent suppression of MYC enhances the sensitivity of cancer cells to cytotoxic agents. Oncotarget 8 (11):17995-18009. doi:10.18632/oncotarget.14929

30. Zhao P, Damerow MS, Stern P, Liu AH, Sweet-Cordero A, Siziopikou K, Neilson JR, Sharp PA, Cheng C (2013) CD44 promotes Kras-dependent lung adenocarcinoma. Oncogene 32 (43):5186-5190. doi:10.1038/onc.2012.542

31. Nishino M, Ozaki M, Hegab AE, Hamamoto J, Kagawa S, Arai D, Yasuda H, Naoki K, Soejima K, Saya H, Betsuyaku T (2017) Variant CD44 expression is enriching for a cell population with cancer stem cell-like characteristics in human lung adenocarcinoma. J Cancer 8 (10):1774-1785. doi:10.7150/jca.19732

32. Cheng C, Yaffe MB, Sharp PA (2006) A positive feedback loop couples Ras activation and CD44 alternative splicing. Genes Dev 20 (13):1715-1720. doi:10.1101/gad.1430906

33. Okamoto I, Kawano Y, Murakami D, Sasayama T, Araki N, Miki T, Wong AJ, Saya H (2001) Proteolytic release of CD44 intracellular domain and its role in the CD44 signaling pathway. J Cell Biol 155 (5):755-762. doi:10.1083/jcb.200108159

34. Su YJ, Lai HM, Chang YW, Chen GY, Lee JL (2011) Direct reprogramming of stem cell properties in colon cancer cells by CD44. EMBO J 30 (15):3186-3199. doi:10.1038/emboj.2011.211

35. Janiszewska M, De Vito C, Le Bitoux MA, Fusco C, Stamenkovic I (2010) Transportin regulates nuclear import of CD44. J Biol Chem 285 (40):30548-30557. doi:10.1074/jbc.M109.075838

36. Tsuda M, Sasaoka Y, Kiso M, Abe K, Haraguchi S, Kobayashi S, Saga Y (2003) Conserved role of nanos proteins in germ cell development. Science 301 (5637):1239-1241. doi:10.1126/science.1085222

37. Julaton VT, Reijo Pera RA (2011) NANOS3 function in human germ cell development. Hum Mol Genet 20 (11):2238-2250. doi:10.1093/hmg/ddr114

38. Chen HC (2005) Boyden chamber assay. Methods Mol Biol 294:15-22

39. Kleinman HK, Jacob K (2001) Invasion assays. Curr Protoc Cell Biol Chapter 12:Unit 12 12. doi:10.1002/0471143030.cb1202s00

40. Shaw LM (2005) Tumor cell invasion assays. Methods Mol Biol 294:97-105

41. Payne RW, Murray DA, Harding SA, Baird DB, Soutar DM (2009) GenStat for Windows (12th Edition) Introduction. VSN International, Hemel Hempstead

Chapter 4

Nanos3 in prostate cancer

Contributions

Evi De Keuckelaere designed, performed and analyzed experiments (Figure 4.1-4.11). Ellen Sanders provided overall technical assistance. Amanda Gonçalves provided technical assistance with microscopy.

4.1 Introduction

Preliminary results in my research group (in collaboration with Dr. Nawrocki-Raby and Prof. Dr. Birembaut, Reims) revealed Nanos3 as a relevant target in prostate tumors. Immunohistochemical staining of human prostate cancer biopsies showed a correlation between Nanos3 expression and tumor aggressiveness. More specifically a higher Nanos3 expression was seen in less differentiated human prostate tumors with higher tumor grades and thus higher aggressiveness of prostate tumor cells (Figure 4.1). *NANOS3* mRNA expression levels were similarly increased in a tumor sample with a high Gleason score compared to normal prostate tissue (data not shown). Furthermore, according to the cBioportal database (*http://cbioportal.org*), frequency of *NANOS3* alteration (amplification) was highest in NEPC as compared to numerous other human tumor types. The study yielding these results reports *NANOS3* amplification in both castration resistant prostate adenocarcinomas (11/63 cases, 17.5%) and castration resistant neuroendocrine prostate cancers (8/44 cases, 18.2%) [1]. Copy-number alteration of the *NANOS3* locus (19p13.12) was also significantly correlated with amplification of the *NANOS1* (10q26.11) and *NANOS2* (19q13.32) locus [1].

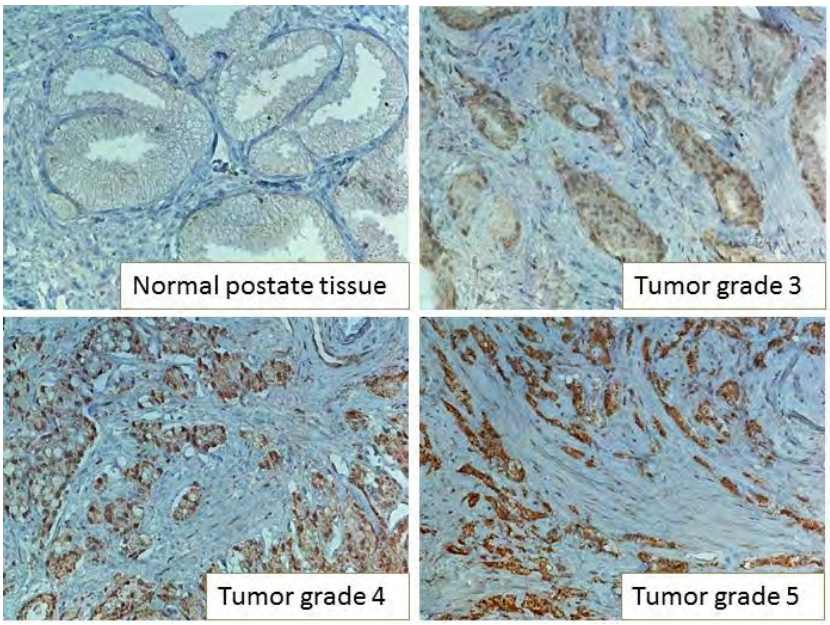

Figure 4.1. Nanos3 expression is associated with tumor grade. Immunohistochemical staining for Nanos3 showed a high expression level in human prostate cancer biopsies, with increasing intensity in higher tumor grades. Normal prostate tissue was negative for Nanos3 staining (Dr. Simon Grelet, personal communication, 2015).

Prostate cancer is the most diagnosed cancer and the third leading cause of cancer death among men in developed countries, with an estimated 8.9% of the total cancer mortality in men [2]. Further research of prostate cancer progression and possible therapeutic targets is therefore highly relevant [2].

Several mouse models exist to investigate prostate cancer, including xenograft and allograft mouse models, oncogene expression models, and knockout models targeting tumor suppressor genes such as *PTEN* (see Chapter 1) [3-5]. The ARR_2/Pb-myc (Hi-Myc) model [6] is an interesting model to investigate the possibility whether Nanos3 expression drives prostate cancer progression. The promoter used is composed of the rat prostate-specific Pb promoter with two additional androgen response elements [7]. Overexpression of the human *MYC* gene in mice of this mouse model is thus prostate-specific and regulated by androgen expression [6]. All mice of this model developed PIN lesions from 2 weeks onwards, which subsequently progress to adenocarcinoma formation detectable at 6 months of age. Prostatic adenocarcinoma is commonly observed in men and similarly to the human situation, in this mouse model tumor progression is associated with a decrease of *Nkx3.1* and an increase of *Pim-1* expression levels [8,9,6]. Metastasis formation is not observed in this Hi-Myc mouse model but we have examined whether this might be induced by additional ectopic Nanos3 expression.

When choosing a genotypically best fitting mouse model, the strain background can also have a big influence on the experiment. As mentioned above mice on an FVB/N background are more susceptible to tumor formation than mice on other backgrounds. Mammary gland lesions induced by the *WAP-TGF-α* transgene occurred more often in mice on an FVB/N background compared to those on a C57BL/6J background [10]. The prevalence of alveolar nodules decreased significantly in the (FVB; C57BL/6J) F1 background. Similarly, FVB/N mice carrying the Hi-Myc transgene turned out to be more susceptible to prostate cancer formation than those on a (FVB/N; C57BL/6) F1 background (Figure 4.2). Metastasis formation was also shown to be dependent on the strain background since only FVB/N mice of the TRAMP model developed bone metastasis unlike those on a C57BL/6 background [11].

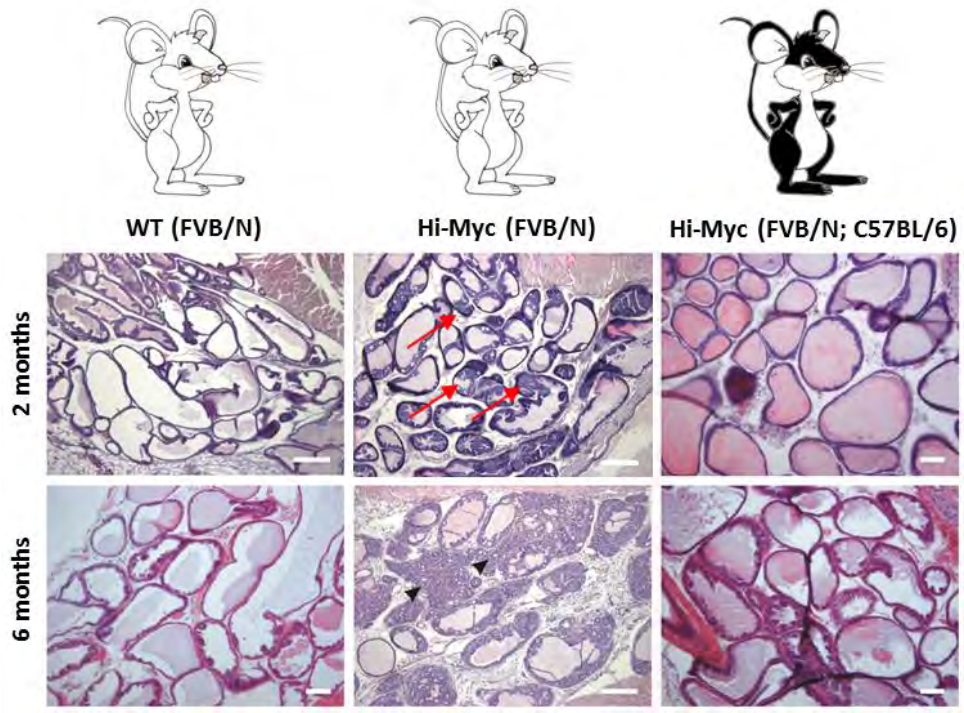

Figure 4.2. FVB/N mice are more susceptible to prostate cancer progression under influence of the Hi-Myc gene in comparison with (FVB/N; C57BL/6) F1 hybrids. H&E stainings of sections of the dorsolateral prostate of wild-type (WT, FVB/N), Hi-Myc (FVB/N) and Hi-Myc (FVB/N; C57BL/6) mice. At the age of two months prostatic intraepithelial neoplasias (red arrows) are only visible in Hi-Myc mice on an FVB/N background. At the age of 6 months adenocarcinoma formation (arrow heads) was observed in these mice while only limited PIN formation is visible in the Hi-Myc mice on the mixed background. Bars: 100 µm. Figure adapted from [12]**.**

To express our human *NANOS3* transgene in a prostate-specific manner we used the Pb-Cre4 transgenic mouse line (official nomenclature: transgene insertion 4, Pradip Roy-Burman; Tg(Pbsn-cre)4Prb) [13]. The same ARR_2/Pb promoter as in the Hi-Myc model is used here to express the Cre recombinase.

4.2 Pb-Cre specific recombination

4.2.1 Female Pb-Cre mice can be used as a "Cre deleter line"

To confirm prostate-specific expression of the Cre recombinase under control of the ARR_2/Pb promotor, Pb-Cre mice were crossed to *ROSA26* reporter (R26R) LacZ mice [14]. $Rosa26^{tg/-}$ mice were crossed with $Pb\text{-}Cre^{+/-}$ mice resulting in mice of four different genotypes (Table 4.1). Mice having both Pb-Cre4 and Rosa26R transgenes and mice only having the Rosa26R transgene were used for lacZ staining. The mice with the latter genotype were used as a negative control. LacZ staining was preceded by a perfusion-based fixation of the organs with 4% PFA. Remarkably, the two female mice tested (75F and 76F) and one male mouse (63M) showed ubiquitous LacZ staining (Figure 4.3). Two of these mice did not even have the Pb-Cre4 gene.

Table 4.1. Offspring obtained after crossing a male $Rosa26R^{tg/-}$ mouse and a female $Pb\text{-}Cre^{+/-}$ mouse.

Ear tag	Gender	Pb-Cre4	Rosa26R
58	M	+/-	tg/-
59	M	+/-	-/-
60	M	+/-	-/-
61	M	+/-	tg/-
62	M	+/-	tg/-
63	M	-/-	tg/-
64	M	+/-	-/-
65	M	+/-	tg/-
66	M	-/-	tg/-
67	M	+/-	tg/-
68	M	-/-	tg/-
69	M	-/-	-/-
70	M	-/-	-/-
71	M	-/-	-/-
72	F	-/-	-/-
73	F	+/-	tg/-
74	F	+/-	-/-
75	F	-/-	tg/-
76	F	+/-	tg/-
77	F	-/-	tg/-

The mice marked in light and dark grey were used for the first and second lacZ staining, respectively.

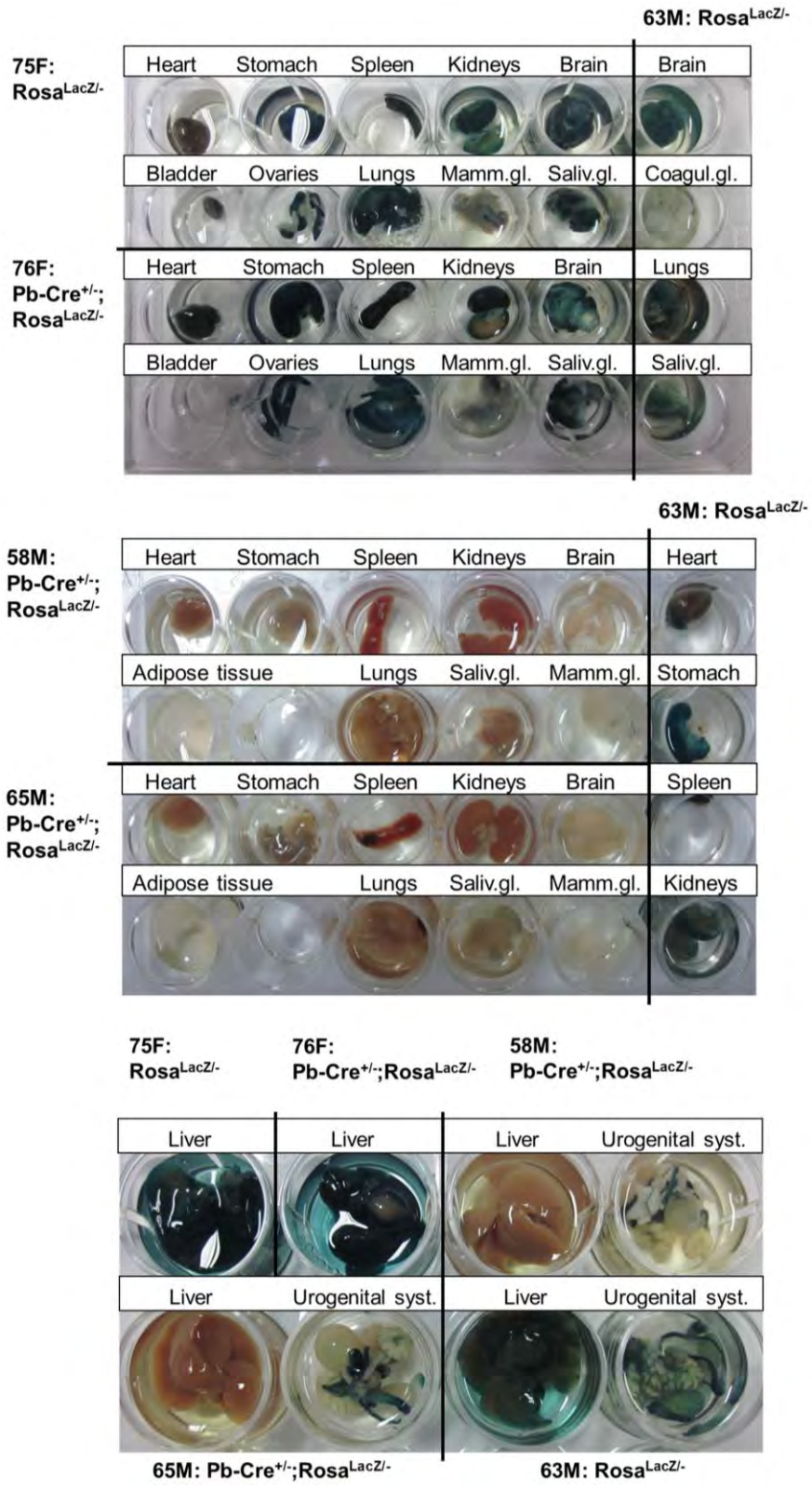

Figure 4.3. Various organs subjected to a LacZ staining. Perfusion-fixed organs were dissected and stained for LacZ. The corresponding mice and their genotypes are mentioned. F, female; M, male; mamm.gl., mammary gland; saliv.gl., salivary gland; urogenital syst., urogenital system.

Repetition of this experiment on new mice gave similar results (data not shown) showing ubiquitous LacZ staining in both tested females and two males. One of the males (62M) with mosaic LacZ overexpression in several tissues analyzed showed a comparable staining of the urogenital system as the male (61M) exhibiting prostate-specific Cre expression (Figure 4.4), similar to males 58 and 65 (Figure 4.3). The limited amount of LacZ staining in the testis corresponds to the previously reported Pb-Cre expression [13]. This and the positive staining of the vas deferens and the seminal vesicles could be attributed to endogenous galactosidase activity seen in wild-type mice [15,16]. This activity can be strain-dependent and differs markedly for several tissues [16]. LacZ staining of the vas deferens is for instance reported to be intense in FVB/N mice while any sign of staining is absent in C57BL/6N mice [16]. In our case the $Rosa^{LacZ}$ mice were on a mixed (B6; 129; Swiss) background while the Pb-Cre mice were on an FVB/N background. Offspring of these mice showed a positive staining of the vas deferens (Figure 4.4).

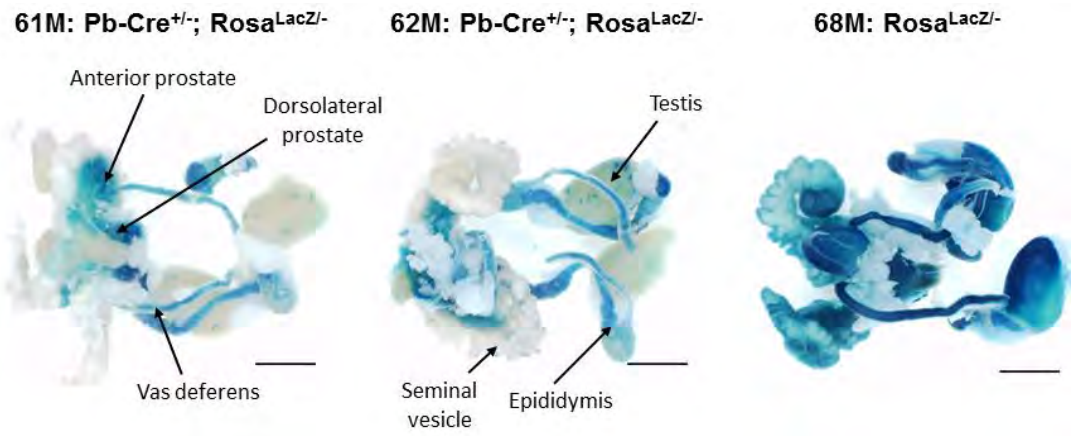

Figure 4.4. LacZ staining of the urogenital system. The corresponding mice and their genotypes are mentioned on top of the figures (see also Table 4.1). M, male. Bars: 5 mm.

4.2.2 Prostate-specific recombination of loxP-flanked transgenes can be obtained by Pb-Cre gene being transmitted through male mice

The ubiquitous/mosaic expression pattern seen in our experiments is reminiscent of Cre expression in the oocyte. It was indeed recently reported that this Pb-Cre mouse can be used for mosaic or prostate-specific gene deletion depending on the gender used to transmit the Pb-Cre gene [17]. Whereas maternal transmission of Pb-Cre causes complete deletion of maternally transmitted floxed alleles, mosaic to complete deletion was seen for paternally transmitted floxed alleles [17]. Paternal transmission of the Pb-Cre gene gives a prostate-

specific recombination of loxP-flanked transgenes. Therefore, our breeding experiments were restarted with consequent use of males to transmit the Pb-Cre gene. Offspring of a female Rosa26$^{tg/tg}$ mouse and a male Pb-Cre$^{+/-}$ mouse were used to finally confirm prostate-specific expression via western blot detection of the Cre-recombinase and lacZ staining of diverse organs (Table 4.2). This time other organs mostly stained negative with few organs showing non-specific staining such as the salivary glands and the epididymis (Figure 4.5). However, unlike the previously reported LacZ staining of C57BL/6N and FVB/N mice [16], we only saw unspecific staining in the salivary glands from the male mice and not in those from the female mice (Figure 4.6).

Table 4.2. Overview of two litters obtained after crossing a female Rosa26R$^{tg/tg}$ mouse with a male Pb-Cre$^{+/-}$ mouse.

Eartag	Gender	Pb-Cre4	Rosa26R	Experiment
1976	M	+/-	tg/-	WB
1977	M	+/-	tg/-	WB
1978	F	-/-	tg/-	WB
1979	F	+/-	tg/-	WB
1980	F	-/-	tg/-	/
1981	F	+/-	tg/-	/
1982	F	+/-	tg/-	/
2214	M	-/-	tg/-	LacZ
2215	M	-/-	tg/-	LacZ
2216	M	+/-	tg/-	LacZ
2217	M	+/-	tg/-	LacZ
2218	M	+/-	tg/-	LacZ
2219	M	+/-	tg/-	LacZ
2220	M	-/-	tg/-	/
2221	M	-/-	tg/-	/
2222	F	+/-	tg/-	LacZ
2223	F	+/-	tg/-	LacZ
2224	F	-/-	tg/-	LacZ
2225	F	+/-	tg/-	/
2226	F	+/-	tg/-	/
2227	F	-/-	tg/-	LacZ

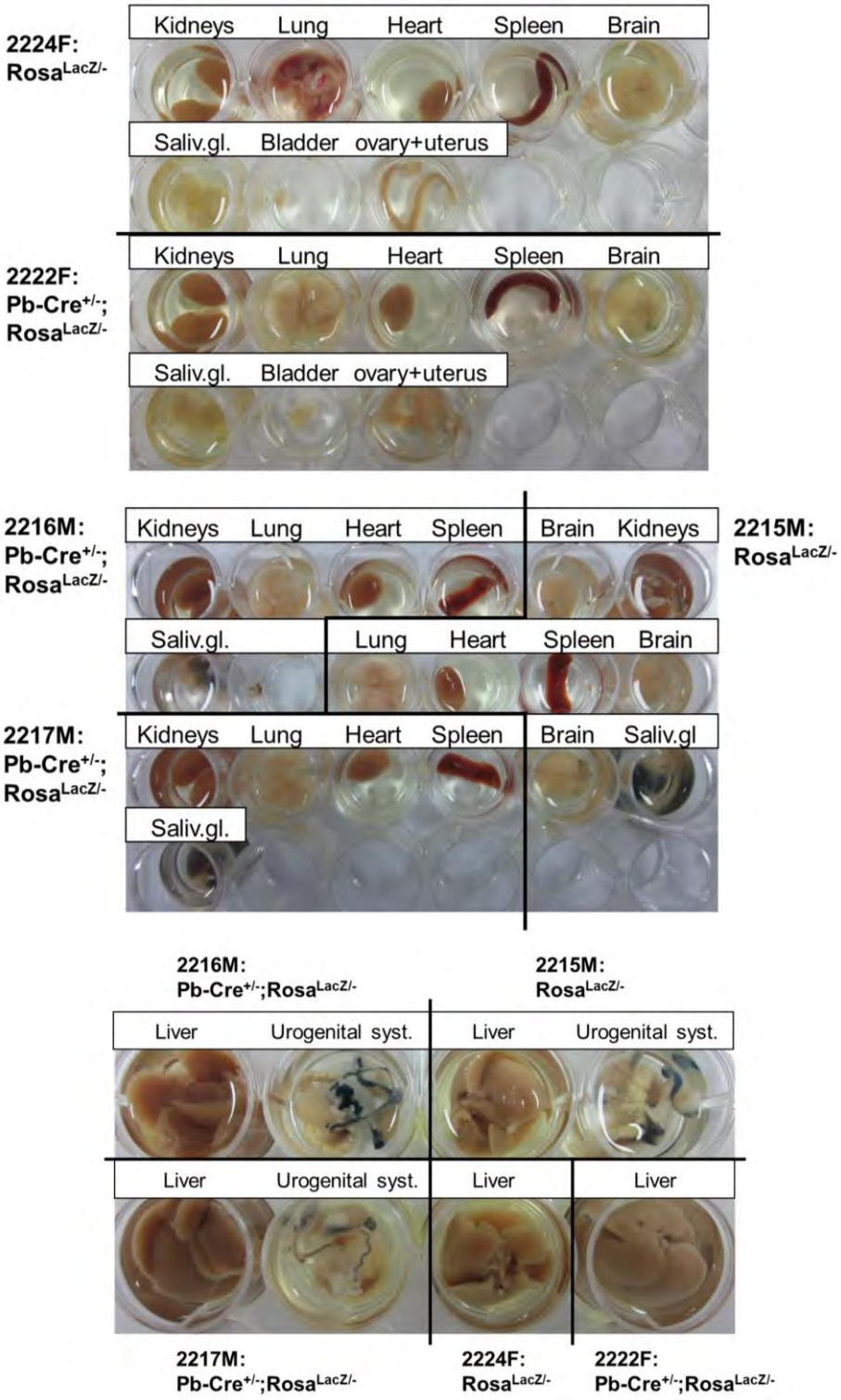

Figure 4.5. Various organs subjected to a LacZ staining. Perfusion fixed organs were dissected and stained for LacZ. The corresponding mice and their genotypes are mentioned. F, female; M, male; mamm.gl., mammary gland; saliv.gl., salivary gland; urogenital syst., urogenital system.

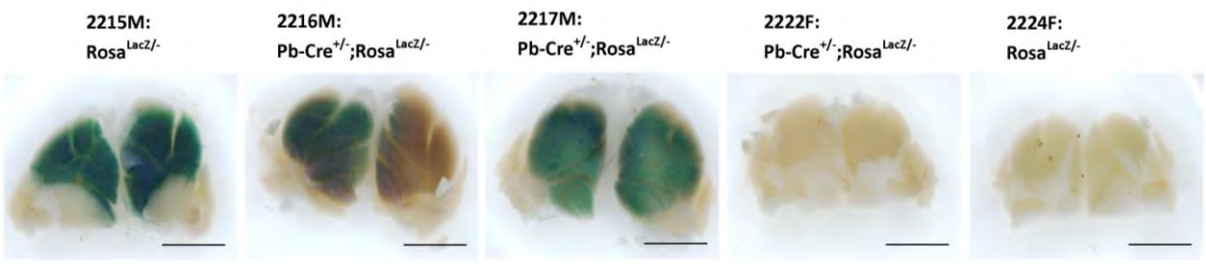

Figure 4.6. Salivary glands stained for β-galactosidase. The male (M) salivary glands showed a lot of background staining in contrast to the lack of staining in the female (F) glands. Bars: 5 mm.

Besides expression in the prostate, few cells in the testes and ovaries also showed Pb-Cre expression, which was not observed in matched controls (Figure 4.7) [13]. Sections of the epididymis from both Cre-positive and Cre-negative Rosa^{LacZ} mice showed clear lacZ staining (Figure 4.7). On western blots the epididymis also showed high expression levels of the Cre-recombinase in Cre-positive Rosa^{LacZ} mice, arguing against merely endogenous β-galactosidase activity (Figure 4.8). A male Cre-negative Rosa^{LacZ} mouse was not available when performing this experiment.

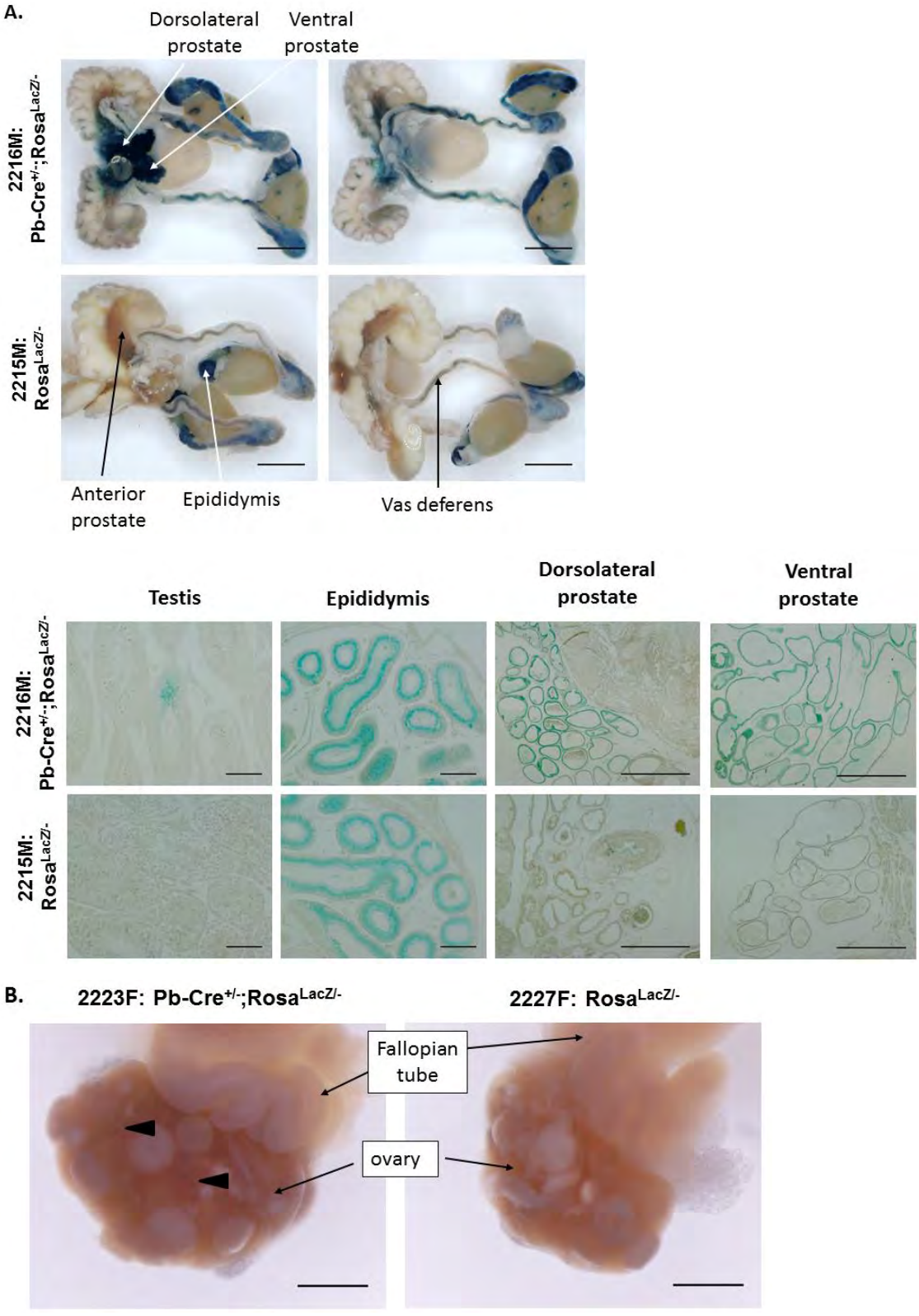

Figure 4.7. Prostate-specific Pb-Cre recombination with only few spots in the testes and ovaries.

Figure legend on the next page.

Figure 4.7. Prostate-specific Pb-Cre recombination with only few spots in the testes and ovaries. A. Pb-Cre induced LacZ expression in the prostate and few spots in the testis with unspecific expression in the vas deferens and epididymis. Bars: 5 mm for the macroscopic pictures, 100 µm for the microscopic pictures of the testis and epididymis, and 500 µm for those of the prostate. **B.** Sparse LacZ staining could be observed in a Pb-Cre expressing ovary (arrowheads) while a matched control ovary was completely negative. Bars: 1 mm. The corresponding mouse numbers and genotypes are mentioned with M standing for male and F for female (see also Table 4.2).

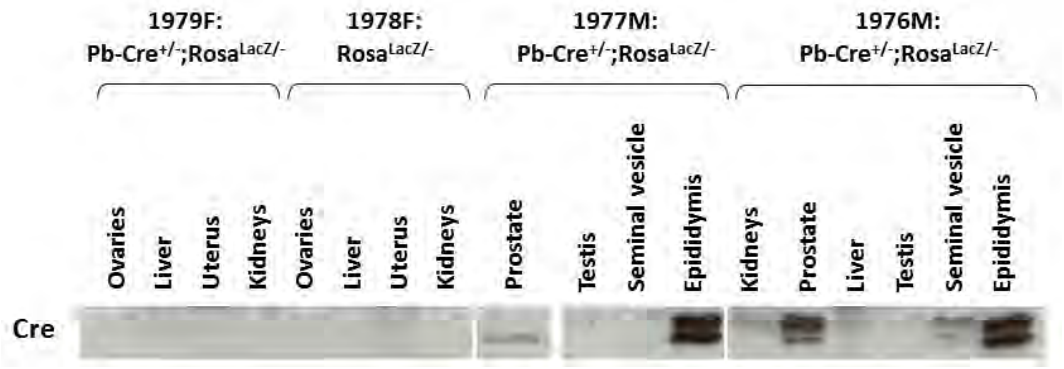

Figure 4.8. Western blot detection of Cre-recombinase expression. Various organs were dissected from $Rosa^{LacZ/-}$ and $Pb\text{-}Cre^{+/-};Rosa^{LacZ/-}$ mice showing Cre-recombinase expression in the prostate and epididymis.

4.3 Nanos3 and prostate tumor progression

To tackle the hypothesis that *NANOS3* might be a relevant oncogene in prostate cancer, prostate-specific Nanos3-expressing mice carrying the Hi-Myc transgene (Nanos3) were compared to two types of control mice bearing the conditional *NANOS3* allele, but with or without the Hi-Myc gene, and with or without Cre activity (Controls 1 and 2):

Control-1: $Nanos3^{LSL/LSL};Pb\text{-}Cre^{-/-};Hi\text{-}Myc^{+/-}$

Control-2: $Nanos3^{LSL/LSL};Pb\text{-}Cre^{-/-};Hi\text{-}Myc^{-/-}$

Nanos3: $Nanos3^{LSL/LSL};Pb\text{-}Cre^{+/-};Hi\text{-}Myc^{+/-}$

Unlike the PIN appearance at the age of 2 weeks reported in the literature [6], we observed PIN lesions around the age of 16 weeks (Figure 4.9A). Moreover, PIN formation was not 100% penetrant, demonstrating the variability of our mouse model. The underlying reason for this delayed tumorigenesis is currently unknown. Similarly as in the study by Ellwood-Yen

et al. [6], FVB/N mice were used by us. PIN lesions were still visible at the age of 24 weeks (Figure 4.9B), eventually progressing to adenocarcinomas around 30 weeks (Figure 4.9C). Adenocarcinoma formation started in the lateral prostate, followed by spreading to the dorsal and ventral part of the prostate. Adenocarcinoma was not observed in the anterior prostate until the age of 30 weeks (partly visible in Figure 4.9C, arrows). GFP staining was only visible in the Nanos3 transgenic mice, confirming correct transgenesis (Figure 4.10). GFP staining was, however, not always observed in the complete tumors (Figure 4.10H).

Human prostate cancer metastasis most commonly occurs in the lymph nodes, lungs, liver, brain and bones. Although metastasis was not reported for Hi-Myc mice [6], we examined the possibility of metastasis formation upon additional Nanos3 expression. Metastasis was, however, absent in all abovementioned mice. A few mice were kept until the age of 58 weeks (Table 4.3), of which two out of four control-1 mice demonstrated lung tumors, possibly metastases (Figure 4.11). Unfortunately, for that age mice with both the Hi-Myc and Nanos3 transgenes were not available. One 58-week old control-2 mouse and three 58-week old mice showing only prostate-specific Nanos3 expression were also available. Lung tumors were not observed in these additional mice.

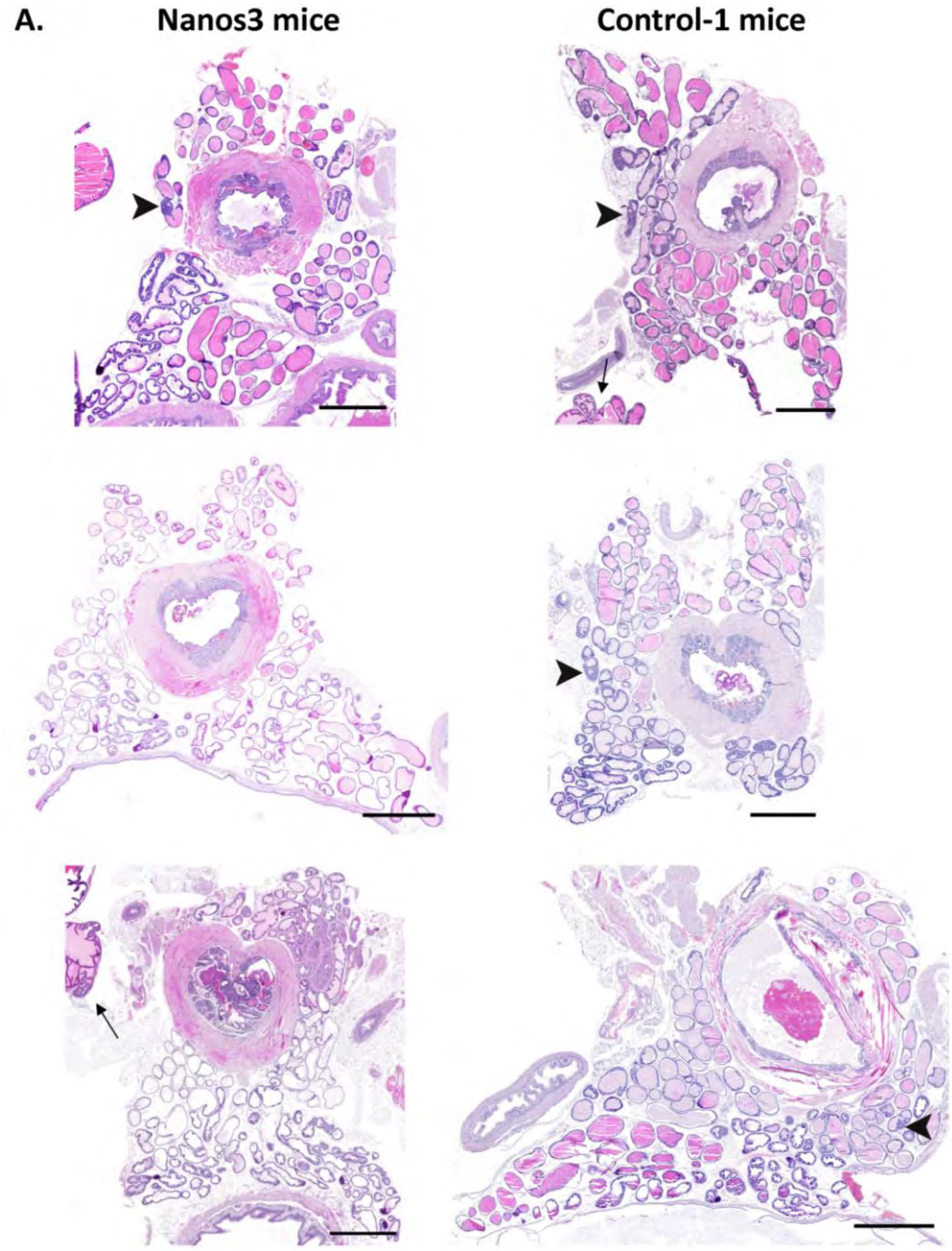

Figure 4.9. H&E stainings of prostate sections of Hi-Myc mice with or without ectopic Nanos3 expression. Prostatic intraepithelial neoplasia (PIN, arrowheads) were visible at the age of 16 **(A)** and 24 weeks **(B)**, progressing to adenocarcinoma around the age of 30 weeks **(C)**. Arrow, part of anterior prostate. This PIN and tumor appearance was the case for both Nanos3 (Nanos3$^{LSL/LSL}$;Pb-Cre$^{+/-}$;Hi-Myc$^{+/-}$) and control-1 (Nanos3$^{LSL/LSL}$;Pb-Cre$^{-/-}$;Hi-Myc$^{+/-}$) mice. **D.** H&E stained prostate sections of two control-2 mice (Nanos3$^{LSL/LSL}$;Pb-Cre$^{-/-}$;Hi-Myc$^{-/-}$) at the age of 16 weeks (left picture) and 58 weeks (right picture). All prostate pictures are oriented with the ventral prostate at the bottom. Bars, 1 mm.

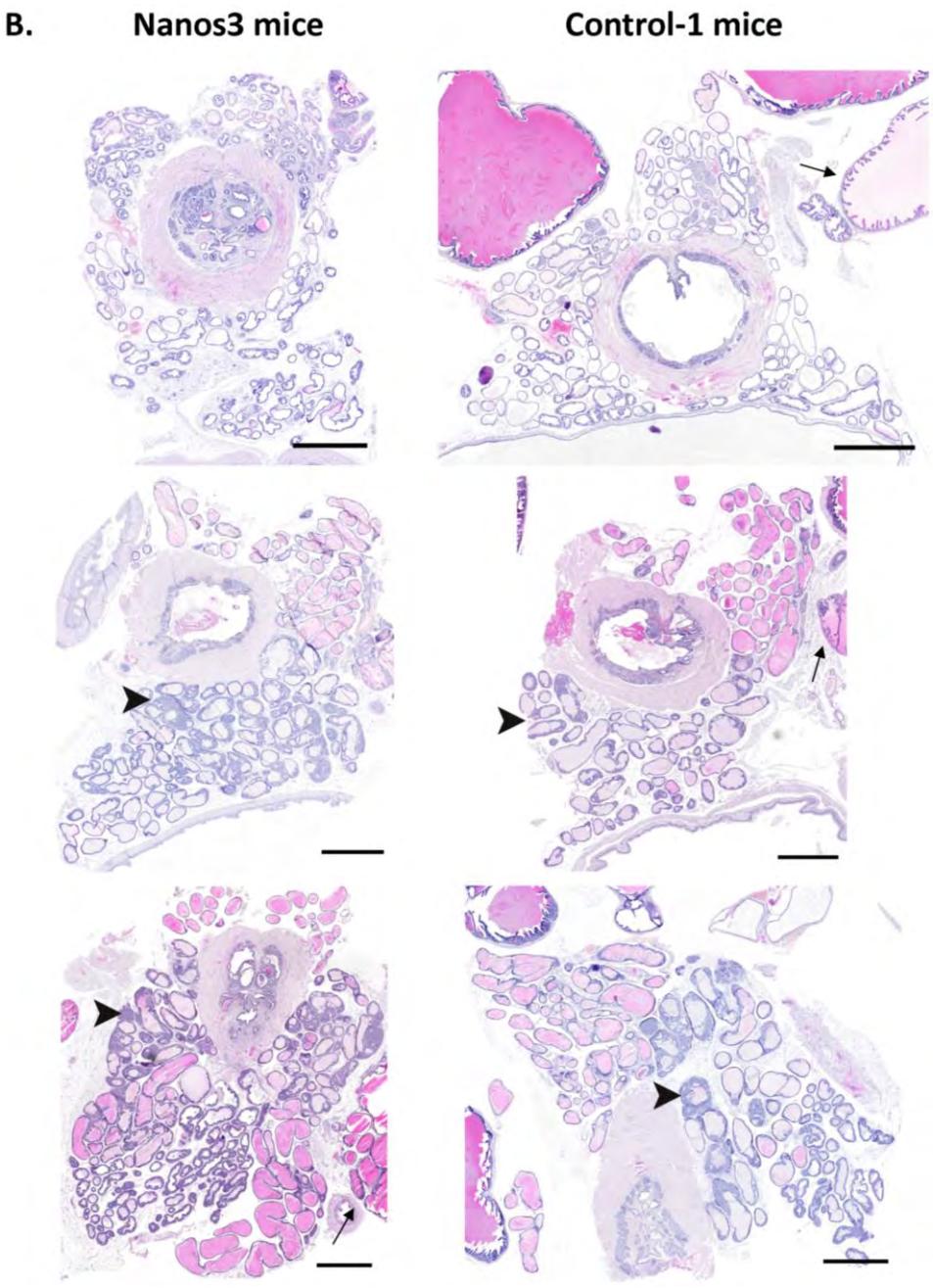

Figure 4.9. H&E stainings of prostate sections of Hi-Myc mice with or without ectopic Nanos3 expression. (Continued)

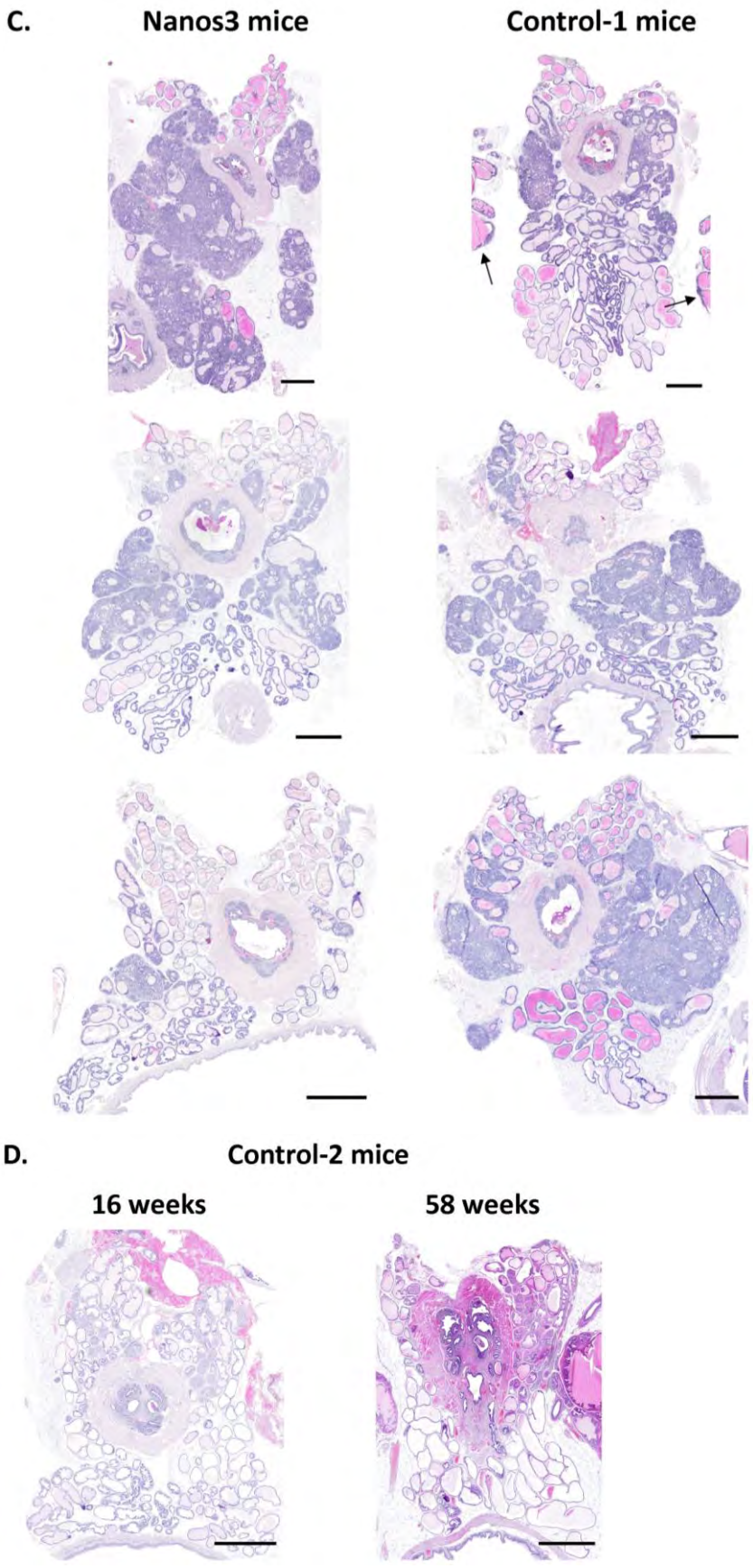

Figure 4.9. H&E stainings of prostate sections of Hi-Myc mice with or without ectopic Nanos3 expression. (Continued)

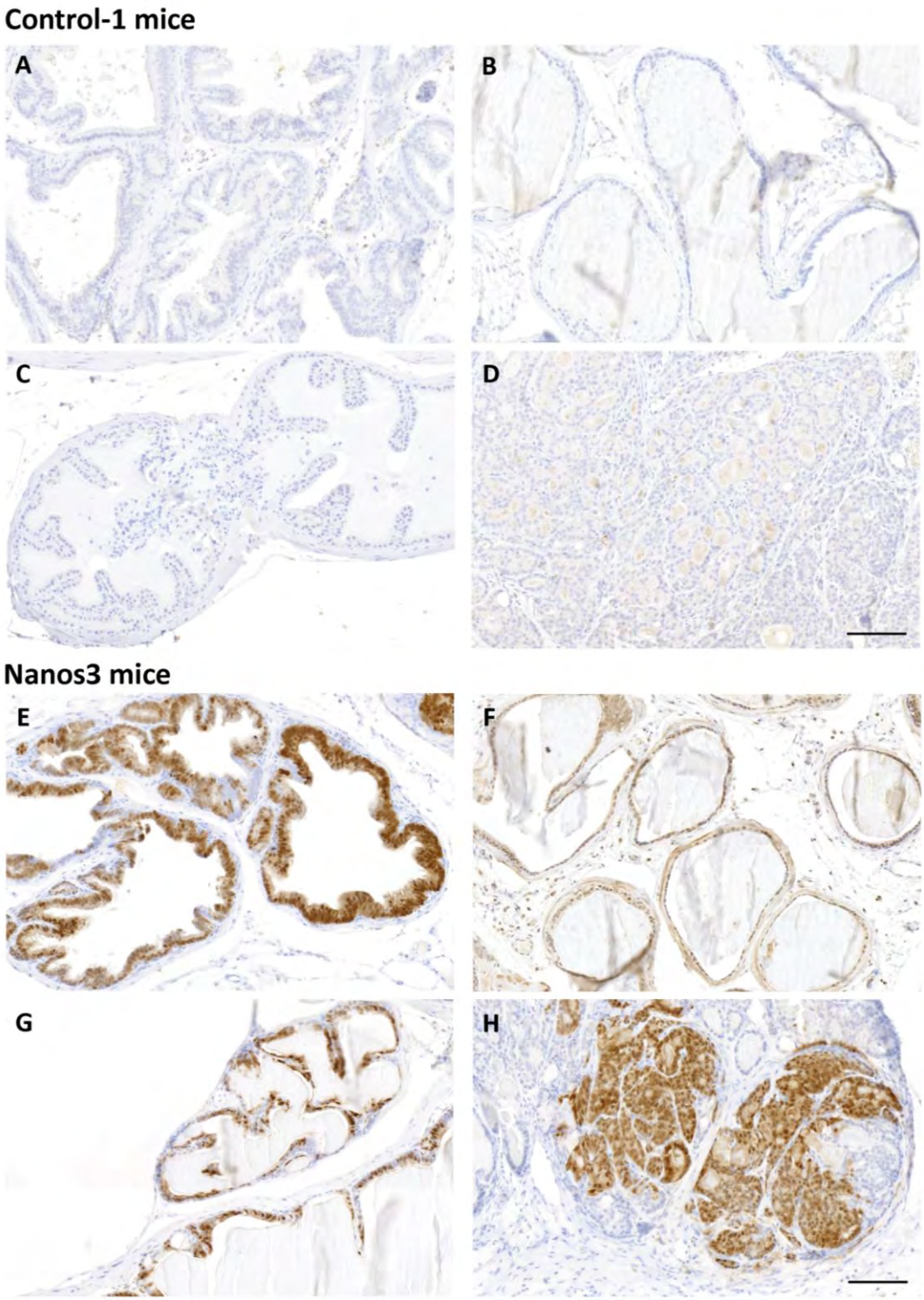

Figure 4.10. GFP staining of prostate sections of control-1 and Nanos3 expressing Hi-Myc mice of 30 weeks old. Ventral (**A** and **E**), dorsal (**B** and **F**), and anterior prostate tissues (**C** and **G**), as well as lateral prostate tumor tissues (**D** and **H**) were stained for GFP. GFP staining was only detected in the Nanos3 transgenic mice (Nanos3$^{LSL/LSL}$;Pb-Cre$^{+/-}$;Hi-Myc$^{+/-}$, panels **E-H**) and was missing in the control-1 mice (Nanos3$^{LSL/LSL}$;Pb-Cre$^{-/-}$;Hi-Myc$^{+/-}$, panels **A-D**). Bars, 100 µm.

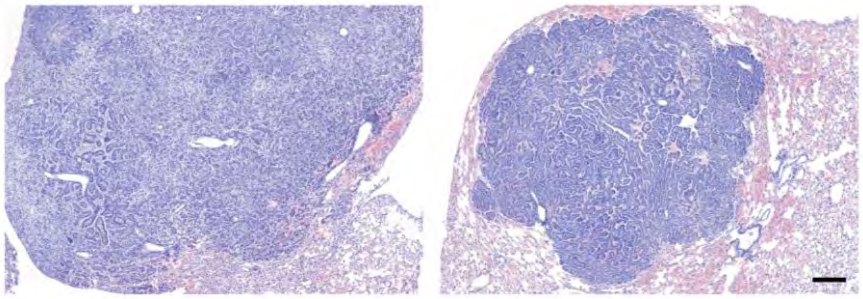

Figure 4.11. Lung tumors in Hi-Myc mice at the age of 58 weeks. H&E stained lung sections, demonstrating tumor formation in two Hi-Myc mice without human Nanos3 expression. Bar, 200 µm.

Table 4.3. A list of prostate cancer model mice available at the age of 58 weeks.

Eartag	Nanos3	Pb-Cre4	Hi-Myc		Experiment	Tumors in other tissues
1214	LSL/LSL	-/-	+/-	Control-1	IHC	Lung
1215	LSL/LSL	-/-	+/-	Control-1	IHC	/
1216	LSL/LSL	-/-	-/-	Control-2	IHC	/
1217	LSL/LSL	-/-	+/-	Control-1	IHC	Lung
1219	LSL/LSL	-/-	+/-	Control-1	IHC	/
1222	LSL/LSL	+/-	-/-		IHC	/
7445	LSL/LSL	+/-	-/-		IHC	/
7446	LSL/LSL	+/-	-/-		IHC	/

As for the lung tumors (Chapter 3), primary cell lines were made from the prostate tumors. However, this proved to be more complicated than for the primary lung cancer cell lines. Given the apparently unaffected prostate tumor progression upon ectopic expression of Nanos3, no further experiments were done.

4.4 Discussion

We first checked mouse prostate-specific expression of transgenes using the ARR_2/Pb promotor, and confirmed the results from a previous report that paternal transmission of the Pb-Cre gene was essential for this [17]. This Cre transgenic mouse model was then used to overexpress Nanos3 in the prostate of the published Hi-Myc mice [6]. Unlike reported in the literature, in our experiments, tumor progression in these mice was remarkably slower with PIN formation only around 16 weeks. At this age, PIN lesions were observed more commonly in Hi-Myc mice without Nanos3 expression as compared to mice with Nanos3 expression. This observation seemed to indicate that Nanos3 might act as a tumor suppressor in the prostate. However, there was a lot of variability between mice with the same genotype and age, and at a later age, no differences could be discerned between the tumor progression of Hi-Myc mice with and without Nanos3 expression.

Genetic background of mice was previously demonstrated to have a huge influence on prostate carcinogenesis. Gene expression analyses of prostates from different strains indeed revealed various differentially expressed genes [18].

However, FVB/N mice were used in both our case and the original Hi-Myc article, reporting PIN lesions from two weeks old [6]. A possible explanation for the delay in tumorigenesis in our experiments could be the presence of unidentified modifiers adjacent to the integrated human *NANOS3* gene. The Nanos3 expression construct was originally inserted in a *ROSA26* allele of G4 ES cells with B6; 129 background. The ROSA26 allele on the 129 background is more likely to give a higher efficiency of recombination [19]. The resulting mice were backcrossed to a C57BL/6 background which were again backcrossed to an FVB/N background (for at least ten generations). 129 or C57BL/6 passenger mutations can still be present [20].

We have also combined this Hi-Myc mouse model with Pcdh9 knockout mice. Control mice of this experiment, with only the Hi-Myc gene, showed PIN lesions at 12 weeks and clear adenocarcinoma formation at 24 weeks of age. This suggests a faster tumor progression in Hi-Myc mice lacking the floxed Nanos3 allele, although this should be further confirmed.

The observed tumors originated in the lateral prostatic lobe. Although prostatic lobes from mice cannot be simply linked with the zones of the human prostate, the dorsolateral lobe is considered to show highest similarity with the peripheral zone of the human prostate. The latter is similarly the preferred zone for human prostate adenocarcinoma formation. At later age, adenocarcinomas were also observed in the ventral and dorsal lobes. However, additional tumor formation in the anterior prostate was only seen in the few available control-1 mice of 58 weeks old. This is consistent with the lower tumorigenesis in the anterior prostate, reported in the Hi-Myc article [6]. The anterior prostate might be less permissive to malignant transformation by the Hi-Myc gene. On the other hand, expression from the ARR_2/Pb promoter is at a lower level in the anterior prostate compared to the other lobes [13]. This was also confirmed in our Cre expression analysis (lacZ experiment).

Lung tumors were observed in two 58-week-old Hi-Myc mice without Nanos3 expression (control-1 mice). At this age I could only investigate four control-1 mice, one control-2 mouse and three mice showing only prostate-specific Nanos3 expression. Without further characterization, it is difficult to state that these lung tumors are indeed metastases originating from the prostate. For instance, immunohistochemical staining for androgen receptor and dorsolateral prostate secretory proteins could confirm their prostatic origin. Spontaneous alveolar/bronchiolar tumor formation has been reported for older FVB/N mice [21]. According to this study, 6 out of 45 FVB/N males revealed lung tumors at the age of 14 months. The possibility thus exist that the observed lung tumors are merely spontaneous without any connection to the prostate tumor.

Unlike seen for our LSL-$KRas^{G12D}$ and LSL-$KRas^{G12D}$;$p53^{fl/fl}$ lung cancer models, ectopic expression of human Nanos3 did not seem to have an influence on the survival and prostate tumor progression of Hi-Myc mice. Thus, the oncogenic effect of Nanos3 might depend on the tissue type or cellular context or both. Our lung models were based on overexpression of the mutant *KRAS* gene with or without the additional loss of *TP53*. The oncogenic role of Nanos3 might depend on overexpression of and cooperation with mutant KRas. Although the *KRAS* gene is mutated in many cancers, *RAS* mutations are not that common in prostate cancer. General overexpression of $KRas^{G12V}$ gives tumors in the lungs only, of mice analyzed at 1 year of age, clearly demonstrating the susceptibility of the lungs to transformation by KRas [22]. Overexpression of ETS proteins, downstream of the MAP kinase cascade, is

however frequently observed in prostate cancer, especially as a result of the *TMPRSS2:ERG* gene fusion [23,24]. Overexpression of a member of the ETS transcription factor family is often associated with loss of *PTEN*, which is also commonly observed in prostate cancer [25,26]. In this way ETS overexpression activates RAS/ERK target genes and *PTEN* deletion activates the PI3K/AKT pathway, whereas in lung cancer *KRAS* mutation activates both ERK and PI3K pathways. It might thus be interesting to look at the influence of ectopic Nanos3 expression on a prostate cancer model with ERG overexpression and loss of *PTEN* [25,27].

According to the cBioPortal (*http://cbioportal.org*) database, *NANOS3* amplification was also frequently observed in ovarian cancer besides prostate cancer (see Chapter 2, Figure 2.3). As mentioned in Chapter 1, *NANOS3* mutations could also be linked with premature ovarian insufficiency (see section 1.1.4). We started investigating the possible role of Nanos3 in ovarian cancer by using an Amhr2-Cre;Pten$^{fl/fl}$;LSL-KRas^{G12D} model. However, because of lack of time and funding, the breeding experiments were ended before any results could be deduced.

In conclusion, ectopic expression of Nanos3 does not seem to influence tumor progression in the Hi-Myc prostate cancer model, on an FVB/N background.

4.5 Materials and methods

Mice and genotyping

Pb-Cre4 (Tg(Pbsn-cre)4Prb) [13], Hi-Myc [6] and our Nanos3$^{LSL/LSL}$ mice were used to obtain our prostate cancer model. *ROSA26* reporter (R26R) LacZ mice [14] were used to assess prostate-specific expression under control of the ARR_2/Pb promotor. All mice were bred and housed in individually ventilated cages in a specific pathogen-free facility. Genotyping was done as mentioned in Chapter 2. Primers used and the corresponding PCR programs can be found in addendum 4 and 5, respectively.

Perfusion and LacZ staining

Mice were anesthetized trough intra-peritoneal injection followed by a heart perfusion starting with +/- 15 ml PBS, till the organs are completely white, and ending with +/- 50-150 ml 4% PFA. The organs of interest were dissected and subjected to a LacZ staining. For this the organs were washed in detergent solution (Table 4.4) for 3 times 30 minutes at RT. This was followed by a one-hour incubation in staining solution (Table 4.5) at RT and a further overnight incubation at 4°C. Pictures were taken in detergent solution, and if the organs needed further treatment to prepare sections, they were fixed overnight in 4% PFA. Pictures were taken with a Canon G15 digital camera, Nikon AZ100M Macroscope or Olympus BX51 Discussion Microscope.

Table 4.4. Detergent solution.

- 50 ml 0.2 M phosphate buffer, pH 7.4
  - 19 ml 0.2 M NaH_2PO_4
  - 81 ml 0.2 M Na_2HPO_4
- 200 µl $MgCl_2$ (1 M)
- 1 ml sodium deoxycholate (1%)
- 500 µl BSA (1%)
- 20 µl NP-40
- 50 ml bidi
- 1250 µl 0.2 M EGTA

Table 4.5. Staining solution.

- 19 ml detergent solution - 1 ml X-gal - 200 µl 500 mM $K_3Fe(CN)_3$ (dissolved in detergent solution) - 200 µl 500 mM $K_4Fe(CN)_3$ (dissolved in detergent solution)

Western blotting

Western blotting of various mouse tissues was carried out as described in detail in Chapter 2. For the primary antibodies used and their respective dilutions, see addendum 2.

Immunohistochemistry

The protocol for IHC stainings is described in detail in Chapter 2. Biotin-conjugated secondary antibodies to rabbit immunoglobulins (Dako, 1:500) were used. Antibody-specific adaptations to the general protocol can be obtained upon simple request. For the antibodies used and their respective dilutions, see addendum 2.

H&E sections and stained sections of the prostate were scanned with the Slide Scanner Axio Scan.Z1 or the Pannoramic Slide Scanner.

4.6 References

1. Beltran H, Prandi D, Mosquera JM, Benelli M, Puca L, Cyrta J, Marotz C, Giannopoulou E, Chakravarthi BV, Varambally S, Tomlins SA, Nanus DM, Tagawa ST, Van Allen EM, Elemento O, Sboner A, Garraway LA, Rubin MA, Demichelis F (2016) Divergent clonal evolution of castration-resistant neuroendocrine prostate cancer. Nat Med 22 (3):298-305. doi:10.1038/nm.4045

2. Torre LA, Bray F, Siegel RL, Ferlay J, Lortet-Tieulent J, Jemal A (2015) Global cancer statistics, 2012. CA Cancer J Clin 65 (2):87-108. doi:10.3322/caac.21262

3. Rea D, Del Vecchio V, Palma G, Barbieri A, Falco M, Luciano A, De Biase D, Perdona S, Facchini G, Arra C (2016) Mouse Models in Prostate Cancer Translational Research: From Xenograft to PDX. Biomed Res Int 2016:9750795. doi:10.1155/2016/9750795

4. Grabowska MM, DeGraff DJ, Yu X, Jin RJ, Chen Z, Borowsky AD, Matusik RJ (2014) Mouse models of prostate cancer: picking the best model for the question. Cancer Metastasis Rev 33 (2-3):377-397. doi:10.1007/s10555-013-9487-8

5. Wu X, Gong S, Roy-Burman P, Lee P, Culig Z (2013) Current mouse and cell models in prostate cancer research. Endocr Relat Cancer 20 (4):R155-170. doi:10.1530/ERC-12-0285

6. Ellwood-Yen K, Graeber TG, Wongvipat J, Iruela-Arispe ML, Zhang J, Matusik R, Thomas GV, Sawyers CL (2003) Myc-driven murine prostate cancer shares molecular features with human prostate tumors. Cancer Cell 4 (3):223-238

7. Zhang J, Thomas TZ, Kasper S, Matusik RJ (2000) A small composite probasin promoter confers high levels of prostate-specific gene expression through regulation by androgens and glucocorticoids in vitro and in vivo. Endocrinology 141 (12):4698-4710. doi:10.1210/endo.141.12.7837

8. Bowen C, Bubendorf L, Voeller HJ, Slack R, Willi N, Sauter G, Gasser TC, Koivisto P, Lack EE, Kononen J, Kallioniemi OP, Gelmann EP (2000) Loss of NKX3.1 expression in human prostate cancers correlates with tumor progression. Cancer Res 60 (21):6111-6115

9. Dhanasekaran SM, Barrette TR, Ghosh D, Shah R, Varambally S, Kurachi K, Pienta KJ, Rubin MA, Chinnaiyan AM (2001) Delineation of prognostic biomarkers in prostate cancer. Nature 412 (6849):822-826. doi:10.1038/35090585

10. Rose-Hellekant TA, Gilchrist K, Sandgren EP (2002) Strain background alters mammary gland lesion phenotype in transforming growth factor-alpha transgenic mice. Am J Pathol 161 (4):1439-1447

11. Gingrich JR, Barrios RJ, Morton RA, Boyce BF, DeMayo FJ, Finegold MJ, Angelopoulou R, Rosen JM, Greenberg NM (1996) Metastatic prostate cancer in a transgenic mouse. Cancer Res 56 (18):4096-4102
12. Kahr I (2012) Functional analysis of the candidate tumor suppressor protein protocadherin-10. Dissertation, University of Ghent
13. Wu X, Wu J, Huang J, Powell WC, Zhang J, Matusik RJ, Sangiorgi FO, Maxson RE, Sucov HM, Roy-Burman P (2001) Generation of a prostate epithelial cell-specific Cre transgenic mouse model for tissue-specific gene ablation. Mech Dev 101 (1-2):61-69
14. Soriano P (1999) Generalized lacZ expression with the ROSA26 Cre reporter strain. Nat Genet 21 (1):70-71. doi:10.1038/5007
15. West DB, Pasumarthi RK, Baridon B, Djan E, Trainor A, Griffey SM, Engelhard EK, Rapp J, Li B, de Jong PJ, Lloyd KC (2015) A lacZ reporter gene expression atlas for 313 adult KOMP mutant mouse lines. Genome Res 25 (4):598-607. doi:10.1101/gr.184184.114
16. Bolon B (2008) Whole mount enzyme histochemistry as a rapid screen at necropsy for expression of beta-galactosidase (LacZ)-bearing transgenes: considerations for separating specific LacZ activity from nonspecific (endogenous) galactosidase activity. Toxicol Pathol 36 (2):265-276. doi:10.1177/0192623307312693
17. Birbach A (2013) Use of PB-Cre4 mice for mosaic gene deletion. PLoS One 8 (1):e53501. doi:10.1371/journal.pone.0053501
18. Bianchi-Frias D, Pritchard C, Mecham BH, Coleman IM, Nelson PS (2007) Genetic background influences murine prostate gene expression: implications for cancer phenotypes. Genome Biol 8 (6):R117. doi:10.1186/gb-2007-8-6-r117
19. Ware CB, Siverts LA, Nelson AM, Morton JF, Ladiges WC (2003) Utility of a C57BL/6 ES line versus 129 ES lines for targeted mutations in mice. Transgenic Res 12 (6):743-746
20. Vanden Berghe T, Hulpiau P, Martens L, Vandenbroucke RE, Van Wonterghem E, Perry SW, Bruggeman I, Divert T, Choi SM, Vuylsteke M, Shestopalov VI, Libert C, Vandenabeele P (2015) Passenger Mutations Confound Interpretation of All Genetically Modified Congenic Mice. Immunity 43 (1):200-209. doi:10.1016/j.immuni.2015.06.011
21. Mahler JF, Stokes W, Mann PC, Takaoka M, Maronpot RR (1996) Spontaneous lesions in aging FVB/N mice. Toxicol Pathol 24 (6):710-716. doi:10.1177/019262339602400606
22. Mainardi S, Mijimolle N, Francoz S, Vicente-Duenas C, Sanchez-Garcia I, Barbacid M (2014) Identification of cancer initiating cells in K-Ras driven lung adenocarcinoma. Proc Natl Acad Sci U S A 111 (1):255-260. doi:10.1073/pnas.1320383110

23. Tomlins SA, Rhodes DR, Perner S, Dhanasekaran SM, Mehra R, Sun XW, Varambally S, Cao X, Tchinda J, Kuefer R, Lee C, Montie JE, Shah RB, Pienta KJ, Rubin MA, Chinnaiyan AM (2005) Recurrent fusion of TMPRSS2 and ETS transcription factor genes in prostate cancer. Science 310 (5748):644-648. doi:10.1126/science.1117679

24. Perner S, Mosquera JM, Demichelis F, Hofer MD, Paris PL, Simko J, Collins C, Bismar TA, Chinnaiyan AM, De Marzo AM, Rubin MA (2007) TMPRSS2-ERG fusion prostate cancer: an early molecular event associated with invasion. Am J Surg Pathol 31 (6):882-888. doi:10.1097/01.pas.0000213424.38503.aa

25. Carver BS, Tran J, Gopalan A, Chen Z, Shaikh S, Carracedo A, Alimonti A, Nardella C, Varmeh S, Scardino PT, Cordon-Cardo C, Gerald W, Pandolfi PP (2009) Aberrant ERG expression cooperates with loss of PTEN to promote cancer progression in the prostate. Nat Genet 41 (5):619-624. doi:10.1038/ng.370

26. King JC, Xu J, Wongvipat J, Hieronymus H, Carver BS, Leung DH, Taylor BS, Sander C, Cardiff RD, Couto SS, Gerald WL, Sawyers CL (2009) Cooperativity of TMPRSS2-ERG with PI3-kinase pathway activation in prostate oncogenesis. Nat Genet 41 (5):524-526. doi:10.1038/ng.371

27. Chen Y, Chi P, Rockowitz S, Iaquinta PJ, Shamu T, Shukla S, Gao D, Sirota I, Carver BS, Wongvipat J, Scher HI, Zheng D, Sawyers CL (2013) ETS factors reprogram the androgen receptor cistrome and prime prostate tumorigenesis in response to PTEN loss. Nat Med 19 (8):1023-1029. doi:10.1038/nm.3216

Chapter 5

Nanos3 interaction partners

Contributions

Evi De Keuckelaere designed, performed and analyzed several experiments (Figure 5.1-5.14). Dr. Vanessa Andries designed, performed and analyzed several experiments (Figure 5.1-5.3). Ellen Sanders contributed to the BioID experiment. Mass spectrometry analysis was performed by the group of Prof. Dr. Kris Gevaert, The Medical Biotechnology Center, Ghent University.

5.1 Introduction

Every eukaryotic cell contains several thousand different proteins, which facilitate a variety of biological processes such as gene expression, cell growth, morphology, proliferation, motility, intercellular communication, apoptosis, etc. Functions of proteins depend on the ability to respond to inter- and intracellular signals or to interact with other biomolecules or both. These biomolecules can for instance be other proteins, carbohydrates, lipids, metabolites, RNA molecules and DNA molecules. Nanos proteins are mainly reported to form a multisubunit translation inhibitor complex with pumilio proteins. This complex has been shown to bind several mRNA targets, leading to their repression by binding several additional proteins such as the CCR4-NOT complex [1]. This complex and other proteins facilitate mRNA deadenylation and degradation, hence inhibiting mRNA translation. Recently, Nanos3 has been reported to negatively regulate E-cadherin at the transcriptional level, and to positively regulate vimentin at the post-transcriptional level [2]. The latter occurs by binding vimentin mRNA and by stimulating its polyadenylation and protecting it from miRNA-mediated repression. Known interaction partners of human Nanos proteins are still very scarce. The search for additional Nanos3-interacting proteins can bring more insight into the function of this protein. For example, no functional role has been attributed to Nanos3 expression in the brain, and proteins mediating Nanos3-directed transcriptional regulation are poorly characterized.

Co-immunoprecipitation (co-IP) followed by mass spectrometry is an elegant method to identify possible interaction partners of proteins of interest in a cell line of your choice [3]. Mass spectrometry on its own was already used to identify proteins that are differently expressed upon ectopic Nanos3 expression in three lung cell lines (see Chapter 2, Figure 2.7). In combination with Nanos3 co-IP this should give an interesting idea of the proteins that interact directly with or form a protein complex with Nanos3. The latter class of proteins also includes indirect interactors. Many techniques exist to verify the binding of possible interaction partners selected on the basis of mass spectrometry or hypothesis-based candidate interaction partners. Yeast two-hybrid screening, originally described by Fields and Song [4], is widely used to detect protein-protein interactions. This technique has several advantages such as the low requirements and costs and the speed and ease by which

several interactions can be checked at the same time. Major disadvantages are the lack of correct post-transcriptional modification and possible incorrect protein folding in yeast. This is less a problem when working with mammalian cells for analysis or confirmation of specific protein-protein interactions. Such methods include co-IP, pull-down assays and the mammalian protein-protein interaction trap (MAPPIT) [5,6]. The first two techniques depend on co-precipitation of interacting proteins with the protein of interest. The interacting proteins are separated from the lysate by using antibodies against the bait protein in co-immunoprecipitations, or against the affinity-tagged bait in pull-down assays. Immunoprecipitated proteins and their interaction partners are detected and identified by separating the proteins using SDS-PAGE followed by western blot analysis. These techniques are, however, only useful for stable interactions, as transient interactions are washed away during the procedures followed. In contrast, MAPPIT allows also for the detection of weak and transient interactions. As for co-IP, also indirect interactions are detected in the latter approach.

Fluorescence based techniques such as Förster resonance energy transfer or fluorescence resonance energy transfer (FRET), bioluminescence resonance energy transfer (BRET) [7] and bimolecular fluorescence complementation (BiFc) [8] can additionally supply information about the intercellular location where the interaction takes place.

5.2 Use of MAPPIT and other methods to confirm the interaction of Nanos3 with candidate partners such as Argonaute proteins

Only 2% of the human genome encodes proteins. Noncoding sequences include introns, regulatory regions and sequences for non-coding RNAs (RNA genes). Examples of non-coding RNAs (ncRNAs) are transfer RNAs (tRNAs), ribosomal RNAs (rRNAs) and small RNAs. The most abundant small RNAs are short-interfering RNAs (siRNAs), miRNAs and PIWI-interacting RNAs (piRNAs). siRNAs and miRNAs are processed by the endoribonuclease, Dicer. siRNAs can also originate from exogenous sources such as viruses, transgenes and introduced double-stranded RNA (dsRNA). Small RNAs interact with members of the Argonaute protein family to exert their functions. While siRNAs and miRNAs interact with proteins from the AGO subclade, piRNAs interact with proteins from the PIWI (P-element-induced whimpy testes) subclade (Table 5.1). siRNAs and miRNAs bound to AGO proteins bind their

complementary mRNA target, which can then be cleaved or translationally repressed. Several mRNA decapping, decay and deadenylation complexes are involved in translational silencing. For miRNA-mediated repression, an interaction between AGO proteins and members of the GW182 protein family is required. These GW182 proteins have for instance been shown to recruit the CCR4-NOT deadenylase complex [9]. RNP complexes consisting of piRNAs and PIWI proteins mainly regulate transposable elements. Regulation of gene expression by PIWI proteins has also been demonstrated, however, few target genes are known so far [10].

Table 5.1. Argonaute family proteins. Adapted from [11].

	AGO		**PIWI**
Expression	All tissues		Germline and cancer
Homologs of human,	AGO1, AGO2, AGO3 and AGO4		PIWIL1 (HIWI), PIWIL2 (HILI), PIWIL3 and PIWIL4 (HIWI2)
mouse and	AGO1, AGO2, AGO3 and AGO4		PIWIL1 (MIWI), PIWIL2 (MILI) and PIWIL4 (MIWI2)
Drosophila	AGO1 and AGO2		PIWI, AUB and AGO3
Bound small RNA	miRNA	siRNA	piRNA
Length (nt)	20-23	20-23	25-31
Biogenesis	Drosha, Dicer	Dicer	Dicer-independent
Precursor	Hairpin-structured RNA	dsRNA	ssRNA
Function	Regulation of mRNA stability and translation	Transposon silencing and protection from viral infection	Transposon silencing and unknown function

Based on the role of Nanos proteins in post-transcriptional regulation and the close interaction with the miRNA regulatory network, interaction of Nanos3 with Argonaute family proteins, Dicer and GW182, also known as TNRC6A, was investigated by MAPPIT. In our research group, a pull-down experiment using Myc-tagged Nanos1 led to the identification of RNA helicase DDX1 as a possible interaction partner (V. Andries *et al*., unpublished). The latter protein was also taken along given the association of DEAD-box RNA helicases with translation initiation, RNA synthesis and degradation [12].

The MAPPIT technique relies on the functional restoration of a defective cytokine receptor upon interaction between bait- and prey-fusion proteins. The bait is fused to the defective receptor and the prey is fused to a part of the receptor containing STAT3 recruitment sites (Figure 5.1). Luciferase activity, depending on cytokine-induced STAT3 signaling, is used as a read-out for interaction. This technique indeed confirmed interaction between each of the three human Nanos proteins and DDX1 (Figure 5.2A), and between Nanos3 and AGO1 to -3 and PIWIL1, PIWIL2 and PIWIL4 proteins, but not with TNRC6A or Dicer (Figure 5.2).

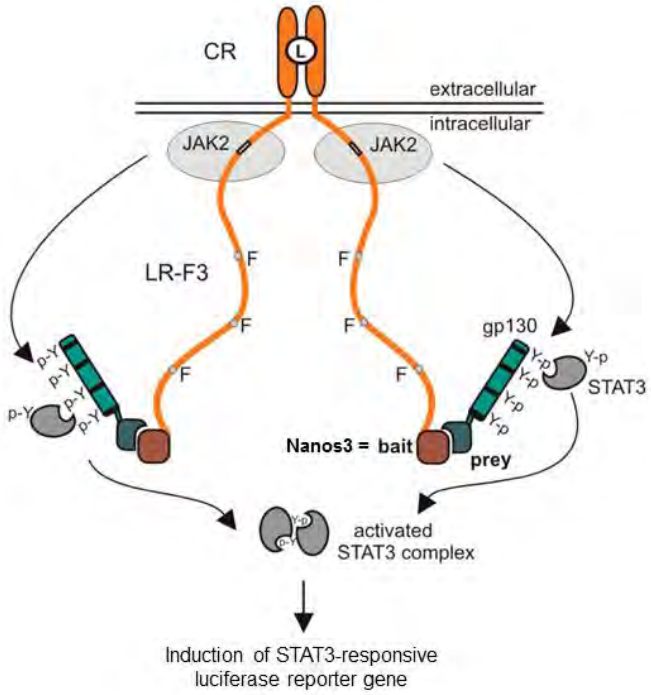

Figure 5.1. MAPPIT concept. The bait, Nanos3 in our case, is fused to a defective cytokine receptor (CR) such as the leptin receptor (LR). The tyrosines (Y) in the intracellular receptor tails were replaced by phenylalanine (F) making them unable to bind STAT3. STAT3 is activated upon leptin (L) stimulation in the presence of the prey, fused to a receptor fragment containing functional STAT3 recruitment sites (gp130). The activated STAT3 complex migrates to the nucleus and induces STAT3-responsive reporter gene expression. Figure adapted from [13].

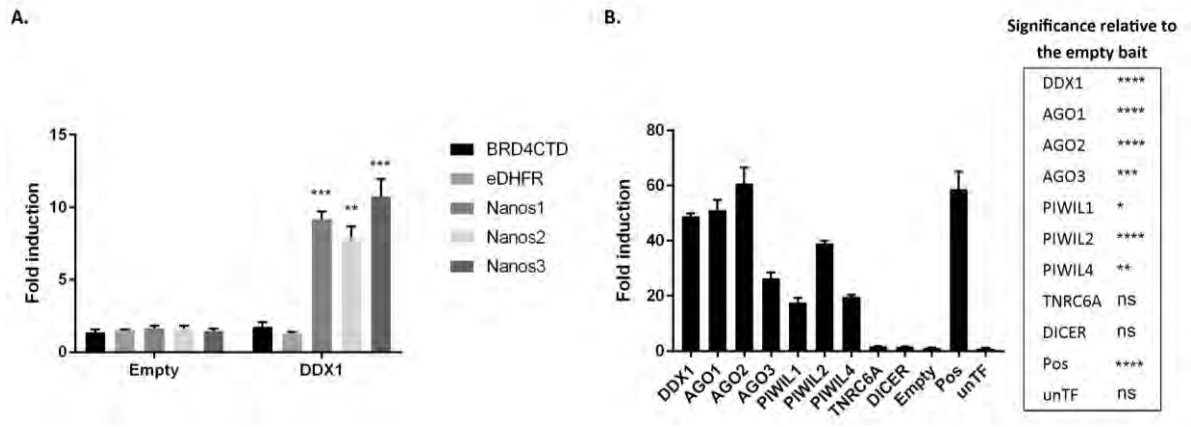

Figure 5.2. Nanos3 interacts with DDX1 and Argonaute family proteins. A. MAPPIT assay revealing interaction of DDX1 with the human Nanos proteins. The empty prey vector served as a negative control and BRD4CTD and eDHFR as irrelevant bait vectors. **B.** MAPPIT assay showing interaction between Nanos3 and several Argonaute proteins. The empty prey vector and untransfected (unTF) cells served as negative controls and REM2 prey, binding the receptor part of the bait-fusion protein, was taken along as a positive control. Luciferase measurements were normalized by β-galactosidase expression. Reporter activities are represented as fold induction of the normalized luciferase activity (leptin-treated *versus* leptin-untreated cells). Three independent replicates were performed. Error bars, SEM; n=3, ns: not significant, *: P≤0.05, **: P≤0.01, ***: P≤0.001, ****: P≤0.0001.

Co-IP was used to confirm these protein-protein interactions, indicated by MAPPIT. To this end, HEK293T cells were transfected with Myc-Nanos3 and Flag-DDX1 constructs. To test if this interaction is RNA-dependent, half of the cell lysate was treated with RNase A. Immunoprecipitations were done with an anti-Myc or irrelevant antibody. The subsequent western blot detection with anti-Myc antibody, anti-Flag antibody or anti-DDX1 antibody demonstrated that DDX1 interacts with Nanos3 in an RNA-dependent manner (Figure 5.3A). Endogenous DDX1 also co-immunoprecipitated with Myc-Nanos3 (Figure 5.3B).

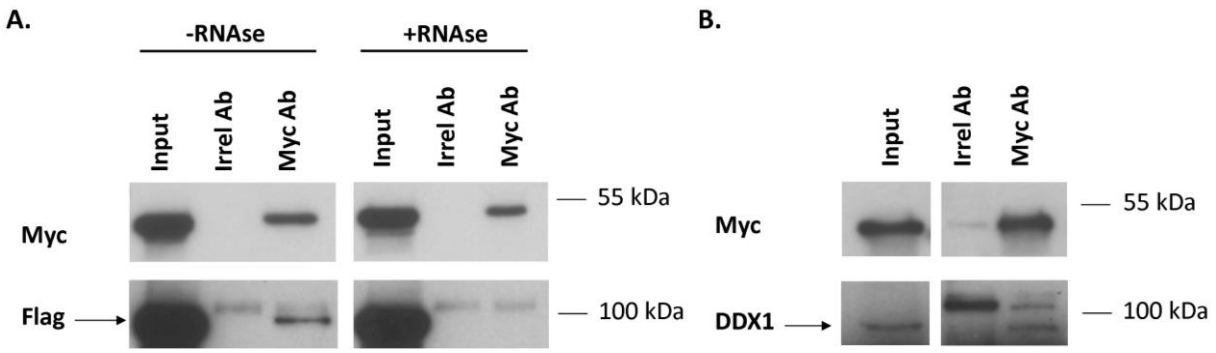

Figure 5.3. DDX1 is an RNA-dependent interaction partner of Nanos3. A. Lysates of HEK293T cells expressing both Myc-Nanos3 and Flag-DDX1 were treated with RNase or left untreated. This was followed by co-immunoprecipitation with an irrelevant (Irrel) or Myc-specific antibody (Ab) and western blot detection of Nanos3 and DDX1 using Myc and Flag antibodies, respectively. **B.** Endogenous DDX1 was similarly co-immunoprecipitated using HEK293T cells overexpressing Myc-Nanos3.

To confirm the interaction with the PIWIL and AGO proteins, the MAPPIT prey constructs were transfected into HEK293T cells together with Myc-Nanos3. These prey constructs include a flag-tag and the gp130 receptor chain harboring STAT3 recruitment sites. Myc-immunoprecipitation was followed by western blotting, showing an interaction between all PIWIL and AGO proteins on the one hand, and Myc-Nanos3 on the other hand (Figure 5.4).

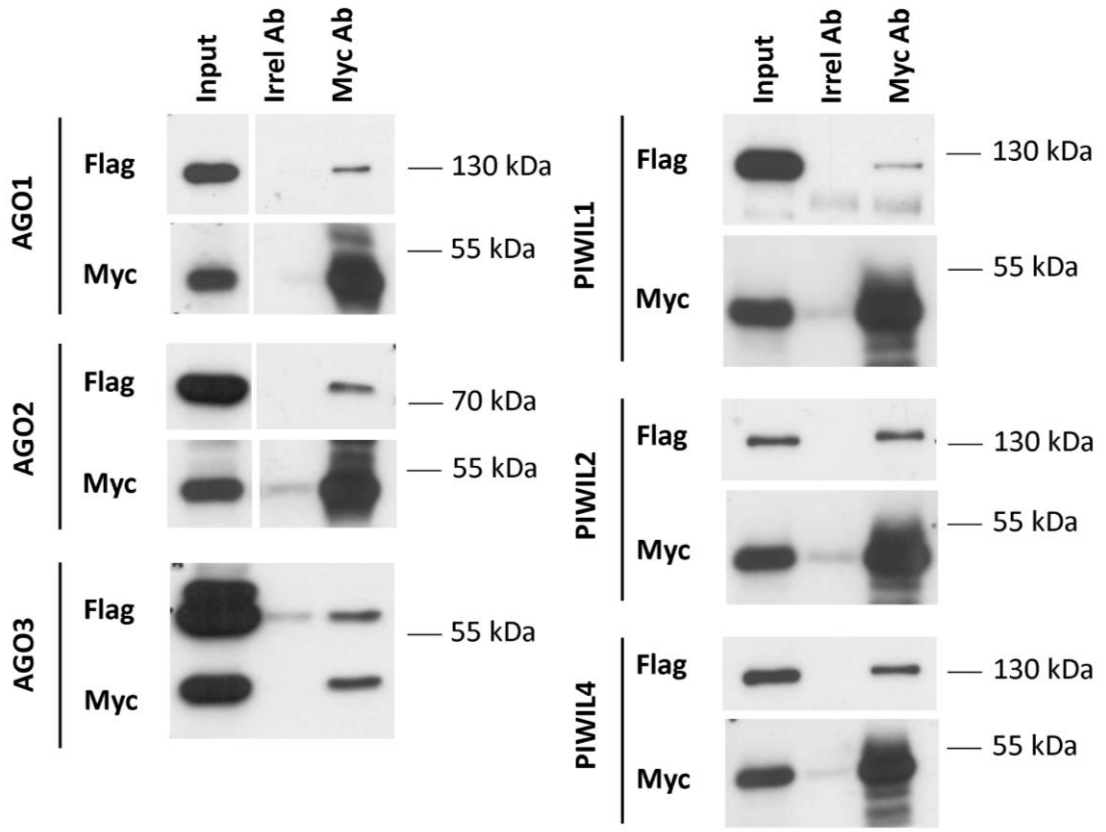

Figure 5.4. Nanos3 interacts with Argonaute family proteins. Immunoprecipitation experiment using HEK293T cells overexpressing Myc-Nanos3 and a flag-tagged protein from the Argonaute family (AGO1, AGO2, AGO3, PIWIL1, PIWIL2 or PIWIL4). Nanos3 was immunoprecipitated using a Myc antibody (Ab), and an irrelevant (irrel) antibody as negative control. Co-immunoprecipitation of the Argonaute family proteins was checked via western blot detection with anti-Flag.

However, the bands for AGO2 and AGO3 ran much lower than expected. The prey constructs were a gift from the lab of Prof. Dr. Jan Tavernier, VIB-UGent, Center for Medical Biotechnology. These were made with sequences from the ORFeome8.1 collection [14], which apparently in case for AGO2 and AGO3 do not represent the complete genes. Argonaute proteins contain four domains, the N-terminal, PAZ (PIWI/Argonaute/Zwille), MID and PIWI domain (Figure 5.5A). The PAZ domain is also found in Dicer and is able to bind the 3' end of the small RNAs [15,16]. The three-dimensional shape of the PIWI domain resembles that of enzymes of the RNaseH family [17]. Mutations in this domain indeed abolish the catalytic activity needed for mRNA target cleavage, also called slicer activity of AGO2 [18]. The cDNA sequence for AGO2, obtained from the ORFeome collection, represents the C-terminal part including almost the complete MID-PIWI domains (Figure

5.5A). The domains depicted in Figure 5.5 are those recognized as the conserved domains by NCBI (the National Center for Biotechnology). The PIWI domain recognized by NCBI (Figure 5.5A) can be further separated in the MID and PIWI domains mentioned above. The ORFeome sequence of AGO3 only includes the N-terminal part of the sequence including the N-terminal domain of argonaute (ArgoN) and almost the complete argonaute linker 1 domain (ArgoL1), between the ArgoN and PAZ domain.

The TNRC6A sequence was also incomplete, only encompassing part of the C-terminal RNA recognition motif (RRM) (Figure 5.5B). Therefore, the lack of Nanos3 interaction in the MAPPIT assay does not necessarily mean that Nanos3 does not interact with TNRC6A. For DDX1 only the 43 N-terminal AA were missing.

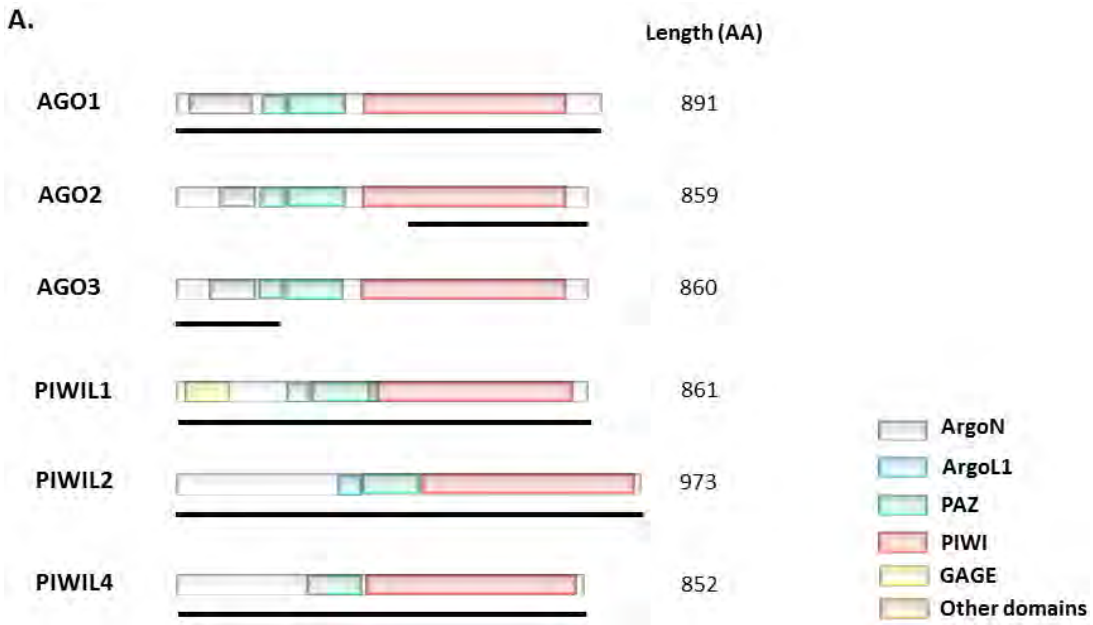

Figure 5.5. Panel A.

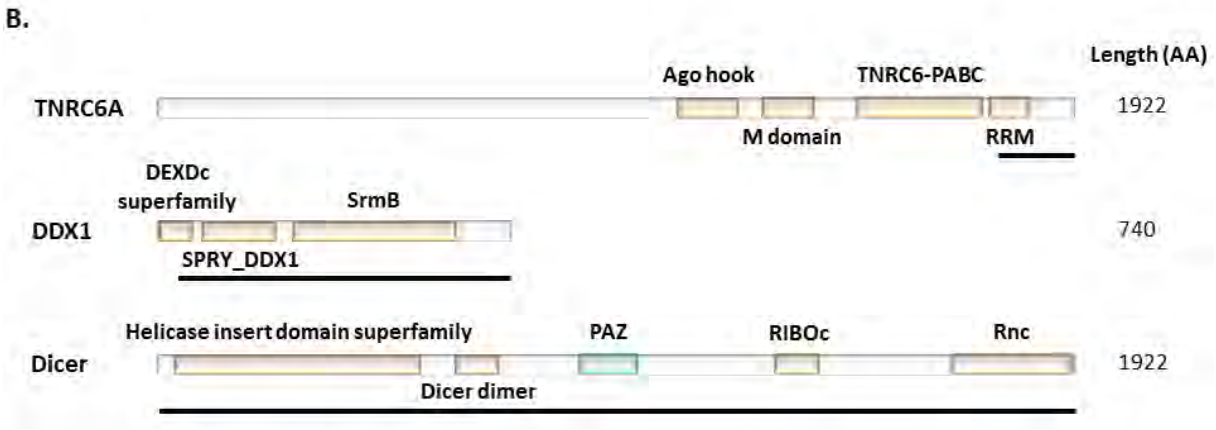

Figure 5.5. Sequences from the ORFeome8.1 collection do not always encompass the complete protein sequence. A. The investigated Argonaute proteins are depicted with their protein domains according to NCBI (*https://www.ncbi.nlm.nih.gov*). The used ORFeome sequences for each of these are depicted by the black line underneath the represented protein. **B.** The ORFeome sequence (black line) for TNRC6A only represents a small C-terminal part of the protein while that for Dicer is complete and that of DDX1 only misses a small N-terminal part of the protein sequence. AA, amino acids; ArgoN, N-terminal domain of argonaute; ArgoL1, argonaute linker 1 domain; PAZ, PIWI/Argonaute/Zwille; PIWI, P-element-induced whimpy testes; Ago hook, argonaute hook; M domain, middle domain; RRM, RNA recognition motif; SPRY, Spla and the Ryanodine receptor; SrmB, Superfamily II DNA and RNA helicases; dicer dimer, dicer dimerization domain; RIBOc, ribonuclease III family; Rnc, dsRNA-specific ribonuclease

New constructs without the gp130 receptor chain were made to confirm the interaction of Nanos3 with AGO1 and the PIWIL proteins. The ORFeome sequences of AGO1 and PIWIL1, -2 and -4 were fused to EGFP and together with Myc-Nanos3 they were overexpressed in HEK293T cells. However, immunoprecipitation using a Myc-antibody followed by EGFP-detection on western blot revealed this time no interaction between Nanos3 and the Argonaute family proteins. When comparing PIWIL protein expression of HEK293T cells transfected with the PIWIL prey constructs from MAPPIT and the EGFP-PIWIL proteins, a typical cytoplasmic staining was observed for the first type of constructs (Figure 5.6). The EGFP-PIWIL constructs seemed to form aggregates and were largely expressed in seemingly dying cells. The same was seen for the EGFP-AGO1 construct. This might explain why an interaction was not observed using the EGFP constructs.

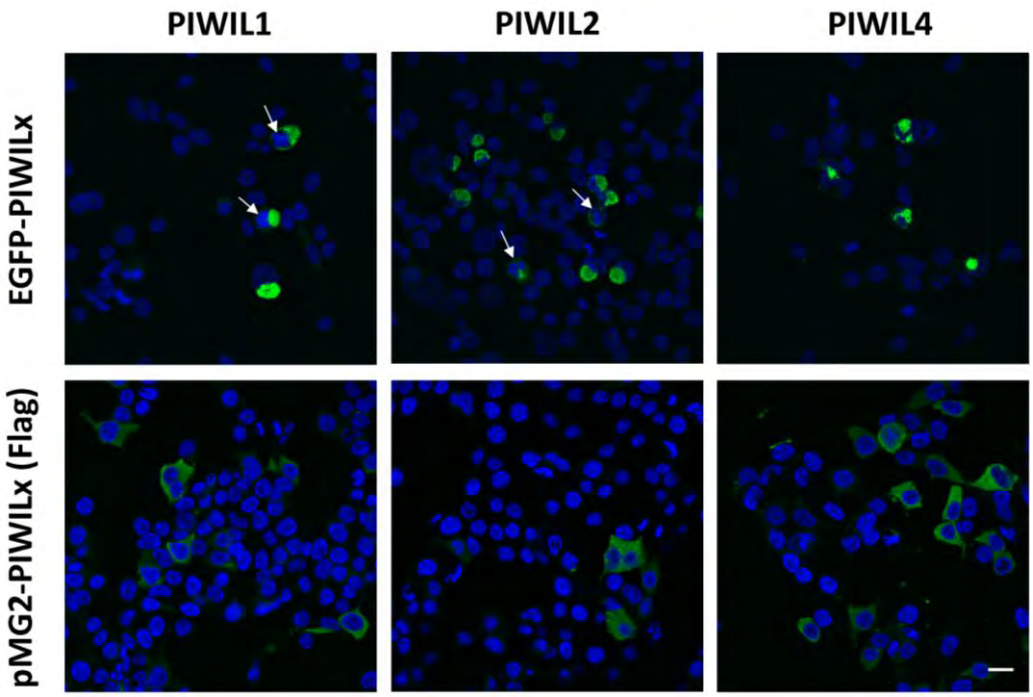

Figure 5.6. Cellular localization of PIWIL expression constructs in HEK293T cells. Immunofluorescent detection of PIWIL proteins in transfected HEK293T cells. The EGFP and pMG2 constructs were detected using an anti-GFP and an anti-Flag antibody, respectively. Bar, 20 µm; arrows, seemingly dying cells.

5.3 Co-IP followed by mass spectrometry

To have a global view on the possible interaction partners of Nanos3 the co-IP protocol was optimized for Nanos3 including the use of bis(sulfosuccinimidyl)suberate (BS3) crosslinkers to link the antibodies to the Protein G Dynabeads® (Life Technologies). Co-IP was done on HEK293T cells transfected with a Nanos3 expression construct. Nanos3 and its associated proteins were eluted and separated on 15% SDS-PAGE gels (see Materials and methods). A small fraction of the elution was used to test immunoprecipitation of the Nanos3 protein through western blotting (Figure 5.7) while the gel loaded with the vast majority of the elution fraction was stained with Coomassie brilliant stain. Differential bands between 22 and 60 kDa were cut out (+/- 22, 25, 30 and 60 kDa, Nanos3 and isotype bands) and subjected to a tryptic digestion for mass spectrometric analysis. Protein identification by LC-MS/MS analysis on the Orbitrap XL mass spectrometer was performed by the group of Prof. Dr. Kris Gevaert, The Medical Biotechnology Center, Ghent University.

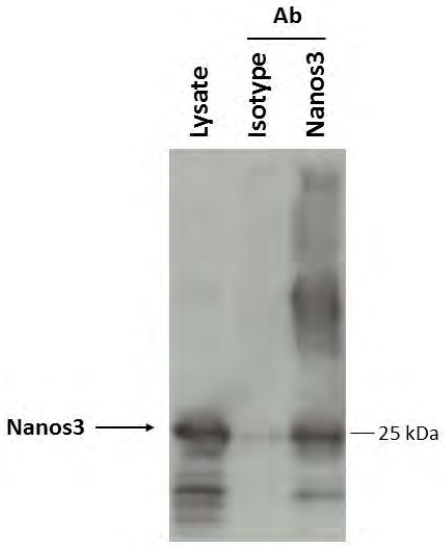

Figure 5.7. Immunoprecipitation of Nanos3 (complexes) in transfected HEK293T cells. HEK293T cells transfected with a Nanos3-expressing plasmid were used in a Nanos3 co-immunoprecipitation experiment. Polyclonal rabbit IgG isotype antibodies (Abs) were used as a negative control. Immunoprecipitation of Nanos3 was confirmed through western blotting using a Nanos3-specific Ab (Proteintech).

Of all the proteins identified, 70 proteins were specific for the bands from the Nanos3 immunoprecipitation (Table 5.2). Nine of these were identified by more than one peptide with a protein coverage ranging from 0.97-15.87%. The protein coverage represents the

percentage of amino acids of the protein covered in the detected peptides. The respective molecular weights of the proteins were more or less in accordance with the molecular weight corresponding to the excised band in which the protein was found. PLAK and TGM5 were two exceptions since they both have an expected molecular weight around 80 kDa and were found in the +/- 22 kDa and +/- 60 kDa band region of the gel, respectively. Unlike for TGM5, the four peptide sequences of PLAK, enriched in the Nanos3 lane, were spread over the complete protein.

Table 5.2. List of 70 proteins that were only traced back in the gel bands obtained after immunoprecipitation with the Nanos3 antibody and not in those from the isotype antibody. The proteins are ranked according to the total number of detected peptides.

Accession number	Protein	Mean score[a]	Mean threshold[b]	Total # of peptides
Q92600	RCD1_HUMAN Cell differentiation protein RCD1 homolog GN[c]=RQCD1	44	20	4
P14923	PLAK_HUMAN Junction plakoglobin GN=JUP	33	19	4
Q9UIV1	CNOT7_HUMAN CCR4-NOT transcription complex subunit 7 GN=CNOT7	47	23	3
Q9BQE4	SELS_HUMAN Selenoprotein S GN=VIMP	48	21	3
Q9NZN8	CNOT2_HUMAN CCR4-NOT transcription complex subunit GN=CNOT2	48	21	3
P62753	RS6_HUMAN 40S ribosomal protein S6 GN=RPS6	42	23	2
O43548	TGM5_HUMAN Protein-glutamine gamma-glutamyltransferase 5 GN=TGM5	26	25	2
Q99741	CDC6_HUMAN Cell division control protein 6 homolog GN=CDC6	39	23	2
P26373	RL13_HUMAN 60S ribosomal protein L13 GN=RPL13	34	22	2
P12235	ADT1_HUMAN ADP/ATP translocase 1 GN=SLC25A4	31	23	1
P15880	RS2_HUMAN 40S ribosomal protein S2 GN=RPS2	20	16	1
P24534	EF1B_HUMAN Elongation factor 1-beta GN=EEF1B2	27	22	1
P48775	T23O_HUMAN Tryptophan 2,3-dioxygenase GN=TDO2	36	21	1
Q07666	KHDR1_HUMAN KH domain-containing, RNA-binding, signal transduction-associated protein 1 GN=KHDRBS1	23	19	1
Q12912	LRMP_HUMAN Lymphoid-restricted membrane protein GN=LRMP	21	19	1
Q14680	MELK_HUMAN Maternal embryonic leucine zipper kinase GN=MELK	24	23	1
Q8IYA6	CKP2L_HUMAN Cytoskeleton-associated protein 2-like GN=CKAP2L	44	23	1
Q9H0U3	MAGT1_HUMAN Magnesium transporter protein 1 GN=MAGT1	41	24	1
Q9HCK1	ZDBF2_HUMAN DBF4-type zinc finger-containing protein 2 GN=ZDBF2	21	20	1
Q9UFF9	CNOT8_HUMAN CCR4-NOT transcription complex subunit 8 GN=CNOT8	53	21	1
Q9Y399	RT02_HUMAN 28S ribosomal protein S2, mitochondrial GN=MRPS2	25	20	1
Q9Y5M8	SRPRB_HUMAN Signal recognition particle receptor subunit beta GN=SRPRB	28	22	1
Q9Y6D6	BIG1_HUMAN Brefeldin A-inhibited guanine nucleotide-exchange protein 1 GN=ARFGEF1	26	24	1
O14908	GIPC1_HUMAN PDZ domain-containing protein GIPC1 GN=GIPC1	23	22	1
O95025	SEM3D_HUMAN Semaphorin-3D GN=SEMA3D	22	20	1
P15586	GNS_HUMAN N-acetylglucosamine-6-sulfatase GN=GNS	25	20	1

Accession number	Protein	Mean score[a]	Mean threshold[b]	Total # of peptides
P50914	RL14_HUMAN 60S ribosomal protein L14 GN=RPL14	40	19	1
Q8N3V7	SYNPO_HUMAN Synaptopodin GN=SYNPO	32	22	1
Q99714	HCD2_HUMAN 3-hydroxyacyl-CoA dehydrogenase type-2 GN=HSD17B10	26	20	1
Q9BW19	KIFC1_HUMAN Kinesin-like protein KIFC1 GN=KIFC1	99	23	1
Q9NX63	CHCH3_HUMAN Coiled-coil-helix-coiled-coil-helix domain-containing protein 3, mitochondrial GN=CHCHD3	44	23	1
Q9UF83	YM012_HUMAN Uncharacterized protein DKFZp434B061	32	21	1
Q9UI43	RRMJ2_HUMAN Putative ribosomal RNA methyltransferase 2 GN=FTSJ2	24	14	1
O75072	FKTN_HUMAN Fukutin GN=FKTN	24	23	1
P30626	SORCN_HUMAN Sorcin GN=SRI	37	23	1
P46778	RL21_HUMAN 60S ribosomal protein L21 GN=RPL21	18	17	1
P61009	SPCS3_HUMAN Signal peptidase complex subunit 3 GN=SPCS3	41	22	1
P62081	RS7_HUMAN 40S ribosomal protein S7 GN=RPS7	31	24	1
Q02413	DSG1_HUMAN Desmoglein-1 OS=Homo sapiens GN=DSG1 PE=1 SV=2	53	17	1
Q5T749	KPRP_HUMAN Keratinocyte proline-rich protein OS=Homo sapiens GN=KPRP PE=1 SV=1	41	24	1
Q9BQ61	CS043_HUMAN Uncharacterized protein C19orf43 OS=Homo sapiens GN=C19orf43 PE=1 SV=1	36	20	1
Q9H8H2	DDX31_HUMAN Probable ATP-dependent RNA helicase DDX31 OS=Homo sapiens GN=DDX31 PE=1 SV=2	39	24	1
A6NNZ2	TBB8L_HUMAN Tubulin beta-8 chain-like protein LOC260334 OS=Homo sapiens PE=1 SV=1	49	24	1
O76014	KRT37_HUMAN Keratin, type I cuticular Ha7 OS=Homo sapiens GN=KRT37 PE=2 SV=3	27	22	1
O94804	STK10_HUMAN Serine/threonine-protein kinase 10 OS=Homo sapiens GN=STK10 PE=1 SV=1	34	23	1
O95159	ZFPL1_HUMAN Zinc finger protein-like 1 GN=ZFPL1	23	22	1
P06239	LCK_HUMAN Tyrosine-protein kinase Lck GN=LCK	33	25	1
P10809	CH60_HUMAN 60 kDa heat shock protein, mitochondrial GN=HSPD1	30	21	1
P11940	PABP1_HUMAN Polyadenylate-binding protein 1 GN=PABPC1	23	20	1
P17987	TCPA_HUMAN T-complex protein 1 subunit alpha GN=TCP1	26	20	1
P22234	PUR6_HUMAN Multifunctional protein ADE2 GN=PAICS	32	20	1
P26368	U2AF2_HUMAN Splicing factor U2AF 65 kDa subunit GN=U2AF2	23	16	1
P30153	2AAA_HUMAN Serine/threonine-protein phosphatase 2A 65 kDa regulatory subunit A alpha isoform GN=PPP2R1A	66	23	1
P34897	GLYM_HUMAN Serine hydroxymethyltransferase, mitochondrial GN=SHMT2	21	19	1
P48643	TCPE_HUMAN T-complex protein 1 subunit epsilon GN=CCT5	92	23	1
P49368	TCPG_HUMAN T-complex protein 1 subunit gamma GN=CCT3	37	17	1
P53367	ARFP1_HUMAN Arfaptin-1 GN=ARFIP1	20	19	1
P60709	ACTB_HUMAN Actin, cytoplasmic 1 GN=ACTB	46	24	1
Q00537	CDK17_HUMAN Cyclin-dependent kinase 17 GN=CDK17	51	23	1
Q12912	LRMP_HUMAN Lymphoid-restricted membrane protein GN=LRMP	20	19	1
Q13547	HDAC1_HUMAN Histone deacetylase 1 GN=HDAC1	27	21	1
Q15361	TTF1_HUMAN Transcription termination factor 1 GN=TTF1	21	20	1
Q6B0I6	KDM4D_HUMAN Lysine-specific demethylase 4D GN=KDM4D	42	24	1

Accession number	Protein	Mean score[a]	Mean threshold[b]	Total # of peptides
Q8N684	CPSF7_HUMAN Cleavage and polyadenylation specificity factor subunit 7 GN=CPSF7	30	23	1
Q96LI5	CNO6L_HUMAN CCR4-NOT transcription complex subunit 6-like GN=CNOT6L	36	20	1
Q96TA2	YMEL1_HUMAN ATP-dependent zinc metalloprotease YME1L1 GN=YME1L1	25	21	1
Q9NRI5	DISC1_HUMAN Disrupted in schizophrenia 1 protein GN=DISC1	28	22	1
Q9P258	RCC2_HUMAN Protein RCC2 GN=RCC2	26	22	1
Q9UF83	YM012_HUMAN Uncharacterized protein DKFZp434B061	24	21	1
Q9UKX7	NUP50_HUMAN Nuclear pore complex protein Nup50 GN=NUP50	25	20	1

[a] a -log function of a p-value calculated at the 95% significance level showing how well the observed spectrum corresponds to the proposed peptides

[b] -10 log score calculated by mascot based on several parameters such as how many peptides in the database have the mass in question, using a significance threshold of 0.05

[c] Gene name

Nanos3 peptides were traced back in the Nanos3-enriched lane as well as in the isotype lane. However, more Nanos3 peptides were detected in the former, indicating a higher amount of Nanos3 protein as is clearly visible after western blot detection (Figure 5.7).

Our relatively short list of candidate interactors of Nanos3 contains several proteins from the CCR4-NOT complex (RCD1, CNOT7, CNOT2, CNOT8 and CNO6L). Recently the human Nanos proteins were indeed found to bind the CCR4-NOT complex through interaction with CNOT1 [1]. Surprisingly CNOT1 was not detected here. Ribosomal proteins are also strongly represented in our list. However, these proteins are very abundant in the cell and often co-precipitate unspecifically. Several other ribosomal proteins were also found back in the isotype control bands.

Given the fairly low number of identified possible Nanos3 interaction partners we decided to repeat the experiment, but this time by using a higher amount of starting proteins. Twenty 175-cm^2 flasks of HEK293T cells were transfected with a Nanos3 expression construct (pdest 12.2 Nanos3cl1) rendering around 67 mg protein that could be used for both the Nanos3 and isotype immunoprecipitation. Instead of eluting the proteins by boiling the beads, a pH-based elution was now chosen (Figure 5.8). This was established to give less background after western blot detection.

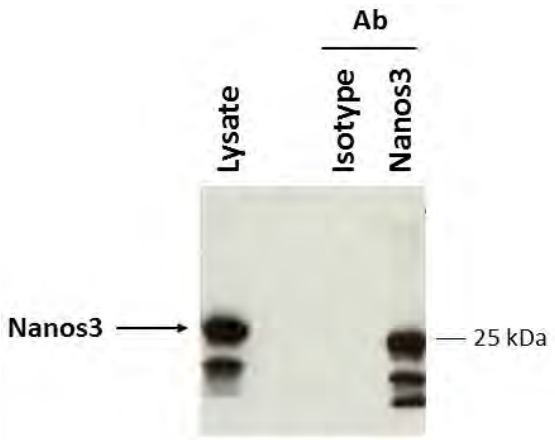

Figure 5.8. Immunoprecipitation of Nanos3 (complexes) in transfected HEK293T cells. Nanos3-expressing HEK293T cells were used in a co-immunoprecipitation experiment to identify interaction partners of Nanos3. Polyclonal rabbit IgG isotype antibodies (Abs) were used as a negative control. A pH-based elution was used to separate the Nanos3 complexes from the beads. Immunoprecipitation of Nanos3 was confirmed through western blotting using a Nanos3-specific Ab (Proteintech).

Five differentially expressed bands (band 1: +/- 15 kDa, band 2: +/- 22 kDa and band 3-5: +/- 25-34 kDa) were cut out of the gel from the lanes loaded with the isotype and Nanos3 eluate. Nanos3 was again found in every Nanos3 band with 8, 12, 44, 78 and 78 peptide counts in band 1-5, respectively. Nanos3 was only detected in two isotype bands with merely 2 and 4 peptide counts.

This time only 25 proteins were uniquely detected in the Nanos3 bands of which two were detected by merely one peptide (Table 5.3). The protein coverage ranged from 0.8-28.6%. As expected CNOT proteins were detected, yet to a lesser extent compared to the previous experiment. Only RCD1 and CNOT7 were found back as possible Nanos3 interaction partners in both experiments. Although, similarly as in the first experiment, several ribosomal proteins were detected in this experiment, none of them matched those that were previously found. This underscores the unspecific binding of these proteins. DDX1 and AGO proteins were not detected despite our abovementioned positive MAPPIT and co-IP results using expression constructs.

Table 5.3. List of 25 unique proteins identified by Nanos3 immunoprecipitation. The proteins are ranked according to the total number of detected peptides.

Accession number	Protein	Mean score[a]	Mean threshold[b]	Total # of peptides
Q92600	RCD1_HUMAN Cell differentiation protein RCD1 homolog GN[c]=RQCD1	55	28	8
Q99569	PKP4_HUMAN Plakophilin-4 GN=PKP4	44	29	6
P62269	RS18_HUMAN 40S ribosomal protein S18 GN=RPS18	77	28	4
Q8TCC3	RM30_HUMAN 39S ribosomal protein L30, mitochondrial GN=MRPL30	43	27	4
Q9Y3C6	PPIL1_HUMAN Peptidyl-prolyl cis-trans isomerase-like 1 GN=PPIL1	38	27	4
Q9UBD9	CLCF1_HUMAN Cardiotrophin-like cytokine factor 1 GN=CLCF1	37	27	3
P04083	ANXA1_HUMAN Annexin A1 GN=ANXA1	31	24	2
Q32NC0	CR021_HUMAN UPF0711 protein C18orf21 GN=C18orf21	27	25	2
Q9NSI2	F207A_HUMAN Protein FAM207A GN=FAM207A	34	26	2
Q9NVE4	CCD87_HUMAN Coiled-coil domain-containing protein 87 GN=CCDC87	28	27	2
Q9UIV1	CNOT7_HUMAN CCR4-NOT transcription complex subunit 7 GN=CNOT7	63	28	2
Q86TB9	PATL1_HUMAN Protein PAT1 homolog 1 GN=PATL1	32	28	2
O95503	CBX6_HUMAN Chromobox protein homolog 6 GN=CBX6	40	28	2
P42126	ECI1_HUMAN Enoyl-CoA delta isomerase 1, mitochondrial GN=ECI1	30	27	2
Q9BPW8	NIPS1_HUMAN Protein NipSnap homolog 1 GN=NIPSNAP1	35	29	2
Q9NX63	MIC19_HUMAN MICOS complex subunit MIC19 GN=CHCHD3	44	29	2
Q9Y224	CN166_HUMAN UPF0568 protein C14orf166 GN=C14orf166	31	30	2
O95299	NDUAA_HUMAN NADH dehydrogenase [ubiquinone] 1 alpha subcomplex subunit 10, mitochondrial GN=NDUFA10	57	28	2
P42766	RL35_HUMAN 60S ribosomal protein L35 GN=RPL35	53	25	2
P46779	RL28_HUMAN 60S ribosomal protein L28 GN=RPL28	39	26	2
P61353	RL27_HUMAN 60S ribosomal protein L27 GN=RPL27	48	29	2
P62263	RS14_HUMAN 40S ribosomal protein S14 GN=RPS14	31	27	2
P62854	RS26_HUMAN 40S ribosomal protein S26 GN=RPS26	29	27	2
P68400	CSK21_HUMAN Casein kinase II subunit alpha GN=CSNK2A1	39	29	1
Q15005	SPCS2_HUMAN Signal peptidase complex subunit 2 GN=SPCS2	30	28	1

[a] a -log function of a p-value calculated at the 95% significance level showing how well the observed spectrum corresponds to the proposed peptides

[b] -10 log score calculated by mascot based on several parameters such as how many peptides in the database have the mass in question, using a significance threshold of 0.05

[c] Gene name

5.4 Proximity-dependent biotin identification (BioID), applied on Nanos3

Although co-IP is a recommended technique to detect interaction partners, the washing steps preclude the detection of transient and weak interactions. BioID is a suitable technique to identify weak and transient interactions in addition to proteins located in the direct neighborhood of the investigated protein. The technique relies on the use of a mutant BirA, a biotin ligase from *E. coli* [19]. This mutant has a lower binding affinity for the biotinyl-5'-AMP intermediate [20]. This leads to premature release of the activated biotin ligand which can interact with nearby primary amine groups (-NH_2) hence performing sequence-unspecific but proximity-dependent biotinylation. We fused the HA-tagged BirA ligase to the C-terminus of Nanos3. The coding DNA sequence of this fusion protein was expressed from a dox-dependent CMV(TetO) promoter and followed by a Flippase (Flp) Recombinase/Recognition Target (FRT) site (see Materials and methods). We used the Flp-In™ T-Rex™ 293 cell line and a flp-recombinase expression vector to stably integrate our expression vector into the FRT-containing locus.

Dox-induced cells were treated with biotin for 24 hours. These induced cells express the Nanos3-BirA-HA construct (Figures 5.9 and 5.10A) and behaved as normal Flp-In™ T-Rex™ 293 cells. The BirA ligation did not seem to affect Nanos3 localization in HEK cells (Figure 5.9). The addition of biotin (50 µM) resulted in BirA-mediated biotinylation and staining for biotin using Alexa Fluor® 488 streptavidin revealed a biotinylation pattern similar to that of the Nanos3-BirA-HA construct (Figure 5.9).

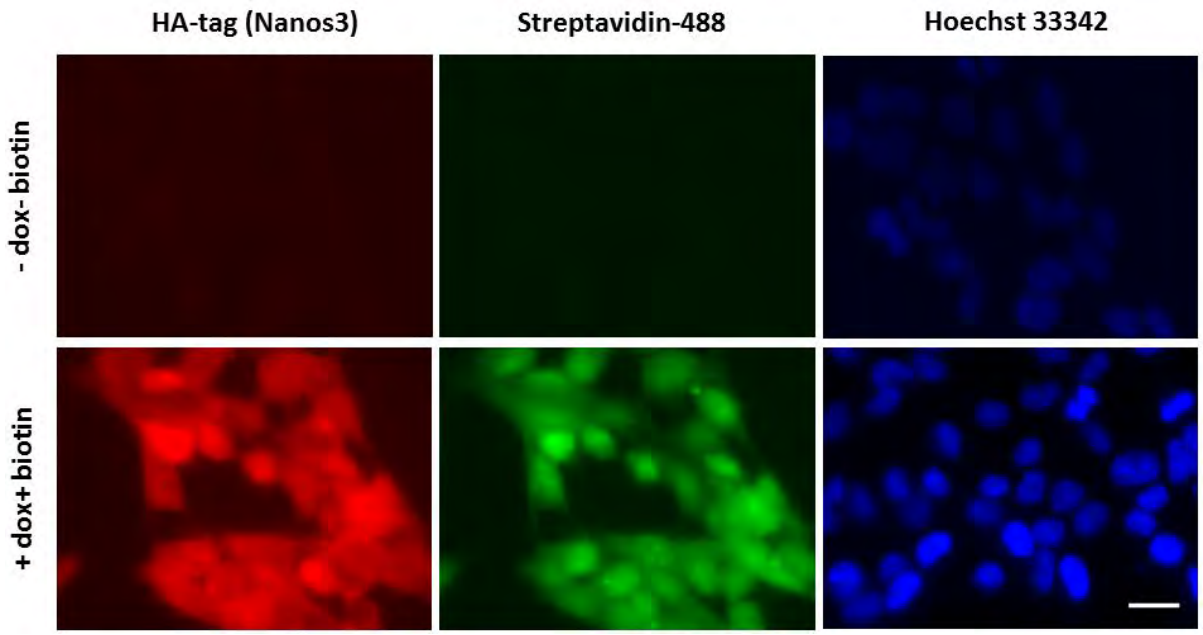

Figure 5.9. Immunocytochemistry to check the inducibility of the Nanos3-biotin ligase plasmid. Flp-In™ T-Rex™ 293 cells transfected with the plasmid containing the *NANOS3* and biotin ligase cDNA were checked for Nanos3 and biotin expression after addition of doxycycline and biotin. This was done using an anti-HA-tag antibody followed by a secondary goat anti-mouse IgG Dylight® 594 antibody for HA-tagged Nanos3 detection and an Alexa Fluor® 488 streptavidin conjugate for biotin detection. Hoechst 33342 was used as a nuclear stain. Bar, 20 µm.

Expression of the Nanos3-BirA-HA fusion protein and its biotinylation were further checked after a pull-down using streptavidin beads. Besides using cells treated with both doxycycline and biotin (+dox+biotin), two negative controls were included: cells that were not induced with dox (-dox+biotin) and cells that were not incubated with biotin (+dox-biotin). The eluate after pull-down was analyzed via western blotting (Figure 5.10B). Detection with the anti-HA antibody also showed some positive staining in the samples without biotin and without doxycycline (Figure 5.10B). These bands were, however, not or barely visible when using HRP-conjugated streptavidin demonstrating massive biotinylation in the +dox+biotin sample (Figure 5.10B). Although these results were not completely what we hoped for, we decided to continue and expand these cells to do the BioID experiment.

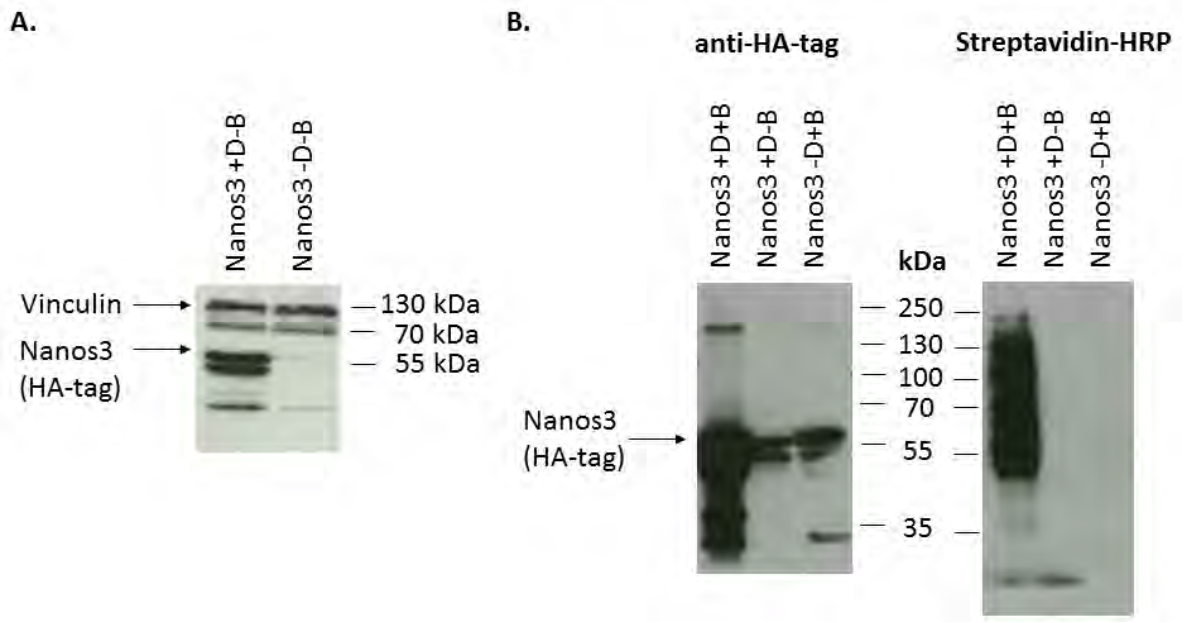

Figure 5.10. Verifying cells stably transfected with the Nanos3-BirA-HA fusion construct for BioID. **A.** Flp-In™ T-Rex™ 293 cells transfected with the Nanos3-biotin ligase plasmid were treated with or without doxycycline (D) and lysed to check for Nanos3 expression via western blotting using an anti-HA-tag antibody. Vinculin was used as a loading control and detected using a vinculin-specific antibody. **B.** Cells treated with or without doxycycline or biotin (B) were used for co-immunoprecipitation with streptavidin-coupled beads. Western blot detection was done with an anti-HA-tag antibody and HRP-conjugated streptavidin.

For the BioID experiment, the cells were induced with dox and incubated with 50 µm biotin (+dox+biotin). After 24 hours of incubation the cells were harvested and streptavidin beads were used to capture the biotinylated proteins from the lysate. This was followed by an on-bead trypsin digestion and by LC-MS/MS analysis of the resulting peptide mixture. The same negative controls as mentioned above were included (+dox-biotin and -dox+biotin). Three replicates were used per condition. This resulted in a list of 422 proteins identified in all three replicates of the +dox+biotin condition and with significantly higher LFQ (label-free quantification) intensity values [21,22] than in the controls (Figure 5.11 and Table S5.1).

The BioID experiment revealed several proteins that were also identified using the co-IP technique such as the top hit RCD1 and other CCR4-NOT proteins: CNOT2, CNOT6L, CNOT7 and CNOT8. Through BioID, additional CCR4-NOT proteins could be detected such as CNOT3, CNOT4, CNOT6, CNOT10, CNOT11 and also CNOT1, a proven direct binding partner of human Nanos3 [1] (Figure 5.12). CNOT4 is not a standard component of the CCR4-NOT complex in

humans but was found to interact with CNOT1 [23]. Gel-filtration analysis identified CNOT4 as part of a smaller protein complex, yet to be studied. TAB182 (TNKS1BP1) was also found in our list and was previously reported to be a stable component of the CCR4-NOT complex in humans [23]. TAB182 is also involved in the repair of double-strand DNA breaks by facilitating the interaction between poly [ADP-ribose] polymerase 1 (PARP-1) and DNA-dependent protein kinase catalytic subunit (DNA-PKcs) [24]. The latter two proteins are, however, not present in our list. TAB182 is also involved in actin organization by facilitating CapZA2 binding to the actin filaments [25]. Decreased TAB182 and CapZA2 expression both lead to an increased invasive capacity of HTC75 fibrosarcoma and pancreatic cancer cells [25]. F-actin-capping proteins, CapZA2 and CapZA1 are also represented in our list.

Figure 5.11. The core proteome of Nanos3. Venn diagram showing the overlap of proteins identified in the Nanos3 proteome (Table S5.1) by BioID as compared to the two different controls.

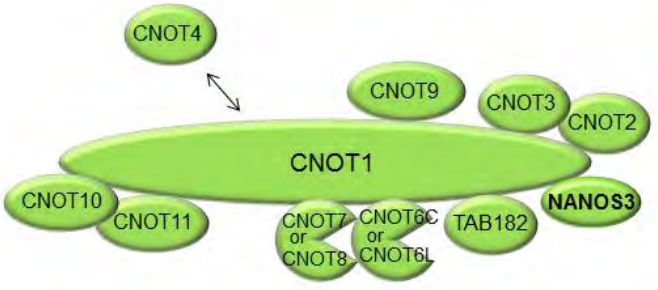

Figure 5.12. Proteins of the CCR4-NOT complex detected with BioID using Nanos3 as a bait. Schematic representation of the CCR4-NOT complex. CNOT4 is not a stable core subunit but its binding to CNOT1 is likely to be regulated.

The two techniques, Co-IP and BioID, also had proteins in common that play a role in polyadenylation such as CPSF7 and PABP1. In addition, eukaryotic translation initiation

factor 1 was found via both methods, congruent with the role of Nanos3 in the regulation of translation.

Histone deacetylase 1 (HDAC1), regulator of chromosome condensation 2 (RCC2), T-complex protein subunit epsilon (CCT5), Patl1 and nuclear pore complex protein Nup50 were also detected in both screens. HDAC1 is a part of the nucleosome remodeling and histone deacetylation (NuRD) complex of which several other subunits such as HDAC2, RBBP7, MTA1 and MTA2 were present in our BioID list. We had two antibodies available detecting respectively HDAC1 and CHD4 of the NuRD complex. Anti-flag beads were used to pull down Nanos3 from lysates of HEK cells transfected with a flag-tagged Nanos3 expression construct (pdcDNA-Flag Nanos3cl4). Untransfected HEK cells were used as a negative control. Western blot detection could not confirm the binding of Nanos3 to endogenous CHD4 and HDAC1, despite their clear presence in the lysate (data not shown). Although several subunits of T-complex protein 1 were detected in both screens, only subunit epsilon was found in both. The chaperonin-containing TCP-1 (CCT) complex is a protein folding complex with several substrates such as actin, tubulin and STAT3 [26-29]. Patl1 is part of the RNA decapping and decay machinery, mentioned further below.

Several other types of proteins such as cyclin-dependent kinases, serine/threonine protein kinases and phosphatases and subunits of the signal peptidase complex were also detected in both screens, although not the same proteins.

Using BioID, Pumilio1 and -2 were also identified as members of the Nanos3 proxeome. Although interaction with the Pumilio proteins has not been shown yet for human Nanos3, interaction between Nanos and Pumilio proteins is seen in several species [30-33] and is thus expected.

Furthermore, from this list we could discern several components of other interesting complexes involved in transcriptional regulation, besides the CNOT proteins. For instance components of the mRNA decapping and decay complex were distinguished such as EDC3, DDX6, DCP1a and XRN1 (Figure 5.13). The lsm/Pat1 complex (Lsm2, -4, -5 and -7 and Patl1, [34,35]) and the RNA-induced silencing complex (RISC; AGO1 to -3, TNRC6A and TNRC6B) are also found back in our list (Figure 5.13). mRNA decapping and decay complexes are known to cluster together and form multi-mRNP assemblies which are seen as P-bodies in the

cytoplasm [36]. Mouse Nanos2 has already been shown to interact with the CCR4-NOT complex in these P-bodies and also Nanos3 is expressed in these discrete foci [37,38]. TNRC6A is involved in miRNA-mediated repression and does this by recruiting the CCR4-NOT complex through CNOT9. The CNOT1-DDX6 interaction is also found to be essential for miRNA-mediated repression [39]. Besides the CCR4-NOT complex, the PAN2-PAN3 deadenylase complex is likewise present in the list. Also the transcription elongation complex was clearly represented (LARP7, MEPCE, BRE1 aka RNF20, KMT2a aka MLL, HEXIM, BRD4, CDK9 and Cyclin K).

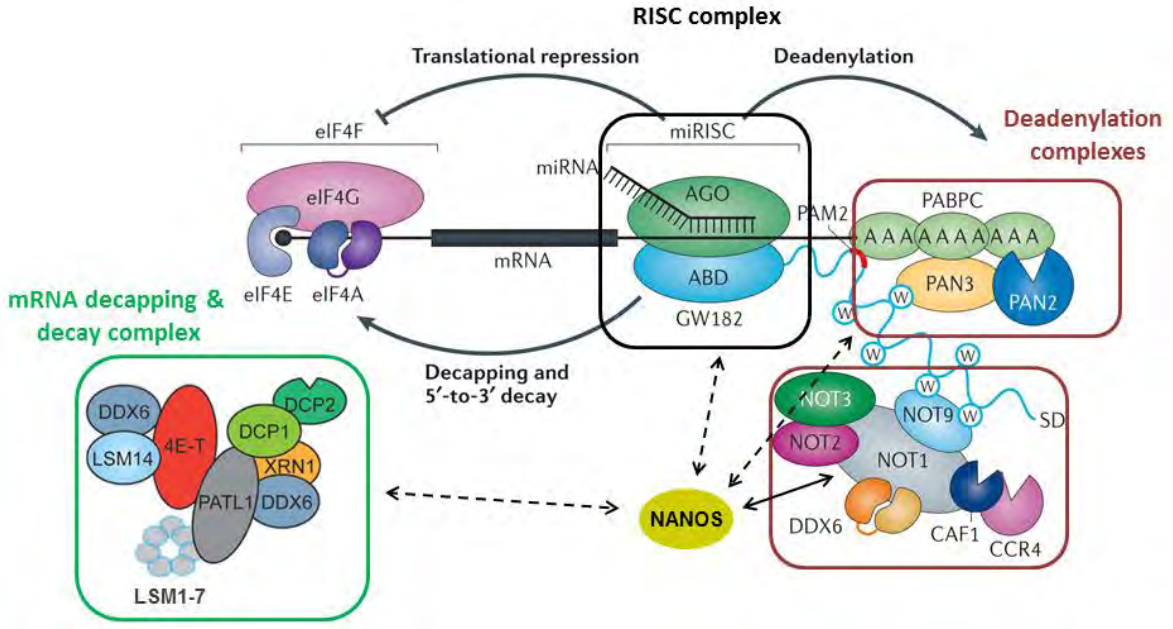

Figure 5.13. mRNA-associated complexes with which Nanos3 possibly associates. Dashed double-sided arrows indicate possible interactions while the full double-sided arrow indicates the reported interaction between Nanos3 and CNOT1 [1]. Figure adapted from [40] and [41].

Since Nanos3 was already reported to be associated with the CCR4-NOT complex, the components of this complex can be considered positive controls for specific proximity with Nanos3 in our analysis. The CNOT proteins with the lowest difference between the +dox+biotin condition and a control condition are CNOT1 and CNOT10 (difference *versus* control 2 (-dox+biotin) equals 3.38). Using this difference as a cut-off, leaves us with 146 proteins (Table 5.4). Several proteins of the abovementioned protein complexes are still represented in this shorter list and are therefore a good starting point to confirm linkage of Nanos3 to these complexes.

Table 5.4. A list of 146 proteins identified by BioID with a difference ≥ 3.38 compared to the controls. The proteins are ranked according to the difference between the +dox+biotin condition and the -dox+biotin condition (control 2).

Protein name	Gene name	Difference[a] (control 1[b])	Difference (control 2[c])
TOX high mobility group box family member 4	*TOX4*	7,85	7,72
Putative adenosylhomocysteinase 2	*AHCYL1*	8,52	7,61
Putative adenosylhomocysteinase 3	*AHCYL2*	7,31	7,41
Probable JmjC domain-containing histone demethylation protein 2C	*JMJD1C*	6,58	7,07
5-3 exoribonuclease 1	*XRN1*	6,53	6,77
Ubiquitin-associated protein 2	*UBAP2*	6,75	6,65
Proliferation-associated protein 2G4	*PA2G4*	6,35	6,56
Nuclear pore complex protein Nup153	*NUP153*	5,59	6,56
Transgelin-2	*TAGLN2*	4,44	6,52
Ankyrin repeat domain-containing protein 17	*ANKRD17*	9,73	6,38
Crk-like protein	*CRKL*	6,98	6,25
Src substrate cortactin	*CTTN*	5,63	6,24
Ran-binding protein 3	*RANBP3*	4,49	6,23
Paired amphipathic helix protein Sin3b	*SIN3B*	7,00	6,20
Bromodomain-containing protein 4	*BRD4*	5,27	6,19
Protein PRRC2A	*PRRC2A*	6,83	6,16
Protein PRRC2C	*PRRC2C*	6,73	6,06
Origin recognition complex subunit 2	*ORC2*	5,09	5,96
SURP and G-patch domain-containing protein 1	*SUGP1*	5,17	5,86
Poly(A) polymerase alpha	*PAPOLA*	5,88	5,78
Serine/threonine-protein phosphatase 1 regulatory subunit 10	*PPP1R10*	6,54	5,75
Protein FAM195B	*FAM195B*	3,95	5,68
MKL/myocardin-like protein 2	*MKL2*	6,59	5,67
Adapter molecule crk	*CRK*	5,40	5,66
Wings apart-like protein homolog	*WAPAL*	5,70	5,65
Zinc finger CCCH domain-containing protein 4	*ZC3H4*	4,54	5,59
TIP41-like protein	*TIPRL*	4,58	5,54
WD repeat and HMG-box DNA-binding protein 1	*WDHD1*	5,15	5,50
Nuclear autoantigenic sperm protein	*NASP*	5,07	5,49
Ubiquitin-associated protein 2-like	*UBAP2L*	7,48	5,45
Roquin-1	*RC3H1*	4,27	5,41
Trinucleotide repeat-containing gene 6B protein	*TNRC6B*	8,03	5,33
Protein PRRC2B	*PRRC2B*	5,71	5,32
Serine/threonine-protein phosphatase 4 regulatory subunit 3A	*SMEK1*	5,90	5,28
Nanos homolog 3	***NANOS3***	**4,82**	**5,28**
Protein argonaute-3	*AGO3*	4,60	5,18
Ubiquitin carboxyl-terminal hydrolase 10	*USP10*	4,94	5,18
Tubulin polyglutamylase complex subunit 2	*TPGS2*	5,76	5,12
Regulation of nuclear pre-mRNA domain-containing protein 2	*RPRD2*	5,43	5,05
Protein SET;Protein SETSIP	*SET;SETSIP*	4,68	5,03
Eukaryotic translation initiation factor 4E transporter	*EIF4ENIF1*	5,52	5,01
Zinc finger protein 318	*ZNF318*	5,70	4,98

Protein name	Gene name	Difference[a] (control 1[b])	Difference (control 2[c])
Probable helicase with zinc finger domain	*HELZ*	3,61	4,95
General transcription factor IIE subunit 1	*GTF2E1*	3,72	4,94
RING finger protein unkempt homolog	*UNK*	4,47	4,94
CCR4-NOT transcription complex subunit 8	*CNOT8*	6,00	4,91
Eukaryotic translation initiation factor 4B	*EIF4B*	5,32	4,85
Ankyrin repeat and KH domain-containing protein 1	*ANKHD1*	7,98	4,82
Roquin-2	*RC3H2*	4,24	4,71
Histone acetyltransferase type B catalytic subunit	*HAT1*	4,11	4,70
Serine/threonine-protein kinase SMG1	*SMG1*	5,47	4,69
Squamous cell carcinoma antigen recognized by T-cells 3	*SART3*	5,25	4,65
Trinucleotide repeat-containing gene 6A protein	*TNRC6A*	7,01	4,63
Protein HEXIM1	*HEXIM1*	3,84	4,62
Vasculin-like protein 1	*GPBP1L1*	3,62	4,61
mRNA-decapping enzyme 1A	*DCP1A*	3,54	4,59
CCR4-NOT transcription complex subunit 6-like	*CNOT6L*	6,46	4,57
Peptidyl-prolyl cis-trans isomerase FKBP3	*FKBP3*	3,70	4,56
Proteasome activator complex subunit 3	*PSME3*	4,30	4,55
Cytochrome b-c1 complex subunit 1, mitochondrial	*UQCRC1*	4,15	4,55
CCR4-NOT transcription complex subunit 2	*CNOT2*	7,93	4,53
RNA polymerase II-associated protein 3	*RPAP3*	4,83	4,50
Inhibitor of Bruton tyrosine kinase	*IBTK*	3,71	4,47
Signal recognition particle 54 kDa protein	*SRP54*	3,97	4,41
CD2-associated protein	*CD2AP*	7,83	4,37
CCR4-NOT transcription complex subunit 4	*CNOT4*	4,57	4,37
Interferon-induced protein with tetratricopeptide repeats 5	*IFIT5*	4,42	4,36
Coiled-coil domain-containing protein 43	*CCDC43*	4,13	4,35
Beta-catenin-like protein 1	*CTNNBL1*	4,80	4,33
Small acidic protein	*SMAP*	4,65	4,32
Eukaryotic translation initiation factor 4 gamma 2	*EIF4G2*	4,61	4,30
Mitochondrial import inner membrane translocase subunit Tim8 A	*TIMM8A*	4,86	4,27
DAZ-associated protein 1	*DAZAP1*	3,44	4,27
Negative elongation factor E	*NELFE*	3,63	4,27
PIH1 domain-containing protein 1	*PIH1D1*	4,12	4,20
Eukaryotic translation initiation factor 1	*EIF1*	4,00	4,18
BRCA1-associated protein	*BRAP*	3,49	4,16
Hepatoma-derived growth factor-related protein 2	*HDGFRP2*	3,40	4,15
Nuclear pore complex protein Nup50	*NUP50*	3,60	4,14
C-Myc-binding protein	*MYCBP*	4,40	4,14
G patch domain and KOW motifs-containing protein	*GPKOW*	3,83	4,13
Epidermal growth factor receptor substrate 15-like 1	*EPS15L1*	5,07	4,13
Negative elongation factor B	*NELFB*	4,15	4,13
Lysine-specific demethylase 3B	*KDM3B*	4,52	4,10
Ataxin-2	*ATXN2*	3,79	4,08
RNA-binding protein 20	*RBM20*	3,44	4,07
Probable ATP-dependent RNA helicase DDX6	*DDX6*	6,04	4,06
Craniofacial development protein 1	*CFDP1*	4,54	4,04

Protein name	Gene name	Difference[a] (control 1[b])	Difference (control 2[c])
Zinc finger CCHC domain-containing protein 2	*ZCCHC2*	4,85	4,04
ATP-dependent RNA helicase DDX42	*DDX42*	5,38	4,03
Cold shock domain-containing protein E1	*CSDE1*	5,57	4,03
28 kDa heat- and acid-stable phosphoprotein	*PDAP1*	4,09	4,03
RNA-binding protein 3	*RBM3*	4,42	4,03
Protein FAM193A	*FAM193A*	5,59	4,02
YTH domain-containing family protein 3	*YTHDF3*	5,19	4,00
Nicolin-1	*NICN1*	3,38	3,97
Cyclin-T1	*CCNT1*	3,54	3,97
SUMO-conjugating enzyme UBC9	*UBE2I*	3,55	3,96
SAP30-binding protein	*SAP30BP*	4,41	3,93
Ubiquitin carboxyl-terminal hydrolase 15	*USP15*	3,89	3,92
Ataxin-2-like protein	*ATXN2L*	6,30	3,92
Coatomer subunit zeta-1	*COPZ1*	4,92	3,90
Fanconi anemia group J protein	*BRIP1*	4,22	3,90
Origin recognition complex subunit 5	*ORC5*	4,60	3,89
Programmed cell death protein 5	*PDCD5*	3,66	3,88
Headcase protein homolog	*HECA*	4,97	3,86
Autophagy-related protein 2 homolog B	*ATG2B*	3,59	3,85
Leucine-rich repeat and WD repeat-containing protein 1	*LRWD1*	3,85	3,85
Nucleoprotein TPR	*TPR*	6,41	3,84
WD repeat-containing protein 82	*WDR82*	6,53	3,84
Acyl-protein thioesterase 2	*LYPLA2*	3,71	3,84
7SK snRNA methylphosphate capping enzyme	*MEPCE*	5,73	3,83
Origin recognition complex subunit 3	*ORC3*	4,18	3,82
mRNA export factor	*RAE1*	3,54	3,80
DNA topoisomerase 3-beta-1	*TOP3B*	6,10	3,77
182 kDa tankyrase-1-binding protein	*TNKS1BP1*	7,76	3,72
CCR4-NOT transcription complex subunit 3	*CNOT3*	6,04	3,71
Pumilio homolog 1	*PUM1*	4,23	3,71
Neuroblast differentiation-associated protein AHNAK	*AHNAK*	5,61	3,66
Far upstream element-binding protein 2	*KHSRP*	6,07	3,65
Cell differentiation protein RCD1 homolog	*RQCD1*	4,36	3,64
AT-rich interactive domain-containing protein 3B	*ARID3B*	4,70	3,64
RNA-binding protein 33	*RBM33*	5,47	3,63
Insulin-degrading enzyme	*IDE*	3,39	3,63
CCR4-NOT transcription complex subunit 6	*CNOT6*	6,82	3,62
Microtubule-associated protein 4	*MAP4*	5,51	3,59
Transcriptional regulator Kaiso	*ZBTB33*	5,42	3,56
Eukaryotic translation initiation factor 2A;Eukaryotic translation initiation factor 2A, N-terminally processed	*EIF2A*	4,39	3,56
Segment polarity protein dishevelled homolog DVL-1;Putative	*DVL1;DVL1P1*	5,19	3,56
Serine-threonine kinase receptor-associated protein	*STRAP*	4,97	3,54
Probable tubulin polyglutamylase TTLL1	*TTLL1*	3,85	3,54
Flap endonuclease 1	*FEN1*	4,93	3,54
CCR4-NOT transcription complex subunit 11	*CNOT11*	4,75	3,53

Protein name	Gene name	Difference[a] (control 1[b])	Difference (control 2[c])
CCR4-NOT transcription complex subunit 7	*CNOT7*	3,85	3,51
Filamin-A	*FLNA*	4,64	3,50
Gametogenetin-binding protein 2	*GGNBP2*	5,04	3,49
Coatomer subunit beta	*COPB2*	5,85	3,47
Uncharacterized protein KIAA1841	*KIAA1841*	5,34	3,47
WD repeat-containing protein 11	*WDR11*	3,81	3,46
Coatomer subunit gamma-2	*COPG2*	4,10	3,46
Transcription elongation factor A protein 1	*TCEA1*	3,94	3,45
T-complex protein 1 subunit theta	*CCT8*	3,89	3,43
Plasminogen activator inhibitor 1 RNA-binding protein	*SERBP1*	4,52	3,41
Caldesmon	*CALD1*	4,99	3,39
CCR4-NOT transcription complex subunit 10	*CNOT10*	3,92	3,38
CCR4-NOT transcription complex subunit 1	*CNOT1*	3,90	3,38

[a] Difference between the mean log2 LFQ intensity values of the +dox+biotin condition and the mentioned control

[b] +dox-biotin

[c] -dox+biotin

To further analyze the Nanos3 proxeome, the proteins from the BioID list were analyzed with Enrichr (*http://amp.pharm.mssm.edu/Enrichr/* [42,43]). This allowed us to gain information on enriched Gene Ontology (GO) terms and pathways (Figure 5.14). Shortening of the poly(A) tail, mRNA splicing, decapping, gene silencing and translation inhibition are among the top 25 biological processes associated with the Nanos3 proxeome (Figure 5.14A and Table 5.5). mRNA binding is the most significantly associated GO molecular function and the top two identified cellular components are the P-body and cytoplasmic stress granule in agreement with previous reports for mouse Nanos2 and Nanos3 proteins [32,37,38,44]. RNA degradation is the top-ranked KEGG pathway (Figure 5.14B), based on the presence of the previously discussed Lsm proteins, DDX6, XRN1, EDC3 and two proteins of the 3'-5' degrading exosome complex, DIS3L and EXOSC4 [45,46].

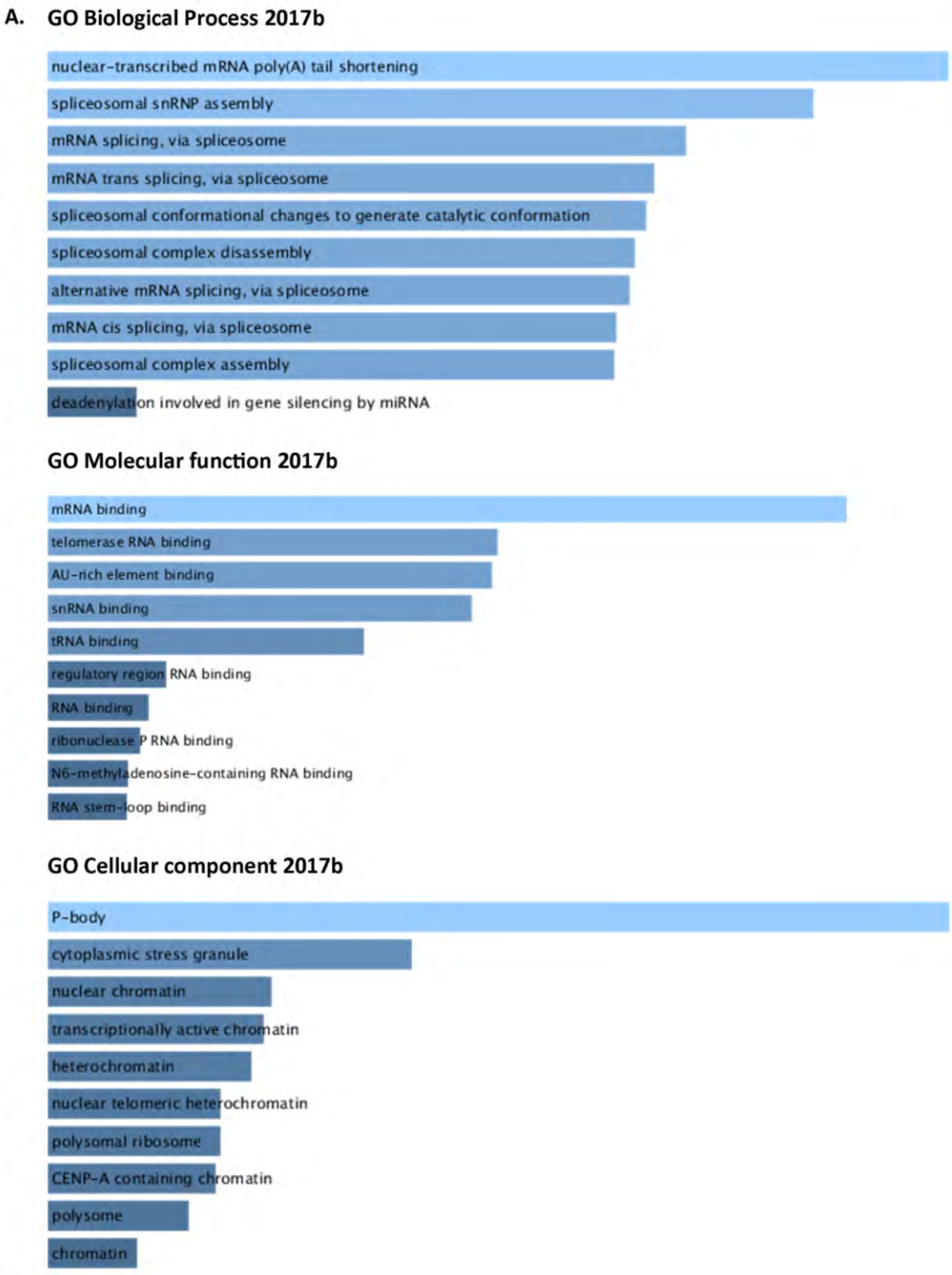

Figure 5.14. Panel A.

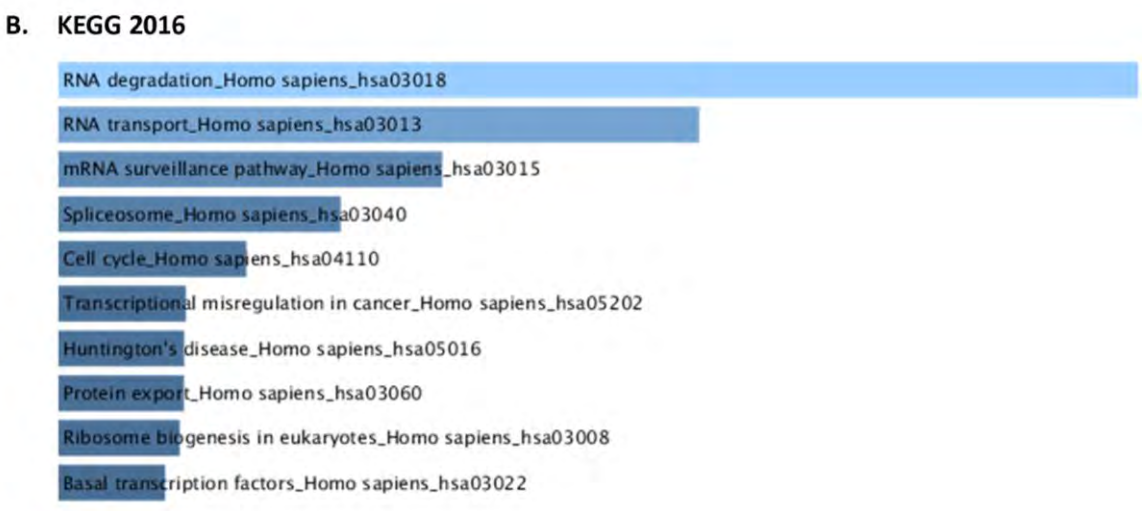

Figure 5.14. Enriched GO terms and pathways associated with the proteins in our BioID list. Enrichr was used to study the proteins from the Nanos3 proxeome, identified using BioID. The ten best hits of the corresponding GO terms (**A**) and KEGG pathways (**B**) are given. The size and the color of the bars correspond to the combined score attributed by Enrichr, with a larger bar and lighter bar color corresponding to a higher score.

Table 5.5. The top 25 entries of the GO biological processes found in our BioID list using Enrichr.

	Biological process	P-value	Adjusted p-value	Z-score	Combined score
1	nuclear-transcribed mRNA poly(A) tail shortening	8,34E-24	3,05E-20	-2.56	153.81
2	spliceosomal snRNP assembly	2,93E-15	2,14E-12	-3.70	149.46
3	mRNA splicing, via spliceosome	6,29E-15	2,38E-12	-3.67	145.37
4	mRNA trans splicing, via spliceosome	4,39E-15	2,29E-12	-3.61	144.34
5	spliceosomal conformational changes to generate catalytic conformation	5,01E-15	2,29E-12	-3.62	144.09
6	spliceosomal complex disassembly	5,01E-15	2,29E-12	-3.61	143.72
7	alternative mRNA splicing, via spliceosome	7,43E-15	2,47E-12	-3.64	143.56
8	mRNA cis splicing, via spliceosome	6,52E-15	2,38E-12	-3.62	143.14
9	spliceosomal complex assembly	1,25E-14	3,79E-12	-3.68	143.06
10	deadenylation involved in gene silencing by miRNA	6,00E-20	1,10E-16	-2.50	127.71
11	regulation of gene silencing by miRNA	2,91E-15	2,14E-12	-2.96	119.35
12	mRNA destabilization	1,70E-11	4,43E-09	-3.45	109.52
13	exonucleolytic nuclear-transcribed mRNA catabolic process involved in deadenylation-dependent decay	1,35E-15	1,64E-12	-2.54	104.57
14	negative regulation of translational initiation	8,14E-11	1,98E-08	-2.96	89.08
15	gene silencing by miRNA	1,32E-11	3,70E-09	-2.68	85.70
16	positive regulation of gene silencing by miRNA	9,91E-11	2,13E-08	-2.79	83.42
17	positive regulation of nuclear-transcribed mRNA catabolic process, deadenylation-dependent decay	3,49E-10	6,72E-08	-2.88	82.65
18	deadenylation-dependent decapping of nuclear-transcribed mRNA	8,71E-11	1,99E-08	-2.65	79.71
19	regulation of translational initiation	1,81E-10	3,67E-08	-2.67	78.37
20	negative regulation of gene silencing by miRNA	1,35E-08	2,23E-06	-3.09	77.31
21	regulation of production of miRNAs involved in gene silencing by miRNA	5,55E-09	9,65E-07	-2.65	68.60
22	regulation of miRNA mediated inhibition of translation	5,55E-09	9,65E-07	-2.64	68.55
23	miRNA mediated inhibition of translation	5,84E-08	8,20E-06	-2.89	68.02
24	miRNA loading onto RISC involved in gene silencing by miRNA	3,13E-08	4,97E-06	-2.69	65.04
25	termination of RNA polymerase II transcription	1,53E-04	0.000009956	-4.13	64.89

5.5 Discussion

Since most proteins exert their function by interacting with other proteins, identification of molecular interaction partners of proteins is of importance for assigning a function to a certain protein.

So far Pumilio2, p120-catenin, β-catenin, SNAPIN, GEMIN3 and CNOT1 are reported interaction partners of human Nanos1 (see Chapter 1 section 1.1.3). Besides CNOT1, no interaction partners have been discovered for Nanos2 and Nanos3 [1]. We detected DDX1, a DEAD box helicase like GEMIN3, in a mass spectrometry analysis of Nanos1 co-immunoprecipitates. Using MAPPIT, we identified DDX1 again, but now as an interaction partners for all three human Nanos proteins. We confirmed this for Nanos3 by performing Nanos3 co-IP followed by western blotting. *DDX1* was originally found to be amplified in two retinoblastoma cell lines [47]. Since *NANOS1* and *NANOS3* mRNAs are also found to be upregulated in pRb-deficient cells [48], the interaction between DDX1 and the Nanos proteins might be relevant in retinoblastoma. Analyzing several adult mouse tissues seemingly restricted *DDX1* mRNA expression to the testis [49]. DDX1 is expressed in spermatogonial stem cells and its expression is lost during differentiation. *CCND2* (cyclin-D2) and *CD9*, two stem cell-associated genes, are targets of DDX1 both in mouse and human germ cell-derived cell lines, proposing a role for DDX1 as stem cell regulator. DDX1 transcriptionally regulates cyclin-D2 by binding to its upstream DNA region [49]. DDX1 is also expressed in human testicular germ cell tumors (TGCT) and is responsible for the tumorigenic capacity of the human embryonal carcinoma-derived cell line, NEC8. Nanos3 was likewise found to be expressed in TGCT [50]. The interaction between DDX1 and Nanos3 proved to be RNA-dependent suggesting that a complex consisting of Nanos3 and DDX1 regulates mRNA transcription. Our collaborators from Reims (Dr. Grelet from the lab of Prof. Dr. Nawrocki-Raby, INSERM, UMR-S 903, University of Reims Champagne-Ardenne) have shown that this interaction is important for the Nanos3-dependent polyadenylation and upregulation of vimentin. DDX1 might be specifically involved in the activating role of Nanos3.

Given the interaction between the miRNA regulatory complex and the Nanos/Pumilio complex (see Chapter 1), interaction of Nanos3 with Argonaute family proteins, Dicer and

TNRC6A was investigated. MAPPIT analysis showed an interaction of Nanos3 with all investigated Argonaute family proteins; PIWIL1, -2 and -4 and AGO1 to -3. In *Drosophila* the piRNA pathway was shown to play a role in early translational repression and in deadenlyation-dependent mRNA degradation of maternal mRNAs such as *nanos* mRNA [51]. In the *Drosophila* l(3)mbt model (see Chapter 1), besides nanos also two PIWI proteins (piwi and aub), as well as vasa (DDX4 in humans) were found to be ectopically expressed and essential in brain tumor growth [52]. There is, however, limited data revealing the exact role of mammalian PIWI proteins in tumorigenesis. All four human PIWI proteins have been found to be expressed in the testis. Elevated expression levels of human PIWI proteins, mainly PIWIL1 and PIWIL2, have been detected in different human cancer types [11,53]. Their encoding genes are also known as cancer testis genes CT80.1 and CT80, respectively.

Confirmation of the interaction between Nanos3 and the Argonaute proteins was done by performing a co-IP experiment using the same constructs as were used for MAPPIT in combination with Myc-tagged Nanos3. However, the AGO2 and -3 constructs yielded smaller protein bands on SDS-PAGE gel as they represent only parts of the complete protein sequences. Argonaute proteins have a bilobal architecture with the N-terminal and the PAZ domain forming one lobe and the MID and PIWI domain forming the second lobe [17]. Lack of a large part of the protein sequence, as is seen for the AGO2 and -3 construct used by us might influence the protein folding and hence the interaction with other proteins. In addition different protein domains, the N-terminal and PIWI domain, were represented by the ORFeome sequences for AGO3 and AGO2, respectively. Their interaction with Nanos3, demonstrated by both MAPPIT and co-IP, is thus rather surprising. Interaction of the full-length proteins without the gp130 receptor chain, present in these MAPPIT prey constructs, should be investigated. When the same AGO1, PIWIL1, -2 and -4 sequences were C-terminally fused to EGFP these showed a different cellular localization pattern than the corresponding MAPPIT bait fusion proteins. No interaction could be seen when using these EGFP protein constructs and Myc-tagged Nanos3, performing a co-IP using the Myc antibody. These constructs should be tested further and additional constructs using a C-terminal reporter might solve this problem. Ideally specific antibodies could be purchased, eliminating the requirement of a tag and additionally allowing to analyze interaction of Nanos3 with the endogenous Argonaute family proteins. It would be interesting to

investigate the domains involved in the mutual interaction. If we consider the interaction of Nanos3 with the N-terminal part of the AGO3 protein on the one hand and with the C-terminal part of the AGO2 protein on the other hand, multiple domains of AGO proteins seem to be involved in binding Nanos3. The PAZ domain does not seem to be sufficient for Nanos3 binding since this is also present in the Dicer protein, and interaction with the latter protein was not demonstrated using MAPPIT.

Also the TNRC6A construct, used in the MAPPIT assay, does not span the complete protein sequence, but merely a small C-terminal part of the protein. Interaction between Nanos3 and TNRC6A can thus not be excluded on the basis of a negative result in the present assay. Even if an interaction between the bait and prey proteins was not seen when the complete protein sequences were covered, as was the case for Dicer, *in vivo* these proteins might still interact. For MAPPIT, the interaction should be able to take place in the cytosol and in some cases fusion of the mutated receptor and the gp130 receptor chain to the bait and prey protein, respectively, might interfere with their mutual interaction.

Furthermore, two more techniques were used to identify new interaction partners of Nanos3. In a first approach, HEK293T cells were transfected with a Nanos3 expression construct. The cell lysates were then used in a co-IP experiment using a rabbit Nanos3-specific antibody (Proteintech) or an IgG isotype control. This technique was repeated once, using more cells and a pH-based elution instead of boiling the bead suspension. In both cases, we obtained a relatively small list comprising several proteins from the CCR4-NOT complex, confirming the reliability of the technique. Surprisingly, CNOT1, which was shown to directly interact with Nanos3 [1], was not detected in these experiments. Similarly, DDX1 and Argonaute proteins were also absent from our list. An important limitation of these experiments is that differentially binding proteins had to be selected on the basis of visualization in SDS-PAGE gels. It is likely that many proteins were not detected that way because they were too scarce and gave no visible differential band compared to the control sample. This shortcoming has now been overcome by using an on-bead digestion method, omitting the need of SDS-PAGE analysis. The only limitation of the newer approach is that the molecular weight of the protein cannot be double-checked. Two interesting, high-ranking hits, plakoglobin (PLAK) and plakophilin-4 (PKP4) were for instance detected in gel bands corresponding to a lower molecular weight than those expected for these proteins.

These hits are, however, interesting since they are both armadillo repeat proteins found in adherens junctions as well as desmosomes [54]. The armadillo repeat domain shares a similar topology with PUM-HD, involved in Nanos3 binding, and human Nanos1 has already been reported to bind to two armadillo proteins, p120-catenin and β-catenin [55]. Furthermore, the fact that few Nanos3 peptides were also detected in the isotype control bands, could be paired with failing identification of a few real interaction partners.

In a second approach, BioID, a fusion protein was made between the Nanos3 protein and a mutant BirA, mediating proximity-dependent biotinylation. Also here the two armadillo proteins previously found to bind Nanos1 [55] were not picked up. Using BioID, β-catenin-like protein 1, CTNNBL1, was traced back in the Nanos3 proxeome. This armadillo protein is involved in splicing and was shown to stimulate proliferation and invasion in ovarian cancer [56]. CTNNBL1 binds CWC15 and associates with the core CDC5L/Prp19 complex of the spliceosome [57]. The CWC15 protein was also present in our BioID list.

The labeling range of the BirA-fusion protein is around 10 nm [58]. However, not all proteins in a radius of 10 nm of the bait are labeled. Protein labeling requires the presence of available primary amines. Biotinylated, low abundance proteins might also escape detection and negative results must thus be regarded with caution. A stable cell line was made expressing the Nanos3-BirA-HA fusion protein in a dox-inducible manner in Flp-In™ T-Rex™ 293 cells. After dox induction and 24 h of incubation with biotin, lysates were used for an immunoprecipitation using streptavidin-coupled beads. Negative controls without doxycycline induction or biotin addition were taken along. The beads and bead-bound proteins were subjected to an on-bead trypsin digestion followed by mass spectrometry. This BioID experiment resulted in a large list of proteins present in the Nanos3 proxeome.

These two techniques for identifying proteins in the proximity of Nanos3 yielded several proteins in common along which the expected CCR4-NOT proteins. Additional CNOT proteins were detected by the BioID approach, including the anticipated CNOT1. Furthermore, proteins involved in polyadenylation and translation were shared between both experiments. Also Patl1, part of the lsm/Pat1 complex involved in mRNA decapping and mRNA decay, was found with both techniques. Moreover additional proteins associated with this complex, such as DDX6, DCP1a and XRN1 and several lsm proteins, were identified using

BioID. Proteins from other interesting complexes, including RISC, the transcription elongation complex and another deadenylation complex, the PAN2-PAN3 deadenylase complex, were similarly found back in our lists. The nanos protein in *Drosophila* was already shown to interact with several subunits of deadenylase and decapping complexes such as NOT1 to -3, PAN2, -3, DCP2 and HPat (Patl1 in humans) [59]. Nanos3 seems to be involved in both transcriptional and post-transcriptional regulation of several genes [60]. The fact that multiple protein members of the molecular complexes, involved in these regulations, are found back in our BioID analysis suggests that these complexes are indeed likely interacting with Nanos3. Enrichr confirmed that most of the proteins detected through BioID are involved in biological processes involving mRNA sequences.

Although not detected in our co-IP experiments, using BioID we also identified the expected Pumilio1 and Pumilio2 as members of the Nanos3 proxeome. This might point to a weak mutual interaction, which might have been lost during the washing steps of the immunoprecipitation protocol.

The previously investigated proteins AGO1 to -3 and TNRC6A from the RISC complex were identified as part of the Nanos3 proxeome. The PIWIL proteins were not detected, but given their mainly germline-specific expression this is not so surprising. Unlike high-throughput techniques, such as yeast two-hybrid analysis of cDNA libraries [61], and array MAPPIT using cDNA libraries [13], the BioID technique is limited to the proteins expressed in the cell line used, Flp-In™ T-Rex™ 293 cells in our case. It would be interesting to perform the BioID experiment in a cancer cell line to see if this would influence the Nanos3 proxeome.

Although DDX1 was not detected using either the co-IP or the BioID approach, other DEAD-box proteins such as EIF4A2 (DDX2B), DDX6, DDX31, DDX42 and DDX46 were found back using at least one of these approaches. EIF4A2 and DDX6 are both linked to the CCR4-NOT complex and have been implicated in miRNA mediated repression [62,39,63]. The role of DDX31 has not been elucidated yet and DDX42 and DDX46 are involved in pre-mRNA splicing [64]. The latter two contribute to the abundance of biological processes involving splicing, and which were detected in the Nanos3 proxeome using Enrichr.

GEMIN3 (DDX20) was previously shown to interact with Nanos1 [65] and AGO2 [66]. GEMIN3, AGO2 and GEMIN4 were identified in an RNP complex containing many miRNAs

[66]. In our BioID list only Gemin5 was detected, which is not a DEAD-box protein. GEMIN3 and GEMIN5 are both part of the SMN complex (see Chapter 1), of which GEMIN5 represents the small nuclear RNA (snRNA) binding protein of the complex [67].

One should keep in mind that both our co-IP experiment followed by mass spectrometry, and the BioID experiment depend on the forced overexpression of Nanos3. This could result in the detection of interaction partners that are not seen under normal conditions, and which can also preclude the detection of natural interaction partners. Negative results should be regarded with caution and especially for these techniques, identified proteins should be validated by use of other methods.

In conclusion the methodology used (MAPPIT, co-IP and mass spectrometry, BioID) further confirmed the link between Nanos3 and the miRNA regulatory system (De Keuckelaere *et al.*, 2018). The suggested interaction between Nanos3 and several mRNA decapping, decay and deadenylase complexes will assist further research concerning the exact function of this protein.

5.6 Materials and methods

Cell lines and transient transfection

HEK293T cells and Flp-In™ T-Rex™ 293 cells were cultured in DMEM containing 10% FCS, supplemented with L-Gln and Na-pyruvate. The latter cells were a gift from the lab of Prof. Dr. Jan Tavernier, VIB-UGent Center for Medical Biotechnology. The cells were seeded in culture flasks or 96-well plates the day before transfection. Transient transfection was performed using the calcium phosphate precipitation method.

Plasmid construction

Sequences of the Argonaute family proteins were purchased from the human ORFeome v8.1 collection [14]. Gateway Technology (Life Technologies Europe) was used to recombine these sequences with an EGFP destination vector (pDEST-EGFP (LMBP 04542), available at Belgian Coordinated Collections of Microorganisms (BCCM)/GeneCorner, Ghent University (*http://www.genecorner.ugent.be/*)). An expression vector for Myc-tagged Nanos3 was already available in the lab, pdcDNA4/TOmyc-NANOS3.

MAPPIT assay

For the first experiment concerning DDX1, *DDX1* cDNA was transferred to the pMG1 vector [5] and *NANOS1*, *NANOS2* and *NANOS3* cDNAs were transferred to the pCLG bait vector [69]. Both destination vectors are gateway-compatible allowing efficient transfer of the cDNA sequences by using Gateway Technology (Life Technologies Europe). In the second experiment pMG2 bait vectors [70] were a gift from the lab of Prof. Dr. Jan Tavernier, VIB-UGent Center for Medical Biotechnology. The cDNA sequences used for the pMG2 bait vectors are obtained from the ORFeome8.1 collection. The pXP2d2-rPAP1-luciferase reporter [71] and irrelevant bait vectors, pCLG-BRD4CTD [69] and pCLL-eDHFR [72] were previously described. For the MAPPIT analysis, 10,000 HEK293T cells were seeded in 96-well plates. One day later, the cells were transiently transfected with the desired bait and prey plasmids in addition to the luciferase reporter plasmid using calcium phosphate transfection. The empty prey and REM2, a prey protein interacting with the leptin receptor part of the bait, were used as a negative and positive control, respectively. One day after transfection, cells were stimulated with leptin (100 ng/ml) for another 24 h or were left untreated. All

conditions were performed in triplicate. Cells were lysed in 50 µl luciferase lysis buffer (25 mM Tris-phosphate pH 7.8, 2 mM DTT, 2 mM CDTA, 10% glycerol, 1% Triton X-100). Luciferase and β-galactosidase activity was measured as described in Chapter 2.

Co-immunoprecipitation

Two days after transfection the HEK293T cells were lysed in lysis buffer containing 10 mM Tris pH 8.0, 150 mM NaCl and 0.5% NP-40 supplemented with protease inhibitors (Complete Mini, Roche). Samples were incubated at 4°C for half an hour, while rotating. The cell debris and insoluble protein fraction were removed by centrifugation. Protein concentration of the supernatant was measured using the DC protein assay kit (Bio-Rad), according to the manufacturer's instructions. For the DDX1 co-IP experiment, part of the lysate was treated with RNase A (100 µg/mL) for 20 min at 37°C. Protein lysates were incubated with Myc-tag-specific or irrelevant antibodies for two hours at 4°C or 30 min at RT, while rotating. This mixture was added to Dynabeads® M-280 sheep anti-mouse IgG beads (Novex, Life technologies) and incubated for a few hours to ON at 4°C, while rotating. After several washes with lysis buffer, the proteins were eluted from the beads by boiling the samples in SDS sample buffer (10 min at 95°C), see below for buffer composition. For the co-IP experiment followed by mass spectrometry Dynabeads® Protein G (Life technologies) were used. These beads were crosslinked, through the use of BS3, with rabbit anti-Nanos3 antibody (Proteintech) or rabbit polyclonal IgG isotype control (Abcam). In the first experiment, elution was carried out with SDS sample buffer and in the second experiment a pH-based elution was performed. Elution was done in two consecutive steps using 40 µl 150 mM glycine-HCl (pH 1.5-2.5) with 500 mM NaCl. The eluates were pooled and neutralized with an alkaline neutralization buffer (1.7 M NaOH). This was followed by a protein extraction using Trichloroacetic acid (TCA) and sodium deoxycholate (SOD). The concentrated eluate, solved in SDS sample buffer, was incubated at 95°C for 10 min. Eluates were separated on an SDS-PAGE gel followed by western blotting as described in Chapter 2 (see addendum 2 for the antibodies used). For mass spectrometry the SDS-PAGE gels were stained with Colloidal Coomassie stain (Invitrogen) according to the manufacturer's instructions. Bands were cut out and submitted for LC-MS/MS analysis.

SDS sample buffer was made as follow (1 ml):

- 80 µl 10% glycerol
- 40 µl 10% SDS
- 40 µl 1M Tris-HCl pH 6.8
- 20 µl 0.5 M EDTA
- 12 µl of BPB dissolved in bidi
- 8 µl β-Mercaptoethanol
- 800 µl bidi

BioID construct and stable cell line generation

pcDNA3.1 MCS-BirA(R118G)-HA was a gift from Kyle Roux (Addgene plasmid # 36047) [19]. The BirA(R118G)-HA sequence from this vector was cut out and inserted in the multiple cloning site of pcDNA4/FRT/TO (LMBP 07073), available at BCCM/GeneCorner, Ghent University (*http://www.genecorner.ugent.be/*). Subsequently, human *NANOS3* cDNA was inserted in front of the BirA(R118G)-HA sequence resulting in the pCLG-CMV (TetO) Nanos3-BirA-HA construct (Figure 5.15).

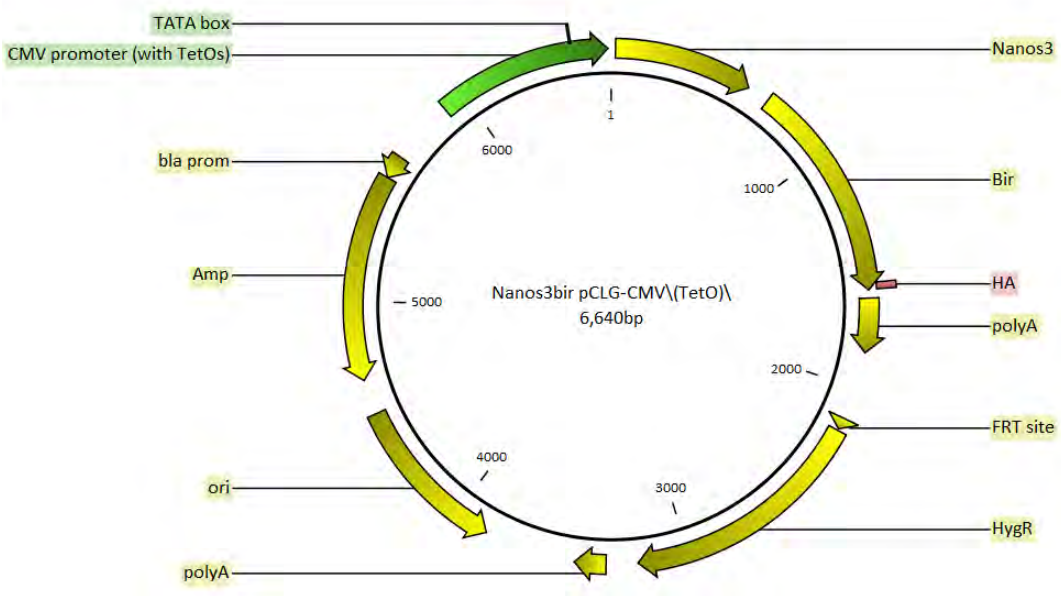

Figure 5.15. The pCLG-CMV(TetO) Nanos3-BirA-HA vector.

Flp-In™ T-Rex™ 293 cells were used for the generation of stable lines using the flp-in system. These cells have an FRT site and were co-transfected with the pOG44 flp-recombinase expression vector and our pCLG-CMV(TetO) Nanos3-BirA-HA expression vector containing an FRT site. Selection of transfected cells was done by adding 100 µg/ml hygromycin and 15 µg/ml blasticidin to the medium during at least 14 days. The Nanos3-BirA-HA fusion protein was expressed after doxycycline induction (1 µg/ml).

Immunofluorescence

Immunofluorescence was performed as described in Chapter 3. For the primary antibodies used and their dilutions, see addendum 2. Goat anti-mouse IgG Dylight® 594 (1/1000) was used as a secondary antibody to detect the anti-HA-tag antibody. For detection of biotinylated proteins an Alexa Fluor™ 488 Streptavidin conjugate (Invitrogen, Thermo Fisher Scientific; 1/500) was used. Pictures were taken with the Olympus CellM fluorescence microscope.

Biotin ligation protocol

Biotin ligation was done as previously described [73]. Briefly, three 175-cm^2 culture flasks of Nanos3-BirA-HA expressing cells were grown in three different conditions: +dox, +biotin; +dox, -biotin; -dox, -biotin. The last two conditions served as negative controls. Each condition was performed in triplicate. Doxycycline (1 µg/ml) was added to the cells when they were seeded and 50 µM biotin was added 24 h before harvesting. Cells were pelleted, washed and frozen at -70°C until purification. After thawing, lysis buffer (50 mM HEPES-NaOH pH 8.0, 100 mM KCl_2, 2 mM EDTA, 0.1% NP-40, 10% glycerol with 1 mM phenylmethylsulfonyl fluoride (PMSF), 1mM DTT and protease inhibitor (Sigma)) was added to the cells and they were placed on ice. After sonication, benzonase nuclease (100 units) was added and the cells were incubated for one hour at 4°C with rotation. The lysates were cleared by centrifugation and added to Dynabeads™ MyOne™ Streptavidin C1 (Life Technologies). After three hours incubation at 4°C with rotation, the beads were washed with a 20 mM Tris-HCl (pH 8.0), 2 mM $CaCl_2$ buffer followed by washing with a 50 mM ammonium bicarbonate buffer (pH 8.0). Washed beads were resuspended in 1 ml 50 mM ammonium bicarbonate and submitted for LC-MS/MS analysis.

Western blotting

Western blotting of Nanos3-BirA-HA-expressing Flp-In™ T-Rex™ 293 cells treated with or without doxycycline (1 µg/ml) was carried out as described in detail in Chapter 2. For the primary antibodies used and their dilutions, see addendum 2.

Mass spectrometry analysis

Protein identification by LC-MS/MS analysis was performed by the group of Prof. Dr. Kris Gevaert, The Medical Biotechnology Center, Ghent University.

Gel bands of interest after immunoprecipitation were washed and an in-gel trypsin digest was performed. After digestion, the peptide mixtures were dried in the SpeedVac, suspended in 30 µL of loading solvent (2% acetonitrile, 0.1% trifluoroacetic acid), transferred to MS compatible vials and analyzed by LC-MS/MS on the Orbitrap XL mass spectrometer. A total volume of 6 µL was injected. The obtained spectra were searched with Mascot Daemon [74] with the search parameters depicted in Table 5.6.

Table 5.6. Parameters that were used for the database search in Mascot Daemon.

Database	*Homo sapiens* (SwissProt)
Enzyme	Trypsin/P
Max. missed cleavages	1
Fixed Modifications	None
Variable Modifications	N-Ac (protein N-terminus) Met Ox Pyro-Glu (N-term Q) Propionamide (C)
Quantitation	None
Peptide tolerance	10 ppm
Instrument	ESI-TRAP
MS/MS tolerance	0.5 Da

N-Ac, N-terminal acetylation; Met Ox, oxidized methionines; Pyro-Glu, N-terminal pyro-glutamic acid (Q); C, cysteine; ppm, parts per million.

BioID samples were incubated for 4 h with 1 µg trypsin (Promega) at 37˚C. After removal of the beads, another 1 µg of trypsin was added and proteins were further digested overnight at 37˚C. Peptides were purified on Omix C18 tips (Agilent), dried and re-dissolved in 20 µl 0.1% formic acid in water/acetonitrile (98:2, v/v) of which 2 µl was injected for LC-MS/MS

analysis on an Ultimate 3000 RSLC nano LC (Thermo Fisher Scientific, Bremen, Germany) in-line connected to a Q Exactive mass spectrometer (Thermo Fisher Scientific). More detailed information can be provided upon request.

Analysis of the Nanos3 proxeome

To elucidate the GO terms and KEGG pathways associated with the protein list identified as the Nanos3 proxeome, we performed an enrichment analysis on the protein list using Enrichr (*http://amp.pharm.mssm.edu/Enrichr/* [42,43]).

Statistical analysis

The MAPPIT data was analyzed with GraphPad Prism 7 performing a two-way ANOVA.

Results obtained by mass spectrometry following a co-IP experiment, were stored in the ms_lims system [75] and analyzed using the "Knime" software program (*http://www.knime.org/*). In this workflow only those peptides were retained that were identified with 95% confidence.

For the BioID data, analysis was performed with MaxQuant (version 1.5.3.30) [21] using the Andromeda search engine with default search settings including a false discovery rate set at 1% on both the peptide and protein level. Proteins were quantified by the MaxLFQ algorithm integrated in the MaxQuant software [22]. Further data analysis was performed with the Perseus software (version 1.5.2.6) after loading the proteinGroups file from MaxQuant. T-tests were performed (FDR=0.01 and S_0=1) for pairwise comparisons of all three conditions (Figure S5.1).

5.7 Supplementary data

Table S5.1. Complete list of 422 proteins found to significantly interact with Nanos3 as observed by BioID. The proteins are ordered alphabetically according to their gene name.

Protein name	Gene name	Difference[a] (control 1[b])	Difference (control 2[c])
ATP-binding cassette sub-family F member 2	*ABCF2*	3,52	1,54
Protein argonaute-1	*AGO1*	5,78	3,04
Protein argonaute-2	*AGO2*	6,94	3,10
Protein argonaute-3	*AGO3*	4,60	5,18
Putative adenosylhomocysteinase 2	*AHCYL1*	8,52	7,61
Putative adenosylhomocysteinase 3	*AHCYL2*	7,31	7,41
Neuroblast differentiation-associated protein AHNAK	*AHNAK*	5,61	3,66
Ankyrin repeat and KH domain-containing protein 1	*ANKHD1*	7,98	4,82
Ankyrin repeat domain-containing protein 17	*ANKRD17*	9,73	6,38
Coatomer subunit delta	*ARCN1*	4,74	3,07
ADP-ribosylation factor GTPase-activating protein 1	*ARFGAP1*	2,38	2,66
Rho guanine nucleotide exchange factor 7	*ARHGEF7*	2,46	2,56
AT-rich interactive domain-containing protein 1A	*ARID1A*	3,77	2,77
AT-rich interactive domain-containing protein 3A	*ARID3A*	2,17	3,19
AT-rich interactive domain-containing protein 3B	*ARID3B*	4,70	3,64
ARPIN	*ARPIN*	2,67	3,06
Activating signal cointegrator 1 complex subunit 2	*ASCC2*	2,62	1,66
Activating signal cointegrator 1 complex subunit 3	*ASCC3*	2,21	1,43
Autophagy-related protein 2 homolog B	*ATG2B*	3,59	3,85
Sodium/potassium-transporting ATPase subunit beta-3	*ATP1B3*	4,31	3,19
ATP synthase subunit beta, mitochondrial	*ATP5B*	2,29	1,90
Ataxin-2	*ATXN2*	3,79	4,08
Ataxin-2-like protein	*ATXN2L*	6,30	3,92
Brain-specific angiogenesis inhibitor 1-associated protein 2-like protein 1	*BAIAP2L1*	2,66	2,36
B-cell receptor-associated protein 31	*BCAP31*	3,03	1,80
BRCA1-associated protein	*BRAP*	3,49	4,16
Bromodomain-containing protein 4	*BRD4*	5,27	6,19
Fanconi anemia group J protein	*BRIP1*	4,22	3,90
Transcription factor BTF3	*BTF3*	2,66	5,04
Protein BTG3	*BTG3*	2,92	3,15
Mitotic checkpoint protein BUB3	*BUB3*	4,41	2,13
UPF0705 protein C11orf49	*C11orf49*	4,83	2,96
Uncharacterized protein C12orf45	*C12orf45*	2,84	2,42
Protein Njmu-R1	*C17orf75*	2,70	2,99
Uncharacterized protein C19orf43	*C19orf43*	2,45	3,93
Caldesmon	*CALD1*	4,99	3,39
Caprin-1	*CAPRIN1*	4,57	3,23
F-actin-capping protein subunit alpha-1	*CAPZA1*	2,36	1,52
F-actin-capping protein subunit alpha-2	*CAPZA2*	3,81	1,44
Coiled-coil domain-containing protein 43	*CCDC43*	4,13	4,35

Protein name	Gene name	Difference[a] (control 1[b])	Difference (control 2[c])
Cyclin-A2	*CCNA2*	3,05	3,25
G2/mitotic-specific cyclin-B1	*CCNB1*	2,09	2,48
Cyclin-K	*CCNK*	3,62	3,00
Cyclin-T1	*CCNT1*	3,54	3,97
T-complex protein 1 subunit epsilon	*CCT5*	4,29	2,34
T-complex protein 1 subunit zeta	*CCT6A*	2,63	2,35
T-complex protein 1 subunit eta	*CCT7*	2,98	2,44
T-complex protein 1 subunit theta	*CCT8*	3,89	3,43
CD2-associated protein	*CD2AP*	7,83	4,37
Cyclin-dependent kinase 2	*CDK2*	4,60	2,04
Cyclin-dependent kinase 9	*CDK9*	4,47	3,21
Protein CDV3 homolog	*CDV3*	2,66	3,91
Centrosomal protein of 44 kDa	*CEP44*	2,47	2,28
Craniofacial development protein 1	*CFDP1*	4,54	4,04
Chromodomain-helicase-DNA-binding protein 8	*CHD8*	4,93	2,24
Cap-specific mRNA (nucleoside-2-O-)-methyltransferase 1	*CMTR1*	2,37	1,96
Calponin-3	*CNN3*	3,86	3,02
CCR4-NOT transcription complex subunit 1	*CNOT1*	3,90	3,38
CCR4-NOT transcription complex subunit 10	*CNOT10*	3,92	3,38
CCR4-NOT transcription complex subunit 11	*CNOT11*	4,75	3,53
CCR4-NOT transcription complex subunit 2	*CNOT2*	7,93	4,53
CCR4-NOT transcription complex subunit 3	*CNOT3*	6,04	3,71
CCR4-NOT transcription complex subunit 4	*CNOT4*	4,57	4,37
CCR4-NOT transcription complex subunit 6	*CNOT6*	6,82	3,62
CCR4-NOT transcription complex subunit 6-like	*CNOT6L*	6,46	4,57
CCR4-NOT transcription complex subunit 7	*CNOT7*	3,85	3,51
CCR4-NOT transcription complex subunit 8	*CNOT8*	6,00	4,91
Coatomer subunit alpha;Xenin;Proxenin	*COPA*	1,65	1,36
Coatomer subunit beta	*COPB1*	3,52	2,33
Coatomer subunit beta	*COPB2*	5,85	3,47
Coatomer subunit epsilon	*COPE*	4,77	2,72
Coatomer subunit gamma-2	*COPG2*	4,10	3,46
Coatomer subunit zeta-1	*COPZ1*	4,92	3,90
Coronin-1B	*CORO1B*	3,52	1,57
Cytochrome c oxidase subunit 7A2, mitochondrial	*COX7A2*	4,10	3,23
Cytoplasmic polyadenylation element-binding protein 4	*CPEB4*	2,93	3,50
Cleavage and polyadenylation specificity factor subunit 2	*CPSF2*	2,08	1,58
Cleavage and polyadenylation specificity factor subunit 3	*CPSF3*	2,13	1,69
Cleavage and polyadenylation specificity factor subunit 6	*CPSF6*	3,27	2,36
Cleavage and polyadenylation specificity factor subunit 7	*CPSF7*	4,44	2,52
Adapter molecule crk	*CRK*	5,40	5,66
Crk-like protein	*CRKL*	6,98	6,25
Cold shock domain-containing protein E1	*CSDE1*	5,57	4,03
Cleavage stimulation factor subunit 2	*CSTF2*	3,90	3,10
Beta-catenin-like protein 1	*CTNNBL1*	4,80	4,33
CTP synthase 1	*CTPS1*	3,20	2,89

Protein name	Gene name	Difference[a] (control 1[b])	Difference (control 2[c])
Src substrate cortactin	*CTTN*	5,63	6,24
Spliceosome-associated protein CWC15 homolog	*CWC15*	3,36	3,27
UPF0428 protein CXorf56	*CXorf56*	3,51	3,02
Uncharacterized protein CXorf57	*CXorf57*	1,93	2,36
DAZ-associated protein 1	*DAZAP1*	3,44	4,27
Drebrin	*DBN1*	4,26	1,41
mRNA-decapping enzyme 1A	*DCP1A*	3,54	4,59
mRNA-decapping enzyme 1B	*DCP1B*	3,06	3,29
Dynactin subunit 4	*DCTN4*	2,39	3,15
ATP-dependent RNA helicase DDX42	*DDX42*	5,38	4,03
Probable ATP-dependent RNA helicase DDX46	*DDX46*	2,54	1,75
Probable ATP-dependent RNA helicase DDX6	*DDX6*	6,04	4,06
ATP-dependent RNA helicase DHX29	*DHX29*	2,50	2,15
Probable ATP-dependent RNA helicase DHX35	*DHX35*	3,07	2,67
Death-inducer obliterator 1	*DIDO1*	3,24	2,50
DIS3-like exonuclease 1	*DIS3L*	2,21	3,73
DnaJ homolog subfamily B member 1	*DNAJB1*	3,10	1,97
DnaJ homolog subfamily C member 17	*DNAJC17*	2,39	1,92
DnaJ homolog subfamily C member 8	*DNAJC8*	3,32	2,86
Dolichol-phosphate mannosyltransferase subunit 1	*DPM1*	3,90	2,50
Dihydropyrimidinase-related protein 2	*DPYSL2*	3,08	3,78
Dihydropyrimidinase-related protein 3	*DPYSL3*	2,60	4,03
Developmentally-regulated GTP-binding protein 1	*DRG1*	4,00	2,04
Segment polarity protein dishevelled homolog DVL-1;Putative segment polarity protein dishevelled homolog DVL1P1	*DVL1;DVL1P1*	5,19	3,56
Segment polarity protein dishevelled homolog DVL-3	*DVL3*	4,82	2,82
Transcription factor E2F6	*E2F6*	3,11	3,13
Enhancer of mRNA-decapping protein 3	*EDC3*	2,58	2,73
Endothelial differentiation-related factor 1	*EDF1*	2,69	3,60
Erythroid differentiation-related factor 1	*EDRF1*	2,79	2,85
EF-hand domain-containing protein D1	*EFHD1*	3,40	2,78
Eukaryotic translation initiation factor 1	*EIF1*	4,00	4,18
Eukaryotic translation initiation factor 1A, X-chromosomal;Eukaryotic translation initiation factor 1A, Y-chromosomal	*EIF1AX;EIF1AY*	2,96	3,29
Eukaryotic translation initiation factor 2A;Eukaryotic translation initiation factor 2A, N-terminally processed	*EIF2A*	4,39	3,56
Eukaryotic translation initiation factor 3 subunit A	*EIF3A*	3,70	2,10
Eukaryotic translation initiation factor 3 subunit F	*EIF3F*	4,27	2,45
Eukaryotic translation initiation factor 3 subunit H	*EIF3H*	4,13	1,75
Eukaryotic translation initiation factor 3 subunit L	*EIF3L*	3,56	2,99
Eukaryotic translation initiation factor 3 subunit M	*EIF3M*	3,99	2,91
Eukaryotic initiation factor 4A-II;Eukaryotic initiation factor 4A-II, N-terminally processed	*EIF4A2*	3,18	2,90
Eukaryotic translation initiation factor 4B	*EIF4B*	5,32	4,85
Eukaryotic translation initiation factor 4E	*EIF4E*	3,13	3,61

Protein name	Gene name	Difference[a] (control 1[b])	Difference (control 2[c])
Eukaryotic translation initiation factor 4E type 2	*EIF4E2*	2,37	2,30
Eukaryotic translation initiation factor 4E transporter	*EIF4ENIF1*	5,52	5,01
Eukaryotic translation initiation factor 4 gamma 1	*EIF4G1*	3,94	3,19
Eukaryotic translation initiation factor 4 gamma 2	*EIF4G2*	4,61	4,30
Eukaryotic translation initiation factor 4 gamma 3	*EIF4G3*	2,85	2,88
Elongator complex protein 4	*ELP4*	2,25	1,82
Protein enabled homolog	*ENAH*	3,56	3,29
Epidermal growth factor receptor substrate 15-like 1	*EPS15L1*	5,07	4,13
ELKS/Rab6-interacting/CAST family member 1	*ERC1*	5,67	2,10
RNA-binding protein EWS	*EWSR1*	4,95	1,39
Exosome complex component RRP41	*EXOSC4*	3,27	4,50
Protein FAM13A	*FAM13A*	4,05	2,58
Protein FAM193A	*FAM193A*	5,59	4,02
Protein FAM193B	*FAM193B*	2,66	3,09
Protein FAM195A	*FAM195A*	3,06	3,52
Protein FAM195B	*FAM195B*	3,95	5,68
Protein FAM91A1	*FAM91A1*	3,07	3,77
Flap endonuclease 1	*FEN1*	4,93	3,54
Peptidyl-prolyl cis-trans isomerase FKBP3	*FKBP3*	3,70	4,56
Filamin-A	*FLNA*	4,64	3,50
Filamin-B	*FLNB*	4,77	2,22
Fragile X mental retardation protein 1	*FMR1*	2,83	2,01
Far upstream element-binding protein 1	*FUBP1*	3,56	2,46
Far upstream element-binding protein 3	*FUBP3*	4,80	2,72
RNA-binding protein FUS	*FUS*	2,82	1,43
Fragile X mental retardation syndrome-related protein 1	*FXR1*	3,23	2,45
Ras GTPase-activating protein-binding protein 1	*G3BP1*	3,32	2,86
Ras GTPase-activating protein-binding protein 2	*G3BP2*	4,11	1,47
GTPase-activating protein and VPS9 domain-containing protein 1	*GAPVD1*	2,79	4,20
H/ACA ribonucleoprotein complex subunit 1	*GAR1*	2,77	3,04
Transcriptional repressor p66-beta	*GATAD2B*	3,40	1,37
GC-rich sequence DNA-binding factor 2	*GCFC2*	1,64	1,47
Gem-associated protein 5	*GEMIN5*	4,92	2,42
Gametogenetin-binding protein 2	*GGNBP2*	5,04	3,49
PERQ amino acid-rich with GYF domain-containing protein 1	*GIGYF1*	2,49	2,04
PERQ amino acid-rich with GYF domain-containing protein 2	*GIGYF2*	2,32	2,32
Vasculin-like protein 1	*GPBP1L1*	3,62	4,61
G patch domain and KOW motifs-containing protein	*GPKOW*	3,83	4,13
G-protein-signaling modulator 1	*GPSM1*	2,27	2,99
General transcription factor IIE subunit 1	*GTF2E1*	3,72	4,94
GTP-binding protein 1	*GTPBP1*	1,97	1,66
Histone acetyltransferase type B catalytic subunit	*HAT1*	4,11	4,70

Protein name	Gene name	Difference[a] (control 1[b])	Difference (control 2[c])
Host cell factor 1;HCF N-terminal chain 1;HCF N-terminal chain 2;HCF N-terminal chain 3;HCF N-terminal chain 4;HCF N-terminal chain 5;HCF N-terminal chain 6;HCF C-terminal chain 1;HCF C-terminal chain 2;HCF C-terminal chain 3;HCF C-terminal chain 4;HCF C-terminal chain 5;HCF C-terminal chain 6	*HCFC1*	3,61	2,36
Histone deacetylase 1	*HDAC1*	4,43	1,46
Histone deacetylase 2	*HDAC2*	2,65	1,78
Hepatoma-derived growth factor-related protein 2	*HDGFRP2*	3,40	4,15
Vigilin	*HDLBP*	2,70	2,62
Headcase protein homolog	*HECA*	4,97	3,86
Probable helicase with zinc finger domain	*HELZ*	3,61	4,95
Protein HEXIM1	*HEXIM1*	3,84	4,62
Minor histocompatibility antigen H13	*HM13*	2,30	4,16
Hematological and neurological expressed 1 protein;Hematological and neurological expressed 1 protein, N-terminally processed	*HN1*	4,02	3,29
Hematological and neurological expressed 1-like protein	*HN1L*	3,36	3,33
Heterogeneous nuclear ribonucleoprotein D-like	*HNRNPDL*	2,04	1,73
Heterogeneous nuclear ribonucleoprotein K	*HNRNPK*	1,99	1,99
Inhibitor of Bruton tyrosine kinase	*IBTK*	3,71	4,47
Insulin-degrading enzyme	*IDE*	3,39	3,63
Interferon-induced protein with tetratricopeptide repeats 5	*IFIT5*	4,42	4,36
Phosphatidylinositol 3,4,5-trisphosphate 5-phosphatase 2	*INPPL1*	2,85	3,32
Integrator complex subunit 9	*INTS9*	1,97	2,18
Probable JmjC domain-containing histone demethylation protein 2C	*JMJD1C*	6,58	7,07
Lysine-specific demethylase 3B	*KDM3B*	4,52	4,10
Far upstream element-binding protein 2	*KHSRP*	6,07	3,65
Uncharacterized protein KIAA1841	*KIAA1841*	5,34	3,47
Kinesin-like protein KIF23	*KIF23*	3,40	2,83
Chromosome-associated kinesin KIF4A	*KIF4A*	2,70	2,61
Histone-lysine N-methyltransferase 2A;MLL cleavage product N320;MLL cleavage product C180	*KMT2A*	2,50	3,27
La-related protein 1	*LARP1*	2,73	2,44
La-related protein 7	*LARP7*	4,55	3,28
Inner nuclear membrane protein Man1	*LEMD3*	3,14	1,37
Leukocyte receptor cluster member 8	*LENG8*	3,75	2,35
LIM domain-containing protein 1	*LIMD1*	3,20	3,81
Lipopolysaccharide-responsive and beige-like anchor protein	*LRBA*	2,27	2,52
Leucine-rich repeat-containing protein 49	*LRRC49*	4,89	2,79
Leucine-rich repeat and WD repeat-containing protein 1	*LRWD1*	3,85	3,85
Protein LSM12 homolog	*LSM12*	3,95	3,10
Protein LSM14 homolog A	*LSM14A*	3,65	2,46
U6 snRNA-associated Sm-like protein LSm2	*LSM2*	5,33	1,95
U6 snRNA-associated Sm-like protein LSm4	*LSM4*	3,77	3,13
U6 snRNA-associated Sm-like protein LSm5	*LSM5*	3,19	2,79

Protein name	Gene name	Difference[a] (control 1[b])	Difference (control 2[c])
U6 snRNA-associated Sm-like protein LSm7	*LSM7*	1,96	2,17
U6 snRNA-associated Sm-like protein LSm8	*LSM8*	3,04	1,43
Acyl-protein thioesterase 2	*LYPLA2*	3,71	3,84
Microtubule-associated protein 4	*MAP4*	5,51	3,59
Myc-associated zinc finger protein	*MAZ*	2,99	2,61
Mediator of RNA polymerase II transcription subunit 12	*MED12*	3,89	2,98
7SK snRNA methylphosphate capping enzyme	*MEPCE*	5,73	3,83
Microsomal glutathione S-transferase 3	*MGST3*	2,65	2,63
MICAL-like protein 1	*MICALL1*	1,84	1,86
MKL/myocardin-like protein 2	*MKL2*	6,59	5,67
Malectin	*MLEC*	2,39	4,02
Myb/SANT-like DNA-binding domain-containing protein 2	*MSANTD2*	2,89	3,43
Metastasis-associated protein MTA1	*MTA1*	2,56	1,50
Metastasis-associated protein MTA2	*MTA2*	3,54	1,34
Mitochondrial carrier homolog 1	*MTCH1*	1,70	2,06
Myotubularin-related protein 9	*MTMR9*	1,70	2,99
C-Myc-binding protein	*MYCBP*	4,40	4,14
Nascent polypeptide-associated complex subunit alpha;Nascent polypeptide-associated complex subunit alpha, muscle-specific form	*NACA*	3,62	1,56
Nucleus accumbens-associated protein 1	*NACC1*	2,74	2,38
Nanos homolog 3	***NANOS3***	**4,82**	**5,28**
Nucleosome assembly protein 1-like 1	*NAP1L1*	2,25	2,00
Nucleosome assembly protein 1-like 4	*NAP1L4*	3,61	3,33
Asparagine--tRNA ligase, cytoplasmic	*NARS*	2,34	2,51
Nuclear autoantigenic sperm protein	*NASP*	5,07	5,49
Negative elongation factor B	*NELFB*	4,15	4,13
Negative elongation factor E	*NELFE*	3,63	4,27
Nicolin-1	*NICN1*	3,38	3,97
Glycylpeptide N-tetradecanoyltransferase 1	*NMT1*	2,87	2,17
RNA-binding protein NOB1	*NOB1*	3,86	3,08
Nuclear ubiquitous casein and cyclin-dependent kinase	*NUCKS1*	2,92	4,47
Cleavage and polyadenylation specificity factor subunit 5	*NUDT21*	3,06	2,18
Nuclear fragile X mental retardation-interacting protein 2	*NUFIP2*	5,22	2,23
Nuclear mitotic apparatus protein 1	*NUMA1*	3,90	3,04
Nuclear pore complex protein Nup153	*NUP153*	5,59	6,56
Nuclear pore complex protein Nup50	*NUP50*	3,60	4,14
Nuclear pore complex protein Nup88	*NUP88*	3,33	2,53
Origin recognition complex subunit 2	*ORC2*	5,09	5,96
Origin recognition complex subunit 3	*ORC3*	4,18	3,82
Origin recognition complex subunit 4	*ORC4*	2,90	4,50
Origin recognition complex subunit 5	*ORC5*	4,60	3,89
Proliferation-associated protein 2G4	*PA2G4*	6,35	6,56
Polyadenylate-binding protein 1;Polyadenylate-binding protein 3	*PABPC1;PABPC3*	1,85	1,52
Polyadenylate-binding protein 4	*PABPC4*	1,76	1,78

Protein name	Gene name	Difference[a] (control 1[b])	Difference (control 2[c])
PAB-dependent poly(A)-specific ribonuclease subunit PAN3	*PAN3*	2,83	3,20
Poly(A) polymerase alpha	*PAPOLA*	5,88	5,78
Protein PAT1 homolog 1	*PATL1*	3,29	3,07
Pre-mRNA cleavage complex 2 protein Pcf11	*PCF11*	3,30	3,66
PCI domain-containing protein 2	*PCID2*	3,44	2,43
PEST proteolytic signal-containing nuclear protein	*PCNP*	2,32	3,58
28 kDa heat- and acid-stable phosphoprotein	*PDAP1*	4,09	4,03
Programmed cell death protein 5	*PDCD5*	3,66	3,88
Protein disulfide-isomerase A5	*PDIA5*	3,64	2,29
PDZ and LIM domain protein 1	*PDLIM1*	2,60	2,67
PDZ and LIM domain protein 5	*PDLIM5*	3,64	2,47
Sister chromatid cohesion protein PDS5 homolog A	*PDS5A*	4,49	2,69
Prefoldin subunit 2	*PFDN2*	2,79	4,02
Prefoldin subunit 6	*PFDN6*	2,54	3,01
PHD finger protein 23	*PHF23*	2,05	2,41
PHD finger protein 3	*PHF3*	3,72	2,09
PIH1 domain-containing protein 1	*PIH1D1*	4,12	4,20
Phosphoinositide 3-kinase regulatory subunit 4	*PIK3R4*	1,86	3,40
Procollagen-lysine,2-oxoglutarate 5-dioxygenase 1	*PLOD1*	4,01	3,33
PMS1 protein homolog 1	*PMS1*	2,69	2,45
DNA polymerase alpha catalytic subunit	*POLA1*	2,74	2,36
Peptidyl-prolyl cis-trans isomerase B	*PPIB*	5,92	3,26
Peptidyl-prolyl cis-trans isomerase-like 4	*PPIL4*	3,27	1,74
Serine/threonine-protein phosphatase PP1-alpha catalytic subunit	*PPP1CA*	4,25	1,51
Serine/threonine-protein phosphatase 1 regulatory subunit 10	*PPP1R10*	6,54	5,75
Polyglutamine-binding protein 1	*PQBP1*	3,48	2,40
DNA primase small subunit	*PRIM1*	2,86	2,76
U4/U6 small nuclear ribonucleoprotein Prp31	*PRPF31*	3,78	1,32
Protein PRRC2A	*PRRC2A*	6,83	6,16
Protein PRRC2B	*PRRC2B*	5,71	5,32
Protein PRRC2C	*PRRC2C*	6,73	6,06
Proteasome activator complex subunit 3	*PSME3*	4,30	4,55
Pumilio homolog 1	*PUM1*	4,23	3,71
Pumilio homolog 2	*PUM2*	2,87	3,03
mRNA export factor	*RAE1*	3,54	3,80
GTP-binding nuclear protein Ran	*RAN*	4,93	2,29
E3 SUMO-protein ligase RanBP2	*RANBP2*	4,21	2,96
Ran-binding protein 3	*RANBP3*	4,49	6,23
Ran GTPase-activating protein 1	*RANGAP1*	3,92	3,12
Ribonucleoprotein PTB-binding 1	*RAVER1*	3,14	1,38
Histone-binding protein RBBP7	*RBBP7*	1,63	1,59
RNA-binding protein 10	*RBM10*	2,97	1,76
Splicing factor 45	*RBM17*	4,68	3,11
RNA-binding protein 20	*RBM20*	3,44	4,07

Protein name	Gene name	Difference[a] (control 1[b])	Difference (control 2[c])
RNA-binding protein 26	*RBM26*	3,26	1,69
RNA-binding protein 3	*RBM3*	4,42	4,03
RNA-binding protein 33	*RBM33*	5,47	3,63
RNA-binding protein 42	*RBM42*	3,05	1,35
Roquin-1	*RC3H1*	4,27	5,41
Roquin-2	*RC3H2*	4,24	4,71
Protein RCC2	*RCC2*	4,15	2,14
Telomere-associated protein RIF1	*RIF1*	3,89	1,94
Serine/threonine-protein kinase RIO2	*RIOK2*	3,22	3,01
E3 ubiquitin-protein ligase BRE1A	*RNF20*	2,94	2,68
RING finger protein 219	*RNF219*	4,18	1,87
mRNA-capping enzyme;Polynucleotide 5-triphosphatase;mRNA guanylyltransferase	*RNGTT*	2,78	3,21
RNA polymerase II-associated protein 3	*RPAP3*	4,83	4,50
Ribonuclease P protein subunit p25-like protein	*RPP25L*	3,02	3,23
Regulation of nuclear pre-mRNA domain-containing protein 2	*RPRD2*	5,43	5,05
Cell differentiation protein RCD1 homolog	*RQCD1*	4,36	3,64
RuvB-like 1	*RUVBL1*	4,19	2,51
RuvB-like 2	*RUVBL2*	2,72	2,45
SAP30-binding protein	*SAP30BP*	4,41	3,93
SAP domain-containing ribonucleoprotein	*SARNP*	2,65	1,54
Squamous cell carcinoma antigen recognized by T-cells 3	*SART3*	5,25	4,65
Protein strawberry notch homolog 1	*SBNO1*	2,32	3,39
Splicing factor, arginine/serine-rich 15	*SCAF4*	2,85	1,92
Succinate dehydrogenase [ubiquinone] flavoprotein subunit, mitochondrial	*SDHA*	2,05	2,68
Septin-2	*SEP2*	3,68	2,26
Septin-7	*SEP7*	3,36	2,23
Septin-9	*SEP9*	3,00	2,44
Plasminogen activator inhibitor 1 RNA-binding protein	*SERBP1*	4,52	3,41
Protein SET;Protein SETSIP	*SET;SETSIP*	4,68	5,03
Splicing factor 1	*SF1*	4,16	2,48
Splicing factor 3A subunit 3	*SF3A3*	2,83	1,81
Endophilin-A2	*SH3GL1*	2,57	3,23
Paired amphipathic helix protein Sin3b	*SIN3B*	7,00	6,20
Spindle and kinetochore-associated protein 3	*SKA3*	2,74	3,13
Small acidic protein	*SMAP*	4,65	4,32
SWI/SNF-related matrix-associated actin-dependent regulator of chromatin subfamily A containing DEAD/H box 1	*SMARCAD1*	2,98	2,32
Serine/threonine-protein phosphatase 4 regulatory subunit 3A	*SMEK1*	5,90	5,28
Serine/threonine-protein kinase SMG1	*SMG1*	5,47	4,69
Protein SMG5	*SMG5*	2,92	1,63
U2 small nuclear ribonucleoprotein B	*SNRPB2*	3,00	1,67
Signal peptidase complex subunit 2	*SPCS2*	2,63	3,97
Signal recognition particle 54 kDa protein	*SRP54*	3,97	4,41

Protein name	Gene name	Difference[a] (control 1[b])	Difference (control 2[c])
Signal recognition particle subunit SRP68	*SRP68*	3,60	3,31
Signal recognition particle subunit SRP72	*SRP72*	4,27	2,43
Cohesin subunit SA-2	*STAG2*	2,66	1,88
Signal transducer and activator of transcription 1-alpha/beta	*STAT1*	3,21	4,39
Serine-threonine kinase receptor-associated protein	*STRAP*	4,97	3,54
Sin3 histone deacetylase corepressor complex component SDS3	*SUDS3*	2,94	4,14
SURP and G-patch domain-containing protein 1	*SUGP1*	5,17	5,86
SURP and G-patch domain-containing protein 2	*SUGP2*	2,65	2,73
Transcription initiation protein SPT3 homolog	*SUPT3H*	1,78	1,94
Transcriptional adapter 1	*TADA1*	2,71	2,98
TATA-binding protein-associated factor 2N	*TAF15*	3,48	1,82
TAF6-like RNA polymerase II p300/CBP-associated factor-associated factor 65 kDa subunit 6L	*TAF6L*	2,65	2,05
Transgelin-2	*TAGLN2*	4,44	6,52
TBC1 domain family member 19	*TBC1D19*	4,59	2,62
TBC1 domain family member 8	*TBC1D8*	1,88	2,08
TATA box-binding protein-like protein 1	*TBPL1*	2,95	3,74
Transcription elongation factor A protein 1	*TCEA1*	3,94	3,45
T-complex protein 1 subunit alpha	*TCP1*	1,63	1,36
Tudor domain-containing protein 3	*TDRD3*	4,16	2,26
Telomeric repeat-binding factor 2	*TERF2*	3,97	1,44
Telomeric repeat-binding factor 2-interacting protein 1	*TERF2IP*	2,60	3,40
Mitochondrial import inner membrane translocase subunit Tim23;Putative mitochondrial import inner membrane translocase subunit Tim23B	*TIMM23;TIMM23B*	1,65	3,07
Mitochondrial import inner membrane translocase subunit Tim8 A	*TIMM8A*	4,86	4,27
TIP41-like protein	*TIPRL*	4,58	5,54
Talin-1	*TLN1*	4,12	3,01
Lamina-associated polypeptide 2, isoform alpha;Thymopoietin;Thymopentin	*TMPO*	4,32	1,64
182 kDa tankyrase-1-binding protein	*TNKS1BP1*	7,76	3,72
Trinucleotide repeat-containing gene 6A protein	*TNRC6A*	7,01	4,63
Trinucleotide repeat-containing gene 6B protein	*TNRC6B*	8,03	5,33
Protein Tob2	*TOB2*	2,66	4,11
Mitochondrial import receptor subunit TOM22 homolog	*TOMM22*	3,23	3,20
Mitochondrial import receptor subunit TOM40 homolog	*TOMM40*	3,17	3,10
Mitochondrial import receptor subunit TOM70	*TOMM70A*	2,29	2,51
DNA topoisomerase 3-beta-1	*TOP3B*	6,10	3,77
Torsin-1A-interacting protein 1	*TOR1AIP1*	2,43	2,77
TOX high mobility group box family member 4	*TOX4*	7,85	7,72
Tubulin polyglutamylase complex subunit 1	*TPGS1*	1,99	1,59
Tubulin polyglutamylase complex subunit 2	*TPGS2*	5,76	5,12
Nucleoprotein TPR	*TPR*	6,41	3,84
Transformation/transcription domain-associated protein	*TRRAP*	3,70	2,52

Protein name	Gene name	Difference[a] (control 1[b])	Difference (control 2[c])
Tumor susceptibility gene 101 protein	*TSG101*	2,15	1,76
Tetratricopeptide repeat protein 13	*TTC13*	2,87	3,18
Tetratricopeptide repeat protein 28	*TTC28*	1,94	1,84
Probable tubulin polyglutamylase TTLL1	*TTLL1*	3,85	3,54
Thioredoxin domain-containing protein 9	*TXNDC9*	1,91	3,27
Ubiquitin-associated protein 2	*UBAP2*	6,75	6,65
Ubiquitin-associated protein 2-like	*UBAP2L*	7,48	5,45
SUMO-conjugating enzyme UBC9	*UBE2I*	3,55	3,96
RING finger protein unkempt homolog	*UNK*	4,47	4,94
Cytochrome b-c1 complex subunit 7	*UQCRB*	2,57	2,85
Cytochrome b-c1 complex subunit 1, mitochondrial	*UQCRC1*	4,15	4,55
Cytochrome b-c1 complex subunit 2, mitochondrial	*UQCRC2*	3,68	1,59
Unconventional prefoldin RPB5 interactor 1	*URI1*	3,10	4,40
Up-regulated during skeletal muscle growth protein 5	*USMG5*	3,24	3,48
Ubiquitin carboxyl-terminal hydrolase 10	*USP10*	4,94	5,18
Ubiquitin carboxyl-terminal hydrolase 15	*USP15*	3,89	3,92
Vesicle-associated membrane protein 3;Vesicle-associated membrane protein 2	*VAMP3;VAMP2*	3,30	4,01
Deubiquitinating protein VCIP135	*VCPIP1*	2,54	3,43
Wings apart-like protein homolog	*WAPAL*	5,70	5,65
WD repeat and HMG-box DNA-binding protein 1	*WDHD1*	5,15	5,50
WD repeat-containing protein 11	*WDR11*	3,81	3,46
WD repeat-containing protein 61;WD repeat-containing protein 61, N-terminally processed	*WDR61*	3,33	2,54
WD repeat-containing protein 70	*WDR70*	4,53	2,91
WD repeat-containing protein 82	*WDR82*	6,53	3,84
WD repeat-containing protein 92	*WDR92*	2,02	2,62
WD repeat domain phosphoinositide-interacting protein 2	*WIPI2*	3,59	3,34
ATPase WRNIP1	*WRNIP1*	4,15	1,60
WW domain-containing oxidoreductase	*WWOX*	2,72	4,06
5-3 exoribonuclease 1	*XRN1*	6,53	6,77
YEATS domain-containing protein 2	*YEATS2*	2,61	2,44
YTH domain-containing family protein 1	*YTHDF1*	4,61	2,14
YTH domain-containing family protein 2	*YTHDF2*	3,37	2,71
YTH domain-containing family protein 3	*YTHDF3*	5,19	4,00
Transcriptional regulator Kaiso	*ZBTB33*	5,42	3,56
Zinc finger CCCH domain-containing protein 4	*ZC3H4*	4,54	5,59
Zinc finger CCCH-type antiviral protein 1	*ZC3HAV1*	2,35	1,31
Zinc finger CCHC domain-containing protein 2	*ZCCHC2*	4,85	4,04
Zinc finger CCHC domain-containing protein 3	*ZCCHC3*	2,16	2,92
Zinc fingers and homeoboxes protein 3	*ZHX3*	3,32	3,66
Zinc finger protein with KRAB and SCAN domains 4	*ZKSCAN4*	2,37	3,22
Protein kinase C-binding protein 1	*ZMYND8*	2,00	3,02
BUB3-interacting and GLEBS motif-containing protein ZNF207	*ZNF207*	4,00	2,60
Zinc finger protein 318	*ZNF318*	5,70	4,98
Zinc finger protein 598	*ZNF598*	2,78	2,31

Protein name	Gene name	Difference[a] (control 1[b])	Difference (control 2[c])
Zinc finger protein 638	*ZNF638*	3,05	2,15
Zyxin	*ZYX*	1,98	2,64

[a] Difference between the mean log2 LFQ intensity values of the +dox+biotin condition and the mentioned control

[b] +dox-biotin

[c] -dox+biotin

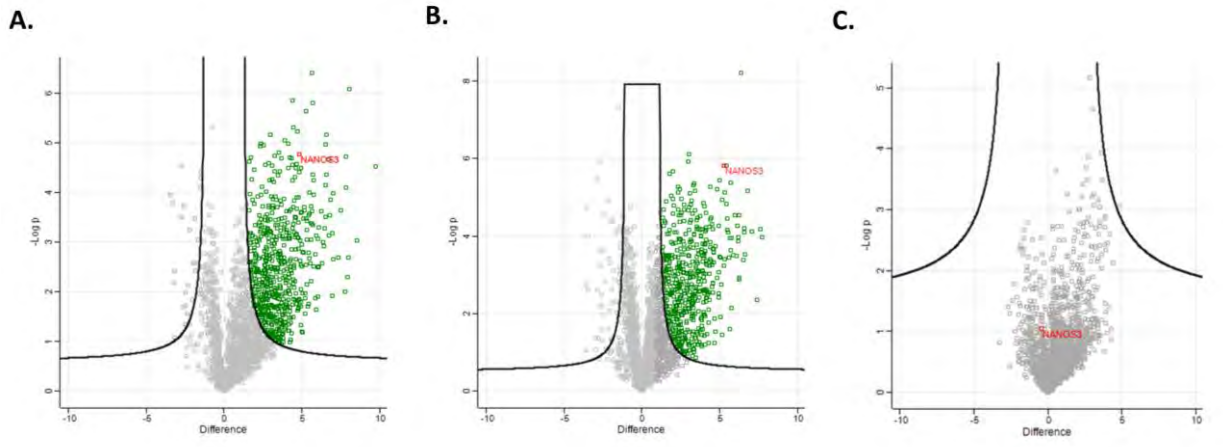

Figure S5.1. Volcano plots showing a pairwise comparison of the three conditions used in the BioID experiment. A. Volcano plot of the +dox+biotin (right) *versus* +dox-biotin (left) condition. **B.** Volcano plot of the +dox+biotin (right) *versus* -dox+biotin (left) condition. **C.** Volcano plot of the -dox+biotin (right) *versus* +dox-biotin (left) condition. Each dot represents an identified and quantified protein. The -Log P value on the Y-axis indicates the statistical significance (taking into account the three replicate samples for each condition), the difference on the X-axis indicates the fold change difference in protein abundance (in $\log_2$) between both samples. Nanos3 is indicated in red and as expected among the most regulated proteins. T-tests were performed for pairwise comparison of all three conditions, FDR=0.01 and S_0=1.

5.8 References

1. Bhandari D, Raisch T, Weichenrieder O, Jonas S, Izaurralde E (2014) Structural basis for the Nanos-mediated recruitment of the CCR4-NOT complex and translational repression. Genes Dev 28 (8):888-901. doi:10.1101/gad.237289.113
2. Grelet S, Andries V, Polette M, Gilles C, Staes K, Martin AP, Kileztky C, Terryn C, Dalstein V, Cheng CW, Shen CY, Birembaut P, Van Roy F, Nawrocki-Raby B (2015) The human NANOS3 gene contributes to lung tumour invasion by inducing epithelial-mesenchymal transition. J Pathol 237 (1):25-37. doi:10.1002/path.4549
3. Free RB, Hazelwood LA, Sibley DR (2009) Identifying novel protein-protein interactions using co-immunoprecipitation and mass spectroscopy. Curr Protoc Neurosci Chapter 5:Unit 5 28. doi:10.1002/0471142301.ns0528s46
4. Fields S, Song O (1989) A novel genetic system to detect protein-protein interactions. Nature 340 (6230):245-246. doi:10.1038/340245a0
5. Eyckerman S, Verhee A, der Heyden JV, Lemmens I, Ostade XV, Vandekerckhove J, Tavernier J (2001) Design and application of a cytokine-receptor-based interaction trap. Nat Cell Biol 3 (12):1114-1119. doi:10.1038/ncb1201-1114
6. Lievens S, Peelman F, De Bosscher K, Lemmens I, Tavernier J (2011) MAPPIT: a protein interaction toolbox built on insights in cytokine receptor signaling. Cytokine Growth Factor Rev 22 (5-6):321-329. doi:10.1016/j.cytogfr.2011.11.001
7. Xu Y, Piston DW, Johnson CH (1999) A bioluminescence resonance energy transfer (BRET) system: application to interacting circadian clock proteins. Proc Natl Acad Sci U S A 96 (1):151-156
8. Hu CD, Chinenov Y, Kerppola TK (2002) Visualization of interactions among bZIP and Rel family proteins in living cells using bimolecular fluorescence complementation. Mol Cell 9 (4):789-798
9. Braun JE, Huntzinger E, Fauser M, Izaurralde E (2011) GW182 proteins directly recruit cytoplasmic deadenylase complexes to miRNA targets. Mol Cell 44 (1):120-133. doi:10.1016/j.molcel.2011.09.007
10. Hashim A, Rizzo F, Marchese G, Ravo M, Tarallo R, Nassa G, Giurato G, Santamaria G, Cordella A, Cantarella C, Weisz A (2014) RNA sequencing identifies specific PIWI-interacting small non-coding RNA expression patterns in breast cancer. Oncotarget 5 (20):9901-9910. doi:10.18632/oncotarget.2476
11. Suzuki R, Honda S, Kirino Y (2012) PIWI expression and function in cancer. Front Genet 3:204. doi:10.3389/fgene.2012.00204

12. Rocak S, Linder P (2004) DEAD-box proteins: the driving forces behind RNA metabolism. Nat Rev Mol Cell Biol 5 (3):232-241. doi:10.1038/nrm1335

13. Lievens S, Vanderroost N, Van der Heyden J, Gesellchen V, Vidal M, Tavernier J (2009) Array MAPPIT: high-throughput interactome analysis in mammalian cells. J Proteome Res 8 (2):877-886. doi:10.1021/pr8005167

14. Yang X, Boehm JS, Yang X, Salehi-Ashtiani K, Hao T, Shen Y, Lubonja R, Thomas SR, Alkan O, Bhimdi T, Green TM, Johannessen CM, Silver SJ, Nguyen C, Murray RR, Hieronymus H, Balcha D, Fan C, Lin C, Ghamsari L, Vidal M, Hahn WC, Hill DE, Root DE (2011) A public genome-scale lentiviral expression library of human ORFs. Nat Methods 8 (8):659-661. doi:10.1038/nmeth.1638

15. Song JJ, Liu J, Tolia NH, Schneiderman J, Smith SK, Martienssen RA, Hannon GJ, Joshua-Tor L (2003) The crystal structure of the Argonaute2 PAZ domain reveals an RNA binding motif in RNAi effector complexes. Nat Struct Biol 10 (12):1026-1032. doi:10.1038/nsb1016

16. Lingel A, Simon B, Izaurralde E, Sattler M (2004) Nucleic acid 3'-end recognition by the Argonaute2 PAZ domain. Nat Struct Mol Biol 11 (6):576-577. doi:10.1038/nsmb777

17. Song JJ, Smith SK, Hannon GJ, Joshua-Tor L (2004) Crystal structure of Argonaute and its implications for RISC slicer activity. Science 305 (5689):1434-1437. doi:10.1126/science.1102514

18. Liu J, Carmell MA, Rivas FV, Marsden CG, Thomson JM, Song JJ, Hammond SM, Joshua-Tor L, Hannon GJ (2004) Argonaute2 is the catalytic engine of mammalian RNAi. Science 305 (5689):1437-1441. doi:10.1126/science.1102513

19. Roux KJ, Kim DI, Raida M, Burke B (2012) A promiscuous biotin ligase fusion protein identifies proximal and interacting proteins in mammalian cells. J Cell Biol 196 (6):801-810. doi:10.1083/jcb.201112098

20. Kwon K, Beckett D (2000) Function of a conserved sequence motif in biotin holoenzyme synthetases. Protein Sci 9 (8):1530-1539. doi:10.1110/ps.9.8.1530

21. Cox J, Mann M (2008) MaxQuant enables high peptide identification rates, individualized p.p.b.-range mass accuracies and proteome-wide protein quantification. Nat Biotechnol 26 (12):1367-1372. doi:10.1038/nbt.1511

22. Cox J, Hein MY, Luber CA, Paron I, Nagaraj N, Mann M (2014) Accurate proteome-wide label-free quantification by delayed normalization and maximal peptide ratio extraction, termed MaxLFQ. Mol Cell Proteomics 13 (9):2513-2526. doi:10.1074/mcp.M113.031591

23. Lau NC, Kolkman A, van Schaik FM, Mulder KW, Pijnappel WW, Heck AJ, Timmers HT (2009) Human Ccr4-Not complexes contain variable deadenylase subunits. Biochem J 422 (3):443-453. doi:10.1042/BJ20090500

24. Zou LH, Shang ZF, Tan W, Liu XD, Xu QZ, Song M, Wang Y, Guan H, Zhang SM, Yu L, Zhong CG, Zhou PK (2015) TNKS1BP1 functions in DNA double-strand break repair though facilitating DNA-PKcs autophosphorylation dependent on PARP-1. Oncotarget 6 (9):7011-7022. doi:10.18632/oncotarget.3137

25. Ohishi T, Yoshida H, Katori M, Migita T, Muramatsu Y, Miyake M, Ishikawa Y, Saiura A, Iemura SI, Natsume T, Seimiya H (2017) Tankyrase-binding protein TNKS1BP1 regulates actin cytoskeleton rearrangement and cancer cell invasion. Cancer Res 77 (9):2328-2338. doi:10.1158/0008-5472.CAN-16-1846

26. Gao Y, Thomas JO, Chow RL, Lee GH, Cowan NJ (1992) A cytoplasmic chaperonin that catalyzes beta-actin folding. Cell 69 (6):1043-1050

27. Yaffe MB, Farr GW, Miklos D, Horwich AL, Sternlicht ML, Sternlicht H (1992) TCP1 complex is a molecular chaperone in tubulin biogenesis. Nature 358 (6383):245-248. doi:10.1038/358245a0

28. Kasembeli M, Lau WC, Roh SH, Eckols TK, Frydman J, Chiu W, Tweardy DJ (2014) Modulation of STAT3 folding and function by TRiC/CCT chaperonin. PLoS Biol 12 (4):e1001844. doi:10.1371/journal.pbio.1001844

29. Yam AY, Xia Y, Lin HT, Burlingame A, Gerstein M, Frydman J (2008) Defining the TRiC/CCT interactome links chaperonin function to stabilization of newly made proteins with complex topologies. Nat Struct Mol Biol 15 (12):1255-1262. doi:10.1038/nsmb.1515

30. Sonoda J, Wharton RP (1999) Recruitment of Nanos to hunchback mRNA by Pumilio. Genes Dev 13 (20):2704-2712

31. Jaruzelska J, Kotecki M, Kusz K, Spik A, Firpo M, Reijo Pera RA (2003) Conservation of a Pumilio-Nanos complex from *Drosophila* germ plasm to human germ cells. Dev Genes Evol 213 (3):120-126. doi:10.1007/s00427-003-0303-2

32. Lolicato F, Marino R, Paronetto MP, Pellegrini M, Dolci S, Geremia R, Grimaldi P (2008) Potential role of Nanos3 in maintaining the undifferentiated spermatogonia population. Dev Biol 313 (2):725-738. doi:10.1016/j.ydbio.2007.11.011

33. Nakahata S, Katsu Y, Mita K, Inoue K, Nagahama Y, Yamashita M (2001) Biochemical identification of *Xenopus* Pumilio as a sequence-specific cyclin B1 mRNA-binding protein that physically interacts with a Nanos homolog, Xcat-2, and a cytoplasmic polyadenylation element-binding protein. J Biol Chem 276 (24):20945-20953. doi:10.1074/jbc.M010528200

34. Bouveret E, Rigaut G, Shevchenko A, Wilm M, Seraphin B (2000) A Sm-like protein complex that participates in mRNA degradation. EMBO J 19 (7):1661-1671. doi:10.1093/emboj/19.7.1661

35. Tharun S (2009) Roles of eukaryotic Lsm proteins in the regulation of mRNA function. Int Rev Cell Mol Biol 272:149-189. doi:10.1016/S1937-6448(08)01604-3

36. Franks TM, Lykke-Andersen J (2008) The control of mRNA decapping and P-body formation. Mol Cell 32 (5):605-615. doi:10.1016/j.molcel.2008.11.001

37. Suzuki A, Igarashi K, Aisaki K, Kanno J, Saga Y (2010) NANOS2 interacts with the CCR4-NOT deadenylation complex and leads to suppression of specific RNAs. Proc Natl Acad Sci U S A 107 (8):3594-3599. doi:10.1073/pnas.0908664107

38. Suzuki A, Niimi Y, Saga Y (2014) Interaction of NANOS2 and NANOS3 with different components of the CNOT complex may contribute to the functional differences in mouse male germ cells. Biol Open 3 (12):1207-1216. doi:10.1242/bio.20149308

39. Mathys H, Basquin J, Ozgur S, Czarnocki-Cieciura M, Bonneau F, Aartse A, Dziembowski A, Nowotny M, Conti E, Filipowicz W (2014) Structural and biochemical insights to the role of the CCR4-NOT complex and DDX6 ATPase in microRNA repression. Mol Cell 54 (5):751-765. doi:10.1016/j.molcel.2014.03.036

40. Jonas S, Izaurralde E (2015) Towards a molecular understanding of microRNA-mediated gene silencing. Nat Rev Genet 16 (7):421-433. doi:10.1038/nrg3965

41. Nishimura T, Padamsi Z, Fakim H, Milette S, Dunham WH, Gingras AC, Fabian MR (2015) The eIF4E-binding protein 4E-T is a component of the mRNA decay machinery that bridges the 5' and 3' termini of target mRNAs. Cell Rep 11 (9):1425-1436. doi:10.1016/j.celrep.2015.04.065

42. Chen EY, Tan CM, Kou Y, Duan Q, Wang Z, Meirelles GV, Clark NR, Ma'ayan A (2013) Enrichr: interactive and collaborative HTML5 gene list enrichment analysis tool. BMC Bioinformatics 14:128. doi:10.1186/1471-2105-14-128

43. Kuleshov MV, Jones MR, Rouillard AD, Fernandez NF, Duan Q, Wang Z, Koplev S, Jenkins SL, Jagodnik KM, Lachmann A, McDermott MG, Monteiro CD, Gundersen GW, Ma'ayan A (2016) Enrichr: a comprehensive gene set enrichment analysis web server 2016 update. Nucleic Acids Res 44 (W1):W90-97. doi:10.1093/nar/gkw377

44. Yamaji M, Tanaka T, Shigeta M, Chuma S, Saga Y, Saitou M (2010) Functional reconstruction of NANOS3 expression in the germ cell lineage by a novel transgenic reporter reveals distinct subcellular localizations of NANOS3. Reproduction 139 (2):381-393. doi:10.1530/REP-09-0373

45. Tomecki R, Kristiansen MS, Lykke-Andersen S, Chlebowski A, Larsen KM, Szczesny RJ, Drazkowska K, Pastula A, Andersen JS, Stepien PP, Dziembowski A, Jensen TH (2010) The human core

exosome interacts with differentially localized processive RNases: hDIS3 and hDIS3L. EMBO J 29 (14):2342-2357. doi:10.1038/emboj.2010.121

46. Staals RH, Bronkhorst AW, Schilders G, Slomovic S, Schuster G, Heck AJ, Raijmakers R, Pruijn GJ (2010) Dis3-like 1: a novel exoribonuclease associated with the human exosome. EMBO J 29 (14):2358-2367. doi:10.1038/emboj.2010.122
47. Godbout R, Squire J (1993) Amplification of a DEAD box protein gene in retinoblastoma cell lines. Proc Natl Acad Sci U S A 90 (16):7578-7582
48. Miles WO, Korenjak M, Griffiths LM, Dyer MA, Provero P, Dyson NJ (2014) Post-transcriptional gene expression control by NANOS is up-regulated and functionally important in pRb-deficient cells. EMBO J 33 (19):2201-2215. doi:10.15252/embj.201488057
49. Tanaka K, Okamoto S, Ishikawa Y, Tamura H, Hara T (2009) DDX1 is required for testicular tumorigenesis, partially through the transcriptional activation of 12p stem cell genes. Oncogene 28 (21):2142-2151. doi:10.1038/onc.2009.89
50. Jorgensen A, Nielsen JE, Almstrup K, Toft BG, Petersen BL, Rajpert-De Meyts E (2013) Dysregulation of the mitosis-meiosis switch in testicular carcinoma in situ. J Pathol 229 (4):588-598. doi:10.1002/path.4154
51. Rouget C, Papin C, Boureux A, Meunier AC, Franco B, Robine N, Lai EC, Pelisson A, Simonelig M (2010) Maternal mRNA deadenylation and decay by the piRNA pathway in the early *Drosophila* embryo. Nature 467 (7319):1128-1132. doi:10.1038/nature09465
52. Janic A, Mendizabal L, Llamazares S, Rossell D, Gonzalez C (2010) Ectopic expression of germline genes drives malignant brain tumor growth in *Drosophila*. Science 330 (6012):1824-1827. doi:10.1126/science.1195481
53. Krishnan P, Ghosh S, Graham K, Mackey JR, Kovalchuk O, Damaraju S (2016) Piwi-interacting RNAs and PIWI genes as novel prognostic markers for breast cancer. Oncotarget 7 (25):37944-37956. doi:10.18632/oncotarget.9272
54. Hatzfeld M, Green KJ, Sauter H (2003) Targeting of p0071 to desmosomes and adherens junctions is mediated by different protein domains. J Cell Sci 116 (Pt 7):1219-1233
55. Strumane K, Bonnomet A, Stove C, Vandenbroucke R, Nawrocki-Raby B, Bruyneel E, Mareel M, Birembaut P, Berx G, van Roy F (2006) E-cadherin regulates human Nanos1, which interacts with p120ctn and induces tumor cell migration and invasion. Cancer Res 66 (20):10007-10015. doi:10.1158/0008-5472.CAN-05-3096
56. Li Y, Guo H, Jin C, Qiu C, Gao M, Zhang L, Liu Z, Kong B (2017) Spliceosome-associated factor CTNNBL1 promotes proliferation and invasion in ovarian cancer. Exp Cell Res 357 (1):124-134. doi:10.1016/j.yexcr.2017.05.008

57. van Maldegem F, Maslen S, Johnson CM, Chandra A, Ganesh K, Skehel M, Rada C (2015) CTNNBL1 facilitates the association of CWC15 with CDC5L and is required to maintain the abundance of the Prp19 spliceosomal complex. Nucleic Acids Res 43 (14):7058-7069. doi:10.1093/nar/gkv643

58. Kim DI, Birendra KC, Zhu W, Motamedchaboki K, Doye V, Roux KJ (2014) Probing nuclear pore complex architecture with proximity-dependent biotinylation. Proc Natl Acad Sci U S A 111 (24):E2453-2461. doi:10.1073/pnas.1406459111

59. Raisch T, Bhandari D, Sabath K, Helms S, Valkov E, Weichenrieder O, Izaurralde E (2016) Distinct modes of recruitment of the CCR4-NOT complex by *Drosophila* and vertebrate Nanos. EMBO J 35 (9):974-990. doi:10.15252/embj.201593634

60. Grelet S, Andries V, Polette M, Gilles C, Staes K, Martin AP, Kileztky C, Terryn C, Dalstein V, Cheng CW, Shen CY, Birembaut P, Van Roy F, Nawrocki-Raby B (2015) The human NANOS3 gene contributes to lung tumour invasion by inducing epithelial-mesenchymal transition. J Pathol. doi:10.1002/path.4549

61. Dreze M, Monachello D, Lurin C, Cusick ME, Hill DE, Vidal M, Braun P (2010) High-quality binary interactome mapping. Methods Enzymol 470:281-315. doi:10.1016/S0076-6879(10)70012-4

62. Meijer HA, Kong YW, Lu WT, Wilczynska A, Spriggs RV, Robinson SW, Godfrey JD, Willis AE, Bushell M (2013) Translational repression and eIF4A2 activity are critical for microRNA-mediated gene regulation. Science 340 (6128):82-85. doi:10.1126/science.1231197

63. Chen Y, Boland A, Kuzuoglu-Ozturk D, Bawankar P, Loh B, Chang CT, Weichenrieder O, Izaurralde E (2014) A DDX6-CNOT1 complex and W-binding pockets in CNOT9 reveal direct links between miRNA target recognition and silencing. Mol Cell 54 (5):737-750. doi:10.1016/j.molcel.2014.03.034

64. Will CL, Urlaub H, Achsel T, Gentzel M, Wilm M, Luhrmann R (2002) Characterization of novel SF3b and 17S U2 snRNP proteins, including a human Prp5p homologue and an SF3b DEAD-box protein. EMBO J 21 (18):4978-4988

65. Ginter-Matuszewska B, Kusz K, Spik A, Grzeszkowiak D, Rembiszewska A, Kupryjanczyk J, Jaruzelska J (2011) NANOS1 and PUMILIO2 bind microRNA biogenesis factor GEMIN3, within chromatoid body in human germ cells. Histochem Cell Biol 136 (3):279-287. doi:10.1007/s00418-011-0842-y

66. Mourelatos Z, Dostie J, Paushkin S, Sharma A, Charroux B, Abel L, Rappsilber J, Mann M, Dreyfuss G (2002) miRNPs: a novel class of ribonucleoproteins containing numerous microRNAs. Genes Dev 16 (6):720-728. doi:10.1101/gad.974702

67. Battle DJ, Lau CK, Wan L, Deng H, Lotti F, Dreyfuss G (2006) The Gemin5 protein of the SMN complex identifies snRNAs. Mol Cell 23 (2):273-279. doi:10.1016/j.molcel.2006.05.036

68. De Keuckelaere E, Hulpiau P, Saeys Y, Berx G, van Roy F (2018) Nanos genes and their role in development and beyond. Cell Mol Life Sci. doi:10.1007/s00018-018-2766-3

69. Yan J, Li Q, Lievens S, Tavernier J, You J (2010) Abrogation of the Brd4-positive transcription elongation factor B complex by papillomavirus E2 protein contributes to viral oncogene repression. J Virol 84 (1):76-87. doi:10.1128/JVI.01647-09

70. Lemmens I, Eyckerman S, Zabeau L, Catteeuw D, Vertenten E, Verschueren K, Huylebroeck D, Vandekerckhove J, Tavernier J (2003) Heteromeric MAPPIT: a novel strategy to study modification-dependent protein-protein interactions in mammalian cells. Nucleic Acids Res 31 (14):e75

71. Eyckerman S, Broekaert D, Verhee A, Vandekerckhove J, Tavernier J (2000) Identification of the Y985 and Y1077 motifs as SOCS3 recruitment sites in the murine leptin receptor. FEBS Lett 486 (1):33-37

72. Risseeuw MD, De Clercq DJ, Lievens S, Hillaert U, Sinnaeve D, Van den Broeck F, Martins JC, Tavernier J, Van Calenbergh S (2013) A "clickable" MTX reagent as a practical tool for profiling small-molecule-intracellular target interactions via MASPIT. ChemMedChem 8 (3):521-526. doi:10.1002/cmdc.201200493

73. Lambert JP, Tucholska M, Go C, Knight JD, Gingras AC (2015) Proximity biotinylation and affinity purification are complementary approaches for the interactome mapping of chromatin-associated protein complexes. J Proteomics 118:81-94. doi:10.1016/j.jprot.2014.09.011

74. Perkins DN, Pappin DJ, Creasy DM, Cottrell JS (1999) Probability-based protein identification by searching sequence databases using mass spectrometry data. Electrophoresis 20 (18):3551-3567. doi:10.1002/(SICI)1522-2683(19991201)20:18<3551::AID-ELPS3551>3.0.CO;2-2

75. Helsens K, Colaert N, Barsnes H, Muth T, Flikka K, Staes A, Timmerman E, Wortelkamp S, Sickmann A, Vandekerckhove J, Gevaert K, Martens L (2010) ms_lims, a simple yet powerful open source laboratory information management system for MS-driven proteomics. Proteomics 10 (6):1261-1264. doi:10.1002/pmic.200900409

CONCLUSIONS AND FUTURE PERSPECTIVES

1 New roles for Nanos proteins?

Lung and prostate cancer are the most frequently diagnosed cancers in men worldwide and belong to the leading causes of cancer death in men [1]. In women, lung cancer is the second most cause of cancer-related death [1]. Preliminary results suggest a role for Nanos3 in both epithelial cancer types (V. Andries *et al*., unpublished results and [2]). Nanos genes encode RBPs that form a protein complex together with their conserved interaction partner, Pumilio. This complex regulates transcript stability and translation after binding NRE sequences, PBE sequences, or both in the 3'UTR of the mRNA targets. *Nanos* genes have been traced back in the most ancestral animals, such as comb jellies. While the genome of *D. melanogaster* only encodes one *nanos* gene, two, three or even four *nanos* genes are encoded by the genomes of other species. These (species-specific) duplications are in all probability associated with new functions.

Human Nanos1 was previously found to be overexpressed in E-cadherin-negative cancer cells and its overexpression promotes invasion in DLD1 cancer cells [3]. In human lung cancer cell lines, Nanos3 expression was recently linked to EMT, as it negatively influences E-cadherin transcription while stimulating vimentin expression [2]. Whether Pumilio is required for these new Nanos3 roles involving transcriptional control and stimulation of protein expression, has not been elucidated. *Nanos* genes in other species have been mostly investigated with respect to their role in germ cells. Whether nanos orthologs in other species besides humans could play a role in cancer should be further investigated. In *Drosophila*, nanos was found to be overexpressed in the *l(3)mbt* brain tumor model. The above mentioned new functions of Nanos3, in addition to the well-studied post-transcriptional repression by Nanos proteins, might be specific to Nanos3 orthologs or to mammalian Nanos paralogs. Also this needs further investigation.

2 Nanos3 expression in human (cancer) cell lines

In Chapter 2, we described our study of Nanos3 expression in several human (cancer) cell lines. In contrast to the Nanos3 expression observed in diverse types of human cancer [4],

Nanos3 overexpression was not generally seen in the human cancer cell lines investigated. Cancer cell lines such as the prostate and ovarian cancer cell lines investigated, which have low expression levels of Nanos3, can however be used to analyze the effect of ectopic Nanos3 expression. To this end, dox-inducible Nanos3 expression constructs can be used. So far, technical difficulties have prevented us from stably transfecting these cell lines.

To tackle the encountered problem of low transfection efficiency, dox-inducible GFP expression constructs were made. Transfection, selection and dox induction could thus be followed by GFP-FACS sorting allowing to obtain the few correctly transfected cells. Although this method, using the same cell line with and without overexpression of the gene of interest, is ideal to avoid variations among different cell lines, the effect of doxycycline addition and the effect of using GFP constructs should be considered. Doxycycline has for instance been shown to influence TNF-α production in endometrial stromal cells. This was observed after a 24-hour treatment with a doxycycline concentration of merely 1 μg/ml [5]. At a higher concentration (5-10 μg/ml) doxycycline affected the invasive potential and cell proliferation of colon cancer cell lines by inhibiting MMP activity [6]. A similar negative effect on cell proliferation and MMP activity was seen in gall bladder carcinoma cell lines upon treatment with 5 and 20 μg/ml doxycycline, respectively [7].

3 The search for Nanos3 mRNA targets

When studying RBPs such as Nanos3, identifying specific mRNA targets is most important. RIP was used by us to capture RNAs associated with Nanos3, in order to identify potential mRNA targets. The RNA obtained after RIP was analyzed using RT-qPCR to assess the binding of possible mRNA targets. The mRNAs encoding proteins, found to be up- or downregulated in our proteome analysis comparing control and Nanos3-expressing lung cells, were analyzed as possible mRNA targets of Nanos3. RIP was performed in SK-LU-1-GFP-Nanos3 and Calu-1-GFP-Nanos3 cells and *SPTAN1* and *PPL* mRNAs were identified as candidate Nanos3 targets. Cotransfecting HEK293T cells with a reporter construct having the 3'UTR of *SPTAN1* cloned behind the luciferase gene and different concentrations of a Nanos3 expression construct, rather suggests an upregulation of spectrin alpha-1 upon Nanos3 overexpression. When repeating the RIP analysis with a second negative control besides the IgG control, that is, the

same lung cancer cell line without Nanos3 expression (Calu-1-GFP-pdest 12.2 cells), *SPTAN1* mRNA was also picked up in the negative control. A lot of background was seen when using the Nanos3 antibody for western blot detection in the RIP setup, suggesting unspecific binding of other proteins. *SPTAN1* mRNA might represent an example of unspecific mRNA binding to the Nanos3 antibody. However, *VIM* mRNA, which is a reported Nanos3 target, was also observed in the negative control, therefore suggesting experimental shortcomings. Calu-1-GFP-pdest 12.2 cells still have a small amount of endogenous Nanos3 expression. However, we also performed the RIP analysis with primary lung cancer cell lines, LuTDco and LuTDNa3 cell lines, obtained from our lung model #3, LSL-KRas^{G12D};p53$^{-/-}$. Although the LuTDco cell lines are completely negative for Nanos3, similar results were obtained as for the Calu-1-GFP-pdest 12.2 cells. It would thus be essential to find out whether optimization of the protocol, another Nanos3-specific antibody or another RIP-kit could improve the results obtained.

Other approaches could be used to analyze the Nanos3-bound mRNAs such as the use of cDNA microarrays [8] or Illumina sequencing of the purified mRNAs. These methods should also allow us to identify mRNA targets without any prior knowledge. RNA sequencing of lung lysates with or without Nanos3 overexpression could also reveal possible mRNA targets.

Unlike previously detected mRNA targets of Nanos proteins, such as hunchback [9], *para* [10,11] and *E2F3* [12], *VIM* mRNA does not have any NRE or PBE sequences, neither in its 3'UTR nor in the coding sequence as was seen for *para* [10]. It would therefore be interesting to investigate how Nanos3 exactly binds the *VIM* mRNA sequence. This might reveal a new binding sequence and new interaction partners involved in Nanos3-mediated post-transcriptional upregulation.

Besides SPTAN1, also SPTBN1 (spectrin β1) was found to be downregulated in lung cell lines upon Nanos3 overexpression. Unlike *SPTAN1*, *SPTBN1* mRNA has both a conserved PBE and NRE sequence in its 3'UTR. Further investigation of Nanos3 binding to *SPTBN1* mRNA could be interesting and could also explain the observed downregulation of SPTAN1 since downregulation of spectrin β1 was previously found to be linked to downregulation of spectrin α1 [13].

Since nanos proteins generally cooperate with pumilio proteins to repress their mRNA targets, we checked whether the proteins that were downregulated upon Nanos3 expression could be traced back in reported lists of mRNA targets for Pumilio1 and Pumilio2 [8]. For Pumilio2, only *CD9* from our list was reported to be an mRNA target. Besides *CD9*, *SPTBN1*, *NEXN*, *AKAP12* and *ARHGDIB* were reported mRNA targets of Pumilio1 [8]. This suggests that Nanos3 rather cooperates with Pumilo1 than with Pumilio2 in our lung cell lines.

Next we checked whether Nanos3 also influences the levels of those mRNAs that correspond to the proteins detected in our proteome analysis. The results from our RT-qPCR analysis were generally in accordance with the proteomic data showing a trend toward downregulation of the RNA level when the associated protein was downregulated upon Nanos3 overexpression, and the other way around. However, significant changes were rarely observed and for some genes the RNA levels differed quite a lot between the biological triplicates of one lung cell line. A difference in cell confluency probably also resulted in a difference in the observed RNA levels.

The “cellular context”, which seems to be different in the lung cancer cell lines, SK-LU-1 and Calu-1, as compared to the transformed HBE4-E6/E7 cell line, might also influence Nanos3-mediated regulation. Both lung cancer cell lines carry *KRas* mutations, with one $KRas^{G12D}$ allele in the SK-LU-1 cell line and two $KRas^{G12C}$ alleles in the Calu-1 cell line. Given the decreased survival and advanced bronchiolar hyperplasia upon ectopic Nanos3 expression in our LSL-$KRas^{G12D}$;$p53^{fl/fl}$;CCSP-$rtTA^{+/-}$;TetO-$Cre^{+/-}$ NSCLC model, oncogenic KRas activation might influence Nanos3-mediated regulation.

4 The role of Nanos3 in NSCLC models

The functions of the Nanos/Pumilio complex concerning germ cell development, including prevention of apoptosis and inhibition of precocious PGC differentiation [14] seem to be highly conserved from flies to mammals, as elegantly demonstrated by the Saga group [15]. The surprisingly dynamic behavior of PGCs under the influence of nanos can be considered an example of non-pathological invasive behavior. Grelet et al. linked Nanos3 to EMT in human NSCLC cell lines in which Nanos3 overexpression or silencing respectively stimulates EMT or

induces mesenchymal-epithelial transition (MET) [16]. As invasion and metastasis are the major causes of mortality in cancer patients, it is crucial to understand the molecular mechanisms underlying the successive stages of cancer progression in order to improve prevention, diagnosis and treatment of cancer. To study the role of Nanos3 *in vivo*, we crossed our Nanos3$^{LSL/LSL}$ mice to mice of the p53$^{fl/fl}$;CCSP-rtTA$^{+/-}$;TetO-Cre$^{+/-}$ (model #1), LSL-KRas^{G12D};CCSP-rtTA$^{+/-}$;TetO-Cre$^{+/-}$ (model #2) or LSL-KRas^{G12D};p53$^{fl/fl}$;CCSP-rtTA$^{+/-}$;TetO-Cre$^{+/-}$ (model #3) NSCLC mouse models. The first model was abandoned since it did not generate the expected adenocarcinomas. In the other two models, mice with ectopic Nanos3 expression showed a significantly reduced survival rate (Figure 1). Model #3, combining mutant KRas expression with loss of *TP53*, was the fastest model and was used for further analysis.

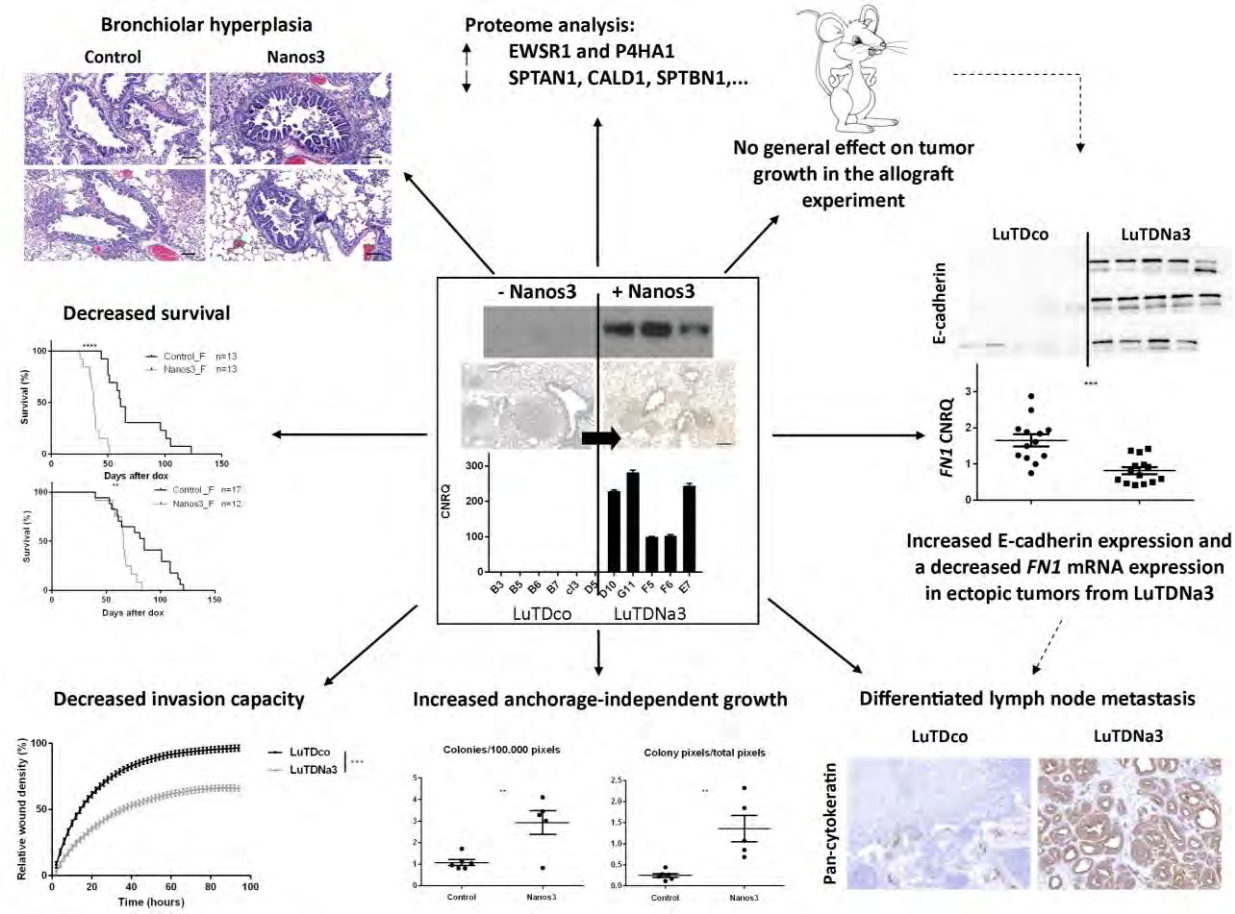

Figure 1. Summary of the effects of ectopic Nanos3 expression obtained from experiments performed on established lung cell lines, primary lung cancer-derived cell lines and our lung cancer mouse model #3. See text for further explanation.

Our NSCLC mice showed a hyperplastic bronchiolar phenotype. NSCLC mice with ectopic expression of Nanos3 showed a more enhanced hyperplastic bronchiolar phenotype compared to the control NSCLC mice. This phenotype might be expected to compromise breathing, although the behavior of the mice did not demonstrate any obvious breathing problems. Bronchiolar hyperplasia might also be secondary to inflammation and might be associated with the activation or inactivation of important stress pathways, which could result in mortality. Otherwise, Nanos3 did not seem to influence tumor progression, as a comparable alveolar tumor percentage and amount of proliferating cells in the lungs was found for both control and Nanos3 NSCLC mice.

Ectopic expression of Nanos3 was, unlike previously seen in NSCLC cell lines [2], not coupled with a change in E-cadherin or vimentin expression in the lung tumors. The reason for this discrepancy is still unclear and further investigations should be conducted to shed light onto this controversy.

Primary lung tumor-derived cell lines from a control and a Nanos3 NSCLC mouse were used to further investigate the influence of Nanos3 *in vitro* and in an allograft experiment. *In vitro* experiments revealed an increased anchorage-independent growth in LuTDNa3 compared to LuTDco cell lines. Surprisingly, the LuTDco cell lines demonstrated an increased invasive capacity through Matrigel, compared to LuTDNa3 cell lines.

These results are in contrast to those from our allograft experiment involving the s.c. injection of three LuTDco and three LuTDNa3 cell lines in five mice each. Even though both groups of mice, injected with either LuTDco or LuTDNa3 cell lines, showed a similar type of lung metastasis, lymph node metastasis (histologically verified) was clearly different in both groups of mice. In mice injected with LuTDNa3 lines F5 and D10, the lymph nodes were almost completely taken over by tumor cells forming a solid differentiated tumor. In mice injected with LuTDco cell lines, lymph node metastases were visible as small groups of undifferentiated neoplastic cells. Lymph node metastasis could not be investigated in mice injected with LuTDNa3 line G11. These mice did not show any enlarged lymph nodes at the time point of death, when the tumors reached approximately 1250 mm^3. These mice were, however, sacrificed much earlier, 34 days after s.c. injection compared to 48-69 days after injection. This because of the increased primary tumor growth compared to the tumors in all

other mice of our experiment. Since the primary tumor growth was not increased in all mice injected with LuTDNa3, compared to mice injected with LuTDco cell lines, this phenotype could not be attributed to Nanos3 expression.

Dissemination of tumor cells can be mediated by entering the lymphatic system or the hematogenous vasculature or by a combination of both. Breast cancer tumors for instance preferably disseminate through the lymphatic system [17]. Nanos3 might play a role in differentiation of disseminated cancer cells in the lymph node microenvironment.

Allograft tumors originating from both LuTDco and LuTDNa3 cell lines were analyzed using western blotting and RT-qPCR. This revealed a higher E-cadherin expression in the Nanos3- and GFP-expressing tumors, only visible at the protein level (Figure 1). At the mRNA level Nanos3-expressing tumors showed a lower *FN1* mRNA level compared to the allografts from LuTDco cell lines. Any further observed differences could not be linked to Nanos3 expression. This is in contrast to the previously reported link between Nanos3 and EMT *in vitro* [2].

Orthotopic injection of the same Nanos3-expressing primary lung cell line, transfected with either a negative control shRNA or a Nanos3-targeting shRNA, might help to further assess the effect of Nanos3. This also offers a tumor environment similar to that where lung cancer normally originates. Since the tumor environment is known to influence the growth of cancer cells, this might render different results compared to *in vitro* experiments and ectopic injections. The orthotopic model would also be interesting to compare (lymph node) metastasis between control and Nanos3-expressing tumor cells.

When analyzing *NANOS3* and *GFP* mRNA expression in our lung cancer model #1, i.e. dox-inducible transgenic mice with *TP53* knockout, some leakage of *NANOS3*/*GFP* expression was observed in transgenic mice that did not receive any dox food. Since the same CCSP-rtTA and TetO-Cre mice were used in lung models #2 and #3, leakage might be expected also in these models. However, since our controls are dox-induced mice without the *NANOS3* transgene, this is not of much importance.

Using the proper controls is essential in experimentation and sometimes less obvious than expected. For instance, mice carrying the CCSP-rtTA transgene have been reported to display

airspace enlargement [18,19]. This should be the case in mice with or without doxycycline exposure, and appeared to be independent of the CCSP promoter since also mice that use the SPC promoter to express the rtTA gene in lung epithelial cells exhibit these abnormalities [19]. This is for instance important when investigating emphysema. In our case, alveolar enlargement was seen in a few lungs or lung parts; however, this did not seem to be consistent with CCSP-rtTA expression (data not shown).

Administration of doxycycline has previously been shown to cause alveolar simplification in neonatal rats [20]. Doxycycline is a pan-MMP inhibitor and MMPs play a functional role in alveolarization [21,22]. We administered doxycycline (625 mg/kg) through the food for a period of two weeks. At this concentration an adult mouse consumes around 1-3 mg of dox per day (100 mg/kg), which is not expected to affect postnatal alveolarization [23].

Gender differences should also be considered. In our lung models (models #2 and #3) there was a remarkable difference in survival between females and males of the same genotype. Since a significantly decreased survival of the Nanos3 NSCLC mice compared to the control NSCLC mice occurred in females only, further experiments were limited to female mice. The reason for this gender difference remains elusive. The different levels of hormones in female and male mice might play a role in this. Hormones play for instance a role in the gender differences concerning the prevalence of asthma at different ages [24]. Higher estrogen levels were previously shown to increase the severity of histamine-induced anaphylaxis in female mice compared to male mice [25]. This could play a role in the higher prevalence of anaphylaxis in women compared to men [26,27]. Several reports also link estrogen to increased lung tumor progression [28]. Furthermore, tobacco smoke negatively influences estrogen metabolism in the lung [29]. Estrogen-driven pathways are likely to interact with the EGFR pathways given the synergistic effect of fulvestrant (ER antagonist) and gefitinib (EGFR inhibitor) on inhibiting ectopic tumor growth of NSCLC cells [30]. More specifically estrogen was previously reported to positively influence tumor progression of the LSL-$KRas^{G12D}$;$p53^{fl/fl}$ mouse model with intranasal Adeno-Cre administration [31].

However, when we compare the difference in survival of female and male NSCLC mice (model #3), there is only a significant gender difference in the mice with ectopic Nanos3

expression (Figure 2). A possible explanation for this could be the involvement of estrogen in Nanos3-mediated changes, although this needs further investigation.

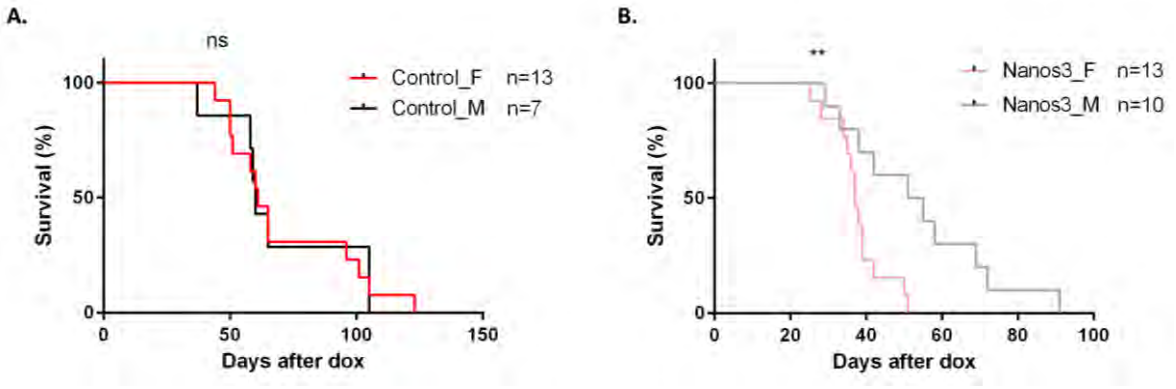

Figure 2. Ectopic Nanos3 expression in the lungs of NSCLC mice (model #3) seems to have an influence on female mice only. A. The survival curves of control female and male NSCLC mice (LSL-KRas^{G12D};p53$^{fl/fl}$;CCSP-rtTA$^{+/-}$;TetO-Cre$^{+/-}$). **B.** The survival curves of Nanos3 female and male NSCLC mice (Nanos3$^{LSL/-}$;LSL-KRas^{G12D};p53$^{fl/fl}$;CCSP-rtTA$^{+/-}$;TetO-Cre$^{+/-}$). Ns: not significant, **: P≤0.01

5 Nanos3 does not stimulate prostate cancer progression of Hi-Myc transgenic mice

To investigate the influence of ectopic Nanos3 expression on prostate cancer progression we used the Hi-Myc prostate cancer model [32] and the Pb-Cre mouse [33]. In combination with our Nanos3 transgenic mouse, the Pb-Cre mouse gave prostate epithelial cell-specific expression of Nanos3 upon paternal transmission of the Pb-Cre transgene [34]. Despite some interesting preliminary data regarding ectopic Nanos3 expression in human prostate cancer, Nanos3 expression did not seem to promote prostate cancer progression in our Hi-Myc mouse model. Afterwards it turned out that this model was not the best choice after all. A lot of variation was seen in the tumor development of our mice and in our hands PIN lesions and tumor initiation were observed at a later age compared to what has been reported in the literature [32] (PIN formation around 16 weeks *versus* 2 weeks).

Given the negative influence of ectopic Nanos3 expression on the survival of female NSCLC mice with a *KRAS* mutation with or without additional loss of *TP53*, it might be interesting to investigate the role of Nanos3 in a prostate cancer model with ERG overexpression and loss

of PTEN [35,36]. In such a mouse model, both the PI3K/AKT pathway and RAS/ERK target genes are activated, as is the case upon $KRas^{G12D}$ expression.

6 Possible interaction partners of Nanos3 and suggested mechanisms of mRNA regulation

Nanos3 is an RBP and was recently shown to repress gene expression at the transcriptional level (*CDH1*) as might be expected, and to stimulate protein expression at the post-transcriptional level (vimentin), which is a novel mechanism for the action of Nanos [2]. Given its interaction with the CCR4-NOT complex [37] and the function of other *Nanos* genes [38], it probably represses several mRNA targets post-transcriptionally. The link between the Nanos/Pumilio complex and the miRNA regulatory complex [38] and the localization of mouse Nanos2 and Nanos3 in P-bodies [39,40], which are also linked with miRNA-mediated repression made us investigate the interaction between Nanos3 and the Argonaute proteins. A previous pull-down experiment for Nanos1 also brought DDX1 to our attention as a possible interaction partner of Nanos proteins. DDX1 has several RNA-associated roles [41], making it plausible that Nanos proteins might bind to DDX1.

Using MAPPIT, we showed an interaction between all human Nanos proteins and DDX1 and the Argonaute proteins investigated (AGO1 to -3, PIWIL1, PIWIL2 and PIWIL4) were also found to interact with Nanos3. This was further confirmed by performing co-immunoprecipitations. For the Argonaute proteins the interaction could only be demonstrated by using the MAPPIT constructs. The use of newly generated expression constructs could not confirm these interactions in a co-IP experiment. As was done for endogenous DDX1, it would be interesting to check the interaction of Nanos3 with the endogenous Argonaute proteins. On the other hand it would also be interesting to generate new constructs, containing parts of the Argonaute proteins, which would enable us to investigate the exact binding sequence needed for interaction of Nanos3 with these proteins.

Although some proteins function on their own, the vast majority of proteins interact with other proteins to execute their functions. The interaction partners of Nanos3 might

determine which mRNA targets are bound in specific environments and whether the formed complexes will stimulate or repress protein expression or stabilize or destabilize the mRNA sequence.

Our collaborators from Reims demonstrated that DDX1 was essential for the Nanos3-mediated upregulation of vimentin in various NSCLC cell lines, more specifically for the lengthening of the poly(A) tail of *VIM* mRNA (S. Grelet *et al*., unpublished). The exact mechanism underlying this DDX1 dependency needs further investigation. Besides binding *VIM* mRNA and thereby regulating vimentin expression, the Nanos3/DDX1 complex is likely to bind other mRNAs. DDX1 could be a Nanos3 interaction partner required for post-transcriptional upregulation while other Nanos3 partners might be involved in the more classical post-transcriptional repression (Figure 3).

Co-IP of endogenous or in our case ectopically expressed proteins and their associated complexes, followed by proteome analysis through mass spectrometry, might allow the discovery of Nanos3 interaction partners without prior knowledge. This might reveal novel mechanisms for Nanos3-mediated (post-)transcriptional regulation.

Besides co-IP using HEK293T cells that overexpress a Nanos3 expression construct, we also performed BioID with a Nanos3-BirA-HA fusion protein stably and inducibly expressed in Flp-In™ T-Rex™ 293 cells. BioID followed by mass spectrometry detected proteins in a 10 nm range of Nanos3 that might bind Nanos3 in a direct or indirect way.

Besides proteins from the CCR4-CNOT complex, which was already reported to bind Nanos3 [37], other proteins involved in polyadenylation and proteins associated with initiation of translation or mRNA decapping and decay were found by us using both co-IP and BioID.

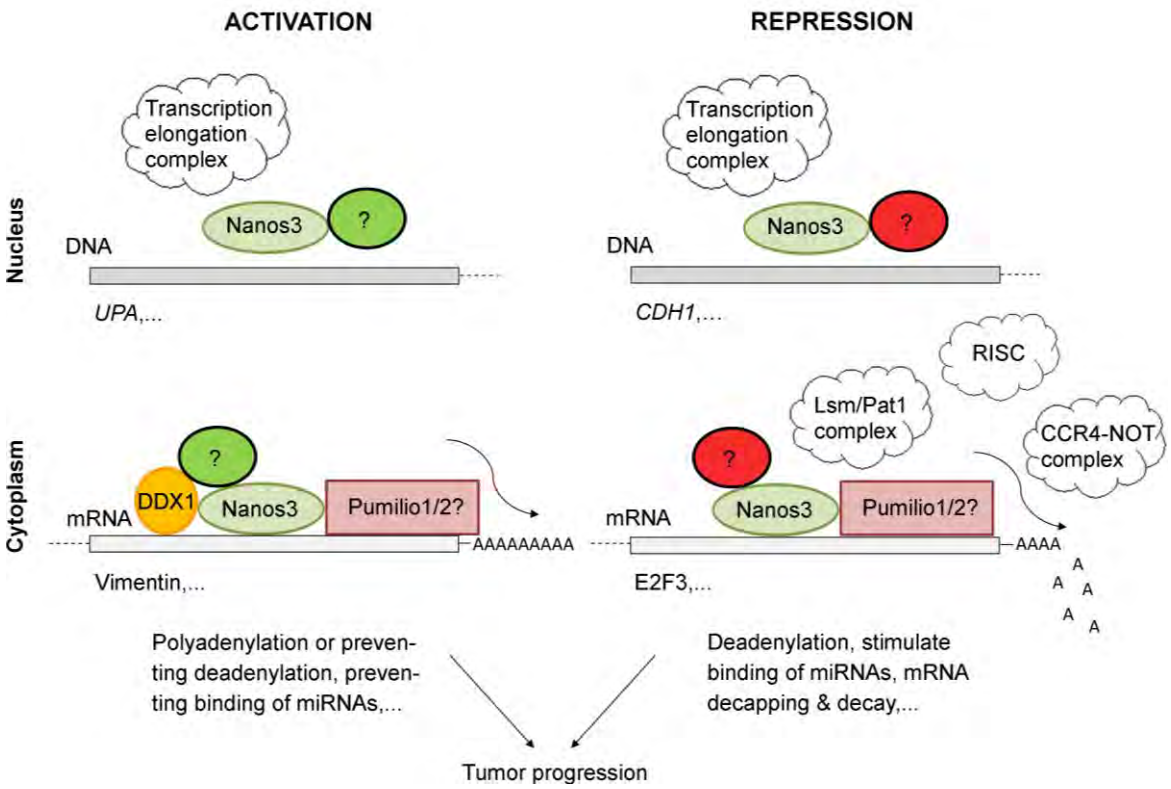

Figure 3. A scheme of the hypothetical functions of Nanos3 and the possible proteins/complexes involved in these functions. This scheme was based upon the reported influence of Nanos3 on the mRNA levels of certain proteins [4,2], on reported mRNA targets of Nanos3 [2,12] and upon our MAPPIT, co-IP and BioID results. Additional unpublished data from our collaborators in Reims linked DDX1 expression to Nanos3-mediated upregulation of vimentin. Complexes are represented by clouds and other unknown proteins involved in positive or negative regulation are represented by green and red ovals, respectively.

Additional proteins from the mRNA decapping and decay complex and proteins from other complexes such as the lsm/Pat1 complex, the PAN2-PAN3 deadenylase complex, the transcription elongation complex and the RNA-induced silencing complex were identified only in case of the BioID method. These complexes might play a role in the Nanos3-mediated transcriptional and post-transcriptional regulation (Figure 3). Most of the above complexes are involved in post-transcriptional repression, consistent with the evolutionarily anticipated role of nanos proteins: formation of a multisubunit translation-inhibitory complex that includes, among other proteins, a pumilio protein.

Nanos3 was previously shown to positively influence *UPA* mRNA expression and to repress *CDH1* mRNA expression in NSCLC cell lines [2] (Figure 3). The mechanism behind these

observed changes at the transcriptional level, has not yet been elucidated. The possibility exists that the influence of Nanos3 on these mRNA expression levels is indirect through post-transcriptional regulation of another regulator. Analysis of our lung tumor-derived lung cancer cells could, however, not confirm these observed changes in *UPA* and *CDH1* mRNA expression levels upon ectopic expression of Nanos3.

Using co-IP we also picked up PLAK and PKP4, two armadillo proteins. These were not identified using the BioID approach. However, another armadillo protein, CTNNBL1, was identified in the Nanos3 proxeome. Given the similarity between the PUM-HD domain and the armadillo repeat domain, Nanos3 might similarly bind and influence the function of such proteins. PLAK and PKP4 are part of the adherens junctions and desmosomes [42]. PPL, another component of the desmosomes, was detected as a possible mRNA target of Nanos3 (Chapter 2). Moreover, Nanos1 was already found to interact with p120-catenin and β-catenin, two other armadillo proteins that are part of the adherens junctions [3]. This could point to a new function of Nanos proteins. It would be interesting to further investigate these possible interaction partners and the biological consequences of the interaction of Nanos proteins with armadillo proteins found in cell-cell junctions.

7 Concluding remarks

Further research should investigate whether *NANOS3* can be considered as a potential oncogene in other cancer types, besides NSCLC. Although our *in vivo* mouse models for NSCLC clearly demonstrated that ectopic Nanos3 expression was paired with a significantly earlier death of these (female) mice, the exact mechanism behind this needs further investigation. The search for Nanos3 interaction partners and mRNA targets in normal and cancer cells might help solving these questions.

Our findings concerning the influence of Nanos3 expression on E-cadherin and vimentin expression could not confirm the previously reported repressive and promoting effect of Nanos3 expression on E-cadherin and vimentin protein levels, respectively [2]. Elucidating the exact mechanism behind these changed expression levels might be needed to explain this discrepancy. Since Nanos proteins have previously not been linked to transcriptional and positive post-transcriptional regulation, this might open up a new way of thinking about the

mechanisms used by Nanos proteins and the relevance of their cytoplasmic *versus* nuclear expression.

The biological function of Nanos3 in the brain is another unexplored territory. Identification of new interaction partners and pathways involved in Nanos3 function, might also help to resolve this.

8 References

1. Torre LA, Bray F, Siegel RL, Ferlay J, Lortet-Tieulent J, Jemal A (2015) Global cancer statistics, 2012. CA Cancer J Clin 65 (2):87-108. doi:10.3322/caac.21262

2. Grelet S, Andries V, Polette M, Gilles C, Staes K, Martin AP, Kileztky C, Terryn C, Dalstein V, Cheng CW, Shen CY, Birembaut P, Van Roy F, Nawrocki-Raby B (2015) The human NANOS3 gene contributes to lung tumour invasion by inducing epithelial-mesenchymal transition. J Pathol 237 (1):25-37. doi:10.1002/path.4549

3. Strumane K, Bonnomet A, Stove C, Vandenbroucke R, Nawrocki-Raby B, Bruyneel E, Mareel M, Birembaut P, Berx G, van Roy F (2006) E-cadherin regulates human Nanos1, which interacts with p120ctn and induces tumor cell migration and invasion. Cancer Res 66 (20):10007-10015. doi:10.1158/0008-5472.CAN-05-3096

4. Grelet S (2014) Implication de Nanos-3 dans l'invasion tumorale broncho-pulmonaire. Dissertation, University of Reims Champagne-Ardenne

5. Li R, Luo X, Pan Q, Zineh I, Archer DF, Williams RS, Chegini N (2006) Doxycycline alters the expression of inflammatory and immune-related cytokines and chemokines in human endometrial cells: implication in irregular uterine bleeding. Hum Reprod 21 (10):2555-2563. doi:10.1093/humrep/del206

6. Onoda T, Ono T, Dhar DK, Yamanoi A, Fujii T, Nagasue N (2004) Doxycycline inhibits cell proliferation and invasive potential: combination therapy with cyclooxygenase-2 inhibitor in human colorectal cancer cells. J Lab Clin Med 143 (4):207-216. doi:10.1016/j.lab.2003.12.012

7. Wang S, Liu C, Liu X, He Y, Shen D, Luo Q, Dong Y, Dong H, Pang Z (2017) Effects of matrix metalloproteinase inhibitor doxycycline and CD147 antagonist peptide-9 on gallbladder carcinoma cell lines. Tumour Biol 39 (10):1010428317718192. doi:10.1177/1010428317718192

8. Galgano A, Forrer M, Jaskiewicz L, Kanitz A, Zavolan M, Gerber AP (2008) Comparative analysis of mRNA targets for human PUF-family proteins suggests extensive interaction with the miRNA regulatory system. PLoS One 3 (9):e3164. doi:10.1371/journal.pone.0003164

9. Wharton RP, Struhl G (1991) RNA regulatory elements mediate control of *Drosophila* body pattern by the posterior morphogen nanos. Cell 67 (5):955-967

10. Muraro NI, Weston AJ, Gerber AP, Luschnig S, Moffat KG, Baines RA (2008) Pumilio binds para mRNA and requires Nanos and Brat to regulate sodium current in *Drosophila* motoneurons. J Neurosci 28 (9):2099-2109. doi:10.1523/JNEUROSCI.5092-07.2008

11. Mee CJ, Pym EC, Moffat KG, Baines RA (2004) Regulation of neuronal excitability through pumilio-dependent control of a sodium channel gene. J Neurosci 24 (40):8695-8703. doi:10.1523/JNEUROSCI.2282-04.2004

12. Miles WO, Tschop K, Herr A, Ji JY, Dyson NJ (2012) Pumilio facilitates miRNA regulation of the E2F3 oncogene. Genes Dev 26 (4):356-368. doi:10.1101/gad.182568.111

13. Hulsmeier J, Pielage J, Rickert C, Technau GM, Klambt C, Stork T (2007) Distinct functions of alpha-Spectrin and beta-Spectrin during axonal pathfinding. Development 134 (4):713-722. doi:10.1242/dev.02758

14. Wang Z, Lin H (2004) Nanos maintains germline stem cell self-renewal by preventing differentiation. Science 303 (5666):2016-2019. doi:10.1126/science.1093983

15. Suzuki A, Tsuda M, Saga Y (2007) Functional redundancy among Nanos proteins and a distinct role of Nanos2 during male germ cell development. Development 134 (1):77-83. doi:10.1242/dev.02697

16. Grelet S, Andries V, Polette M, Gilles C, Staes K, Martin AP, Kileztky C, Terryn C, Dalstein V, Cheng CW, Shen CY, Birembaut P, Van Roy F, Nawrocki-Raby B (2015) The human NANOS3 gene contributes to lung tumour invasion by inducing epithelial-mesenchymal transition. J Pathol. doi:10.1002/path.4549

17. Rahman M, Mohammed S (2015) Breast cancer metastasis and the lymphatic system. Oncol Lett 10 (3):1233-1239. doi:10.3892/ol.2015.3486

18. Perl AK, Wert SE, Loudy DE, Shan Z, Blair PA, Whitsett JA (2005) Conditional recombination reveals distinct subsets of epithelial cells in trachea, bronchi, and alveoli. Am J Respir Cell Mol Biol 33 (5):455-462. doi:10.1165/rcmb.2005-0180OC

19. Sisson TH, Hansen JM, Shah M, Hanson KE, Du M, Ling T, Simon RH, Christensen PJ (2006) Expression of the reverse tetracycline-transactivator gene causes emphysema-like changes in mice. Am J Respir Cell Mol Biol 34 (5):552-560. doi:10.1165/rcmb.2005-0378OC

20. Hosford GE, Fang X, Olson DM (2004) Hyperoxia decreases matrix metalloproteinase-9 and increases tissue inhibitor of matrix metalloproteinase-1 protein in the newborn rat lung: association with arrested alveolarization. Pediatr Res 56 (1):26-34. doi:10.1203/01.PDR.0000130658.45564.1F

21. Oblander SA, Zhou Z, Galvez BG, Starcher B, Shannon JM, Durbeej M, Arroyo AG, Tryggvason K, Apte SS (2005) Distinctive functions of membrane type 1 matrix-metalloprotease (MT1-MMP or MMP-14) in lung and submandibular gland development are independent of its role in pro-MMP-2 activation. Dev Biol 277 (1):255-269. doi:10.1016/j.ydbio.2004.09.033

22. Atkinson JJ, Holmbeck K, Yamada S, Birkedal-Hansen H, Parks WC, Senior RM (2005) Membrane-type 1 matrix metalloproteinase is required for normal alveolar development. Dev Dyn 232 (4):1079-1090. doi:10.1002/dvdy.20267

23. Whitsett JA, Perl AK (2006) Conditional control of gene expression in the respiratory epithelium: A cautionary note. Am J Respir Cell Mol Biol 34 (5):519-520. doi:10.1165/rcmb.F310

24. Carey MA, Card JW, Voltz JW, Arbes SJ, Jr., Germolec DR, Korach KS, Zeldin DC (2007) It's all about sex: gender, lung development and lung disease. Trends Endocrinol Metab 18 (8):308-313. doi:10.1016/j.tem.2007.08.003

25. Hox V, Desai A, Bandara G, Gilfillan AM, Metcalfe DD, Olivera A (2015) Estrogen increases the severity of anaphylaxis in female mice through enhanced endothelial nitric oxide synthase expression and nitric oxide production. J Allergy Clin Immunol 135 (3):729-736 e725. doi:10.1016/j.jaci.2014.11.003

26. Webb LM, Lieberman P (2006) Anaphylaxis: a review of 601 cases. Ann Allergy Asthma Immunol 97 (1):39-43. doi:10.1016/S1081-1206(10)61367-1

27. Gonzalez-Perez A, Aponte Z, Vidaurre CF, Rodriguez LA (2010) Anaphylaxis epidemiology in patients with and patients without asthma: a United Kingdom database review. J Allergy Clin Immunol 125 (5):1098-1104 e1091. doi:10.1016/j.jaci.2010.02.009

28. Hsu LH, Chu NM, Kao SH (2017) Estrogen, Estrogen Receptor and Lung Cancer. Int J Mol Sci 18 (8). doi:10.3390/ijms18081713

29. Peng J, Xu X, Mace BE, Vanderveer LA, Workman LR, Slifker MJ, Sullivan PM, Veenstra TD, Clapper ML (2013) Estrogen metabolism within the lung and its modulation by tobacco smoke. Carcinogenesis 34 (4):909-915. doi:10.1093/carcin/bgs402

30. Stabile LP, Lyker JS, Gubish CT, Zhang W, Grandis JR, Siegfried JM (2005) Combined targeting of the estrogen receptor and the epidermal growth factor receptor in non-small cell lung cancer shows enhanced antiproliferative effects. Cancer Res 65 (4):1459-1470. doi:10.1158/0008-5472.CAN-04-1872

31. Hammoud Z, Tan B, Badve S, Bigsby RM (2008) Estrogen promotes tumor progression in a genetically defined mouse model of lung adenocarcinoma. Endocr Relat Cancer 15 (2):475-483. doi:10.1677/ERC-08-0002

32. Ellwood-Yen K, Graeber TG, Wongvipat J, Iruela-Arispe ML, Zhang J, Matusik R, Thomas GV, Sawyers CL (2003) Myc-driven murine prostate cancer shares molecular features with human prostate tumors. Cancer Cell 4 (3):223-238

33. Wu X, Wu J, Huang J, Powell WC, Zhang J, Matusik RJ, Sangiorgi FO, Maxson RE, Sucov HM, Roy-Burman P (2001) Generation of a prostate epithelial cell-specific Cre transgenic mouse model for tissue-specific gene ablation. Mech Dev 101 (1-2):61-69

34. Birbach A (2013) Use of PB-Cre4 mice for mosaic gene deletion. PLoS One 8 (1):e53501. doi:10.1371/journal.pone.0053501

35. Carver BS, Tran J, Gopalan A, Chen Z, Shaikh S, Carracedo A, Alimonti A, Nardella C, Varmeh S, Scardino PT, Cordon-Cardo C, Gerald W, Pandolfi PP (2009) Aberrant ERG expression cooperates with loss of PTEN to promote cancer progression in the prostate. Nat Genet 41 (5):619-624. doi:10.1038/ng.370

36. Chen Y, Chi P, Rockowitz S, Iaquinta PJ, Shamu T, Shukla S, Gao D, Sirota I, Carver BS, Wongvipat J, Scher HI, Zheng D, Sawyers CL (2013) ETS factors reprogram the androgen receptor cistrome and prime prostate tumorigenesis in response to PTEN loss. Nat Med 19 (8):1023-1029. doi:10.1038/nm.3216

37. Bhandari D, Raisch T, Weichenrieder O, Jonas S, Izaurralde E (2014) Structural basis for the Nanos-mediated recruitment of the CCR4-NOT complex and translational repression. Genes Dev 28 (8):888-901. doi:10.1101/gad.237289.113

38. De Keuckelaere E, Hulpiau P, Saeys Y, Berx G, van Roy F (2018) Nanos genes and their role in development and beyond. Cell Mol Life Sci. doi:10.1007/s00018-018-2766-3

39. Suzuki A, Igarashi K, Aisaki K, Kanno J, Saga Y (2010) NANOS2 interacts with the CCR4-NOT deadenylation complex and leads to suppression of specific RNAs. Proc Natl Acad Sci U S A 107 (8):3594-3599. doi:10.1073/pnas.0908664107

40. Suzuki A, Niimi Y, Saga Y (2014) Interaction of NANOS2 and NANOS3 with different components of the CNOT complex may contribute to the functional differences in mouse male germ cells. Biol Open 3 (12):1207-1216. doi:10.1242/bio.20149308

41. Rocak S, Linder P (2004) DEAD-box proteins: the driving forces behind RNA metabolism. Nat Rev Mol Cell Biol 5 (3):232-241. doi:10.1038/nrm1335

42. Hatzfeld M, Green KJ, Sauter H (2003) Targeting of p0071 to desmosomes and adherens junctions is mediated by different protein domains. J Cell Sci 116 (Pt 7):1219-1233

ADDENDUM

Addendum 1. Production of Nanos3 antibodies

Since the commercial Nanos3 antibody (Proteintech) gives a lot of background in western blot and IHC assays, an attempt was done to make our own Nanos3-specific polyclonal and monoclonal antibodies. For the polyclonal antibodies a peptide corresponding to the C-terminus of Nanos3 was used (P1540, NH_2-KKLVRPDKAKTQDTGH-COOH) (Figure 1A). This peptide was first coupled to KLH (Keyhole limpet hemocyanin), to stimulate the immune reaction, and was then injected into rabbits after which bleedings were collected (Figure 1B). Sera were tested for the presence of antibodies against Nanos3. Pre-immune serum was used as a negative control. Enzyme-linked immunosorbent assay (ELISA) was done to test the specificity of the antibodies for the Nanos3 protein. I purified polyclonal antibodies from a bleeding (serum) by using a column with the immobilized peptide used to make these antibodies (P1540) (see further for Materials and methods of this section). The elution fractions of interest were pooled and dialyzed against a 25 mM HEPES, 140 mM NaCl (pH 7.5) buffer to obtain purified antibodies. These polyclonal antibodies (G379) gave good results on lysates from cells with overexpression of Nanos3 (see 2.2.3; Figure 2.15A) but were apparently not sensitive enough to detect the endogenous Nanos3 protein.

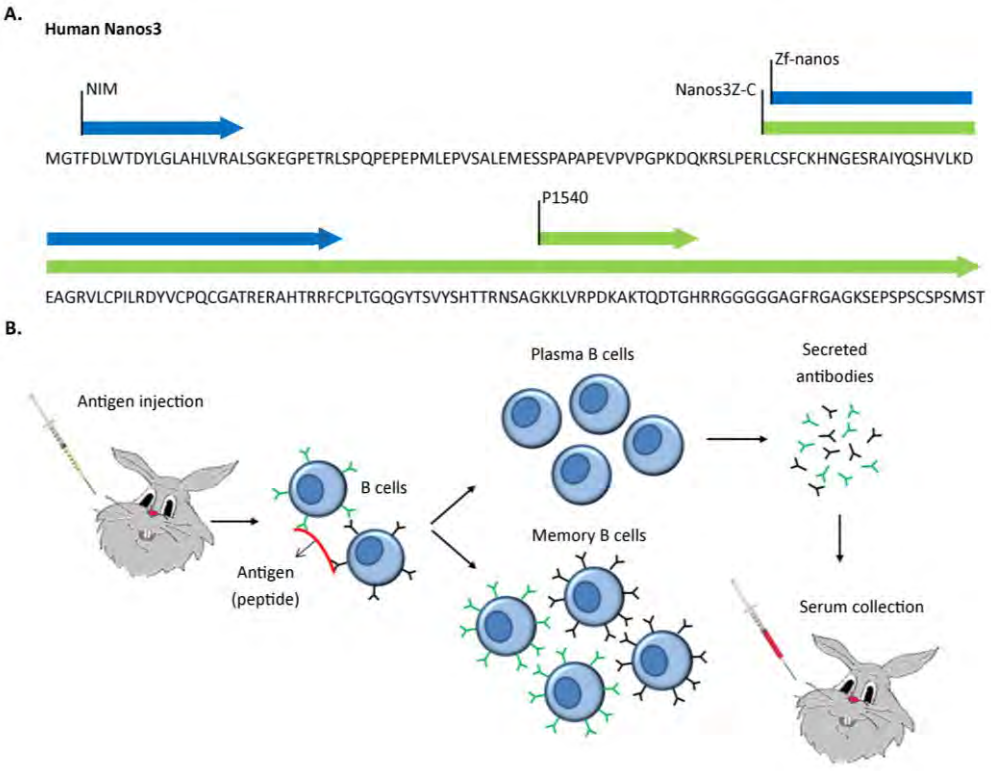

Figure 1. The production of Nanos3 antibodies. A. Peptides used for the in-house production of Nanos3 antibodies (green arrows). The Nanos3 regions; NIM (NOT1 interacting motif) and Zf-nanos (zinc finger domain of nanos proteins) are depicted with blue arrows. **B.** Schematic diagram of the production of polyclonal antibodies for Nanos3 using P1540.

A much longer peptide corresponding to the C-terminal part of Nanos3 (Nanos3Z-C, recombinant protein purified by the VIB Protein Service Facility (PSF)), including the Zf-nanos domain, was used to produce monoclonal antibodies (Figure 1A). This peptide was used in my research group for immunization of C57BL/6 mice. Blood of these mice was checked for antibodies with ELISA in comparison with pre-immune serum. Splenocytes of antibody producing mice were fused with Sp2/0-Ag14 myeloma cells and selected in HAT medium (hypoxanthine-aminopterin-thymidine medium). In this way the unfused immortal myeloma and B-cells will die, leaving only the B-cell-myeloma hybrids (hybridomas) alive. Clones were repetitively screened for Nanos3 specificity using ELISA, with maltose binding protein (MBP) as a negative control. Positive clones were finally frozen. I grew the Nanos3 hybridoma 7g1 clone 8 and analyzed unpurified and purified medium, undiluted or diluted, for Nanos3 specificity (Nanos3Z-C) performing ELISA (Figure 2). A 1 to 1000 dilution of serum from the immunized mice was used as a positive control and mLIF (mouse leukemia inhibitory factor) was used as a negative control. Initially I purified the antibodies from the hybridoma

medium by using sheep anti-mouse IgG-coupled beads. However, after diluting the eluted antibody, specific reactivity of the Nanos3 antibody was rapidly lost (Figure 2A). Using protein A-coupled beads to purify the antibody was even less successful (Figure 2B). During this second type of purification the remaining medium after purification was also tested for reactivity with Nanos3Z-C. The ELISA results demonstrated that Nanos3 antibodies were still present in this medium and purification was therefore inefficient. However, the hybridoma medium itself already proofed adequate to detect Nanos3 in immunofluorescence experiments of Nanos3-expressing cells and in protein lysates. As for the polyclonal Nanos3 antibody, detection was also limited to high levels of Nanos3 (Figure 3). The commercial Nanos3 antibody (Proteintech) was therefore preferred.

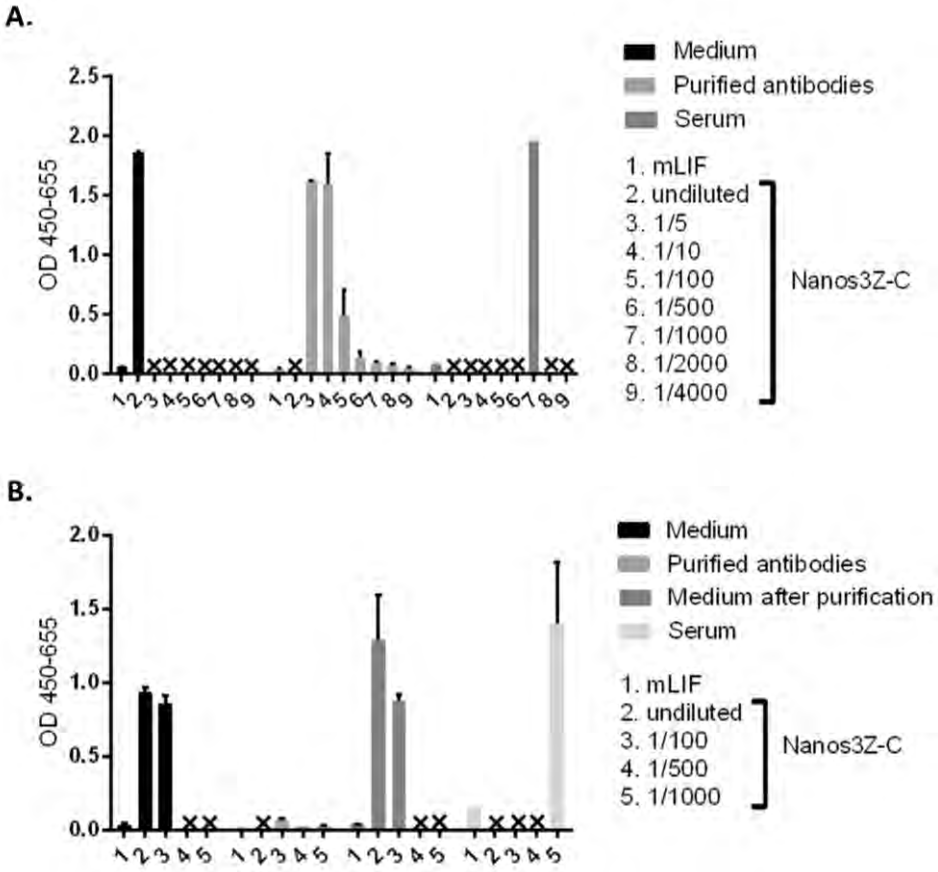

Figure 2. Nanos3 specificity of the in-house produced monoclonal antibodies. Antibodies in the medium of hybridoma cells and purified antibodies, undiluted or diluted, were checked with ELISA for reactivity with the Nanos3Z-C peptide. Serum from the immunized mice and mLIF were used as a positive and negative control, respectively. Antibodies were purified with sheep anti-mouse IgG beads **(A)** or protein A beads **(B)**. To check if the purification with the protein A beads was efficient, medium from which the antibodies were already purified, was also analyzed **(B)**. X, not checked; error bars, SEM; n=2.

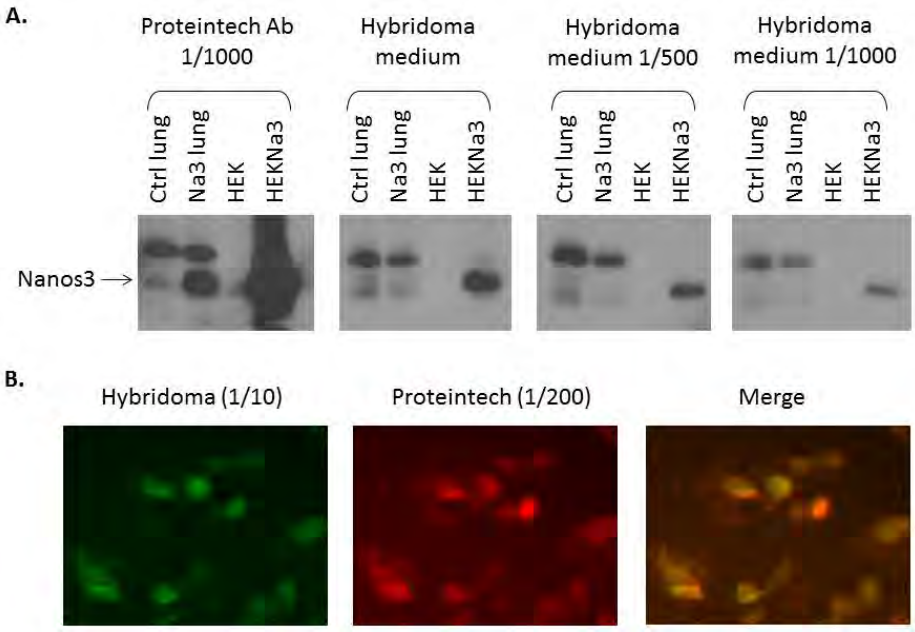

Figure 3. Nanos3 monoclonal antibodies for western blot and immunofluorescence detection of Nanos3. The hybridoma medium could be used to detect overexpression of Nanos3 (Na3) in HEK293T cells using western blotting **(A)** and immunofluorescence **(B)**. In contrast to the hybridoma antibodies, the commercial antibody could detect Nanos3 when it was present in lower levels in lung lysates. For this experiment, lungs with and without ectopic Nanos3 expression were used (see Chapter 3 section 3.2, lung cancer model 3).

Materials and methods

Cell culture

Nanos3 hybridoma cells, generated in-house by Katrien Staes, were cultured in RPMI containing 10% fetal calf serum (FCS), supplemented with 2 mM L-Glutamine (L-Gln), 0.4 mM Na-pyruvate, 100 nM non-essential AA (NEAA) and BM Condimed H1 (Roche). Finally, sodium bicarbonate (Gibco, Life technologies) was added (2.2 g/L) to prevent quick acidification of the medium. HEK293T cells were cultured in DMEM containing 10% FCS, supplemented with L-Gln and Na-pyruvate. Cells were kept at 37°C in a CO_2 incubator (5%) or CO_2 was manually added to 5% in closed recipients, after which cells were grown in a hot room (37°C).

Transient transfection of HEK293T cells

Calcium phosphate ($Ca_3(PO_4)_2$) transfection was done to overexpress Nanos3 (expression construct pdest 12.2 Nanos3cl1) in HEK293T cells. Briefly, 2.5 million cells were seeded in a 75-cm^2 cell culture flask in 15 ml medium. The following day the cells were transfected with the Nanos3 construct and refreshed six hours later. 48 hours after transfection, cells were harvested for western blotting and RT-qPCR analyses.

Affinity purification of polyclonal antibodies

Antibody purification was done by using the SulfoLink® kit (Pierce) according to the manufacturer's instructions. Briefly, the serum sample from the immunized rabbit was loaded, in 1.5-ml fractions, on a P1540-coupled D-Salt™ Polyacrylamide desalting column. The column flow was stopped (bottom cap) for 30 min between each fraction to allow sufficient binding of the sample. This was followed by two washing steps with 6 ml degassed PBS (wash buffer). Antibodies were eluted by passing a 100-mM glycine (pH 2.6) buffer through the column. Fractions of 1 ml were collected and neutralized with 1 M Tris-HCl (pH 8.5-9). The fractions with the highest absorbance at 280 nm were pooled and dialyzed with the Slide-A-lyser (Thermo Scientific) against a 25 mM HEPES, 140 mM NaCl (pH 7.5) buffer.

Antibody purification of monoclonal antibodies

Dynabeads® M-280 sheep anti-mouse IgG beads (Novex, Life technologies) or Dynabeads™ protein A (Invitrogen, Life technologies) were used to purify antibodies from hybridoma medium. Prior to use, beads (50 µl) were washed twice with PBS. The medium containing Ig's was added to the beads and incubated at 4°C, overnight (ON). Beads were washed several times with PBS after which the antibodies were eluted with 0.1 M glycine-HCl (pH 2.5).

ELISA

96-well plates were coated with Nanos3Z-C peptide or mLIF (negative control) in 0.1 M carbonate buffer, pH 9.6 to a final concentration of 2 µg/ml. The plates were incubated ON at 4°C after which they were washed three times with tap water followed by a wash with PBST (PBS with 0.1% Tween 20 (Sigma-Aldrich)). Plates were then incubated with blocking

buffer (PBS + 1% BSA) for 1.5 hours at room temperature (RT). Undiluted or serially diluted (in equal amounts of PBST and blocking buffer) supernatants of hybridoma cell cultures were applied to the ELISA plate. Serum from the immunized mouse was used as a positive control. The plates were incubated for another 1.5 hours at RT after which they were washed again three times with tap water and once with PBST. Plates were then incubated with an HRP-coupled secondary anti-mouse antibody (1:3000; Dako). Development was done by adding TMB substrate (30 min, BD OptEIA^{TM}, BD Biosciences) and was stopped by adding 1 M H_2SO_4 solution. The plates were read in a microplate absorbance reader (iMark^{TM}, Bio-Rad) at 450 nm with 655 nm as background reading.

Western blotting

Cells were lysed as mentioned in Chapter 2. Protein concentration of the supernatants was measured using the DC protein assay kit (Bio-Rad) and total protein (20 µg for HEK293T lysates, 80 µg for the lung) was separated by SDS-PAGE on a 15% polyacrylamide gel. Wet blotting was performed as mentioned in Chapter 2. For the primary antibodies used and their dilutions, see addendum 4.

Immunofluoresence

Immunofluorescence was performed as described in Chapter 2.

Addendum 2. Antibodies used for western blotting (WB), immunohistochemistry (IHC), immunofluorescence (IF) and immunoprecipitation (IP).

Antigen	Type	Company	Working dilution	Technique	Note
Actin	Mouse monoclonal	MP biomedicals	1/10000	WB	
CC10/CCSP	Rabbit polyclonal	Millipore	1/4000	IHC	
CD31	Rat monoclonal	BD Pharmingen	1/50	IHC	
CD44v6	Rat monoclonal	Genetex	1/300	IHC	
CHD4	Rabbit polyclonal	Abcam	1/2000	WB	dissolve in TBST (Tris-buffered saline, 0.1% Tween 20)
Cre	Mouse monoclonal	Abcam	1/500	WB	
Cre	Mouse monoclonal	Abcam	1/1000	WB	
DDX1	Rabbit polyclonal	Proteintech	1/250	WB & IP	
DDX1	Mouse monoclonal	BD Transduction Laboratories	/	IP	
E-cadherin	Rabbit monoclonal	Cell signaling	1/200	IF	
E-cadherin	Mouse monoclonal	BD Transduction Laboratories	1/500	IHC	
E-cadherin (Rat-DECMA1)	Rat monoclonal	Sigma-Aldrich	1/1000	WB	

Antigen	Type	Company	Working dilution	Technique	Note
Flag	Mouse monoclonal	Sigma	1/1000	IF & WB	
Flag-HRP	Mouse monoclonal	Sigma	1/1000	WB	
GFP	Rabbit monoclonal	Cell Signaling technology	1/200	IHC & IF	clone D5.1
GFP	Mouse monoclonal	Roche	1/1000	WB	clones 7.1 and 13.1
GFP	Mouse monoclonal	Abcam	1/500	IF	IgG2A
HA-tag	Mouse monoclonal	Sigma	1/1000	WB & IP	
HA-tag	Mouse monoclonal	Eurogentec	1/500	IF	
HDAC	Rabbit polyclonal	Abcam	1/5000	WB	
Ki67	Rat monoclonal	DakoCytomation	1/30	IHC	
Myc	Mouse monoclonal	in-house made	/	IP	
Myc	Rabbit polyclonal	Santa Cruz	1/300	IHC	
Myc-HRP	Mouse monoclonal	Invitrogen, Thermo Fisher Scientific	1/1000	WB	
Nanos3	Rabbit polyclonal	Proteintech	1/1000 1/200	WB, IHC, IF & IP	
Nanos3	Rabbit polyclonal	in-house made	1/500	WB	
Nanos3	Mouse monoclonal	in-house made	several	WB, IF & ELISA	

Antigen	Type	Company	Working dilution	Technique	Note
Pan-cytokeratin	Mouse monoclonal	Abcam	1/1800	IHC	
pH3 (Ser10)	Rabbit polyclonal	Bethyl laboratories	1/500	IHC	
Sox2	Rabbit monoclonal	Abcam	1/200	IHC	
SPC	Rabbit polyclonal	Millipore	1/4000	IHC	
SPTAN1 (fodrin)	Mouse monoclonal	Enzo	1/250	IHC	
Vimentin	Rabbit polyclonal	Genetex	1/1000	WB	
Vimentin	Guinea pig polyclonal	Fitzgerald	1/1000	IHC	
Vinculin	Mouse monoclonal	Sigma	1/400	WB	
β-catenin	Rabbit polyclonal	Sigma	1/2000	IF	

Addendum 3. A list of the RT-qPCR primers used.

Gene name	Forward primer (5'-3')	Reverse primer (5'-3')
GFP	GAGCTGAAGGGCATCGACTT	TCTGCTTGTCGGCCATGAT
Human genes		
NANOS3 **(1)**	CGCAAACACAACGGCGAGTC	CGGGTGGTGTGGCTGTAGA
NANOS3 **(2)**	CAGGGCTACACCTCCGTCTACA	ACTTCCCGGCACCTCTGAAACC
NANOS1	TGTGGAGTACTTCCGTGCTG	TCAGCTCCTGGAACGACTAC
NANOS2	GCTGCCACCCTTCGACATGTGGA	GCTGGTGTGAGGAGTAGACGTGG
VIM	GACAATGCGTCTCTGGCACGTCTT	TCCTCCGCCTCCTGCAGGTTCTT
CDH1 **(1)**	GCCTCCTGAAAAGAGAGTGGAAG	TGGCAGTGTCTCTCCAAATCCG
CDH1 **(2)**	GGGTACACGCTGGGAAACAT	GACAATGCGTCTCTGGCACGTCTT
EWSR1	AAAGGCGATGCCACAGTGTCCT	TCATTGGAGGCTTCTTCCGAGC
P4HA1	GCCAAAGCTCTGTTACGTCTCC	CAAAGCAGTCCTCAGCCGTTAG
EPHX1	GTTTTCCACCTGGACCAATACGG	TGGTGCCTGTTGTCCAGTAGAG
DDX21	TGGACTCAGAGGGCAGCAGTTA	TGTCTCCATGCAAGGACTGAGC
RPLP1	CAATGCCCTCATTAAAGCAGCCG	CCCTACATTGCAGATGAGGCTC
CALD1	AGAAAAGCAGTGGTGTCAAATCG	CCAGTCTGCTGTCAATCTTGGA
SPTAN1	CTGAAGGTCTCATGGCAGAGGA	CACGGTGTGAACCATCAGACGA
SPTBN1	GGGGTCCCATGACATCGTG	CCGGTGTTTGTGTATCAGTGC
NEXN	AAGAGCGAGCAAGAAGGAGAGC	GTGAGTAAATGGAGCCTCGCTTT
AKAP12	AGAAAGGAGCCCTGAACGGTCA	CCGCTGACTTAGTAGCCATCTC
ARHGDIB	CGTTCAGCACACCTACAGGACT	TTGGGAGCCTCCTCAACTGGAG
BANF1	TGGCTGGGATTGGTGAAGTCCT	CGCCACAAGTGTCTTTCAGCCA
SDPR	GCGGTCAAAGAGCGCATGGATA	AAACACGCTGGCAGGGATCTCA
CD9	TCGCCATTGAAATAGCTGCGGC	CGCATAGTGGATGGCTTTCAGC
CRIP1	GCCTGAAGTGCGAGAAATGTGG	CCCAAACATGGCTGCGTAGCAG

FKBP3	GGAGTAGGCAAAGTTATCAGAGG	GCTGTCCTTTCTTTCCGTAAGCC
HIST1H2BK	TACAACAAGCGCTCGACCAT	TAGCGCTGGTGTACTTGGTG
PPL	GGCTGCAGAATCTGGAGTTTGC	CTCAGTCTCCTCATCCAGTTCC
CNN1	ACAAGAGCGGAGATTTGAGCCG	TCATAGAGGTGACGCCGTGTAC
SLUG	GCCAAACTACAGCGAACTGGA	TGTGGTATGACAGGCATGGAG
PLAU	GGCTTAACTCCAACACGCAAGG	CCTCCTTGGAACGCATCTTCAG
OCLN	TCAAACCGAATCATTATGCACCA	AGATGGCAATGCACATCACAA
MMP-14	CCTTGGACTGTCAGGAATGAGG	TTCTCCGTGTCCATCCACTGGT
PUM1	GCAAACATCGATGGCCTACT	TCTTCCCTCCAGAGCAAGTG
PUM2	GCAAAATATCGAAGTGCTTCA	TCAACTATATGTCCAATCAAG
Housekeeping genes		
ACTB	CTGGAACGGTGAAGGTGACA	AAGGGACTTCCTGTAACAATGCA
GAPDH	CGACCACTTTGTCAAGCTCA	AGGGGAGATTCAGTGTGGTG
SDHA	TGGGAACAAGAGGGCATCTG	CCACCACTGCATCAAATTCATG
UBC	ATTTGGGTCGCGGTTCTTG	TGCCTTGACATTCTCGATGGT
HMBS	GGCAATGCGGCTGCAA	GGGTACCCACGCGAATCAC
HPRT1	TGACACTGGCAAAACAATGCA	GGTCCTTTTCACCAGCAAGCT
MATR3	CGGCAGGAATAGGCCTTCTT	CGTGCAGTACCCTGGTTCATC
OAZ1	AGAGACGCAGCGGAGGTTTT	TCTGGCGAAGCAGTGGCTAT
Mouse genes		
Nanos3	ATGGGGACTTTCAATCTTTGGAC	GTTTGCAGAATGAACATAAGCGT
Ocln	TGGCAAGCGATCATACCCAGAG	CTGCCTGAAGTCATCCACACTC
Fn1	AGACTCGAGGCGGAAATTCC	CCCTGCGACCCTCAGAAGT
Vim	CGGAAAGTGGAATCCTTGCAGG	AGCAGTGAGGTCAGGCTTGGAA
Cdh1	GGTCATCAGTGTGCTCACCTCT	GCTGTTGTGCTCAAGCCTTCAC
Cdh2	AGCGCAGTCTTACCGAAGG	TCGCTGCTTTCATACTGAACTTT

Plau	AGAAGCGACCCTGGTGCTATGT	CCACACTGGAAGCCTTGTTGGT
Zeb1	TTGCGTGTCAGGCATGGAT	GAAAACGGCTGTGAACCAAAA
Zeb2	GGCAAGGCCTTCAAGTACAA	AAGCGTTTCTTGCAGTTTGG
Housekeeping genes		
Tbp	TCTACCGTGAATCTTGGCTGTAAA	TTCTCATGATGACTGCAGCAAA
Hmbs	GAAACTCTGCTTCGCTGCATT	TGCCCATCTTTCATCACTGTATG
ActB	GCTTCTAGGCGGACTGTTACTGA	GCCATGCCAATGTTGTCTCTTAT
B2m	ATGCACGCAGAAAGAAATAGCAA	AGCTATCTAGGATATTTCCAATTTTTGAA
Gapdh	TGTGTCCGTCGTGGATCTGA	TTGCTGTTGAAGTCGCAGGAG
Hprt1	AGTGTTGGATACAGGCCAGAC	CGTGATTCAAATCCCTGAAGT
Rpl13A	CCTGCTGCTCTCAAGGTTGTT	TGGTTGTCACTGCCTGGTACTT
Sdha	CTTGAATGAGGCTGACTGTG	ATCACATAAGCTGGTCCTGT
Ubc	AGCCCAGTGTTACCACCAAG	ACCCAAGAACAAGCACAAGG
Ywhaz	TAAATGGTCTGTCACCGTCT	GGAAATACTCGGTAGGGTGT
Calm2	AGAGCTTCGCCATGTGATG	CAATGTCTTCACTTCGCTGTC
Oaz1	ATTGCTGTTTAAGATGGTCAGG	GGGGAGGTGACACTATTTTTCC

Addendum 4. A list of the primers used for genotyping.

Allele	Primer name	Primer sequence	Amplicon size (bp)
Rosa floxed (Nanos3 mouse)	G1	5’-TAGGTAGGGGATCGGGACTCT-3’	1300
	G2	5’-GCGAAGAGTTTGTCCTCAACC-3’	
Cre	Cre_F	5'-TGCCACGACCAAGTGACAGCAATG-3'	374
	Cre_R	5'-AGAGACGGAAATCCATCGCTCG-3'	
Nanos3-IRES-eGFP	Nanos3_F	5'-AAGGATCAGAAGCGCAGCCT-3'	488
	Nanos3_R	5'-GGGCGGAATTCGATATCAAG-3'	
Rosa	Rosa_F	5'-AAAGTCGCTCTGAGTTGTTAT-3'	wt: 603 floxed: 300
	Rosa_R1	5'-GGAGCGGGAGAAATGGATATG-3'	
	Rosa_R2	5'-GCGAAGAGTTTGTCCTCAACC-3'	
Nanos3 deletion	Nanosdel_F	5'-GGCGCAGTAGTCCAGGGTTTCCTTG-3'	floxed: 355 deletion: +/- 600
	Nanosdel_R1	5'-AGCCGGTTGGCGCTACCGGT-3'	
	Nanosdel_R2	5'-GCCGTTGTGTTTGCAGAAAGAGCA-3'	
LSL-KRas^{G12D}	KRas_F	5'-ATGTCTTTCCCCAGCACAGT-3'	wt: 452 floxed: 327
	KRas_R1	5'-TCCGAATTCAGTGACTACAGATG-3'	
	KRas_R2	5'-CTAGCCACCATGGCTTGAGT-3'	
CCSP-rtTA	CCSP-rtTA_F	5'-AAAATCTTGCCAGCTTTCCCC-3'	584
	CCSP-rtTA_R	5'-ACTGCCCATTGCCCAAACAC-3'	
p53	p53_F	5'-AAGGGGTATGAGGGACAAGG-3'	wt: 431 floxed: 584
	p53_R	5'-GAAGACAGAAAAGGGGAGGG-3'	
p53 deletion	p53del_F	5'-CACAAAAACAGGTTAAACCCAG-3'	612
	p53del_R	5'-GAAGACAGAAAAGGGGAGGG-3'	
Pb-Cre4	Pb-Cre4_F	5'-CTGAAGAATGGGACAGGCATTG-3'	393
	Pb-Cre4_R	5'-CATCACTCGTTGCATCGACC-3'	
Hi-Myc	Hi-Myc_F	5'-AAACATGATGACTACCAAGCTTGGC-3'	177
	Hi-Myc_R	5'-ATGATAGCATCTTGTTCTTAGTCTTTTTC TTAATAGGG-3'	

Addendum 5. The PCR programs executed for the corresponding PCR products.

PCR product	enzyme system	# cycles	denaturing step	annealing step	Elongation step
Rosa floxed (Nanos3 mouse)	Qiagen Taq	35	94°C 1 min	57°C 1 min	72°C 1.5 min
Cre	GoTaq	35	93°C 30 sec	58°C 30 sec	72°C 30 sec
Nanos3	Qiagen Taq	35	94°C 30 sec	60°C 30 sec	72°C 45 sec
Rosa	GoTaq	40	93°C 30 sec	58°C 30 sec	72°C 45 sec
Nanos3 deletion	KAPA2G	39	94°C 30 sec	60°C 30 sec	72°C 45 sec
KRas	Invitrogen Taq	35	94°C 30 sec	60°C 30 sec	72°C 45 sec
CCSP-rtTA	KAPA2G	35	94°C 30 sec	60°C 30 sec	72°C 45 sec
p53	Qiagen Taq	35	93°C 30 sec	58°C 30 sec	72°C 30 sec
p53 deletion	Qiagen Taq	35	94°C 30 sec	60°C 30 sec	72°C 45 sec
Pb-Cre4	Qiagen Taq	35	94°C 30 sec	60°C 30 sec	72°C 30 sec
Hi-Myc	Invitrogen Taq	35	94°C 30 sec	55°C 30 sec	72°C 30 sec

CURRICULUM VITAE

PERSONALIA

Name:	Evi De Keuckelaere
Address:	Overbroekkouterslag 11A
	9850 Merendree
Contact:	+32 493 73 45 06
	evidekeuckelaere@gmail.com
Date of birth:	19-02-1990
LinkedIn account:	*https://www.linkedin.com/in/evi-de-keuckelaere-15896978/*

EDUCATION

2013-2018	Ph.D., Biochemistry and Biotechnology - UGent
2012-2013	Laboratory animal science (FELASA Cat. C) - UGent
2008-2013	Master in Biochemistry and Biotechnology - UGent
2008-2011	Bachelor in Biochemistry and Biotechnology - UGent
2005-2007	Science and mathematics - Emmaüsinstituut, Aalter

WORKING EXPERIENCE

2018-current	**Compliance scientist** at Alcon-Novartis (USG Professionals)
2013-2018	**PhD student** at the university of Ghent, VIB, Inflammation Research Center The role of Nanos3 in tumor progression Promoters: Prof. Dr. Frans Van Roy and Prof. Dr. Geert Berx FWO Fellowship; period: 01/10/2013 - 30/09/2017

TRAINING

Scientific writing – Basic microscopy course (VIB BIC) – CLC Main Workbench Training – Ingenuity pathway analysis (IPA) training – Statistics in GraphPad Prism – Analyzing flow cytometry data using FlowJo (Bits) – Basic statistics in R (Bits) – Image editing (GIMP)

ACADEMIC ACTIVITIES

- Unit and room responsible of tissue culture (TC) (2016-2017)
- Member of the organizing committee of the VIBes congress (2017)
- Member of the organizing committee of the PhD day of the VIB seminar (2015)
- Room responsible of the DNA room (2014-2015)
- Supervisor of a research project 2nd master, Erasmus student (5 months, 2015-2016)
- Supervisor of a research project 1st master (6 weeks, 2015)

PARTICIPATION SYMPOSIA AND CONFERENCES

Poster presenter at the 6th Oncopoint meeting organized by CRIG (Cancer Research Institute Ghent), in collaboration with ION (Immuno-Oncology Network) and CEDAR-IC (Cell Death Activity Regulation in Inflammation and Cancer) held 28/02/2018 at 'het Pand' in Gent/Belgium

Chair at the VIBes in biosciences held 27-29/09/2017 at 'het Pand' in Gent/Belgium

Oral presentation at the IRC department (VIB-UGent); Hot Science, 2016

Poster presenter at the Belgian Society of Cell and Developmental Biology meeting on Cell Adhesion and Communication held 13-14/10/16 at 'het Pand' in Gent/Belgium

Poster presenter at the PhD Symposium held 17/03/16 at Campus Ledeganck/Belgium

Poster presenter at the Belgian Society for Cell and Developmental Biology FWO-IUAP meeting on Developmental programming and organ repair held 23-24/11/15 at 'het Provinciehuis' in Leuven/Belgium

Poster presenter at the SFB '15 held 10-14/03/15 in Freiburg/Germany

Participant at the IUAP network DevRepair meeting held at 08/12/14 in Rotterdam

Poster presenter at the 23rd EACR Congress held 05-08/07/14 in Munich/Germany

Poster presenter at the annual VIB seminar at Residents Duinse Polders in Blankenberge/Belgium

PUBLICATIONS

Evi De Keuckelaere, Paco Hulpiau, Yvan Saeys, Geert Berx and Frans van Roy
Nanos genes and their role in development and beyond. Cellular and Molecular Life Sciences (ISI-IF: 5.788) (Published, *https://doi.org/10.1007/s00018-018-2766-3*)

Ismail Sahin Gul, Jens Staal, Paco Hulpiau, **Evi De Keuckelaere**, Kai Kamm, Tom Deroo, Ellen Sanders, Katrien Staes, Yasmine Driege, Yvan Saeys, Rudi Beyaert, Ulrich Technau, Bernd Schierwater and Frans van Roy.
GC content of early metazoan genes and its impact on gene expression levels in mammalian cell lines. Genome Biology and Evolution (ISI-IF: 4.487) (Published, *https:// doi: 10.1093/gbe/evy040*)

Evi De Keuckelaere, Vanessa Andries, Katrien Staes, Ellen Sanders, Geert Berx and Frans van Roy.
A new mouse model to study the role of ectopic Nanos3 expression in lung cancer (In preparation)

Nicolas Skrypek, Kenneth Bruneel, Cindy Vandewalle, Eva De Smedt, **Evi De Keuckelaere**, Bieke Soen, Joachim Taminau, Niels Vandamme and Geert Berx
ZEB2 stably represses RAB25 expression through epigenetic regulation with SIRT1 and DNMTs during epithelial-to-mesenchymal transition (In preparation)

PUBLICATIONS

Cellular and Molecular Life Sciences
https://doi.org/10.1007/s00018-018-2766-3

Cellular and Molecular Life Sciences

REVIEW

Nanos genes and their role in development and beyond

Evi De Keuckelaere[1,2,3,4] · Paco Hulpiau[1,2] · Yvan Saeys[1,5] · Geert Berx[3,4] · Frans van Roy[1,2]

Received: 11 October 2017 / Revised: 22 January 2018 / Accepted: 29 January 2018

Abstract
The hallmark of Nanos proteins is their typical $(CCHC)_2$ zinc finger motif (zf-nanos). Animals have one to four *nanos* genes. For example, the fruit fly and demosponge have only one *nanos* gene, zebrafish and humans have three, and *Fugu rubripes* has four. *Nanos* genes are mainly known for their evolutionarily preserved role in germ cell survival and pluripotency. Nanos proteins have been reported to bind the C-terminal RNA-binding domain of Pumilio to form a post-transcriptional repressor complex. Several observations point to a link between the miRNA-mediated repression complex and the Nanos/Pumilio complex. Repression of the E2F3 oncogene product is, indeed, mediated by cooperation between the Nanos/Pumilio complex and miRNAs. Another important interaction partner of Nanos is the CCR4–NOT deadenylase complex. Besides the tissue-specific contribution of Nanos proteins to normal development, their ectopic expression has been observed in several cancer cell lines and various human cancers. An inverse correlation between the expression levels of human Nanos1 and Nanos3 and E-cadherin was observed in several cancer cell lines. Loss of E-cadherin, an important cell–cell adhesion protein, contributes to tumor invasion and metastasis. Overexpression of Nanos3 induces epithelial–mesenchymal transition in lung cancer cell lines partly by repressing E-cadherin. Other than some most interesting data from *Nanos* knockout mice, little is known about mammalian Nanos proteins, and further research is needed. In this review, we summarize the main roles of Nanos proteins and discuss the emerging concept of Nanos proteins as oncofetal antigens.

Keywords Nanos · Pumilio · Germ cell specification · Cancer · Phylogeny · RNA-binding protein · RNA regulation · Multiprotein complexes · Cancer testis antigen · pRb deficiency

Introduction

Nanos was originally discovered and studied in *Drosophila melanogaster* (fruit fly) [1]. Nanos proteins belong to a highly conserved protein family found in both vertebrates and invertebrates. In *D. melanogaster*, the *nanos* gene was primarily found to be essential for anterior–posterior axis polarity, abdomen formation, and germ cell development [1–3]. The Nanos protein establishes a multisubunit translation-inhibitory complex with Pumilio, its RNA-binding partner. The genomes of mouse and other mammals contain three Nanos-encoding genes, *Nanos1*, *Nanos2*, and *Nanos3*. Nanos homologs exist in several other species, such as *Caenorhabditis elegans*, *Xenopus laevis*, and *Danio rerio* (summarized in Table 1). The germ stem cell function of Nanos orthologs is conserved from invertebrates to mammals such as *Mus musculus* (Nanos2 and Nanos3) [4] and *Homo sapiens* (Nanos3) [5]. Two essential characteristics of germline cells are that they can give rise to all the cell types present in the adult (totipotency) and that they are immortal, passing on their genetic information to an endless series of generations. Nanos protein expression has also been linked to increased cell migration and invasion [6, 7]. Ectopic expression of *Nanos1* mRNA and Nanos3 protein has been observed in

✉ Frans van Roy
frans.vanroy@ugent.be

1 VIB-UGent Center for Inflammation Research, Technologiepark 927, 9052 Ghent, Belgium

2 Molecular Cell Biology Unit, Department of Biomedical Molecular Biology, Ghent University, Technologiepark 927, 9052 Ghent, Belgium

3 Molecular and Cellular Oncology Laboratory, Department of Biomedical Molecular Biology, Ghent University, Technologiepark 927, 9052 Ghent, Belgium

4 Cancer Research Institute Ghent (CRIG), Ghent, Belgium

5 Department of Applied Mathematics, Computer Science and Statistics, Ghent University, Krijgslaan 281, S9, 9000 Ghent, Belgium

Published online: 03 February 2018

GC content of early metazoan genes and its impact on gene expression levels in mammalian cell lines

Ismail Sahin Gul[1,2], Jens Staal[1,2], Paco Hulpiau[1,2], Evi De Keuckelaere[1,2], Kai Kamm[5], Tom Deroo[1,2], Ellen Sanders[1,2], Katrien Staes[1,2], Yasmine Driege[1,2], Yvan Saeys[1,3], Rudi Beyaert[1,2], Ulrich Technau[4], Bernd Schierwater[5] and Frans van Roy[1,2*]

[1] Center for Inflammation Research, VIB, Ghent, Belgium

[2] Department of Biomedical Molecular Biology, Ghent University, Ghent, Belgium

[3] Department of Basic Medical Sciences, Ghent University, Ghent, Belgium

[4] Department of Molecular Evolution and Development, Faculty of Life Sciences, University of Vienna

[5] ITZ, Division of Ecology and Evolution, Stiftung Tieraerztliche Hochschule Hannover, Germany

* Author for correspondence: Frans van Roy, Department of Biomedical Molecular Biology & Center for Inflammation Research, Ghent University & VIB, FSVM Building, Technologiepark 927, B-9052 Ghent, Belgium, frans.vanroy@ugent.be

ACKNOWLEDGEMENTS

Jaren geleden en zelf maanden geleden kon ik hier alleen maar van dromen, maar nu is het eindelijk zover. Ik heb onderweg veel geleerd, zowel op wetenschappelijk als op persoonlijk vlak. Het verwezenlijken van dit doctoraat lukte echter niet zonder de hulp en steun van een hoop collega's, vrienden en familie.

In de eerste plaats wil ik graag Prof. Dr. em. **Frans Van Roy** bedanken. Jouw deur stond altijd open en ik apprecieerde het feit dat je complimenten kon geven als het goed was. Ook na je pensioen kon ik steeds met al mijn vragen bij jou terecht en heb je nog de tijd gevonden om mijn doctoraat volledig na te lezen.

Vanessa, jij begeleidde mij doorheen mijn eerste jaren van mijn doctoraat en al vlug bleek dat jij op elke vraag wel een antwoord wist. Als enige postdoc in ons labo had het volledige team ontzettend veel aan jou. Ook tijdens mijn laatste jaar was je er voor mij en kon je me motiveren om dit doctoraat tot een goed einde te brengen. Woorden schieten te kort om je hiervoor te bedanken. **Katrien** en **Ellen**, jullie waren ook een vaste waarde van het labo en stonden steeds klaar om uitleg te geven, al dan niet over werk-gerelateerde zaken. **Sahin**, you are a good teacher and it was nice talking to you about scientific and other stuff. **Vidhya**, you brought life in the lab! Partly by letting us taste some Indian "zero spicy" (= very spicy) food and partly by starting to organize girls nights with **Jolien**, **Nathalie** and **Ana**. **Jolien**, ik zal die fantastische jenever avond en nacht nooit vergeten! **Koen**, jij gaat steeds recht op je doel af, dat bewonder ik aan jou. **Jolanda** jij hebt me in het labo binnengebracht voor mijn thesis en hebt me voorgesteld voor dit doctoraat. **Mara**, jij hebt me wegwijs gemaakt tijdens mijn eerste weken in het labo (thesisjaar). ik herinner me jou als een glimlachende blok energie op hoge hakken. **Eleonora**, keep up the Italian spirit, your perseverance will bring you where you want to be.

Tenslotte werd ik voor het einde van mijn doctoraat opgevangen door de groep van Prof. Dr. **Geert Berx**. Bedankt Geert om u open te stellen voor Nanos3 en mij vertrouwen in te spreken.

Niels, een hardwerkende, vriendelijke kerel die altijd de laatste roddels weet en die mij met open armen in de unit heeft ontvangen. **Bieke** en **Nele**, met jullie kon ik ongegeneerd mijn enthousiasme over mijn neefje delen. **Bieke**, de wereld ligt aan je voeten, nu alleen nog kiezen wat je ermee gaat doen. **Nele**, je bent erg gedreven en gaat recht op je doel af, niemand zal jou kunnen tegenhouden van dat dan ook te bereiken! **Eva**, bedankt om het zonnetje van de 'Berx unit' te zijn. Tegenslagen maken jou alleen maar sterker en geven je nog meer inspiratie. Je ben er bijna! **Joachim**, jij bent supervriendelijk en bij jou kon ik ook terecht met kleine vraagjes of verhaaltjes over het bouwen van een huis. **Kenneth**, het was aangenaam om met jou te babbelen. Je bent goed bezig en met jouw

zelfstandigheid zal je het nog ver brengen. Jij komt er zeker, misschien wel al dansend. **Gillian**, jouw inzet en passie voor het werk typeren jou. Je zorgde ook voor sfeer en stond altijd klaar voor een feestje, jij vindt overal wel tijd voor. **Nicolas**, you always had time for a question, thank you for sharing some of your knowledge. **Sven**, bij jou kon ik steeds een enthousiaste update krijgen over verschillende series. Jouw project loopt al goed, als het zo verder gaat kom je er in 'no time'.

Steven en **Tim**, jullie ervaring, inspanning en wijsheid zijn ongelofelijk. Er is ook nog altijd plaats voor een grapje en plezier. Steven, ik denk maar aan de groene lichtgevende veters op de trouw van Eva. **Sarah**, jij bent de rust zelve. In al de chaos voer jij elke experiment goed en georganiseerd uit. **Kelly**, bedankt voor al je hulp en steun. Ik waardeer het enorm hoe je de laatste loodjes voor mij wat lichter hebt gemaakt.

Verder zou ik graag nog zoveel mensen van het gebouw willen bedanken; **Marita** en **Ann** die steeds klaarstaan met hun altijd aanwezige glimlach. De collega's in het animalarium, in het bijzonder **Céline** en **Korneel**, voor de goede zorgen voor mijn muizen. **Marnik** voor de statistische hulp. **Paco** voor de hulp bij de fylogenetische analyse. **Maria** for your everlasting smile and the chats in the hallway and in the library. Ik ben zeker dat ik nog verschillende mensen ben vergeten, ook aan hen een grote dankjewel!

Dan wil ik ook nog mijn vrienden buiten het werk bedanken waarmee ik fantastische momenten heb beleefd en tegen wie ik ook steeds mijn verhaal kon vertellen. Ik denk maar aan **Nastia, Eline, David, Ester, Steven, Joke, Elise…**

Verder wil ik ook nog mijn **ouders** bedanken, die me de vrije keuze gaven omtrent mijn studies en me altijd volledig gesteund hebben. Ik kan niet genoeg dankbaarheid tonen voor wat jullie voor mij gedaan hebben en nog steeds doen. **Ann**, als mijn grote zus en doctor in de toegepaste biologische wetenschappen begreep jij ook wanneer ik liever niet weer die vraag hoorde "hoe zit het nu met je doctoraat?". Door **Maarten** en jou werd ik vorig jaar de trotse meter van **Ewoud**. Een lief ventje als hij kan steeds een glimlach op mijn gezicht toveren, wat tijdens het laatste jaar soms wel van pas kwam. En tenslotte, **Jeroen**, samen een huis bouwen is niet altijd even gemakkelijk, dit in combinatie met het laatste jaar van mijn doctoraat maakte het er niet makkelijker op. Bedankt voor al je begrip en jouw zalige massages. Er staan ons nog veel mooie momenten te wachten, ik ben nu volledig klaar om de wereld met jou verder te verkennen!